Development and Mechanistic Studies of Short, Cationic and Broad-Spectrum Antimicrobial Peptides

A Dissertation Submitted to the
Indian Institute of Technology Guwahati

As Partial Fulfilment for the Award of Degree of
Doctor of Philosophy in Chemistry

Submitted by

TANUMOY SARKAR

Roll No.-186122042

Department of Chemistry

Indian Institute of Technology Guwahati

Supervised by

DR. SUNANDA CHATTERJEE

Associate Professor

Department of Chemistry

Indian Institute of Technology Guwahati

Department of Chemistry

Indian Institute of Technology Guwahati

Guwahati, Assam- 781039, India

December 2024

Declaration

I do hereby declare that the matter embodied in this thesis entitled "**Development and Mechanistic Studies of Short, Cationic and Broad-Spectrum Antimicrobial Peptides**" has been carried out by me under the supervision of **Dr. Sunanda Chatterjee**, Associate Professor, during the period July 2018 to November 2024, at the department of Chemistry, Indian Institute of Technology Guwahati (IITG), India. The work presented here has not been submitted for the award of any other degree or diploma at any other Institution.

In keeping with the general practice of reporting scientific observations, due acknowledgements have been made whenever the work described is based on the findings of the other investigators.

TANUMOY SARKAR
IIT Guwahati
December 2024

Certificate by the Supervisor

This is to certify that the thesis entitled "**Development and Mechanistic Studies of Short, Cationic and Broad-Spectrum Antimicrobial Peptides**" submitted by **Mr. TANUMOY SARKAR** (Roll number - 186122042) for the award of Ph.D. degree from the Department of Chemistry, IIT Guwahati is absolutely based on his own research work under my supervision. This thesis or any part of it has not been submitted for any degree/ diploma or any academic award anywhere before.

DR. SUNANDA CHATTERJEE
Associate Professor
Department of Chemistry
Indian Institute of Technology Guwahati
Guwahati, Assam -781039
Email: sunanda.c@iitg.ac

Acknowledgements

Ph.D. has been an exciting journey. A journey that has taught in life many lessons, helped gather experiences, gather wisdom, find ways of adapting to new challenges, looking at things from different perspectives and all these summing up to the effort of becoming a better student, a better learner. I feel lucky enough of waking up each morning in one of the most beautiful campuses and endeavoured educational institutes in the country, IIT Guwahati. The life in the campus was truly a bliss helping a lot to deal with the academic stress that one encounters being a research scholar. First and foremost, I would like to express my sincere gratitude to my supervisor **Dr. Sunanda Chatterjee**, Associate professor, Department of Chemistry, IIT Guwahati, for her all her guidance, support, motivation and inspiration throughout. She has been an excellent mentor. My immense gratitude towards **Dr. Priyadarshi Satpati**, Associate professor, Department of Biosciences and Bioengineering, IIT Guwahati, for providing with all the supports that strengthened my work and enormous help that I received from him over the entire period. I learnt a lot from his valuable knowledge and in-depth experiences.

My heartful thanks and humble gratitude towards the chairperson of my doctoral committee, **Prof. Debapratim Das**, Professor, Department of Chemistry, IIT Guwahati. His valuable insights and continuous evaluation of my work at different stages led me to this stage of successful completion of my work and writing of the thesis. I also express my gratefulness towards doctoral committee members **Dr. Kalyan Raidongia**, Associate professor, Department of Chemistry, IIT Guwahati and **Dr. Dipankar Srimani**, Associate professor, Department of Chemistry, IIT Guwahati for their considerable suggestions in wrapping up my work.

My sincere thanks to all my past lab mates **Dr. Karabi Roy**, **Dr. Gopal Pandit**, **Dr. Swapna Debnath** and **Dr. Monikha Chetia** for their kind cooperation and help in carrying out my work. I would also like to thank my present lab mates **Ms. Maitery Yadav**, **Ms. Jyoti Gangwar** and **Ms. Shrutimoyee Gogoi** their consistent cooperation and help in carrying forward my work. My special thanks to our master's students **Arnab**, **Tanya**, **Rahul** and **Suresh** who assisted me in many ways during the project work carried out by them in our lab.

I would further like to whole heartedly express my gratitude towards **Dr. Suvankar Ghosh** and **Mr. Vignesh S.R.** for all the collaborative work on MD simulations that strengthened my

experimental data. I am also thankful to **Dr. Rajkumar Parshottambhai Thummer**, Assistant professor, Department of Biosciences and Bioengineering, IIT Guwahati and his students **Pradeep Kumar Sundaravadivelu** and **Ronima K.R.** for helping me out with the MTT assays.

I deeply acknowledge my Ph.D. batchmates and friends **Debjyoti**, **Sandeep**, **Dr. Sagnik**, **Vinay**, **Tirupati**, **Altaf**, **Samir**, **Tamal**, **Dr. Arin**, **Bittu**, **Dr. Sabina**, **Dr. Rinki**, **Priyanka (Adhikari), Prangobinda, Dr. Chang, Dr. Bapan, Dr. Shankhadeep, Monuranjan** and **Dr. Pallab** for their help, support and assistance received in various forms during the academic journey.

I would like to thank all the research scholars working in the department of Chemistry. **Dr. Kanu Das**, **Dr. Araghni Bhattacharya**, **Dr. Sourav Das**, **Dr. Basab Kanti Das**, **Dr. Debasish Barman**, **Dr. Abhijit Roy**, **Priyam Ghosh**, **Partha Pratim Nath**, **Malay Kumar Baroi**, **Arup Samanta**, **Priyam Das**, **Avisekh Sarkar** are some of the names that deserve special mentioning.

I acknowledge **The Central Instruments Facility (CIF), IIT Guwahati** for the state-of-the-art instrument facilities. I my express sincere thanks to all the operators who operated ITC, FESEM, FETEM and MALDI-TOF instruments and helped me in acquiring data using those instruments whenever I required. I would also like to thank **North East Centre for Biological Sciences and Healthcare Engineering (NECBH)**, IIT Guwahati for the Flow Assisted Cell Sorting and FESEM imaging facilities that I used quite a few times. I would also like to thank the **Centre for Nanotechnology, IIT Guwahati** for letting me use their confocal instrument for acquiring some confocal images.

I acknowledge **The Department of Chemistry, IIT Guwahati** for providing me with the platform to work, learn and carry forward my research. Working in the department was a truly wonderful experience, surrounded by some of the brightest minds of the country in the field. I convey my sincere thanks to all the faculty members of the Department of Chemistry, as I received helps from many of them in different times while carrying out my research.

I further acknowledge **IIT Guwahati** as an institute for providing us with the best of the facilities not only in the terms of academic context, but also in terms of excellent accommodation facilities, modern games and sport facilities as well as good health care facilities.

Finally, and most importantly I express my strongest gratitude towards my grandmother and my mother without whom nothing would have been possible in my life till date and I dedicate this thesis work to them.

TANUMOY SARKAR

IIT Guwahati

December 2024

Abstract

The rising threat of antimicrobial resistance and the failure of the conventional antibiotics to tackle the crisis has necessitated the need for alternatives to the conventional antibiotics existing in the markets. Peptide based antimicrobial agents or antimicrobial peptides (AMPs) may be thought of an alternative to the existing ineffective drugs, as many of these have shown excellent prospects with superior properties including lesser scope for the microbes to develop resistance against them. However, these peptides also have certain limitations like salt-sensitivity, protease degradability, high cytotoxicity, along with high cost of production, that are to be addressed to make them commercially available in the clinics. Chemical modifications of the naturally occurring AMPs or *de novo* design of AMPs can provide us with essential avenues to tackle their limitations and render them effective *in vivo*. Our thesis is an attempt to design AMPs countering many of their inherent limitations discussed in the following chapters:

Chapter 1: Chapter 1 is an extensive literature survey on the antimicrobial peptides. In this chapter, we have discussed in details the cause of antimicrobial resistance, and the relevance of antimicrobial peptides in this context. We have provided examples of several AMPs that have been isolated from the natural sources from the early times of their discovery up till the recent times, and their limitations. Chemical modification techniques or *de novo* design methods that have been utilized to develop AMPs with desired characteristics have also been discussed comprehensively. We have also discussed the mode/ mechanism of actions of these peptides. Finally, we have provided examples of some the antimicrobial peptides that have made in their way to the clinics and are in wide range of use.

Chapter 2: Protease susceptibility is one of the major drawbacks the AMPs composed of L-amino acids. In this chapter, we modified two of our previously reported peptides P4 and P5 through a substitution of L-amino acids with D-amino acids. Partially D-substituted peptides P4A/P4B/P5A/P5B resulted in a loss of their activity tested against different microbial strains while fully D-substituted peptides, P4C and P5C were either found to retain their antimicrobial potencies or were accompanied with a marginal increase in their activity. D-peptides retained their non-cytotoxic and non-hemolytic nature. L-peptides P4/P5 degraded in the presence of the proteolytic enzymes and serum, while the D-peptides P4C/P5C were found to be completely protease and serum stable. The cause of proteolytic stability was addressed through MD simulations studies. MD simulations showed that the relative distance between the scissile peptide

carbonyl and that of the hydroxyl group of the seine-195 of the catalytic triad (H57, D102, and S195) of the proteases increased upon L → D substitution, making it difficult for the catalytic site to approach and act on the scissile bonds of the D-peptides. Also, binding of trypsin/chymotrypsin to the L peptides were energetically far more favourable compared to that of the D-peptides. Several biophysical, spectroscopic and microscopic techniques together established the membranolytic nature of the developed peptides P4C and P5C.

Chapter 3: In this chapter, we have employed alchemical free energy simulations (ΔΔG) to design potent AMPs and experimentally validated their anticipated antimicrobial potency against Gram-negative bacteria *A. baumannii*, Gram-positive bacteria Methicillin-resistant *S. aureus*, and fungus *C. albicans*. Taking our previously reported AMP P4 (LKWLKKL-NH_2) as the template, we designed a series of eight P4-analog peptides by side-chain substitutions [W3→ F3($P4^{W3F}$)/ Y3($P4^{W3Y}$)/ A3($P4^{W3A}$); L4→W4($P4^{L4W}$)/ F4($P4^{L4F}$)/ Y4($P4^{L4Y}$)/A4 ($P4^{L4A}$); W3L4 →A3A4 ($P4^{W3A,L4A}$)] at the positions 3 and 4 of the peptide. Using alchemical simulations, we calculated the difference in binding affinity (ΔΔG) between P4 and its analogs to the simple bacterial membrane-mimetic bilayer. These simulations revealed the underlying thermodynamics of peptide-bilayer selectivity and ranked the peptides based on the strength of their computed binding affinities to the bilayer. *In silico* ranking of peptides matched perfectly with the experimental antimicrobial efficacy. Adding a second tryptophan residue in P4 by substituting L4→W4 yielded $P4^{L4W}$, significantly improving the bilayer binding affinity and enhancing the antimicrobial potency against all the strains by 2-5 folds. Substitution of W3→F3/Y3 diminished the antimicrobial activity, while W3/W3L4→A3/A3A4 severely destabilized the peptide: bilayer complex, leading to the loss of activity of $P4^{W3A}$/$P4^{W3A,L4A}$. Peptides were unstructured both in the free state in water as well as in the presence of membrane mimic SDS, and the potent peptides displayed a membranolytic mode of action against the pathogens. We established that ΔΔG calculated from alchemical simulations were sufficiently reliable to draw quantitative conclusions regarding the effect of peptide mutations on the energetics of peptide: bilayer binding and its link to the structure and antimicrobial activity. Thus, alchemical simulations could be a tool for the rational design of short broad-spectrum membranolytic AMPs.

Chapter 4: In this chapter, we designed modified analogs of a naturally occurring peptide jelleine I, with an aim of increasing its antimicrobial potency and protease resistance. Phenylalanine residue in the sequence of the parent peptide was substituted with tryptophan in all the modified

analogs J1-J4. The charge of the designed peptides J1-J4 was systematically increased from +2 to +5, through the incorporation of a non-standard cationic amino acid Dab (analog of Lys) for inducing the protease resistance to the designed peptides. With the replacement of polar and hydrophobic amino acid residues with cationic Dab residue along the series of J1-J4 peptides, the hydrophobic-hydrophilic balance of the peptides was systematically diminished. J3 and J4 emerged to be the most active, among all the designed peptides against both Gram-positive and Gram-negative bacteria as well as fungus *C. albicans*. J3 was a better antimicrobial than J4 in the presence of physiological concentration of salt (150 mM NaCl), and displayed a faster killing kinetics compared to that of J4, though the latter had a higher charge over the former. J3 and J4 were protease (trypsin) and serum resistant. Both J3 and J4 were non-cytotoxic towards the mammalian cell lines within the range of their microbicidal concentrations. The antimicrobial potencies of these small cationic peptides were independent of any secondary structural requirements, and mostly governed by the electrostatic interaction in between the AMPs and the negatively charged microbial membranes. The designed peptides J3 and J4 were found to be membranolytic in nature. J3 with a lower positive charge than J4, was a better AMP compared to the latter, and hence it may be concluded that the optimum hydrophobic-hydrophilic balance is a very important parameter to be considered while designing synthetic AMPs.

Chapter 5: In this chapter, we designed two broad-spectrum cationic octapeptides WRL and LWRF, rich in arginine and tryptophan and both bearing a net charge of +4. The peptide WRL was found to be more potent compared to that of LWRF, tested against a number of Gram-negative and Gram-positive bacterial strains as well as fungus *C. albicans*, both in the absence and in the presence of the salts. The enhanced efficacy of the WRL was attributed to the presence of two tryptophan residues in WRL, one of them being at the N-terminus, over the only non-terminal tryptophan residue in LWRF. CD spectroscopy revealed that both the peptides were unstructured in their free state in water, but adopted a partial helical conformation in the presence of membrane mimetics. MD simulations revealed that in the case of WRL, both the tryptophan residues were found to be properly anchored inside hydrophobic pockets of the membrane bilayer in contrast to LWRF, where the sole tryptophan was pointing towards the water. This led to better peptide membrane interaction for WRL compared to LWRF. Both the cationic peptides were membranolytic in their mechanism of action and were established through several spectroscopic, microscopic and biophysical experiments. The peptide membrane interaction was primarily driven

by the electrostatic interactions as seen from the MD simulations. Both the peptides were non-cytotoxic and non-hemolytic well within the range of their microbicidal concentrations, however LWRF appeared to be more selective of the two. This study conclusively demonstrated that for cationic peptides of similar charge, number and the position of the tryptophan residues played a crucial role in determining the efficacy of the AMPs, owing to the critical role played by tryptophan in the initial peptide membrane interactions. However, one must also be aware that selectivity towards membrane binding decreased with the increase in the number of tryptophan residues. Hence, selecting an optimum number of tryptophan residues is crucial in striking a balance between high antimicrobial potency and membrane selectivity.

Chapter 6: Secondary structures of the AMPs are found to play an important role in their activity. In this chapter, we have reported *de novo* design of two short amphipathic peptides RR-12 (12 aa res; charge: +5) and FL-13 (13 aa res; charge: +6) based on the helical wheel projections. The peptides displayed broad-spectrum antimicrobial activity tested against a number of Gram-negative and Gram-positive bacterial strains, including MRSA as well as fungus *Candida albicans,* with low $MIC_{90\%}$ values ranging in between 2-7.5 μM. Peptides were highly salt-tolerant, as well as non-cytotoxic and non-hemolytic within the range of their microbicidal concentrations. Peptides displayed very fast bactericidal/fungicidal activities. Peptide RR-12 lost its activity to some extent in the presence of serum, while for the peptide FL-13 the extent of loss in its activity in the presence of serum was less pronounced. Peptides were unstructured in water but adopted alpha helices in the presence of bacterial membrane mimic SDS as well as LPS, implying that the peptides might adopt alpha helical structures when interacting with the bacterial cells and this might be the plausible reason for its excellent potency. Peptides were mebranolytic in nature and established through several assays like PI assay, NPN assay, DiSC 3(5) assay, FESEM/FETEM imaging of the peptide treated microbes, live cell NMR experiments, confocal imaging etc. The peptide-membrane/ membrane mimetic interactions at the atomic levels were understood using MD simulations. Thus, this work adds two new synthetic α-alpha helical peptides to the library of membranolytic broad-spectrum antimicrobial peptides that are non-cytotoxic/non-hemolytic. This work re-establishes the importance of hydrophilic-hydrophobic balance, positive charge, and primary sequence of the peptides, in designing potent antimicrobial peptides.

Chapter 7: In this chapter, we have discussed about the future directions.

Contents

Chapter 1: Introduction

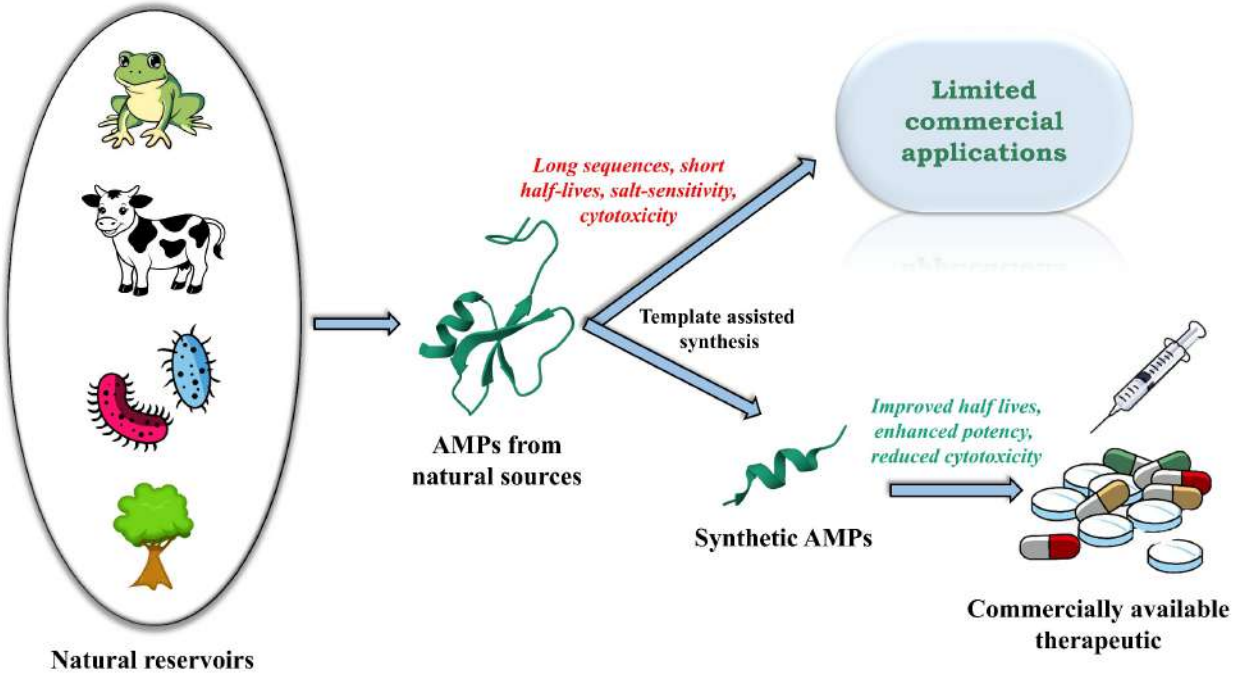

1.1. Microorganisms

Microbes or microorganisms are a class of living organisms that are too tiny to be seen with the naked eyes.[1] Microbes are found almost everywhere: air, water, soil, and even inside the body of other living organisms.[2-3] Microbes can be classified as bacteria, fungi, protozoans, protists, archaea etc.[4] Viruses are also considered as microorganisms although there is a controversy whether they are living or not.[5] Bacteria and archaea are prokaryotic microorganisms whereas protozoans, protists and fungi are eukaryotic forms of microorganisms. Microbes vary widely in their shape and though they are mostly unicellular, the existence of multicellular microbes is also known.[6-8] Most microbes are neutral to other living organisms. Some microbes are even beneficial for other living organisms. Many of the microbes are involved in the process of digestion of food, absorption of nutrients, production of vitamins and minerals, fighting of harmful infections and microbes throughout the living systems.[9-12] Microbes are also beneficial in the sense as many of bacteria and yeasts are used in the production of fermented food and beverages like bread, cheese, yogurt, curd, pickles, beer and wine.[13-16] However, a small percentage of the microbes are harmful for their hosts which they infect and may lead to some life-threatening diseases.[17]

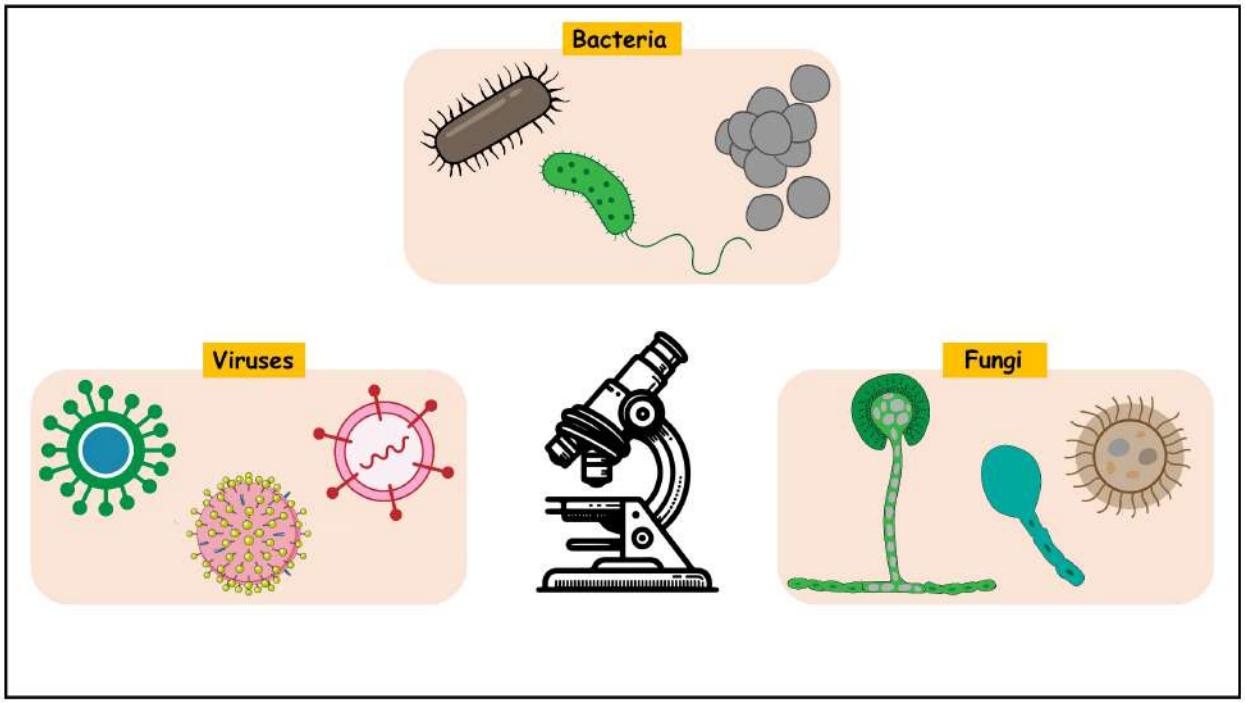

Figure 1.1. Pathogenic microorganisms.

1.2. Disease causing microorganisms

Most infectious diseases are caused by the three main types of microorganisms: viruses, bacteria, fungi.

1.2.1 Viruses

These are a class of microbes that are capable of replicating only after infecting the host. These microbes work by hijacking the cellular machinery of the host. Viruses contain some small nucleic acid sequences in the form of either DNA or RNA enclosed in a shell of protein. Some viruses may additionally be enclosed in membrane envelops made of lipids. Viruses may assume different shapes mostly being spherical or rod-like. Viruses spread and infect humans through various means like air, fecal-oral contact, sexual contact, insects/ mosquitoes, through animals and in many cases because of careless treatment procedures.[18] The table below enlists various diseases caused by different viruses spread through different modes of action.

Table 1.1. Diseases caused by different viruses.[18-23]

Virus	Symptoms	Mode of transfer
SARS-CoV	Fever, cough, tiredness	Airborne transmission
Influenza virus	Fever, chills, muscle aches, cough	Airborne transmission
Rhinovirus	Sore throat, runny nose, coughing, sneezing	Airborne transmission
Measles virus	High fever, cough, runny nose	Airborne transmission
Respiratory syncytial virus (RSV)	Cough, runny nose, congestion, sneezing	Airborne transmission
Adenovirus	Sore throat, sneezing, runny nose, cough	Airborne transmission
Poliovirus	Fever, fatigue, headache, vomiting	Fecal-oral

Hepatitis A	Diarrhea, vomiting, gastric pain	Fecal-oral
Dengue	Fever with nausea, vomiting, rash	Mosquito bites
HIV	Immunodeficiency, Kaposi's sarcoma	Sexual transmission
Hepatitis B	Abdominal pain, dark urine, fever	Sexual transmission
Ebola	Fever, headache, muscle pain and chills	Blood or body fluids
Nipah	Mild to severe symptoms including encephalitis and death	Fruit bats mostly, pigs and other animals may also act as carriers

1.2.2. Bacteria

Bacteria are prokaryotic, single cellular microorganisms believed to evolve roughly 3 billion years ago i.e., they are the oldest life forms that evolved on earth.[24-25] Bacteria are found everywhere on earth starting from air to deep inside earth's crust and they are majorly present in the bodies of other living organisms.[26] Human body is a host to almost as many bacterial cells as the number of eukaryotic cells that constitute it.[27] Majority of the bacterial species carry their genetic information in the form of a double stranded circular DNA.[28] Bacteria can be classified based on different aspects but most commonly they are classified based on their staining characteristics into two categories namely Gram-positive and Gram-negative.[29] Gram-positive and Gram-negative bacteria differ in their constitution of cell wall.[30-31] Bacteria adopt different shapes likes spheres or cocci, rods or bacilli, and spirals or helixes (spirochetes).[8] Majority of the bacteria are harmless to their hosts, some of them even beneficial like the bacteria present in the gut of humans are associated with process of digestion, absorption of nutrients, synthesis of vitamins and are therefore important factors for human health.[32] Less than 1% of the total bacteria are found to be harmful for their host causing illness. Bacteria is responsible for several diseases in humans, some of them being fatal. The table below lists diseases caused by different bacteria.

Table 1.2. Diseases caused by different bacteria.[33-40]

Bacteria	Name of the disease	Site of infection	Symptoms	Type	Mode of transfer
Mycobacterium tuberculosis	Tuberculosis	Lungs	Fever, night sweats, weight loss	Gram-positive	Airborne transmission
Streptococcus pneumonia	Pneumonia	Lungs	Fever, chest pain, cough	Gram-positive	Airborne transmission
Staphylococcus aureus	*Staphylococcus aureus* infection	Skin and soft tissue, lungs	Skin with blisters, abscesses; sometimes pneumoniae	Gram-positive	Physical contact with infected person
Pseudomonas aeruginosa	Pseudomonas infection	Chest, urinary tract, wound and blood	Coughing and difficulty breathing, urinary tract infections, pain, wound	Gram-negative	Food, surgical equipment, physical contact
Neisseria gonorrhoeae	Gonorrhea	Genitals, rectum, throat	Burning sensation while urinating	Gram-negative	Sexual intercourse
Klebsiella pneumoniae	*Klebsiella pneumoniae* infections	Bloodstream, urinary tract, meningitis, wound	Fever, cough, chest pain, pain while urinating	Gram-negative	Physical contact with infected person
Acinetobacter baumannii	*Acinetobacter baumannii* infection	Pneumonia, bloodstream, meningitis, wound and surgical site, urinary tract	Fever and chills, rash for bloodstream infections, pain or burning sensation for UTIs, flu-like symptoms for meningitis	Gram-negative	Contact with an infected person or environment that has the bacteria
Escherichia coli	*Escherichia coli* infection	Mainly gut, urinary tract	Diarrhea, stomach cramping	Gram-negative	Contaminated food/ water

1.2.3. Fungi

Fungi are a class of eukaryotic organisms constituting a separate kingdom in the classification of living organisms. Fungi have a distinct nucleus containing genetic material, a rigid cell wall composed of chitin that surrounds their plasma membrane and usually are much bigger in size

when compared to that of the bacterial cells. Single-celled fungi are called yeasts while those having long threads like filamentous structures are called hyphae. Unlike bacteria, in most cases fungi cannot invade a healthy host. They are called opportunist pathogens as they are found to infect immunocompromised patients with relative ease.[41] Most fungi like bacteria are harmless to humans, only a few selective number of species being responsible for diseases. The table below enlists different fungal species and diseases caused by them.

Table 1.3. Diseases caused by different fungi.[42-49]

Fungi	Name of the disease	Symptoms	Mode of transfer
***Candida* spp.** *C. albicans* *C. glabrata* *C. tropicalis* *C. parapsilosis* *C. krusei*	Candidiasis	**Vaginal candidiasis:** itching, burning and discharge **Candidiasis in the mouth and throat:** white patches, burning or itchy sensation **Candidiasis in the esophagus:** difficulty in swallowing **Invasive candidiasis:** fever and chills	Contact with infected people or contaminated surfaces
***Aspergillus* spp.** *A. fumigatus* *A. flavus* *A. terreus* *A. brasiliensis*	Aspergillosis	**Allergic bronchopulmonary aspergillosis (ABPA):** infection in lungs causing inflammation **Allergic Aspergillus aspergillosis:** infections in sinuses **Chronic pulmonary aspergillosis:** severe infections in lungs **Cutaneous (skin) aspergillosis:** aspergillus entering body through cuts or burns **Invasive aspergillosis:** Starts from lungs, goes on infecting brain, heart, kidneys.	Inhalation of airborne mold spores
***Cryptococcus* spp.** *C. neoformans* *C. gattii*	Cryptococcosis	**Lung infection:** Cough, pain on chest, difficulties in breathing **Meningitis:** Headache, blurred vision, depression, agitation, and confusion **Skin infection:** Rash, bumps filled with pus on skin or open sores	Inhalation of spores
Histoplasma capsulatum	Histoplasmosis	**Acute:** mild flu, fever, headache, chills, cough, muscle ache, fatigue	Inhalation of spores

		Chronic: severe infections in mouth, liver, central nervous system, skin and adrenal glands	
Coccidioides immitis	Coccidioidomycosis	**Acute:** fever, cough, tiredness, headache, difficulties in breathing, rashes on legs and arms **Chronic:** weight-loss, cough, pain in chest, sputum with blood, nodules in the lungs **Disseminated:** nodules, ulcers and skin lesions; lesions in different bones; swollen joints; meningitis	Inhalation of spores
Blastomyces dermatitidis	Blastomycosis	Fever, cough, breathing troubles, chest pain, pain in muscles, weight loss, tiredness, skin infections on hands and feet, severe forms of infections may hit brain, spinal cord, stomach, intestines and kidneys	Inhalation of spores

1.3. Antibiotics

The usage of antimicrobial compounds to treat infections has been in practice for millennia by humans. Usage of mouldy breads, beverages like beer or medicinal soils to treat wounds were quite common in the ancient times. The microbes present in them could produce a variety of antimicrobial compounds capable of treating infections. The usages of herbs which are a source of a wide variety of antimicrobial compounds to treat infections is quite common in Indian and Chinese culture. Presence of tetracyclines in the traces of human skeleton discovered in the modern-day Nubia also speculates the usage of antibiotics in the ancient era. Antibiotics are a class of antimicrobial drugs known for their ability to kill or inhibit the growth of bacteria. Salvarsan, discovered by Paul Ehrlich, was the first antibiotic used clinically followed by the discovery of Prontosil (a sulfanilamide-based drug) by Gerhard Domagk having broad-spectrum antimicrobial clinical usage. Alexender Fleming was credited with the discovery of the first antibiotic obtained from the natural source Penicillin. Norman Heatley, Howard Florey, and Ernst Chain later were involved in its isolation, purification and mass production for usage as a drug. Selman Waksman in another important name in the field of antibiotics who first introduced the word ‘antibiotic’ and is credited with the discovery of several antibiotics like actinomycin, streptomycin, and neomycin in the 1940s.[50-51]

Antibiotics may be classed into different categories based on their mechanism of action:

***(1) Antibiotics targeting cell wall*:**

β-lactams interact with the penicillin binding proteins present in the bacterial cell walls thereby inhibiting the synthesis of new peptidoglycans leading to disruption of peptidoglycan layers and hence resulting in cell death. Examples: penicillins, cephalosporins, monobactams, carbapenems.[52-54] **Glycopeptides** on the other hands prevent binding of D-alanyl D-alanine portion of peptide present in the peptidoglycan subunits to the penicillin binding proteins inhibiting cell wall synthesis, for example vancomycin.[55-57]

(2) Antibiotics targeting bacterial membranes:

Polymyxins are a class of antibiotics that target the lipopolysaccharide present on the outer membranes of Gram-negative bacteria leading to membrane damage and cell death. Examples: Polymyxin B and Polymyxin E. **Daptomycin,** a lipopeptide is another example of this category of antibiotics that inserts itself in the bacterial membrane leading to membrane rupture and hence cell death.[58-60]

(3) Antibiotics inhibiting biosynthesis of proteins:

Aminoglycosides are a class of antibiotics that binds to the 30s subunits of bacterial ribosomal leading to faulty protein synthesis responsible for membrane disruption. Streptomycin, gentamycin, neomycin and kanamycin represent this class of antibiotics. **Tetracyclines** are another class of antibiotics that also binds to the 30s subunits, blocks their association with the tRNAs, inhibits protein synthesis and induces cell death. Tetracycline, doxycycline and tigecycline are some examples belonging to the tetracyclines class of antibiotics. **Macrolides** (erythromycin, azithromycin etc.), **lincosamides** (lincomycin, clindamycin) and **chloramphenicol** represent different class of antibiotics that bind to the 50s ribosomal subunits blocking peptide bond formation between the amino acids. **Oxazolidinones** (linezolid) also represent a class of 50s ribosomal subunit binding antibiotics that inhibits complex formation between the 50s and 30s subunits.[61-63]

(4) Antibiotics inhibiting nucleic acid synthesis:

Fluoroquinolones (ciprofloxacin, levofloxacin, ofloxacin etc.) are a class of antibiotics capable of blocking DNA replication by inhibiting the activity of DNA gyrase. **Rifamycin** (rifampin) is a drug that blocks transcription by inhibiting RNA polymerase activity.[64-67]

(5) Antibiotics inhibiting metabolic pathways:

Sulphonamides (sulfamethoxazole, dapsone) are a class of antibiotics that function as antimetabolites acting as competitive inhibitors for metabolic enzymes. Sulphonamides block the production of dihydrofolic acid by inhibiting the enzyme involved in its production. This process leads to an inhibition of folic acid synthesis required for the biosynthesis of pyrimidines and purines which in turn is necessary for nucleic acid synthesis. **Trimethoprim** is another antibiotic belonging to this category that blocks the production of tetrahydrofolic acid and consequently the synthesis of folic acid and hence nucleic acids.[68-69]

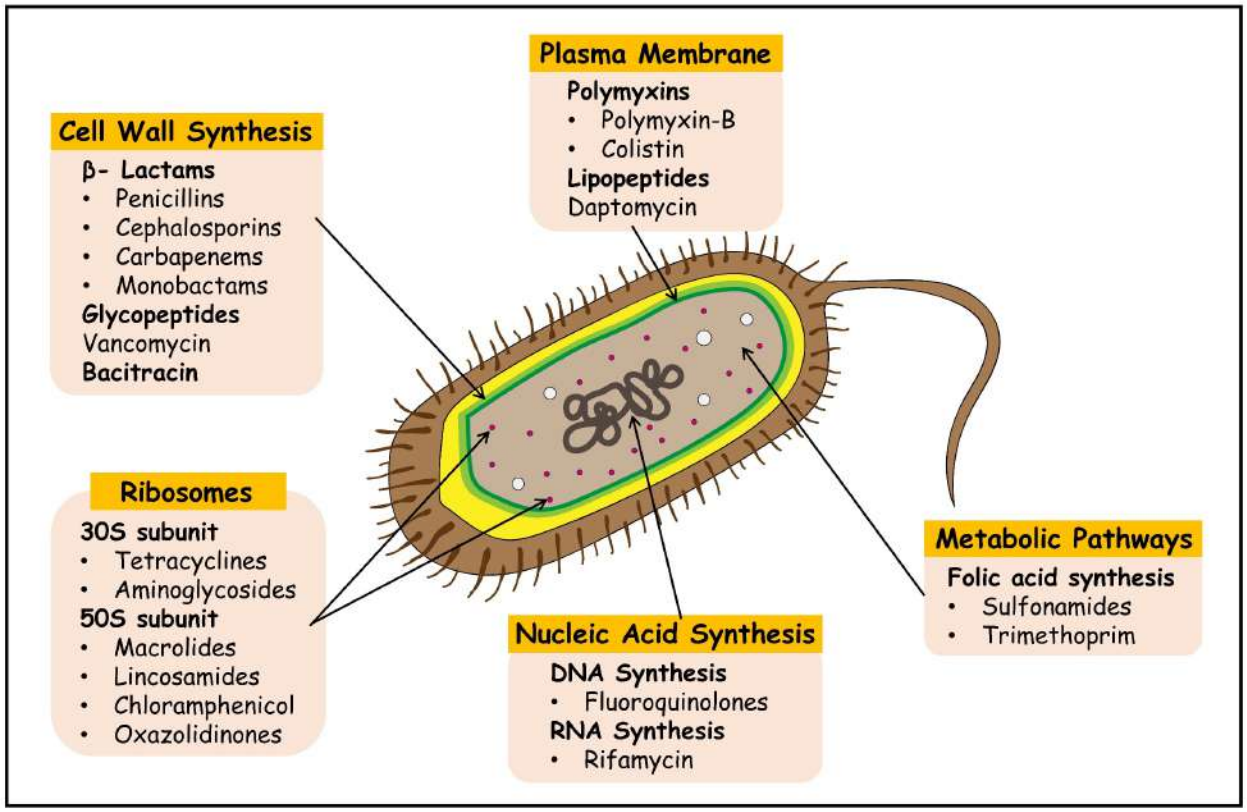

Figure 1.2. Targets within a bacterial cell for different classes of antibiotics.

1.4. Antifungal drugs

Antifungal drugs mostly operate by targeting the cell membranes of fungi. Fungi differ slightly in their membrane composition from that of the mammals. Ergosterol is the key sterol that constitutes the fungal membrane, unlike the cholesterol in mammals. Hence targeting ergosterol may serve as a route to eliminate fungi selectively without damaging the host's cells. **Azoles** are a class of antifungal medicines that kill fungi blocking the biosynthetic pathway for the synthesis of

ergosterol. **Imidazoles** (miconazole, ketoconazole, clotrimazole etc.), **triazoles** (fluconazole, itraconazole) and **allylamines** (terbinafine) are some subcategories of this azole class of antifungals. **Polyenes** are another class of antifungal drugs known to create pores in the plasma membrane by binding to the ergosterol. Amphotericin B (AmpB), natamycin, and nystatin are three major examples of polyenes. **Thiocarbamates** (tolnaftate) and **morpholines** (amorolfine, fenpropimorph) are also two other classes of antifungal drug that inhibit ergosterol synthesis. **Echinocandins** are a relatively new class of antifungal drugs that inhibit fungal cell wall synthesis by acting as inhibitors of 1,3-β-D-glucan synthase, the enzyme necessary for the synthesis of an important constituent of the fungal cell walls, namely β -glucan.[70-71]

1.5. Antimicrobial drug resistance

In nature evolution is a natural process. Microbes are in a continuous mode of evolution in order to combat the antimicrobial compounds produced by other microorganisms. Usage of antimicrobial drugs have furthered fueled up this process of evolution. Factors like excessive usage of antimicrobial compounds, their injudicious usage, incomplete dosages etc., have led to a situation known as antimicrobial resistance in which the conventional drugs known to treat certain infections are no longer effective. Repeated use of an antimicrobial compound against a species of microbe over time may lead to mutations in their chromosomes eventually making them resistant to that specific drug. These mutated chromosomes passed on to the subsequent generations will eventually give rise to a population of microbes having resistant genes. Horizontal gene transfers between microbes through plasmids or transposons may also be a reason for the development of antimicrobial resistance in some microbes.[72] A microbe may resist a drug in several mechanistic ways.[73-75]

(1) Prevention of cellular uptake of antimicrobial drugs into the cells or efflux of antimicrobial drugs from the cells

Prevention of cellular uptake may involve a change in the lipid composition of the microbial membrane, decrease in the number of porin channels or porin channel selectivity.[76] Small hydrophobic molecules like β-lactams or quinolines that are capable of invading the bacterial cells through the porins suffer resistance because of this mechanism.[77] Carbapenem resistance acquired in *Pseudomonas aeruginosa* is because of decrease in the number of porin channels.[78] Efflux pumps on the other hand are a class of membrane proteins in both Gram-negative and Gram-

positive bacteria involved in pumping the antibiotics out of the cytoplasm before they can reach their targets.[79] Resistance to many of the antibiotics like β-lactams, macrolides, tetracyclines, fluoroquinolones etc., are acquired through efflux pumps.[80]

(2) Enzymes inactivation

Resistance may also be acquired against different antibiotics through the resistant genes that encode enzymes that bring about chemical modification or hydrolysis of antibiotics.[81] β-lactamases are enzymes that are known to hydrolyze β-lactams having ester and amide bonds.[82] Aminoglycoside-modifying enzymes (AMEs) are enzymes that reduce affinity of a modified molecule to the ribosomal subunits providing resistance. Aminoglycosides and fluoroquinolones are examples of drugs that become ineffective because of AMEs.[83] Chloramphenicol transacetylase is an enzyme responsible for acetylation of the hydroxyl groups of chloramphenicol hence making it unavailable to bind with the ribosomal units.[84]

(3) Target modifications

Different group of antibiotics have a different set of targets in a bacterial cell and hence any structural changes or modifications of the target prevents binding of the antibiotics at their targeted sites making them ineffective. Changes in the structure of ribosomal subunits provides resistance to tetracyclines and aminoglycoside,[85] changes in the structure of LPS provides resistance to polymyxins,[86] mutations in DNA gyrase leads to fluoroquinolones resistance,[87] changes in the cell wall precursor leads to glycopeptide resistance,[88] mutations in RNA polymerase provides resistance to rifampicin.[89]

(4) Target overproduction or Enzymatic bypass

In many cases, resistance against a particular antimicrobial is acquired by a microbe through the expression of an excessive amount of the target enzyme so that there are sufficient free enzymes for the microbes to carry out their enzymatic functions even after antimicrobial binding.[90] Microbes may also develop resistance through the process of enzymatic bypass in which the microbe avoids the target enzyme for its functioning. Resistance to sulfonamide is known to take place by both these mechanisms.[91]

(5) Target mimicry

This is a strategy in which the microbes produce proteins that prevent antimicrobials from binding to their targets. MfpA protein produced by *Mycobacterium tuberculosis* binds DNA gyrase, preventing binding of fluoroquinolones to DNA gyrase.[92-94]

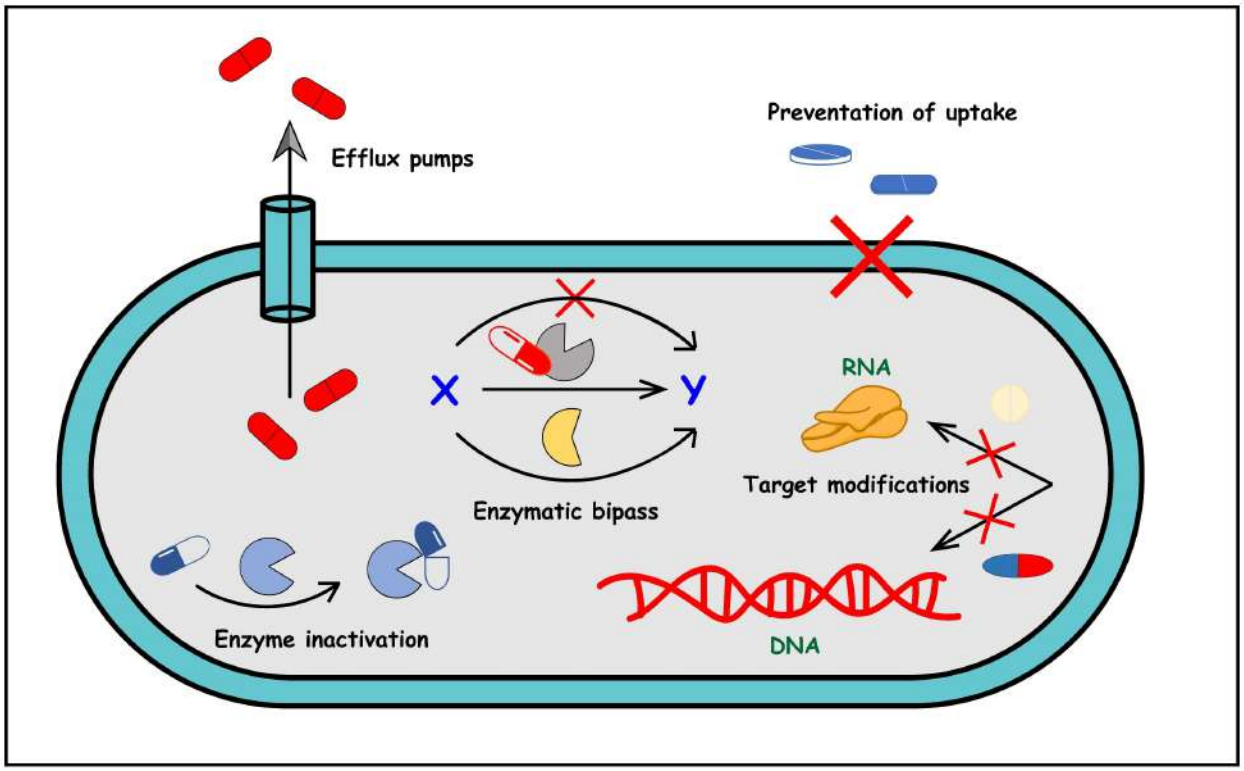

Figure 1.3. Different strategies adopted by microbes to develop resistance against antimicrobial drugs.

1.6. Antimicrobial Resistance (AMR) and its consequences

Antimicrobial Resistance (AMR) is a phenomenon in which the existing drugs available to treat the infections caused by microbes become ineffective. The most common form of antimicrobial resistance is antibiotic resistance in bacteria, where bacteria develop resistance to the antibiotics to which they are exposed. Resistance to antimicrobials is also reported in fungi, viruses and even in the parasites.[95] Repeated exposure of a drug to a microbe may lead to mutations making way for the newer generations of microbes with better adaptability to the exposed drug, making it ineffective. Microbes may also further transfer their genes to other microbes fueling the speed of antimicrobial resistance. Excessive, inappropriate or incomplete dosages of antimicrobials in health and non-health sectors (farming and animal husbandry), poor hygiene and sanitation facilities and overall lack of newer drugs to tackle the crisis are some of the leading causes responsible for the rapid spread of antimicrobial resistance.[96-97]

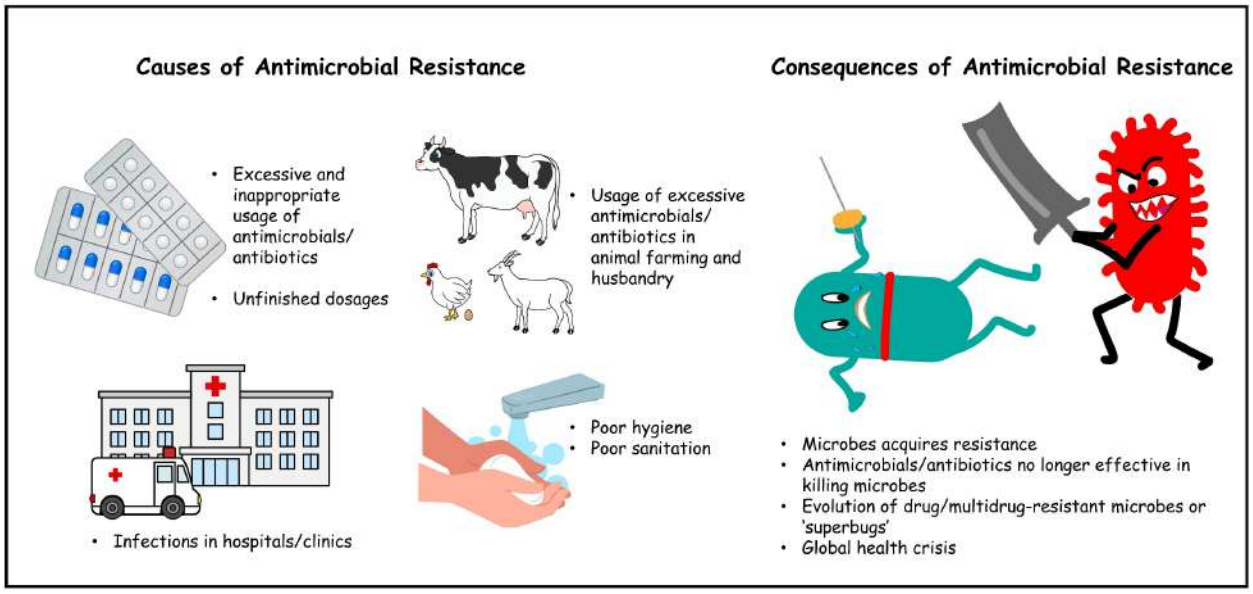

Figure 1.4. Causes of antimicrobial resistance and its consequences.

Antimicrobial resistance has given birth to some of the fatal drug resistant bacteria like methicillin-resistant *Staphylococcus aureus* (MRSA), vancomycin-resistant *Enterococcus* (VRE), multidrug-resistant *Mycobacterium tuberculosis* (MDR-TB) and carbapenemase-producing *Enterobacterales* (CPE).[98-100] Several species of *Aspergillus* and *Candida* have also shown to develop resistance against certain classes of antifungal drugs.[101] A study carried out by the Lancet reveals as many as five million deaths took place in 2019 alone, as a result of infections caused by resistant microbes. This figure is expected to increase many folds in the coming decades, if this situation is not dealt with seriousness.[102-103]

1.7. Antimicrobial peptides

Antimicrobial peptides, also known as host defense peptides[104-105] are a class of small protein molecules found in almost all classes of living organisms including animals, plants and microorganisms.[106-107] These peptides serve as the first line of defense in a host's intrinsic immunity system by resisting the invasion of pathogenic microbes like bacteria, viruses, fungi and sometimes even parasites.[108] These peptides, primarily synthesized as the secondary metabolites have also been found to have anti- inflammatory, anti-tumor/ anti-cancer properties in many of the cases in addition to their antimicrobial properties.[109] These peptides have lengths varying up to 100 residues and may adopt different secondary structures like alpha-helices, beta-sheets, random coils or a combination of these.[110-111] Most antimicrobial peptides carry a net positive charge,

although they may also be neutral or negatively charged.[112-113] Most of these peptides are also found to be considerably rich in hydrophobic amino acids other than the positively charged amino acids.[114-115] Peptide length, sequence, secondary structures, net positive charge and hydrophobic-hydrophilic balance are important parameters that are crucial for these peptides to display their antimicrobial activity. Antimicrobial peptides are known to realize their activity through various modes of action like membrane lysis,[116] intracellular targeting[117] and modulation of immune response.[118] Cationic AMPs mostly kill via membranolytic modes of action i.e., by targeting the microbial membrane leading to membrane rupture followed by cell death. Intracellular modes of action of AMPs involve inhibition of regular cellular processes by binding the bacterial DNA, RNA or membrane proteins.[109,119-120]Antimicrobial peptides may also exert their activity indirectly through immunomodulatory responses via recruitment and activation of immune cells, enhanced pathogen clearance and controlled inflammation.[121] The multiple mechanisms of action of AMPs are distinctly different from that of fixed intracellular targets of the conventional antibiotics, making them less prone to generate antimicrobial resistance in microbes, and hence better candidates to combat drug-resistant microbes.[122-123]

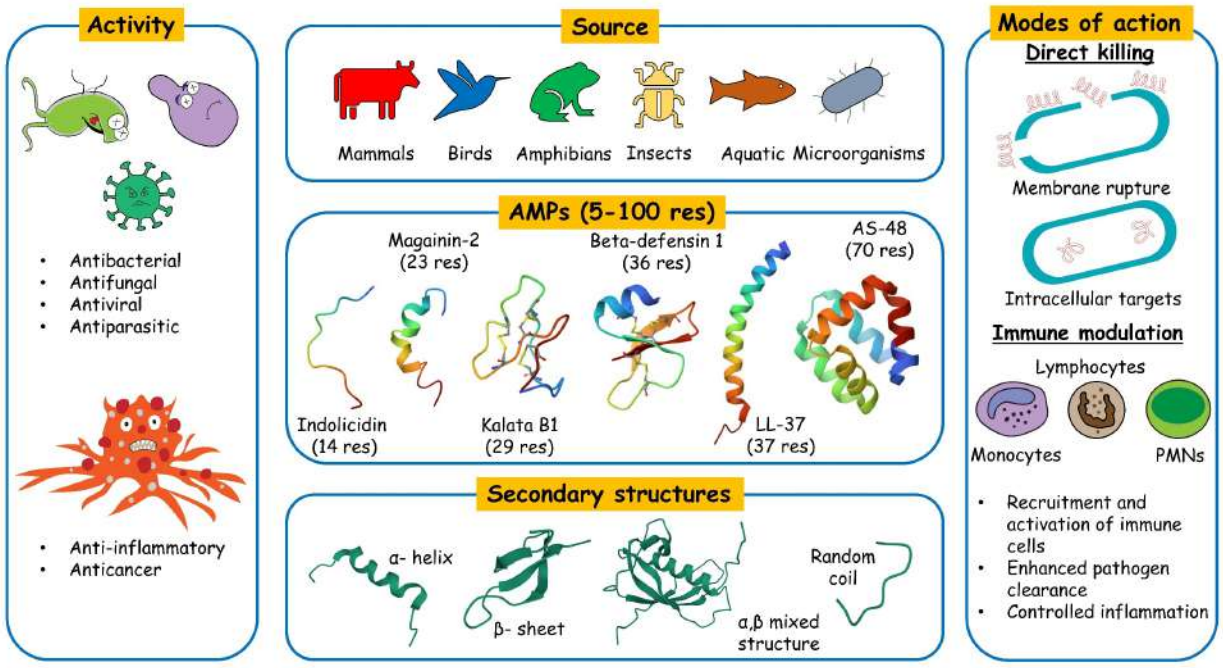

Figure 1.5. An introduction to antimicrobial peptides: length, source, secondary structures, activity and modes of action.

1.8. Antimicrobial peptides from natural sources

Antimicrobial peptides or AMPs have been isolated from almost all classes of living organisms including bacteria, archaea, protists, fungi, plants and animals. 3146 antimicrobial peptides from different natural sources have been identified or isolated till date as enlisted in the Antimicrobial Peptide Database (https://aps.unmc.edu/).[124]

Nisin (1928) was the first peptide based antimicrobial compound to be discovered, although its structure was established much later.[125-127] This was followed by the discovery of Gramicidin (1939), isolated from *Brevibacillus brevis* and effective against pneumococci infection.[128-130] Purothionins (1942) present in endosperms of wheat and other cereals species are a class of disulfide-rich basic antimicrobial peptides.[131] Purothionins exist in three isomeric forms namely: α1-purothionin, α2-purothionin and β-purothionin[132-135] and have considerable antimicrobial activity against different species of *Pseudomonas*, *Xanthomonas* and *Corynebacterium*.[136] Decapeptide Gramicidin S (1944) discovered by G.F. Gause was the first cyclic antimicrobial peptide to be discovered (antibiotics) and used clinically.[137-138]

Polymyxins (1947) are a class of another cationic antimicrobial compounds consisting of five different compounds (Polymyxin A-E). Polymyxin B and polymyxin E (also known as colistin) are only two from the group that are in clinical usage.[139-140] Polymyxin B and colistin are more selective in their activity against Gram-negative bacteria and are known to act by interacting with the negatively charged lipopolysaccharides present on the outer membrane of Gram-negative bacteria.[141-143] Colistin is considered as one the last resort antibiotics for its high cytotoxicity and lethal antimicrobial activity.[144]

Melittin (1967) is a peptide of insect origin that constitutes the primary bioactive component (40-60% of the dry weight) of the venom of European honey bee (*Apis mellifera*)[145-146] It is a linear cationic peptide with a chain length comprising of 26 amino acid residues, having significant hydrophobic characteristics as well as the ability to adopt α-helical conformation.[147-149] Melittin also has anti-cancer[150] and anti-diabetic[151] properties in addition to its excellent antimicrobial properties.[152-155]

Cecropins (1980) are class of insect-derived antimicrobial peptides, first isolated from the hemolymph of *Hyalophora cecropia* or giant silk moths. Cecropin A, cecropin B were the first two

peptides in the category to be isolated from *Hyalophora cecropia* and hence were named after the species.[156-157] Peptides with structural similarities to cecropins obtained from other species of insects like papiliocin,[158] sarcotoxin[159] and stomoxyn[160] etc., were subsequently discovered and added to the cecropins group of peptides.[161] Cecropins in general have length varying from 31-39 amino acids, generally adopt alpha helical secondary structures having broad spectrum antimicrobial activity against Gram-positive, Gram-negative bacteria, as well as fungi.[162-164] Some of the cecropins have also been identified to have considerable anti-cancer potentials.[165]

Daptomycin (1986) is a cyclic lipopeptide and among only a few of the antimicrobial peptides till date approved by the FDA for usage as a clinical drug.[166-167] Daptomycin is highly active against Gram-positive bacteria and is widely used to treat skin infections caused by *Staphylococcus aureus*.[168-169] Daptomycin has a mechanism different from most of the other antimicrobial peptides as it damages bacterial membrane by membrane depolarization inducing leakage of ions.[170-171]

Magainins (1987), are a family of antimicrobial peptides, that were isolated from the skin of frog *Xenopus laevis*. Magainins, in general represents two peptides magainin 1 and magainin 2, both of which are composed of 23 amino residues and have broad-spectrum antimicrobial activity against Gram-positive, Gram-negative bacteria as well as fungi.[172-173] These peptides are unstructured in water, however, adopt α-helices in the presence of bacterial membranes.[174-177] PGLa and peptides with structural similarities are also included in the magainins family of peptides.[178]

Tachyplesin (1988) is an antimicrobial peptide originally isolated from horseshoe crab *(Tachypleus tridentatus)* having a length of 17 amino acid residues and containing two disulfide bridges.[179] Tachyplesin has a β-hairpin structure and has potential antimicrobial activity against a wide range of microbes.[180]

Histatins (1988) are a class of histidine rich antimicrobial peptides secreted into the human saliva by salivary glands.[181] These are a group of 12 proteins: histatin-1-12. Histatin-1, histatin 3 and histatin 5 are three of the most common histatins and present as original sequences in the human saliva, while histatin 2 is a proteolytic fragment of histatin 1 and remaining histatins are proteolytic fragments of histatin 3.[182] Histatins are associated with several functions in the oral cavity and also have been found to have considerable antimicrobial potencies.[183-186]

Bactenecin (1988), an antimicrobial peptide containing 12 amino acid residues isolated from bovine neutrophils is the first peptide to be discovered and classified under cathelicidins. Two of the cysteine residues present in the peptide form a disulfide bond giving a folded structure to the peptide.[187]. Bactenecin is known to display excellent antimicrobial activity against Gram-negative bacteria, however it is also known to display considerable cytotoxicity.[188-190]

Apidaecins (1989) are a class of antimicrobial peptides isolated from the lymph fluid of the honeybee (*Apis melifera*). These peptides are 18-20 amino acid residues long and are highly rich in proline, usually unstructured and are known to be active against a wide range of microbes.[191-192]

PR-39 (1991), named after the high content of proline (P) and arginine (R) in its sequence and having a total of 39 amino acid residues, isolated from the intestine of pig, is another antimicrobial peptide categorized under the cathelicidin group.[193-195] This peptide is found to exhibit broad-spectrum antimicrobial activity against a number of microbes including some multidrug-resistant variants.[196-198] This peptide has an intracellular mode of action unlike majority of the antimicrobial peptides that kill via a membranolytic mode of action.[199]

Human α-Defensins are a group of six antimicrobial peptides: HNP 1 (1985), HNP 2 (1985), HNP 3 (1985), HNP4, HD 5 (1992) and HD 6 (1993).[200-204] HNP 1-4 are expressed in the human neutrophils and hence are named as named as human neutrophil peptides, while the other two peptides HD5 and HD6 are expressed in the human intestine by Paneth cells.[205-206] Human α-Defensins were found to be highly active against a wide range of microbes.[207] β-defensin are another class of antimicrobial peptides abundantly found in bovine sources, humans and also in birds.[208-211] hBD 1 (1995),[212] hBD 2 (1997),[213] hBD 3 (2001)[214] and hBD 4 (2001)[215] are some of the widely studied human beta defensins peptides.

Indolicidin (1992) is an antimicrobial peptide with a length of 13 amino acid residues, present in the bovine neutrophils.[216] This is a peptide with high arginine content and is known to display antimicrobial activity against a wide range of Gram-negative and Gram-positive bacteria as well as fungi, having a membranolytic mode of action.[217-220]

Protegrins (1993) are a class of antimicrobial peptides isolated from the porcine leukocytes, containing 16-18 residues of amino acids, having double disulfide bridges and hence β-sheet

structures.[221] These peptides have broad-spectrum antimicrobial activities against a variety of microbes.[222-223]

Esculentins (1994) are a class of AMPs that represent a large number of peptides isolated from the skin secretions of a wide variety of frog species. Esculentins are active against Gram-positive, Gram-negative bacteria as well as fungi.[224-226]

Temporins are a group of antimicrobial peptides first isolated in 1996 from the skin of frog *Rana temporaria*,[227] with numbers exceeding more than 130 till date.[228] Temporins have been isolated from different genera of frogs like *Lithobates*, *Pelophylax*, *Hylarana*, *Odorrana*, *Amolops* etc.[229] Temporins have a sequence length ranging from 8-17 amino acid residues, most being of 13 residues.[229-230] These peptides contain arginine mostly as the basic amino acid imparting positive charge, although lysine residues are also present as the basic amino acid in many of the sequences. Overall, they bear a charge of 0 to +3 and are in general are amidated at the C- terminus.[230-231] Temporins, generally unstructured in water, are known to adopt α-helices in the presence of microbial membranes or membrane mimics.[232-233] Temporins kill bacteria via a membranolytic mode of action. Initially they interact with the lipopolysaccharide of the outer membrane of Gram-negative bacteria or lipoteichoic acid of the Gram-positive bacteria, followed by inner membrane permeation and finally cellular rupture.[229,234-235]

Thanatin (1996) is a 21 amino acid containing antimicrobial peptide first isolated from the spined soldier bug or *Podisus maculiventris*.[236] This AMPs has a disulfide linkage due the presence of two cysteine residues in it and hence has a β-hairpin structure in both solution as well as in the presence of microbial membrane mimics.[236-239] Thanatin is known to exhibit excellent antimicrobial potency against a wide range of Gram-negative, Gram-positive bacteria and fungi, both *in vivo* and *in vitro*, and having both membranolytic as well as intracellular modes of action.[240-241]

Buforins (1996) are antimicrobial peptides first isolated from the stomach tissue of the Asian toad *Bufo bufo gargarizans*.[242] Buforin I is an antimicrobial peptide, 39 amino acid residues long, while buforin II, a derivative of buforin I, is an antimicrobial peptide with 21 amino acid residues. Both the peptides are highly active against a wide range of Gram-negative, Gram-positive bacteria as well as fungi, buforin II being superior in its activity than buforin I.[243]

Cyclotides are a class of antimicrobial peptides obtained from the plant sources, that are typically 28-37 amino acid residues long and having a cyclic cystine knot (cck). These peptides are head to tail cyclized and interconnected through three disulfide bridges linking the six cysteine residues in the sequences.[244-246] Kalata B1 (1999) belonging to the Möbius family of cyclotides is one the most studied antimicrobial peptides from the group.[247-248]

Ponericins (2001), isolated from ant species *Pachycondyla goeldii* are a group of fifteen peptides, grouped into three classes G, L and W, having significant antimicrobial activities against Gram-positive and Gram-negative bacteria.[249] Dermcidin (2001) is an antimicrobial peptide of human origin that is secreted into the sweat, by sweat glands, having broad-spectrum antimicrobial activity retained over a broad pH range as well as in high salt concentrations.[250]

Halocidin (2002) is a 33 amino acid containing peptide containing two sub-units having lengths of 18 and 15 amino acid residues, linked together by a disulfide bridge. Halocidin was isolated was from *Halocynthia aurantium and* showed considerable activity against both the Gram-negative as well as the Gram-positive bacteria.[251]

Plectasin (2005) categorised as a defensin is an antimicrobial peptide from the fungus source *Pseudoplectania nigrella* that could cure mice of pneumonia while displaying no cytotoxicity.[252]

Lasioglossins (2009) are a group of three fifteen amino acid residues peptides lasioglossin I, lasioglossin II and lasioglossin III, having antimicrobial activity against Gram-negative/ Gram-positive bacteria, anti-cancer potencies while displaying low hemolysis.[253]

Lucifensin (2010), is an antimicrobial peptide composed of 40 amino acid residues, with three disulfide bridges and are secreted in to the wounds as a disinfectant by blowfly (*Lucilia sericata*) larvae during a medical process call maggot therapy.[254] Lucifensin is categorized as an insect defensin I and has better activity against Gram-positive bacteria compared to that of Gram-negative bacteria.[255]

Temporin-SHf (2010), isolated from the skin of the frog *Pelophylax saharica* is an eight-residue antimicrobial peptide with high phenylalanine content displaying broad spectrum antimicrobial activity against a wide range of Gram-positive/Gram-negative bacteria and yeasts while adopting α helices seen in the presence of membrane mimics.[256]

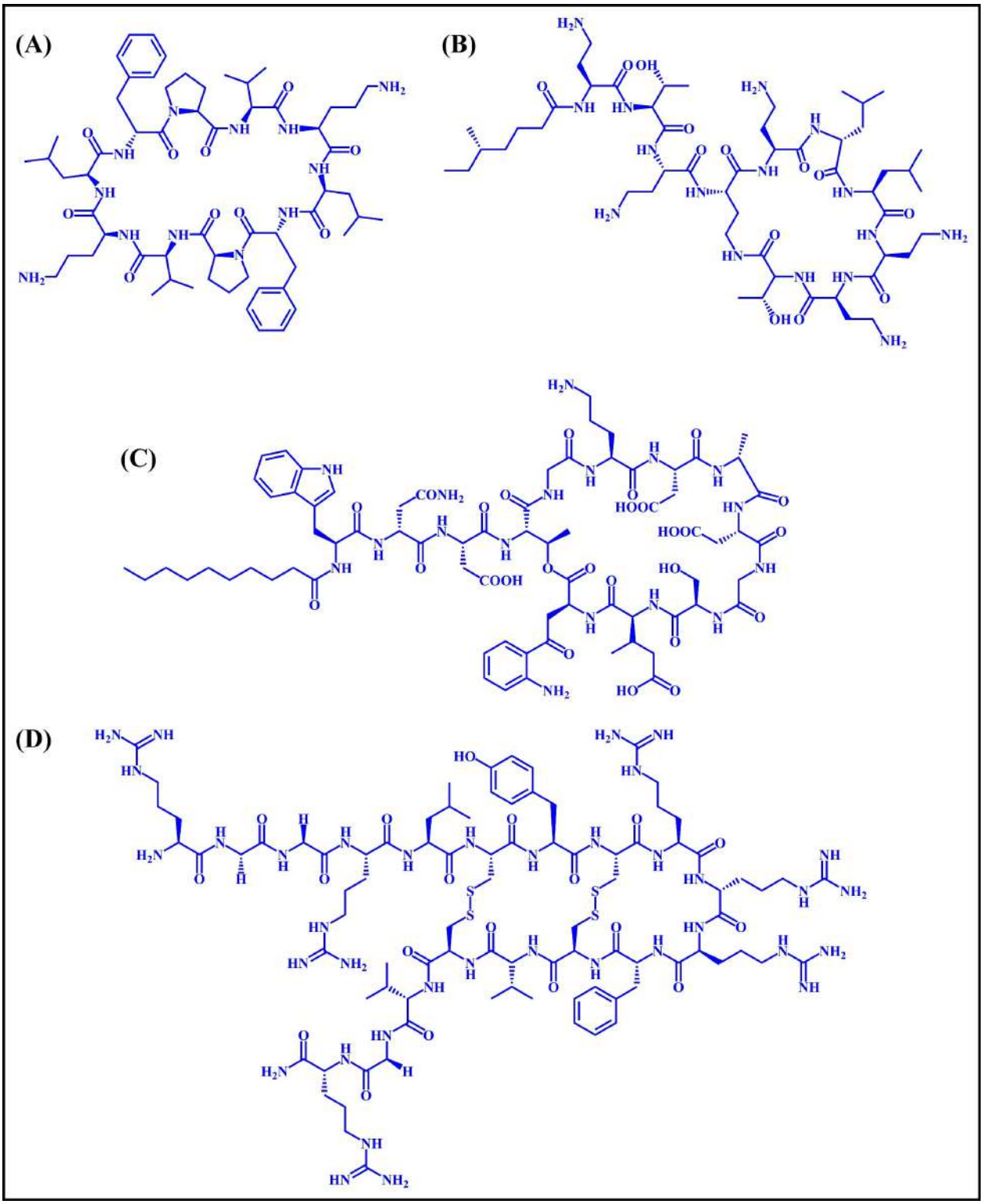

Figure 1.6. Some examples of antimicrobial peptides (AMPs) isolated from nature: (A) Gramicidin S, (B) Colistin or Polymyxin E, (C) Daptomycin and (D) Protegrin 1.

Gageotetrins A-C (2014) are three lipopeptides isolated from a marine *Bacillus subtilis*, that showed potent antimicrobial activity with no cytotoxicity.[257] Copsin (2014) is an antimicrobial peptide isolated from the fungus *Coprinopsis cinerea,* capable of killing bacteria by inhibiting their cell wall synthesis.[258]

Teixobactin (2015), isolated from the soil bacteria *Eleftheria terrae*, is a macrocyclic depsipeptide. It contains some unusual amino acids like l-allo-enduracididine and methylated phenylalanine, and is found to be very potent against Gram-positive bacteria with absence of resistance development in microbes against itself.[259] Teixobactin kill microbes by inhibiting cell wall synthesis.[260]

cPcAMP1 and its derivative cPcAMP1/26 (2016) isolated from the unicellular protist *Paramecium caudatum* displayed considerable antibacterial activity interacting with the LTA/LPS present in the outer membranes of the microbes.[261]

Lugdunin (2016) is a cyclic non-ribosomal peptide, isolated from the nasal bacteria *Staphylococcus lugdunensis* present in the humans and found to be bactericidal against *Staphylococcus aureus*.[262]

Urumin (2017) isolated from the skin of frog *Hydrophylax bahuvistara* is a 27 amino acid residue antimicrobial peptide discovered in the recent times and was found to display antiviral activity against influenza viruses.[263]

Tur1A and Tur1B (2018) are two proline rich antimicrobial peptides, isolated from the sea dolphin *Tursiops truncates* that displayed bacterial killing. Tur1A had a non-membranolytic mode of action of killing microbes. It inhibited protein synthesis by binding to the ribosomes.[264]

Very recently a 30 mer peptide Nv-CATH (2022) discovered from skin of the frog *Nanorana ventripunctata*, displayed broad-spectrum antibacterial activity against both Gram-negative and Gram-positive bacteria. It was additionally found to display immunomodulatory properties by repressing the production of NO, IL-6, TNF-α, and IL-1β.[265] The AMPs from the natural sources as discussed above are summarized in the table 1.4 below.

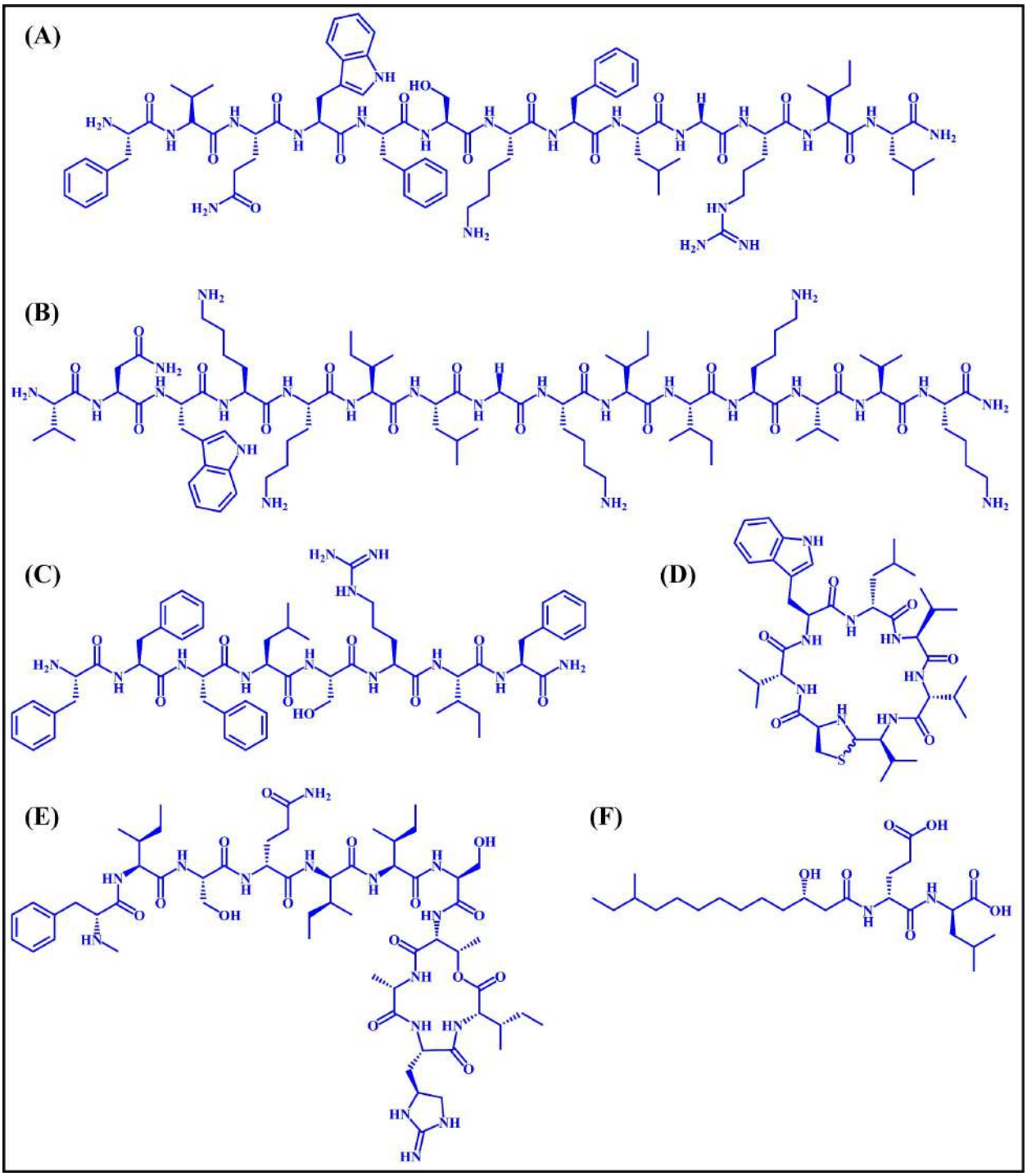

Figure 1.7. Chemical structure of of some antimicrobial peptides (AMPs) isolated from nature: (A) Temporin L, (B) Lasioglossin III, (C) Temporin SHf, (D) Lugdunin, (E) Teixobactin and (F) Gageotetrin A.

Table 1.4. Antimicrobial peptides (AMPs) from natural sources.[125-265]

AMP	Source	Physiological Properties	Targets/ Modes of action
Nisin	*Lactococcus lactis*	34 aa res; polycyclic peptide; contains uncommon amino acids	Gram-positive bacteria; pore formation and cell wall synthesis inhibition
Gramicidin	*Brevibacillus brevis*	Mixture Gramicidin A, B and C each having 2 isomers and 15 aa res	Gram-positive bacteria; act as a channel forming ionophores inducing pore formation
Gramicidin S	*Brevibacillus brevis*	Cyclodecapeptide; contains uncommon amino acids; β-sheet structure	Gram-negative/Gram-positive bacteria; disruption of membrane through formation of ionophores
Purothionins	Endosperm of wheat	Contains 8 cysteines forming 4 disulfide bridges	Different species of *Pseudomonas*, *Xanthomonas* and *Corynebacterium*
Polymyxin B	*Bacillus polymyxa*	Cyclic lipodecapeptide	Gram-negative bacteria; binds to the LPS of Gram-negative bacteria
Polymyxin E (Colistin)	*Bacillus polymyxa*	Cyclic lipodecapeptide	Gram-negative bacteria; binds to the LPS of Gram-negative bacteria
Melittin	Honeybee (*Apis mellifera*)	26 aa res; consists of two α-helical segments joined in a "bent rod" configuration	Gram-negative/Gram-positive bacteria; antitumor activity; membrane lysis
Cecropins	Insects; first isolated from *Hyalophora cecropia*	31-39 aa res; adopt α-helices in the presence of membrane/ membrane mimics	Gram-negative/Gram-positive bacteria and fungi; anticancer activity; membrane binding driven by electrostatic interactions and pore formation
Daptomycin	*Streptomyces roseosporus*	Cyclic lipopeptide	Gram-positive bacteria; binds to the cell membranes
Magainin	Skin of frog *Xenopus laevis*	Two types: Magainin A & B, both 23 aa res; adopt α-helices	Gram-negative/Gram-positive bacteria and fungi; membrane lysis

Tachyplesin	Horseshoe crab (*Tachypleus tridentatus*)	17 aa res; β-hairpin structure	Gram-negative/Gram-positive bacteria and fungi; membrane lysis driven by electrostatics
Histatin	Human saliva	Histidine rich; Histatin 1: 38 aa res; Histatin 3: 32 aa res; Histatin 5: 24 aa res	Antifungal; disruption of plasma membrane
Apidaecins	honeybee (*Apis mellifera*)	Proline rich; 18-20 aa res; unstructured	Gram-negative bacteria; binding with outer membrane
PR-39	Porcine	Proline & arginine rich; 39 aa res	Gram-negative/Gram-positive bacteria; inhibits protein & DNA synthesis; immunomodulatory activities
Human Neutrophil Peptides 1-4 (HNP 1-4)	Human neutrophils	HNP1: 30 res; HNP 2: 29 res; HNP 3: 30 res; HNP 3: 33 res	Gram-negative/Gram-positive bacteria, fungi and enveloped viruses; membranolytic interactions; immunomodulatory activities
Human α-Defensins 5	Paneth cells of human small intestine	32 aa res; 3 disulfide bridges	Gram-negative/Gram-positive bacteria; membrane lysis
Protegrins	Porcine leukocytes	16-18 aa res; 2 disulfide bridges; anti-parallel β-strand structure	Antibacterial, antifungal; membrane disruption
Esculentins	Skins of different species of frogs e.g., *Rana esculenta, Rana palustris*	Esculatin 1a: 46 aa res; Esculatin 2a: 46 aa res; α- helical structure	Gram-negative/Gram-positive bacteria and fungi; membrane binding interactions
Temporins	Skin of different genres of frogs including *Rana, Lithobates*, *Pelophylax*, *Hylarana*, *Odorrana*, *Amolops*	8-17 aa res; adopts α- helical structure in the presence of membranes	Gram-negative/Gram-positive bacteria; interaction with LPS or LTA present on the outer membrane of bacteria

Thanatin	*Podisus maculiventris*	21 aa res; 1 disulfide linkage; β-hairpin structure	Gram-negative/Gram-positive bacteria and fungi; membranolytic as well as intracellular mode of action
Buforin	Asian toad *Bufo bufo gargarizans*	Buforin 1: 39 aa res; Buforin 2: 21 aa res; adopt α- helices	Gram-negative/Gram-positive bacteria and fungi; inhibits the cellular functions by binding to DNA and RNA
Kalata B1	*Oldenlandia affinis*	Belongs to Möbius family of cyclotides; 29 aa res; head to tail cyclized with three disulfide bridges	Gram-negative bacteria; membrane lysis
Ponericins	Ant *Pachycondyla goeldii*	24-31 aa res; 3 sub-categories: Ponericin G, W and L; adopts α- helical structure in the presence of membranes	Gram-negative/Gram-positive bacteria; membrane lysis
Dermcidin	Human sweat glands	47 aa res; hexameric linear α-helical bundle structure	Gram-negative/Gram-positive bacteria and fungi; binds to the microbial envelops and signals inhibition of RNA/protein synthesis
Halocidin	*Halocynthia aurantium*	Total 33 aa res: two linear peptides one of 15 aa res and another of 18 aa res linked by a disulfide bond	Gram-negative/Gram-positive bacteria and fungi; membrane lysis
Lasioglossin III	*Lasioglossum laticeps*	15 aa res; α-helical in the presence of membranes	Gram-negative/Gram-positive bacteria; membranolytic as well as intracellular targets
Lucifensins	Blowfly *Lucilia sericata*	40 aa res; three disulfide bridges	Gram-negative/Gram-positive bacteria; membrane lysis
Temporin-SHf	Skin of frog *Pelophylax saharica*	8 aa res; high phenylalanine content; adopts α- helix in the presence of membranes	Gram-negative/Gram-positive bacteria and fungi; disrupts the acyl chain packing of anionic lipid bilayer
Gageotetrins	Marine *Bacillus subtilis*	Gageotetrin A: lipo-dipeptide; Gageotetrin B & C: lipo-tetrapeptide	Fungi; membrane lysis

Copsin	Inky cap mushroom *Coprinopsis cinerea*	57 aa res; contains one α-helix followed by two β-strands and is stabilized by six disulfide bonds	Gram-positive; inhibits the cell wall synthesis
Teixobactin	Gram-negative bacteria *Eleftheria terrae*	11 aa res; macrocyclic; contains unusual and D-amino acids	Gram-positive bacteria including drug-resistant strains; inhibition of cell wall synthesis
CPcAMP1/26	Protist *Paramecium caudatum*	CPcAMP1: 91 res; CPcAMP1/26: 26 res; adopt α-helical structure in the presence of membrane mimics	Gram-negative/Gram-positive bacteria; bind to LPS/LTS, induce membrane permeabilization, depolarization and increase in intracellular ROS levels
Lugdunin	*Staphylococcus lugdunensis* present in human nose	Cyclic; consists of 6 aa res and a thiazolidine moiety	Gram-positive bacteria including drug-resistant strains; inhibits target bacteria by dissipating their membrane potential
Urumin	Skin of frog *Hydrophylax bahuvistara*	27 aa res	Influenza A virus; targets glycoprotein hemagglutinin and destroys influenza virions
Tur1A	Bottlenose Dolphin *Tursiops truncates*	32 aa res; Proline-rich	Gram-negative bacteria; inhibits protein synthesis by binding with the ribosomal tunnel
Nv-CATH	Skin of the frog *Nanorana ventripunctata*	30 aa res	Gram-negative/Gram-positive bacteria; immunomodulatory activities

1.9. Classification of Antimicrobial peptides (AMPs)

Antimicrobial peptides can be classified based on different aspects like (a) source, (b) secondary structures, (c) activity and (d) amino acid content.[106]

1.9.1. Classification based on source

Antimicrobial peptides have been isolated from different sources like mammals, insects, amphibians, marine organisms, plants and microorganisms. Defensins, cathelicidins, histatins, lactoferricin, dermcidin, protegrins etc., are examples some of the AMPs studied widely that have been isolated from different mammalian sources including humans, bovine, cattle etc.[266-269] Insects are a source of innumerous antimicrobial peptides like insect defensins, cecropins, attacins, lebocins, drosocin, diptericins, metchnikowin, ponericins, jelleines, apisimin, pyrrhocoricin, persulcatusin, melittin etc.[270] Almost one fourth of the total number of AMPs enlisted in the Antimicrobial Peptide Database or APD3 (https://aps.unmc.edu/) are from the amphibian sources and have been isolated mostly from the skins of frogs or toads.[271] Temporins, bombinins, aureins, maximin, brevinins, gaegurins, esculentins, magainins, dermaseptins, tigerinins, nigrocins, japanicins, palustrins, ranatuerins etc., are some of the AMPs that have been isolated from the amphibians.[272-273]A large number of AMPs with varying lengths, secondary structures, amphiphilicity have also been isolated from a wide variety marine organisms till date like clavanins, styelins, piscidins, halocyntin, hedistin, myxinidin, pleurocidin, arasins, astacidins, chrysophsins, crustins, hepcidins, myticins, aurelin, damicornin, penaeidins, strongylocins, tachyplesins, poliphemusins, discodermin A etc.[274-277] Plants too produce a large number of AMPs that are broadly classified into different categories like thionins, plant defensins, hevein-like peptides, knottins, stable-like peptides, lipid transfer proteins, snakins, cyclotides, α-hairpinin family etc.[278-282] Several antimicrobial peptides have been isolated from the microorganisms like bacteria, fungi and protozoans.[283] Nisin, mersacidin, pediocins, lactococcins, acidocins are some AMPs produced by lactic acid bacteria.[284] Enterocins are produced by *E. faecium*,[285] iturins are produced by *Bacillus* sp.,[286] viscosins, amphisin, tolaasin and syringomycins are produced by *Pseudomonas* sp.,[287] gramicidins are produced by *B. brevis*[128-129, 137], subtilosin A is produced by *B. subtilis*,[288] lacticin 3147 is produced by *Lactococcus lactis*[289] etc. Plectasin produced by *Pseudoplectania nigrella* is an AMP of fungal origin.[252]

1.9.2. Classification based on secondary structures

Antimicrobial peptides can be classified into different categories based on their secondary structures: α-helical peptides, β-sheet peptides, β hairpin peptides, αβ mixed structure peptides, extended peptides, looped peptides and cyclic peptides.[290-294] α-helical peptides are typically amphipathic peptides that may have α-helical secondary structure (in water) or may adopt α-helical conformation in the presence of membranes or membrane mimetics. Melittin, magainin 2,

cecropins, LL-37, clavanin etc., are some peptides with α-helical structures.[295-298] β-sheet peptides have β-strands linked through disulfide bridges that form sheet-like structures. Defensins from humans, animals and plants, bovine lactoferrin, protegrins are some of the AMPs having β-sheet structures.[299-301] β-hairpin peptides are peptides having hairpin-like structure stabilized by disulfide bridges or hydrogen-bonding interactions. Tachyplesin I from horseshoe crab and thanatin from spined soldier bug are examples of AMPs with β-hairpin structures.[302-303] Mixed peptides are AMPs having a combination of both α-helices and β-sheets. Peptides belonging to the cis-defensins superfamily are a class of peptides having both α-helical as well as β-sheet structure within the same molecule e.g., plant C8 defensin NaD1, human beta-defensins 1 (hBD1) etc.[304-305] Extended peptides are AMPs that adopt no specific regular conformations like α-helices or β-sheets and are generally rich in certain amino acid residues like proline, arginine, tryptophan glycine etc., like indolicidin and histatins etc.[306-307,181] Looped peptides are peptides forming loops or cycles through disulfide linkages e.g., cyclotides from plants.[308] Cyclic peptides are peptides that are head to tail cyclized (i.e. bond between the N- and C-termini). Gramicidin S, tyrocidine, polymyxins, daptomycin, echinomycin, cyclosporin A, aureobasidin A are typical cyclic AMPs.[137,309-314]

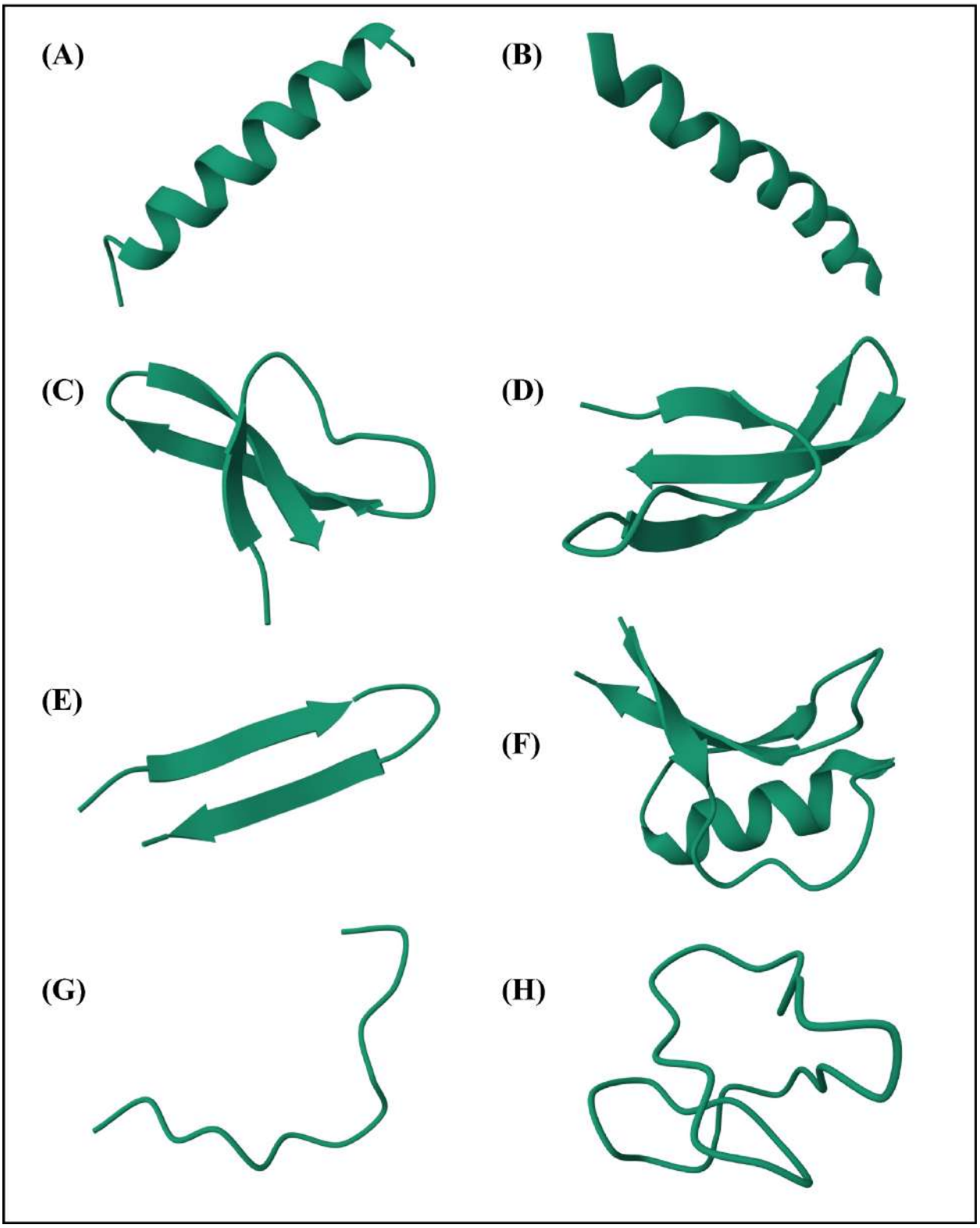

Figure 1.8. Secondary structures of some representative antimicrobial peptides collected from PDB. (A) Magainin 2 (α-helical, PDB id: 2MAG), (B) Clavanin (α-helical, PDB id: 6C41), (C)

HNP (β-sheet, PDB id: 3HJD), (D) Human alpha-defensin 1 (β-sheet, PDB id: 3LVX), (E) Tachyplesin I (β-hairpin, PDB id: 2RTV), (F) NaD1 (αβ mixed, PDB id: 4AAZ), (G) Indolicidin (extended/ random coil, PDB id: 1G89), (H) Kalata B1 (looped, PDB id: 1K48).

1.9.3. Classification based on activity

Antimicrobial peptides can also be classified based on their activity: antibacterial peptides, antifungal peptides, antiviral peptides, antiparasitic peptides, anti-inflammatory peptides, anti-cancer peptides etc.[315] Antibacterial peptides constitute the majority of the antimicrobial peptides isolated from natural sources. Some AMPs have broad spectrum antimicrobial activities against both Gram-positive and Gram-negative bacteria, while others may be selective against either of the Gram-positive or Gram-negative bacteria.[316] Most antibacterial peptides have a membranolytic mode of action, however some may have intracellular targets (modes of action in details have been discussed later).[317] α and β-defensins from different sources, cathelicidins, magainins, cecropins, protegrins, melittin etc., are some major classes of the antibacterial peptides.[318-319] Antifungal peptides constitute the second most abundant peptides in the library of AMPs after the antibacterial peptides. Antifungal AMPs like antibacterial peptides may target the fungal membranes or may have intracellular targets.[320-322] Several peptides belonging to α and β-defensins, protegrins, cathelicidins, histatins, dermaseptins, magainins, cecropins group of AMPs have antifungal activities.[323-324] Certain peptides have also been found to have antiviral properties. Peptides may target viruses in different mechanistic ways: (a) it can directly disrupt the viral envelops thereby damaging the virions and hence their ability to infect; (b) it can prevent the interactions between the viral surface proteins and the host cell receptors by binding to them; (c) it may even inhibit the replication of viral genomes by binding to viral nucleic acids or interfering with the viral polymerase enzyme.[263,325-328] Several peptides belonging to revinins, caerins, circulins, cycloviolacins, dermaseptins, esculatins, human beta defensins (1, 2 & 3), human neutrophil peptides (5 & 6), LL-37 are typical AMPs with antiviral properties.[329] Antiparasitic peptides are peptides with activity against protozoa (such as *Plasmodium* spp., *Trypanosoma* spp., and *Leishmania* spp.) or helminths (parasitic worms). Membrane disruption, prevention of parasites from invading host cells by binding to and neutralizing surface molecules essential for host-cell recognition and entry, disruption of intracellular processes are some of the mechanistic steps by which these peptides function. Bombinins, temporins, dermaseptins, melittin, apidaecins, cecropins, tachyplesin, clavanins, cecropins, thionins, tyrocidines, histatins and indolicidin are

some of the examples of the antiparasitic peptides.[330-331] Some of the antimicrobial peptides in addition to their antimicrobial activities may exert anti-inflammatory responses by suppressing the pro-inflammatory cytokines or promoting the anti-inflammatory cytokines, neutralizing toxins like LPS (inducers of inflammation) produced by the Gram-negative bacteria or by recruitment of immune cells to the site of infection or inflammation. LL-37, human beta defensin 3, papiliocin, dCATH are some representatives of anti-inflammatory AMPs.[332-333] Anticancer properties of many AMPs have also been detected. AMPs utilizes different methods to eliminate cancer cells including direct disruption of membranes, binding with different intracellular targets to induce apoptosis or through immune response modulation by generations of cytokines. Melittin, mastoparan, cecropins, aureins, dermaseptins, lactoferricin B, magainins, buforins, human neutrophils peptides 1, 2 & 3, citropins, tachyplesin, polyphemusins, piscidins are some examples of antimicrobial peptides with anti-cancer activities.[334-337]A few of the AMPs belonging to brevinins, esculatins, temporins, ranatuerins, magainins, pseudhymenochirins etc., were found to have anti-diabetic properties.[338]

1.9.4. Classification based on specific amino acids rich sequences

AMPs may also be classified based on the abundance of specific amino acids in their sequences like proline rich AMPs, tryptophan-arginine rich AMPs, histidine rich AMPs, glycine rich AMPs etc.[106,339] Proline rich AMPs are AMPs with high proline contents in their sequences and are mostly abundant in a wide variety of insects, crustaceans and mammals. Apidaecins, abaecin from honeybee *apis mellifera*, drosocin from fruit fly *Drosophila melanogaster* are some proline rich AMPs derived from insects. Arasin1 from spider crab *Hyas Araneus*, penaeidins isolated from shrimps belong to proline rich AMPs derived from crustaceans. Bac 5 and Bac 7 derived from cows, PR-39 derived from porcine source are examples of mammalian derived proline rich AMPs.[340-341] Proline rich AMPs in general has a non-membranolytic mode of action e.g., binding with the 70s subunit of the ribosomes and thereby inhibiting protein synthesis, binding and inhibition of heat shock protein DnaK or protein-folding protein GroEL.[342-345] AMPs with high content of tryptophan and arginine in their sequences are quite common in different sources in the nature.[346-347] The reason for the co-occurrence of arginine and tryptophan in many of the AMPs is the parallel or stacked arrangement between them that is energetically favourable.[348] Tryptophan has a high affinity for the membrane bilayers because of the unique hydrophobicity-hydrophilicity character associated with it, enabling its easy insertion into the membrane bilayers,[349-350] while

arginine because of its positively charged guanidine group can strongly interact with the components of the negatively charged surfaces of microbial membranes such as lipopolysaccharide, teichoic acid, or phosphatidyl glycerol phospholipid headgroups.[346] Hence, tryptophan-arginine rich peptides generally operate via a membranolytic mode of action. Indolicidin and lactoferricin from the bovine source, tritrpticin from the porcine source are some of the eminent examples from this group.[217,300,351] Peptides with high histidine percentages in their sequences like histatins in humans,[181,352] sherpins from shepherd's purse (*Capsella bursa-pastoris*),[353] histidine-rich glycoprotein,[354] AMPs derived from hard ticks,[355] clavanins,[356] Gad-1 and Gad-2 from Atlantic cod[357] etc., constitute another classification. Primarily these peptides inhibit microbes through a membrane disruption mechanism and have effect of pH on their activities.[358-359] Many AMPs also have a significant percentage of glycine residues present in them and they are classified as glycine rich AMPs like attacins,[360] gloverins,[361] diptericins,[362] armadillidins,[363] acanthoscurrin,[364] hyastatin[365] serrulin[366] sherpins[353] etc. Smaller size of the glycine side chain provides AMPs with the flexibility and conformational adaptability crucial for the peptide's ability to adopt various structures that are necessary for interacting with and disrupting microbial membranes.[367]

1.10. Limitations of the Antimicrobial peptides isolated from natural sources

Although more than 3000 antimicrobial peptides from different sources have been isolated till date, not even a dozen of them are in use clinically or have been commercialized.[368] There are several factors responsible that limit the usage of antimicrobial peptides as commercial antibiotics.[369] Most of the AMPs discovered till date have failed the clinical trials, many of these have shown excellent *in vitro* activities but have diminished *in vivo* activities. The first reason that limits the usage of AMPs is their salt-sensitivity i.e. reduction of antimicrobial activity in the presence of physiological concentrations of different salts.[370-373] Secondly, even if the peptides are less sensitive in the presence of salts, proteases or peptidases (protein cleaving enzymes) present in the biological systems degrade the peptides into smaller fragments thus reducing their effectiveness.[374-375]Short half-lives of many of the peptides due to their degradation in the presence of proteases/peptidases restrain their therapeutic potentials. Thirdly, serum present in humans (or other mammals) containing different proteins may interact with the AMPs to reduce their efficacies.[376-377] Apart from these many of these peptides display cytotoxicity and induce

hemolysis at concentrations close to their antimicrobial therapeutic dosages.[378-379] And finally, unfavorable economic viability for large scale commercial production is another factor that restrict their mass scale production.[380] Other factors like protein folding responsible for antimicrobial activities of many of the naturally occurring AMPs may not be induced in synthetically manufactured sequences. Thus, all these factors possess some serious challenges in the path of antimicrobial peptides or AMPs from the natural sources to be commercialized and used clinically.

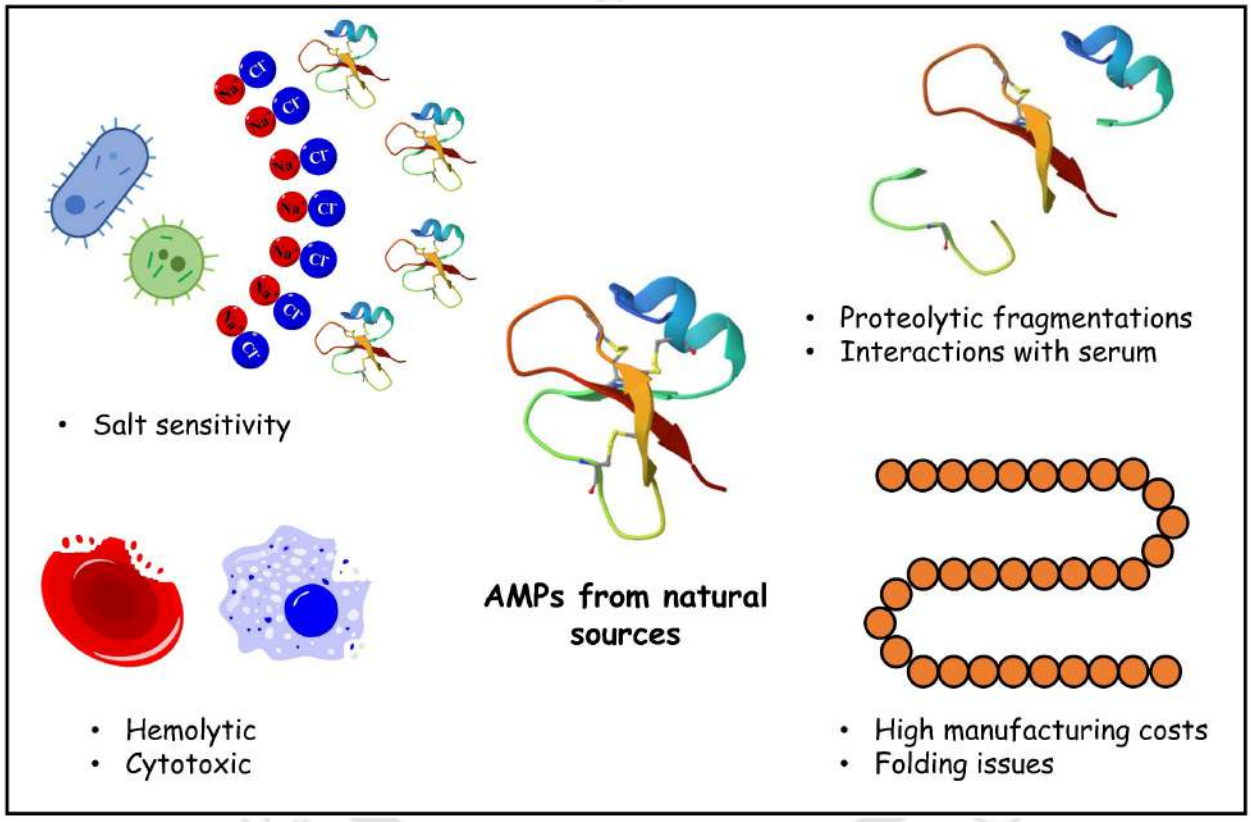

Figure 1.9. Limitations of AMPs obtained from nature restraining them for clinical usages.

1.11. Synthetic antimicrobial peptides

The limitations of the naturally antimicrobial peptides have been discussed in the previous section. AMPs can be tailored to generate synthetic AMPs based on their chain lengths, secondary structures, net charge, hydrophobicity and amphiphilicity, to circumvent their shortcomings and make them therapeutically superior. Design strategies of AMPs mainly include template-assisted design, *de novo* design, and computer aided design. Modifications of AMPs may also involve sequence truncations, deletions or substitutions of specific amino acids, modifications based on physicochemical properties (hydrophobicity, charge), secondary structures, termini alterations (N-

terminal acetylation, C-terminal amidation), incorporation/substitution of unnatural amino acids, substitution with D-amino acids, lipidation, cyclisation etc.[106,381-383] Various strategies adopted to enhance the potency of natural AMPs and to overcome their inherent shortcomings are systematically discussed here in details.

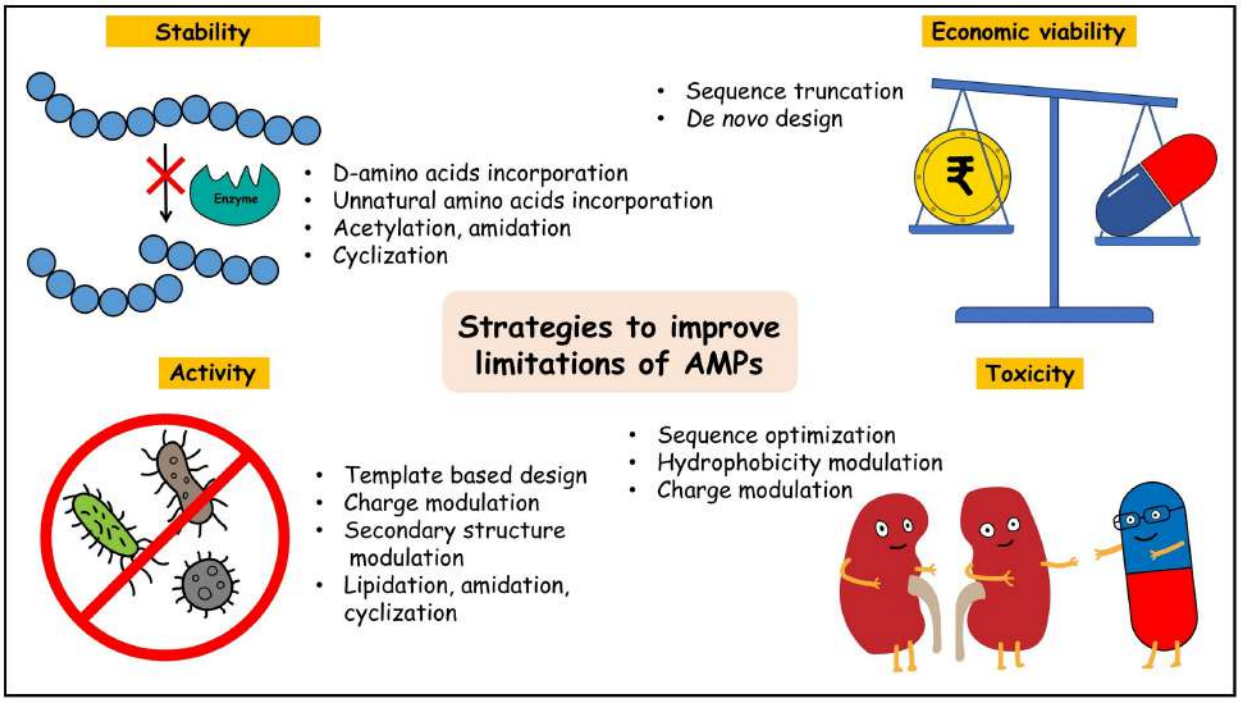

Figure 1.10. Strategies to improve the limitations of antimicrobial peptides.

1.11.1. Template based design of AMPs

This method involves the design of new antimicrobial peptides by modification of the existing antimicrobial peptide sequences as the templates. This method leverages known structures, sequences and characteristics of effective AMPs to guide the design process, aiming to produce new peptides that are both potent and selective against target microorganisms. AMP sequences with known characteristics like secondary structures, net charge, hydrophobicity, activity are chosen as templates. Modifications of the sequences may involve replacement of certain amino acids with more hydrophobic or charged residues to enhance interactions with the bacterial membranes and/or to reduce cytotoxicity. An increase in the antimicrobial activity of the peptide magainin 2 was observed upon extension of its length through the addition of basic amino acids i.e. either lysine or arginine both at the N-terminus as well as the C-terminus. Extension of the peptide length led to an increase in the helical content of modified peptides and hence an overall

improvement in the antimicrobial activity of the peptides were observed both against Gram-negative and Gram-positive bacteria.[384] Magainin 2 amide modified by increasing the net charge from +3 to +7 showed an increasing antimicrobial activity with increasing charge, however the peptide with +5 charge was found to be the most selective among all having optimum characteristics such as enhanced antimicrobial activity and minimal increase in the hemolytic activity. Peptides with higher charge showed a simultaneous increase in their hemolytic activity, the selectivity of such peptides could be increased by reduction of the hydrophobicity of the hydrophobic helix surface.[385] MSI-78, designed with magainin 2 as template through the incorporation of several additional lysine substituents, increased its ability to form helix in the presence of the membranes.[386] Another work revealed that stapling of a truncated magainin 2 derivative (17 amino acid residue fragment responsible for the antimicrobial activity of magainin 2) between its first and fifth position led to an enhanced antimicrobial activity with the retention of insignificant hemolytic activity.[387] CP-11 is a modified analogue of indolicidin modified by increase of net positive charge through incorporation of additional lysine residues to the peptide sequence keeping the chain length fixed. CP-11 showed an enhanced antimicrobial activity against a number of Gram-negative, Gram-positive and fungal strains, compared to that of the parent sequence indolicidin. CP-11C, the carboxymethylated analogue of CP-11, showed higher activity compared to that of CP-11.[388] A disulfide-bonded cyclic analogue of the peptide CP-11, cycloCP-11 displayed an overall reduced antimicrobial activity compared to that of the linear analogue. However, the cyclic analogue displayed longer stability and better retention of antimicrobial ability in the presence of trypsin compared to that of the linear analogue.[389] An increase in the net positive charge added at the C and the N termini of the peptide bactenecin and its linear analogue led to an overall increase in antimicrobial activities of the modified peptides.[390] TP1[F4A], TP1[I11A], and TP1[C3A,C16A], designed by a systematic amino acid replacement of template tachyplesin-1, led to an improvement of the therapeutic indexes with enhanced broad spectrum activity and low hemolytic activity.[391] Modified analogues of FK-13 (residues 17-29 of LL-37), FK-13-a1 and FK-13-a7, modified through incorporation of additional arginine and tryptophan residues as the substituents, showed enhanced therapeutic indexes compared to that of the parent sequence.[392] Several other LL-37 template based truncated and modified peptides with enhanced antimicrobial properties include GF-17, 17BIPHE2,[393] 17tF-W.[394] IG-13-1 and IG-13-2 are two modified analogues of truncated LL-37 engineered through varying charge and hydrophobicity that could

inhibit the formation of *Streptococcus mutans* at low concentrations, along with display of anti-inflammatory properties.[395] Modulation of the core antimicrobial motif of bovine lactoferrin (LfcinB6) through the increase of net positive charge and balance of hydrophobicity led to a peptide 5L with high antimicrobial activity against *Enterococcus faecium* compared to the parent peptide accompanied by low mammalian cell cytotoxicity.[396] OMN6, a 40 amino acid residue disulfide bridged cyclic analogue of the peptide cecropin A, displayed good activity against several Gram-negative bacteria including some multidrug-resistant strains, enhanced proteolytic stability and no cytotoxicity.[397] Truncation and modification of a peptide Cecropin 4 into a 18 amino acid residue peptide C18 obtained through variation of the charge and hydrophobicity balance, demonstrated high antibacterial activity against Gram-negative, Gram-positive bacteria and yeasts.[398] Pap12-1**,** a truncated derivative of the papiliocin, modified into different sequences by increase of the cationicity and amphipathicity, showed enhanced antimicrobial potencies compared to that of their parent analogue. Pap12-6, having tryptophan at the C-terminus was found to be most potent amongst all the designed peptides. It also displayed anti-inflammatory activity and low cytotoxicity.[399] N-15 Cath-2, the 15-residue long N-terminal fragment of the antimicrobial peptide CATH-2, was modified into several analogues based on a balance of charge, aliphatic character and amphipathicity. Of all the designed peptides, peptide DP1 (LLK) appeared to be the most potent of all having an overall increase in the antimicrobial activity with the simultaneous decrease in the toxicity and hence a superior therapeutic index.[400] Template assisted modification of temporin B through alanine scanning at different position of the sequence led to peptide TB_G6A with enhanced antimicrobial ability. TB_G6A further modified through addition of two lysine residues at the N-terminus produced a peptide TB_KKG6A. The modified peptide TB_KKG6A was more potent than TB_G6A and displayed broad-spectrum antimicrobial activity.[401] Another study on temporin B showed that its hydrophobic enhancement at the N-terminus and cationic enhancement at the C-terminus enhanced its membrane interactions and hence antimicrobial activity.[402] Template based modification of the antimicrobial peptide temporin-WY2, into a perfect amphipathic analogue QUB-142 and two lysine-clustered analogues 6K-WY2 and 6K-1426 showed an overall increased antimicrobial activity as well as enhanced therapeutic index compared to that of the parent peptides.[403]

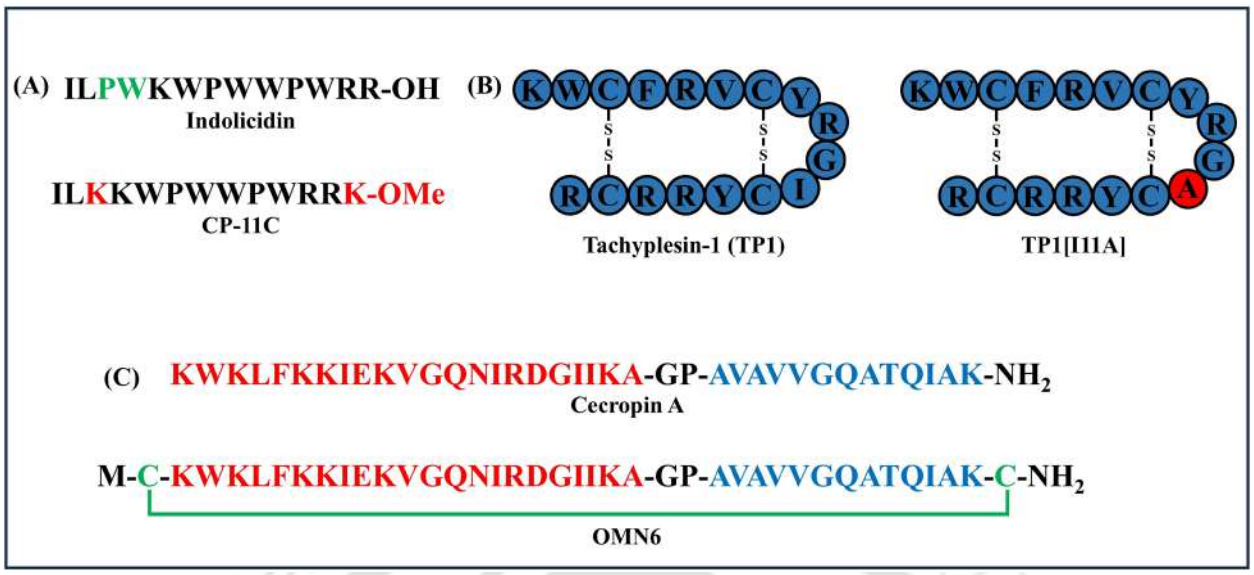

Figure 1.11. Template assisted design of antimicrobial peptides. (A) Template assisted modification of CP-11C[388] from indolicidin; (B) Design of TP1[I11A] based on tachyplesin-1 (TP1)[391] and (C) OMN6[397] modified from cecropin A. All the modified analogues displayed superior activity compared to that of their parent sequence.

1.11.2. De novo design of AMPs

AMP design strategies often rely on the consideration of empirical factors like length, charge, hydrophobicity, amphipathicity, secondary structures etc. *De novo* design of antimicrobial peptides refers to design of peptides not by modification of any existing sequences, but design of novel peptides sequences based on theoretical models and principles of amphipathicity, charge, helical structure, length etc. This design strategy generally utilizes selected amino acid residues which are highly abundant in the natural AMP sequences. For example, WLBU2 is a synthetic peptide designed based on a helical wheel model, derived through optimization of cationic and hydrophobic properties for superior antimicrobial activity. WLBU2 showed excellent activity against Gram-negative *Pseudomonas aeruginosa* as well as Gram-positive *Staphylococcus aureus* both in the presence as well as in the absence of salts, together with high selectivity.[404] *De novo* design of peptides with sequences $(KLAKKLA)_3$, $(KLAKLAK)_3$, $(KALKALK)_3$, $(KLGKKLG)_3$ and $(KAAKKAA)_3$ showed good antimicrobial activity against Gram-negative and Gram-positive bacteria, with the first three being cytotoxic, while the latter two being non-cytotoxic against 3T3 mouse fibroblast.[405] Peptides with designed sequences $G(IIKK)_nI\text{-}NH_2$ (n = 1, 2, 3 or 4) were screened against several Gram-positive and Gram-negative bacteria as well as cancer cells and

normal mammalian cells. Peptide with the sequence $G(IIKK)_3I\text{-}NH_2$ appeared to be the most selective among all, having potent antibacterial and antitumor activity in addition to minimum cytotoxicity against healthy mammalian cells.[406] A series of 11 undecapeptide isomers having the general formula L5K5W were designed and synthesized. The position of the tryptophan in the sequence was varied from residue 1 to residue 11 in the sequences. Although the peptides displayed similar antimicrobial activities but there were significant differences in their hemolytic activity based on the position of tryptophan in the sequences. Peptide W7 (L5K5W7) displayed highest therapeutic potential amongst all the peptides.[407] Series of peptides designed with repeating units of $(WRX)_n$, where X represents I, L, F, W or K and n = 2, 3, 4, or 5 and were screened against a number of Gram-positive and Gram-negative bacteria including some multidrug-resistant bacteria. $(WRK)_4$ and $(WRK)_5$ appeared to have the most optimum selectivity for bacterial membranes over the mammalian cell membranes.[408] Triblock amphiphilic peptides ($K_nF_mK_n$): $K_2F_6K_2$, $K_3F_6K_3$, $K_4F_6K_4$, $K_4F_8K_4$ were synthesized and screened against Gram-negative *E. coli* and Gram-positive *S. aureus*. All the peptides displayed some extent of antimicrobial activity against both the strains, $K_3F_6K_3$ being the most potent of all with activity comparable to many of the naturally occurring AMPs, while displaying very low cytotoxicity.[409]

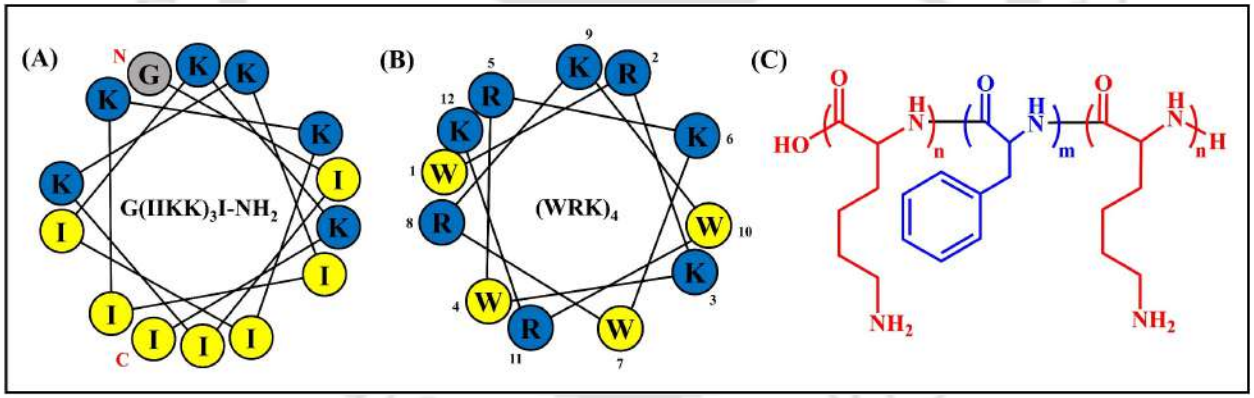

Figure 1.12. *De novo* design of AMPs. Helical wheel projection for the design of : (A) $G(IIKK)_3I\text{-}NH_2$[406]; (B) $(WRK)_4$[408] and (C) Chemical structure of Triblock amphiphilic peptides with general formula ($K_nF_mK_n$).[409]

1.11.3. Modification of AMPs by deletions or substitutions of amino acids

AMPs require a minimum number of amino acid residues in their sequences for their antimicrobial activity. Synthesis of large sequences of AMPs is not commercially viable, and thus sequences can be shortened by deletion of individual/ stretches amino acid residue(s) from their sequences, that

may not affect their antimicrobial activity. Substitution of certain amino acids with certain others in the sequences of many of AMPs are found to result in enhancement of the antimicrobial activity or reduction of cytotoxicity. Buforin II is a 21 amino acid bearing antimicrobial peptide having a random coil region at the N-terminus (1-4 aa res), followed by an extended helical region (5-10 aa res), a hinge (11 aa res) and finally another α-helical region (12-21 aa res) at the C-terminal. An increase in the antimicrobial activity was observed upon truncation of the random coil region.[410] Similarly, the truncated derivatives of LL-37 like KR-12 (residues 18 to 29 of LL-37) and FK-13-NH_2 (residues 17 to 29), retained their antimicrobial activities upon truncation.[411-413] Deletion of the either of 15th or 16th residue, or both of the 16th and 17th residues simultaneously from the sequence of a 21 mer peptide thanatin, resulted in an increased antimicrobial activity of the truncated peptides against Gram-positive bacteria.[414] C-terminal truncated peptide PC-13 (16 mer) displayed an enhanced activity against *Neisseria gonorrhoeae* compared to that of its parent sequence Protegrin 1 (18 mer).[415] Replacement of glutamic acid with glutamine in the 19th position in the sequence of the peptide magainin 2 as well as its amidation at the C-terminus yielded a peptide 19Q-MG2a, while phenylalanine at the 12th position substituted with tryptophan yielded 12W-MG2, both of which were found to have enhanced antimicrobial activity compared to that of their parent analogue magainin 2.[416] Replacement of E16 and K25 with two L residues and Q22, D26 and N30 with three K residues in the sequence of an antimicrobial peptide K^{15}-V^{32} [part of human cathelicidin LL-37 (L1-S37)] produced a peptide LLKKK which was far more superior than its parent analogue.[417] Replacement of all the arginine residues by lysine residues in the sequences of the peptide tritrpticin and its modified analogue SYM11,[418] to peptides TRK and SYM11KK respectively, led to an increased antimicrobial activity and decreased hemolytic activity.[419]

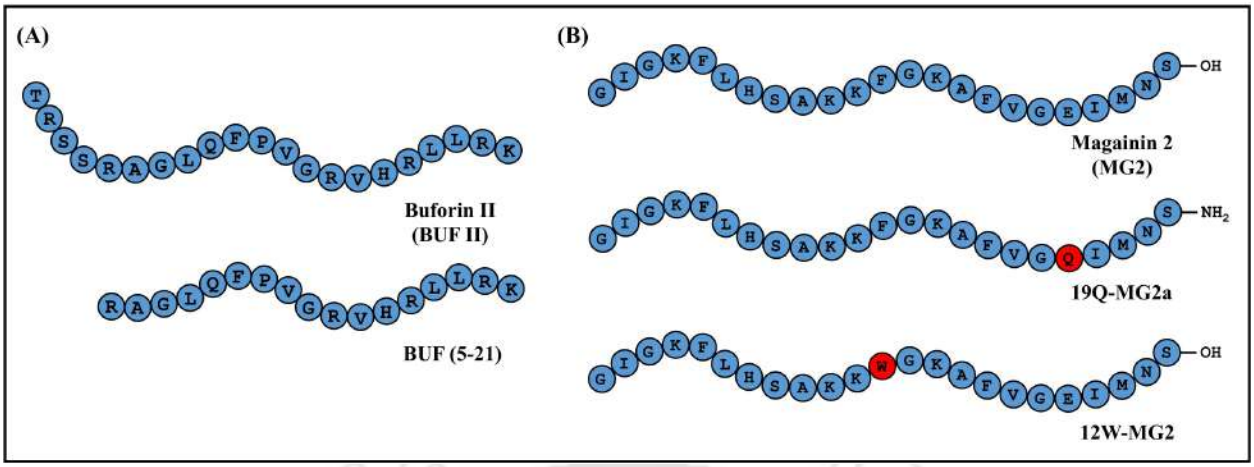

Figure 1.13. Modification of AMPs through sequence truncation or amino acid substitution. (A) Truncation of Buforin II (BUF II) to shorter analogue BUF (5-21) with enhanced antimicrobial activity.[410] (B) Amino acid substitution in the sequence of Magainin 2 (MG2) to produce 19Q-MG2a and 12W-MG2a with enhanced activity.[416]

1.11.4. N-terminal acetylation and C-terminal amidation

N-terminal acetylation or C-terminal amidation serves as another effective way to increase the efficacy of the antimicrobial peptides. N-acetylation of the AMPs may lead to an increase in the helicity of the peptides or the enzymatic stability of the peptides, while C-terminal amidation is an effective strategy to strengthen the structural stability and an increase in net positive charge leading to enhanced antimicrobial ability.[420] C-terminal amidation of a short arginine-tryptophan containing peptide Lfc1 led to an increase in the antimicrobial activity of the modified peptide, while N-terminal acetylation led to a decrease in the antimicrobial activity but increased protease resistance.[421] N-terminal acetylation of a synthetic octapeptide L1A led to an increased affinity and improved lytic efficiency against anionic vesicles as well as an increase in its helicity content.[422] A follow up study showed that acetylated form of the peptide L1A was able to penetrate deeper into the inside regions of the membranes.[423] N-terminal acetylation of a peptide L163 to L163-Ac led to an increase in its antimicrobial ability against certain microbes, along with an increased tolerance to temperature, pH, plasma and trypsin with the retention of low toxicity.[424] Removal of the C-terminal amidation of the peptide eumenine mastoparan-AF (INLLKIAKGIIKSL-NH_2) to its unmasked form INLLKIAKGIIKSL-COO^-, showed a reduction in helical content in the presence of the membrane mimics as established through CD, NMR and MD simulations.[425] C-terminal deamination of a peptide maximim H5 was found to be accompanied with a reduced

helical content, lower hemolytic activity and lower penetration ability into the membrane mimics of erythrocytes.[426] C-terminal amidation of the peptides Aurein 2.6-COOH and aurein 3.1-COOH revealed an increase in the helical propensity in the presence of lipid bilayers.[427] Amidation of a peptide N6 at the C-terminus to generate N6NH2 resulted in an overall enhancement of the antimicrobial ability in addition to improved trypsin resistance, reduced hemolytic activity and enhanced inner and outer membrane permeation.[428] C-amidated form the peptide maculatin 1.1 displayed superior antimicrobial activity, better membrane disruptive ability compared to that of the peptide in its acidic form.[429]

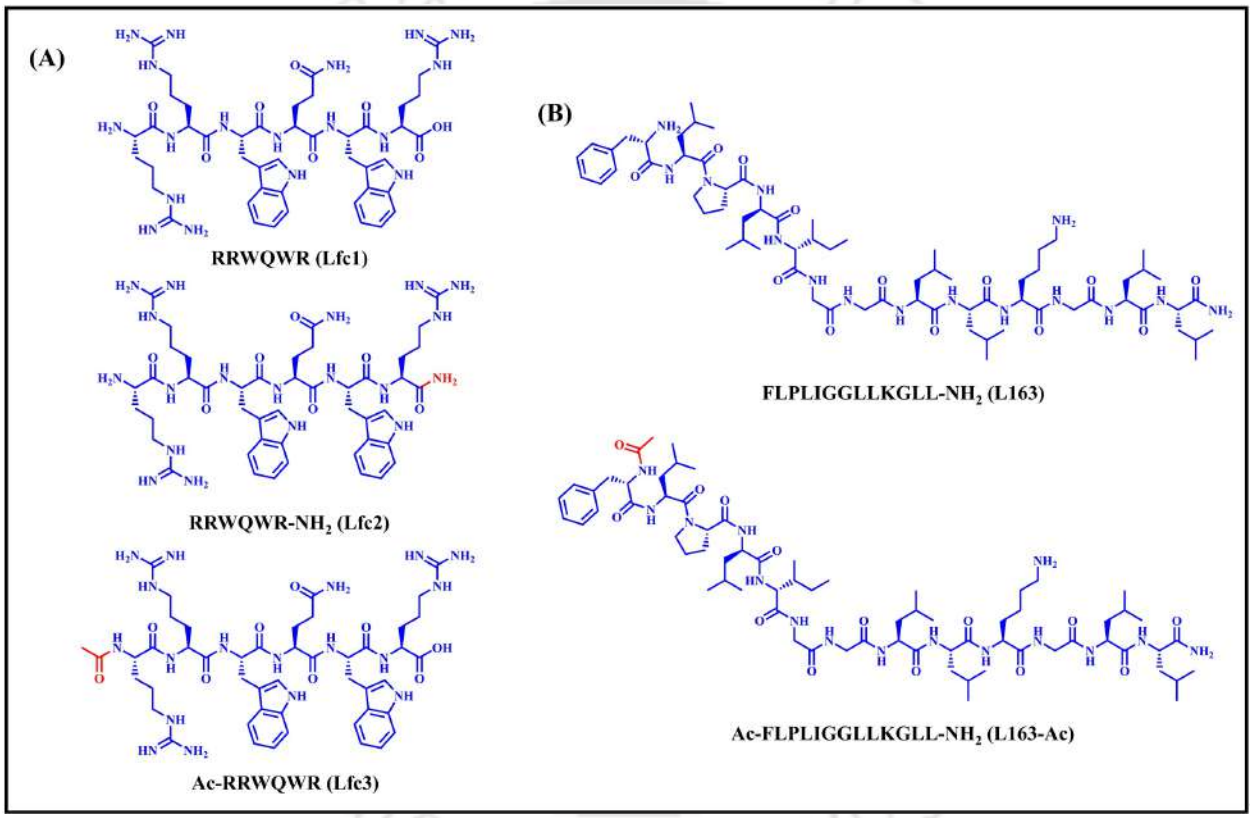

Figure 1.14. (A) Amidation of a peptide RRWQWR (Lfc1) produces a peptide with enhanced activity (Lfc2), while acetylation produces peptide with enhanced stability (Lfc3).[421] (B) Amidation of a peptide LPLIGGLLKGLL-NH_2 (L163) produces peptide with increased antimicrobial potency L163-Ac.[424]

1.11.5. Incorporation or substitution with D- amino acids

Naturally occurring amino acids in the sequences of proteins or peptides are almost exclusively composed of L-configuration. Hence, peptides composed of L-amino acids are prone to proteolytic

degradation if administered in the biological systems rendering them less effective. Inversion in stereochemistry of the amino acids in the peptide sequences from L to D is characterized with a significant proteolytic stability. Inclusion of D-amino acids also do not tend to decrease the antimicrobial potency of the peptides, and sometimes even results in enhanced activity.[430-432] D-enantiomers of the peptides cecropin A, magainin 2 amide and melittin as well as two synthetic chimeric cecropin-melittin hybrid peptides were found to be completely enzyme resistant and were almost equally as active as the L-isomers.[433] D-amino acids substituted at the C-terminus or the N-terminus or at the both ends of a peptide KKVVFKVKFKK to generate several diastereomers did not alter their antimicrobial activities, however stability of the modified peptides in serum improved significantly.[434] Diastereomeric isomer of a peptide K_6L_9, injected intravenously to cure neutropenic mice from the infections caused by drug resistant *Pseudomonas aeruginosa* and *Acinetobacter baumannii* showed effective results, while the all L-isomer was ineffective.[435] M33-D, the D-isomer analogue of a branched peptide M33, displayed a remarkable improvement in its antimicrobial activity against Gram-positive microbes compared that of its parent analogue along with complete resistance against bacterial proteases. Additionally, mice infected with *S. aureus* showed a 100% survival upon being treated with M33-D, compared to 0% survival with M33.[436] D-CopA3, enantiomeric counterpart of the peptide CopA3 retained its antifungal activity and non-hemolytic nature. The D-enantiomer however displayed complete trypsin stability and maintained antifungal activity in the presence of the trypsin, while the L-isomer degraded and lost its activity in the presence of trypsin.[437] II-D, with the peptide sequence $i(llkk)_2i$, an all D-amino acid containing peptide exhibited enhanced antimicrobial activity against different strains of *M. tuberculosis* compared to that of its all L-amino acid containing counterpart, with a 4 times improvement in the selectivity index.[438] An all D-amino acids containing peptide klkllllllklk-NH_2 exhibited superior antimicrobial activity compared to its all L-amino acid containing counterpart, with complete protease resistance. The enhanced activity of the D-enantiomer was attributed to its better binding to the peptidoglycan of *S. aureus* compared to that of the L-isomer.[439] All D-amino acid substitution of a peptide Polybia-CP to its enantiomeric form D-CP, and partial substitution of one of its lysine with D-lys to the diastereomeric peptide D-lys-CP resulted in an enhanced proteolytic resistance against trypsin and chymotrypsin for both the modified peptides.[440] Partial or full D-substitution of a peptide W3R6 to D-Arg-W3R6 and D-W3R6 respectively led to an increased proteolytic stability of the modified peptides.[441] Lipidated D-enantiomeric form of

bactenecin, dBacK-(cap) was far superior in its antimicrobial activity with very low MIC values compared to that its parent analogue.[442]

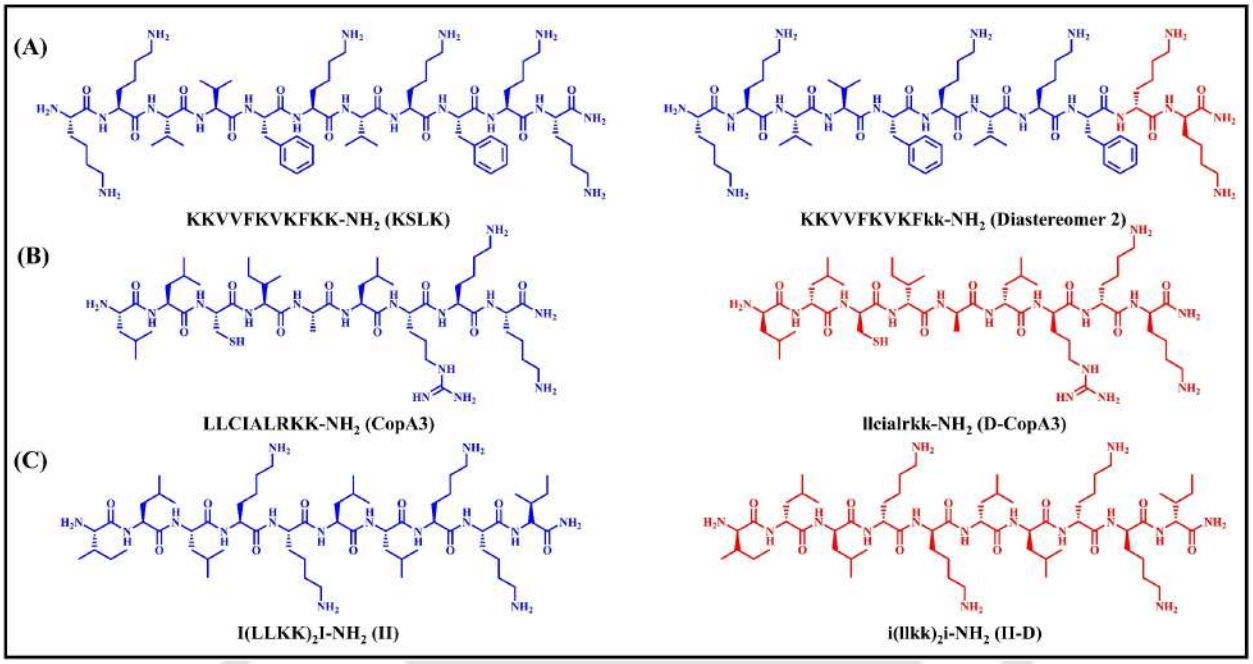

Figure 1.15. Incorporation of D-amino acids in the sequences of antimicrobial peptides. (A) Substitution of the two C-terminal residues of peptide KSLK with D-amino acids showed enhanced serum stability.[434] (B) All-D enantiomer, D-CopA3 was completely stable compared to that of its all L-isomer CopA3.[437] (C) All-D enantiomer, II-D displayed enhanced activity compared to that of its all L-isomer II.[438]

1.11.6. Incorporation or substitution with unnatural amino acids

Proteolytic instability of the naturally occurring AMPs can be overcome by the substitution of natural amino acid residues with unnatural amino acids in the sequences of the AMPs or by the design of AMPs containing unnatural amino acids. Unnatural amino acids incorporated in the AMP sequences are not recognized by the proteolytic enzymes present in the physiological systems, thus making the peptides stable. Modifications of the backbone or introduction of new functional groups in the side chains of peptides, through the incorporation of unnatural amino acids may improve their interactions with the microbial membranes, decrease cytotoxicity or result in better selectivity. β-amino acids, γ-amino acids, α,α-disubstituted amino acids, analogues of lysine or arginine with elongated/shortened side chains, fluorinated, methylated side chain modified amino acids etc., have been effectively incorporated or substituted into the AMP sequences.[431-432] Lysine

at the N-terminus of a 11 residue peptide, MP was replaced with three different unnatural amino acids with increasing positive charge [(+2) to (+4)] to yield three modified peptides MPU1-3. The modified peptides bearing unnatural amino acids with increased net positive charge and bulkier size led to an increased stability against the serum protease with an overall retention of antimicrobial activity.[443] Substitution of Aib at different positions in the sequence of a peptide Temporin-1DRa, resulted in variation of their antimicrobial activities. Aib substituted at positions 4, 8 and 10 increased helicity percentages of the peptides, their antimicrobial activity as well as cytotoxicity. Substitution of Aib at the position 6 significantly reduced the activity of the peptide, while substitutions at positions 1, 2, 3, 5 and 7 did not induce any considerable changes in the activities both in terms of antimicrobial potency or cytotoxicity. Substitution effected at positions 9, 13 and 14 produced to be fruitful amongst all, producing analogues with overall better selectivity.[444] A series of peptides incorporating unnatural amino acids residues like Tic (tetrahydroisoquinolinecarboxylic acid) and Oic (octahydroindolecarboxylic acid) were designed based on the sequence of magainin 2 as a template. Some of the designed peptides also incorporated other unnatural amino acid residues like β-alanine, diaminopropionic acid, 4-fluorophenylalanine, 4-nitrophenylalanine, GABA, γ-aminobutyric acid, D-lysine, D-phenylalanine in addition to the Tic or Oic units. Antimicrobial screening of the designed peptides revealed that different peptides had different potency against different microbes based on their membrane composition. Minute changes in the structure or the position of the constituent amino acids might lead to significant differences in their potency against a particular strain.[445] Substitution of all the arginine residues in the sequence of a peptide Sub3 with an unnatural amino acid α-amino-3-guanidino-propionic acid (Agp), led to an enhanced serum stability of the resulting peptide without any reduction in the antimicrobial activity.[446] A peptide Api88, with an unnatural ornithine residue at the N-terminus linked to N,N,N,N-tetramethylguanidine was designed based on the template of the peptide apidaecin 1b. The modified peptide Api88 displayed excellent antimicrobial activity against a wide range of Gram-negative bacteria without inducing *in vitro*/ *in vivo* cytotoxicity even at very high concentrations.[447] The peptide Api88 however showed very low half-life in the presence of mouse serum. Removal of amidation at the C-terminus with free acid as well as substitution of the Arg-17 with L-ornithine or L-homoarginine increased the serum stability of the modified peptides by more than twenty folds. However, only the modified peptide with free acid at the C-terminus could retain its antimicrobial activity.[448] Replacement of the

histidine residues with unnatural substituents β-naphthylalanine or β-(4,4'-biphenyl)alanine led to an increased salt-tolerance of the modified peptides.[370] Similarly, end tagging of β-naphthylalanine in the sequence of a short Trp-rich antimicrobial peptide S1 produced analogue with enhanced antimicrobial activity and higher resistance to salts.[373] Replacement of the lysine with ornithine at the position 5 and 9 of an antimicrobial peptide Cbf-14 yielded the modified analogue Cbf-14-2 with enhanced antimicrobial activity. Cbf-14-2 also displayed low hemolysis and low cytotoxicity and a higher percent of alpha-helical content than that of the parent sequence Cbf-14.[449] Natural amino acids in the sequence of a peptide C18G were substituted with different unnatural amino acids of varying lengths. All the leucine residues were systematically replaced with norleucine, norvaline, cyclohexylalanine and aminobutyric acid in the sequence of the parent peptide C18G to produce peptides C18G-Nle, C18G-Nva, C18G-Cha and C18G-Abu respectively. An overall enhancement of activity was observed for the peptide C18G-Nle. C18G-Nva somewhat retained its antimicrobial activity while the other analogues i.e. C18G-Cha and C18G-Abu lost their antimicrobial activities in comparison to the parent peptide C18G.[450]

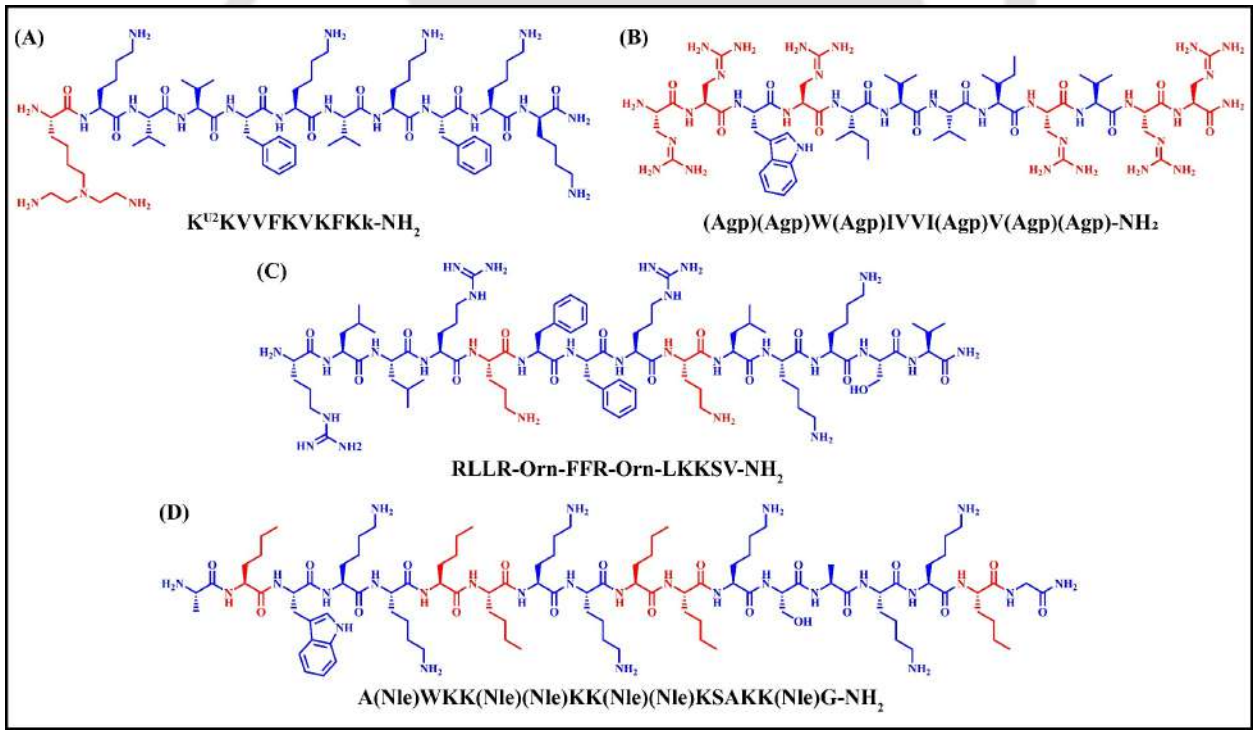

Figure 1.16. Peptides containing unnatural amino acids (highlighted in red) in their sequences. (A) MPU2[443] (B) Sub3-Agp[446] (C) Cbf-14-2[449] and (D) C18G-Nle.[450]

1.11.7. Lipidation of antimicrobial peptides

Lipidation or introduction of lipids into the sequences of antimicrobial peptides is another effective strategy to overcome the limitations of the naturally occurring AMPs. Lipidation increases the hydrophobicity and permeability of antimicrobial peptides through enhanced interactions with the microbial membranes. It may also help in reduction of toxicity toward mammalian cells, thereby enhancing selectivity. Proteolytic stability may also get enhanced on introduction of lipid moieties in the AMP sequences. Lipids may be incorporated at different sites of antimicrobial peptides like at the N-terminus, at the C-terminus or at the side chain. Effective incorporation of cholesterol and fatty acids of different lengths into AMPs are shown to have considerable effect on their properties.[451-453] Incorporation of fatty acyl chains C-8, C-10 and C-12 at the N-terminus of an antimicrobial peptide CG 117-136 resulted in an enhanced activity with increased helical content, better ability to disrupt lipid membranes compared to the that of parent peptide, while retaining non-cytotoxicity *in vivo*.[454] Tetrapeptides with sequence KXXK (X = L, A, G, K, or E), amidated at the C-terminus and having one D-amino acid were conjugated with fatty acids of chain length 12,14 and 16. Fatty acids conjugation rendered the peptides sequences with antimicrobial potency. Peptides C16-KGG*K*, C16-KA*A*K and C16-KK*K*K were found to be most active amongst all, while C12-KA*A*K and C16-GIG*K* (Italics word denote D-amino acids) were the least potent.[455] Fatty acid conjugation of an 18-residue peptide AKK led to increased antimicrobial activity parallelly with increase in chain lengths from C-12 to C-18, compared to that of the unconjugated parent peptide sequence. Conjugation with chain lengths beyond C-18 i.e. C-20 led to a decrease in the antimicrobial potency owing to increased self-assembling property (low CMC).[456] N-terminus of three peptide scaffolds composed of 3, 4, and 5 ornithine residues were acylated with myristic acid, palmitic acid, and stearic acid to yield nine lipopeptides. The peptides displayed very good antimicrobial activity with high selectivity against microbial cells over the mammalian cells, membranolytic modes of action, stability in human blood plasma and adversity towards resistance development. The most potent of the series LP-16, also displayed *in vivo* antimicrobial activity in infected mice.[457] Peptide dimers conjugated with fatty acid moieties resulted in enhanced interactions with the lipopolysaccharides with better permeabilization resulting in improved activity against Gram-negative bacteria. Fatty acids with chain lengths of 8-12 carbon showed maximum selectivity.[458] Side chain of lysine lipidated with a C8 acyl chain and added to the C-terminus or N-terminus of a peptide sequence RWRWRW-NH_2 showed improved

antimicrobial activity without altering the mechanism of action of the parent peptide.[459] A heptapeptide BA250 was conjugated with fatty acids of length 8-14 carbons both at the C-terminus and the N-terminus. The lipopeptides displayed potent antimicrobial activity against a number of clinical isolates of *P. aeruginosa,* with BA250-C10 (BA250 conjugated with fatty acid of chain length having 12 carbons linked at the C-terminus) being the most potent of all. BA250-C10 also displayed potent biofilm inhibition properties and showed enhanced potency in combination with antibiotics like colistin or tobramycin.[460] Saturated, unsaturated, methoxylated and methyl-branched fatty acids of different chain lengths (C8-C20) conjugated to the N-terminus of a peptide A2 (IKQVKKLFKK) resulted in an enhanced activity of the modified peptides against Gram-positive/ Gram-negative bacteria and fungus. Peptides conjugated with fatty acids of chain length C8 and C14 exhibited better antibacterial activity, while those conjugated with methoxylated and enoic fatty acids appeared to be superior antifungal agents.[461] Conjugation of a C-14 fatty acid moiety to the N-terminus of small dipeptides or tripeptides containing lysine or arginine residues endowed the ultra-short peptide sequences with potent antimicrobial properties. C14-RRR, was considerably salt, serum and pH tolerant. The designed peptides had a membranolytic modes of action and could both inhibit or disrupt biofilm formations.[462] 4-methylhexanoic acid conjugated to the N-terminus of a peptide fragment derived from the human autophagy 16 polypeptide displayed excellent activity against *S. aureus* with MIC values in the nano to low micromolar ranges, and very good activity against Gram-negative pathogenic strains of *P. aeruginosa* and *E. coli.*[463] Three lipopeptides, with the general formula of $C_nH_{2n+1}CO$-D-Phe-Dab-Dab-Leu-NH_2 (n = 11, 13, or 15) were designed and synthesized. The designed peptides could penetrate the lipid membranes mimicking bacterial membranes. The peptides were more potent towards Gram-positive bacteria compared to that of the Gram-negative bacteria while displaying low levels of hemolysis.[464] KR-12 (a fragment of LL-37) was acylated with fatty acids of chain lengths C2-C14. Peptides with C4-C14 were far superior in their antimicrobial activity compared to that the C2 derivative. The C8 derivative was the most potent of all with lowest MIC values against a wide range of microbes. C-14 with higher aggregation properties inhibited its antimicrobial abilities compared to that of the C-8 derivative with lesser aggregation properties.[465] A lipopeptide LP20, was constructed by incorporation of palmitic acid at the N-terminus of a cathelicidin derived peptide P-20. LP20 designed to have nanomicelle formulations displayed a higher helical content in the presence of bacterial membrane mimics, better trypsin stability and an overall increase in its

antimicrobial activity tested against a number of microbes compared to that of the parent sequence of LP20.[466] Short fatty acids (C2-C10) were attached to the ε-amino of Lys8 and Lys13 of a peptide WL (WLKKLKKKLKKLKKK) to yield five double-site lipidated peptides. Peptides with C2-C8 conjugations displayed an improvement in their antimicrobial activities while that with the C10 conjugation lost its activity compared to that of the parent WL. C6 conjugated WL or WL-C_6 appeared to be the most potent amongst all having lowest overall MIC values. WL-C_6 studied further revealed it to be potent against a number of drug-resistant strains, non-cytotoxic, considerably salt tolerant and significantly protease resistant displaying membranolytic modes of action.[467]

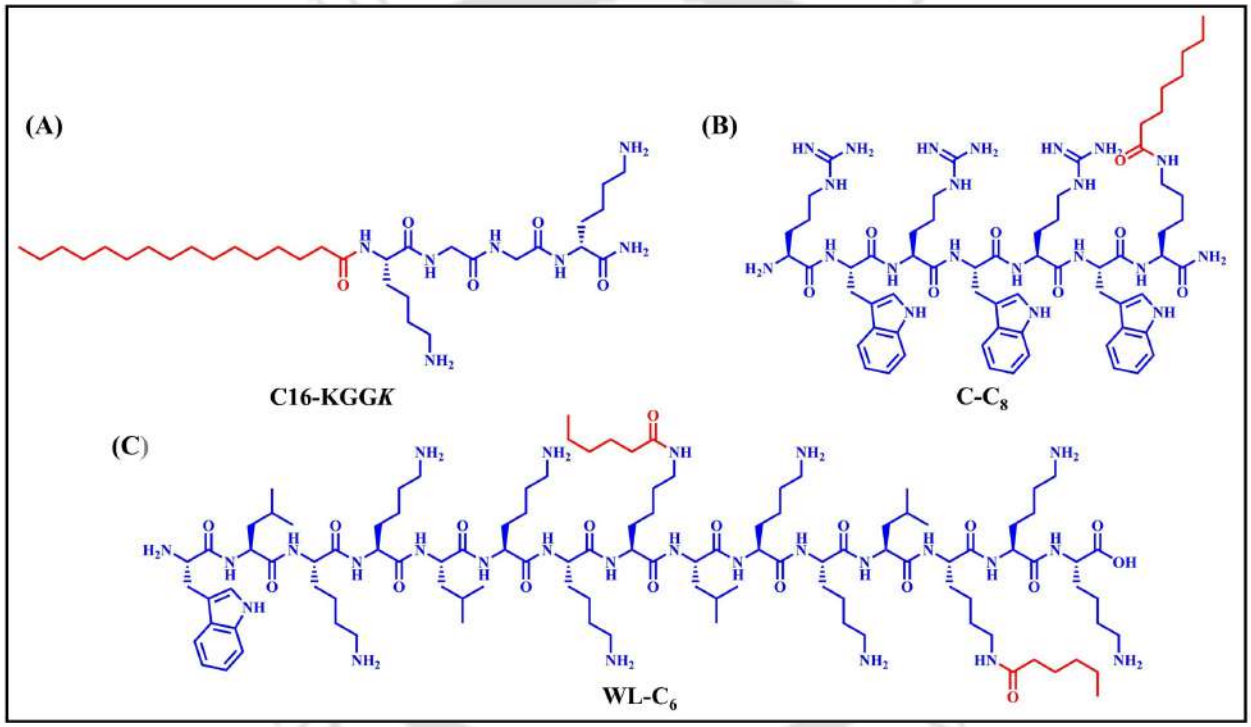

Figure 1.17. Lipidated peptides. (A) C16-KGG*K*[455] (B) C-C_8[459] and (C) WL-C_6.[467]

1.11.8. Cyclisation of antimicrobial peptides

Cyclisation of peptides or design of cyclic peptides offers another solution to overcome many of the drawbacks of the existing AMPs. Cyclic peptides in many of the cases have been found to be antimicrobially more potent, proteolytically more stable and less cytotoxic compared to their liner analogues. Cyclic peptides might be formed by bond formation in between the amino acids of the peptide sequences through disulfide bridges, head to tail amide bond formation or through side chain-side chain linkages.[468-469] A series of eight or six residue cyclic peptides composed altering

D and L amino acid residues were designed and synthesized. The cyclic D, L-α-peptides were found to be effective against both Gram-positive and Gram-negative bacteria with low cytotoxicity, proteolytic stability and membrane permeation mode of action. Linear analogue designed for one such cyclic peptide with high antimicrobial activity was found to have significantly reduced activity.[470] A pronounced improvement in the antimicrobial activity was observed on head to tail cyclization of a hexapeptide with arginine and tryptophan. Cyclized analogue with a conformational rigidity provided an amphipathic structure with positive charges at the one end and aromatic groups at the other, increasing the depths of penetration into lipid bilayers.[471] Self-assembling cyclic D,L-α-peptides were incorporated with D-glucosamine ($GlcNH_2$), D-galactose (Gal), or D-mannose (Man) glycosyl side chains. Specific glycosylation of the peptides reduced cytotoxicity while retaining the antimicrobial potencies of the peptides.[472] A series of 13 pseudopeptides composed of α-amino and aza-β^3-amino acids were designed based on *de novo* principles and synthesized. The peptides named as antimicrobial cyclic pseudopeptides or ACCP 1-13 showed potency against a variety of microbes. Aza-β^3-amino acids incorporation ensured hydrophobicity and rigid backbones necessary for biological activities. The pseudopeptides were also proteolytically far more stable with enhanced half-lives compared to that of some naturally occurring AMPs.[473] Peptidomimetic lipidated cyclic γ-AA peptides were found to display a broad-spectrum antimicrobial activity against a number of Gram-negative and Gram-positive strains along with potent anti-inflammatory activity.[474] A number of cyclic cell penetrating cyclic peptides, and their analogues were synthesized and screened for their antimicrobial activity. Cyclic peptide [R_4W_4] was found to be most potent against MRSA, with MIC value few folds lower compared to that of its linear analogue. Lipidation of the cyclic peptide [KRRRRR] with octanoyl, dodecanoyl or hexadecanoyl chains led to a significant improvement in antimicrobial activity of the conjugated analogues against MRSA.[475] Antimicrobial bridged bicyclic peptides (AMBPs) designed the concept of chemical space displayed activity against *Pseudomonas aeruginosa*. Two of the AMBPs discovered were also capable of inhibiting biofilms and were found to increase the activity of polymyxin-B in synergy.[476] A number of peptides cyclized via a xylene double thioether bridge connecting the terminal cysteines placed at the ends of linear sequences composed of alternating D and L-amino acids (composed of lysine and tryptophan residues) were designed and synthesized. The synthesized peptides displayed potent antimicrobial activity against Gram-negative *Pseudomonas aeruginosa* and Gram-positive *Bacillus subtilis*.

Amongst all the designed peptides, RH11 with sequence [CwWkKkKkWwC] was found to be most potent of all and was additionally active against several clinal isolates of *Pseudomonas aeruginosa*. RH11 was found to interact with the bacterial membranes to form lipid-peptide aggregates.[477] ZY-4, a 17-residue peptide cyclized through disulfide bridge between two cysteines placed at the position 2 and at position 16 was designed and synthesized. The linear sequence of ZY-4 was adopted through modification of a previously reported AMP Cathelicidin-BF-15. ZY-4 displayed excellent antimicrobial activity against *P. aeruginosa*, *A. baumannii* and some clinical multidrug-resistant (MDR) strains. ZY-4 also showed improved proteolytic stability *in vivo*, stability against the development of resistance and biofilm eradication properties.[478] A cyclic peptide OIR3 with the sequence Cyclo-$(IR)_3P(IR)_3P$ was found to have low MIC values against a number of Gram-positive and Gram-negative bacteria tested. The MIC value of the cyclic peptide OIR3 was found to be 2-32 times superior compared to that of its linear analogue IR3 with sequence $(IR)_3P(IR)_3P$. OIR3 disrupted cells through a membranolytic mode of action. OR3 additionally displayed anti-inflammatory properties through inhibition of TNF-α, IL-1β and IL-6 mRNA expression.[479] IDR-1018, an antimicrobial peptide was cyclized via three strategies: head-to-tail cyclization (C1), side-chain-to-tail cyclization (C2), and a disulfide bond cross-linkage (C3). An improvement in the proteolytic stability was observed for all the three modified analogues C1, C2 and C3. An overall enhancement in the antimicrobial activity was observed for the peptide C-2 compared to that of the parent sequence. C-2 also displayed anti-inflammatory activity and ability to reduce bacterial loads of *Staphylococcus aureus* in murine skin infection model.[480] A total of ten analogues of the peptide tyrocidine A (Tyrc A) was designed through a sequential replacement of the hydrophobic residues (Asn, Gln and Tyr) and then the hydrophilic residues (Val and Leu) with ornithine (Orn) residues. The modified peptides assumed a positive charge in between +2 and +6. Peptide 8 with a sequence cyclo-(^{D}FPF^{D}FOOOOOL) and having a net charge of +5 was the peptide with overall best antimicrobial activity and low hemolysis. Peptide 9 and 10 with a net positive charge of +5 and +6 respectively, however showed a diminished activity. Peptide 8 was found to diffuse membrane in a detergent like manner.[481]

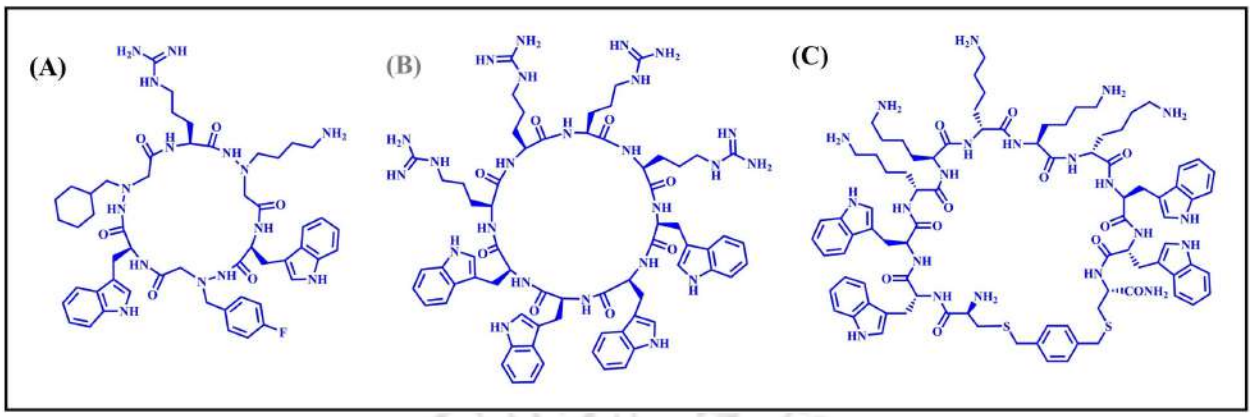

Figure 1.18. Synthetic cyclic peptides. (A) ACCP-7[473] (B) [R_4W_4][475] and (C) RH11.[477]

1.12. Mechanism of action of antimicrobial peptides

Mechanism of action of antimicrobial peptides can be broadly classified into two categories: direct killing mechanism and immune modulation. Direct killing may further involve membrane target mechanism or non-membrane target mechanisms.[106,332,482-484]

1.12.1. Membrane target mechanism

Before understanding the membrane target mechanism of the antimicrobial peptides, an insight of the microbial cell envelopes is important. There is a distinct difference in the membrane composition of Gram-negative bacterial, Gram-positive bacterial and fungal cell envelopes with that of mammalian cell membranes.[485-487] The envelope of the Gram-negative bacteria is composed of three layers. The inner membrane is constituted out of a bilayer of phospholipids mainly composed of phosphatidylethanolamine (PE), phosphatidylglycerol (PG), and cardiolipin (CL) along with some membrane proteins.[488] This is followed by a thin layer of peptidoglycan. The final outer membrane is composed of an unsymmetric bilayer: an inner leaflet majorly constituted by phospholipid constituents (PE, PG), while the outer leaflet mostly constituted by lipopolysaccharides (large molecular entities composed of lipids and polysaccharides). Outer membrane is additionally found to contain porins, a type of channel forming proteins that is involved in the process of uptake of nutrients, balance of ions etc., and some lipoproteins that helps in anchoring of the outer membrane to the peptidoglycan and provide structural stability.[489-490] Gram-positive bacteria is composed of two layers and unlike the Gram-negative bacteria is devoid of the outermost membrane. The inner membrane is similar to that of the Gram-negative bacteria and is composed of a bilayer of phospholipids (PE, PG, CL) with some proteins embedded in it.

The peptidoglycan layer, however in the case of Gram-positive bacteria is much thicker compared to that of Gram-negative bacteria and contains entities like teichoic acids or lipoteichoic acids embedded in it that are responsible for several functionalities.[491]

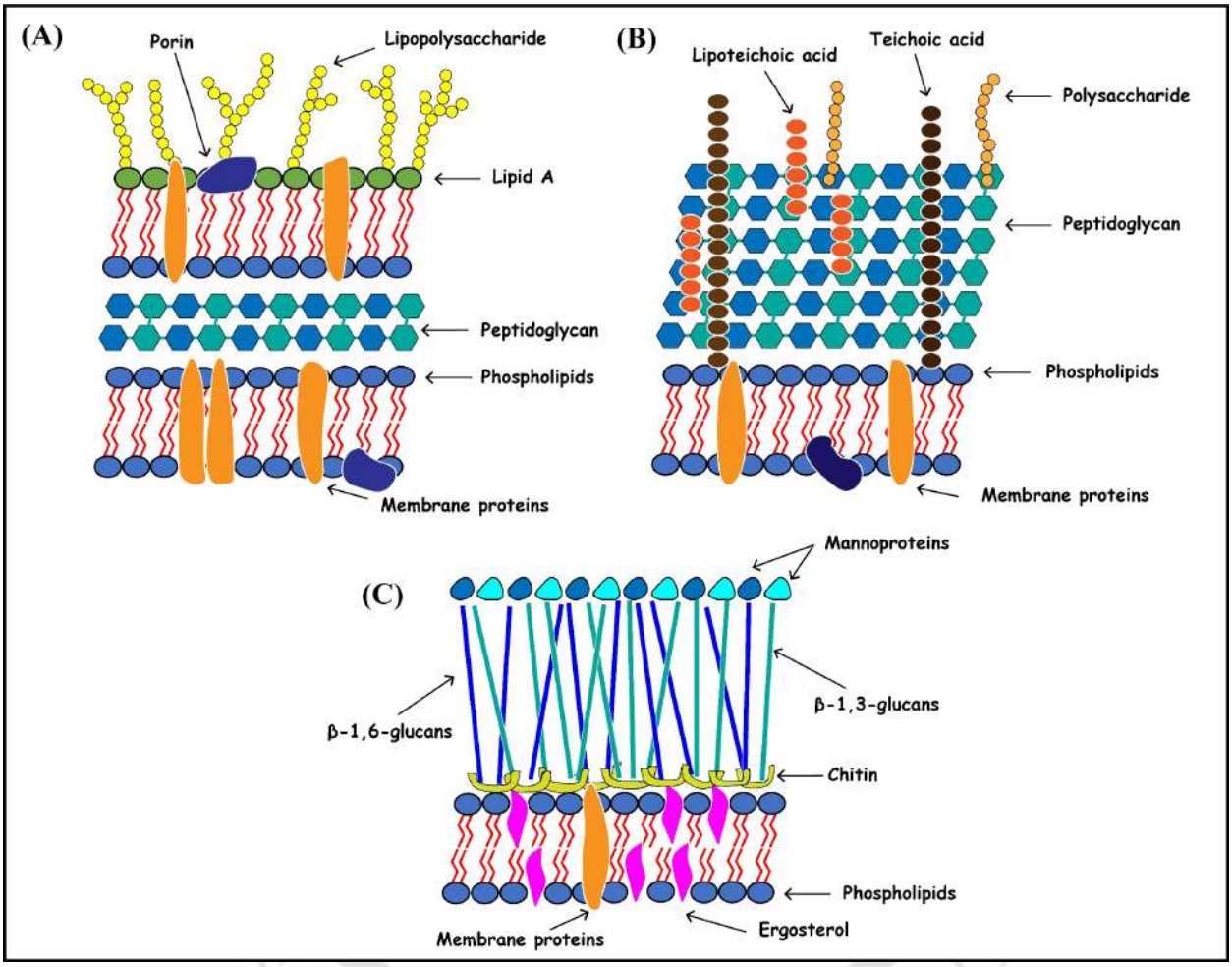

Figure 1.19. Membrane envelope constitution of (A) Gram-negative bacteria, (B) Gram-positive bacteria, (C) fungus.

Fungal cell envelopes too are composed of two layers: an inner cytoplasmic membrane and an outer cell wall. The inner plasma membrane is a bilayer mainly composed of phospholipids in the form of phosphatidylcholine (PC), phosphatidylethanolamine (PE), phosphatidylserine (PS) and phosphatidylinositol (PI) along with sterol molecules ergosterol, imparting the membrane with fluidity and stability, and some integral membrane proteins. Some other units like sphingolipids and glycoproteins also contribute to the plasma membrane constitution. The cell wall surrounding the plasma membrane is mainly composed of three units namely chitin, β-glucans and

mannoproteins. Chitins are long-chain polymers of N-acetylglucosamine constituting the inner part of the cell wall, β-glucans constitute the fibrous mesh in between, while the mannoproteins constitute the outer surface of the fungal cell wall.[486,492] Mammalian cell membranes are far less complex with no outer layers and represent a single bilayer of phospholipids embedded with cholesterol endowing the cells with stability and mobility. The bilayer also contains membrane proteins involved in transportation, reception and enzymatic functions, and carbohydrate units in the form of glycolipids and glycoproteins responsible for several functions. The phospholipids that constitute the membrane bilayer in mammalian cells are mainly phosphatidylcholine (PC), phosphatidylserine (PS), phosphatidylethanolamine (PE) and sphingomyelin (SM).[487,493-494]

Now, having understood the membrane composition of the bacterial, fungal and mammalian cells, it is worth mentioning that bacterial surfaces carry a negative charge arising from phospholipids with net negative charge like phosphatidylglycerol (PG) and cardiolipin (CL), a considerable percentage of what constitutes the membrane bilayers.[495-496] In addition to that a significant negative charge originates from the lipid A part of the lipopolysaccharides in Gram-negative bacteria and teichoic acids in case of Gram-positive bacteria.[497-499] This negatively charged surface provides the cationic antimicrobial peptides, a platform to interact with microbial membranes due to obvious electrostatic reasons. Outer leaflet of the bilayer constituting the mammalian membranes are mainly composed of neutral phosphatidylcholine (PC) and sphingolipids (SL), rendering no electrostatic advantage for the binding of the positively charged AMPs.[500-501] AMPs are also known to interact with the negatively charged fungal surfaces. The surface of the fungal membranes carries negative charges mainly originating from the phosphate groups of mannoproteins.[502] Glucuronic acid residues from cell wall constituting polysaccharides and sialic acids originating from the glycoproteins and glycolipids may also contribute to the negative charges in the fungal membranes.[503]

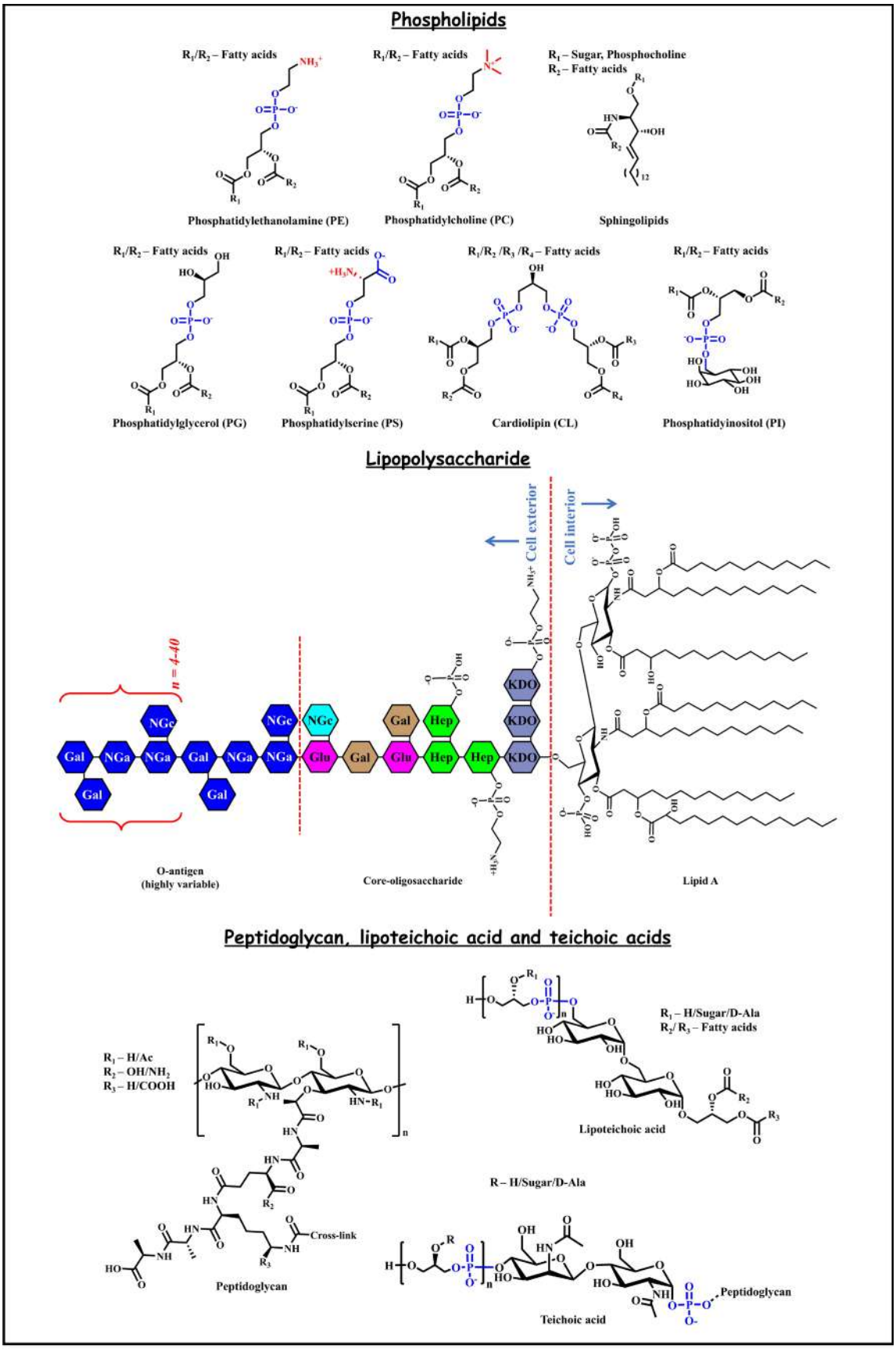

Figure 1.20. Chemical structure of different constituents of microbial membranes. Topmost panel: different types of phospholipids constituting membranes; middle panel: lipopolysaccharide constituting Gram-negative bacterial membrane; lower panel: Chemical structure of peptidoglycan, lipoteichoic acid and teichoic acid constituting Gram-positive bacterial membranes.

Driven by electrostatics, once an AMP associates itself with the microbial membranes, disruption of membranes may take place through various proposed models like barrel-stave model, toroidal model, carpet model or detergent model.[504-506] In the barrel-stave model, AMPs in their monomeric form first aggerate on the membrane surface and then undergo oligomerization. Oligomers having α-helical AMP units then descends into the hydrophobic cores of the membrane bilayers forming pores. The hydrophobic face of the peptides interacting with the hydrophobic tails of the phospholipids helps their insertion into the membranes.

The hydrophobic inner core forms the passage for the ions and water into the cells resulting in membrane disruption. [507-508] Alamethicin is an AMP known to disrupt microbial membrane based on this model.[509] In the toroidal pore model, the hydrophilic part of an AMP associates with the polar headgroups of the phospholipids and induce curvature in the membranes to form ring-like pores without being dissociated from the membranes. Magainin, aurein 2.2, melittin etc., are known to disrupt membranes following the toroidal pore model.[510-512] In the carpet-like model, AMPs get attached the microbial membranes parallelly, driven by hydrophilic-anionic interactions. Peptides adopt helical structure in contact with negatively charged membranes. After a sufficient number of these AMP units are accumulated (over a threshold number) on the membranes resembling carpets, the AMPs inserts into the membrane lipids with their hydrophobic surface facing the lipids, leading to the breakage of the bilayer structure. Dermaseptin, protegrin-1, aurein 1.2 etc., are some AMPs that follow the carpet model of disruption.[513-515] The detergent model is an extension of the carpet model. The membranes follow same method of disruption as in the case of the carpet model followed by dissolution of the membrane fragments upon disruption.[516]

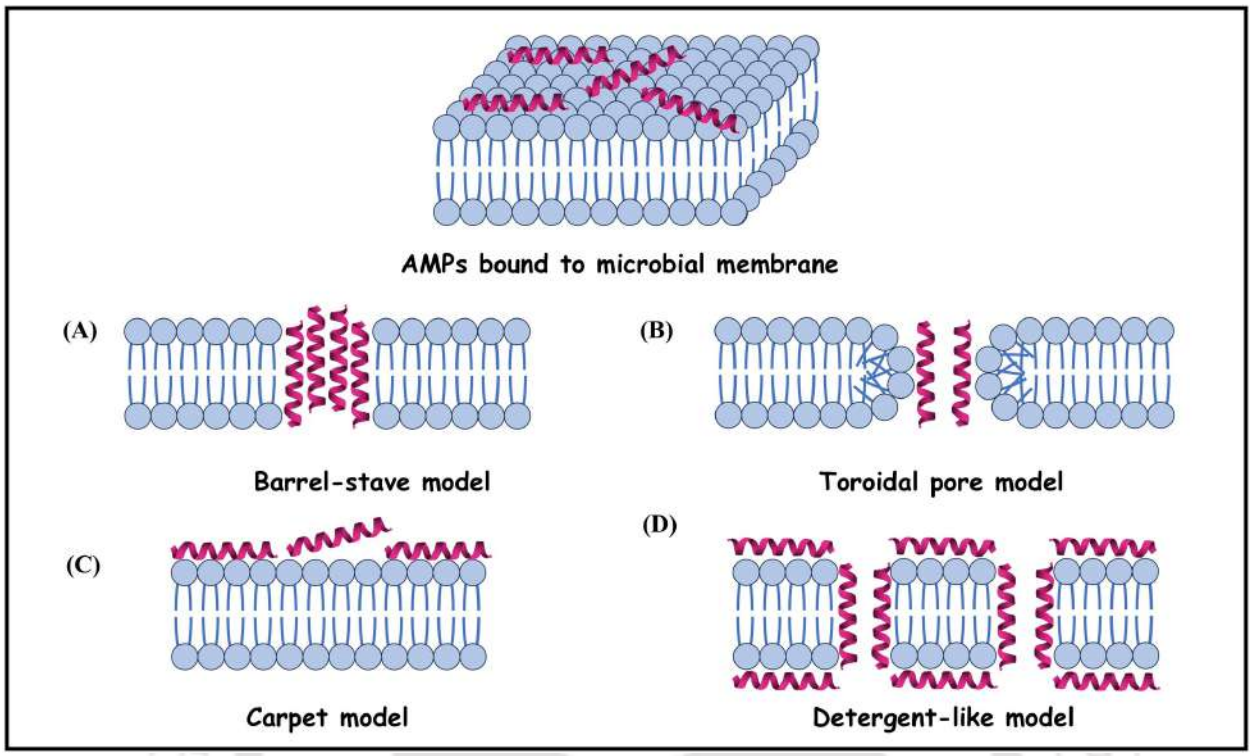

Figure 1.21. Different models of microbial membrane disruption: (A) Barrel-stave model, (B) Toroidal pore model, (C) Carpet model and (D) Detergent-like model.

1.12.2. Non-membrane target mechanism

Other than direct target on the microbial membranes, AMPs may exercise microbial killing through several non-membranolytic modes of action.[517] These may involve inhibition of cell wall synthesis e.g. as exhibited by nisin, vancomycin.[518-519] AMPs like these tend to bind with the lipid II, an important precursor responsible for cell wall biosynthesis.[520] AMPs like HNP 1or teixobactin are also found to display bactericidal abilities by binding to the lipid II precursor of the cell wall and thereby inhibiting cell wall biosynthesis.[521,260] Some AMPs are known to act on microbes through inhibition of protein synthesis. Several proline rich AMPs belong to this category of AMPs that inhibit protein synthesis via binding to the ribosomes.[343] For example, $Bac7_{1-35}$ is an AMP that binds to ribosomes to inhibit protein translation.[522] Tur1A is another example of an AMP that inhibits bacterial protein synthesis by binding to the ribosome and blocking the translation.[264] Oncocin, Api137 are some other AMPs that inhibit protein synthesis through termination of translation.[523-524] Some AMPs are also capable of displaying antimicrobial activities involving their interactions with the nucleic acids. Buforin II, Tachyplesin I and Indolicidin are known to display bactericidal action upon binding to the microbial DNA.[219,243,525] Some AMPs like Pse-T2

are known to display bactericidal action by interacting with the microbial DNAs preventing replication and transcription.[526] Some AMPs are even capable of inducing cell deaths through inhibition of cell division, e.g. 20 residue amino acid containing APP, histatin 5 etc.[527-528] Several AMPs are also known to be associated with inhibition of enzymatic activities, leading to cell death.[529-532]

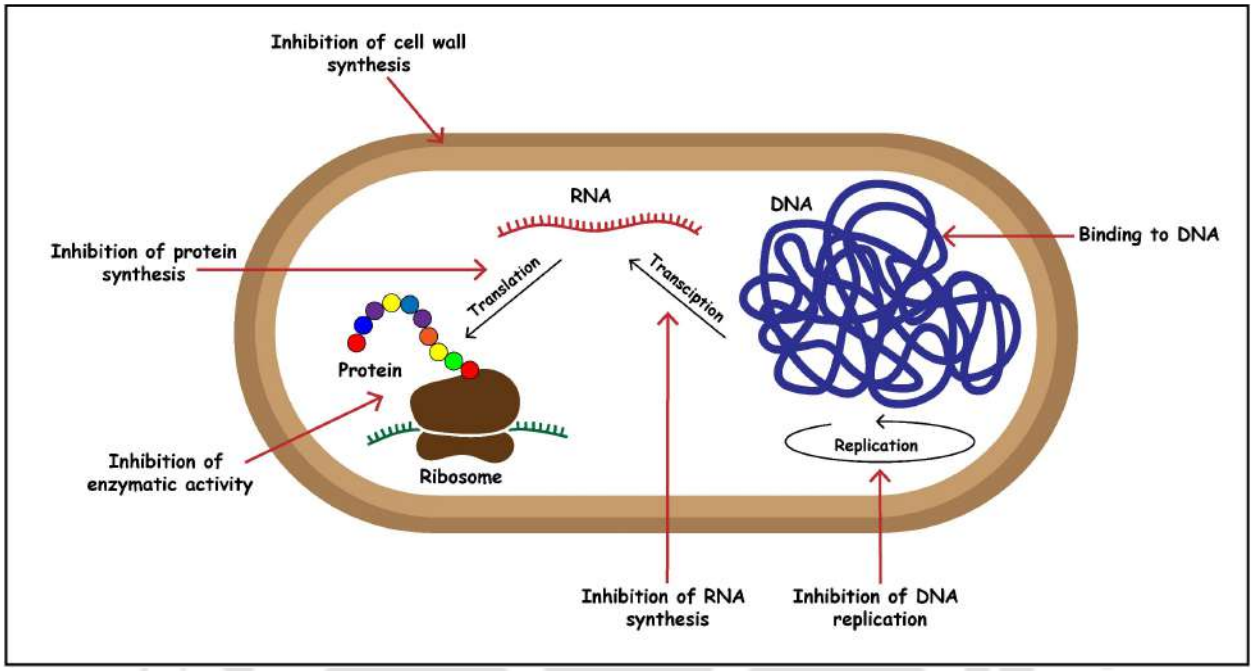

Figure 1.22. Different intracellular targets of antimicrobial peptides.

1.12.3. Immune modulation

Other than direct action on the microbes, AMPs are also capable of acting on the microbes through indirect immune modulation and neutralizing them.[118,533]. AMPs are known to assist in the recruitment and activation of immune cells. AMPs may induce migration of immune cells such as neutrophils, monocytes or dendritic cells to the site of infection contributing to efficient immune defense mechanism.[534] Examples of these type include LL-37,[535] human beta defensins,[536] human neutrophil defensins (HNP 1-3),[537] C18G[538] etc. AMPs also activate immune cells and enhance pathogen killing by stimulation of macrophages and neutrophils to produce cytokines and chemokines resulting in improved inflammatory response that helps to clear infections. LL-37 activates various immune cells through multiple receptors such as FPR2, P2X7 and TLRs.[539] Defensins can activate immune cells such as dendritic cells and macrophages by interacting with

TLRs inducing secretion of pro-inflammatory cytokines and chemokines.[540] Hepcidin activates macrophages inducing the production of inflammatory cytokines such as IL-6.[541]

1.13. Antimicrobial peptides in clinical applications

Although a large number of AMPs have been separated from different sources till date but only a few of them have been approved for clinical usages.[368,542-543] Gramicidin, bacitracin, colistin (polymyxin E), daptomycin, vancomycin, oritavancin, dalbavancin, telavancin etc., are some of the known AMPs that are widely used in clinical applications. Gramicidin (Gramicidin D) is a mixture of three linear peptides Gramicidin A, B and C. This was first isolated from the bacteria *Bacillus brevis* and is used to treat a number of infections alone or in combination with other antibiotics.[544] Gramicidin is mostly used for tropical applications in skin infections and also for treating infections related to eyes, throat and nose.[545] Colistin, also known as polymyxin E is a cyclic lipopeptide, especially active against Gram-negative bacteria like *P. aeruginosa, A. baumannii, K. pneumoniae* and many of their drug-resistant varieties. It has a membrane disrupting mechanism initiated through attack on the lipopolysaccharides present on the outer membranes of Gram-negative bacterial envelopes. It is considered as a last resort medicines for treating severe bacterial infections including pneumoniae, urinary tract infections, meningitis, skin infections etc. Colistin is marketed as its inactive prodrug colistin methanesulfonate (CMS) administered orally or intravenously.[142,546-549] Daptomycin, also marketed as cubicin is a cyclic lipopeptide widely used in treatment of serious skin and soft tissue infections caused by Gram-positive bacteria. Daptomycin has been found to be highly effective in treating infections caused by many drug-resistant bacteria like methicillin-susceptible and methicillin-resistant *Staphylococcus aureus* (MSSA/MRSA), vancomycin-resistant *S. aureus*, vancomycin-resistant Enterococci (VRE) etc. It has a membrane targeting mechanism initiated through membrane binding followed by membrane depolarization and rapid lysis.[167,169,550] It was approved by the FDA in 2003, and marks one of the most significant progresses in the history of antimicrobial peptide research.[551] Vancomycin, a tricyclic glycopeptide is another drug that had been approved the FDA for its excellent antimicrobial activity against Gram-positive bacteria including several drug-resistant strains like MRSA, MSSA. It is widely used in the treatment of infections related to skins and soft tissues, lower respiratory tract, enterocolitis, endocarditis etc. It is usually administered as intravenous injections for majority of the infections because of its poor bioavailability. However, for intestinal

infections caused by *Clostridioides difficile* it is taken orally. Vancomycin has a cell wall targeting mechanism in which it inhibits the cell wall biosynthesis through inhibition of the polymerization of peptidoglycans.[552-557] Oritavancin is a semi-synthetic peptide with structural similarities to vancomycin, intended for treating Gram-positive infections like acute bacterial skin and skin structure infections. It acts via inhibition of cell wall synthesis through inhibition of transglycosylation and inhibition of transpeptidation as well as membrane disruption.[558-562] Dalbavancin is a semisynthetic cyclic lipopeptide, structurally very similar to vancomycin and oritavancin, approved by FDA in 2014. It is used primarily for the treatment of acute bacterial skin and skin structure infections (ABSSSI) caused by Gram-positive bacteria, including resistant strains such as methicillin-resistant *Staphylococcus aureus* (MRSA). Dalbavancin, like vancomycin, binds to the D-alanyl-D-alanine terminus of the peptidoglycan precursors inhibiting cell wall synthesis. Dalbavancin also inhibits transpeptidase, the enzyme responsible for cross-linking the peptidoglycan layers in the bacterial cell wall. Another important feature of this AMP is its extended half-life making it once in a week antibiotic without the need for multiple dosages. Although approved for ABSSSI, clinical trials conducted at different stages have shown its ability to heal osteomyelitis, an infection that needs long treatments with deeper penetrations in bones, both of which are satisfied by dalbavancin.[563-567] Telavancin like oritavancin and dalbavancin is a semi-synthetic derivative of vancomycin. It is primarily used in the treatment of complicated skin and skin structure infections (cSSSI) and hospital-acquired and ventilator-associated bacterial pneumonia (HABP/VABP), particularly those caused by *Staphylococcus aureus*, including methicillin-resistant strains (MRSA). It has a dual mode of action i.e. inhibition of cell wall synthesis similar to that of vancomycin accompanied by membrane disruption induced by membrane depolarization.[568-570] Several AMPs are under different phases of clinical trials. D2A21 intended for burn wound infections, SGX942 intended for oral mucositis, PXL01 intended for post-surgical adhesions, POL7080 intended for *P. aeruginosa* and *K. pneumoniae* infections, p2TA (AB103) intended for soft tissue infections, Omiganan (CLS001) intended for rosacea, Ramoplanin (NTI-851) intended for VRE, *C. difficile* infections are in their phase III trials. EA-230 intended for sepsis and renal failure protection, Delmitide (RDP58) intended for inflammatory bowel disease, Ghrelin intended for chronic respiratory failure, C16G2 intended for tooth decay by *Streptococcus mutans*, DPK-060 intended for acute external otitis, PAC113 intended for oral candidiasis, LTX-109 (Lytixar) intended for Gram-positive MRSA skin infections, OP-145

intended for chronic middle ear infection, hLF1-11 intended for MRSA, *K. pneumoniae*, *L. monocytogenes* infections, Wap-8294A2 (Lotilibcin) intended for Gram-positive bacterial infections etc., are some other AMPs currently under phase II or phase I clinical trials.[571-572]

Table 1.5. Antimicrobial peptides in clinical usages.[542-570]

Name	Source	Treatment	Mode of action	Mode of administration
Colistin	Soil bacteria *Paenibacillus polymyxa*	Infections caused by Gram-negative bacteria including pneumonia, bloodstream infections, urinary tract infections etc.	Membrane disruption; binding of LPS	Intravenous or oral
Daptomycin	*Streptomyces roseosporus*	Infections caused by Gram-positive bacteria including MRSA, VRE	Membrane disruption initiated through membrane depolarization	Intravenous
Vancomycin	Soil bacteria *Amycolatopsis orientalis*	Severe skin & soft tissue infections, MRSA infections, endocarditis, pneumonia, meningitis etc.	Inhibition of cell wall synthesis; binds to D-alanyl-D-alanine	Intravenous or oral
Oritavancin	Semi-synthetic derivative of vancomycin	Acute bacterial skin and skin structure infections (ABSSSI) caused by Gram-positive bacteria	Inhibition of cell wall synthesis; inhibits transglycosylation and transpeptidation	Intravenous
Dalbavancin	Semi-synthetic derivative of vancomycin	Acute bacterial skin and skin structure infections (ABSSSI) caused by Gram-positive bacteria	Inhibition of cell wall synthesis; binds to D-alanyl-D-alanine & inhibits cross-linking between peptidoglycan layers	Intravenous
Telavancin	Semi-synthetic derivative of vancomycin	Complicated skin and skin structure infections (cSSSI) & Hospital-acquired and Ventilator-associated bacterial pneumonia (HABP/VABP) caused by Gram-positive bacteria	Inhibition of cell wall synthesis; inhibits cross-linking of peptidoglycan layers; membrane disruption	Intravenous

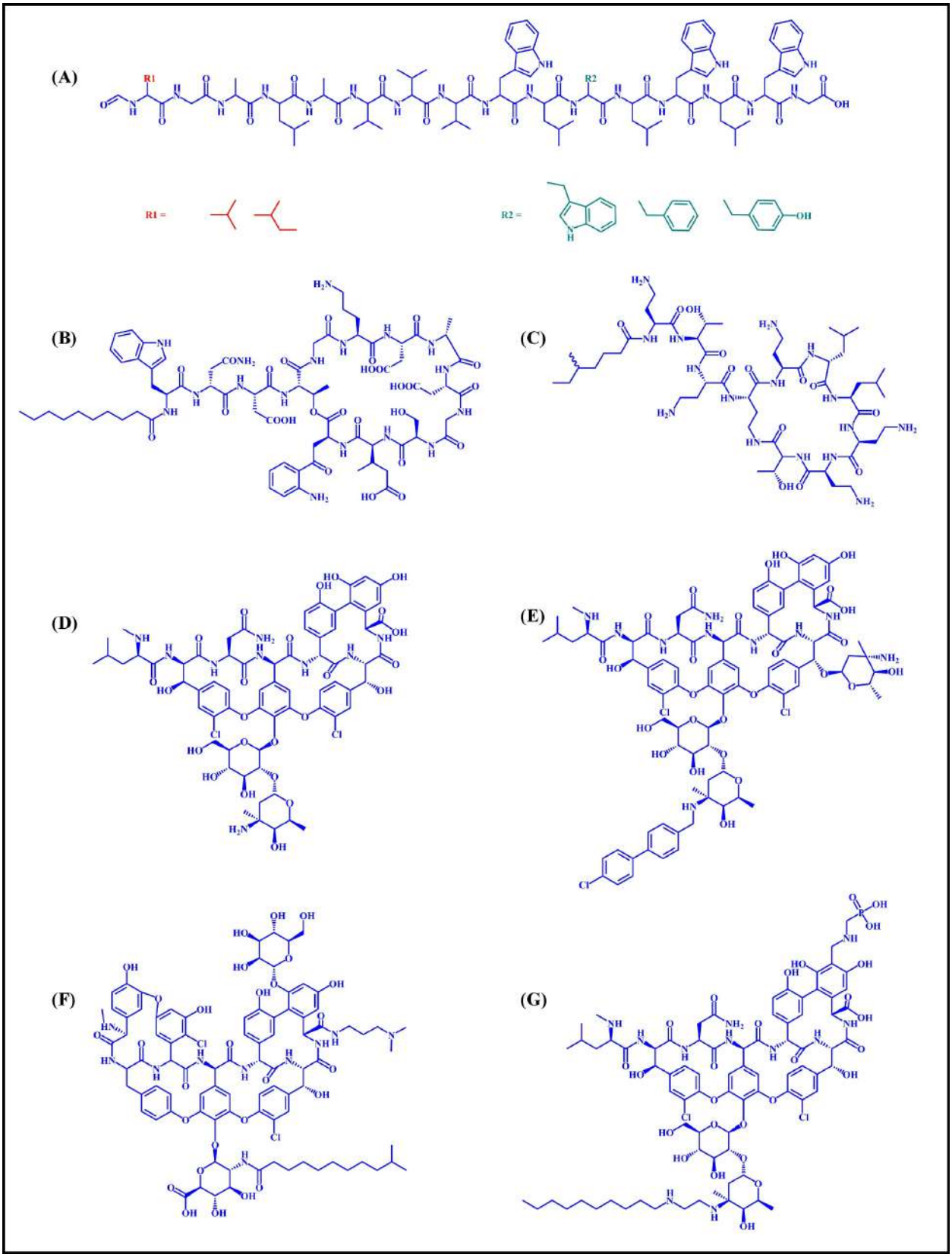

Figure 1.23. Chemical structure of some of the antimicrobial peptides commercially available as

antibiotics. (A) Gramicidin (R2 = Tryptophan: Gramicidin A; R2 = Phenylalanine: Gramicidin B and R2 = Tyrosine: Gramicidin C; each of the Gramicidin has two variants based on R1: valine variant and isoleucine variant) (B) Daptomycin (C) Colistin (Polymyxin E) (D) Vancomycin (E) Oritavancin (F) Dalbavancin (G) Telavancin.

1.14. Aim of the thesis

Driven by the need for the development of alternate antimicrobials in dealing with infections caused by pathogens, and inspired by the potential of antimicrobial peptides (AMPs) as therapeutic molecules, this thesis intended to develop AMPs that addressed their present shortcomings. The aim(s) of our thesis were as follows:

Development of

(1) Membranolytic AMPs: Design and synthesis of membrane active peptides as these provide greater challenges for the microbes to grow resistance against, compared to antimicrobials that target the intracellular functions.

(2) Short AMPs: Synthesis of large sequences of peptides incur high cost and long times for manufacturing, making them expensive and hence commercially inviable. We aimed to address this issue through the design of short/ ultrashort peptides, that are both cost effective as well as time convenient. Small peptide sequences also helped circumvent the problems arising from misfolding and aggregation of longer peptides.

(3) Protease and serum stable AMPs: Proteolytic enzymes present in the physiological systems as well as in the serum present in the blood are known to cleave peptides/ proteins into smaller fragments making them less effective/ineffective against the microbes. We aimed to address this issue through the incorporation of D-amino acids or unnatural amino acids in the peptide sequences making them proteolytically stable.

(4) Salt sensitive AMPs: As membranolytic peptides involve the electrostatic interactions with the negatively charged microbial surfaces, presence of ionic salts in the systems are known to hinder their activity. Our design principles aimed to involve proper hydrophilicity-hydrophobicity balance to make them completely/partially resistant to the presence of salts.

(5) Non-Cytotoxic AMPs: Our design principles aimed at proper charge/hydrophobicity modulation to promote non-cytotoxicy as well as non-hemolytic characteristics to the peptides.

(6) Alternate method for design of broad-spectrum membrane active AMPs: We also proposed a new approach of designing broad-spectrum AMPs, based on calculation of the relative binding affinity of peptides (ΔΔG), involved in binding to simple microbial membrane mimetic models (in collaboration).

References

1. Parker, N.; Schneegurt, M.; Tu, A.H.T.; Forster, B.M.; Lister, P. An Invisible World. In *Microbiology*, 1st ed.; OpenStax, **2016**; pp 9-33.

2. Locey, K.J.; Lennon, J.T. Scaling laws predict global microbial diversity. *Proc. Natl. Acad. Sci. USA* **2016**, *113* (21), 5970-5975.

3. Editorial. Microbiology by numbers. *Nat. Rev. Microbiol.* **2011**, *9* (9), 628.

4. Pitt, T.L.; Barer, M.R. Classification, identification and typing of micro-organisms. *Med. Microbiol.* **2012**, 24-38.

5. Koonin, E.V.; Starokadomskyy, P. Are viruses alive? The replicator paradigm sheds decisive light on an old but misguided question. *Stud. Hist. Philos. Biol. Biomed. Sci.* **2016**, *59*, 125-34.

6. Young, K.D. Bacterial morphology: why have different shapes? *Curr. Opin. Microbiol.* **2007**, *10* (6), 596-600.

7. Basic Biology of Oral Microbes. In *Atlas of Oral Microbiology* **2015**, 1-14.

8. Young, K.D. The selective value of bacterial shape. *Microbiol. Mol. Biol. Rev*. **2006**, *70* (3), 660-703.

9. Gorbach, S.L. Microbiology of the Gastrointestinal Tract. In *Medical Microbiology*, 4th ed.; University of Texas Medical Branch at Galveston, Galveston (TX), **1996**, Chapter 95.

10. Stevens, C.E.; Hume, I.D. Contributions of microbes in vertebrate gastrointestinal tract to production and conservation of nutrients. *Physiol. Rev.* **1998**, *78* (2), 393-427.

11. Valdes, A.M.; Walter, J.; Segal, E.; Spector, T.D. Role of the gut microbiota in nutrition and health. *BMJ*. **2018**, *361*, k2179.

12. Tellez, G.; Higgins, S. E.; Donoghue, A. M.; Hargis, B. M. Digestive Physiology and the Role of Microorganisms1. *J. Appl. Poultry Res.* **2006**, *15* (1), 136-144.

13. Varzakas, T. Microbiology of Fermented Foods and Beverages. *Foods* **2020**, *9* (11), 1660.

14. Tamang, J.P.; Shin, D.H.; Jung, S.J.; Chae, S.W. Functional Properties of Microorganisms in Fermented Foods. *Front. Microbiol*. **2016**, *7*, 578.

15. Sharma, R.; Garg, P.; Kumar, P.; Bhatia, S.K.; Kulshrestha, S. Microbial Fermentation and Its Role in Quality Improvement of Fermented Foods. *Fermentation.* **2020**, *6* (4), 106.

16. Rappuoli, R.; Young, P.; Ron, E.; Pecetta, S.; Pizza, M. Save the microbes to save the planet. A call to action of the International Union of the Microbiological Societies (IUMS). *One Health Outlook* **2023**, *5* (1), 5.

17. Fierer, J.; Looney, D.; Kok, M.; Pechère, J.C. Nature and Pathogenicity of Micro-organisms. *Infectious Diseases,* 3rd ed.; **2010**, *1*, 3-29.

18. Taylor, M.W. What Is a Virus?. In *Viruses and Man: A History of Interactions*; Springer International Publishing: Cham, Switzerland, **2014**, pp 23-40.

19. Wang, C.C.; Prather, K.A.; Sznitman, J.; Jimenez, J.L.; Lakdawala, S.S.; Tufekci, Z., Marr, L.C. Airborne transmission of respiratory viruses. *Science* **2021**, *373* (6558), eabd9149.

20. Zuckerman, A.J. Hepatitis Viruses. In *Medical Microbiology*, 4th ed.; University of Texas Medical Branch at Galveston, Galveston (TX), **1996**, Chapter 70.

21. Wolbert, J.G.; Rajnik, M.; Swinkels, H.M.; Higginbotham, K. Poliomyelitis. In *StatPearls (Internet)*; StatPearls Publishing, Treasure Island (FL), **2024**.

22. Hollingshead, C.M.; Swinkels, H.M.; Shah, S. Ebola Virus Disease. In *StatPearls (Internet)*; StatPearls Publishing, Treasure Island (FL), **2024**.

23. Banerjee, S.; Gupta, N.; Kodan, P.; Mittal, A.; Ray, Y.; Nischal, N.; Soneja, M.; Biswas, A.; Wig, N. Nipah virus disease: A rare and intractable disease. *Intractable Rare. Dis. Res*. **2019**, *8* (1), 1-8.

24. Introduction to Bacteriology. In *Medical Microbiology*, 4th ed.; University of Texas Medical Branch at Galveston, Galveston (TX), **1996**.

25. Alegado, R.A.; King, N. Bacterial influences on animal origins. *Cold Spring Harb. Perspect. Biol*. **2014**, *6* (11), a016162.

26. Fredrickson, J.K.; Onstott, T.C. Microbes deep inside the earth. *Sci Am*. **1996**, *275* (4), 68-73.

27. Sender, R.; Fuchs, S.; Milo, R. Revised Estimates for the Number of Human and Bacteria Cells in the Body. *PLoS Biol*. **2016**, *14* (8), e1002533.

28. Toro, E.; Shapiro, L. Bacterial chromosome organization and segregation. *Cold Spring Harb. Perspect. Biol*. **2010**, *2* (2), a000349.

29. Bartholomew, J.W.; Mittwer, T. The Gram stain. *Bacteriol. Rev*. **1952**, *16* (1), 1-29.

30. Rohde, M. The Gram-Positive Bacterial Cell Wall. *Microbiol. Spectr*. **2019**, *7* (3), 10.1128/microbiolspec.gpp3-0044-2018.

31. Work, E. Biochemistry of the bacterial cell wall. *Nature* **1957**, *179*, 841-847.

32. Zhang, Y.J.; Li, S.; Gan, R.Y.; Zhou, T.; Xu, D.P.; Li, H.B. Impacts of gut bacteria on human health and diseases. *Int. J. Mol. Sci*. **2015**, *16*, 7493-7519.

33. Smith, I. Mycobacterium tuberculosis pathogenesis and molecular determinants of virulence. *Clin. Microbiol Rev*. **2003**, *16* (3), 463-496.

34. Marquart, M.E. Pathogenicity and virulence of *Streptococcus pneumoniae*: Cutting to the chase on proteases. *Virulence* **2021**, *12* (1), 766-787.

35. Iglewski, B.H. Pseudomonas. In *Medical Microbiology*, 4th ed.; University of Texas Medical Branch at Galveston, Galveston (TX), **1996**, Chapter 27.

36. Mueller, M.; Tainter, C.R. Escherichia coli Infection. In *StatPearls (Internet)*; StatPearls Publishing, Treasure Island (FL), **2024**.

37. Ashurst, J.V.; Dawson, A. Klebsiella Pneumonia. In *StatPearls (Internet)*; StatPearls Publishing, Treasure Island (FL), **2024**.

38. Taylor, T.A., Unakal, C.G. Staphylococcus aureus Infection. In *StatPearls (Internet)*; StatPearls Publishing, Treasure Island (FL), **2024**.

39. Tong, S.Y.C.; Davis, J.S.; Eichenberger, E.; Holland, T.L.; Fowler, V.G. Jr. Staphylococcus aureus infections: epidemiology, pathophysiology, clinical manifestations, and management. *Clin. Microbiol. Rev*. **2015**, *28* (3), 603-661.

40. Howard, A.; O'Donoghue, M.; Feeney, A.; Sleator, R.D. Acinetobacter baumannii: an emerging opportunistic pathogen. *Virulence* **2012**, *3* (3), 243-250.

41. de Pauw, B.E. What are fungal infections? *Mediterr. J. Hematol. Infect. Dis*. **2011**, *3* (1), e2011001.

42. Soliman, S.S.M. Editorial: *Candida* spp.-transmission, pathogenesis, host-pathogen interaction, prevention, and treatment. *Front. Microbiol*. **2023**, *14*, 1258837.

43. Spampinato, C.; Leonardi, D. *Candida* infections, causes, targets, and resistance mechanisms: traditional and alternative antifungal agents. *Biomed. Res. Int*. **2013**, *2013*, 204237.

44. Sellon, D.C.; Kohn, C. Aspergillosis. In *Equine Infectious Disease*, 2nd ed.; **2013**, 421-434.e4.

45. Jenks, J.D.; Hoenigl, M. Treatment of Aspergillosis. *J. Fungi (Basel)* **2018**, *4* (3), 98.

46. Maziarz, E.K.; Perfect, J.R. Cryptococcosis. *Infect. Dis. Clin. North Am*. **2016**, *30* (1), 179-206.

47. Mittal, J.; Ponce, M.G.; Gendlina, I.; Nosanchuk, J.D. Histoplasma Capsulatum: Mechanisms for Pathogenesis. In *Fungal Physiology and Immunopathogenesis*; Springer International Publishing: Cham, Switzerland, **2018**, *422*, pp 157-191.

48. Kirkland, T.N.; Fierer, J. Coccidioides immitis and posadasii; A review of their biology, genomics, pathogenesis, and host immunity. *Virulence* **2018**, *9* (1), 1426-1435.

49. McBride, J.A.; Gauthier, G.M.; Klein, B.S. Clinical Manifestations and Treatment of Blastomycosis. *Clin. Chest Med*. **2017**, *38* (3), 435-449.

50. Hutchings, M.I.; Truman, A.W.; Wilkinson, B. Antibiotics: past, present and future. *Curr. Opin. Microbiol*. **2019**, *51*, 72-80.

51. Chin, K.W.; Tiong, H.L.M.; Luang-In, V.; Ma, N.L. An overview of antibiotic and antibiotic resistance. *Environmental Advances* **2023**, *11*, 100331.

52. Bush, K.; Bradford, P.A. β-Lactams and β-Lactamase Inhibitors: An Overview. *Cold Spring Harb. Perspect. Med*. **2016**, *6* (8), a025247.

53. Zhou, J.; Cai, Y.; Liu, Y.; An, H.; Deng, K.; Ashraf, M.A.; Zou, L.; Wang. J. Breaking down the cell wall: Still an attractive antibacterial strategy. *Front. Microbiol*. **2022**, *13*, 952633.

54. Epand, R.M.; Walker, C.; Epand, R.F.; Magarvey, N.A. Molecular mechanisms of membrane targeting antibiotics. *Biochim. Biophys. Acta* **2016**, 1858 (5), 980-987.

55. Sarkar, P.; Yarlagadda, V.; Ghosh, C.; Haldar, J. A review on cell wall synthesis inhibitors with an emphasis on glycopeptide antibiotics. *Medchemcomm*. **2017**, *8* (3), 516-533.

56. Buijs, N. P.; Matheson, E. J.; Cochrane, S. A.; Martin, N. I. Targeting membrane-bound bacterial cell wall precursors: a tried and true antibiotic strategy in nature and the clinic. *Chem. Commun.* **2023**, 59 (50), 7685-7703.

57. Butler, M.S.; Hansford, K.A.; Blaskovich, M.A.T.; Halai, R.; Cooper, M.A. Glycopeptide antibiotics: back to the future. *J. Antibiot.* **2014**, *67* (9), 631-644.

58. Hurdle, J.G.; O'Neill, A.J.; Chopra, I.; Lee, R.E. Targeting bacterial membrane function: an underexploited mechanism for treating persistent infections. *Nat. Rev. Microbiol*. **2011**, *9* (1), 62-75.

59. Ledger, E.V.K.; Sabnis, A.; Edwards, A.M. Polymyxin and lipopeptide antibiotics: membrane-targeting drugs of last resort. *Microbiology (Reading)* **2022**, *168* (2), 001136.

60. Gray, D.A.; Wenzel, M. More Than a Pore: A Current Perspective on the In Vivo Mode of Action of the Lipopeptide Antibiotic Daptomycin. *Antibiotics (Basel)* **2020**, *9* (1), 17.

61. Arenz, S.; Wilson, D.N. Bacterial Protein Synthesis as a Target for Antibiotic Inhibition. *Cold Spring Harb. Perspect. Med*. **2016**, *6* (9), a025361.

62. Lin, J., Zhou, D., Steitz, T.A., Polikanov, Y.S., Gagnon, M.G. Ribosome-Targeting Antibiotics: Modes of Action, Mechanisms of Resistance, and Implications for Drug Design. *Annu. Rev. Biochem*. **2018**, *87*, 451-478.

63. Polikanov, Y.S., Aleksashin, N.A., Beckert, B., Wilson, D.N. The Mechanisms of Action of Ribosome-Targeting Peptide Antibiotics. *Front. Mol. Biosci*. **2018**, *5*, 48.

64. Cambau, E.; Guillard, T. Antimicrobials that affect the synthesis and conformation of nucleic acids. *Rev. Sci. Tech*. **2012**, *31* (1), 77-87.

65. Santos, J.A.; Lamers, M.H. Novel Antibiotics Targeting Bacterial Replicative DNA Polymerases. *Antibiotics (Basel)* **2020**, *9* (11), 776.

66. Bhattacharjee, M.K. Antibiotics That Inhibit Nucleic Acid Synthesis. In *Chemistry of Antibiotics and Related Drugs*; Springer International Publishing: Cham, Switzerland, **2016**; pp. 109-128.

67. Hu, Y.; Coates, A.R.M.; Mitchison, D.A. Sterilizing activities of fluoroquinolones against rifampin-tolerant populations of Mycobacterium tuberculosis. *Antimicrob. Agents Chemother*. **2003**, *47* (2), 653-657.

68. Manelbaum, M. Action of Sulphonamides and their Derivatives on Bacteria. *Nature* **1941**, *147*, 266-267.

69. Ovung, A.; Bhattacharyya, J. Sulfonamide drugs: structure, antibacterial property, toxicity, and biophysical interactions. *Biophys. Rev*. **2021**, *13* (2), 259-272.

70. Ghannoum, M.A.; Rice, L.B. Antifungal agents: mode of action, mechanisms of resistance, and correlation of these mechanisms with bacterial resistance. *Clin. Microbiol. Rev*. **1999**, *12* (4), 501-517.

71. Dixon, D.M.; Walsh, T.J. Antifungal Agents. In *Medical Microbiology*, 4th ed.; University of Texas Medical Branch at Galveston, Galveston (TX), **1996**, Chapter 76.

72. Prestinaci, F.; Pezzotti, P.; Pantosti, A. Antimicrobial resistance: a global multifaceted phenomenon. *Pathog. Glob. Health* **2015**, *109* (7), 309-318.

73. Darby, E.M.; Trampari, E.; Siasat, P.; Gaya, M.S.; Alav, I.; Webber, M.A.; Blair, J.M.A. Molecular mechanisms of antibiotic resistance revisited. *Nat. Rev. Microbiol*. **2023**, *21* (5), 280-295.

74. Munita, J.M.; Arias, C.A. Mechanisms of Antibiotic Resistance. *Microbiol. Spectr*. **2016**, *4* (2), 10.1128/microbiolspec.

75. Kapoor, G.; Saigal, S.; Elongavan, A. Action and resistance mechanisms of antibiotics: A guide for clinicians. *J. Anaesthesiol. Clin. Pharmacol*. **2017**, *33* (3), 300-305.

76. Delcour, A.H. Outer membrane permeability and antibiotic resistance. *Biochim. Biophys. Acta* **2009**, *1794* (5), 808-816.

77. Kim, S.W.; Lee, J.S.; Park, S.B.; Lee, A.R.; Jung, J.W.; Chun, J.H.; Lazarte, J.M.S.; Kim, J.; Seo, J.S.; Kim, J.H.; Song, J.W.; Ha, M.W.; Thompson, K.D.; Lee, C. R.; Jung, M.; Jung, T.S. The Importance of Porins and β-Lactamase in Outer Membrane Vesicles on the Hydrolysis of β-Lactam Antibiotics. *Int. J. Mol. Sci*. **2020**, *21* (8), 2822.

78. Codjoe, F.S.; Donkor, E.S. Carbapenem Resistance: A Review. *Med. Sci. (Basel)* **2018**, *6* (1), 1.

79. Gaurav, A.; Bakht, P.; Saini, M.; Pandey, S.; Pathania, R. Role of bacterial efflux pumps in antibiotic resistance, virulence, and strategies to discover novel efflux pump inhibitors. *Microbiology (Reading)* **2023**, *169* (5), 001333.

80. Sun, J.; Deng, Z.; Yan, A. Bacterial multidrug efflux pumps: mechanisms, physiology and pharmacological exploitations. *Biochem. Biophys. Res. Commun*. **2014**, *453* (2), 254-267.

81. Liu, Y.; Li, R.; Xiao, X.; Wang, Z. Molecules that Inhibit Bacterial Resistance Enzymes. *Molecules* **2019**, *24* (1), 43.

82. Tooke, C.L.; Hinchliffe, P.; Bragginton, E.C.; Colenso, C.K.; Hirvonen, V.H.A.; Takebayashi, Y.; Spencer, J. β-Lactamases and β-Lactamase Inhibitors in the 21st Century. *J. Mol. Biol*. **2019**, *431* (18), 3472-3500.

83. Ramirez, M.S.; Tolmasky, M.E. Aminoglycoside modifying enzymes. *Drug Resist. Updat*. **2010**, *13* (6), 151-171.

84. Biswas, T.; Houghton, J.L.; Garneau-Tsodikova, S.; Tsodikov, O.V. The structural basis for substrate versatility of chloramphenicol acetyltransferase CATI. *Protein Sci*. **2012**, *21* (4), 520-530.

85. Garneau-Tsodikova, S.; Labby, K.J. Mechanisms of Resistance to Aminoglycoside Antibiotics: Overview and Perspectives. *Medchemcomm*. **2016**, *7* (1), 11-27.

86. Olaitan, A.O.; Morand, S.; Rolain, J.M. Mechanisms of polymyxin resistance: acquired and intrinsic resistance in bacteria. *Front. Microbiol*. **2014**, *5*, 643.

87. Weigel, L.M.; Steward, C.D.; Tenover, F.C. gyrA mutations associated with fluoroquinolone resistance in eight species of Enterobacteriaceae. *Antimicrob. Agents Chemother*. **1998**, *42* (10), 2661-2667.

88. Lebreton, F.; Cattoir, V. Resistance to Glycopeptide Antibiotics. In *Bacterial Resistance to Antibiotics - From Molecules to Man*. **2019**, pp 51-80.

89. Molodtsov, V.; Scharf, N.T.; Stefan, M.A.; Garcia, G.A.; Murakami, K.S. Structural basis for rifamycin resistance of bacterial RNA polymerase by the three most clinically important RpoB mutations found in Mycobacterium tuberculosis. *Mol. Microbiol*. **2017**, *103* (6), 1034-1045.

90. Chopra, I. Over-expression of target genes as a mechanism of antibiotic resistance in bacteria. *J. Antimicrob. Chemother*. **1998**, *41* (6), 584-588.

91. Then, R.L. Mechanisms of resistance to trimethoprim, the sulfonamides, and trimethoprim-sulfamethoxazole. *Rev. Infect. Dis*. **1982**, *4* (2), 261-269.

92. Andriole, V.T. The quinolones: past, present, and future. *Clin. Infect. Dis*. **2005**, *15* (41), S113-S119.

93. Hegde, S.S.; Vetting, M.W.; Roderick, S.L.; Mitchenall, L.A.; Maxwell, A.; Takiff, H.E.; Blanchard, J.S. A fluoroquinolone resistance protein from Mycobacterium tuberculosis that mimics DNA. *Science* **2005**, *308* (5727), 1480-1483.

94. Zhang, Y.J.; Li, X.J.; Mi, K.X. Mechanisms of fluoroquinolone resistance in Mycobacterium tuberculosis. *Yi Chuan* **2016**, *38* (10), 918-927.

95. Tang, K.W.K.; Millar, B.C.; Moore, J.E. Antimicrobial Resistance (AMR). *Br. J. Biomed. Sci*. **2023**, *80*, 11387.

96. Larsson, D.G.J.; Flach, C.F. Antibiotic resistance in the environment. *Nat. Rev. Microbiol.* **2022**, *20* (5), 257-269.

97. Irfan, M.; Almotiri, A.; AlZeyadi, Z.A. Antimicrobial Resistance and Its Drivers-A Review. *Antibiotics* **2022**, *11* (10), 1362.

98. Calfee, D.P. Methicillin-resistant Staphylococcus aureus and vancomycin-resistant enterococci, and other Gram-positives in healthcare. *Curr. Opin. Infect Dis*. **2012**, *25* (4), 385-394.

99. Seung, K.J.; Keshavjee, S.; Rich, M.L. Multidrug-Resistant Tuberculosis and Extensively Drug-Resistant Tuberculosis. *Cold Spring Harb. Perspect. Med*. **2015**, *5* (9), a017863.

100. Patel, B.; Hopkins, K.L.; Freeman, R.; Pople, D.; Brown, C.S.; Robotham, J.V. Carbapenemase-producing Enterobacterales: a challenge for healthcare now and for the next decade. *Infect Prev. Pract*. **2020**, *2* (3), 100089.

101. Vitiello, A.; Ferrara, F.; Boccellino, M.; Ponzo, A.; Cimmino, C.; Comberiati, E.; Zovi, A.; Clemente, S.; Sabbatucci, M. Antifungal Drug Resistance: An Emergent Health Threat. *Biomedicines* **2023**, *11* (4), 1063.

102. Antimicrobial Resistance Collaborators. Global burden of bacterial antimicrobial resistance in 2019: a systematic analysis. *Lancet* **2022**, *399* (10325), 629-655.

103. Aggarwal, R.; Mahajan, P.; Pandiya, S.; Bajaj, A.; Verma, S.K.; Yadav, P.; Kharat, A.S.; Khan, A.U.; Dua, M.; Johri, A.K. Antibiotic resistance: a global crisis, problems and solutions. *Crit. Rev. Microbiol*. **2024**, *50* (5), 896-921.

104. Mookherjee, N.; Anderson, M.A.; Haagsman, H.P.; Davidson, D.J. Antimicrobial host defence peptides: functions and clinical potential. *Nat. Rev. Drug Discov*. **2020**, *19* (5), 311-332.

105. Kim, J.; Cho, B.H.; Jang, Y.S. Understanding the Roles of Host Defense Peptides in Immune Modulation: From Antimicrobial Action to Potential as Adjuvants. *J. Microbiol. Biotechnol*. **2023**, *33* (3), 288-298.

106. Huan, Y.; Kong, Q.; Mou, H.; Yi, H. Antimicrobial Peptides: Classification, Design, Application and Research Progress in Multiple Fields. *Front. Microbiol*. **2020**, *11*, 582779.

107. Kumar, P.; Kizhakkedathu, J.N.; Straus, S.K. Antimicrobial Peptides: Diversity, Mechanism of Action and Strategies to Improve the Activity and Biocompatibility In Vivo. *Biomolecules* **2018**, *8* (1), 4.

108. Steinstraesser, L.; Kraneburg, U.M.; Hirsch, T.; Kesting, M.; Steinau, H.U.; Jacobsen, F.; Al-Benna, S. Host Defense Peptides as Effector Molecules of the Innate Immune Response: A Sledgehammer for Drug Resistance? *Int. J. Mol. Sci.* **2009**, *10* (9), 3951-3970.

109. Zhang, Q.Y.; Yan, Z.B.; Meng, Y.M.; Hong, X.Y.; Shao, G.; Ma, J.J.; Cheng, X.R.; Liu, J.; Kang, J.; Fu, C.Y. Antimicrobial peptides: mechanism of action, activity and clinical potential. *Mil. Med. Res*. **2021**, *8* (1), 48.

110. Wang, G. Unifying the classification of antimicrobial peptides in the antimicrobial peptide database. *Methods Enzymol*. **2022**, *663*, 1-18.

111. Liang, Y.; Zhang, X.; Yuan, Y.; Bao, Y.; Xiong, M. Role and Modulation of the Secondary Structure of Antimicrobial Peptides to Improve Selectivity. *Biomater. Sci.* **2020**, *8* (24), 6858-6866.

112. Jiang, Z.; Vasil, A.I.; Hale, J.D.; Hancock, R.E.W.; Vasil, M.L.; Hodges, R.S. Effects of net charge and the number of positively charged residues on the biological activity of amphipathic alpha-helical cationic antimicrobial peptides. *Biopolymers* **2008**, *90* (3), 369-383.

113. Bahar, A.A.; Ren, D. Antimicrobial Peptides. *Pharmaceuticals* **2013**, *6* (12), 1543-1575.

114. Yin, L.M.; Edwards, M.A.; Li, J.; Yip, C.M.; Deber, C.M. Roles of hydrophobicity and charge distribution of cationic antimicrobial peptides in peptide-membrane interactions. *J. Biol. Chem*. **2012**, *287* (10), 7738-7745.

115. Chen, Y.; Guarnieri, M.T.; Vasil, A.I.; Vasil, M.L.; Mant, C.T.; Hodges, R.S. Role of Peptide Hydrophobicity in the Mechanism of Action of α-Helical Antimicrobial Peptides. *Antimicrob. Agents Chemother.* **2007**, *51* (4), 1398-1406.

116. Li J.; Koh, J.J.; Liu, S.; Lakshminarayanan, R.; Verma, C.S.; Beuerman, R.W. Membrane Active Antimicrobial Peptides: Translating Mechanistic Insights to Design. *Front. Neurosci*. **2017**, *11*, 73.

117. Le, C.F.; Fang, C.M.; Sekaran, S.D. Intracellular Targeting Mechanisms by Antimicrobial Peptides. *Antimicrob. Agents Chemother*. **2017**, *61* (4), e02340-16.

118. Guryanova, S.V.; Ovchinnikova, T.V. Immunomodulatory and Allergenic Properties of Antimicrobial Peptides. *Int. J. Mol. Sci*. **2022**, *23* (5), 2499.

119. Benfield, A.H.; Henriques, S.T. Mode-of-Action of Antimicrobial Peptides: Membrane Disruption vs. Intracellular Mechanisms. *Front. Med. Technol*. **2020**, *2*, 610997.

120. Talapko, J.; Meštrović, T.; Juzbašić, M.; Tomas, M.; Erić, S.; Aleksijević, L.H.; Bekić, S.; Schwarz, D.; Matić, S.; Neuberg, M.; Škrlec, I. Antimicrobial Peptides-Mechanisms of Action, Antimicrobial Effects and Clinical Applications. *Antibiotics* **2022**, *11* (10), 1417.

121. Li, H.; Niu, J.; Wang, X.; Niu, M.; Liao, C. The Contribution of Antimicrobial Peptides to Immune Cell Function: A Review of Recent Advances. *Pharmaceutics* **2023**, *15* (9), 2278.

122. Xuan, J.; Feng, W.; Wang, J.; Wang, R.; Zhang, B.; Bo, L.; Chen, Z.S.; Yang, H.; Sun, L. Antimicrobial peptides for combating drug-resistant bacterial infections. *Drug Resist. Updat*. **2023**, *68*, 100954.

123. Ji, S.; An, F.; Zhang, T.; Lou, M.; Guo, J.; Liu, K.; Zhu, Y.; Wu, J.; Wu, R. Antimicrobial peptides: An alternative to traditional antibiotics. *Eur. J. Med. Chem*. **2024**, *265*, 116072.

124. Wang, G.; Li, X.; Wang, Z. APD3: the antimicrobial peptide database as a tool for research and education. *Nucleic Acids Res*. **2016**, *44* (D1), D1087-109393.

125. Rogers, L.A. The inhibiting effect of *Streptococcus lactis* on *Lactobacillus bulgaricus*. *J. Bacteriol*. **1928**, *16* (5), 321-325.

126. Field, D.; de Ullivarri, M.F.; Ross, R.P.; Hill, C. After a century of nisin research - where are we now? *FEMS Microbiol. Rev*. **2023**, *47* (3), fuad023.

127. Shin, J.M.; Gwak, J.W.; Kamarajan, P.; Fenno, J.C.; Rickard, A.H.; Kapila, Y.L. Biomedical applications of nisin. *J. Appl. Microbiol*. **2016**, *120* (6), 1449-1465.

128. Dubos, R.J. Studies on a bactericidal agent extracted from a soil *Bacillus*: I. Preparation of the agent. Its activity in vitro. *J. Exp. Med*. **1939**, *70* (1), 1-10.

129. Herrell, W.E.; Heilman, D. Experimental and clinical studies on gramicidin. *J. Clin. Invest*. **1941**, *20* (5), 583-591.

130. Zerfas, B.L.; Joo, Y.; Gao, J. Gramicidin A Mutants with Antibiotic Activity against Both Gram-Positive and Gram-Negative Bacteria. *ChemMedChem*. **2016**, *11* (6), 629-636.

131. Balls, A.K.; Hale, W.S.; and Harris, T.H. A Crystalline Protein Obtained from a Lipoprotein of Wheat Flour. *Cereal Chemistry* **1942**, *19*, 279-288.

132. Richard, J.A.; Kelly, I.; Marion, D.; Auger, M.; Pézolet, M. Structure of beta-purothionin in membranes: a two-dimensional infrared correlation spectroscopy study. *Biochemistry* **2005**, *44* (1), 52-61.

133. De Caleya, R.F.; Hernandez-Lucas, C.; Carbonero, P.; Garcia-Olmedo, F. Gene expression in alloploids: genetic control of lipopurothionins in wheat. *Genetics* **1976**, *83* (4), 687-699.

134. Clore, G.M.; Sukumaran, D.K.; Gronenborn, A.M.; Teeter, M.M.; Whitlow, M.; Jones, B.L. Nuclear magnetic resonance study of the solution structure of alpha 1-purothionin. Sequential resonance assignment, secondary structure and low resolution tertiary structure. *J. Mol. Biol*. **1987**, *193* (3), 571-578.

135. Rao, U.; Stec, B.; Teeter, M.M. Refinement of purothionins reveals solute particles important for lattice formation and toxicity. Part 1: alpha1-purothionin revisited. *Acta Crystallogr. D. Biol. Crystallogr.* **1995**, *51* (6), 904-913.

136. De Caleya R.F., Gonzalez-Pascual, B.; García-Olmedo, F.; Carbonero, P. Susceptibility of phytopathogenic bacteria to wheat purothionins in vitro. *Appl. Microbiol*. **1972**, *23* (5), 998-1000.

137. Gause, G.F.; Brazhnikova, M. Gramicidin *S* and its use in the Treatment of Infected Wounds. *Nature* **1944**, *154*, 703.

138. Llamas-Saiz A.L.; Grotenbreg, G.M.; Overhand, M.; van Raaij, M.J. Double-stranded helical twisted beta-sheet channels in crystals of gramicidin S grown in the presence of trifluoroacetic and hydrochloric acids. *Acta Crystallogr. D. Biol. Crystallogr*. **2007**, *63* (3), 401-407.

139. Gupta, S.; Govil, D.; Kakar, P.N.; Prakash, O.; Arora, D.; Das, S.; Govil, P.; Malhotra, A. Colistin and polymyxin B: a re-emergence. *Indian. J. Crit. Care. Med*. **2009**, *13* (2), 49-53.

140. Storm, D.R.; Rosenthal, K.S.; Swanson, P.E. Polymyxin and related peptide antibiotics. *Annu. Rev. Biochem*. **1977**, *46*, 723-763.

141. Schindler, M.; Osborn, M.J. Interaction of divalent cations and polymyxin B with lipopolysaccharide. *Biochemistry* **1979**, *18* (20), 4425-4430.

142. Li, J.; Nation, R.L.; Milne, R.W.; Turnidge, J.D.; Coulthard, K. Evaluation of colistin as an agent against multi-resistant Gram-negative bacteria. *Int. J. Antimicrob. Agents* **2005**, *25* (1), 11-25.

143. Newton, B.A. The properties and mode of action of the polymyxins. *Bacteriol. Rev*. **1956**, *20* (1), 14-27.

144. Mondal, A.H.; Khare, K.; Saxena, P.; Debnath, P.; Mukhopadhyay, K.; Yadav, D. A Review on Colistin Resistance: An Antibiotic of Last Resort. *Microorganisms.* **2024**, *12* (4), 772.

145. Raghuraman, H.; Chattopadhyay, A. Melittin: a membrane-active peptide with diverse functions. *Biosci. Rep*. **2007**, *27* (4-5), 189-223.

146. Chen, J.; Guan, S.M.; Sun, W.; Fu, H. Melittin, the Major Pain-Producing Substance of Bee Venom. *Neurosci. Bull*. **2016**, *32* (3), 265-272.

147. Ratcliffe, N.A.; Mello, C.B.; Garcia, E.S.; Butt, T.M.; Azambuja, P. Insect natural products and processes: new treatments for human disease. *Insect Biochem. Mol. Biol*. **2011**, *41* (10), 747-769.

148. Yang, H.; Ma, R.; Chen, J.; Xie, Q.; Luo, W.; Sun, P.; Liu, Z.; Guo, J. Discovery of Melittin as Triple-Action Agent: Broad-Spectrum Antibacterial, Anti-Biofilm, and Potential Anti-Quorum Sensing Activities. *Molecules* **2024**, *29* (3), 558.

149. Dempsey, C.E.; Butler, G.S. Helical structure and orientation of melittin in dispersed phospholipid membranes from amide exchange analysis in situ. *Biochemistry* **1992**, *31* (48), 11973-11977.

150. Rady, I.; Siddiqui, I.A.; Rady, M.; Mukhtar, H. Melittin, a major peptide component of bee venom, and its conjugates in cancer therapy. *Cancer Lett*. **2017**, *402*, 16-31.

151. Hossen, M.S.; Gan, S.H.; Khalil, M.I. Melittin, a Potential Natural Toxin of Crude Bee Venom: Probable Future Arsenal in the Treatment of Diabetes Mellitus. *Journal of Chemistry* **2017**, *2017*, 4035626.

152. Askari, P., Namaei, M.H., Ghazvini, K.; Hosseini, M. *In vitro* and *in vivo* toxicity and antibacterial efficacy of melittin against clinical extensively drug-resistant bacteria. *BMC Pharmacol. Toxicol.* **2021**, *22*, 42.

153. Lima, W.G.; de Brito, J.C.M.; Cardoso, V.N.; Fernandes, S.O.A. In-depth characterization of antibacterial activity of melittin against Staphylococcus aureus and use in a model of non-surgical MRSA-infected skin wounds. *Euro. J. of Pharm. Sci*. **2020**, *156*, 105592.

154. Dosler, S.; Gerceker, A.A. In vitro activities of antimicrobial cationic peptides; melittin and nisin, alone or in combination with antibiotics against Gram-positive bacteria. *J. Chemother*. **2012**, *24* (3), 137-43.

155. Memariani, H.; Memariani, M.; Shahidi-Dadras, M.; Nasiri, S.; Akhavan, M.M.; Moravvej, H. Melittin: from honeybees to superbugs. *Appl. Microbiol. Biotechnol*. **2019**, *103* (8), 3265-3276.

156. Hultmark, D.; Steiner, H.; Rasmuson, T.; Boman, H.G. Insect immunity. Purification and properties of three inducible bactericidal proteins from hemolymph of immunized pupae of Hyalophora cecropia. *Eur. J. Biochem*. **1980**, *106* (1), 7-16.

157. Steiner, H.; Hultmark, D.; Engström, Å.; Bennich, H.; Boman, H.G. Sequence and specificity of two antibacterial proteins involved in insect immunity. *Nature* **1981**, *292* (5820), 246-248.

158. Kim, J.K.; Lee, E.; Shin, S.; Jeong, K.; Lee, J.Y.; Bae, S.Y.; Kim, S.H.; Lee, J.; Kim, S.R.; Lee, D.G.; Hwang, J.S.; Kim, Y. Structure and function of papiliocin with antimicrobial and anti-inflammatory activities isolated from the swallowtail butterfly, Papilio xuthus. *J. Biol. Chem*. **2011**, *286* (48), 41296-41311.

159. Okada, M.; Natori, S. Primary structure of sarcotoxin I, an antibacterial protein induced in the hemolymph of Sarcophaga peregrina (flesh fly) larvae. *J. Biol. Chem*. **1985**, *260* (12), 7174-7177.

160. Landon, C.; Meudal, H.; Boulanger, N.; Bulet, P.; Vovelle, F. Solution structures of stomoxyn and spinigerin, two insect antimicrobial peptides with an alpha-helical conformation. *Biopolymers* **2006**, *81* (2), 92-103.

161. Brady, D.; Grapputo, A.; Romoli, O.; Sandrelli, F. Insect Cecropins, Antimicrobial Peptides with Potential Therapeutic Applications. *Int. J. Mol. Sci.* **2019**, *20* (23), 5862.

162. Sato, H.; Feix, J.B. Peptide-membrane interactions and mechanisms of membrane destruction by amphipathic alpha-helical antimicrobial peptides. *Biochim. Biophys. Acta* **2006**, *1758* (9), 1245-1256.

163. Moore, A.J.; Beazley, W.D.; Bibby, M.C.; Devine, D.A. Antimicrobial activity of cecropins. *J. Antimicrob. Chemother*. **1996**, *37* (6), 1077-1089.

164. Andrä, J.; Berninghausen, O.; Leippe, M. Cecropins, antibacterial peptides from insects and mammals, are potently fungicidal against Candida albicans. *Med. Microbiol. Immunol*. **2001**, *189* (3), 169-173.

165. Suttmann, H.; Retz, M.; Paulsen, F.; Harder, J.; Zwergel, U.; Kamradt, J.; Wullich, B.; Unteregger, G.; Stöckle, M.; Lehmann, J. Antimicrobial peptides of the Cecropin-family show potent antitumor activity against bladder cancer cells. *BMC Urol*. **2008**, *8*, 5.

166. Eisenstein, B.I.; Oleson, F.B. Jr.; Baltz, R.H. Daptomycin: from the mountain to the clinic, with essential help from Francis Tally, MD. *Clin. Infect. Dis*. **2010**, *50* (1), S10-5.

167. Heidary, M.; Khosravi, A.D.; Khoshnood, S.; Nasiri, M.J.; Soleimani, S.; Goudarzi, M. Daptomycin. *J. Antimicrob. Chemother*. **2018**, *73* (1), 1-11.

168. Pokorny, A.; Almeida, P.F. The Antibiotic Peptide Daptomycin Functions by Reorganizing the Membrane. *J. Membr. Biol*. **2021**, *254* (1), 97-108.

169. Carpenter, C.F.; Chambers, H.F. Daptomycin: another novel agent for treating infections due to drug-resistant gram-positive pathogens. *Clin. Infect. Dis*. **2004**, *38* (7), 994-1000.

170. Huang, H.W. DAPTOMYCIN, its membrane-active mechanism vs. that of other antimicrobial peptides. *Biochim. Biophys. Acta. Biomembr*. **2020**, *1862* (10), 183395.

171. Miller, W.R.; Bayer, A.S.; Arias, C.A. Mechanism of Action and Resistance to Daptomycin in Staphylococcus aureus and Enterococci. *Cold Spring Harb. Perspect. Med*. **2016**, *6* (11), a026997.

172. Zasloff, M. Magainins, a class of antimicrobial peptides from Xenopus skin: isolation, characterization of two active forms, and partial cDNA sequence of a precursor. *Proc. Natl. Acad. Sci. USA* **1987**, *84* (15), 5449-5453.

173. Bechinger, B.; Juhl, D.W.; Glattard, E.; Aisenbrey, C. Revealing the Mechanisms of Synergistic Action of Two Magainin Antimicrobial Peptides. *Front. Med. Technol*. **2020**, *2*, 615494.

174. Zasloff, M.; Martin, B.; Chen, H.C. Antimicrobial activity of synthetic magainin peptides and several analogues. *Proc. Natl. Acad. Sci. USA* **1988**, *85* (3), 910-913.

175. Khandelia, H.; Ipsen, J.H.; Mouritsen, O.G. The impact of peptides on lipid membranes. *Biochim. Biophys. Acta* **2008**, *1778* (7-8), 1528-1536.

176. Matsuzaki, K. Why and how are peptide-lipid interactions utilized for self-defense? Magainins and tachyplesins as archetypes. *Biochim. Biophys. Acta* **1999**, *1462* (1-2), 1-10.

177. Jacob, L.; Zasloff, M. Potential therapeutic applications of magainins and other antimicrobial agents of animal origin. *Ciba. Found. Symp*. **1994**, *186*, 197-216.

178. Soravia, E.; Martini, G.; Zasloff, M. Antimicrobial properties of peptides from Xenopus granular gland secretions. *FEBS Lett*. **1988**, *228* (2), 337-340.

179. Nakamura, T.; Furunaka, H.; Miyata, T.; Tokunaga, F.; Muta, T.; Iwanaga, S.; Niwa, M.; Takao, T.; Shimonishi, Y. Tachyplesin, a class of antimicrobial peptide from the hemocytes of the horseshoe crab (Tachypleus tridentatus). Isolation and chemical structure. *J. Biol. Chem*. **1988**, *263* (32), 16709-16713.

180. Liu, C.; Qi, J.; Shan, B.; Ma, Y. Tachyplesin Causes Membrane Instability That Kills Multidrug-Resistant Bacteria by Inhibiting the 3-Ketoacyl Carrier Protein Reductase FabG. *Front. Microbiol.* **2018**, *9*, 825.

181. Oppenheim, F.G.; Xu, T.; McMillian, F.M.; Levitz, S.M.; Diamond, R.D.; Offner, G.D.; Troxler, R.F. Histatins, a novel family of histidine-rich proteins in human parotid secretion. Isolation, characterization, primary structure, and fungistatic effects on Candida albicans. *J. Biol. Chem*. **1988**, *263* (16), 7472-7.

182. Khurshid, Z.; Najeeb, S.; Mali, M,; Moin, S.F.; Raza, S.Q.; Zohaib, S.; Sefat, F.; Zafar, M.S. Histatin peptides: Pharmacological functions and their applications in dentistry. *Saudi Pharm. J*. **2017**, *25* (1), 25-31.

183. Kavanagh, K.; Dowd, S. Histatins: antimicrobial peptides with therapeutic potential. *J. Pharm. Pharmacol*. **2004**, *56* (3), 285-289.

184. Vitorino, R.; Lobo, M.J.C.; Duarte, J.R.; Ferrer-Correia, A.J.; Domingues, P.M.; Amado, F.M.L. The role of salivary peptides in dental caries. *Biomed. Chromatogr*. **2005**, *19* (3), 214-222.

185. Tsai, H.; Bobek, L.A. Human salivary histatins: promising anti-fungal therapeutic agents. *Crit. Rev. Oral Biol. Med*. **1998**, *9* (4), 480-497.

186. Helmerhorst, E.J.; Hof, W.V.; Veerman, E.C.I.; Simoons-Smit, I.; Amerongen, A.V.N. Synthetic histatin analogues with broad-spectrum antimicrobial activity. *Biochem J*. **1997**, *326* (1), 39-45.

187. Romeo, D.; Skerlavaj, B.; Bolognesi, M.; Gennaro, R. Structure and bactericidal activity of an antibiotic dodecapeptide purified from bovine neutrophils. *J. Biol. Chem*. **1988**, *263* (20), 9573-9575.

188. Wu, M.; Hancock, R.E.W. Interaction of the cyclic antimicrobial cationic peptide bactenecin with the outer and cytoplasmic membrane. *J. Biol. Chem*. **1999**, *274* (1), 29-35.

189. Sun, C.; Gu, L.; Hussain, M.A.; Chen, L.; Lin, L.; Wang, H.; Pang, S.; Jiang, C.; Jiang, Z.; Hou, J. Characterization of the Bioactivity and Mechanism of Bactenecin Derivatives Against Food-Pathogens. *Front. Microbiol*. **2019**, *10*, 2593.

190. Radermacher, S.W.; Schoop, V.M.; Schluesener, H.J. Bactenecin, a leukocytic antimicrobial peptide, is cytotoxic to neuronal and glial cells. *J. Neurosci. Res*. **1993**, *36* (6), 657-662.

191. Casteels, P.; Ampe, C.; Jacobs, F.; Vaeck, M.; Tempst, P. Apidaecins: antibacterial peptides from honeybees. *EMBO J*. **1989**, *8* (8), 2387-2391.

192. Li, W.F.; Ma, G.X.; Zhou, X.X. Apidaecin-type peptides: biodiversity, structure-function relationships and mode of action. *Peptides*. **2006**, *27* (9), 2350-2359.

193. Agerberth, B.; Lee, J.Y.; Bergman, T.; Carlquist, M.; Boman, H.G.; Mutt, V.; Jörnvall, H. Amino acid sequence of PR-39. Isolation from pig intestine of a new member of the family of proline-arginine-rich antibacterial peptides. *Eur. J. Biochem*. **1991**, *202* (3), 849-854.

194. Fan, F.; Wu, Y.; Liu, J. Expression and purification of two different antimicrobial peptides, PR-39 and Protegrin-1 in Escherichia coli. *Protein Expr. Purif*. **2010**, *73* (2), 147-151.

195. Holani, R.; Shah, C.; Haji, Q.; Inglis, G.D.; Uwiera, R.R.E.; Cobo, E.R. Proline-arginine rich (PR-39) cathelicidin: Structure, expression and functional implication in intestinal health. *Comp. Immunol. Microbiol. Infect. Dis*. **2016**, *49*, 95-101.

196. Veldhuizen, E.J.A.; Schneider, V.A.F.; Agustiandari, H.; van Dijk, A.; Tjeerdsma-van Bokhoven J.L.M.; Bikker, F.J.; Haagsman, H.P. Antimicrobial and immunomodulatory activities of PR-39 derived peptides. *PLoS One* **2014**, *9* (4), e95939.

197. Linde, C.M.A.; Hoffner, S.E.; Refai, E.; Andersson, M. In vitro activity of PR-39, a proline-arginine-rich peptide, against susceptible and multi-drug-resistant Mycobacterium tuberculosis. *J. Antimicrob. Chemother*. **2001**, *47* (5), 575-580.

198. Ramanathan, B.; Davis, E.G.; Ross, C.R.; Blecha, F. Cathelicidins: microbicidal activity, mechanisms of action, and roles in innate immunity. *Microbes Infect*. **2002**, *4* (3), 361-372.

199. Boman, H.G.; Agerberth, B.; Boman, A. Mechanisms of action on Escherichia coli of cecropin P1 and PR-39, two antibacterial peptides from pig intestine. *Infect Immun*. **1993**, *61* (7), 2978-2984.

200. Ganz, T.; Selsted, M.E.; Szklarek, D.; Harwig, S.S.; Daher, K.; Bainton, D.F.; Lehrer, R.I. Defensins. Natural peptide antibiotics of human neutrophils. *J. Clin. Invest*. **1985**, *76* (4), 1427-1435.

201. Harwig, S.S.; Park, A.S.; Lehrer, R.I. Characterization of defensin precursors in mature human neutrophils. *Blood* **1992**, *79* (6), 1532-1537.

202. Jones, D.E.; Bevins, C.L. Paneth cells of the human small intestine express an antimicrobial peptide gene. *J. Biol. Chem*. **1992**, *267* (32), 23216-23225.

203. Jones, D.E.; Bevins, C.L. Defensin-6 mRNA in human Paneth cells: implications for antimicrobial peptides in host defense of the human bowel. *FEBS Lett*. **1993**, *315* (2), 187-192.

204. Szyk, A.; Wu, Z.; Tucker, K.; Yang, D.; Lu, W.; Lubkowski, J. Crystal structures of human alpha-defensins HNP4, HD5, and HD6. *Protein Sci*. **2006**, *15* (12), 2749-2760.

205. Lehrer, R.I.; Lu, W. α-Defensins in human innate immunity. *Immunol Rev*. **2012**, *245* (1), 84-112.

206. Wu, Z.; Ericksen, B.; Tucker, K.; Lubkowski, J.; Lu, W. Synthesis and characterization of human alpha-defensins 4-6. *J. Pept. Res*. **2004**, *64* (3), 118-25.

207. Ericksen, B.; Wu, Z.; Lu, W.; Lehrer, R.I. Antibacterial activity and specificity of the six human {alpha}-defensins. *Antimicrob. Agents Chemother*. **2005**, *49* (1), 269-275.

208. Daneshi, M.; Caton, J.S.; Caixeta, L.S.; Eftekhari, Z.; Ward, A.K. Expression, Regulation, and Function of β-Defensins in the Bovine Mammary Glands: Current Knowledge and Future Perspectives. *Animals (Basel)* **2023**, *13* (21), 3372.

209. Gurao, A.; Kashyap, S.K.; Singh, R. β-defensins: An innate defense for bovine mastitis. *Vet World* **2017**, *10* (8), 990-998.

210. Pazgier, M.; Hoover, D.M.; Yang, D.; Lu, W.; Lubkowski, J. Human beta-defensins. *Cell Mol. Life Sci*. **2006**, *63* (11), 1294-1313.

211. Sugiarto, H.; Yu, P.L. Avian antimicrobial peptides: the defense role of beta-defensins. *Biochem. Biophys. Res. Commun*. **2004**, *323* (3), 721-727.

212. Bensch, K.W.; Raida, M.; Mägert, H.J.; Schulz-Knappe, P.; Forssmann, W.G. hBD-1: a novel beta-defensin from human plasma. *FEBS Lett*. **1995**, *368* (2), 331-335.

213. Harder, J.; Bartels, J.; Christophers, E.; Schröder, J.M. A peptide antibiotic from human skin. *Nature* **1997**, *387* (6636), 861.

214. Harder, J.; Bartels, J.; Christophers, E.; Schroder, J.M. Isolation and characterization of human beta -defensin-3, a novel human inducible peptide antibiotic. *J. Biol. Chem*. **2001**, *276* (8), 5707-5713.

215. Prahl, A.; Pazgier, M.; Alexandratos, J.; Lubkowski, J. Human β-defensin 4 - defensin without the "twist". *Postepy Biochem*. **2016**, *62* (3), 349-361.

216. Selsted, M.E.; Novotny, M.J.; Morris, W.L.; Tang, Y.Q.; Smith, W.; Cullor, J.S. Indolicidin, a novel bactericidal tridecapeptide amide from neutrophils. *J. Biol. Chem*. **1992**, *267* (7), 4292-4295.

217. Young-Speirs, M.; Drouin, D.; Cavalcante, P.A.; Barkema, H.W.; Cobo, E.R. Host defense cathelicidins in cattle: types, production, bioactive functions and potential therapeutic and diagnostic applications. *Int. J. Antimicrob. Agents* **2018**, *51* (6), 813-821.

218. Benincasa, M.; Scocchi, M.; Pacor, S.; Tossi, A.; Nobili, D.; Basaglia, G.; Busetti, M.; Gennaro, R. Fungicidal activity of five cathelicidin peptides against clinically isolated yeasts. *J. Antimicrob. Chemother*. **2006**, *58* (5), 950-959.

219. Subbalakshmi, C.; Sitaram, N. Mechanism of antimicrobial action of indolicidin. *FEMS Microbiol. Lett*. **1998**, *160* (1), 91-96.

220. Falla, T.J.; Karunaratne, D.N.; Hancock, R.E.W. Mode of action of the antimicrobial peptide indolicidin. *J. Biol. Chem*. **1996**, *271* (32), 19298-19303.

221. Kokryakov, V.N.; Harwig, S.S.L.; Panyutich, E.A.; Shevchenko, A.A.; Aleshina, G.M.; Shamova, O.V.; Korneva, H.A.; Lehrer, R.I. Protegrins: leukocyte antimicrobial peptides that combine features of corticostatic defensins and tachyplesins. *FEBS Lett*. **1993**, *327* (2), 231-236.

222. Sokolov, Y.; Mirzabekov, T.; Martin, D.W.; Lehrer, R.I.; Kagan, B.L. Membrane channel formation by antimicrobial protegrins. *Biochim. Biophys. Acta* **1999**, *1420* (1-2), 23-29.

223. Drin, G.; Temsamani, J. Translocation of protegrin I through phospholipid membranes: role of peptide folding. *Biochim. Biophys. Acta* **2002**, *1559* (2), 160-170.

224. Simmaco, M.; Mignogna, G.; Barra, D.; Bossa, F. Antimicrobial peptides from skin secretions of Rana esculenta. Molecular cloning of cDNAs encoding esculentin and brevinins and isolation of new active peptides. *J. Biol. Chem*. **1994**, *269* (16), 11956-11961.

225. Conlon, J.M.; Kolodziejek, J.; Nowotny, N. Antimicrobial peptides from ranid frogs: taxonomic and phylogenetic markers and a potential source of new therapeutic agents. *Biochim. Biophys. Acta* **2004**, *1696* (1), 1-14.

226. Goraya, J.; Wang, Y.; Li, Z.; O'Flaherty, M.; Knoop, F.C.; Platz, J.E.; Conlon, J.M. Peptides with antimicrobial activity from four different families isolated from the skins of the North American frogs Rana luteiventris, Rana berlandieri and Rana pipiens. *Eur. J. Biochem*. **2000**, *267* (3), 894-900.

227. Simmaco, M.; Mignogna, G.; Canofeni, S.; Miele, R.; Mangoni, M.L.; Barra, D. Temporins, antimicrobial peptides from the European red frog Rana temporaria. *Eur. J. Biochem*. **1996**, *242* (3), 788-792.

228. Romero, S.M.; Cardillo, A.B.; Ceron, M.C.M.; Camperi, S.A.; Giudicessi, S.L. Temporins: An Approach of Potential Pharmaceutic Candidates. *Surg. Infect. (Larchmt)*. **2020**, *21* (4), 309-322.

229. D'Andrea, L.D.; Romanelli, A. Temporins: Multifunctional Peptides from Frog Skin. *Int. J. Mol. Sci*. **2023**, *24* (6), 5426.

230. Mangoni, M.L.; Shai, Y. Temporins and their synergism against Gram-negative bacteria and in lipopolysaccharide detoxification. *Biochim. Biophys. Acta* **2009**, *1788* (8), 1610-1619.

231. Conlon, J.M.; Kolodziejek, J.; Nowotny, N. Antimicrobial peptides from the skins of North American frogs. *Biochim. Biophys. Acta* **2009**, *1788* (8), 1556-1563.

232. D'Abramo, M.; Rinaldi, A.C.; Bozzi, A.; Amadei, A.; Mignogna, G.; Di Nola, A.; Aschi, M. Conformational behavior of temporin A and temporin L in aqueous solution: A computational/experimental study. *Biopolymers* **2006**, *81* (3), 215-224.

233. Zhao, H.; Kinnunen, P.K.J. Binding of the antimicrobial peptide temporin L to liposomes assessed by Trp fluorescence. *J. Biol. Chem*. **2002**, *277* (28), 25170-25177.

234. Mangoni, M.L. Temporins, anti-infective peptides with expanding properties. *Cell. Mol. Life Sci*. **2006**, *63* (9), 1060-1069.

235. Mahalka, A.K.; Kinnunen, P.K.J. Binding of amphipathic alpha-helical antimicrobial peptides to lipid membranes: lessons from temporins B and L. *Biochim. Biophys. Acta* **2009**, *1788* (8), 1600-1609.

236. Fehlbaum, P.; Bulet, P.; Chernysh, S.; Briand, J.P.; Roussel, J.P.; Letellier, L.; Hetru, C.; Hoffmann, J.A. Structure-activity analysis of thanatin, a 21-residue inducible insect defense peptide with sequence homology to frog skin antimicrobial peptides. *Proc. Natl. Acad. Sci. USA* **1996**, *93* (3), 1221-1215.

237. Dash, R.; Bhattacharjya, S. Thanatin: An Emerging Host Defense Antimicrobial Peptide with Multiple Modes of Action. *Int. J. Mol. Sci*. **2021**, *22* (4), 1522.

238. Sinha, S.; Ng, W.J.; Bhattacharjya, S. NMR structure and localization of the host defense antimicrobial peptide thanatin in zwitterionic dodecylphosphocholine micelle: Implications in antimicrobial activity. *Biochim. Biophys. Acta. Biomembr*. **2020**, *1862* (11), 183432.

239. Sinha, S.; Zheng, L.; Mu, Y.; Ng, W.J.; Bhattacharjya, S. Structure and Interactions of A Host Defense Antimicrobial Peptide Thanatin in Lipopolysaccharide Micelles Reveal Mechanism of Bacterial Cell Agglutination. *Sci Rep*. **2017**, *7* (1), 17795.

240. Ma, B.; Fang, C.; Lu, L.; Wang, M.; Xue, X.; Zhou, Y.; Li, M.; Hu, Y.; Luo, X.; Hou, Z. The antimicrobial peptide thanatin disrupts the bacterial outer membrane and inactivates the NDM-1 metallo-β-lactamase. *Nat. Commun*. **2019**, *10* (1), 3517.

241. Javadmanesh, A.; Mohammadi, E.; Mousavi, Z.; Azghandi, M.; Tanhaiean, A. Antibacterial effects assessment on some livestock pathogens, thermal stability and proposing a probable reason for different levels of activity of thanatin. *Sci. Rep*. **2021**, *11* (1), 10890.

242. Park, C.B.; Kim, M.S.; Kim, S.C. A novel antimicrobial peptide from Bufo bufo gargarizans. *Biochem. Biophys. Res. Commun*. **1996**, *218* (1), 408-413.

243. Cho, J.H.; Sung, B.H.; Kim, S.C. Buforins: histone H2A-derived antimicrobial peptides from toad stomach. *Biochim. Biophys. Acta* **2009**, *1788* (8), 1564-1569.

244. Craik, D.J.; Daly, N.L.; Bond, T.; Waine, C. Plant cyclotides: A unique family of cyclic and knotted proteins that defines the cyclic cystine knot structural motif. *J. Mol. Biol*. **1999**, *294* (5), 1327-1336.

245. Weidmann, J.; Craik, D.J. Discovery, structure, function, and applications of cyclotides: circular proteins from plants. *J. Exp. Bot*. **2016**, *67* (16), 4801-4812.

246. Pelegrini, P.B.; Quirino, B.F.; Franco, O.L. Plant cyclotides: an unusual class of defense compounds. *Peptides* **2007**, *28* (7), 1475-1481.

247. Henriques, S.T.; Huang, Y.H.; Chaousis, S.; Sani, M.A.; Poth, A.G.; Separovic, F.; Craik, D.J. The Prototypic Cyclotide Kalata B1 Has a Unique Mechanism of Entering Cells. *Chem. Biol*. **2015**, *22* (8),1087-1097.

248. Huang, Y.H.; Colgrave, M.L.; Daly, N.L.; Keleshian, A.; Martinac, B.; Craik, D.J. The biological activity of the prototypic cyclotide kalata b1 is modulated by the formation of multimeric pores. *J. Biol. Chem*. **2009**, *284* (31), 20699-20707.

249. Orivel, J.; Redeker, V.; Le Caer J.P.; Krier, F.; Revol-Junelles, A.M.; Longeon, A.; Chaffotte, A.; Dejean, A.; Rossier, J. Ponericins, new antibacterial and insecticidal peptides from the venom of the ant Pachycondyla goeldii. *J. Biol. Chem*. **2001**, *276* (21), 17823-17829.

250. Schittek, B.; Hipfel, R.; Sauer, B.; Bauer, J.; Kalbacher, H.; Stevanovic, S.; Schirle, M.; Schroeder, K.; Blin, N.; Meier, F.; Rassner, G.; Garbe, C. Dermcidin: a novel human antibiotic peptide secreted by sweat glands. *Nat. Immunol*. **2001**, *2* (12), 1133-1137.

251. Jang, W.S.; Kim, K.N.; Lee, Y.S.; Nam, M.H.; Lee, I.H. Halocidin: a new antimicrobial peptide from hemocytes of the solitary tunicate, Halocynthia aurantium. *FEBS Lett*. **2002**, *521* (1-3), 81-86.

252. Mygind, P.H.; Fischer, R.L.; Schnorr, K.M.; Hansen, M.T.; Sönksen, C.P.; Ludvigsen, S.; Raventós, D.; Buskov, S.; Christensen, B.; De Maria, L.; Taboureau, O.; Yaver, D.; Elvig-Jørgensen, S.G.; Sørensen, M.V.; Christensen, B.E.; Kjaerulff, S.; Frimodt-Moller, N.; Lehrer, R.I.; Zasloff. M.; Kristensen, H.H. Plectasin is a peptide antibiotic with therapeutic potential from a saprophytic fungus. *Nature* **2005**, *437* (7061), 975-980.

253. Cerovský, V.; Budesínský, M.; Hovorka, O.; Cvacka, J.; Voburka, Z.; Slaninová, J.; Borovicková, L.; Fucík, V.; Bednárová, L.; Votruba, I.; Straka, J. Lasioglossins: three novel antimicrobial peptides from the venom of the eusocial bee Lasioglossum laticeps (Hymenoptera: Halictidae). *Chembiochem*. **2009**, *10* (12), 2089-2099.

254. Andersen, A.S.; Sandvang, D.; Schnorr, K.M.; Kruse, T.; Neve, S.; Joergensen, B.; Karlsmark, T.; Krogfelt, K.A. A novel approach to the antimicrobial activity of maggot debridement therapy. *J. Antimicrob. Chemother*. **2010**, *65* (8), 1646-1654.

255. Ceřovský, V.; Bém, R. Lucifensins, the Insect Defensins of Biomedical Importance: The Story behind Maggot Therapy. *Pharmaceuticals (Basel)* **2014**, *7* (3), 251-264.

256. Abbassi, F.; Lequin, O.; Piesse, C.; Goasdoué, N.; Foulon, T.; Nicolas, P.; Ladram, A. Temporin-SHf, a new type of phe-rich and hydrophobic ultrashort antimicrobial peptide. *J. Biol. Chem*. **2010**, *285* (22), 16880-16892.

257. Tareq, F.S.; Lee, M.A.; Lee, H.S.; Lee, Y.J.; Lee, J.S.; Hasan, C.M.; Islam, M.T.; Shin, H.J. Gageotetrins A-C, noncytotoxic antimicrobial linear lipopeptides from a marine bacterium Bacillus subtilis. *Org. Lett*. **2014**, *16* (3), 928-931.

258. Essig, A.; Hofmann, D.; Münch, D.; Gayathri, S.; Künzler, M.; Kallio, P.T.; Sahl, H.G.; Wider, G.; Schneider, T.; Aebi, M. Copsin, a novel peptide-based fungal antibiotic interfering with the peptidoglycan synthesis. *J. Biol. Chem*. **2014**, *289* (50), 34953-34964.

259. Ling, L.L.; Schneider, T.; Peoples, A.J.; Spoering, A.L.; Engels, I.; Conlon, B.P.; Mueller, A.; Schäberle, T.F.; Hughes, D.E.; Epstein, S.; Jones, M.; Lazarides, L.; Steadman, V.A.; Cohen, D.R.; Felix, C.R.; Fetterman, K.A.; Millett, W.P.; Nitti, A.G.; Zullo, A.M.; Chen, C.; Lewis, K. A new antibiotic kills pathogens without detectable resistance. *Nature* **2015**, *517* (7535), 455-459.

260. Shukla, R.; Lavore, F.; Maity, S.; Derks, M.G.N.; Jones, C.R.; Vermeulen, B.J.A.; Melcrová, A.; Morris, M.A.; Becker, L.M.; Wang, X.; Kumar, R.; Medeiros-Silva, J.; van Beekveld, R.A.M.; Bonvin, A.M.J.J.; Lorent, J.H.; Lelli, M.; Nowick, J.S.; MacGillavry, H.D.; Peoples, A.J.; Spoering, A.L.; Ling, L.L.; Hughes, D.E.; Roos, W.H.; Breukink, E.; Lewis, K.; Weingarth, M. Teixobactin kills bacteria by a two-pronged attack on the cell envelope. *Nature* **2022**, *608* (7922), 390-396.

261. Cui, P.; Dong, Y.; Li, Z.; Zhang, Y.; Zhang, S. Identification and functional characterization of an uncharacterized antimicrobial peptide from a ciliate Paramecium caudatum. *Dev. Comp. Immunol.* **2016**, *60*, 53-65.

262. Zipperer, A.; Konnerth, M.C.; Laux, C.; Berscheid, A.; Janek, D.; Weidenmaier, C.; Burian, M.; Schilling, N.A.; Slavetinsky, C.; Marschal, M.; Willmann, M.; Kalbacher, H.; Schittek, B.; Brötz-Oesterhelt, H.; Grond, S.; Peschel, A.; Krismer, B. Human commensals producing a novel antibiotic impair pathogen colonization. *Nature* **2016**, *535* (7613), 511-516.

263. Holthausen, D.J.; Lee, S.H.; Kumar, V.T.; Bouvier, N.M.; Krammer, F.; Ellebedy, A.H.; Wrammert, J.; Lowen, A.C.; George, S.; Pillai, M.R.; Jacob, J. An Amphibian Host Defense Peptide Is Virucidal for Human H1 Hemagglutinin-Bearing Influenza Viruses. *Immunity* **2017**, *46* (4), 587-595.

264. Mardirossian, M.; Pérébaskine, N.; Benincasa, M.; Gambato, S.; Hofmann, S.; Huter, P.; Müller, C.; Hilpert, K.; Innis, C.A.; Tossi, A.; Wilson, D.N. The Dolphin Proline-Rich Antimicrobial Peptide Tur1A Inhibits Protein Synthesis by Targeting the Bacterial Ribosome. *Cell Chem. Biol*. **2018**, *25* (5), 530-539.e7.

265. Shi, J.; Wu, J.; Chen, Q.; Shen, Y.; Mi, K.; Yang, H.; Mu, L. A Frog-Derived Cathelicidin Peptide with Dual Antimicrobial and Immunomodulatory Activities Effectively Ameliorates *Staphylococcus aureus*-Induced Peritonitis in Mice. *ACS Infect. Dis.* **2022**, *8* (12), 2464-2479.

266. Huttner, K.M.; Bevins, C.L. Antimicrobial Peptides as Mediators of Epithelial Host Defense. *Pediatr. Res.* **1999**, *45*, 785-794.

267. Wang, G. Human antimicrobial peptides and proteins. *Pharmaceuticals (Basel)* **2014**, *7* (5), 545-594.

268. Kumar, R.; Ali, S.A.; Singh, S.K.; Bhushan, V.; Mathur, M.; Jamwal, S.; Mohanty, A.K.; Kaushik, J.K.; Kumar, S. Antimicrobial Peptides in Farm Animals: An Updated Review on Its Diversity, Function, Modes of Action and Therapeutic Prospects. *Vet. Sci*. **2020**, *7* (4), 206.

269. Valdez-Miramontes, C.E.; De Haro-Acosta, J.; Aréchiga-Flores, C.F.; Verdiguel-Fernández, L.; Rivas-Santiago, B. Antimicrobial peptides in domestic animals and their applications in veterinary medicine. *Peptides* **2021**, *142*, 170576.

270. Wu, Q.; Patočka, J.; Kuča, K. Insect Antimicrobial Peptides, a Mini Review. *Toxins (Basel)* **2018**, *10* (11), 461.

271. Patocka, J.; Nepovimova, E.; Klimova, B.; Wu, Q.; Kuca, K. Antimicrobial Peptides: Amphibian Host Defense Peptides. *Curr. Med. Chem*. **2019**, *26* (32), 5924-5946.

272. Rollins-Smith, L.A. The importance of antimicrobial peptides (AMPs) in amphibian skin defense. *Dev. Comp. Immunol*. **2023**, *142*, 104657.

273. Xiao, Y.; Liu, C.; Lai, R. Antimicrobial peptides from amphibians. *Biomolecular Concepts* **2011**, *2* (1-2), 27-38.

274. Falanga, A.; Lombardi, L.; Franci, G.; Vitiello, M.; Iovene, M.R.; Morelli, G.; Galdiero, M.; Galdiero, S. Marine Antimicrobial Peptides: Nature Provides Templates for the Design of Novel Compounds against Pathogenic Bacteria. *Int. J. Mol. Sci.* **2016**, *17* (5), 785.

275. Tincu, J.A.; Taylor, S.W. Antimicrobial peptides from marine invertebrates. *Antimicrob. Agents Chemother*. **2004**, *48* (10), 3645-3654.

276. Wu, R.; Patocka, J.; Nepovimova, E.; Oleksak, P.; Valis, M.; Wu, W.; Kuca, K. Marine Invertebrate Peptides: Antimicrobial Peptides. *Front. Microbiol*. **2021**, *12*, 785085.

277. Guryanova, S.V.; Balandin, S.V.; Belogurova-Ovchinnikova, O.Y.; Ovchinnikova, T.V. Marine Invertebrate Antimicrobial Peptides and Their Potential as Novel Peptide Antibiotics. *Mar. Drugs*. **2023**, *21* (10), 503.

278. Lima, A.M.; Azevedo, M.I.G.; Sousa, L.M.; Oliveira, N.S.; Andrade, C.R.; Freitas, C.D.T.; Souza, P.F.N. Plant antimicrobial peptides: An overview about classification, toxicity and clinical applications. *Int. J. Biol. Macromol*. **2022**, *214*, 10-21.

279. Zou, F.; Tan, C.; Shinali, T.S.; Zhang, B.; Zhang, L.; Han, Z.; Shang, N. Plant antimicrobial peptides: a comprehensive review of their classification, production, mode of action, functions, applications, and challenges. *Food Funct*. **2023**, *14* (12), 5492-5515.

280. Tam, J.P.; Wang, S.; Wong, K.H.; Tan, W.L. Antimicrobial Peptides from Plants. *Pharmaceuticals (Basel)* **2015**, *8* (4), 711-757.

281. Broekaert, W. F.; Cammue, B. P. A.; De Bolle, M. F. C.; Thevissen, K.; De Samblanx, G. W.; Osborn, R. W.; Nielson, K. Antimicrobial Peptides from Plants. *Critical Reviews in Plant Sciences*. **1997**, *16* (3), 297-323.

282. Li, J.; Hu, S.; Jian, W.; Xie, C.; Yang, X. Plant antimicrobial peptides: structures, functions, and applications. *Bot. Stud*. **2021**, *62* (1), 5.

283. Singh, N.; Abraham, J. Ribosomally synthesized peptides from natural sources. *J. Antibiot.* **2014***, 67* (4), 277-289.

284. Drider, D.; Fimland, G.; Héchard, Y.; McMullen, L.M.; Prévost, H. The continuing story of class IIa bacteriocins. *Microbiol. Mol. Biol. Rev*. **2006**, *70* (2), 564-582.

285. Wu, Y.; Pang, X.; Wu, Y.; Liu, X.; Zhang, X. Enterocins: Classification, Synthesis, Antibacterial Mechanisms and Food Applications. *Molecules* **2022**, *27* (7), 2258.

286. Dunlap, C.A.; Bowman, M.J.; Rooney, A.P. Iturinic Lipopeptide Diversity in the *Bacillus subtilis* Species Group - Important Antifungals for Plant Disease Biocontrol Applications. *Front. Microbiol*. **2019**, *10*, 1794.

287. Raaijmakers, J.M.; de Bruijn, I.; de Kock, M.J.D. Cyclic lipopeptide production by plant-associated Pseudomonas spp.: diversity, activity, biosynthesis, and regulation. *Mol. Plant Microbe Interact*. **2006**, *19* (7), 699-710.

288. Babasaki, K.; Takao, T.; Shimonishi, Y.; Kurahashi, K. Subtilosin A, a new antibiotic peptide produced by Bacillus subtilis 168: isolation, structural analysis, and biogenesis. *J. Biochem*. **1985**, *98* (3), 585-603.

289. McAuliffe, O.; Ryan, M.P.; Ross, R.P.; Hill, C.; Breeuwer, P.; Abee, T. Lacticin 3147, a broad-spectrum bacteriocin which selectively dissipates the membrane potential. *Appl. Environ. Microbiol*. **1998**, *64* (2), 439-445.

290. Giuliani, A.; Pirri, G.; Nicoletto, S. Antimicrobial peptides: an overview of a promising class of therapeutics. *Open Life Sciences* **2007**, *2* (1), 1-33.

291. Hafeez, A.B.; Jiang, X.; Bergen, P.J.; Zhu, Y. Antimicrobial Peptides: An Update on Classifications and Databases. *Int. J. Mol. Sci.* **2021**, *22* (21), 11691.

292. Büyükkiraz, M.E.; Kesmen, Z. Antimicrobial peptides (AMPs): A promising class of antimicrobial compounds. *J. Appl. Microbiol*. **2022**, *132* (3), 1573-1596.

293. Lee, H.T.; Lee, C.C.; Yang, J.R.; Lai, J.Z.C.; Chang, K.Y. A large-scale structural classification of antimicrobial peptides. *Biomed. Res. Int*. **2015**, *2015*, 475062.

294. Panteleev, P.V.; Bolosov, I.A.; Balandin, S.V.; Ovchinnikova, T.V. Structure and Biological Functions of β-Hairpin Antimicrobial Peptides. *Acta Naturae* **2015**, *7* (1), 37-47.

295. Huang, Y.; Huang, J.; Chen, Y. Alpha-helical cationic antimicrobial peptides: relationships of structure and function. *Protein & Cell* **2010**, *1* (2), 143-152.

296. Yi, H.Y.; Chowdhury, M.; Huang, Y.D.; Yu, X.Q. Insect antimicrobial peptides and their applications. *Appl. Microbiol. Biotechnol.* **2014***, 98*, 5807-5822.

297. Oren, Z.; Lerman, J.C.; Gudmundsson, G.H.; Agerberth, B.; Shai, Y. Structure and organization of the human antimicrobial peptide LL-37 in phospholipid membranes: relevance to the molecular basis for its non-cell-selective activity. *Biochem J*. **1999**, *341* (3), 501-513.

298. Lee, I.H.; Zhao, C.; Cho, Y.; Harwig, S.S.L.; Cooper, E.L.; Lehrer, R.I. Clavanins, alpha-helical antimicrobial peptides from tunicate hemocytes. *FEBS Lett*. **1997**, *400* (2), 158-162.

299. Lehrer, R.I.; Bevins, C.L.; Ganz, T. Defensins and Other Antimicrobial Peptides and Proteins. *Mucosal Immunology*, 3rd ed.; **2005**, 95-110.

300. Hwang, P.M.; Zhou, N.; Shan, X.; Arrowsmith, C.H.; Vogel, H.J. Three-dimensional solution structure of lactoferricin B, an antimicrobial peptide derived from bovine lactoferrin. *Biochemistry* **1998**, *37* (12), 4288-4298.

301. Ostberg, N.; Kaznessis, Y. Protegrin structure-activity relationships: using homology models of synthetic sequences to determine structural characteristics important for activity. *Peptides* **2005**, *26* (2), 197-206.

302. Vernen, F.; Harvey, P.J.; Dias, S.A.; Veiga, A.S.; Huang, Y.H.; Craik, D.J.; Lawrence, N.; Henriques, S.T. Characterization of Tachyplesin Peptides and Their Cyclized Analogues to Improve Antimicrobial and Anticancer Properties. *Int. J. Mol. Sci*. **2019**, *20* (17), 4184.

303. Abdullah, S.J.; Mu, Y.; Bhattacharjya, S. Structures, Interactions and Activity of the N-Terminal Truncated Variants of Antimicrobial Peptide Thanatin. *Antibiotics* **2024**, *13* (1), 74.

304. Shafee, T.M.A.; Lay, F.T.; Phan, T.K.; Anderson, M.A.; Hulett, M.D. Convergent evolution of defensin sequence, structure and function. *Cell. Mol. Life Sci.* **2017**, *74*, 663-682.

305. Shafee, T.M.A.; Lay, F.T.; Hulett, M.D.; Anderson, M.A. The Defensins Consist of Two Independent, Convergent Protein Superfamilies. *Mol. Bio. and Evolution*. **2016**, *33* (9), 2345-2356.

306. Takahashi, D.; Shukla, S.K.; Prakash, O.; Zhang, G. Structural determinants of host defense peptides for antimicrobial activity and target cell selectivity. *Biochimie* **2010**, *92* (9), 1236-1241.

307. Friedrich, C.L.; Rozek, A.; Patrzykat, A.; Hancock, R.E.W.; Structure and mechanism of action of an indolicidin peptide derivative with improved activity against gram-positive bacteria. *J. Biol. Chem*. **2001**, *276* (26), 24015-24022.

308. Ojeda, P.G.; Cardoso, M.H.; Franco, O.L. Pharmaceutical applications of cyclotides. *Drug Discov. Today* **2019**, *24* (11), 2152-2161.

309. Loll, P.J.; Upton, E.C.; Nahoum, V.; Economou, N.J.; Cocklin, S. The high resolution structure of tyrocidine A reveals an amphipathic dimer. *Biochim. Biophys. Acta* **2014**, *1838* (5), 1199-1207.

310. Mohapatra, S.S.; Dwibedy, S.K.; Padhy, I. Polymyxins, the last-resort antibiotics: Mode of action, resistance emergence, and potential solutions. *J. Biosci.* **2021***, 46*, 85.

311. Micklefield, J. Daptomycin structure and mechanism of action revealed. *Chem. Biol*. **2004**, *11* (7), 887-888.

312. Ughetto, G.; Wang, A.H.J.; Quigley, G.J.; van der Marel, G.A.; van Boom, J.H.; Rich, A. A comparison of the structure of echinomycin and triostin A complexed to a DNA fragment. *Nucleic Acids Res*. **1985**, *13* (7), 2305-2323.

313. The structure of a new cyclosporin A solvated form. *Zeitschrift für Kristallographie - Crystalline Materials* **1996**, *211* (5), 313-318.

314. Takesako, K.; Kuroda, H.; Inoue, T.; Haruna, F.; Yoshikawa, Y.; Kato, I.; Uchida, K.; Hiratani, T.; Yamaguchi, H. Biological properties of aureobasidin A, a cyclic depsipeptide antifungal antibiotic. *J. Antibiot. (Tokyo)* **1993**, *46* (9), 1414-1420.

315. Vanzolini, T.; Bruschi, M.; Rinaldi, A.C.; Magnani, M.; Fraternale, A. Multitalented Synthetic Antimicrobial Peptides and Their Antibacterial, Antifungal and Antiviral Mechanisms. *Int. J. Mol. Sci*. **2022**, *23* (1), 545.

316. Rizzetto, G.; Gambini, D.; Maurizi, A.; Candelora, M.; Molinelli, E.; Cirioni, O.; Brescini, L.; Giacometti, A.; Offidani, A.; Simonetti, O. Our Experience over 20 Years: Antimicrobial Peptides against Gram Positives, Gram Negatives, and Fungi. *Pharmaceutics* **2023**, *15* (1), 40.

317. Li, X.; Zuo, S.; Wang, B.; Zhang, K.; Wang, Y. Antimicrobial Mechanisms and Clinical Application Prospects of Antimicrobial Peptides. *Molecules* **2022**, *27* (9), 2675.

318. Boman, H.G. Antibacterial peptides: basic facts and emerging concepts. *J. Intern. Med*. **2003**, *254* (3), 197-215.

319. Marr, A.K.; Gooderham, W.J.; Hancock, R.E.W. Antibacterial peptides for therapeutic use: obstacles and realistic outlook. *Curr. Opin. Pharmacol*. **2006**, *6* (5), 468-472.

320. De Lucca, A.J.; Walsh, T.J. Antifungal peptides: novel therapeutic compounds against emerging pathogens. *Antimicrob. Agents Chemother*. **1999**, *43* (1), 1-11.

321. Li, T.; Li, L.; Du, F.; Sun, L.; Shi, J.; Long, M.; Chen, Z. Activity and Mechanism of Action of Antifungal Peptides from Microorganisms: A Review. *Molecules* **2021**, *26* (11), 3438.

322. Freitas, C.G.; Felipe, M.S. *Candida albicans* and Antifungal Peptides. *Infect Dis. Ther.* **2023,** *12*, 2631-2648.

323. de Ullivarri M.F.; Arbulu, S.; Garcia-Gutierrez, E.; Cotter, P.D. Antifungal Peptides as Therapeutic Agents. *Front Cell Infect. Microbiol*. **2020**, *10*, 105.

324. Struyfs. C.; Cammue, B.P.A.; Thevissen, K. Membrane-Interacting Antifungal Peptides. *Front. Cell Dev. Biol*. **2021**, *9*, 649875.

325. Brice, D.C.; Toth, Z.; Diamond, G. LL-37 disrupts the Kaposi's sarcoma-associated herpesvirus envelope and inhibits infection in oral epithelial cells. *Antiviral Res*. **2018**, *158*, 25-33.

326. Marcocci, M. E.; Amatore, D.; Villa, S.; Casciaro, B.; Aimola, P.; Franci, G.; Grieco, P.; Galdiero, M.; Palamara, A. T.; Mangoni, M. L.; Nencioni, L. The Amphibian Antimicrobial Peptide Temporin B Inhibits *In Vitro* Herpes Simplex Virus 1 Infection. *Antimicrob. Agents Chemother*. **2018**, *62* (5), e02367-17.

327. de Angelis, M.; Casciaro, B.; Genovese, A.; Brancaccio, D.; Marcocci, M.E.; Novellino, E.; Carotenuto, A.; Palamara, A.T.; Mangoni, M.L.; Nencioni, L. Temporin G, an amphibian antimicrobial peptide against influenza and parainfluenza respiratory viruses: insights into biological activity and mechanism of action. *FASEB J*. **2021**, *35* (2), e21358.

328. Wachinger, M.; Kleinschmidt, A.; Winder, D.; von Pechmann, N.; Ludvigsen, A.; Neumann, M.; Holle, R.; Salmons, B.; Erfle, V.; Brack-Werne, R. Antimicrobial peptides melittin and cecropin inhibit replication of human immunodeficiency virus 1 by suppressing viral gene expression. *J. Gen. Virol*. **1998**, *79* (4), 731-740.

329. Loffredo, M.R.; Nencioni, L.; Mangoni, M.L.; Casciaro, B. Antimicrobial peptides for novel antiviral strategies in the current post-COVID-19 pandemic. *J. Pept. Sci*. **2024**, *30* (1), e3534.

330. Nogrado, K.; Adisakwattana, P.; Reamtong, O. Antimicrobial peptides: On future antiprotozoal and anthelminthic applications. *Acta Trop*. **2022**, *235*, 106665.

331. Pretzel, J.; Mohring, F.; Rahlfs, S.; Becker, K. Antiparasitic peptides. *Adv. Biochem. Eng. Biotechnol*. **2013**, *135*, 157-192.

332. Luo, Y.; Song, Y. Mechanism of Antimicrobial Peptides: Antimicrobial, Anti-Inflammatory and Antibiofilm Activities. *Int. J. Mol. Sci*. **2021**, *22* (21), 11401.

333. Schuerholz, T.; Brandenburg, K.; Marx, G. Antimicrobial peptides and their potential application in inflammation and sepsis. *Crit. Care*. **2012**, *16* (2), 207.

334. Qu, B.; Yuan, J.; Liu, X.; Zhang, S.; Ma, X.; Lu, L. Anticancer activities of natural antimicrobial peptides from animals. *Front. Microbiol*. **2024**, *14*, 1321386.

335. Kordi, M.; Borzouyi, Z.; Chitsaz, S.; Asmaei, M.H.; Salami, R.; Tabarzad, M. Antimicrobial peptides with anticancer activity: Today status, trends and their computational design. *Arch. Biochem. Biophys*. **2023**, *733*, 109484.

336. Gaspar, D.; Veiga, A.S.; Castanho, M.A.R.B. From antimicrobial to anticancer peptides. A review. *Front. Microbiol*. **2013**, *4*, 294.

337. Dong, Z.; Zhang, X.; Zhang, Q.; Tangthianchaichana, J.; Guo, M.; Du, S.; Lu, Y. Anticancer Mechanisms and Potential Anticancer Applications of Antimicrobial Peptides and Their Nano Agents. *Int. J. Nanomedicine*. **2024**, *19*, 1017-1039.

338. Soltaninejad, H.; Zare-Zardini, H.; Ordooei, M.; Ghelmani, Y.; Ghadiri-Anari, A.; Mojahedi, S.; Hamidieh, A.A. Antimicrobial Peptides from Amphibian Innate Immune System as Potent Antidiabetic Agents: A Literature Review and Bioinformatics Analysis. *J. Diabetes Res*. **2021**, *2021*, 2894722.

339. Decker, A.P.; Mechesso, A.F.; Wang, G. Expanding the Landscape of Amino Acid-Rich Antimicrobial Peptides: Definition, Deployment in Nature, Implications for Peptide Design and Therapeutic Potential. *Int. J. Mol. Sci*. **2022**, *23* (21), 12874.

340. Mishra, A.K.; Choi, J.; Moon, E.; Baek, K.H. Tryptophan-Rich and Proline-Rich Antimicrobial Peptides. *Molecules* **2018**, *23* (4), 815.

341. Welch, N.G.; Li, W.; Hossain, M.A.; Separovic, F.; O'Brien-Simpson, N.M.; Wade, J.D. (Re)Defining the Proline-Rich Antimicrobial Peptide Family and the Identification of Putative New Members. *Front. Chem*. **2020**, *8*, 607769.

342. Scocchi, M.; Tossi, A.; Gennaro, R. Proline-rich antimicrobial peptides: converging to a non-lytic mechanism of action. *Cell Mol. Life Sci*. **2011**, *68* (13), 2317-2330.

343. Graf, M.; Mardirossian, M.; Nguyen, F.; Seefeldt, A.C.; Guichard, G.; Scocchi, M.; Innis, C.A.; Wilson, D.N. Proline-rich antimicrobial peptides targeting protein synthesis. *Nat. Prod. Rep*. **2017**, *34* (7), 702-711.

344. Krizsan, A.; Volke, D.; Weinert, S.; Sträter, N.; Knappe, D.; Hoffmann, R. Insect-derived proline-rich antimicrobial peptides kill bacteria by inhibiting bacterial protein translation at the 70S ribosome. *Angew. Chem. Int. Ed. Engl*. **2014**, *53* (45), 12236-12239.

345. Gagnon, M.G.; Roy, R.N.; Lomakin, I.B.; Florin, T.; Mankin, A.S.; Steitz, T.A. Structures of proline-rich peptides bound to the ribosome reveal a common mechanism of protein synthesis inhibition. *Nucleic Acids Res*. **2016**, *44* (5), 2439-2450.

346. Chan, D.I.; Prenner, E.J.; Vogel, H.J. Tryptophan- and arginine-rich antimicrobial peptides: structures and mechanisms of action. *Biochim. Biophys. Acta* **2006**, *1758* (9), 1184-1202.

347. Straus, S.K. Tryptophan- and arginine-rich antimicrobial peptides: Anti-infectives with great potential. *Biochim. Biophys. Acta Biomembr*. **2024**, *1866* (3), 184260.

348. Minoux, H.; Chipot, C. Cation-π Interactions in Proteins: Can Simple Models Provide an Accurate Description?. *J. Am. Chem. Soc.* **1999**, *121* (44), 10366-10372.

349. Yau, W.M.; Wimley, W.C.; Gawrisch, K.; White, S.H. The preference of tryptophan for membrane interfaces. *Biochemistry* **1998**, *37* (42), 14713-14718.

350. Petersen, F.N.R.; Jensen, M.Ø.; Nielsen, C.H. Interfacial tryptophan residues: a role for the cation-pi effect? *Biophys. J*. **2005**, *89* (6), 3985-3996.

351. Lawyer, C.; Pai, S.; Watabe, M.; Borgia, P.; Mashimo, T.; Eagleton, L.; Watabe, K. Antimicrobial activity of a 13 amino acid tryptophan-rich peptide derived from a putative porcine precursor protein of a novel family of antibacterial peptides. *FEBS Lett*. **1996**, *390* (1), 95-98.

352. Dong, N.; Wang, C.; Zhang, T.; Zhang, L.; Xue, C.; Feng, X.; Bi, C.; Shan, A. Bioactivity and Bactericidal Mechanism of Histidine-Rich β-Hairpin Peptide Against Gram-Negative Bacteria. *Int. J. Mol. Sci*. **2019**, *20* (16), 3954.

353. Park, C.J.; Park, C.B.; Hong, S.S.; Lee, H.S.; Lee, S.Y.; Kim, S.C. Characterization and cDNA cloning of two glycine- and histidine-rich antimicrobial peptides from the roots of shepherd's purse, Capsella bursa-pastoris. *Plant Mol. Biol*. **2000**, *44* (2), 187-197.

354. Poon, I.K.H.; Patel, K.K.; Davis, D.S.; Parish, C.R.; Hulett, M.D. Histidine-rich glycoprotein: the Swiss Army knife of mammalian plasma. *Blood*. **2011**, *117* (7), 2093-2101.

355. Lai, R.; Takeuchi, H.; Lomas, L.O.; Jonczy, J.; Rigden, D.J.; Rees, H.H.; Turner, P.C. A new type of antimicrobial protein with multiple histidines from the hard tick, Amblyomma hebraeum. *FASEB J.* **2004**, *18* (12), 1447-1449.

356. van Kan, E.J.M.; Demel, R.A.; Breukink, E.; van der Bent, A.; de Kruijff, B. Clavanin permeabilizes target membranes via two distinctly different pH-dependent mechanisms. *Biochemistry* **2002**, *41* (24), 7529-7539.

357. McDonald, M.; Mannion, M.; Pike, D.; Lewis, K.; Flynn, A.; Brannan, A.M.; Browne, M.J.; Jackman, D.; Madera, L.; Coombs, M.R.P.; Hoskin, D.W.; Rise, M.L.; Booth, V. Structure-function relationships in histidine-rich antimicrobial peptides from Atlantic cod. *Biochim. Biophys. Acta* **2015**, *1848* (7), 1451-1461.

358. Lee, I.H.; Cho, Y.; Lehrer, R.I. Effects of pH and salinity on the antimicrobial properties of clavanins. *Infect Immun*. **1997**, *65* (7), 2898-2903.

359. Kacprzyk, L.; Rydengård, V.; Mörgelin, M.; Davoudi, M.; Pasupuleti, M.; Malmsten, M.; Schmidtchen, A. Antimicrobial activity of histidine-rich peptides is dependent on acidic conditions. *Biochim. Biophys. Acta* **2007**, *1768* (11), 2667-2680.

360. Buonocore, F.; Fausto, A.M.; Pelle, G.D.; Roncevic, T.; Gerdol, M.; Picchietti, S. Attacins: A Promising Class of Insect Antimicrobial Peptides. *Antibiotics (Basel)* **2021**, *10* (2), 212.

361. Yi, H.Y.; Deng, X.J.; Yang, W.Y.; Zhou, C.Z.; Cao, Y.; Yu, X.Q. Gloverins of the silkworm Bombyx mori: structural and binding properties and activities. *Insect Biochem Mol. Biol*. **2013**, *43* (7), 612-625.

362. Reichhart, J.M.; Meister, M.; Dimarcq, J.L.; Zachary, D.; Hoffmann, D.; Ruiz, C.; Richards, G.; Hoffmann, J.A. Insect immunity: developmental and inducible activity of the Drosophila diptericin promoter. *EMBO J*. **1992**, *11* (4), 1469-1477.

363. Becking, T.; Delaunay, C.; Cordaux, R.; Berjeaud, J.M.; Braquart-Varnier, C.; Verdon, J. Shedding Light on the Antimicrobial Peptide Arsenal of Terrestrial Isopods: Focus on Armadillidins, a New Crustacean AMP Family. *Genes (Basel)* **2020**, *11* (1), 93.

364. Lorenzini, D.M.; da Silva, P.I. Jr.; Fogaça, A.C.; Bulet, P.; Daffre, S. Acanthoscurrin: a novel glycine-rich antimicrobial peptide constitutively expressed in the hemocytes of the spider Acanthoscurria gomesiana. *Dev. Comp. Immunol*. **2003**, *27* (9), 781-791.

365. Sperstad, S.V.; Haug, T.; Vasskog, T.; Stensvåg, K. Hyastatin, a glycine-rich multi-domain antimicrobial peptide isolated from the spider crab (Hyas araneus) hemocytes. *Mol. Immunol*. **2009**, *46* (13), 2604-2612.

366. de Jesus Oliveira, T.; de Oliveira, U.C.; da Silva Junior, P.I. Serrulin: A Glycine-Rich Bioactive Peptide from the Hemolymph of the Yellow *Tityus serrulatus* Scorpion. *Toxins (Basel)* **2019**, *11* (9), 517.

367. Pirtskhalava, M.; Vishnepolsky, B.; Grigolava, M.; Managadze, G. Physicochemical Features and Peculiarities of Interaction of AMP with the Membrane. *Pharmaceuticals (Basel)* **2021**, *14* (5), 471.

368. Chen, C.H.; Lu, T.K. Development and Challenges of Antimicrobial Peptides for Therapeutic Applications. *Antibiotics (Basel)* **2020**, *9* (1), 24.

369. Han, Y.; Zhang, M.; Lai, R.; Zhang, Z. Chemical modifications to increase the therapeutic potential of antimicrobial peptides. *Peptides* **2021,** *146*, 170666.

370. Yu H.Y.; Tu C.H.; Yip B.S.; Chen H.L.; Cheng H.T.; Huang K.C.; Lo H.J.; Cheng J.W. Easy strategy to increase salt resistance of Antimicrobial Peptides. *Antimcrob. Agents Chemother*. **2011**, *55* (10), 4918-4921.

371. Goldman, M.J.; Anderson, G.M.; Stolzenberg, E.D.; Kari, U.P.; Zasloff, M.; Wilson, J.M. Human beta-defensin-1 is a salt-sensitive antibiotic in lung that is inactivated in cystic fibrosis. *Cell* **1997**, *88* (4), 553-560.

372. Kandasamy, S.K.; Larson, R.G. Effect of salt on the interactions of antimicrobial peptides with zwitterionic lipid bilayers. *Biochim. Biophys. Acta* **2006**, *1758* (9), 1274-1284.

373. Chu, H.L.; Yu, H.Y.; Yip, B.S.; Chih, Y.H.; Liang, C.W.; Cheng, H.T.; Cheng, J.W. Boosting salt resistance of short antimicrobial peptides. *Antimicrob. Agents Chemother*. **2013**, *57* (8), 4050-4052.

374. Bergmann, M.; Ross, W. F. On proteolytic enzymes: X. The enzymes of papain and their activation. *J. Biol. Chem*. **1936**, *114*, 717-726.

375. Starr, C.G.; Wimley, W.C. Antimicrobial peptides are degraded by the cytosolic proteases of human erythrocytes. *Biochim. Biophys. Acta Biomembr*. **2017**, *1859* (12), 2319-2326.

376. Tang, W.H.; Wang, C.F.; Liao, Y.D. Fetal bovine serum albumin inhibits antimicrobial peptide activity and binds drug only in complex with α1-antitrypsin. *Sci. Rep*. **2021**, *11* (1), 1267.

377. Schneider, E.K.; Huang, J.X.; Carbone, V.; Han, M.; Zhu, Y.; Nang, S.; Khoo, K.K.; Mak, J.; Cooper, M.A.; Li, J.; Velkov, T. Plasma Protein Binding Structure-Activity Relationships Related to the N-Terminus of Daptomycin. *ACS Infect Dis*. **2017**, *3* (3), 249-258.

378. Hancock, R.E.W.; Falla, T.; Brown, M. Cationic bactericidal peptides. *Adv. Microb. Physiol*. **1995**, *37*, 135-175.

379. Bacalum, M.; Radu, M. Cationic Antimicrobial Peptides Cytotoxicity on Mammalian Cells: An Analysis Using Therapeutic Index Integrative Concept. *Int. J. Pept. Res. Ther.* **2015,** *21*, 47-55.

380. Nazarian-Firouzabadi, F.; Torres, M.T.; de la Fuente-Nunez, C. Recombinant production of antimicrobial peptides in plants. *Biotechnol. Adv*. **2024**, *71*, 108296.

381. Chen, N.; Jiang, C. Antimicrobial peptides: Structure, mechanism, and modification. *Eur. J. Med. Chem*. **2023**, *255*, 115377.

382. Lai, Z.; Yuan, X.; Chen, H.; Zhu, Y.; Dong, N.; Shan A. Strategies employed in the design of antimicrobial peptides with enhanced proteolytic stability. *Biotechnol. Adv*. **2022**, *59*, 107962.

383. Gan, B.H.; Gaynord, J.; Rowe, S.M.; Deingruber, T.; Spring, D.R. The multifaceted nature of antimicrobial peptides: current synthetic chemistry approaches and future directions. *Chem. Soc. Rev.* **2021**, *50* (13), 7820-7880.

384. Bessalle, R.; Haas, H.; Goria, A.; Shalit, I.; Fridkin, M. Augmentation of the antibacterial activity of magainin by positive-charge chain extension. *Antimicrob. Agents Chemother*. **1992**, *36* (2), 313-317.

385. Dathe, M.; Nikolenko, H.; Meyer, J.; Beyermann, M.; Bienert, M. Optimization of the antimicrobial activity of magainin peptides by modification of charge. *FEBS Lett*. **2001**, *501* (2-3), 146-150.

386. Hallock, K.J.; Lee, D.K.; Ramamoorthy, A. MSI-78, an analogue of the magainin antimicrobial peptides, disrupts lipid bilayer structure via positive curvature strain. *Biophys. J*. **2003**, *84* (5), 3052-3060.

387. Hirano, M.; Saito, C.; Yokoo, H.; Goto, C.; Kawano, R.; Misawa, T.; Demizu, Y. Development of Antimicrobial Stapled Peptides Based on Magainin 2 Sequence. *Molecules* **2021**, *26* (2), 444.

388. Falla, T.J.; Hancock, R.E.W. Improved activity of a synthetic indolicidin analog. *Antimicrob. Agents Chemother.* **1997**, *41* (4), 771-775.

389. Rozek, A.; Powers, J.P.S.; Friedrich, C.L.; Hancock, R.E.W. Structure-based design of an indolicidin peptide analogue with increased protease stability. *Biochemistry* **2003**, *42* (48), 14130-14138.

390. Wu, M.; Hancock, R.E.W. Improved derivatives of bactenecin, a cyclic dodecameric antimicrobial cationic peptide. *Antimicrob. Agents Chemother*. **1999**, *43* (5), 1274-1276.

391. Edwards, I.A.; Elliott, A.G.; Kavanagh, A.M.; Blaskovich, M.A.T.; Cooper, M.A. Structure-Activity and -Toxicity Relationships of the Antimicrobial Peptide Tachyplesin-1. *ACS Infect Dis.* **2017**, *3* (12), 917-926.

392. Rajasekaran, G.; Kim, E.Y.; Shin, S.Y. LL-37-derived membrane-active FK-13 analogs possessing cell selectivity, anti-biofilm activity and synergy with chloramphenicol and anti-inflammatory activity. *Biochim. Biophys. Acta Biomembr*. **2017**, *1859* (5), 722-733.

393. Mishra, B.; Golla, R.M.; Lau, K.; Lushnikova, T.; Wang, G. Anti-Staphylococcal Biofilm Effects of Human Cathelicidin Peptides. *ACS Med. Chem. Lett*. **2015**, *7* (1), 117-121.

394. Narayana, J.L.; Mishra, B.; Lushnikova, T.; Golla, R.M.; Wang, G. Modulation of antimicrobial potency of human cathelicidin peptides against the ESKAPE pathogens and in vivo efficacy in a murine catheter-associated biofilm model. *Biochim. Biophys. Acta Biomembr*. **2019**, *1861* (9), 1592-1602.

395. Chen, Z.; Yang, G.; Lu, S.; Chen, D.; Fan, S.; Xu.; Wu, B.; He, J. Design and antimicrobial activities of LL-37 derivatives inhibiting the formation of Streptococcus mutans biofilm. *Chem. Biol. Drug Des*. **2019**, *93* (6), 1175-1185.

396. Mishra, B.; Felix, L.; Basu, A.; Kollala, S.S.; Chhonker, Y.S.; Ganesan, N.; Murry, D.J.; Mylonakis, E. Design and Evaluation of Short Bovine Lactoferrin-Derived Antimicrobial Peptides against Multidrug-Resistant *Enterococcus faecium*. *Antibiotics* **2022**, *11* (8), 1085.

397. Mandel, S.; Michaeli, J., Nur, N.; Erbetti, I.; Zazoun, J.; Ferrari, L.; Felici, A.; Cohen-Kutner, M.; Bachnoff, N. OMN6 a novel bioengineered peptide for the treatment of multidrug resistant Gram-negative bacteria. *Sci. Rep.* **2021**, *11* (1), 6603.

398. Peng, J.; Mishra, B.; Khader, R.; Felix, L.; Mylonakis, E. Novel Cecropin-4 Derived Peptides against Methicillin-Resistant *Staphylococcus aureus*. *Antibiotics (Basel)* **2021**, *10* (1), 36.

399. Kim, J.; Jacob, B.; Jang, M.; Kwak, C.; Lee, Y.; Son, K.; Lee, S.; Jung, I.D.; Jeong, M.S.; Kwon, S.H.; Kim, Y. Development of a novel short 12-meric papiliocin-derived peptide that is effective against Gram-negative sepsis. *Sci. Rep*. **2019**, *9* (1), 3817.

400. Sharma, P.; Sharma, S.; Joshi, S.; Barman, P.; Bhatt, A.; Maan, M.; Singla, N.; Rishi, P.; Ali, M.E.; Preet, S.; Saini, A. Design, characterization and structure-function analysis of novel antimicrobial peptides based on the N-terminal CATH-2 fragment. *Sci. Rep*. **2022**, *12* (1), 12058.

401. Avitabile, C.; Netti, F.; Orefice, G.; Palmieri, M.; Nocerino, N.; Malgieri, G.; D'Andrea, L.D.; Capparelli, R.; Fattorusso, R.; Romanelli, A. Design, structural and functional characterization of a Temporin-1b analog active against Gram-negative bacteria. *Biochim. Biophys. Acta* **2013**, *1830* (6), 3767-1375.

402. Manzo, G.; Ferguson, P.M.; Gustilo, V.B.; Hind, C.K.; Clifford, M.; Bui, T.T.; Drake, A.F.; Atkinson, R.A.; Sutton, J.M.; Batoni, G.; Lorenz, C.D.; Phoenix, D.A.; Mason, A.J. Minor sequence modifications in temporin B cause drastic changes in antibacterial potency and selectivity by fundamentally altering membrane activity. *Sci Rep*. **2019**, *9* (1),1385.

403. Liao, F.; Ye, Z.; Cheng, J.; Zhu, J.; Chen, X.; Zhou, X.; Wang, T.; Jiang, Y.; Ma, C.; Zhou, M.; Chen, T.; Shaw, C.; Wang, L. Discovery and engineering of a novel peptide, Temporin-WY2, with enhanced in vitro and in vivo efficacy against multi-drug resistant bacteria. *Sci. Rep*. **2024**, *14* (1), 18769.

404. Deslouches, B.; Phadke, S.M.; Lazarevic, V.; Cascio, M.; Islam, K.; Montelaro, R.C.; Mietzner, T.A. De novo generation of cationic antimicrobial peptides: influence of length and tryptophan substitution on antimicrobial activity. *Antimicrob Agents Chemother*. **2005**, *49* (1), 316-322.

405. Javadpour, M.M.; Juban, M.M.; Lo, W.C.J.; Bishop, S.M.; Alberty, J.B.; Cowell, S.M.; Becker, C.L.; McLaughlin, M.L. De novo antimicrobial peptides with low mammalian cell toxicity. *J Med Chem*. **1996**, *39* (16), 3107-3113.

406. Hu, J.; Chen, C.; Zhang, S.; Zhao, X.; Xu, H.; Zhao, X.; Lu, J.R. Designed antimicrobial and antitumor peptides with high selectivity. *Biomacromolecules* **2011**, *12* (11), 3839-3843.

407. Kim, S.J.; Kim, J.S.; Lee, Y.S.; Sim, D.W.; Lee, S.H.; Bahk, Y.Y.; Lee, K.H.; Kim, E.H.; Park, S.J.; Lee, B.J.; Won, H.S. Structural characterization of de novo designed L5K5W model peptide isomers with potent antimicrobial and varied hemolytic activities. *Molecules* **2013**, *18* (1), 859-876.

408. Zhong C.; Zhang, F.; Yao, J.; Zhu, Y.; Zhu, N.; Zhang, J.; Ouyang, X.; Zhang, T.; Li, B.; Xie, J.; Ni, J. New Antimicrobial Peptides with Repeating Unit against Multidrug-Resistant Bacteria. *ACS Infect. Dis*. **2021**, *7* (6), 1619-1637.

409. Huang, T.; Qian, Y.; Fu, X.; Huang, S.; Li, Y.; Zhou, C. De Novo Design of Triblock Amphiphilic Short Antimicrobial Peptides. *ACS Appl. Polym*. *Mater.* **2020**, *2* (9), 3988-3992.

410. Park, C.B.; Yi, K.S.; Matsuzaki, K.; Kim, M.S.; Kim, S.C. Structure-activity analysis of buforin II, a histone H2A-derived antimicrobial peptide: the proline hinge is responsible for the cell-penetrating ability of buforin II. *Proc. Natl. Acad. Sci. USA* **2000**, *97* (15), 8245-8250.

411. Wang, G. Structures of human host defense cathelicidin LL-37 and its smallest antimicrobial peptide KR-12 in lipid micelles. *J. Biol. Chem*. **2008**, *283* (47), 32637-32643.

412. Ramírez-Ledesma, M.G.; Rodríguez, M.C.; Alva-Murillo, N.; Avila, E.E. The antimicrobial peptides LL-37, KR-20, FK-13 and KR-12 inhibit the growth of a sensitive and a metronidazole-resistant strain of *Trichomonas vaginalis*. *Parasitol. Res.* **2022**, *121*, 3503-3512.

413. Li, X.; Li, Y.; Han, H.; Miller, D.W.; Wang, G. Solution structures of human LL-37 fragments and NMR-based identification of a minimal membrane-targeting antimicrobial and anticancer region. *J. Am. Chem. Soc.* **2006**, *128* (17), 5776-5785.

414. Lee, M.K.; Cha, L.N.; Lee, S.H.; Hahm, K.S. Role of amino acid residues within the disulfide loop of thanatin, a potent antibiotic peptide. *J. Biochem. Mol. Biol*. **2002**, *35* (3), 291-296.

415. Qu, X.D.; Harwig, S.S.; Shafer, W.M.; Lehrer, R.I. Protegrin structure and activity against *Neisseria gonorrhoeae*. *Infect. Immun*. **1997**, *65* (2), 636-639.

416. Matsuzaki, K.; Sugishita, K.; Harada, M.; Fujii, N.; Miyajima, K. Interactions of an antimicrobial peptide, magainin 2, with outer and inner membranes of Gram-negative bacteria. *Biochim. Biophys. Acta* **1997**, *1327* (1), 119-130.

417. Nagaoka, I.; Kuwahara-Arai, K.; Tamura, H.; Hiramatsu, K.; Hirata, M. Augmentation of the bactericidal activities of human cathelicidin CAP18/LL-37-derived antimicrobial peptides by amino acid substitutions. *Inflamm. Res*. **2005**, *54* (2), 66-73.

418. Nagpal, S.; Gupta, V.; Kaur, K.J.; Salunke, D.M. Structure-function analysis of tritrypticin, an antibacterial peptide of innate immune origin. *J. Biol. Chem*. **1999**, *274* (33), 23296-23304.

419. Yang, S.T.; Shin, S.Y.; Lee, C.W.; Kim, Y.C.; Hahm, K.S.; Kim, J.I. Selective cytotoxicity following Arg-to-Lys substitution in tritrpticin adopting a unique amphipathic turn structure. *FEBS Lett*. **2003**, *540* (1-3), 229-233.

420. Kang, S.J.; Nam, S.H.; Lee, B.J. Engineering Approaches for the Development of Antimicrobial Peptide-Based Antibiotics. *Antibiotics* **2022**, *11* (10), 1338.

421. Nguyen, L.T.; Chau, J.K.; Perry, N.A.; de Boer, L.; Zaat, S.A.J.; Vogel, H.J. Serum stabilities of short tryptophan- and arginine-rich antimicrobial peptide analogs. *PLoS One* **2010**, *5* (9), e12684.

422. Zanin, L.P.M.; de Araujo, A.S.; Juliano, M.A.; Casella, T.; Nogueira, M.C.L.; Neto J.R. Effects of N-terminus modifications on the conformation and permeation activities of the synthetic peptide L1A. *Amino Acids* **2016**, *48* (6), 1433-1444.

423. Alvares, D.S.; Wilke, N.; Neto, J.R. Effect of N-terminal acetylation on lytic activity and lipid-packing perturbation induced in model membranes by a mastoparan-like peptide. *Biochim. Biophys. Acta Biomembr*. **2018**, *1860* (3), 737-748.

424. Li, D.; Yang, Y.; Li, R.; Huang, L.; Wang, Z.; Deng, Q.; Dong, S. N-terminal acetylation of antimicrobial peptide L163 improves its stability against protease degradation. *J. Pept. Sci*. **2021**, *27* (9), e3337.

425. Sforça, M.L.; Oyama, S.; Canduri, F.; Lorenzi, C.C.B.; Pertinhez, T.A.; Konno, K.; Souza, B.M.; Palma, M.S.; Neto, J.R.; Azevedo, W.F. Jr.; Spisni, A. How C-terminal carboxyamidation alters the biological activity of peptides from the venom of the eumenine solitary wasp. *Biochemistry* **2004**, *43* (19), 5608-5617.

426. Dennison, S.R.; Mura, M.; Harris, F.; Morton, L.H.G.; Zvelindovsky, A.; Phoenix, D.A. The role of C-terminal amidation in the membrane interactions of the anionic antimicrobial peptide, maximin H5. *Biochim. Biophys. Acta Biomembr*. **2015**, *1848* (5), 1111-1118.

427. Mura, M.; Wang, J.; Zhou, Y.; Pinna, M.; Zvelindovsky, A.V.; Dennison, S.R.; Phoenix, D.A. The effect of amidation on the behaviour of antimicrobial peptides. *Eur. Biophys. J.* **2016**, *45* (3), 195-207.

428. Han, H.; Li, T.; Wang, Z.; Teng, D.; Mao, R.; Hao, Y.; Yang, N.; Wang, X.; Wang, J. Improved Stability and Activity of a Marine Peptide-N6NH2 against *Edwardsiella tarda* and Its Preliminary Application in Fish. *Mar. Drugs*. **2020**, *18* (12), 650.

429. Zhu, S.; Li, W.; O'Brien-Simpson, N.; Separovic, F.; Sani, M.A. C-terminus amidation influences biological activity and membrane interaction of maculatin 1.1. *Amino Acids* **2021**, *53* (5), 769-777.

430. Kapil, S.; Sharma, V. D-Amino acids in antimicrobial peptides: a potential approach to treat and combat antimicrobial resistance. *Can. J. Microbiol*. **2021**, *67* (2), 119-137.

431. Du, Y.; Li, L.; Zheng, Y.; Liu, J.; Gong, J.; Qiu, Z.; Li, Y.; Qiao, J.; Huo, Y.X. Incorporation of Non-Canonical Amino Acids into Antimicrobial Peptides: Advances, Challenges, and Perspectives. *Appl. Environ. Microbiol*. **2022**, *88* (23), e0161722.

432. Wang, X.; Yang, X.; Wang, Q.; Meng, D. Unnatural amino acids: promising implications for the development of new antimicrobial peptides. *Crit. Rev. Microbiol*. **2023**, *49* (2), 231-255.

433. Wade, D.; Boman, A.; Wåhlin, B.; Drain, C.M.; Andreu, D.; Boman, H.G.; Merrifield, R.B. All-D amino acid-containing channel-forming antibiotic peptides. *Proc. Natl. Acad. Sci. USA* **1990**, *87* (12), 4761-4765.

434. Hong, S.Y.; Oh, J.E.; Lee, K.H. Effect of D-amino acid substitution on the stability, the secondary structure, and the activity of membrane-active peptide. *Biochem. Pharmacol*. **1999**, *58* (11), 1775-1780.

435. Braunstein, A.; Papo, N.; Shai, Y. In vitro activity and potency of an intravenously injected antimicrobial peptide and its DL amino acid analog in mice infected with bacteria. *Antimicrob. Agents Chemother*. **2004**, *48* (8), 3127-3129.

436. Falciani, C.; Lozzi, L.; Pollini, S.; Luca, V.; Carnicelli, V.; Brunetti, J.; Lelli, B.; Bindi, S.; Scali, S.; Di Giulio, A.; Rossolini, G.M.; Mangoni, M.L.; Bracci, L.; Pini, A. Isomerization of an antimicrobial peptide broadens antimicrobial spectrum to gram-positive bacterial pathogens. *PLoS One* **2012**, *7* (10), e46259.

437. Choi, H.; Hwang, J.S.; Kim, H.; Lee, D.G. Antifungal effect of CopA3 monomer peptide via membrane-active mechanism and stability to proteolysis of enantiomeric D-CopA3. *Biochem. Biophys. Res. Commun*. **2013**, *440* (1), 94-98.

438. Khara, J.S.; Priestman, M.; Uhía, I.; Hamilton, M.S.; Krishnan, N.; Wang, Y.; Yang, Y.Y.; Langford, P.R.; Newton, S.M.; Robertson, B.D.; Ee, P.L.R. Unnatural amino acid analogues of membrane-active helical peptides with anti-mycobacterial activity and improved stability. *J. Antimicrob. Chemother*. **2016**, *71* (8), 2181-2191.

439. Manabe, T.; Kawasaki, K. D-form KLKLLLLLKLK-NH_2 peptide exerts higher antimicrobial properties than its L-form counterpart via an association with bacterial cell wall components. *Sci. Rep.* **2017**, *7*, 43384.

440. Jia, F.; Wang, J.; Peng, J.; Zhao, P.; Kong, Z.; Wang, K.; Yan, W.; Wang, R. D-amino acid substitution enhances the stability of antimicrobial peptide polybia-CP. *Acta Biochim. Biophys. Sin. (Shanghai)* **2017**, *49* (10), 916-925.

441. Li, Y.; Liu, T.; Liu, Y.; Tan, Z.; Ju, Y.; Yang, Y.; Dong, W. Antimicrobial activity, membrane interaction and stability of the D-amino acid substituted analogs of antimicrobial peptide W3R6. *J. Photochem. Photobiol. B.* **2019**, *200*, 111645.

442. Sim, J.Y.; Kim, S.; Lee, J.; Lim, H.; Kim, H.H.; Park, Z.Y.; Kim, J.I. A significantly enhanced antibacterial spectrum of D-enantiomeric lipopeptide bactenecin. *Biochem. Biophys. Res. Commun*. **2019**, *514* (2), 497-502.

443. Oh, J.E.; Lee, K.H. Synthesis of novel unnatural amino acid as a building block and its incorporation into an antimicrobial peptide. *Bioorganic Med. Chem*. **1999**, *7* (12), 2985-2990.

444. Conlon, J.M.; Al-Kharrge, R.; Ahmed, E.; Raza, H.; Galadari, S.; Condamine, E. Effect of aminoisobutyric acid (Aib) substitutions on the antimicrobial and cytolytic activities of the frog skin peptide, temporin-1DRa. *Peptides* **2007**, *28* (10), 2075-2080.

445. Hicks, R.P.; Bhonsle, J.B.; Venugopal, D.; Koser, B.W.; Magill, A.J. De novo design of selective antibiotic peptides by incorporation of unnatural amino acids. *J. Med. Chem*. **2007**, *50* (13), 3026-3036.

446. Knappe, D.; Henklein, P.; Hoffmann, R.; Hilpert, K. Easy strategy to protect antimicrobial peptides from fast degradation in serum. *Antimicrob. Agents Chemother*. **2010**, *54* (9), 4003-4005.

447. Czihal, P.; Knappe, D.; Fritsche, S.; Zahn, M.; Berthold, N.; Piantavigna, S.; Müller, U.; Van Dorpe, S.; Herth, N.; Binas, A.; Köhler, G.; De Spiegeleer, B.; Martin, L.L.; Nolte, O.; Sträter, N.; Alber, G.; Hoffmann, R. Api88 is a novel antibacterial designer peptide to treat systemic infections with multidrug-resistant Gram-negative pathogens. *ACS Chem. Biol*. **2012**, *7* (7), 1281-1291.

448. Berthold, N.; Czihal, P.; Fritsche, S.; Sauer, U.; Schiffer, G.; Knappe, D.; Alber, G.; Hoffmann, R. Novel apidaecin 1b analogs with superior serum stabilities for treatment of infections by gram-negative pathogens. *Antimicrob. Agents Chemother*. **2013**, *57* (1), 402-409.

449. Kang, W.; Liu, H.; Ma, L.; Wang, M.; Wei, S.; Sun, P.; Jiang, M.; Guo, M.; Zhou, C.; Dou, J. Effective antimicrobial activity of a peptide mutant Cbf-14-2 against penicillin-resistant bacteria based on its unnatural amino acids. *Eur. J. Pharm. Sci*. **2017**, *105*, 169-177.

450. Hitchner, M.A.; Necelis, M.R.; Shirley, D.; Caputo, G.A. Effect of Non-natural Hydrophobic Amino Acids on the Efficacy and Properties of the Antimicrobial Peptide C18G. *Probiotics Antimicrob. Proteins* **2021**, *13* (2), 527-541.

451. Rounds, T.; Straus, S.K. Lipidation of Antimicrobial Peptides as a Design Strategy for Future Alternatives to Antibiotics. *Int. J. Mol. Sci*. **2020**, *21* (24), 9692.

452. Rezende, S.B.; Oshiro, K.G.N.; Júnior, N.G.O.; Franco, O.L.; Cardoso, M.H. Advances on chemically modified antimicrobial peptides for generating peptide antibiotics. *Chem. Commun.* **2021**, *57* (88), 11578-11590.

453. Bellavita, R.; Braccia, S.; Galdiero, S.; Falanga, A. Glycosylation and Lipidation Strategies: Approaches for Improving Antimicrobial Peptide Efficacy. *Pharmaceuticals (Basel)* **2023**, *16* (3), 439.

454. Mak, P.; Pohl, J.; Dubin, A.; Reed, M.S.; Bowers, S.E.; Fallon, M.T.; Shafer, W.M. The increased bactericidal activity of a fatty acid-modified synthetic antimicrobial peptide of human cathepsin G correlates with its enhanced capacity to interact with model membranes. *Int. J. Antimicrob. Agents* **2003**, *21* (1), 13-19.

455. Makovitzki, A.; Avrahami, D.; Shai, Y. Ultrashort antibacterial and antifungal lipopeptides. *Proc. Natl. Acad. Sci. USA* **2006**, *103* (43), 15997-6002.

456. Chu-Kung, A.F.; Nguyen, R.; Bozzelli, K.N.; Tirrell, M. Chain length dependence of antimicrobial peptide-fatty acid conjugate activity. *J. Colloid. Interface Sci*. **2010**, *345* (2), 160-167.

457. Lohan, S.; Monga, J.; Cameotra, S.S.; Bisht, G.S. In vitro and in vivo antibacterial evaluation and mechanistic study of ornithine based small cationic lipopeptides against antibiotic resistant clinical isolates. *Eur. J. Med. Chem*. **2014**, *88*, 19-27.

458. Koh, J.J.; Lin, H.; Caroline, V.; Chew, Y.S.; Pang, L.M.; Aung, T.T.; Li, J.; Lakshminarayanan, R.; Tan, D.T.; Verma, C.; Tan, A.L.; Beuerman, R.W.; Liu, S. N-Lipidated Peptide Dimers: Effective Antibacterial Agents against Gram-Negative Pathogens through Lipopolysaccharide Permeabilization. *J. Med. Chem*. **2015**, *58* (16), 6533-6548.

459. Wenzel, M.; Schriek, P.; Prochnow, P.; Albada, H.B.; Metzler-Nolte, N.; Bandow, J.E. Influence of lipidation on the mode of action of a small RW-rich antimicrobial peptide. *Biochim. Biophys. Acta* **2016**, *1858* (5), 1004-1011.

460. de Gier, M.G.; Albada, H.B.; Josten, M.; Willems, R.; Leavis, H.; van Mansveld, R.; Paganelli, F.L.; Dekker, B.; Lammers, J.W.J.; Sahl, H.G.; Metzler-Nolte, M. Synergistic Activity of a Short Lipidated Antimicrobial Peptide (LipoAMP) and Colistin or Tobramycin against Pseudomonas aeruginosa from Cystic Fibrosis Patients. *Med. Chem. Commun*. **2016**, *7* (1), 148-156.

461. Húmpola, M.V.; Rey, M.C.; Carballeira, N.M.; Simonetta, A.C.; Tonarelli, G.G. Biological and structural effects of the conjugation of an antimicrobial decapeptide with saturated, unsaturated, methoxylated and branched fatty acids. *J. Pept. Sci*. **2017**, *23* (1), 45-55.

462. Mishra, B.; Lushnikova, T.; Wang, G. Small lipopeptides possess anti-biofilm capability comparable to daptomycin and vancomycin. *RSC Adv*. **2015**, *5* (73), 59758-59769.

463. Varnava, K.G.; Mohid, S.A.; Calligari, P.; Stella, L.; Reynison, J.; Bhunia, A.; Sarojini, V. Design, Synthesis, Antibacterial Potential, and Structural Characterization of N-Acylated Derivatives of the Human Autophagy 16 Polypeptide. *Bioconjug. Chem*. **2019**, *30* (7), 1998-2010.

464. Juhaniewicz-Dębińska, J.; Lasek, R.; Tymecka, D.; Burdach, K.; Bartosik, D.; Sęk, S. Physicochemical and Biological Characterization of Novel Membrane-Active Cationic Lipopeptides with Antimicrobial Properties. *Langmuir* **2020**, *36* (43), 12900-12910.

465. Kamysz, E.; Sikorska, E.; Jaśkiewicz, M.; Bauer, M.; Neubauer, D.; Bartoszewska, S.; Barańska-Rybak, W.; Kamysz, W. Lipidated Analogs of the LL-37-Derived Peptide Fragment KR12-Structural Analysis, Surface-Active Properties and Antimicrobial Activity. *Int. J. Mol. Sci.* **2020**, *21* (3), 887.

466. Zou, P.; Liu, J.; Li, X.; Yaseen, M.; Yao, J.; Liu, L.; Luo, L.; Wang, H.; Shi, X.; Li, Z.; Sun, T.; Gao, Y.; Gao, C.; Li, L. L. A Membrane Curvature Modulated Lipopeptide to Broadly Combat Multidrug-Resistant Bacterial Pneumonia with Low Resistance Risk. *ACS Nano* **2022**, *16* (12), 20545- 20558.

467. Lai, Z.; Chen, H.; Yuan, X.; Tian, J.; Dong, N.; Feng, X.; Shan, A. Designing double-site lipidated peptide amphiphiles as potent antimicrobial biomaterials to combat multidrug-resistant bacteria. *Front. Microbiol*. **2022**, *13*, 1074359.

468. He, T.; Qu, R.; Zhang, J. Current synthetic chemistry towards cyclic antimicrobial peptides. *Pept. Sci.* **2022**, *28* (6), e3387.

469. Lai, S.; Zhang, Q.; Jin, L. Natural and Man-Made Cyclic Peptide-Based Antibiotics. *Antibiotics (Basel)* **2023**, *12* (1), 42.

470. Fernandez-Lopez, S.; Kim, H.S.; Choi, E.C.; Delgado, M.; Granja, J.R.; Khasanov, A.; Kraehenbuehl, K.; Long, G.; Weinberger, D.A.; Wilcoxen, K.M.; Ghadiri, M.R. Antibacterial agents based on the cyclic D,L-alpha-peptide architecture. *Nature* **2001**, *412* (6845), 452-455.

471. Dathe, M.; Nikolenko, H.; Klose, J.; Bienert, M. Cyclization increases the antimicrobial activity and selectivity of arginine- and tryptophan-containing hexapeptides. *Biochemistry* **2004**, *43* (28), 9140-9150.

472. Motiei, L.; Rahimipour, S.; Thayer, D.A.; Wong, C.H.; Ghadiri, M.R. Antibacterial cyclic D,L-alpha-glycopeptides. *Chem. Commun.* **2009**, (25), 3693-3695.

473. Laurencin, M.; Amor, M.; Fleury, Y.; Baudy-Floc'h, M. De novo cyclic pseudopeptides containing aza-β3-amino acids exhibiting antimicrobial activities. *J. Med. Chem*. **2012**, *55* (24), 10885-10895.

474. Li, Y.; Smith, C.; Wu, H.; Padhee, S.; Manoj, N.; Cardiello, J.; Qiao, Q.; Cao, C.; Yin, H.; Cai, J. Lipidated cyclic γ-AApeptides display both antimicrobial and anti-inflammatory activity. *ACS Chem. Biol*. **2014**, *9* (1), 211-217.

475. Oh, D.; Sun, J.; Shirazi, A.N.; LaPlante, K.L.; Rowley, D.C.; Parang, K. Antibacterial activities of amphiphilic cyclic cell-penetrating peptides against multidrug-resistant pathogens. *Mol. Pharm*. **2014**, *11* (10), 3528-3536.

476. Di Bonaventura, I.; Jin, X.; Visini, R.; Probst, D.; Javor, S.; Gan, B.H.; Michaud, G.; Natalello, A.; Doglia, S.M.; Köhler, T.; van Delden, C.; Stocker, A.; Darbre, T.; Reymond, J.L. Chemical space guided discovery of antimicrobial bridged bicyclic peptides against *Pseudomonas aeruginosa* and its biofilms. *Chem. Sci*. **2017**, *8* (10), 6784-6798.

477. He, R.; Di Bonaventura, I.; Visini, R.; Gan, B.H.; Fu, Y.; Probst, D.; Lüscher, A.; Köhler, T.; van Delden, C.; Stocker, A.; Hong, W.; Darbre, T.; Reymond, J.L. Design, crystal structure and

atomic force microscopy study of thioether ligated d,l-cyclic antimicrobial peptides against multidrug resistant *Pseudomonas aeruginosa*. *Chem. Sci*. **2017**, *8* (11), 7464-7475.

478. Mwangi, J.; Yin, Y.; Wang, G.; Yang, M.; Li, Y.; Zhang, Z.; Lai, R. The antimicrobial peptide ZY4 combats multidrug-resistant *Pseudomonas aeruginosa* and *Acinetobacter baumannii* infection. *Proc. Natl. Acad. Sci. USA* **2019**, *116* (52), 26516-26522.

479. Dong, N.; Wang, C.; Li, X.; Guo, Y.; Li, X. Simplified Head-to-Tail Cyclic Polypeptides as Biomaterial-Associated Antimicrobials with Endotoxin Neutralizing and Anti-Inflammatory Capabilities. *Int. J. Mol. Sci*. **2019**, *20* (23), 5904.

480. Etayash, H.; Pletzer, D.; Kumar, P.; Straus, S.K.; Hancock, R.E.W. Cyclic Derivative of Host-Defense Peptide IDR-1018 Improves Proteolytic Stability, Suppresses Inflammation, and Enhances In Vivo Activity. *J. Med. Chem*. **2020**, *63* (17), 9228-9236.

481. Zhu, J.; Hu, C.; Zeng, Z.; Deng, X.; Zeng, L.; Xie, S.; Fang, Y.; Jin, Y.; Alezra, V.; Wan, Y. Polymyxin B-inspired non-hemolytic tyrocidine A analogues with significantly enhanced activity against gram-negative bacteria: How cationicity impacts cell specificity and antibacterial mechanism. *Eur. J. Med. Chem*. **2021**, *221*, 113488.

482. Shai, Y. Mode of action of membrane active antimicrobial peptides. *Biopolymers* **2002**, *66* (4), 236-248.

483. Ulm, H.; Wilmes, M.; Shai, Y.; Sahl, H.G. Antimicrobial host defensins - specific antibiotic activities and innate defense modulation. *Front. Immunol.* **2012**, *3*, 249.

484. Li, S.; Wang, Y.; Xue, Z.; Jia, Y.; Li, R.; He, C.; Chen, H. The structure-mechanism relationship and mode of actions of antimicrobial peptides: A review. *Trends Food Sci. Technol.* **2021**, *109*, 103-115.

485. Silhavy, T.J.; Kahne, D.; Walker, S. The bacterial cell envelope. *Cold Spring Harb. Perspect Biol.* **2010**, *2* (5), a000414.

486. Garcia-Rubio, R.; de Oliveira, H.C.; Rivera, J.; Trevijano-Contador, N. The Fungal Cell Wall: *Candida*, *Cryptococcus*, and *Aspergillus* Species. *Front. Microbiol*. **2020**, *10*, 2993.

487. Cockcroft, S. Mammalian lipids: structure, synthesis and function. *Essays Biochem*. **2021**, *65* (5), 813-845.

488. Bogdanov, M.; Pyrshev, K.; Yesylevskyy, S.; Ryabichko, S.; Boiko, V.; Ivanchenko, P.; Kiyamova, R.; Guan, Z.; Ramseyer, C.; Dowhan, W. Phospholipid distribution in the cytoplasmic membrane of Gram-negative bacteria is highly asymmetric, dynamic, and cell shape-dependent. *Sci. Adv*. **2020**, *6* (23), eaaz6333.

489. Beveridge, T.J. Structures of gram-negative cell walls and their derived membrane vesicles. *J. Bacteriol*. **1999**, *181* (16), 4725-4733.

490. Schwechheimer, C.; Kuehn, M.J. Outer-membrane vesicles from Gram-negative bacteria: biogenesis and functions. *Nat. Rev. Microbiol*. **2015**, *13* (10), 605-619.

491. Rajagopal, M.; Walker, S. Envelope Structures of Gram-Positive Bacteria. *Curr. Top Microbiol. Immunol*. **2017**, *404*, 1-44.

492. Gow, N.A.R. Latge, J.; Munro, C.A. The Fungal Cell Wall: Structure, Biosynthesis, and Function. *Microbiol. Spectr*. **2017**, *5* (3), 10.1128/microbiolspec.funk-0035-2016.

493. Virtanen, J.A.; Cheng, K.H.; Somerharju, P. Phospholipid composition of the mammalian red cell membrane can be rationalized by a superlattice model. *Proc. Natl. Acad. Sci. USA*. **1998**, *95* (9), 4964-4969.

494. Luchini, A.; Vitiello, G. Mimicking the Mammalian Plasma Membrane: An Overview of Lipid Membrane Models for Biophysical Studies. *Biomimetics* **2021**, *6* (1), 3.

495. Matsumoto, K.; Kusaka, J.; Nishibori, A.; Hara, H. Lipid domains in bacterial membranes. *Mol. Microbiol*. **2006**, *61* (5), 1110-1117.

496. Oliver, P.M.; Crooks, J.A.; Leidl, M.; Yoon, E.J.; Saghatelian, A. Weibel, D.B. Localization of Anionic Phospholipids in Escherichia coli Cells. *J. Bacteriol*. **2014**, 1*96* (19), 3386-3398.

497. Lüderitz, O.; Freudenberg, M. A.; Galanos, C.; Lehmann, V.; Rietschel, E. T.; Shaw, D. H. Lipopolysaccharides of Gram-Negative Bacteria. In *Current Topics in Membranes and Transport*; Elsevier, **1982**, *17*, pp 79-151.

498. Di Lorenzo, F.; Duda, K.A.; Lanzetta, R.; Silipo, A.; De Castro, C.; Molinaro, A. A Journey from Structure to Function of Bacterial Lipopolysaccharides. *Chem. Rev*. **2022**, *122* (20), 15767-15821.

499. Malanovic, N.; Lohner, K. Gram-positive bacterial cell envelopes: The impact on the activity of antimicrobial peptides. *Biochim. Biophys. Acta* **2016**, *1858* (5), 936-946.

500. van der Veen, J.N.; Kennelly, J.P.; Wan, S.; Vance, J.E.; Vance, D.E.; Jacobs, R.L. The critical role of phosphatidylcholine and phosphatidylethanolamine metabolism in health and disease. *Biochim. Biophys. Acta Biomembr*. **2017**, *1859* (9), 1558-1572.

501. Körner, C.; Fröhlich, F. Compartmentation and functions of sphingolipids. *Curr. Opin. Cell Biol*. **2022**, *74*, 104-111.

502. Ebrahimi, H.; Siavoshi, F.; Jazayeri, M.H.; Sarrafnejad, A.; Saniee, P.; Mobini, M. Physicochemical properties of intact fungal cell wall determine vesicles release and nanoparticles internalization. *Heliyon* **2023**, *9* (3), e13834.

503. Masuoka, J. Surface glycans of Candida albicans and other pathogenic fungi: physiological roles, clinical uses, and experimental challenges. *Clin. Microbiol. Rev*. **2004**, *17* (2), 281-310.

504. Pandidan, S.; Mechler, A. Latest developments on the mechanism of action of membrane disrupting peptides. *Biophys. Rep*. **2021**, *7* (3), 173-184.

505. Wimley, W.C. Describing the mechanism of antimicrobial peptide action with the interfacial activity model. *ACS Chem. Biol*. **2010**, *5* (10), 905-917.

506. Dho, M.; Candian, V.; Tedeschi, R. Insect Antimicrobial Peptides: Advancements, Enhancements and New Challenges. *Antibiotics* **2023**, *12* (6), 952.

507. Baumann, G.; Mueller, P. A molecular model of membrane excitability. *J. Supramol. Struct*. **1974**, *2* (5-6), 538-557.

508. Boheim, G. Statistical analysis of alamethicin channels in black lipid membranes. *J. Membr. Biol.* **1974**, *19* (3), 277-303.

509. Laver, D.R. The barrel-stave model as applied to alamethicin and its analogs reevaluated. *Biophys. J.* **1994**, *66* (2), 355-359.

510. Ludtke, S.J.; He, K.; Heller, W.T.; Harroun, T.A.; Yang, L.; Huang, H.W. Membrane pores induced by magainin. *Biochemistry* **1996**, *35* (43), 13723-13728.

511. Cheng, J.T.J.; Hale, J.D.; Elliot, M.; Hancock, R.E.W.; Straus, S.K. Effect of membrane composition on antimicrobial peptides aurein 2.2 and 2.3 from Australian southern bell frogs. *Biophys. J.* **2009**, *96* (2), 552-565.

512. Yang, L.; Harroun, T.A.; Weiss, T.M.; Ding, L.; Huang, H.W. Barrel-stave model or toroidal model? A case study on melittin pores. *Biophys. J*. **2001**, *81* (3), 1475-1485.

513. Pouny, Y.; Rapaport, D.; Mor, A.; Nicolas, P.; Shai, Y. Interaction of antimicrobial dermaseptin and its fluorescently labeled analogues with phospholipid membranes. *Biochemistry* **1992**, *31* (49), 12416-12423.

514. Mani, R.; Buffy, J.J.; Waring, A.J.; Lehrer, R.I.; Hong, M. Solid-state NMR investigation of the selective disruption of lipid membranes by protegrin-1. *Biochemistry*. **2004**, *43* (43), 13839-13848.

515. Fernandez, D.I.; Le Brun, A.P.; Whitwell, T.C.; Sani, M.A.; James, M.; Separovic, F. The antimicrobial peptide aurein 1.2 disrupts model membranes via the carpet mechanism. *Phys. Chem. Chem. Phys*. **2012**, *14* (45), 15739-15751.

516. Ostolaza, H.; Bartolomé, B.; de Zárate, I.O.; de la Cruz, F.; Goñi, F.M. Release of lipid vesicle contents by the bacterial protein toxin alpha-haemolysin. *Biochim. Biophys. Acta* **1993**, *1147* (1), 81-88.

517. Cardoso, M.H.; Meneguetti, B.T.; Costa, B.O.; Buccini, D.F.; Oshiro, K.G.N.; Preza, S.L.E.; Carvalho, C.M.E.; Migliolo, L.; Franco, O.L. Non-Lytic Antibacterial Peptides That Translocate Through Bacterial Membranes to Act on Intracellular Targets. Int. *J. Mol. Sci*. **2019**, *20* (19), 4877.

518. Iancu, C.; Grainger, A.; Field, D.; Cotter, P.D.; Hill, C.; Ross, R.P. Comparison of the Potency of the Lipid II Targeting Antimicrobials Nisin, Lacticin 3147 and Vancomycin Against Gram-Positive Bacteria. *Probiotics Antimicrob. Proteins* **2012**, *4* (2), 108-115.

519. Loll, P.J.; Axelsen, P.H. The structural biology of molecular recognition by vancomycin. *Annu. Rev. Biophys. Biomol. Struct*. **2000**, *29*, 265-289.

520. Breukink, E.; de Kruijff, B. Lipid II as a target for antibiotics. *Nat. Rev. Drug Discov*. **2006**, *5* (4), 321-332.

521. de Leeuw, E.; Li, C.; Zeng, P.; Li, C.; Diepeveen-de Buin, M.; Lu, W.Y.; Breukink, E.; Lu, W. Functional interaction of human neutrophil peptide-1 with the cell wall precursor lipid II. *FEBS Lett*. **2010**, *584* (8), 1543-1548.

522. Mardirossian, M.; Grzela, R.; Giglione, C.; Meinnel, T.; Gennaro, R.; Mergaert, P.; Scocchi, M. The host antimicrobial peptide Bac71-35 binds to bacterial ribosomal proteins and inhibits protein synthesis. *Chem. Biol*. **2014**, *21* (12), 1639-1647.

523. Roy, R.N.; Lomakin, I.B.; Gagnon, M.G.; Steitz, T.A. The mechanism of inhibition of protein synthesis by the proline-rich peptide oncocin. *Nat. Struct. Mol. Biol*. **2015**, *22* (6), 466-469.

524. Florin, T.; Maracci, C.; Graf, M.; Karki, P.; Klepacki, D.; Berninghausen, O.; Beckmann, R.; Vázquez-Laslop, N.; Wilson, D.N.; Rodnina, M.V.; Mankin, A.S. An antimicrobial peptide that inhibits translation by trapping release factors on the ribosome. *Nat. Struct. Mol. Biol*. **2017**, *24* (9), 752-757.

525. Yonezawa, A.; Kuwahara, J.; Fujii, N.; Sugiura, Y. Binding of tachyplesin I to DNA revealed by footprinting analysis: significant contribution of secondary structure to DNA binding and implication for biological action. *Biochemistry* **1992**, *31* (11), 2998-3004.

526. Kang, H.K.; Seo, C.H.; Luchian, T.; Park, Y. Pse-T2, an Antimicrobial Peptide with High-Level, Broad-Spectrum Antimicrobial Potency and Skin Biocompatibility against Multidrug-Resistant Pseudomonas aeruginosa Infection. *Antimicrob. Agents Chemother*. **2018**, *62* (12), e01493-18.

527. Li, L.; Sun, J.; Xia, S.; Tian, X.; Cheserek, M.J.; Le, G. Mechanism of antifungal activity of antimicrobial peptide APP, a cell-penetrating peptide derivative, against Candida albicans: intracellular DNA binding and cell cycle arrest. *Appl. Microbiol. Biotechnol*. **2016**, *100* (7), 3245-3253.

528. Helmerhorst, E.J.; Troxler, R.F.; Oppenheim, F.G. The human salivary peptide histatin 5 exerts its antifungal activity through the formation of reactive oxygen species. *Proc. Natl. Acad. Sci USA* **2001**, *98* (25), 14637-14642.

529. Kragol, G.; Lovas, S.; Varadi, G.; Condie, B.A.; Hoffmann, R.; Otvos, L. Jr. The antibacterial peptide pyrrhocoricin inhibits the ATPase actions of DnaK and prevents chaperone-assisted protein folding. *Biochemistry* **2001**, *40* (10), 3016-3026.

530. Braffman,N.R.; Piscotta, F.J.; Hauver, J.; Campbell, E.A.; Link, A.J.; Darst, S.A. Structural mechanism of transcription inhibition by lasso peptides microcin J25 and capistruin. *Proc. Natl. Acad. Sci. USA* **2019**, *116* (4), 1273-1278.

531. Yang, H.; Fu, J.; Zhao, Y.; Shi, H.; Hu, H.; Wang, H. Escherichia coli PagP Enzyme-Based De Novo Design and In Vitro Activity of Antibacterial Peptide LL-37. *Med. Sci. Monit*. **2017**, *23*, 2558-2564.

532. Shu, G.; Chen, Y.; Liu, T.; Ren, S.; Kong, Y. Antimicrobial Peptide Cathelicidin-BF Inhibits Platelet Aggregation by Blocking Protease-Activated Receptor 4. *Int. J. Pept. Res. Ther*. **2019**, *25*, 349-358.

533. Lai, Y.; Gallo, R.L. AMPed up immunity: how antimicrobial peptides have multiple roles in immune defense. *Trends Immunol*. **2009**, *30* (3), 131-141.

534. Saha, S.; Barik, D.; Biswas, D. AMPs as Host-Directed Immunomodulatory Agents against Skin Infections Caused by Opportunistic Bacterial Pathogens. *Antibiotics (Basel)* **2024**, *13* (5), 439.

535. Yang, D.; Chen, Q.; Schmidt, A.P.; Anderson, G.M.; Wang, J.M.; Wooters, J.; Oppenheim, J.J.; Chertov, O. LL-37, the neutrophil granule- and epithelial cell-derived cathelicidin, utilizes formyl peptide receptor-like 1 (FPRL1) as a receptor to chemoattract human peripheral blood neutrophils, monocytes, and T cells. *J. Exp. Med*. **2000**, *192* (7), 1069-1074.

536. Soruri, A.; Grigat, J.; Forssmann, U.; Riggert, J.; Zwirner, J. beta-Defensins chemoattract macrophages and mast cells but not lymphocytes and dendritic cells: CCR6 is not involved. *Eur. J. Immunol.* **2007**, *37* (9), 2474-2486.

537. Yang, D.; Chen, Q.; Chertov, O.; Oppenheim, J.J. Human neutrophil defensins selectively chemoattract naive T and immature dendritic cells. *J. Leukoc. Biol*. **2000**, *68* (1), 9-14.

538. Valdivia-Silva, J.; Medina-Tamayo, J.; Garcia-Zepeda, E.A. Chemokine-Derived Peptides: Novel Antimicrobial and Antineoplasic Agents. *Int. J Mol. Sci*. **2015**, *16* (6), 12958-12985.

539. Mookherjee, N.; Brown, K.L.; Bowdish, D.M.E.; Doria, S.; Falsafi, R.; Hokamp, K.; Roche, F.M.; Mu, R.; Doho, G.H.; Pistolic, J.; Powers, J.P.; Bryan, J.; Brinkman, F.S.L.; Hancock, R.E.W. Modulation of the TLR-mediated inflammatory response by the endogenous human host defense peptide LL-37. *J. Immunol*. **2006**, *176* (4), 2455-2464.

540. Yang, D.; Biragyn, A.; Hoover, D.M.; Lubkowski, J.; Oppenheim, J.J. Multiple roles of antimicrobial defensins, cathelicidins, and eosinophil-derived neurotoxin in host defense. *Annu. Rev. Immunol*. **2004**, *22*, 181-215.

541. Nemeth, E.; Rivera, S.; Gabayan, V.; Keller, C.; Taudorf, S.; Pedersen, B.K.; Ganz, T. IL-6 mediates hypoferremia of inflammation by inducing the synthesis of the iron regulatory hormone hepcidin. *J. Clin. Invest*. **2004**, *113* (9), 1271-1276.

542. Greber, K.E.; Dawgul, M. Antimicrobial Peptides Under Clinical Trials. *Curr. Top. Med. Chem*. **2017**, *17* (5), 620-628.

543. Cresti, L.; Cappello, G.; Pini, A. Antimicrobial Peptides towards Clinical Application-A Long History to Be Concluded. *Int. J. Mol. Sci*. **2024**, *25* (9), 4870.

544. Burkhart, B.M.; Gassman, R.M.; Langs, D.A.; Pangborn, W.A.; Duax, W.L.; Pletnev, V. Gramicidin D conformation, dynamics and membrane ion transport. *Biopolymers*. **1999**, *51* (2), 129-144.

545. Hallett, J.W.; Wolkowicz, M.I.; Leopold, I.H. Ophthalmic use of neosporin. *Am. J. Ophthalmol*. **1956**, *41*, 850-853.

546. Nation, R.L.; Li, J. Colistin in the 21st century. *Curr. Opin. Infect. Dis*. **2009**, *22* (6), 535-543.

547. Bergen, P.J.; Li, J.; Rayner, C.R.; Nation, R.L. Colistin methanesulfonate is an inactive prodrug of colistin against Pseudomonas aeruginosa. *Antimicrob. Agents Chemother*. **2006**, *50* (6), 1953-1958.

548. Owen, R.J.; Li, J.; Nation, R.L.; Spelman, D. In vitro pharmacodynamics of colistin against Acinetobacter baumannii clinical isolates. *J. Antimicrob. Chemother*. **2007**, *59* (3), 473-477.

549. Poudyal, A.; Howden, B.P.; Bell, J.M.; Gao, W.; Owen, R.J.; Turnidge, J.D.; Nation, R.L.; Li, J. In vitro pharmacodynamics of colistin against multidrug-resistant Klebsiella pneumoniae. *J. Antimicrob. Chemother.* **2008**, *62* (6), 1311-1318.

550. Gonzalez-Ruiz, A.; Gargalianos-Kakolyris, P.; Timerman, A.; Sarma, J.; Ramallo, V.J.G.; Bouylout, K.; Trostmann, U.; Pathan, R.; Hamed, K. Daptomycin in the Clinical Setting: 8-Year Experience with Gram-positive Bacterial Infections from the EU-CORE(SM) Registry. *Adv. Ther*. **2015**, *32* (6), 496-509.

551. Sauermann, R.; Rothenburger, M.; Graninger, W.; Joukhadar, C. Daptomycin: a review 4 years after first approval. *Pharmacology* **2008**, *81* (2), 79-91.

552. Wilhelm, M.P. Vancomycin. *Mayo Clin. Proc*. **1991**, *66* (11), 1165-1170.

553. Levine, D.P. Vancomycin: A History. *Clin. Infect. Dis*. **2006**, *42* (1), S5-S12.

554. Geraci, J.E.; Wilson, R.E. Vancomycin Therapy for Infective Endocarditis. *Rev. Infect. Dis*. **1981**, *3* (2), S250-S258.

555. Chiu, C.Y.; Sarwal, A.; Feinstein, A.; Hennessey, K. Effective Dosage of Oral Vancomycin in Treatment for Initial Episode of *Clostridioides difficile* Infection: A Systematic Review and Meta-Analysis. *Antibiotics (Basel)* **2019**, *8* (4), 173.

556. Watanakunakorn, C. Mode of action and in-vitro activity of vancomycin. *J. Antimicrob. Chemother.* **1984**, *14* (D), 7-18.

557. Reynolds, P.E. Structure, biochemistry and mechanism of action of glycopeptide antibiotics. *Eur. J. Clin. Microbiol. Infect. Dis*. **1989**, *8* (11), 943-950.

558. Crandon, J.; Nicolau, D. P. Oritavancin: A Potential Weapon in the Battle Against Serious Gram-Positive Pathogens. *Future Microbiology* **2008**, *3* (3), 251-263.

559. Brade, K.D.; Rybak, J.M.; Rybak, M.J. Oritavancin: A New Lipoglycopeptide Antibiotic in the Treatment of Gram-Positive Infections. *Infect. Dis. Ther.* **2016**, *5* (1), 1-15.

560. Domenech, O.; Francius, G.; Tulkens, P. M.; Van Bambeke, F.; Dufrene, Y.; Mingeot-Leclercq, M. P. Interactions of oritavancin, a new lipoglycopeptide derived from vancomyicn, with phospholipid bilayers: effect on membrane permeability and nanoscale lipid membrane organization. *Biochim. Biophys. Acta* **2009**, *1788* (9), 1832-1840.

561. Zhanel, G.G.; Schweizer, F.; Karlowsky, J.A. Oritavancin: Mechanism of Action. *Clin. Infect. Dis*. **2012**, *54* (3), S214-S219.

562. Belley, A.; McKay, G.A.; Arhin, F.F.; Sarmiento, I.; Beaulieu, S.; Fadhil, I.; Parr, T.R. Jr, Moeck, G. Oritavancin disrupts membrane integrity of Staphylococcus aureus and vancomycin-resistant enterococci to effect rapid bacterial killing. *Antimicrob. Agents Chemother*. **2010**, *54* (12), 5369-5371.

563. Chen, A.Y.; Zervos, M.J.; Vazquez, J.A. Dalbavancin: a novel antimicrobial. *Int. J. Clin. Pract*. **2007**, *61* (5), 853-863.

564. Smith, J.R.; Roberts, K.D.; Rybak, M.J. Dalbavancin: A Novel Lipoglycopeptide Antibiotic with Extended Activity Against Gram-Positive Infections. *Infect. Dis. Ther.* **2015**, *4* (3), 245-258.

565. Molina, K.C.; Miller, M.A.; Mueller, S.W.; Van Matre, E.T.; Krsak, M.; Kiser, T.H. Clinical Pharmacokinetics and Pharmacodynamics of Dalbavancin. *Clin. Pharmacokinet*. **2022**, *61* (3), 363-374.

566. Rappo, U.; Puttagunta, S.; Shevchenko, V.; Shevchenko, A.; Jandourek, A.; Gonzalez, P.L.; Suen, A.; Casullo, V.M., Melnick, D.; Miceli, R.; Kovacevic, M.; De Bock, G.; Dunne, M.W.

Dalbavancin for the Treatment of Osteomyelitis in Adult Patients: A Randomized Clinical Trial of Efficacy and Safety. *Open Forum Infect. Dis*. **2019**, *6* (1), ofy331.

567. Dunne, M.W.; Puttagunta, S.; Sprenger, C.R.; Rubino, C.; Van Wart, S.V.; Baldassarre, J. Extended-duration dosing and distribution of dalbavancin into bone and articular tissue. *Antimicrob. Agents Chemother*. **2015**, *59* (4), 1849-1855.

568. Plotkin, P.; Patel, K.; Uminski, A.; Marzella, N. Telavancin (vibativ), a new option for the treatment of gram-positive infections. *P. T*. **2011**, *36* (3), 127-138.

569. Damodaran, S.E.; Madhan, S. Telavancin: A novel lipoglycopeptide antibiotic. *J. Pharmacol. Pharmacother.* **2011**, *2* (2), 135-137.

570. Wenzler, E.; Rodvold, K.A. Telavancin: the long and winding road from discovery to food and drug administration approvals and future directions. *Clin. Infect. Dis*. **2015**, *61* (2), S38-S47.

571. Koo, H.B.; Seo, J. Antimicrobial peptides under clinical investigation. *Pep. Sci.* **2019**, *111* (5), e24122.

572. Magana, M.; Pushpanathan, M.; Santos, A.L.; Leanse, L.; Fernandez, M.; Ioannidis, A.; Giulianotti, M.A.; Apidianakis, Y.; Bradfute, S.; Ferguson, A.L.; Cherkasov, A.; Seleem, M.N.; Pinilla, C.; de la Fuente-Nunez, C.; Lazaridis, T.; Dai, T.; Houghten, R.A.; Hancock, R.E.W.; Tegos, G.P. The value of antimicrobial peptides in the age of resistance. *Lancet Infect. Dis*. **2020**, *20* (9), e216-e230.

Chapter 2: Mechanism of Protease Resistance of D-Amino Acid Residue Containing Cationic Antimicrobial Heptapeptides

NH_3^+-L (K/R) WL (K/R) (K/R) L-$CONH_2$

P4/P5 : All L Peptides

P4C/P5C : All D Peptides

- ✓ Antimicrobial
- ✓ Non-cytotoxic
- ✓ Non-haemolytic

- **Complete Serum/Protease resistance for D peptides**

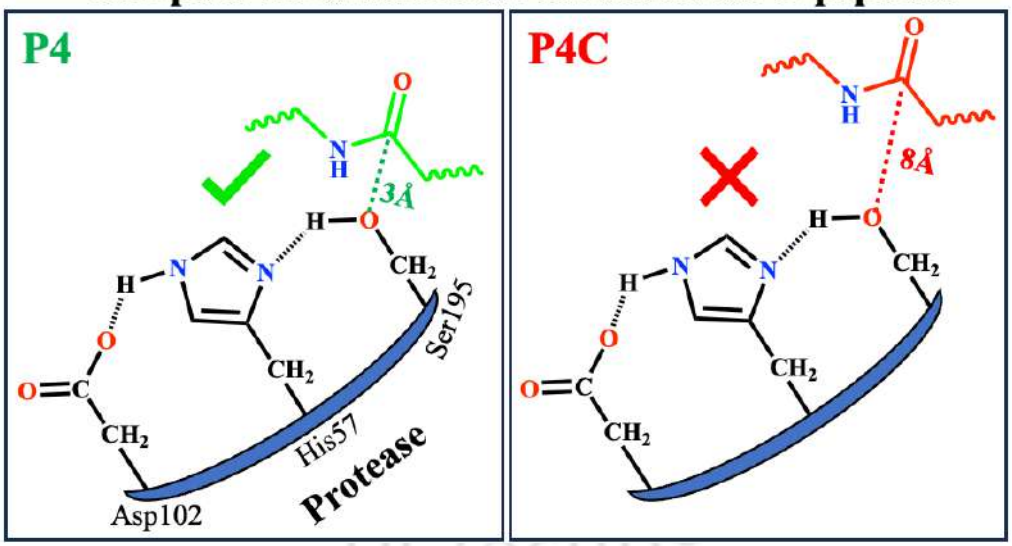

2.1. Introduction

Antimicrobial peptides as a class of molecules although have a huge potential for therapeutic usages, but there are certain limitations associated with them restrict their ample clinical applications.[1] Proteolytic susceptibility of naturally occurring peptides or L-amino acid containing peptides is one such drawback.[2] Proteases or proteolytic enzymes are biocatalysts, basically made of large protein molecules, and are capable of protein/polypeptide degradation.[3] Proteases are specific in their action, and the substrates should fit into their active sites for efficient catalysis to take place.[4] Changes brought in the stereochemistry or structure of the substrate is accompanied with a failure in its recognition by the proteases rendering them inactive. Proteolytic enzymes present proteases that are present in the blood or the gut, are capable of targeting natural AMPs composed of L-amino acid residues, resulting in their short half-lives. To circumvent this problem, different kinds of strategies have been reported in the literature like the incorporation of a single or multiple D-amino acid residue(s)[5-7] or unnatural amino acid residue(s)[6-9] in the sequence of natural AMPs. While such mutations led to protease resistance, in many instances, they were accompanied by a decrease in activity or an increase in the cytotoxicity/ hemolytic ability of the analogues.[6,10-14] In many instances incorporation of D-amino acids in the sequences of the peptides were accompanied with increased antimicrobial activity, reduced cytotoxicity in addition their enhanced proteolytic stability.[15-23] In a study by Ye et al., complete D-amino acid substitution of a peptide L-GL13K (GKIIKLKASLKLL-NH_2) except at the N-terminal to DGL13K (Gkiiklkaslkll-NH_2), led to a faster initiation of self-assembly accompanied by enhanced antimicrobial activity.[24] Fatty acids conjugated to the side chains of D-amino acids resulted in peptides with excellent antimicrobial activity, anti-inflammatory activity, and endotoxin neutralization ability.[25] Substitution of L-Val by D-Val in the peptide WLBU2 resulted in an improved protease resistance, enhanced activity against biofilm growth, reduced toxicity to the white blood cells and erythrocytes, improved safety in mice, and significant improvement of therapeutic index.[26]

Although the knowledge of imparting protease resistance to peptides by using the D-amino acid residues is common and widely used, the mechanism of acquiring stability against proteases is vaguely understood. There are very few studies,[27-29] to the best of our knowledge, which actually demonstrate the mechanism of enhanced stability development in atomic details and with thermodynamic understanding. In the present study, we have developed a library of short cationic

peptides (P4A-C and P5A-C) containing few or all-D-amino acid residues from two moderately active AMPs P4 and P5 earlier developed by our research group,[30] with an intention of developing protease-resistant AMPs. We have studied the antimicrobial potency and the mechanism of action of these AMPs using various biological assays and biophysical/ spectroscopic experiments. We have performed in-depth MD simulations and unravelled the atomic details that impart protease stability to the D-amino acid containing peptides.

2.2. Results

2.2.1. Design and synthesis of peptides

P4 and P5, earlier reported by our group, exhibited broad-spectrum antimicrobial properties against several ESKAPE pathogens and pathogenic fungal strains.[30] These peptides were non-cytotoxic, non-hemolytic, and membranolytic in their mode of action. However, as these peptides were composed of all natural amino acid residues, they were proteolytically susceptible. Here, in this work, we wanted to develop protease resistance in these peptides and probe the plausible reason for the resistance development in detail. For this, we modified peptides P4 and P5 by substituting: (A) all cationic L-amino acid residues (lysine or arginine), (B) all hydrophobic L-amino acid residues (leucine and tryptophan), and (C) all constituent L-amino acid residues with D-amino acid residues (Figure 2.1 and Table 2.1). P4A, P4B, P5A, and P5B peptides had mixed chirality, while peptides P4C and P5C were homochiral with all-D-amino acid residues (Figure 2.1). All designed peptides were synthesized and purified as mentioned in the experimental section and thereafter characterized using analytical HPLC (Figures A1-A6, Appendix A), ESI-MS (Figures A7-A12, Appendix A), and ^{1}H NMR (Figures A13-A18, Appendix A). All peptides used in this study were >95% pure by HPLC analysis.

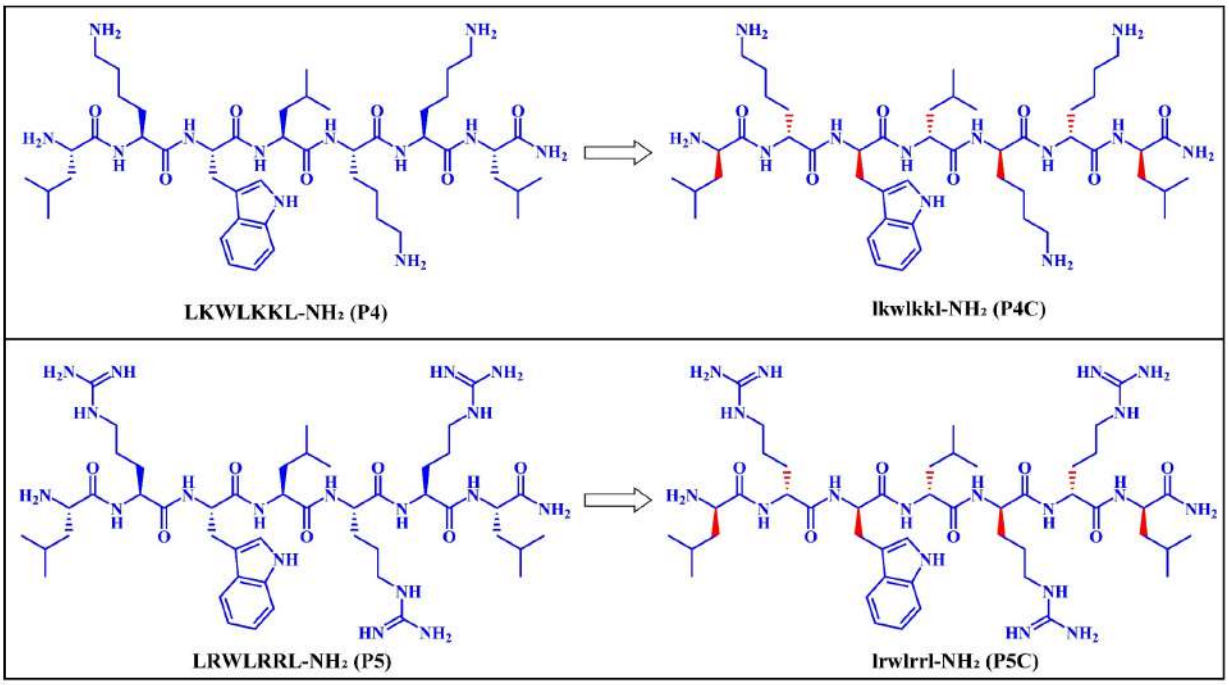

Figure 2.1. Schematic diagram of P4 / P4C (upper panel) and P5 /P5C (lower panel). Capital/ small alphabets denote L-/D- amino acid residues.

Table 2.1. Physicochemical properties of P4, P4A-C P5, P5A-C. Capital/small alphabets denote the L-/D-amino acid residues respectively.

Peptide	Sequence	No. of res.	Charge	Calculated mass $[M+H]^+$ (Da)	Observed mass (Da)	Retention time (min)
P4 (Control)	LKWLKKL-NH_2	7	+4	927.6502	$[M+H]^+$-927.6855	8.75
P4A	LkWLkkL-NH_2	7	+4	927.6502	$[M+H]^+$-927.6832; $[M+2H]^{2+}$-464.3464; $[M+3H]^{3+}$-309.8997.	8.78
P4B	lKwlKKl-NH_2	7	+4	927.6502	$[M+H]^+$-927.6832; $[M+2H]^{2+}$- 464.3221; $[M+3H]^{3+}$- 309.8829	8.80
P4C	lkwlkkl-NH_2	7	+4	927.6502	$[M+H]^+$-927.6855; $[M+2H]^{2+}$- 464.3483; $[M+3H]^{3+}$- 309.9014	9.16
P5 (Control)	LRWLRRL-NH_2	7	+4	1011.6687	$[M+H]^+$- 1012.6678	9.00
P5A	LrWLrrL-NH_2	7	+4	1011.6687	$[M+2H]^{2+}$- 506.8559; $[M+3H]^{3+}$- 338.2400	8.86
P5B	lRwlRRl-NH_2	7	+4	1011.6687	$[M+2H]^{2+}$- 506.3615; $[M+3H]^{3+}$- 337.9113	9.13

P5C	lrwlrrl-NH_2	7	+4	1011.6687	$[M+2H]^{2+}$- 506.3613; $[M+3H]^{3+}$- 337.9109	9.43

** Retention time refers to the time required for a particular peptide to travel through a chromatography column and reach the detector after being injected into the system. HPLC traces of these peptides were acquired using an increasing gradient of acetonitrile (10-100%) over a period of 20 minutes.

2.2.2. Antimicrobial potency of the peptides

Determination of Minimum Inhibitory Concentration (MIC)

The minimum inhibitory concentration ($MIC_{90\%}$) values of the peptides were determined against several strains of ESKAPE pathogens, namely, *Pseudomonas aeruginosa* and *Klebsiella pneumoniae* (Gram-negative), *Staphylococcus aureus* and Methicillin-resistant *Staphylococcus aureus* (Gram-positive), and fungus *Candida albicans* (Table 2.2 and Figures A19-A21, Appendix A). Peptide analogues with mixed chirality (P4A-B and P5A-B) lost their activity against most of the tested microbial strains, with P4 analogues being affected to a greater extent than the P5 analogues. Interestingly, the all-D analogues P4C and P5C, not only retained their activity, but rather showed an overall improved activity against both Gram-positive and Gram-negative bacterial strains. The activity of the all-D-peptides increased considerably in the case of *C. albicans* (Table 2.2). Following the similar trend as in the L-peptides, P5C containing the Arg residue was more active than P4C containing the Lys residue. This might be attributed to the guanidino group present in the side chain of Arg in comparison to the primary amino group present in the side chain of Lys.[31]

Table 2.2. $MIC_{90\%}$ of P4, P4A, P4B, P4C, P5, P5A, P5B and P5C against *P. aeruginosa*, *K. pneumonia, S. aureus, MRSA* and *C. albicans*. Improved MICs of the all-D-peptides against the bacterial and fungal strains are highlighted in bold.

Peptides	**$MIC_{90\%}$ (μM)**				
	Gram-negative		Gram-positive		Fungus
Bacterial strains	*P. aeruginosa*	*K. pneumoniae*	*S. aureus*	Methicillin-resistant *S. aureus*	*C. albicans*
P4	30	50	80	200	30
P4A	200	200	>200	200	50

P4B	>200	>200	>200	>200	80
P4C	**20**	**40**	**60**	**80**	**10**
P5	20	40	40	40	10
P5A	40	50	200	40	20
P5B	40	100	200	30	20
P5C	20	**30**	**30**	**20**	**5**

Determination of MIC in the presence of salts

As one of the other weaknesses of AMPs lies in the salt sensitivity of their antimicrobial activity, we determined the MIC of the most active all-D-peptides (P4C and P5C) in the presence of phosphate-buffered saline (PBS, pH 7.4, 10 mM strength) against Gram-negative *P. aeruginosa* and *K. pneumoniae*, Gram-positive *S. aureus*, MRSA, and fungus *C. albicans* (Figure A22, Appendix A). It was found that P4C was not salt-tolerant against all of the tested strains and completely lost their activity. However, P5C was partially salt-tolerant against *P. aeruginosa*, *S. aureus* and *C. albicans* in the presence of PBS (MIC ~ 50 μM), while they completely lost their activity against *K. pneumonia* in the presence of PBS (Table 2.3).

Table 2.3. $MIC_{90\%}$ of the peptides P4C and P5C against *K. pneumoniae*, *S. aureus, Methicillin-resistant S. aureus and C. albicans* in PBS. The $MIC_{90\%}$ values of the peptides in the absence of salts have also been presented for the comparison purpose.

Peptides / Bacterial strains	**$MIC_{90\%}$ (μM)**				
	P. aeruginosa	*K. pneumoniae*	*S. aureus*	*Methicillin-resistant S. aureus*	*C. albicans*
P4C (in PBS)	>200	>200	>200	>200	100
P4C (in the absence of salts)	20	40	60	80	10
P4C (in PBS)	50	>200	50	100	50
P5C (in the absence of salts)	20	30	30	20	5

We further studied the antimicrobial activity of P4C and P5C against *P. aeruginosa* in the presence of physiological concentrations of various metal salts like 1.25 mM Ca^{2+}, 1 Mm Mg^{2+}, 150 mM Na^{+}, 4 μM Fe^{3+}, and 8 μM Zn^{2+} (Figure A23, Appendix A & Table 3). It was found that P4C

retained its activity almost completely in the presence of Fe^{3+} and Zn^{2+} ions. The activity of P4C varied in the order $Ca^{2+} < Mg^{2+} < Na^{+}$. P5C, on the other hand, could completely retain its activity in the presence of Ca^{2+}, Fe^{3+}, and Zn^{2+} ions and lost its activity only moderately in the presence of Mg^{2+} and Na^{+} ions. Overall, P5C had a better salt tolerance than P4C against a larger number of microbes and a greater variety of metal ions.

Table 2.4. $MIC_{90\%}$ of P4C and P5C against *P. aeruginosa* in the presence of 1.25 mM Ca^{2+}, 1 mM Mg^{2+}, 150 mM Na^{+}, 4 µM Fe^{3+} and 8 µM Zn^{2+}.

Peptides	**$MIC_{90\%}$ (µM)**					
	In absence of salts	Ca^{2+}	Mg^{2+}	Na^{+}	Fe^{3+}	Zn^{2+}
P4C	20	60	100	200	30	30
P5C	20	20	60	100	20	20

Time-kill kinetics

With the intention of determining the time required for complete bactericidal action of the peptides, a time-kill kinetics assay was performed at their respective MICs for P4C, P5C, and their parent peptides P4 and P5 against *P. aeruginosa*, *K. pneumoniae*, and *S. aureus* (Figure 2.2). P5 was seen to have a faster killing kinetics compared to P4 against *K. pneumoniae* and *S. aureus* and similar killing kinetics against *P. aeruginosa*. In similar lines, in the all-D-amino acid containing peptides, P5C had a faster killing kinetics compared to P4C against *P. aeruginosa* and *S. aureus* and similar killing kinetics against *K. pneumoniae*. In all of the strains tested, all-D-analogues had a faster killing kinetics than the corresponding all-L-analogues. For example, against *P. aeruginosa*, P4C showed almost complete inhibition at 45 min in comparison to P4 at 60 min, while P5C showed almost complete inhibition at 30 min in comparison to P5 at 60 min. Similar trends were also followed against *K. pneumoniae* and *S. aureus* (Figure 2.2).

Thus, summarizing all antimicrobial assays, the all-D-peptides P4C/P5C were slightly more potent and faster killing than their L counterparts P4/P5, with P5C distinctly superior over P4C. P5C also had better salt resistance of its antimicrobial activity than P4C.

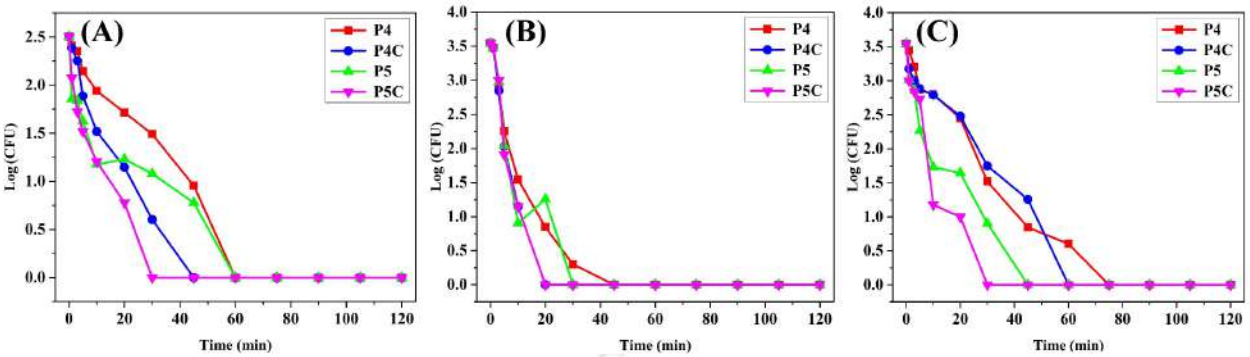

Figure 2.2. Bactericidal activity (log CFU) of the peptides P4, P4C, P5, and P5C against (A) *P. aeruginosa*, (B) *K. pneumoniae*, and (C) *S. aureus* plotted as a function of time.

2.2.3. Activity towards mammalian Cells

Cytotoxicity assay

For being applied as antimicrobial therapeutics, non-cytotoxicity toward mammalian cells is an important virtue of the AMPs. Thus, we tested the effect of all-D-peptides P4C/P5C along with their respective L counterparts P4/P5 on a healthy mammalian cell line human dermal fibroblasts (HDFs) using the MTT assay. To check if the AMPs had an anticancer property, the MTT assay was also performed against a cancer cell line HeLa. None of the four peptides displayed cytotoxicity against either cell lines in the range of their bactericidal concentrations (Figure 2.3).

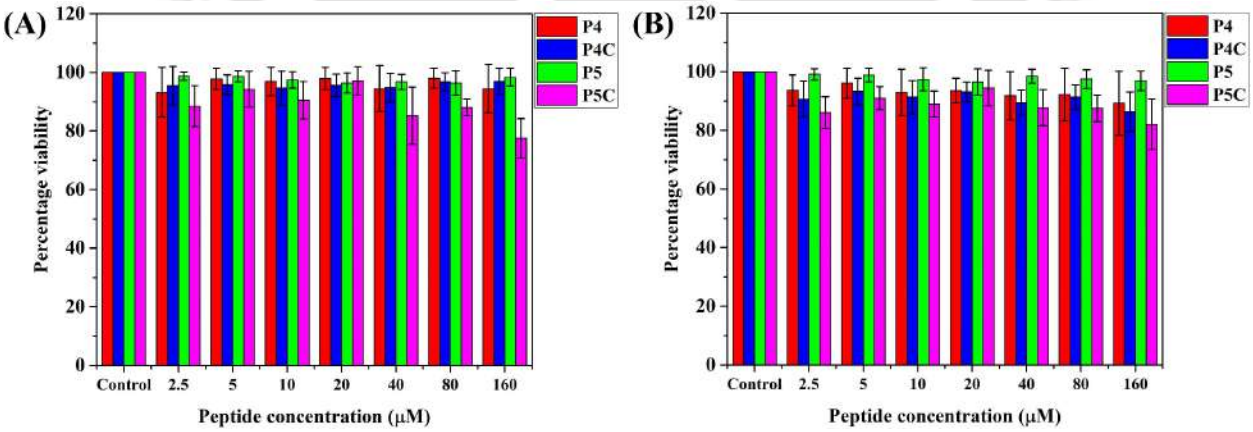

Figure 2.3. MTT assay of P4, P4C, P5, and P5C against (A) HDF and (B) HeLa cells. The percentage viability of the cells was determined upon incubating them with increasing concentrations of peptides and subsequently performing the MTT assay. All experiments were performed in triplicates.

Hemolytic activity

The extent of hemolysis induced by the all-D-peptides P4C/P5C and their all-L counterparts P4/P5 was determined. Human red blood cells (RBCs) of concentration 1% were used for the assay. It was found that both P4C/P5C and their respective L analogues P4/P5 were almost non-hemolytic (<5%) to human RBCs at their bactericidal concentrations (Figure 2.4).

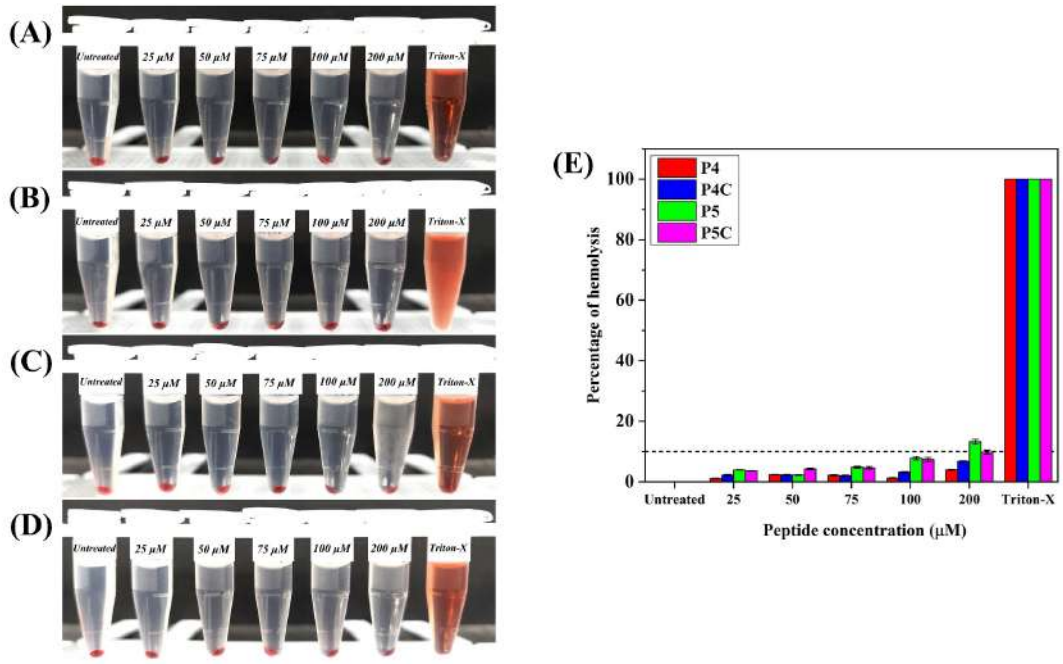

Figure 2.4. Microcentrifuge tubes containing 1 percent human RBCs centrifuged post incubation for 1 h with the peptides (A) P4, (B) P4C, (C) P5 and (D) P5C of increasing concentrations. Untreated cells were maintained as the negative control, while cells treated with 1% Triton-X 100 was the positive control for the experiment. (E) Bar diagrams depicting the percentage of hemolysis induced by the peptides treated with increasing concentrations of the peptides relative that of the untreated cells and cells treated with 1% Triton-X 100.

2.2.4. Protease stability of AMPs

Chemical integrity in the presence of enzymes

Protease degradability is one of the biggest bottlenecks in the commercial success of AMPs. To test the protease resistance of P4C, P5C, and their L counterparts, they were subjected to treatment with proteases. Protease trypsin specifically cleaves the peptide at the C-terminus of cationic

residues lysine or arginine, chymotrypsin cleaves at the C-terminus of aromatic residues phenylalanine, tyrosine, or tryptophan, while proteinase-K cleaves the peptide bonds adjacent to the carboxylic group of aliphatic, hydrophobic, and aromatic amino acid residues with blocked amino groups. All four peptides were incubated with an equimolar mixture of chymotrypsin, trypsin, and proteinase-K. The peptide-enzyme mixtures were incubated for different time intervals, viz., 30 min and 6 h. The reaction mixtures were analysed using analytical HPLC and MALDI-MS.

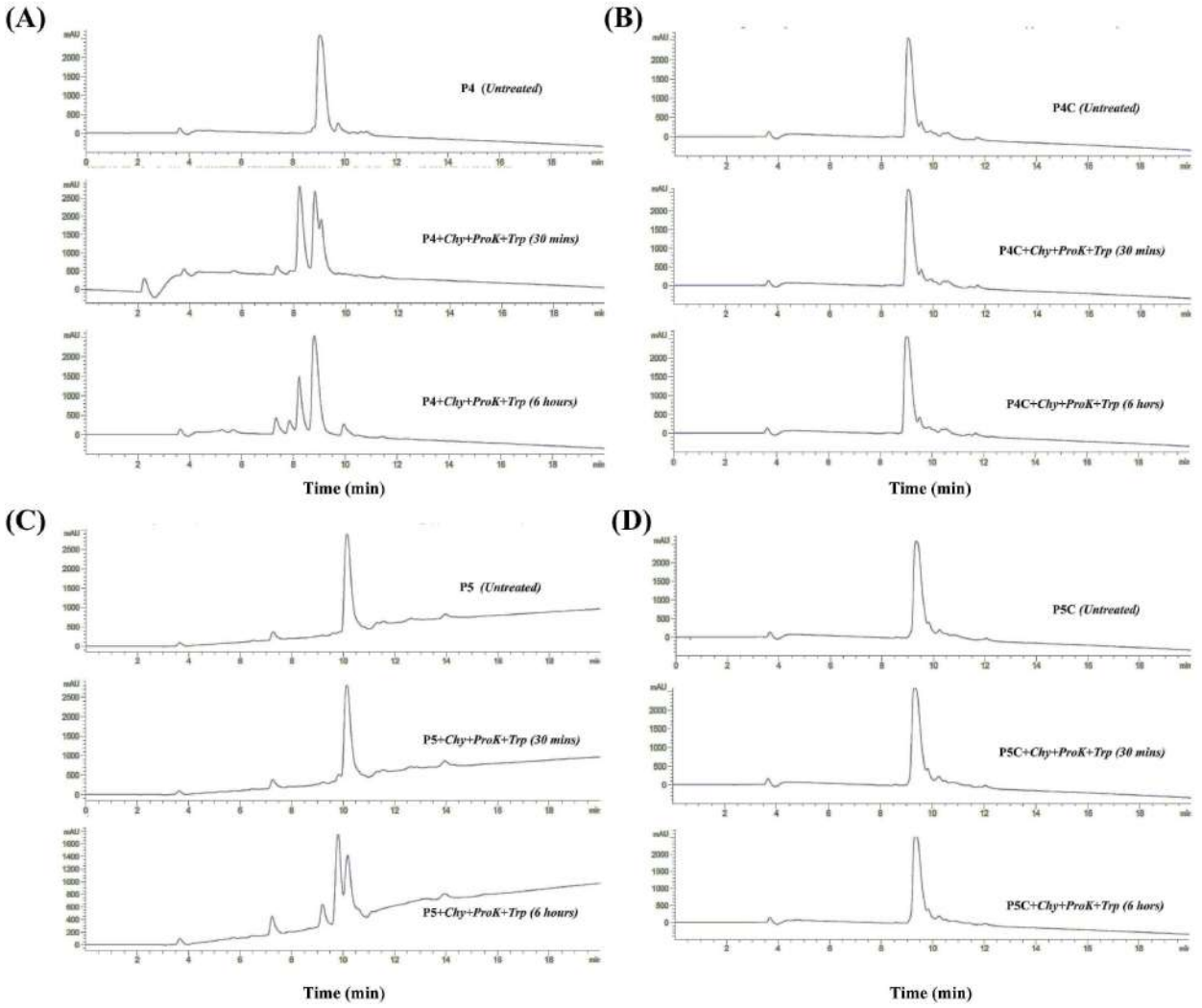

Figure 2.5. Analytical HPLC traces of (A) P4, (B) P4C, (C) P5 and (D) P5C acquired at 214 nm in their untreated form (topmost panels) and after being incubated with an equimolar mixture of chymotrypsin, proteinase K, and trypsin for a period of 30 min (middle panels) and 6 h (bottom panels).

Figure 2.5 shows the analytical HPLC chromatograms of P4/P4C and P5/P5C incubated with the enzyme mixtures quenched after different incubation periods. While the all-L-amino acid containing peptides P4 and P5 degraded significantly, the all-D-amino acid containing analogues P4C and P5C were completely resistant to the enzyme cocktail studied till 6 h. MALDI analysis of the reaction mixture of P4, P4C, P5, and P5C treated with the enzyme cocktail for 30 min and 6 h (Figures A24-A35, Appendix A) proved the presence of various degraded peptide fragments for P4 at both the time points and P5 at the later time point but none in the case of P4C and P5C even up to 6 h. Thus, unlike their L counterparts, the chemical integrity of the all-D-peptides P4C and P5C was retained in the presence of the enzyme cocktail. In other words, the all-D-peptides were stable against protease degradation.

Antimicrobial activity of P5C in the presence of enzymes

Peptides P5 and P5C incubated with equimolar cocktails of the enzyme trypsin, chymotrypsin, and proteinase K for 6 h were quenched and tested for their antimicrobial activity against *P. aeruginosa* (Figure 2.6). While P5 completely lost its activity and showed $MIC_{90\%}$ at 200 μM, $MIC_{90\%}$ of P5C increased marginally to 30 μM ($MIC_{90\%}$ of untreated P5C against *P. aeruginosa*: 20 μM). This clearly established that not only did P5C retain its chemical integrity upon being incubated with enzyme cocktail but also retained most of its antimicrobial potency in contrast to the all-L-peptide P5.

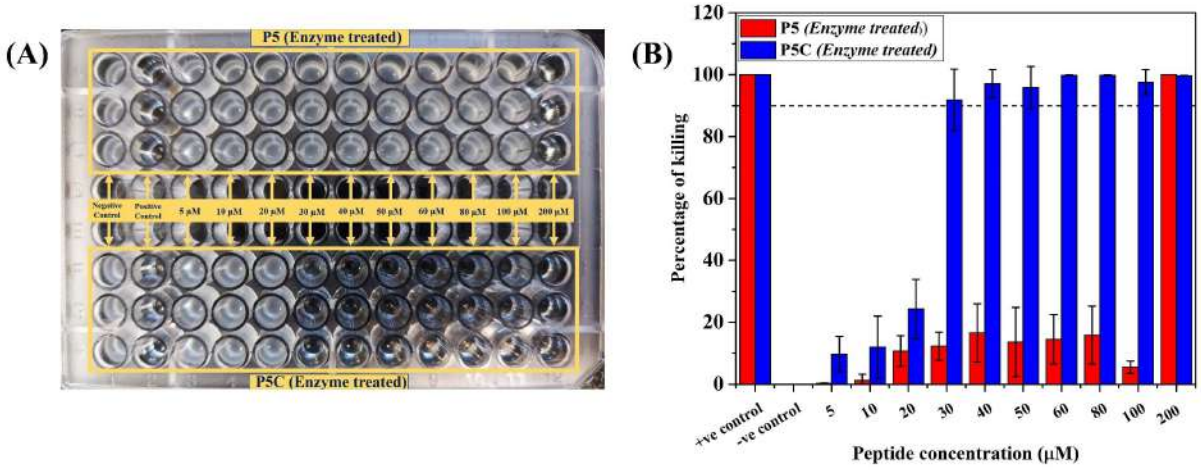

Figure 2.6. (A) Microtiter plate showing the growth of *P. aeruginosa* treated with increasing concentrations of peptides P5 and P5C (preincubated with a mixture of enzymes containing trypsin, chymotrypsin and proteinase-K for a period of 6 h) and the corresponding (B) Bar

diagrams showing the percentage killing of the bacterial cells corresponding to different concentrations of the respective peptides.

Serum stability determination

As the AMPs would have to encounter the human serum upon intravenous administration, we checked the serum stability of both the all-L and D-peptides P4, P5, P4C, and P5C. The peptides were incubated with serum for different time intervals, viz., 30 min, 1, 3, 6, and 24 h. Thereafter, the samples were analysed by analytical HPLC (Figures A36-A39, Appendix A) and MALDI spectroscopy (Figure A40-A43, Appendix A). While the chemical integrity of the all-D-peptides P4C and P5C remained 100% intact even after 24 h of incubation with the serum, the all-L peptides P4 and P5 started degrading just after 30 min of their incubation. After 24 h of serum incubation, more than 60% of P4 and almost 100% of P5 were degraded [Figure 2.7(A)]. The potency of the peptides (P4, P4C, P5, and P5C) against *P. aeruginosa* in the presence of 50% serum was estimated [Figure 2.7(B)]. $MIC_{90\%}$ of P4C and P5C was 20 μM (same as in the absence of serum, $MIC_{90\%}$ = 20 μM, see Table 2.2).

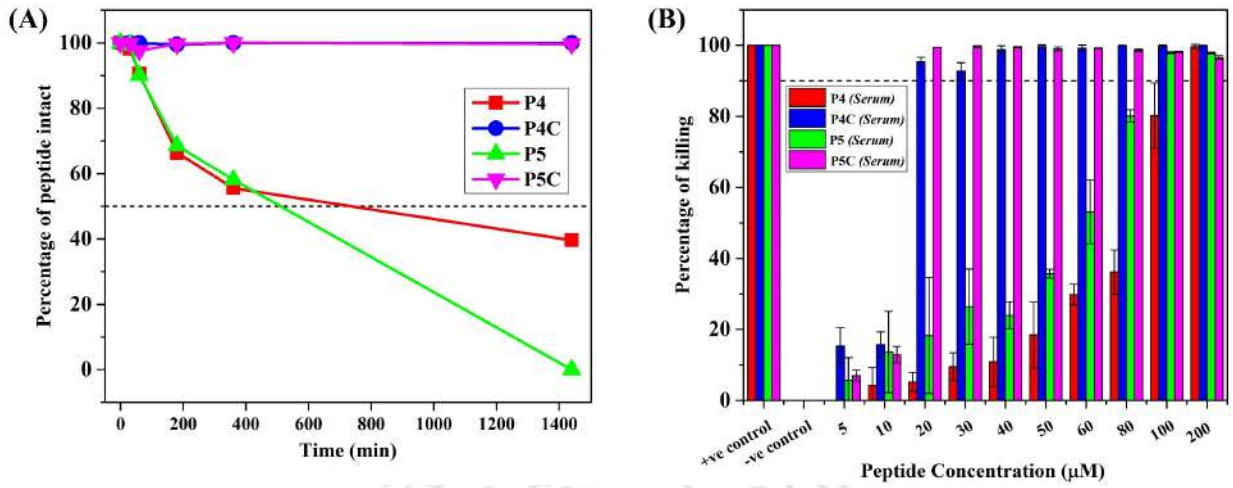

Figure 2.7. (A) Percentage of peptides P4, P4C, P5 and P5C remaining intact after being incubated with serum collected from human blood for various time interval points. (B) Potency of the peptides against *P. aeruginosa* in the presence of serum. $MIC_{90\%}$ was calculated from the microbroth dilution assay. The control experiment was performed in the presence of 10 μM Polymyxin B, and other readings were normalized against it.

Thus, the potency of the D-peptides against *P. aeruginosa* was found to be independent of the serum. However, $MIC_{90\%}$ was increased for P4 and P5 to 200 μM and 100 μM, respectively, in the

presence of serum. In the absence of serum, the $MIC_{90\%}$ for P4 and P5 was 30 μM and 20 μM, respectively (Table 2.2). The loss of activity of the L-peptides in the presence of serum corroborated with the results obtained from HPLC analysis (Figures A36-A39, Appendix A) and was attributed to peptide degradation. Thus, from the studies on the protease stability of the peptides, it can be concluded that the all-D-peptides were completely protease-resistant and serum-stable in contrast to their L counterparts, thus improving their therapeutic prospect.

2.2.5. Interaction of AMPs with the membranes/membrane mimics

Most cationic peptides are reported to be membrane active in their mode of action.[32-38] This involves the initial membrane association of the peptide, followed by the permeation, destabilization, depolarization, and eventual disruption of the membrane. As our designed peptides are cationic in nature, we have investigated their membrane association ability and other related effects on the membrane destabilization using several spectroscopic, biophysical, and microscopic tools.

Membrane permeability assays

NPN (1-*N*-phenylnaphthylamine) dye usually shows enhanced fluorescence upon binding to membrane lipids. NPN cannot bind to membrane lipids of the living bacterial cells due to the impermeability of the outer barrier of the bacterial cells. Once the bacterial cells are ruptured, NPN molecules can easily penetrate through the outer membrane and can bind the membrane lipids showing an enhancement in the fluorescence intensity. Thus, an enhancement of fluorescence intensity of NPN is proportional to the extent of outer membrane permeability. 70 and 89% enhancement in the fluorescence intensity of NPN was observed upon incubation of 0.5× and 1× MICs of P4C [Figure 2.8(A)], while 76 and 97% enhancement was observed upon incubation of 0.5× and 1× MICs of P5C [Figure 2.8(B)] with the *P. aeruginosa* cells. This indicated that the outer membrane permeability of P5C was greater than that of P4C. Propidium iodide (PI) generates high fluorescence signal upon intercalating with the DNA bases. As PI is impermeable through a healthy membrane, an enhancement of PI intensity upon incubating the AMPs with the live cells acts as a marker for the inner membrane permeability. Enhanced intensity of PI fluorescence was observed upon incubating *P. aeruginosa* cells with P4C and P5C for 40 min at their respective 0.5× and 1× MICs [Figure 2.8(C) & (D)]. 0.5× and 1× MICs of P4C induced 12 and 39% leakage of the cells [Figure 2.8(C)], while 33 and 47% of leakage was observed for 0.5× and 1× MICs of

P5C [Figure 2.8(D)]. Thus, P5C had greater inner membrane permeability in Gram-negative bacteria compared to P4C.

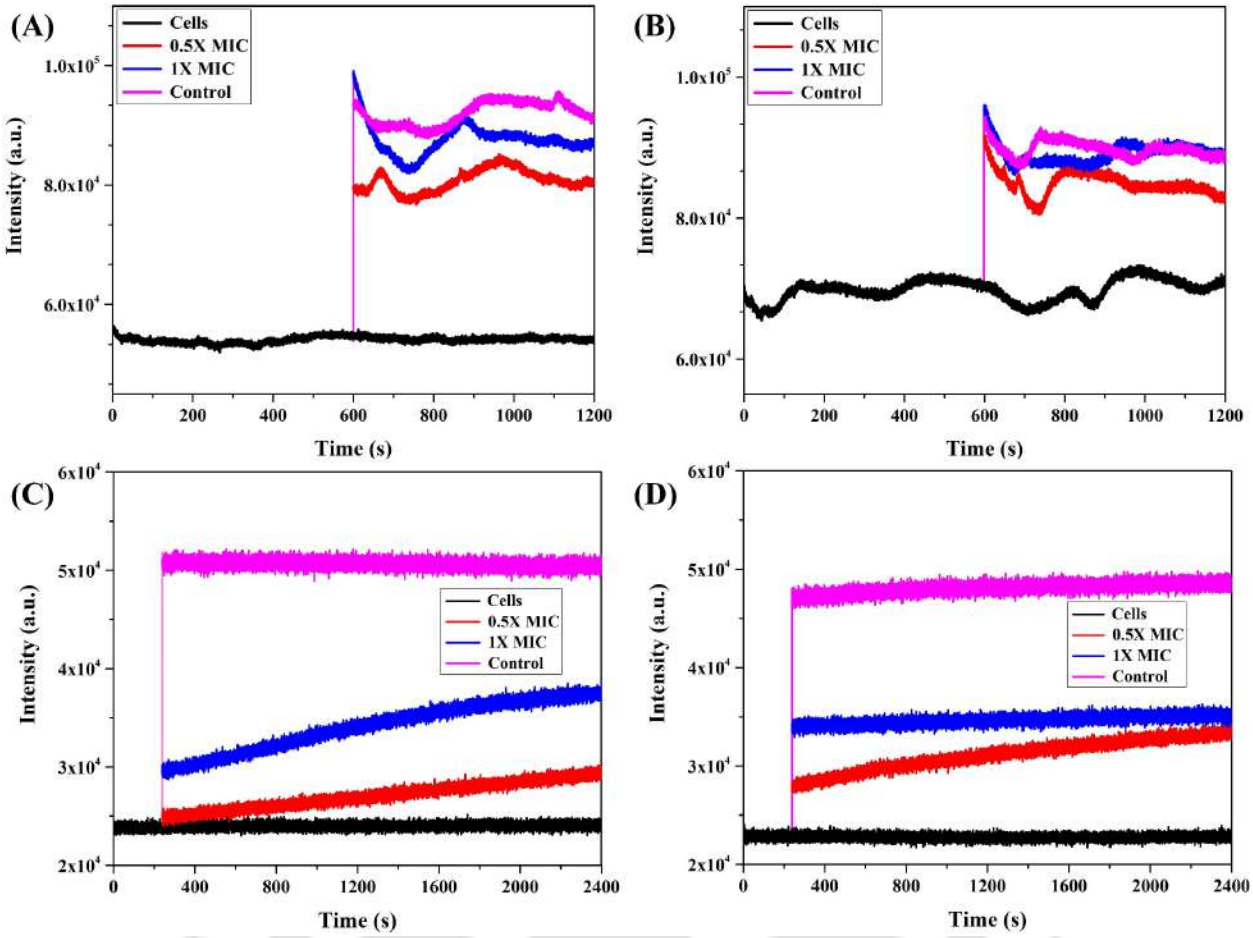

Figure 2.8. Outer membrane and inner membrane permeability. Fluorescence spectra showing the enhanced fluorescence intensity of *P. aeruginosa* cell suspensions containing NPN incubated with respective 0.5X, 1X MICs of (A) P4C, (B) P5C and 0.1% Triton X-100 (positive control). Enhanced intensity of PI was observed for *P. aeruginosa* cells treated with respective 0.5X and 1X MICs of (C) P4C, (D) P5C and 0.1% Triton X-100.

Fluorescence blueshift experiments with membrane mimics

Intrinsic fluorescence properties of tryptophan present in P4C and P5C were used to study the interaction of these peptides with the microbial membrane mimic sodium dodecyl sulfate (SDS) and mammalian membrane mimic dodecylphosphocholine (DPC) [Figures 2.9(A) & A44(A)-(D), Appendix A]. Membrane association of the AMPs causes a change in the microenvironment of the Trp residue, leading to a shift in the fluorescence signal (λ_{max}). Increasing concentrations of SDS

and DPC were added to the peptides P4C and P5C at their respective MICs, with their ratio ranging from 0.25 to 20 times the concentration of the peptides. The blue shift of the λ_{max} values were determined to be 17 nm and 8 nm was observed for P4C and P5C, respectively, when they were titrated against SDS (20× of their MICs). No such shift in the fluorescence maxima of Trp was observed upon titrating the peptides against increasing concentration of DPC [Figures 2.9(A)]. This conclusively suggested selective association of the peptides with the SDS over DPC, probably owing to the favourable electrostatic interaction between the cationic AMPs and the negatively charged SDS. This experiment establishes the selectivity of the peptides toward the microbial cells over the mammalian cells, making it antimicrobial but noncytotoxic.

Live cell blue shift experiment

Next, we studied the interaction of the peptides with live *P. aeruginosa* cells by monitoring the intrinsic fluorescence of the tryptophan residue of P4C and P5C. A clear blue shift of ~20 nm was observed for both P4C and P5C in the presence of $\sim 10^7$ cells [Figures 2.9(B) & A44(E)-(F), Appendix A]. This established the membrane-associative nature of P4C and P5C, with the latter being more efficient than the former.

Solvent accessibility experiments

Extent of solvent accessibility of the tryptophan residues of the free peptides P4C/P5C and in the complex with microbial and mammalian membrane mimics [P4C-D8PG (dioctanoylphosphatidylglycerol) (1:20)/P5C-D8PG (1:20) and P4C-DPC (1:20)/P5CDPC (1:20)] were determined from the Stern-Volmer constant (K_{SV}) using a static quencher, acrylamide. It was observed that the K_{SV} values for both peptides P4C and P5C in the free state as well as in the presence of DPC were higher when compared to that of D8PG, implying higher solvent accessibility in the free state and in the presence of DPC in comparison to that of D8PG [Figures 2.9(C) & (D)]. Lesser solvent accessibility of the Trp residue in D8PG indirectly suggested interaction or binding of P4C/P5C to D8PG in contrast to DPC, suggesting a selectivity of interaction toward the microbial membrane mimics.

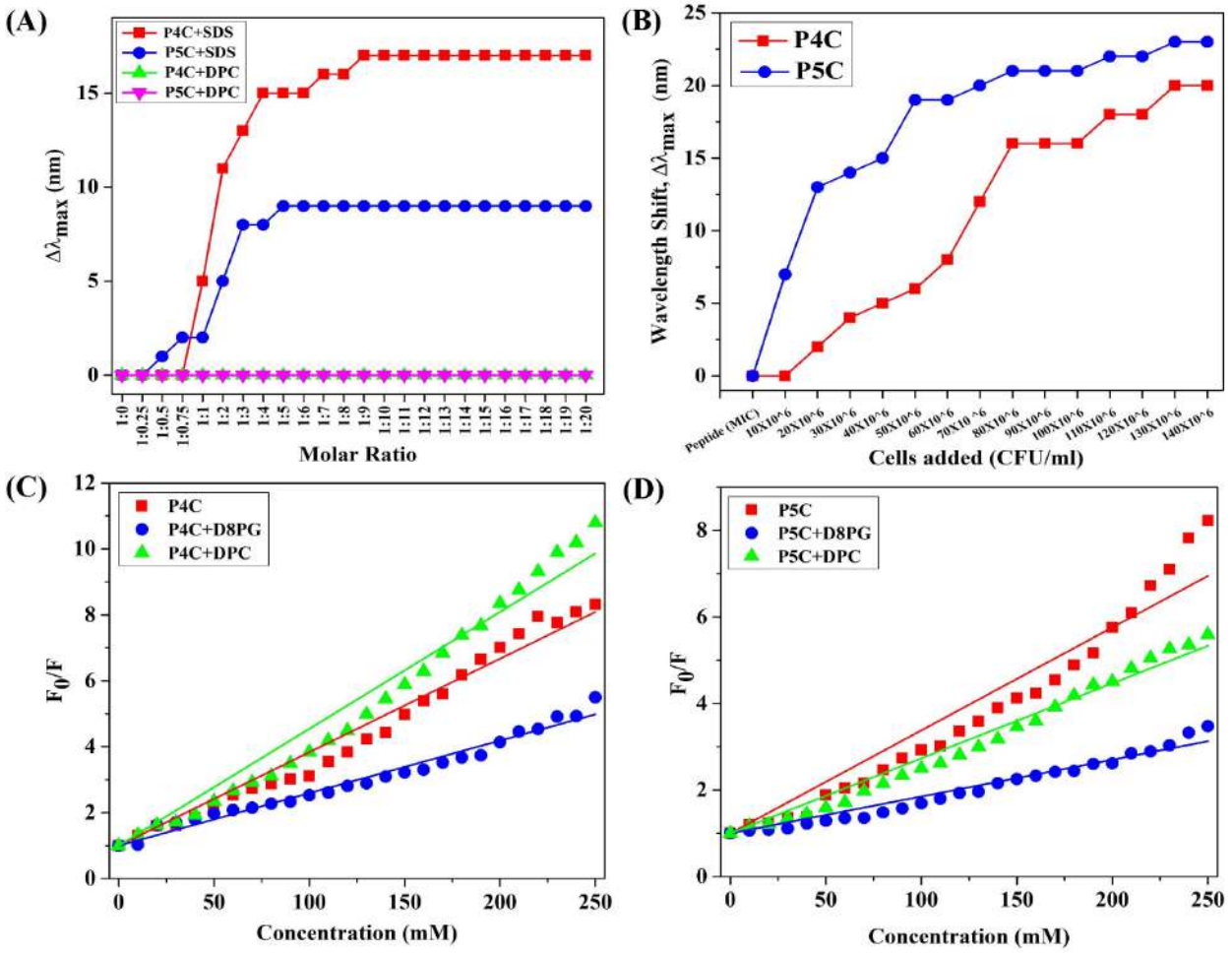

Figure 2.9. Blue shift experiments using intrinsic fluorescence of tryptophan present in P4C and P5C. (A) $\Delta\lambda_{max}$ values of P4C and P5C upon interaction with SDS (bacterial membrane mimic) and DPC (mammalian membrane mimic). (B) $\Delta\lambda_{max}$ values of peptide P4C and P5C upon interaction with the live cells of *P. aeruginosa.* Solvent accessibility of the Trp residue for (C) P4C and (D) P5C in the free state as well as in the presence of D8PG (bacterial membrane mimic) and DPC.

Isothermal titration calorimetry (ITC)

Isothermal titration calorimetry (ITC) was performed to understand the thermodynamics of the interaction between the lipopolysaccharide (LPS, present in the outermost layer of Gram-negative bacteria) and the peptides P4C/P5C (Figure 2.10). Solutions of P4C and P5C (3 mM each) dissolved in phosphate buffer (PB, 10 mM, pH 7.4) were titrated against 100 µM (above the CMC value of LPS) LPS extracted from *P. aeruginosa*. A volume of 2 µL of peptide was injected into the LPS each time. Isotherms obtained for both P4C and P5C were fitted using a single binding

site model. A comparison of the K_D values obtained for P4C and P5C suggested a better interaction of the peptide P5C with the LPS when compared to that of P4C (Table 2.5). Interactions of the peptides P4C and P5C (0.5 mM each) with DPC were also studied using ITC. Isotherms obtained for P4C and P5C, both fitted using a one binding site model, showed little to almost no interaction of the peptides with DPC (Figure 2.10). Thus, selectivity in membrane interaction of P4C/P5C was established by ITC, which explained the high antimicrobial potency in combination with non-cytotoxicity toward mammalian cells.

Table 2.5. Thermodynamic parameters for the interaction of P4C and P5C with LPS extracted from *P. aeruginosa*.

Thermodynamic parameters	LPS	
	P4C	P5C
Model	One binding site	One binding site
Temperature	310 K (37 °C)	310 K (37 °C)
ΔH (cal.mol^{-1})	-1.808×10^{4}	-5.424×10^{3}
ΔS (cal.mol^{-1}.deg^{-1})	- 41.30	0.675
N	0.417	1.41
K_A (M^{-1})	5.08×10^{3}	9.33×10^{3}
ΔG (cal.mol^{-1})	-5.277×10^{3}	-5.633×10^{3}
K_D (μM)	196.85	107.18

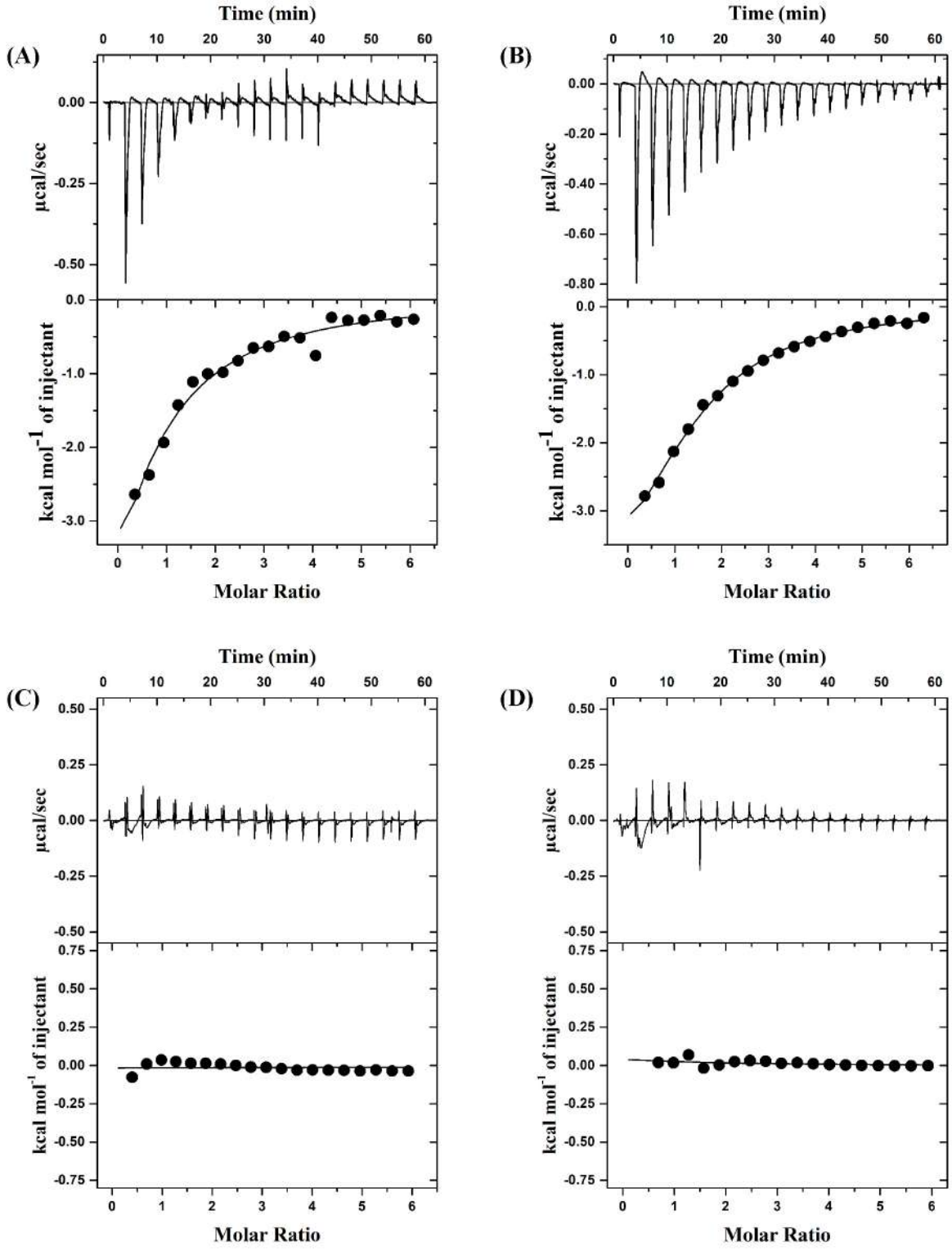

Figure 2.10. ITC curves showing the interactions of (A) P4C with (B) P5C with LPS extracted from *P. aeruginosa.* Interactions of (C) P4C and (D) P5C were studied against DPC.

Secondary structures of the peptides

Secondary structures of all peptides were determined in water (free state), in the presence of SDS/DPC, and in 50% TFE (helix promoting solvent) using CD spectroscopy (Figure 2.11). Both homo- and heterochiral peptides mostly adopted a random coil structure in the free state as well as in the presence of membrane mimics SDS and DPC. Thus, it can be concluded that the activity of these small cationic peptides P4C and P5C was independent of the prerequisite of these peptides to adopt any specific secondary structure.

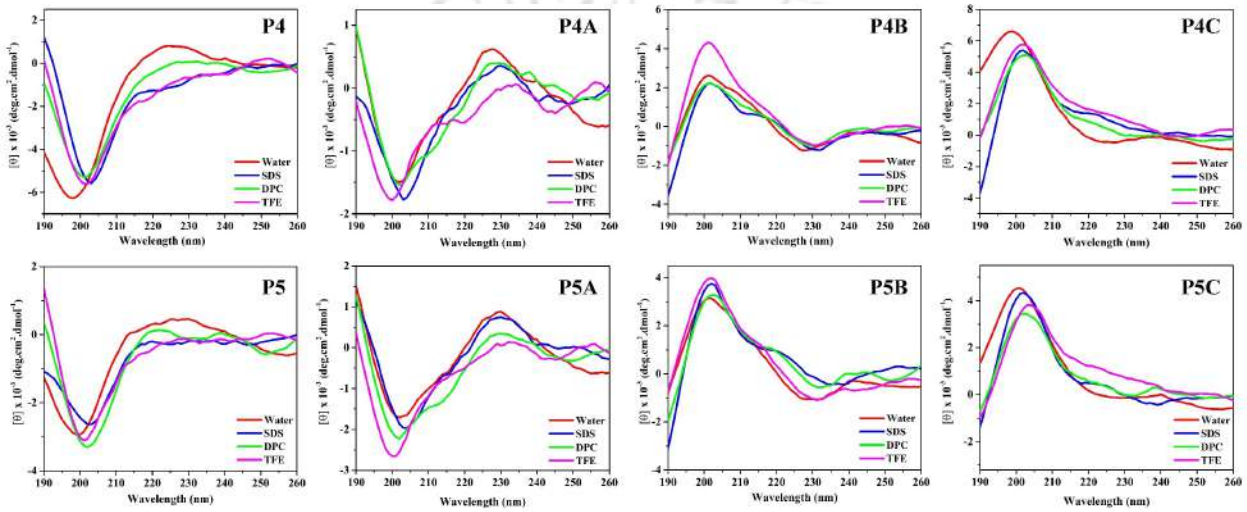

Figure 2.11. CD spectra of the peptides P4, P4A, P4B, P4C, P5, P5A, P5B, P5C in their free state in water as well as in bacterial membrane mimic SDS (30 mM), mammalian membrane mimic DPC (10 mM) and 50 % TFE.

2.2.6. Mechanism of action of the AMPs

Live cell NMR

Time-dependent interaction of the peptide P4C with the cells of *P. aeruginosa* was studied using ^{1}H NMR. ^{1}H NMR was recorded for the peptide in the free state and upon incubation with *P. aeruginosa* cells for various time intervals. Broadening of peaks was observed for the peptide when incubated with the cells (Figures 2.12), suggesting interaction between the peptide P4C and the microbial cells. The appearance of new peaks, which intensified over time, was also observed upon incubation of the peptides with the cells. These new peaks might be attributed to the metabolites that were released from the cells upon membrane lysis caused due to incubation of the peptide with the cells, suggesting membranolytic mode of action of the peptides.

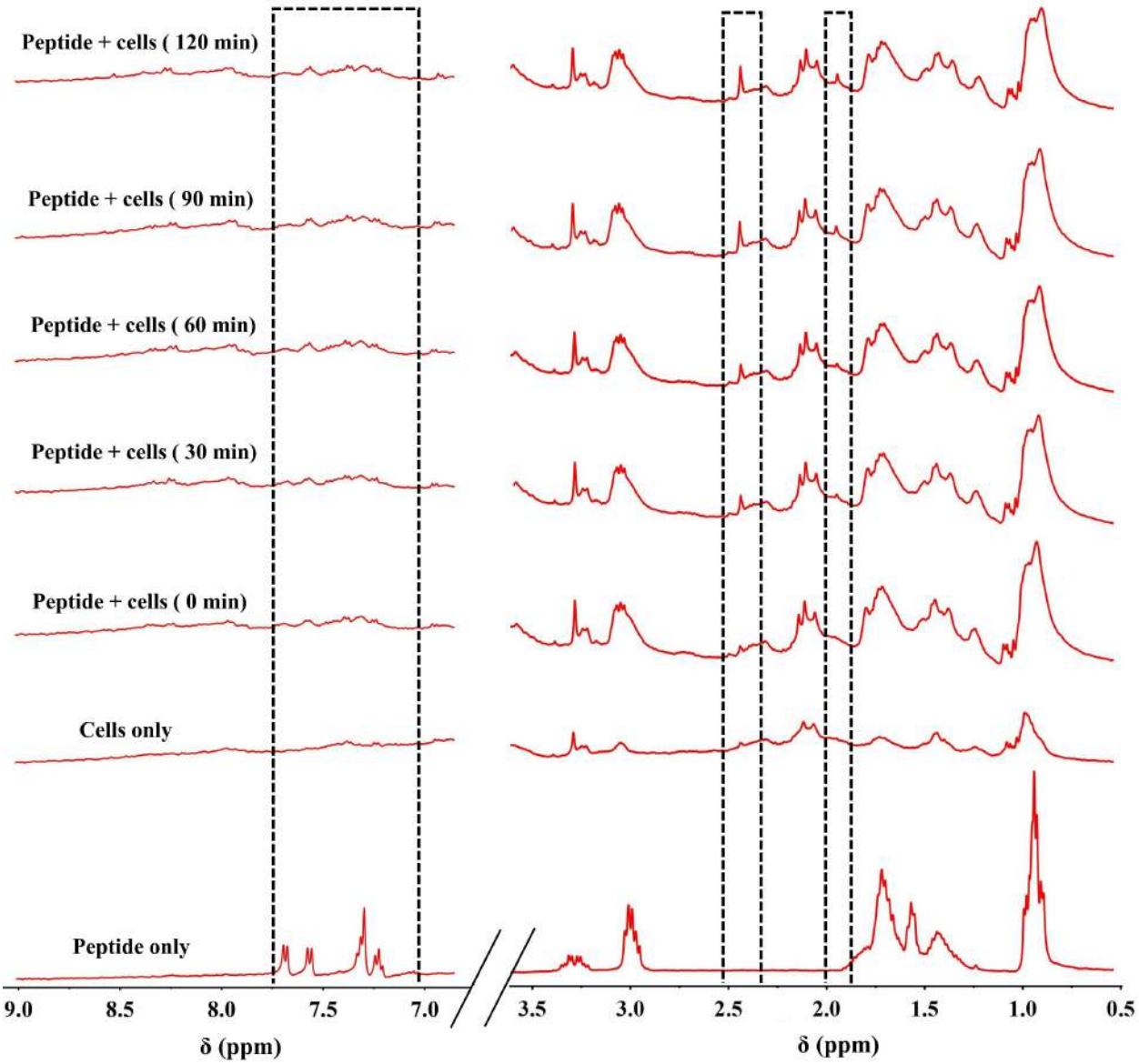

Figure 2.12. 400 MHz stacked ^{1}H 1D NMR spectra of P4C (1 mM), *P. aeruginosa* cells (10^{8} cells) , and P4C incubated with *P. aeruginosa* cells at different time points at room temperature. The appearance of new signals in the spectra of the peptide-cells mixture which intensified with increasing time is attributed to the release of metabolites or cellular matrixes from the cells as a results of membrane lysis and have been highlighted in black boxes.

Flow-assisted cell sorting (FACS)

As mentioned earlier, PI can permeate through the disrupted membranes of lysed/dead cells and bind with the DNA, generating enhanced fluorescence. Hence, PI staining of the cells is an indication of membrane disruption and subsequent cell death. In the untreated cells, only 5.9% of

the cells were PI-stained as shown by flow assisted cell sorting (FACS) data, representing the dead cell population in the negative control (Figure 2.13). On being treated with 1× and 2× MICs of P4C, 70.5 and 87.4% of the cells were PI-stained or lysed, respectively. 1× and 2× MICs of P5C stained and thus lysed 81.3 and 87.2% of the cells, respectively. This established that the designed AMPs were membrane disruptive in their mode of action.

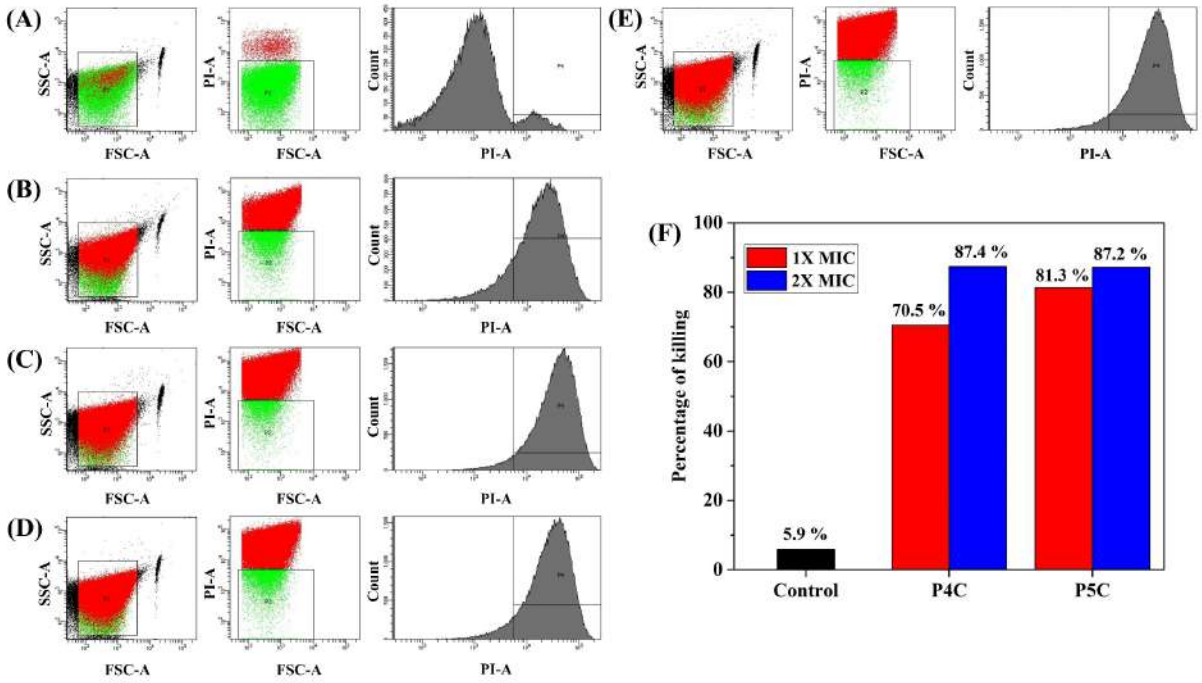

Figure 2.13. FACS histograms showing the permeability of PI in the (A) untreated, (B, C) 1× and 2× MICs of P4C-treated, and (D, E) 1× and 2× MICs of P5C-treated *P. aeruginosa* cells, respectively. (F) Bar diagram showing the percentage killing of *P. aeruginosa* cells incubated with 1× and 2× MICs of P4C and P5C, respectively.

FESEM images of the peptide-treated bacteria

To directly visualize the effect of membranolytic P4C and P5C on the *P. aeruginosa* cell membranes, FESEM images of the cells in their untreated forms as well treated with the peptides at their respective 1×, 2×, and 4× MICs were acquired [Figure 2.14(A)]. The untreated cells that showed a smooth surface, unruptured membrane, and characteristic shape, developed membrane damage and rupture accompanied by shape deformation upon treatment with the peptides P4C or P5C, establishing the membranolytic mode of action of the peptides. Membrane damages were proportional to the concentration of the peptides used.

FETEM images of the peptide-treated bacteria

Peptide treated bacterial cells were further visualized with the help of FETEM imaging [Figure 2.14(B)]. While untreated bacterial cells were seen to be typically rod-shaped, having smooth membrane, peptide-treated bacterial cells were found to be deformed, damaged, and uneven at the edges, indicating membrane lysis.

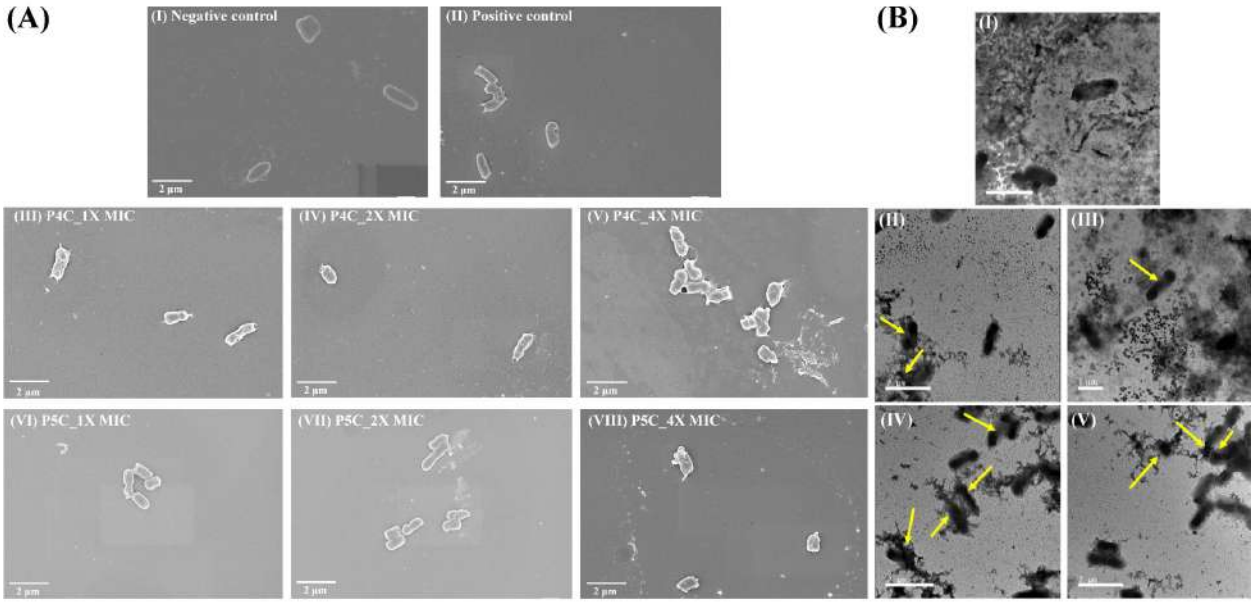

Figure 2.14. FESEM and FETEM imaging of *P. aeruginosa* cells. (A) FESEM images of (I) Untreated, (II) Polymyxin-B (positive control) treated, (III-V) 1X, 2X and 4X MIC of P4C treated and (VI-VII) 1X, 2X and 4X MIC of P5C treated *P. aeruginosa* cells respectively. (B) FETEM images of (I) Untreated, (II-III) 1X, 2X MIC of P4C treated and (IV-V) 1X, 2X MIC of P5C treated *P. aeruginosa* cells respectively.

Confocal images

To determine the translocation ability of the AMPs across the cell membranes, *P. aeruginosa* cells (10^6 CFU/mL) were incubated with 5(6)-carboxyfluorescein tagged P4C and P5C at concentrations corresponding to their respective MICs for 5 min. Confocal images were acquired at the bright field and also at the FITC excitation (Figure 2.15). Green fluorescence was observed throughout the cells, indicative of cellular uptake of the AMPs via membrane translocation and unspecific localization throughout the cytoplasm. This observation suggested that there might be other secondary modes of action of the AMPs in addition to its primary membranolytic mode of action.

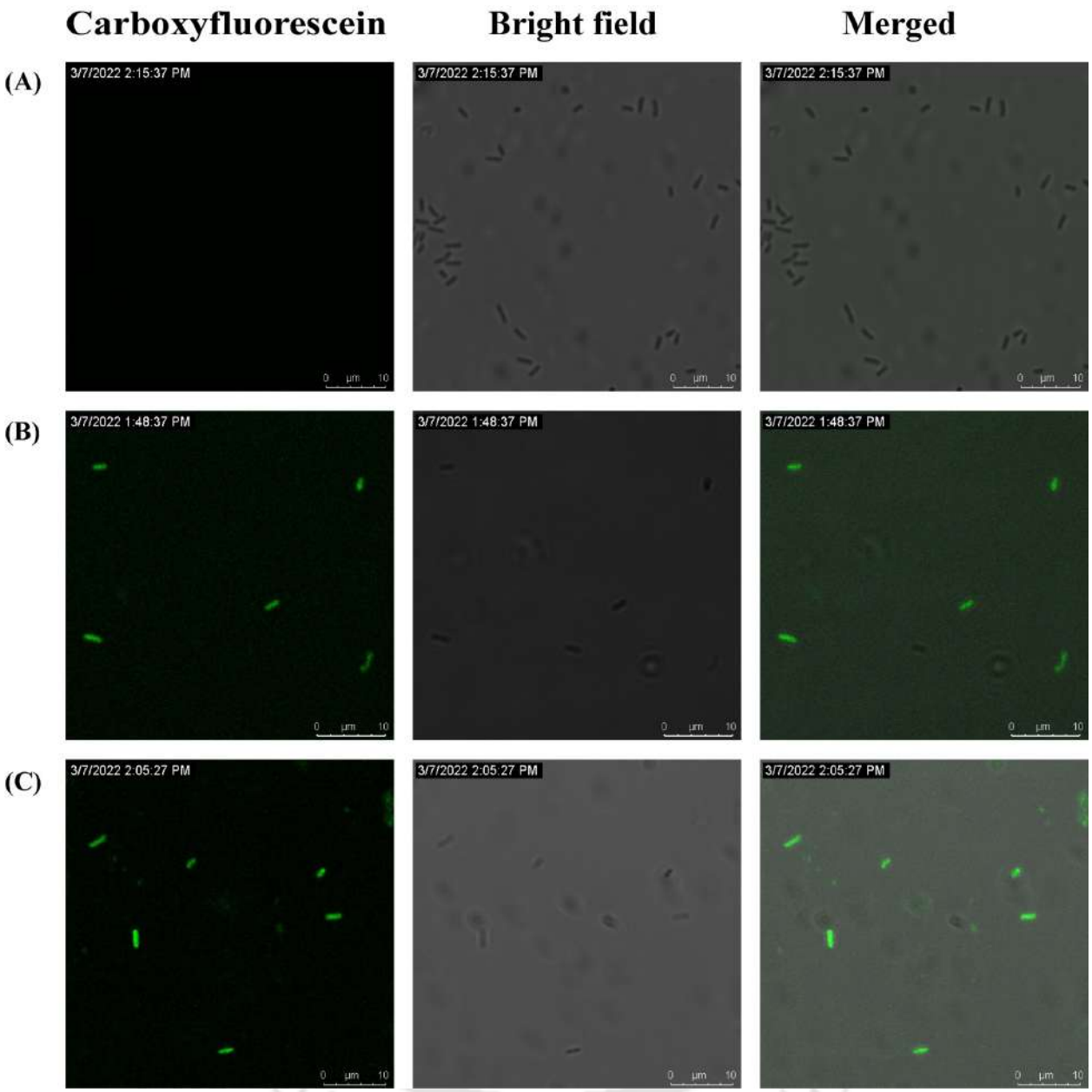

Figure 2.15. Confocal images of *P. aeruginosa* cells. (A) Untreated cells (negative control); Cells treated with (B) Cf-P4C and (C) Cf-P5C.

2.2.7. Insights from MD simulations

P4C/P5C in the presence and absence of membrane-mimetic SDS micelle

MD simulations of the peptides (P4C and P5C in aqueous medium) in the presence and in the absence of the membrane mimicking SDS micelle demonstrated that the peptides lacked secondary structures (random coil) throughout the MD trajectories (Figure 2.16). The CD spectrum of these peptides (Figure 2.11) in an aqueous environment (in the presence and absence of a micellar

environment) also confirmed the random coil structure corroborating the computational observations.

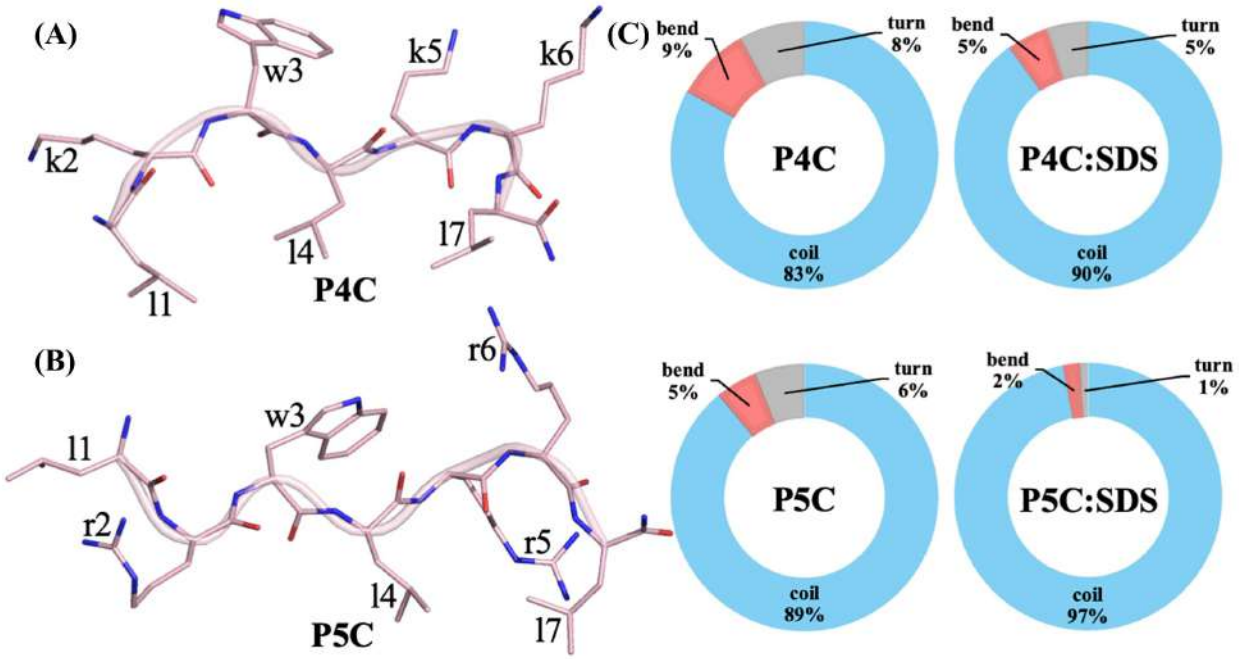

Figure 2.16. (A) P4C and (B) P5C structure in water after 200 ns simulation. (C) The donut chart represents the secondary structure percentage of the peptide during the simulation (last 100 ns of 200 ns simulation) in the absence (P4C, P5C) and presence (P4C: SDS, P5C: SDS) of the SDS micelle.

MD structure of the P4C/P5C:micelle complex (Figure 2.17) revealed that the structural stability involves (a) direct and water-mediated salt-bridge interactions between the cationic peptide tips and the anionic surface of the SDS micelle, (b) shielding of the hydrophobic peptide side chains from water by placing the hydrophobic side chains into the aliphatic core of the micelle, and (c) fulfilling the peptide backbone hydrogen bonding obligation by bonding with the water molecules and the sulfates of the SDS micelle. Simulations demonstrated that the side chains of tryptophan (W3) and leucine (L4) of the P4C/P5C were on the same side relative to the backbone and buried in the dry hydrophobic core of the SDS micelle, where the indole NH proton satisfied its hydrogen-bonding requirement by forming hydrogen bonds with the anionic phosphates of the micelle (Figure 2.17). Tryptophan fluorescence experiments confirmed the blueshift of the intrinsic tryptophan fluorescence emission maxima in response to the peptide:SDS micelle binding [Figure 2.9(A)], corroborating the MD structures in which the tryptophan side chain was inserted into the

hydrophobic core of the micelle (Figure 2.17). The peptide structure and the peptide:micelle interaction network of the D-peptides (P4C or P5C; Figure 2.17) were found to be more or less identical to that of L-peptides (P4 and P5) reported previously.[30-31] The arginine-peptide P5C:SDS complex contained a higher number of salt-bridge interactions and a lower number of water molecules relative to the lysine- peptide P4C:SDS complex (Figure 2.17).

Energetics of P4C/P5C: micelle binding

The absolute P4C/ P5C:SDS micelle-binding affinity (ΔG_{bind}) was estimated using the MM/PBSA method employing the MD trajectory of the P4C/P5C:SDS complex as the input. Peptide binding to the micelle was disfavoured by the desolvation (ΔG_{pb}, polar term) and loss of entropy ($T\Delta S$), the former being significant [Figure 2.17(C)]. However, the unfavourable desolvation was offset by the favourable noncovalent interactions between the peptide and the SDS micelle [ΔE_{ele} and ΔE_{vdw}; the former being noticeable; Figure 2.17(C)]. The magnitude of the nonpolar free-energy component associated with the peptide:micelle binding (ΔG_{SA}) was small and similar for P4C and P5C. Stronger micelle-binding affinity of the arginine-peptide (ΔG_{bind} P5C ~ -21 kcal/mol) relative to its lysine analogue (ΔG_{bind} P4C ~ -17 kcal/mol) was evident. Arginine-peptides (P5C/P5) were preferred by $\sim 3-4$ kcal/mol for SDS micelle binding relative to their lysine analogues (P4C/P4). The binding affinity (ΔG_{bind}) was found to be marginally dependent [$\sim$ 1 kcal/mol, Figure 2.17(C)] on the stereochemistry of the peptide (“L” or “D”).

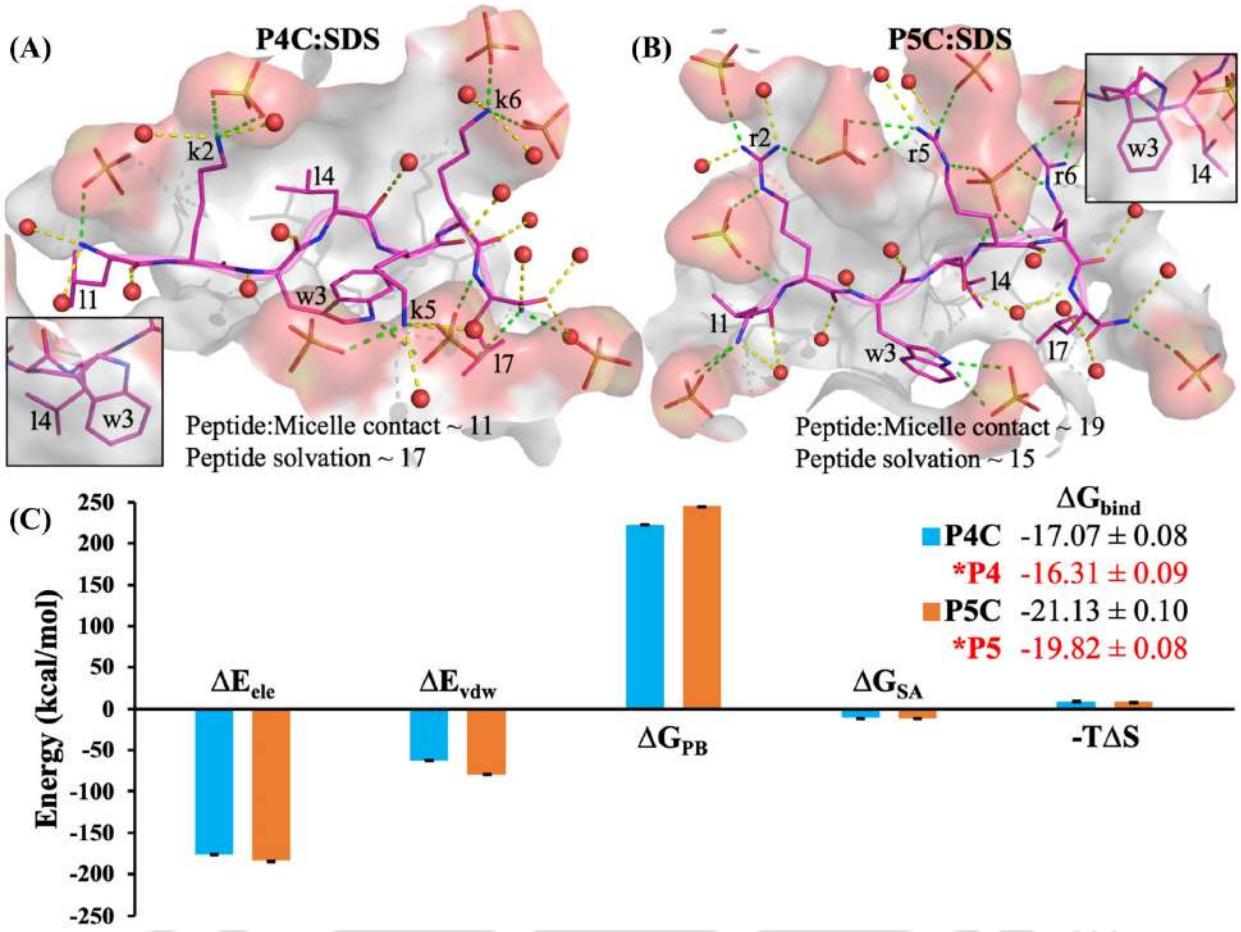

Figure 2.17. Zoomed in view of the representative MD structures of (A) P4C: SDS and (B) P5C: SDS complexes. Micelle surface is represented in red and grey, the peptide backbone in magenta cartoon with sticks (red: oxygen, blue: nitrogen), and the interaction network in dashed line (green: direct peptide-micelle interactions, yellow: interaction with the water molecules in red spheres). Hydrogens are not shown for clarity. Higher peptide: micelle electrostatic contact (heavy atom distance < 3.5 Å; green broken line) and lower peptide solvation (water molecules within 3.5 Å of the peptide) are evident for arginine peptide P5C: SDS complex relative to the P4C: SDS complex. Inset highlights that the side-chain of W3 and L4 are on the same side relative to the peptide backbone. (C) Peptide: micelle binding affinity (ΔG_{bind} in kcal/mol) and its components (ΔE_{ele}: electrostatic energy, ΔE_{vdw}: van der Waals energy, ΔG_{PB}: polar solvation free energy, ΔG_{SA}: non-polar solvation free energy, and $T\Delta S$: entropy contribution) are estimated using MM/PBSA approach. Blue/Orange bars represent binding free energy components for P4C/P5C binding to SDS micelle. Binding is favored by peptide: micelle interactions (ΔE_{ele} and ΔE_{vdw}), but disfavored by desolvation term (ΔG_{PB}).[31]

MD simulations of peptides in complex with serine proteases (trypsin and chymotrypsin)

Experiments confirmed protease resistance (Figures 2.5 and A24-A35, Appendix A) and marginal improvement of the antimicrobial activity (Table 2.2) for the D-peptides (P4C/P5C) relative to the L-peptides (P4/P5). Though there are several reports of protease-resistant peptides in the literature, there is a dearth of studies where the mechanism of peptide selectivity and protease resistance has been probed in terms of atomic structure and its link to thermodynamics. To gain insight into the mechanisms of protease stability and peptide-protease recognition, the peptide: protease complex models were subjected to MD simulations (see methods). Two types of serine proteases (trypsin and chymotrypsin) in complex with P4/P5 and P4C/P5C were simulated. Although trypsin and chymotrypsin have high sequence and structural similarities, they differ in their substrate specificity. Trypsin favours cationic residues (lysine and arginine), whereas chymotrypsin favours aromatic amino acids (phenylalanine, tyrosine, and tryptophan).[39-40] Three key regions of proteases are (i) the side chain binding pocket (promotes specificity), (ii) the catalytic triad (ensures catalysis), and (iii) the nonspecific main chain binding pocket (provides stability).

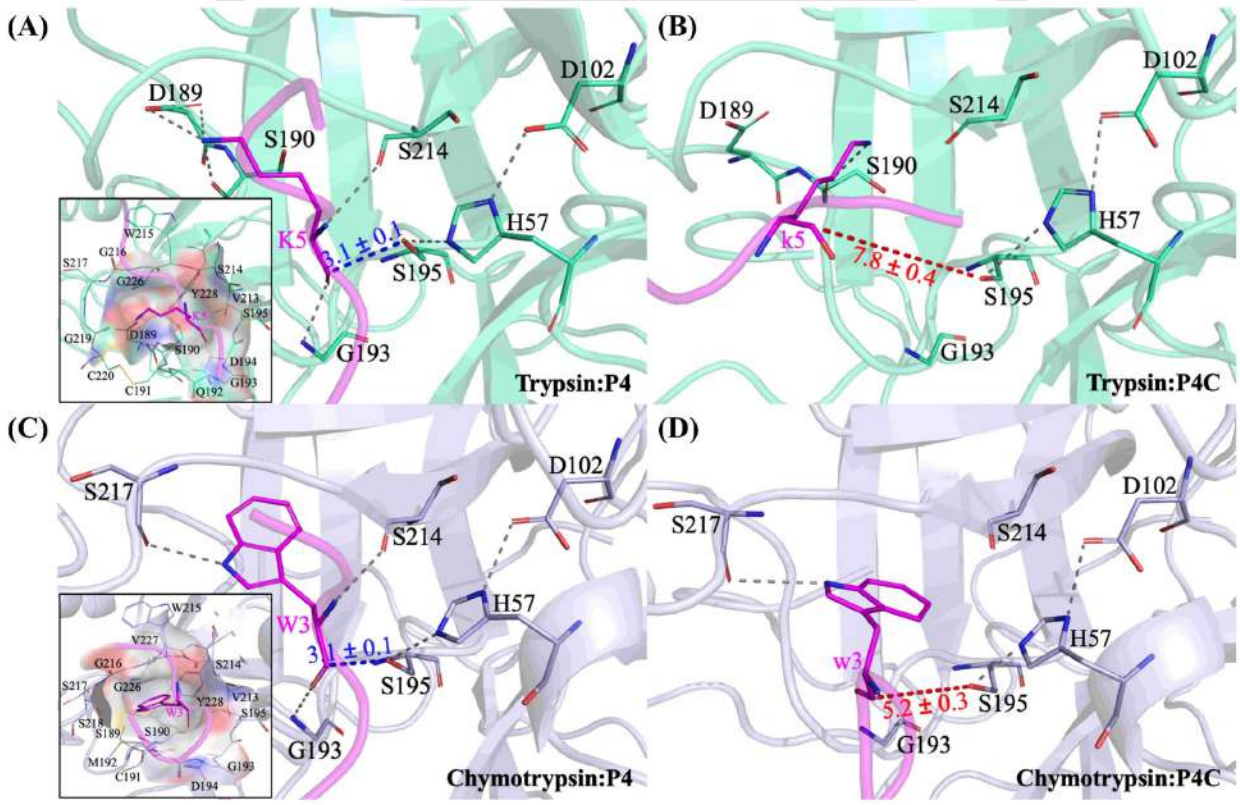

Figure 2.18. A close-up view of the binding pocket of trypsin (upper panel, teal green) and chymotrypsin (bottom panel, light blue) containing scissile bond (K5-K6/W3-L4, magenta) of the

peptide. Interactions between the peptide and protein are highlighted by grey dashed lines (heavy atom distances < 3.4 Å) together with the stick representation of the interacting residues. Side-chain binding pocket residues within 3.4 Å of K5/W3 (in surface representation), catalytic triad (S195, H57, and D102), and non-specific main-chain binding residues (viz., S214, G193) are shown. MD trajectory averaged distance between the scissile carbonyl and catalytic S195 is given (standard deviation as error), indicating catalytically active (blue broken-like) and inactive (red broken-line) conformations.

MD structures [Figure 2.18(A)] revealed that the trypsin: P4 complex was stabilized by (1) the electrostatic interaction involving the cationic tip of the lysine (K5 of P4) and the protease (residues G219, S190, and D189) in the side chain binding pocket and (2) main chain hydrogen bonding between P4 and the protein (viz., G193, S214 etc.). The proximity of the scissile peptide backbone (carbonyl group of K5) and the catalytic triad (S195, H57, D102) in the trypsin:P4 complex was evident in the MD structures [Figure 2.18(A)]. The presence of negatively charged D189 in the catalytic pocket justified the specificity of trypsin for cationic amino acid residues (lysine or arginine). The distance between the hydroxyl oxygen of serine residue (S195 of protease) and scissile carbonyl (K5 of P4) was ~3 A [Figure 2.18(A)]. The proximity and correct relative orientation of the scissile peptide backbone (K5 of P4) and the catalytic triad implied facile proteolysis in the trypsin pocket [Figure 2.18(A)]. The disruption of the main chain interactions, along with the increase in the relative distance between the carbonyl carbon of K5 and S195 (~8 A) in the trypsin protease, was evident in response to L → D conversion [Figures 2.18(B) and 2.19]. Thus, the protease resistance of the D-peptide was most probably related to the (1) destabilization of the D-peptide:protease complexes and (2) increase of the distance between the sessile carbonyl (of the peptide) and nucleophilic serine (S195 of the catalytic triad). The trypsin:P5 complex was stable throughout the MD simulations. However, it is noteworthy that a complete dissociation of P5C from the trypsin protease was observed during the MD simulation. The preference of chymotrypsin for the hydrophobic residues was evident by the existence of a large nonpolar side chain binding pocket [Figures 2.18(C)] well suited for the accommodation of the planar aromatic side chains (viz., Phe, Tyr, and Trp). The indole nitrogen (−NH) of tryptophan formed a hydrogen bond with the main chain of Ser217 [Figures 2.18(C) & (D)]. Like trypsin protease, P4 → P4C conversion increased the distance between the scissile backbone (W3−L4)

and the nucleophilic serine residue (Ser195) that most probably hindered catalysis [Figures 2.19]. However, the relative positions of the catalytic triad in the proteases (trypsin and chymotrypsin) were independent of the nature (L or D) of the bound peptide (P4 or P4C or P5 or P5C).

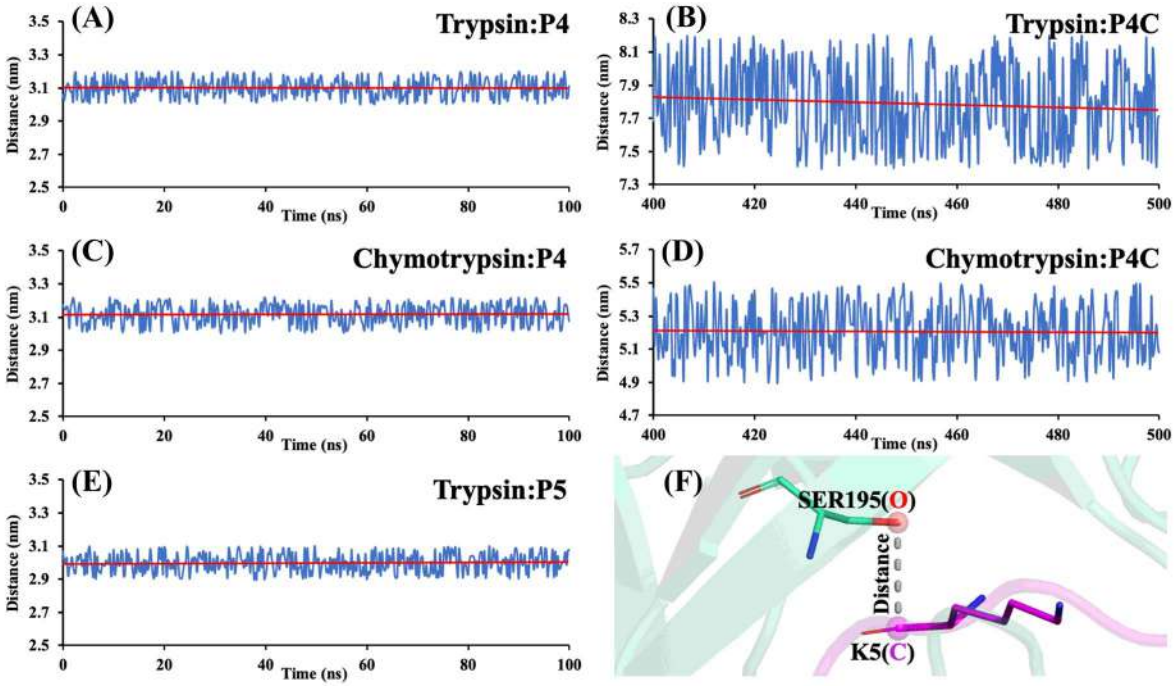

Figure 2.19. Heavy atom distance between SER195(O atom) and scissile residue (C atom) in the last 100 ns MD trajectory of (A) Trypsin:P4, (B) Trypsin:P4C, (C) Chymotrypsin:P4, (D) Chymotrypsin:P4C, and (E) Trypsin:P5. Blue line = distance versus time plot, and the Red line = Running average distance. (F) Pictorial representation of the SER195(O atom) and scissile residue (C atom) distance.

Energetics of protease-peptide binding

The free energy of protease: peptide binding (ΔG, Table 2.6 & Table A2, Appendix A) was determined by umbrella sampling simulations (reaction coordinate ξ; Figure A45, Appendix A). The results revealed two key features: (1) P4→P4C mutation (i.e, L→D conversion) strongly disfavored protease binding ($\Delta\Delta G = \Delta G^{P4C} - \Delta G^{P4} \sim +22$ and +9.5 kcal/mol for the trypsin and the chymotrypsin respectively). Thus, L→D mutation destabilized the protein: protease complex. Interestingly, the P5→P5C mutation resulted in peptide dissociation from the trypsin protease. (2) Binding affinity of P4 (ΔG ~ -23 kcal/mol) and P5 (ΔG ~ -22 kcal/mol) peptides to the trypsin protease differed by less than 1 kcal/mol (Table 2.6). The weak discrimination of trypsin protease

implied that both the L-peptides differing in their cationic side-chain (lysine: P4 or arginine: P5) were likely to bind the trypsin protease with more or less equal strength.

Table 2.6. Average protease: peptide binding affinity (in kcal/mol) estimated by employing "steered molecular dynamics followed by umbrella sampling" simulations. Bootstrapping errors (100 cycles) are given after ±. [#]Dissociation of P5C observed. [ND]Simulation was not performed.

Peptides	Trypsin	Chymotrypsin
P4	–22.79 ± 0.42	–14.34 ± 0.67
P4C	–1.24 ± 0.37	–4.86 ± 0.35
P5	–21.98 ± 0.98	ND
P5C	#	ND

MD simulation of the mixed-chiral peptide P4B in the presence of SDS micelle was also performed to gain insight into its loss of activity. The hydrophobic residues in the middle region of the mixed-chiral-peptide P4B could not be accommodated in the aliphatic core of the micelle during the simulation (Figure 2.20), indicating poor association, and a plausible explanation for the loss of potency.

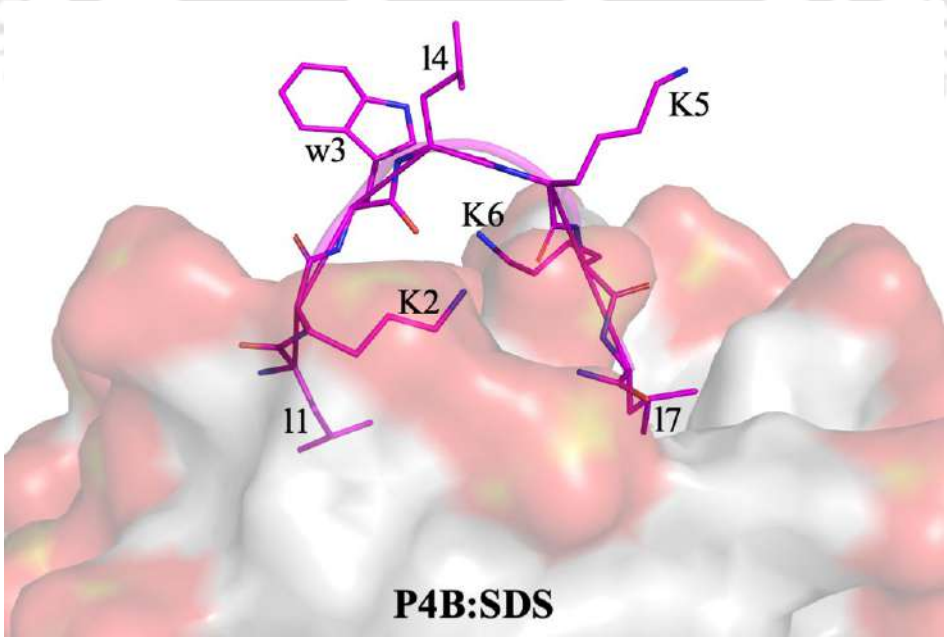

Figure 2.20. Final snap after 200 ns of production dynamics (peptide P4B in magenta, SDS micelle in surface representation). Water molecules and hydrogens are not shown for clarity.

Trypsin: AMP enzyme kinetics

To complement our computational claim, we performed protease activity assay in which the trypsin from porcine pancreas was used as the enzyme for the peptide substrates (P4, P4C, P5, and P5C). The progress of the reaction was estimated by the HPLC method. Michaelis−Menten equation was fitted to estimate the kinetic parameters (Km and Vmax, Figure 2.21). Michaelis constant (Km) is inversely related to the peptide:enzyme binding affinity. Clearly, the D-peptides (P4C and P5C) did not undergo peptide degradation (Figure 2.21) contrary to the L-peptides (P4, P5). Computational analysis estimated severe loss of the peptide:enzyme binding affinity (by ≥10 kcal/mol) in response to D → L transformation of the peptide, thus corroborating the kinetic data (Figure 2.21). Similar Km values for the L-peptides [Km (P4) = 1.85 mM and Km (P5) = 0.95 mM] indicated that both the peptides (P4 and P5) bound to the trypsin enzyme with more or less similar affinity, corroborating our computational prediction (i.e., binding affinity of P4 and P5 to trypsin differed by <1 kcal/mol).

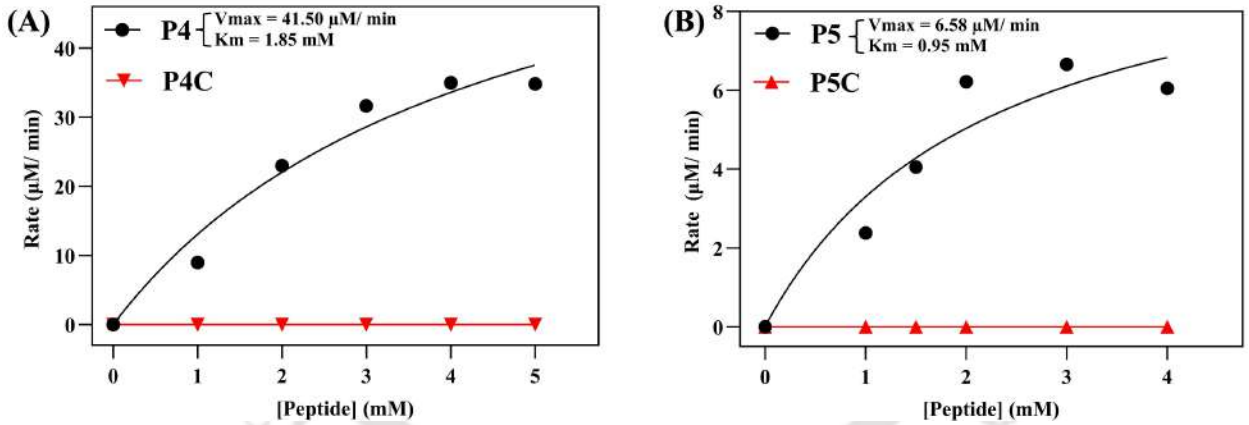

Figure 2.21. Kinetic parameters from the trypsin activity assay using our synthetic peptides as substrate: (A) P4 and P4C, (B) P5 and P5C. The data are fitted to the Michaelis-Menten equation; Rate = $\frac{V_{max}\,[peptide]}{K_M + [peptide]}$. K_m is the Michaelis-Menten constant, V_{max} is the maximum velocity. Peptide degradation was not observed for the D-peptides P4C and P5C.

Our simulations highlighted two key aspects: (1) high free energy of the D-peptide: protease complex was likely to drive dissociation, and (2) even if the high energy D-peptide: protease complex was populated, the chemical step was likely to be disfavoured (supported by the large relative distance between the scissile D-peptide carbonyl and the catalytic triad of the protease in the MD structures, Figure 2.18). The origin of trypsin-protease stability of the D-peptides was thus

attributed to both the poor binding and the slow catalytic step, the former most probably being the prominent factor.

2.3. Discussion

We have established that both the all-D-peptides P4C and P5C had slightly improved activity (lower MICs and faster killing kinetics, Table 2.2) toward most of the microbial strains that were screened in the study in comparison to their L counterparts. Binding affinities of the all-L-(P5/P5) and D-(P4C/P5C) peptides toward SDS micelles (microbial membrane mimic) were almost similar, with a slightly favoured binding for the all-D-peptides, explaining their better antimicrobial potency. The improvement of the antimicrobial activity observed experimentally, in response to L → D conversion, might also be attributed to the greater stability of the D-peptides with respect to the L-peptides toward the exopeptidases that are secreted by the microorganisms. It was also observed that the P5C was more active both in the absence and presence of salts, faster in its killing kinetics, and better membranolytic than the P4C. This might be attributed to the presence of arginine residue with the guanidine side chain in the former in comparison to the primary amine-containing side chain of lysine present in the later.[31] Indeed, arginine-peptides are known to display stronger antimicrobial, membranolytic, and cell-penetrating abilities relative to their lysine analogues.[31,41-42] Our MD simulation studies suggested that Lys(P4/P4C) → Arg(P5/ P5C) conversion favoured micelle binding [Figure 2.17(C)] by increasing peptide:micelle contact [Figure 2.17(A) & (B)]. The favourable micelle-binding affinity of arginine-peptides (P5/ P5C) relative to the lysine-peptides (P4/P4C) justified the experimentally observed higher potency of the former. It was also interesting to note that P4C and P5C remained noncytotoxic and non-hemolytic toward both mammalian cell lines and RBCs.

P4C and P5C were completely protease-resistant and serum stable in their activity in contrast to the all-L-peptides (Figures 2.5, 2.7, A24-A43, Appendix A). In an attempt to understand the underlying details of the protease resistance of the all-D peptides, the binding affinity of the peptides toward serine protease trypsin was computed. The L → D conversion yielded a very high energetic penalty disfavouring protease:(P4C/P5C) binding (Table 2.5). Disruption of intermolecular interactions (Figure 2.18) rationalized the high energy of the protease:P4C/ P5C complexes. The MD structures showed that the L → D conversion altered the relative distance of scissile carbonyl (of the peptide) and catalytic triad (of the protease) without altering the relative

positions of the catalytic residues (residue Ser195, His57, and Asp102) (Figure 2.18). While the L-peptides bound to the active site of the enzyme in a fashion that brought the serine side chain proximal to the peptide backbone, facilitating the nucleophilic attack of the Ser195 OH to the electrophilic carbonyl carbon present at the C-terminus of the positively charged amino acid residue (Lys/arg), D-peptides bound in a manner where the two counterparts were distally located making the nucleophilic attack difficult. This in turn led to the protease resistance of the all-D-peptides over the all-L analogues. Thus, the key effects of the L (P4/P5) → D (P4C/P5C) conversion in achieving proteolytic stability (Figure 2.18) were found to be 2-fold. First, from the energetic viewpoint, the L → D conversion disfavoured the protease:(P4C/P5C) binding affinity by disrupting intermolecular interactions. High free energy of the Trypsin: P5C complex drove P5C dissociation from the trypsin protease. Second, from the structural viewpoint, the scissile carbonyl group of the peptide in the protease:P4C/P5C complex was placed far away (inactive conformation) from the catalytic serine residue (catalytic triad) that hindered catalysis.

Microbes are known to be secreting exopeptidases,[43-44] which can degrade AMPs composed of L-amino acid residues, thereby rendering them less effective in the *in vitro* experiments, as performed in this study. Thus, the resistance of the D-peptides toward peptidases might be the contributing factor to their increased potency, which is reflected in their lower MICs and their faster killing kinetics compared to their all-L counterparts.

MD simulation studies showed that the peptides (P4, P4C, P5, and P5C) adopted a random coil structure in the presence and absence of micelle, in line with the CD experiments (Figure 2.11 & 2.16), establishing that the activity of these small cationic peptides was independent of their structure.

2.4. Conclusion

In this study, we have successfully developed small, protease resistant all-D cationic peptides with enhanced antimicrobial potency and faster killing kinetics in comparison to their L counterparts while remaining noncytotoxic and non-hemolytic at the same time. We have established that L → D conversion marginally favoured the binding of the all-D-peptides toward the SDS micelles in comparison to their all-L counterparts, thus explaining the similar antimicrobial activity for both the all-L and D-peptides, while it forged a huge differential binding of the all-L-peptides P4/P5

with respect to the all-D analogues P4C/P5C toward serine proteases, rendering complete protease stability for the all-D-peptides with respect to the all-L counterparts. Competent binding of the L-peptides at the binding pocket of the protease made the sessile peptide bond amenable to the nucleophilic attack by Ser195 OH, thus leading to protease susceptibility. Conversely, incompetent binding of the D-peptides led to distant location of the sessile peptide bond from the nucleophilic serine, which caused the acquired protease stability of the all-D-peptides. Thus, this study for the first time offered a general and complete understanding of the protease stability developed in the peptides containing D-amino acids from atomic structure and thermodynamic angles.

2.5. Methods

2.5.1. Materials

Rink amide resin, Fmoc-protected amino acids: [Fmoc-Leu-OH, Fmoc-D-Leu-OH, Fmoc-Lys(Boc)-OH, Fmoc-D-Lys(Boc)-OH, Fmoc-Arg(Pbf)-OH, Fmoc-D-Arg- (Pbf)-OH, Fmoc-Trp (Boc)-OH, and Fmoc-D-Trp (Boc)- OH], and peptide coupling reagents (HBTU and HOBt) were purchased from GL Biochem Ltd., Shanghai, China. N,N-Diisopropylethylamine (DIPEA) was purchased from Spectrochem Pvt. Ltd., Mumbai, India. N,N-Dimethylformamide (DMF), and trifluoroacetic acid (TFA) were purchased from Merck Life Science Pvt. Ltd., Mumbai, India. Dichloromethane (DCM) and HPLC-grade acetonitrile (ACN) were purchased from Finar Limited, Ahmedabad, India. Monosodium phosphate (NaH_2PO4), disodium phosphate (Na_2HPO_4), sodium chloride (NaCl), potassium chloride (KCl), monopotassium phosphate (KH_2PO4), calcium chloride ($CaCl_2$), magnesium chloride ($MgCl_2$), ferric chloride ($FeCl_3$), and zinc chloride ($ZnCl_2$) were purchased from Merck Life Science Pvt. Ltd., Mumbai, India. Nutrient broth, BHI broth, chymotrypsin, and proteinase K were purchased from Himedia Laboratories Pvt. Ltd., Mumbai, India. 1,2-Dioctanoyl-*sn-glycero*-3-phospho-(1′-*rac*-glycerol) (sodium salt) (D8PG) and DPC were purchased from Avanti Polar Lipids, Inc., USA. Sodium dodecyl sulfate, N-phenyl-1-naphthylamine, propidium iodide, 2,2,2-trifluoroethanol (TFE), LPS extracted from *Pseudomonas aeruginosa*, acrylamide, glutaraldehyde, deuterium oxide (D_2O), 5(6)-carboxyfluorescein, Triton X-100, α-cyano-4-hydroxycinnamic acid, and trypsin (porcine pancreas) were purchased from Sigma-Aldrich, St. Louis, USA.

2.5.2. Synthesis of peptides

All peptides were synthesized using a solid-phase peptide synthesis strategy using rink amide resin and Fmoc-protected amino acids. Each of the peptides was synthesized using the protocol as follows. The resin was swelled in a mixture of DMF and DCM which was then followed by deprotection of Fmoc using a solution of 20% piperidine in DMF. Three equivalents of Fmoc-protected amino acid (C-terminal amino acid in the sequence of the peptide), 3-equiv of the coupling reagents HBTU and HOBt each, and 6-equiv of DIPEA were mixed together in DMF and added to the resin and allowed to couple. Post coupling, the reaction mixture was drained out, and the resin was thoroughly washed using DMF and DCM. The resin was then capped using a solution containing 70% DMF, 20% acetic anhydride, and 10% pyridine. The capped resin was washed and subsequently deprotected to link the second amino acid as described for the first amino acid. The process of capping, deprotection, and coupling of amino acids was continued in the same way until all amino acids were assembled on the peptide. The Fmoc at the N-terminal amino acid was finally deprotected, and the peptide was cleaved off from the resin using a mixture of TFA, triisopropylsilane, and water (TFA:TIS:H2O = 96:2.5:1.5). The cleaved peptide was precipitated in cold ether, and the crude peptide was obtained.

2.5.3. Purification and characterization of peptides

The crude peptides were dissolved in mili-Q water and injected into a C-18 reverse phase column (Luna 5 µm C18(2) 100 Å, size: 250×21.2 mm) using a water/ACN solvent system each containing 0.1% of TFA. The peptides were eluted using the water/ACN solvent system with an increasing percentage of ACN. The purified peptides were lyophilized and used for further studies. The purified peptides were characterized using analytical HPLC, ESI-MS, and ^{1}H NMR studies. Analytic HPLC traces of the peptides were acquired by injecting 20 µL of the solution into a C-18 reverse phase analytic column (Thermoscientific, Biobasic-18, dimension: 150 × 4.6, particle size: 5 μ) using water/ACN and a linear gradient of increasing ACN percentages from 5 to 100% for 20 min. UV wavelengths corresponding to 214 and 280 nm were used for the analysis. HPLC traces were acquired using an Agilent 1260 Infinity II analytic HPLC system (Agilent Technologies). ESI-MS spectra of the peptides were acquired using an Agilent-Q-TOF 6500 mass spectrometer. ^{1}H NMR spectra of the peptides dissolved in D_2O were acquired on a Bruker Avance III 600 MHz NMR spectrometer.

2.5.4. Determination of MIC

$MIC_{90\%}$ values were determined against two Gram-negative strains *P. aeruginosa* and *K. pneumoniae*, two Gram-positive strains *S. aureus* and Methicillin-resistant *S. aureus*, and a fungus strain *C. albicans*. Gram-negative strains were cultured in nutrient broth (NB), Gram-positive strains in BHI broth at 37 °C, and the fungus *Candida albicans* in YPD media at 25 °C. Bacterial (or fungal) cells at their mid-logarithmic phases were washed using PB (10 mM, pH-7.4) and serially diluted to the order of 10^5 CFU/mL. In a 96-well microtiter plate, in each of the wells, 50 µL of the cell suspension was added to another 50 µL of the peptide solution diluted at various concentrations, starting from a peptide stock solution of 1 mM strength. Untreated cells were considered to be the negative control, while cells treated with polymyxin-B, a well-known antibacterial agent, was taken to be the positive control for the bacterial strains. Amphotericin-B was used as the positive control against the fungal strains. Cell-peptide mixtures were then incubated at 37 °C and 25 °C, respectively, for the bacterial and fungal cells, for a period of 4 h inside an orbital shaker incubator with uniform shaking of 150 rpm. After 4 h of incubation, 100 µL of the respective media were added to the wells of the 96-well microtiter plates and kept for overnight growth at the same temperature and shaking conditions as mentioned above. Post incubated mixtures were then subjected to optical density (OD) value measurements at 600 nm. Percentage killing of the bacterial/fungal samples incubated with various concentrations of the peptides was then determined from the OD values obtained at 600 nm and compared with the OD values obtained for the negative control and positive control, respectively. All experiments were performed in a set of triplicates, and each of the experiments was repeated at least twice.

$MIC_{90\%}$ of the peptides against all strains was also determined in the presence of salts. For the salt-tolerant experiment, PBS (10 mM) of pH 7.4 was used, instead of PB (10 mM) for MIC determination. Exactly, the same protocol was followed in this case, as described above. Washing, resuspensions, and dilutions of the cells, as well as preparation of peptide stock solutions and their dilutions, were carried out in PBS instead of PB.

$MIC_{90\%}$ values of the peptides were also determined against *P. aeruginosa* in the presence of 1.25 mM Ca^{2+}, 1 mM Mg^{2+}, 150 mM Na^{+}, 4 µM Fe^{3+}, and 8 µM Zn^{2+}. To a PB solution of pH 7.4 and strength 10 mM, weighed amounts of different metal salts were added so as to obtain the concentrations of the metal ions as mentioned above. The basic protocol for the determination of

the MIC values remained the same as mentioned previously, except for the fact that respective metal salts containing PB were used for the purpose of washing and dilutions of the cells, as well as for the dilution of the peptides and preparation of the peptide stock solutions in each case.

2.5.5. Time-kill kinetics

P. aeruginosa, *K. pneumoniae*, and *S. aureus* were grown in their respective media. Bacterial cells obtained at their midlogarithmic phases after consecutive washings were serially diluted to the order of 10^5 CFU/mL in PB solution (pH 7.4, 10 mM). 50 µL of the cell suspensions were added to 50 µL of the peptides at their respective MIC values determined previously and incubated for different time intervals. 5 µL of the cell-peptide mixture at each incubated time interval was withdrawn and pipetted on solidified agar plate rich in media, spread uniformly on the agar plate using a cell-spreader, sealed with a parafilm strip, and allowed to incubate at 37 °C overnight. Post incubation, plates were visualized and photographed, and the colonies were counted for each of the plates. The number of colonies at each time interval point were counted and plotted as a function of log CFU vs time.

2.5.6. Cell survival assay or MTT assay

HDF and HeLa cells were seeded at a density of 2000 and 5000 cells/well, respectively, in a 96-well plate. Consequently, the cells were treated with different concentrations of peptides in triplicates ranging from 0 to 160 µM for 24 h. Post treatment, the cells were incubated with 0.25 mg/mL of 3-(4,5-dimethylthiazol-2-yl)-2,5-diphenyltetrazolium bromide (MTT) and were further incubated at 37 °C for 2 h. Then, the formazan crystals formed were dissolved using dimethyl sulfoxide, and the readings were taken at 570 nm with 650 nm as the reference using a multiplate reader (Multiskan GO, Thermo-Scientific). The percentage of survival of the cells was calculated. Experiments were repeated at least twice.

2.5.7. Hemolytic activity

Human blood was collected in an EDTA vial from a healthy donor. Blood was centrifuged at 5000 rpm for 10 min. The serum obtained as the supernatant was discarded, while RBCs precipitated as the pellet was washed with PBS (10 mM, pH 7.4) and resuspended in the same buffer. 1 mL of the 1% washed RBCs were then treated with peptides of different concentrations in PBS and kept incubated for 1 h. Untreated RBCs and those treated with 1% of Triton X-100 were used as the negative and positive controls, respectively. At the end of the incubation period, peptide incubated

RBCs, untreated RBCs as well as those treated with 1% Triton-X 100 were centrifuged. 100 µL of the supernatants were pipetted out on a 96-well sterile plate, and their OD values were determined at 540 nm. Percentage hemolysis was determined by comparing the OD values of the peptide-incubated RBCs with that of the untreated and 1% Triton X-100 treated RBCs.

2.5.8. FACS

P. aeruginosa cells at their midlog phase were centrifuged, washed, and resuspended in PB (10 mM, pH 7.4). The OD value of the resuspended cells was determined, and the cells were adjusted to have a final OD value of 0.1. 1 mL of these cell suspensions were treated with 1× MICs and 2 × MICs of the respective peptides along with 10 µL of PI (stock solution: 1 mM) solution and incubated for 40 min. Untreated cells of the same OD value treated with PI were used as the negative control for the experiment. Cell sorting data was acquired using a BD LSR Fortessa flow cytometry analyzer at an operating wavelength of 488 nm. One hundred thousand events were recorded each of the times. BD FACS Diva software was used to analyze the percentage of live and dead cells.

2.5.9. CD

Secondary structures of the peptides in the free state as well as in the presence of membrane mimics were determined using CD spectroscopy. CD spectra of 50 µM of the peptide solutions in mili-Q water, 30 mM SDS solution, 10 mM DPC solution, and in 50% TFE were recorded. The spectra were acquired by pipetting out 250 µL of each of the solutions in a 300 µL Hemla quartz cuvette of 1 mm path length. A wavelength range of 190-260 nm, a scanning rate of 100 nm/ min, a data pitch of 1 nm, a response time of 4 s, and a bandwidth of 1 s were the parameters used while acquiring the spectra. Spectra were acquired using a JASCO J-1500 CD spectrometer.

2.5.10. Protease-resistant experiment

A mixture of chymotrypsin, proteinase K, and trypsin in the ratio of 1:1:1 (each of the enzymes at a strength of 1 mg/mL) was added to each of the peptides and incubated at 37° C for two time intervals of 30 min and 6 h. Post incubation, the reactions were quenched by an equal volume of ACN solution containing 1% TFA. An analytic reverse phase column (Thermo-scientific, Biobasic-18, dimension: 150 × 4.6, particle size: 5 μ) was used to acquire the HPLC traces of the enzyme-incubated peptides and untreated peptides with an increasing ACN percentage of 5-100%

at a flow rate of 1 mL/ min for 20 min. The elution of the peptides or peptide fragments was monitored at an UV wavelength of 214 nm. All traces were acquired using an Agilent 1260 Infinity II analytic HPLC system (Agilent Technologies). Untreated and enzyme-treated peptides were further subjected to characterization using MALDI-TOF. Spectra were acquired using a Bruker Autoflex Speed MALDI-TOF mass spectrometer (Bruker).

2.5.11. MIC determination of P5 and P5C in the presence of enzymes

To a solution of P5 and P5C (10 mM), a mixture of three enzymes, chymotrypsin, proteinase-K, and trypsin (1 mg/mL each), was added and incubated for a period of 6 h at a temperature of 37 °C. Post incubation, the reactions were quenched using 1% TFA in ACN. Enzyme-quenched peptide solutions were then diluted to a final concentration of 1 mM. $MIC_{90\%}$ of enzyme-treated P5 and P5C was determined using the microbroth dilution assay as described earlier.

2.5.12. Serum stability experiment

Human blood collected from a healthy volunteer was centrifuged to obtain the serum as the supernatant. Peptide stock solution each of strength 10 mM was prepared using PBS (10 mM, pH 7.4) as the solvent. To 20 µL of each of these peptide solutions (10 mM), another 20 µL of the serum was added. Peptide serum mixtures were incubated for different time intervals, viz., 30 min, 1, 3, 6, and 24 h. Peptides incubated with serum post incubation period were subjected to quenching using an equal volume of a mixture of ACN, methanol, and water (ACN: MeOH: H_2O = 8:1:1). Addition of this mixture resulted in the formation of a white precipitate due to coagulation of the serum. This precipitated sample was then centrifuged at 8000 rpm for 10 min, and the supernatant was collected. Untreated peptides adjusted to the same final concentrations as that of the peptides treated with serum were used as the negative control. Peptides treated with serum for different time intervals were subjected to analytical HPLC, and the percentage of intact peptides was quantified by determining the area under the peptide peaks (for serum treated peptides) and comparing the same with the area under the peaks for untreated peptides using Agilent Open Lab CDS software.

2.5.13. Determination of peptide potency in the presence of serum ($MIC_{90\%}$)

The serum was obtained as described above. *P. aeruginosa* cells, grown until mid-log phase were centrifuged, washed with PB (10 mM, pH 7.4), and were finally suspended in serum to the order of 10^5 CFU/mL using serial dilution method. To 50 µL of this cell suspension in serum, another 50

µL of the peptides diluted at different concentrations in PB (10 mM, pH 7.4) ranging from 5 to 200 µM were added. This peptide-cell mixture was incubated at 37 °C under continuous orbital shaking for 4 h, which was followed by addition of another 100 µL of NB media kept incubated overnight. Untreated cells were the negative control, while the cells treated with 10 µM polymyxin-B was used as the positive control for the experiment. Post incubation, the OD values corresponding to the different concentrations of the peptides were determined at 600 nm, and the $MIC_{90\%}$ values of the peptides were determined in reference to the negative and positive controls.

2.5.14. Inner membrane permeation assay

P. aeruginosa cells were washed with PB (pH 7.4) and were diluted to a final strength of 10^6 CFU/mL. To 1 mL of this cell suspensions, PI dye was added at a final concentration of 10 µM and kept incubated for 30 min at 37 °C under constant shaking conditions. The fluorescence of the cell suspension containing PI was monitored for a period of 2400 s at room temperature. The fluorescence spectra of this cell suspension treated with 0.5× MIC, 1× MIC of P4C, P5C, and 0.1% Triton X-100 (positive control) were also monitored one after the other. The excitation wavelength was set at 535 nm with a slit width of 10 nm, while the emission wavelength was set at 617 nm also having a slit width of 10 nm. All spectra were acquired using a Fluoromax Spectrofluorometer (Horiba Scientific).

2.5.15. Outer membrane permeation assay

10 µM NPN dye was added to 1 mL of *P. aeruginosa* cells (10^6 CFU/mL), obtained after centrifugation, washing, and serial dilution of the cells in PB. This cell suspension containing NPN was incubated at 37 °C under constant orbital shaking for a period of 30 min and then subjected to fluorescence measurement for 1200 s excited by an excitation wavelength of 350 nm having a slit width of 5 nm and by an emission wavelength of 410 having a slit width of 5 nm using a Fluoromax Spectrofluorometer (Horiba scientific). After the spectra for the untreated cells were acquired, cells treated with 0.5× MIC, 1×MIC of P4C, P5C, and 0.1% of Triton X-100 (positive control) were also studied, and their respective spectra were acquired.

2.5.16. Blue shift experiment

Intrinsic fluorescence properties of tryptophan residue present in P4C and P5C were used to study their interaction with the bacterial membrane mimic SDS as well as the mammalian membrane

mimic DPC. 1 mL of the peptides at their respective MIC values were taken on a fluorescence cuvette and titrated against increasing concentrations of SDS or DPC (0.25-20 times the concentrations of the peptides). Peptide solutions were excited by an excitation wavelength of 280 nm and 10 nm slit width, and the fluorescence spectra were acquired over a wavelength range of 300-450 nm using a Fluoromax Spectrofluorometer (Horiba scientific).

2.5.17. Live cell blue shift experiments

P. aeruginosa cells washed with PB (10 mM, pH 7.4) were concentrated to a final strength of 10^9 CFU/mL. Increasing concentrations of this cell suspension (10 µL at each step) were added to P4C and P5C at their respective MICs. The fluorescence spectra of the peptides (MICs) alone and upon addition of the cell suspensions at each step were recorded at an excitation wavelength of 280 nm, 5 nm slit width, and in the wavelength range of 295-450 nm. All spectra were acquired using a Fluoromax Spectrofluorometer (Horiba scientific). The $\Delta\lambda$ shift values were plotted against the increasing number of cells.

2.5.18. Solvent accessibility experiment

P4C and P5C at their respective MIC values were titrated against D8PG (a bacterial membrane mimic) and DPC (a mammalian membrane mimic) up to a concentration of 20 times the concentration of the peptides. These peptide-D8PG complexes [P4C-D8PG (1:20) and P5C-D8PG (1:20)] and the peptide-DPC complexes [P4C-DPC (1:20) and P5C-DPC (1:20)] together with the free peptides at their respective MIC values were titrated against an increasing concentration of acrylamide solution, a static quencher varying from 10 to 250 mM. The fluorescence spectra of the free peptides and the peptides in the form of their complexes at the beginning and after addition of acrylamide each time were acquired over a wavelength range of 295−450 nm having a slit width of 10 nm and an excitation wavelength of 280 nm using a Fluoromax Spectrofluorometer (Horiba Scientific). The intensity of the peptides and the peptide-D8PG/DPC complexes at their λmax values was determined from the spectra acquired and fitted to a linear plot following the Stern-Volmer equation.

2.5.19. ITC

Interaction P4C and P5C with LPS (extracted from *P. aeruginosa*) and DPC (a mammalian membrane mimic) were studied using ITC. A solution of the LPS of strength 100 µM (above the

critical micellar concentration value of LPS) in PB (pH 7.4 and strength 10 mM) was prepared, thoroughly vortexed, and sonicated before the start of the experiment. Peptide solutions of the strength 30 times (3 mM) the strength of the LPS solution were prepared using the same PB solution. The reaction was set up at 37 °C, and 2 µL of the peptides were injected each time into the cell for 20 consecutive times, maintaining a uniform stirring speed of 350 rpm. Post titration, the plots corresponding to each titration were fitted to a one-binding site model and thermodynamic parameters such as association constant (Ka), enthalpy change (ΔH), Gibb's free energy change (ΔG), and entropy change (ΔS) were determined.

Next, the binding affinity of P4C and P5C was determined against DPC. Peptide solutions of strength 0.5 mM were prepared using PB (10 mM, pH 7.4) and 280 µL of each of the peptides were placed in the cell. DPC solution 40 times (20 mM) the concentration of the peptides prepared in the same buffer was loaded in the syringe. 2 µL of the DPC solution was titrated against the peptides for 20 consecutive times spanning over a period of 1 h, maintaining a speed of 350 rpm and a temperature of 37 °C. DPC titrated against both the peptides was fitted to a one-binding site model and the thermodynamic parameters were determined from the fitted curves. All the ITC experiments were performed on a iTC 200 Microcalorimeter (Make: GE Health Care).

2.5.20. Live cell NMR experiment

P. aeruginosa cells washed in PB (10 mM, pH 7.4) were concentrated to a final concentration of 10^8 cells/CFU using a PB solution (10 mM, pH 6.5) and 10% D_2O. ^1H NMR spectra for the untreated cells, peptides P4C and P5C (1 mM, prepared in PB of pH 6.5 and 10% D_2O), and the cells treated with P4C and P5C (1 mM) for different time intervals were acquired on a Bruker 400 MHz NMR spectrometer. All spectra were recorded at room temperature.

2.5.21. FESEM imaging of the peptide-treated bacterial cells

Freshly grown *P. aeruginosa* were diluted to the order of 10^6 CFU/mL. 50 µL of these cells were treated with another 50 µL of the peptides P4C and P5C at their respective 1× MIC, 2× MIC, and 4× MICs and incubated for 2 h at 37 °C. Untreated cells were maintained as the negative control. Post incubation, both peptide-treated and untreated cells were fixed with 2.5% glutaraldehyde and further incubated and subsequently washed. The washed cells were finally resuspended in the same buffer and casted on silicon wafers and allowed to dry overnight. Dried

samples were then washed with various percentages of ethyl alcohol and redried. FESEM images were captured after gold-coating of the silicon wafers containing the bacterial samples using a field emission scanning electron microscope (Zeiss, Model: Gemini 300).

2.5.22. FETEM imaging of the peptide-treated bacterial cells

P. aeruginosa cells washed and diluted to the order of 10^6 CFU/mL were treated with 1× MICs and 2×MICs of the peptides P4C and P5C. The cell-peptide mixtures were kept incubated for a period of 2 h at 37 °C with continuous shaking. Each of 3 µL of the untreated cells and those of the cells treated with 1×and 2× MICs of the peptides were then casted on TEM grids followed by staining with 1% uranyl acetate solution. The samples were dried and FETEM images were captured using a field emission transmission electron microscope (JEOL, Model: 2100 F).

2.5.23. Confocal images

P. aeruginosa obtained from a fresh grown culture were diluted to a concentration of 10^6 CFU/mL. 5(6)-carboxyfluorescein tagged P4C (Cf-P4C) and P5C (Cf-P5C) at concentrations corresponding to the respective $MIC_{90\%}$ of P4C and P5C were added to the cells and incubated at room temperature for 5 min. 5 µL of the cells (untreated, Cf-P4C-treated and Cf-P5C-treated) were pipetted on the surface of a clean glass slide and covered with a coverslip for acquiring the images. Fluorescent images were captured at 488 nm using a TCS SP8 confocal microscope and Leica software.

2.5.24. Simulation setup for the synthesized peptides in the presence and absence of SDS micelles

Extended conformation of the peptides (P4C and P5C; N- and C-terminals were capped with $-NH_3^+$ and $-CONH_2$, respectively) were modelled using PyMOL.[45] The peptide was kept at the center of a cubic water box and subjected to MD simulations (Table A1, Appendix A). The simulation box was neutralized by adding chloride ions (Cl^-). CHARM-GUI Membrane Builder[46-47] was used to model the SDS micelle (simplest bacterial membrane-mimetic system), which included 60 SDS molecules. The SDS micelle was placed at the center of a cubic water box and neutralized by adding 60 Na^+ counterions. The resulting simulation box was subjected to minimization, equilibration, and production MD simulations. The final structure of the solvated micelle was selected for studying peptide:micelle binding. The peptides (P4C, P5C) were initially

placed ~2 nm away from the micelle surface (Figure A46 & Table A1, Appendix A) and subjected to MD simulations. The production MD trajectories of the P4C/P5C:SDS micelle complex were used for structural analysis and binding affinity estimation. Simulations were triplicated to ensure adequate sampling and convergence. Peptide:micelle-binding affinity was estimated using MM/PBSA method. Previously adopted methodology[31] for the binding affinity estimation of the L peptides (P4 and P5) to the micelle has been adopted for this work as well.

2.5.25. Simulation setup for peptide-bound proteases

X-ray structure of bovine trypsin protease (223 residues) in complex with squash-inhibitor (PDB 2BTC; resolution = 1.5 A)[48] was retrieved from the RCSB database.[49] Squash-inhibitor is a 29 amino acid residue long peptide sequence. Only seven residues (sequence: RVCPKIL) from the N-terminal of the squash inhibitor were selected and mutated to model P4-bound trypsin complex (PDB 2BTC as template). Modelling P4 (sequence: LKWLKKL) in complex with trypsin was achieved by mutating the side chains except for the fifth and seventh residues of the truncated inhibitor. It should be noted that the fifth residue of the N-terminal of the squash-inhibitor was the lysine residue (containing the scissile carbonyl group), which was recognized by the side chain binding pocket of the trypsin protease. The high-resolution X-ray structure of the ligand-free bovine trypsin protease (PDB 4I8G; resolution = 0.8 A)[50] was also retrieved and compared with the protease structure of PDB 2BTC. The structure of the trypsin protease was found to be more or less identical (heavy atom RMSD ~ 0.29 A) in the PDB 2BTC and PDB 4I8G. Thus, it might be argued that the structure of the trypsin protease was independent of the inhibitor binding. We overlaid the structure of the P4-bound trypsin protease (using PDB 2BTC as a template) to the high resolution X-ray structure of free trypsin protease (PDB 4I8G) and deleted the peptide in the former. The resulting model of P4 bound to trypsin protease (template PDB 4I8G) was subjected to MD simulation. Models of the trypsin:P5 complex were obtained by mutating Lys → Arg (second, fifth, and sixth positions) in the trypsin:P4 complex. Models of D-peptide (P4C/P5C) bound trypsin were obtained by altering the stereochemistry (L → D conversion) of the peptide residues in the trypsin:P4/P5 complexes. The models of the complex were generated using PyMOL[45] software.

Similarly, the X-ray structure of chymotrypsin with the ligand (*n*-acetyl-leucil-phenylalanine aldehyde) bound at the active site (PDB 1GGD; resolution = 1.5 A)[51] was retrieved and used as a

template for modelling the chymotrypsin:P4 complex. The phenylalanine residue of the ligand was found to be placed in the hydrophobic side chain binding pocket of chymotrypsin. Thus, phenylalanine of the ligand (in PDB 1GGD) was mutated to tryptophan (W3) and then extended on both sides to model the chymotrypsin:P4 complex. Chymotrypsin:P4C complexes were modelled as described for the trypsin complexes.

The protease:peptide complexes were solvated, and monovalent ions (Cl^-) were added to neutralize the simulation box (Table A1, Appendix A). The resulting simulation setup was subjected to energy minimization, equilibration, and production dynamics. During equilibration (at *NPT* ensemble), the atomic restraints were gradually removed (from all heavy atoms → Cα atoms only → finally, no restraints). CHARMM36m[52] force field was used to describe the biomolecular system. CHARMM-modified TIP3P[53-54] water model was used to describe water molecules. Each simulation system was triplicated by differing the initial velocities. MD trajectories were visualized using VMD[55] and PyMOL.[45] The final MD structure of the protein:peptide complex was selected and subjected to the center of mass pulling simulations (steered molecular dynamics). Protein:peptide dissociation event cannot be captured by conventional MD simulations. Center of mass pulling (SMD) generates structures along the biased dissociation pathway (Figure A47, Appendix A). Each SMD structure (of the biased dissociation pathway) was considered the starting configuration for the equilibrium umbrella sampling simulation. A series of umbrella sampling windows were combined using the weighted histogram analysis method (WHAM)[56-57] for estimating the potential of mean force (PMF or free-energy profile of dissociation). The adopted methodology has been extensively explained elsewhere.[31] SMD (at a pulling rate = 0.0005 nm/ps) generated a total of 21 windows separated by a spacing of 0.1 nm (in COM distance). Each window was subjected to 500 ps equilibration followed by 50 ns of umbrella sampling simulations at the *NPT* ensemble. A total of ~1.05 μs of umbrella sampling simulations were used to estimate the free-energy profile (PMF) using WHAM. To ensure reliability and achieve convergence, each system was triplicated with different initial velocities, which makes a total of a ~3.15 μs production umbrella sampling for every system. A total of (3.15 × 5) ~ 15.75 μs umbrella sampling simulations have been used for estimating the binding affinities (Tables 2.6 & Table A2, Appendix A).

2.5.26. Enzyme kinetics: trypsin protease activity assay

Peptide substrates (P4 or P4C in PB of strength 10 mM and pH 7.4) of various concentrations (1, 2, 3, 4, and 5 mM) were added to the commercially purchased porcine pancreas trypsin enzyme (10 μM). The substrate was incubated with the trypsin enzyme for different time intervals (5, 15, 30 min, 1, 3, 6, 12, and 24 h) under continuous shaking conditions at room temperature. The reaction was quenched with TFA after each incubation periods, and the concentration of the product (degraded peptide) was estimated from the HPLC peaks. The concentration of the product was plotted as a function of time, and the initial rates were calculated from the region where the concentration increased linearly with time. The initial rates as a function of substrate-concentration were plotted and fitted with the Michaelis-Menten equation for estimating the kinetic parameters (Figure 2.21). Same methodology was adopted for P5 and P5C (substrate: 1, 1.5, 2, 3, and 4 mM). Peptide degradation was not observed for the D peptides P4C and P5C.

References

1. Lei, J.; Sun, L.; Huang, S.; Zhu, C.; Li, P.; He, J.; Mackey, V.; Coy, D. H.; He, Q. The antimicrobial peptides and their potential clinical applications. *Am. J. Transl. Res.* **2019**, *11*, 3919-3931.
2. Sarkar, T.; Chetia, M.; Chatterjee, S. Antimicrobial Peptides and Proteins: From Nature's Reservoir to the Laboratory and Beyond. *Front. Chem.* **2021**, *9*, 691532.

3. López-Otín, C.; Bond, J.S. Proteases: multifunctional enzymes in life and disease. *J. Biol. Chem*. **2008**, *283*, 30433-30437.

4. Robinson, P. K. Enzymes: principles and biotechnological applications. *Essays Biochem.* **2015**, *59*, 1-41.

5. Weinstock, M. T.; Francis, J. N.; Redman, J. S.; Kay, M. S. Protease-resistant peptide design-empowering nature's fragile warriors against HIV. *Biopolymers* **2012**, *98*, 431-442.

6. Lu, J.; Xu, H.; Xia, J.; Ma, J.; Xu, J.; Li, Y.; Feng, J. D-and Unnatural amino acid Substituted Antimicrobial Peptides with Improved Proteolytic Resistance and Their Proteolytic Degradation Characteristics. *Front. Microbiol.* **2020**, *11*, 563030.

7. Oliva, R.; Chino, M.; Pane, K.; Pistorio, V.; De Santis, A.; Pizzo, E.; D' Errico, G.; Pavone, V.; Lombardi, A.; Vecchio, V. D.; Notomista, E.; Nastri, F.; Petraccone, L. Exploring the role of unnatural amino acids in antimicrobial peptides. *Sci. Rep.* **2018**, *8*, 8888.

8. Hitchner, M. A.; Necelis, M. R.; Shirley, D.; Caputo, G. A. Effect of Non-natural Hydrophobic Amino Acids on the Efficacy and Properties of the Antimicrobial Peptide C18G. *Probiotics Antimicrob. Proteins* **2021**, *13*, 527-541.

9. He, S.; Yang, Z.; Li, X.; Wu, H.; Zhang, L.; Shan, A.; Wang, J. Boosting stability and therapeutic potential of proteolysis-resistant antimicrobial peptides by end-tagging *β*-naphthylalanine. *Acta Biomater.* **2023**, *164*, 175-194.

10. Jimenez, E. C.; Watkins, M.; Juszczak, L. J.; Cruz, L. J.; Olivera, B. M. Contryphans from Conus textile venom ducts. *Toxicon* **2001**, *39*, 803-808.

11. Soutourina, J.; Plateau, P.; Blanquet, S. Metabolism of D-aminoacyl- tRNAs in Escherichia coli and Saccharomyces cerevisiae cells. *J. Biol. Chem.* **2000**, *275*, 32535-32542.

12. Bardaweel, S. K.; Abu-Dahab, R.; Almomani, N. F. An in vitro based investigation into the cytotoxic effects of D-amino acids. *Acta Pharm.* **2013**, *63*, 467-478.

13. Grishin, D. V.; Zhdanov, D. D.; Pokrovskaya, M. V.; Sokolov, N. N. D-amino acids in nature, agriculture and biomedicine. *All Life* **2020**, *13*, 11-22.

14. Li, Y.; Liu, T.; Liu, Y.; Tan, Z.; Ju, Y.; Yang, Y.; Dong, W. Antimicrobial activity, membrane interaction and stability of the Damino acid substituted analogs of antimicrobial peptide W3R6. *J. Photochem. Photobiol. B* **2019**, *200*, 111645.

15. Jia, F.; Wang, J.; Peng, J.; Zhao, P.; Kong, Z.; Wang, K.; Yan, W.; Wang, R. D-amino acid substitution enhances the stability of antimicrobial peptide polybia-CP. *Acta Biochim. Biophys. Sin. (Shanghai)* **2017**, *49*, 916-925.

16. Kapil, S.; Sharma, V. D-Amino acids in antimicrobial peptides: a potential approach to treat and combat antimicrobial resistance. *Can. J. Microbiol.* **2021**, *67*, 119-137.

17. Li, H.; Anuwongcharoen, N.; Malik, A. A.; Prachayasittikul, V.; Wikberg, J. E.; Nantasenamat, C. Roles of d-Amino Acids on the Bioactivity of Host Defense Peptides. *Int. J. Mol. Sci.* **2016**, *17*, 1023.

18. Hamamoto, K.; Kida, Y.; Zhang, Y.; Shimizu, T.; Kuwano, K. Antimicrobial activity and stability to proteolysis of small linear cationic peptides with D-amino acid substitutions. *Microbiol. Immunol.* **2002**, *46*, 741-749.

19. Kaminki, H. M.; Feix, J. B. Effects of D-Lysine Substitutions on the Activity and Selectivity of Antimicrobial peptide CM15. *Polymers* **2011**, *3*, 2088-2106.

20. Di Grazia, A.; Cappiello, F.; Cohen, H.; Casciaro, B.; Luca, V.; Pini, A.; Di, Y. P.; Shai, Y.; Mangoni, M. L. D-Amino acids incorporation in the frog skin-derived D-peptide esculentin-1a(1-21)NH_2 is beneficial for its multiple functions. *Amino Acids* **2015**, *47*, 2505-2519.

21. Zaet, A.; Dartevelle, P.; Daouad, F.; Ehlinger, C.; Quile`s, F.; Francius, G.; Boehler, C.; Bergthold, C.; Frisch, B.; Prevost, G.; Lavalle, P.; Schneider, F.; Haikel, Y.; Boutigue, M. H. M.; Marban, C. D-Cateslytin, a new antimicrobial peptide with therapeutic potential. *Sci. Rep.* **2017**, *7*, 15199.

22. Sun, S.; Zhao, G.; Huang, Y.; Cai, M.; Yan, Q.; Wang, H.; Chen, Y. Enantiomeric Effect of d-Amino Acid Substitution on the Mechanism of Action of α-Helical Membrane-Active Peptides. *Int. J. Mol. Sci.* **2018**, *19*, 67.

23. Manabe, T.; Kawasaki, K. D-form KLKLLLLLKLK-NH_2 peptide exerts higher antimicrobial properties than its L-form counterpart via an association with bacterial cell wall components. *Sci. Rep.* **2017**, *7*, 43384.

24. Ye, Z.; Zhu, X.; Acosta, S.; Kumar, D.; Sang, T.; Aparicio, C. Self-assembly dynamics and antimicrobial activity of all l- and d-amino acid enantiomers of a designer peptide. *Nanoscale* **2019**, *11*, 266− 275.

25. Zhong, C.; Zhu, N.; Zhu, Y.; Liu, T.; Gou, S.; Xie, J.; Yao, J.; Ni, J. Antimicrobial peptides conjugated with fatty acids on the side chain of D-amino acid promises antimicrobial potency against multidrug-resistant bacteria. *Eur. J. Pharm. Sci.* **2020**, *141*, 105123.

26. Di, Y. P.; Lin, Q.; Chen, C.; Montelaro, R. C.; Doi, Y.; Deslouches, B. Enhanced therapeutic index of an antimicrobial peptide in mice by increasing safety and activity against multidrugresistant bacteria. *Sci. Adv.* **2020**, *6*, eaay6817.

27. Garton, M.; Nim, S.; Stone, T. A.; Wang, K. E.; Deber, C. M.; Kim, P. M. Method to generate highly stable D-amino acid analogs of bioactive helical peptides using a mirror image of the entire PDB. *Proc. Natl. Acad. Sci. USA* **2018**, *115*, 1505-1510.

28. Eberle, R. J.; Sevenich, M.; Gering, I.; Scharbert, L.; Strodel, B.; Lakomek, N. A.; Santur, K.; Mohrlu¨der, J.; Coronado, M. A.; Willbold, D. Discovery of All-d-Peptide Inhibitors of SARS-CoV-2 3C-like Protease. *ACS Chem. Biol.* **2023**, *18*, 315-330.

29. Hernandez Gonzalez, J. E.; Eberle, R. J.; Willbold, D.; Coronado, M. A. A Computer-Aided Approach for the Discovery of D-Peptides as Inhibitors of SARS-CoV-2 Main Protease. *Front. Mol. Biosci.* **2022**, *8*, No. 816166.

30. Pandit, G.; Ilyas, H.; Ghosh, S.; Bidkar, A. P.; Mohid, S. A.; Bhunia, A.; Satpati, P.; Chatterjee, S. Insights into the Mechanism of Antimicrobial Activity of Seven-Residue Peptides. *J. Med. Chem.* **2018**, *61*, 7614-7629.

31. Ghosh, S.; Sarkar, T.; Chatterjee, S.; Satpati, P. Bridging Thermodynamics, Antimicrobial Activity, and pH Sensitivity of Cationic Membranolytic Heptapeptides-A Computational and Experimental Study. *J. Chem. Inf Model.* **2023**, *63*, 2393-2408.

32. Hancock, R. E. W.; Lehrer, R. Cationic peptides: a new source of antibiotics. *Trends Biotechnol.* **1998**, *16*, 82-88.

33. Geitani, R.; Moubareck, C. A.; Touqui, L.; Sarkis, D. K. Cationic antimicrobial peptides: alternatives and/or adjuvants to antibiotics active against methicillin-resistant Staphylococcus aureus and multidrug-resistant Pseudomonas aeruginosa. *BMC Microbiol.* **2019**, *19*, 54.

34. Rivera-Sanchez, S. P.; Agudelo-Gongora, H. A.; On˜ate-Garzon, J.; Florez-Elvira, L. J.; Correa, A.; London˜o, P. A.; London˜o-Mosquera, J. D.; Aragon-Muriel, A.; Polo-Ceron, D.; Ocampo-Iban˜ez, I. D. Antibacterial Activity of a Cationic Antimicrobial Peptide against Multidrug-Resistant Gram-Negative Clinical Isolates and Their Potential Molecular Targets. *Molecules* **2020**, *25*, 5035.

35. Hancock, R. E. W.; Rozek, A. Role of membranes in the activities of antimicrobial cationic peptides. *FEMS Microbiology Letters* **2002**, *206*, 143-149.

36. Kundu, R. Cationic Amphiphilic Peptides: Synthetic Antimicrobial Agents Inspired by Nature. *ChemMedChem.* **2020**, *15*, 1887-1896.

37. Wenzel, M.; Chiriac, A. I.; Otto, A.; Zweytick, D.; May, C.; Schumacher, C.; Gust, R.; Albada, H. B.; Penkova, M.; Kramer, U.; Erdmann, R.; Metzler-Nolte, N.; Straus, S. K.; Bremer, E.; Becher, D.; Brotz-Oesterhelt, H.; Sahl, H. G.; Bandow, J. E. Small cationic antimicrobial peptides delocalize peripheral membrane proteins. *Proc. Natl. Acad. Sci. USA* **2014**, *111*, E1409-E1418.

38. Omardien, S.; Brul, S.; Zaat, S. A. J. Antimicrobial Activity of Cationic Antimicrobial Peptides against Gram-Positives: Current Progress Made in Understanding the Mode of Action and the Response of Bacteria. *Front. Cell Dev. Biol.* **2016**, *4*, 111.

39. Ma, W.; Tang, C.; Lai, L. Specificity of trypsin and chymotrypsin: loop-motion-controlled dynamic correlation as a determinant. *Biophys. J.* **2005**, *89*, 1183-1193.

40. Vajda, T.; Szabo, T. Specificity of trypsin and alpha chymotrypsin towards neutral substrates. *Acta Biochim. Biophys. Acad. Sci. Hung.* **1976**, *11*, 287-294.

41. Amand, H. L.; Fant, K.; Norden, B.; Esbjorner, E. K. Stimulated endocytosis in penetratin uptake: effect of arginine and lysine. *Biochem. Biophys. Res. Commun.* **2008**, *371*, 621-625.

42. Mitchell, D. J.; Kim, D. T.; Steinman, L.; Fathman, C. G.; Rothbard, J. B. Polyarginine enters cells more efficiently than other polycationic homopolymers. *J. Pept Res.* **2000**, *56*, 318-325.

43. Gonzales, T.; Robert-Baudouy, J. Bacterial aminopeptidases: properties and functions. *FEMS Microbiol. Rev.* **1996**, *18*, 319-344.

44. Akbarian, M.; Khani, A.; Eghbalpour, S.; Uversky, V. N. Bioactive Peptides: Synthesis, Sources, Applications, and Proposed Mechanisms of Action. *Int. J. Mol. Sci.* **2022**, *23*, 1445.

45. Schrödinger, L.L.C. *The PyMOL Molecular Graphics System, Version 2.4.0*; **2010**. https://pymol.org/2/ (accessed May 2021).

46. Lee, J.; Cheng, X.; Swails, J. M.; Yeom, M. S.; Eastman, P. K.; Lemkul, J. A.; Wei, S.; Buckner, J.; Jeong, J. C.; Qi, Y.; Jo, S.; Pande, V. S.; Case, D. A.; Brooks, C. L.; MacKerell, A. D.; Klauda, J. B.; Im, W. CHARMM-GUI Input Generator for NAMD, GROMACS, AMBER, OpenMM, and CHARMM/OpenMM Simulations Using the CHARMM36 Additive Force Field. *J. Chem. Theory Comput.* **2016**, *12*, 405-413.

47. Wu, E. L.; Cheng, X.; Jo, S.; Rui, H.; Song, K. C.; Davila- Contreras, E. M.; Qi, Y.; Lee, J.; Monje-Galvan, V.; Venable, R. M.; Klauda, J. B.; Im, W. CHARMM-GUI Membrane Builder towards Realistic Biological Membrane Simulations. *J. Comput. Chem.* **2014**, *35*, 1997-2004.

48. Helland, R.; Berglund, G. I.; Otlewski, J.; Apostoluk, W.; Andersen, O. A.; Willassen, N. P.; Smalas, A. O. High-Resolution Structures of Three New Trypsin-Squash-Inhibitor Complexes: A Detailed Comparison with Other Trypsins and Their Complexes. *Acta Crystallogr. D Biol. Crystallogr.* **1999**, *55*, 139-148.

49. Burley, S. K.; Bhikadiya, C.; Bi, C.; Bittrich, S.; Chao, H.; Chen, L.; Craig, P. A.; Crichlow, G. V.; Dalenberg, K.; Duarte, J. M.; Dutta, S.; Fayazi, M.; Feng, Z.; Flatt, J. W.; Ganesan, S.; Ghosh, S.; Goodsell, D. S.; Green, R. K.; Guranovic, V.; Henry, J.; Hudson, B. P.; Khokhriakov, I.; Lawson, C. L.; Liang, Y.; Lowe, R.; Peisach, E.; Persikova, I.; Piehl, D. W.; Rose, Y.; Sali, A.; Segura, J.; Sekharan, M.; Shao, C.; Vallat, B.; Voigt, M.; Webb, B.; Westbrook, J. D.; Whetstone, S.; Young, J. Y.; Zalevsky, A.; Zardecki, C. RCSB Protein Data Bank (RCSB.Org): Delivery of Experimentally-Determined PDB Structures alongside One Million Computed Structure Models of Proteins from Artificial Intelligence/Machine Learning. *Nucleic Acids Res.* **2023**, *51*, D488-D508.

50. Liebschner, D.; Dauter, M.; Brzuszkiewicz, A.; Dauter, Z. On the reproducibility of protein crystal structures: five atomic resolution structures of trypsin. *Acta Crystallogr. D Biol. Crystallogr.* **2013**, *69*, 1447-1462.

51. Neidhart, D.; Wei, Y.; Cassidy, C.; Lin, J.; Cleland, W. W.; Frey, P. A. Correlation of low-barrier hydrogen bonding and oxyanion binding in transition state analogue complexes of chymotrypsin. *Biochemistry* **2001**, *40*, 2439-2447.

52. Huang, J.; Rauscher, S.; Nawrocki, G.; Ran, T.; Feig, M.; de Groot, B. L.; Grubmüller, H.; MacKerell, A. D., Jr. CHARMM36m: an improved force field for folded and intrinsically disordered proteins. *Nat. Methods.* **2017**, *14*, 71-73.

53. Jorgensen, W. L.; Chandrasekhar, J.; Madura, J. D.; Impey, R. W.; Klein, M. L. Comparison of Simple Potential Functions for Simulating Liquid Water. *J. Chem. Phys.* **1983**, *79*, 926-935.

54. Bussi, G.; Donadio, D.; Parrinello, M. Canonical sampling through velocity rescaling. *J. Chem. Phys.* **2007**, *126*, 014101.

55. Humphrey, W.; Dalke, A.; Schulten, K. VMD: visual molecular dynamics. *J. Mol. Graph.* **1996**, *14*, 33-38.

56. Kumar, S.; Rosenberg, J. M.; Bouzida, D.; Swendsen, R. H.; Kollman, P. A. The Weighted Histogram Analysis Method for Free-Energy Calculations on Biomolecules. *I. The Method. J. Comput. Chem.* **1992**, *13*, 1011-1021.

57. Hub, J. S.; de Groot, B. L.; van der Spoel, D. g_wham_A Free Weighted Histogram Analysis Implementation Including Robust Error and Autocorrelation Estimates. *J. Chem. Theory Comput.* **2010**, *6*, 3713-3720.

Chapter 3: Alchemical Simulation Aided *De novo* Design of Membrane Active Antimicrobial Hepta-Peptides

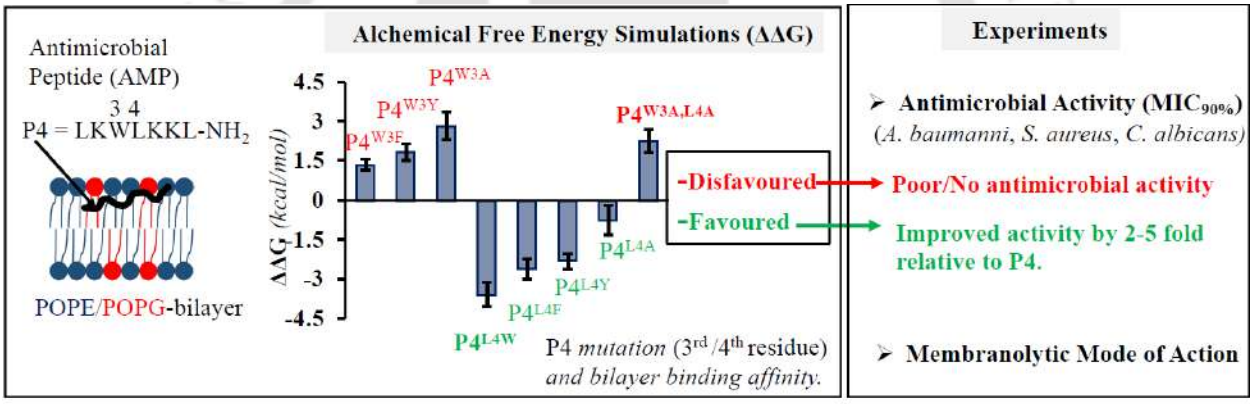

- ΔΔG ranks the antimicrobial potency of the cationic ultra-short membranolytic peptides.
- $P4^{L4W}$ ($P4^{W3A}$, $P4W^{3A,L4A}$) was predicted and verified as the most potent (inactive) membranolytic AMP.

3.1. Introduction

In an earlier study, we synthesized a short, cationic, and membranolytic heptapeptide P4 (LKWLKKL-NH_2 charge = +4) with moderate broad-spectrum membranolytic activity against several ESKAPE pathogens and fungal strains *in vitro*.[1] However, P4 was inactive against Methicillin-resistant *S. aureus* (MRSA). Being membranolytic, the peptide: cell-membrane association was a prerequisite for the manifestation of the antimicrobial activity of P4. The composition of the negatively charged bacterial membrane is rather complex, including the plasma membrane, cell wall, embedded proteins, small molecules, etc. Thus, computational models of the cell membranes (in atomic details) are limited by size and complexity. Membrane-mimetic micelles or bilayer models are simple, popular models used for studying peptide: membrane interactions. Recently, employing computer simulations on peptide: micelle/bilayer complexes, we successfully designed and synthesized a potent pH-sensitive P4-derivative AMP against acid-resistant *E. Coli*.[2] MD simulations (peptide binding to micelles) were successful in explaining the differential potency and cytotoxicity of 14-residue long cationic AMP (LL-14: LKWLKKLLKWLKKL-NH_2; doubling the P4 sequence) upon L→V mutation. We demonstrated that a slight decrease in the peptide hydrophobicity (Leu →Val mutation at the N-terminal of LL-14) could strongly disfavour SDS-micelle binding affinity by $\Delta\Delta G \sim 8$ kcal/mol, by weakening peptide: micelle electrostatic interactions. We highlighted the strong correlation between hydrophobicity and electrostatics in terms of atomic interactions and energetics of peptide: micelle complex.[3] In another study, we showed that Lys/Arg spacer length modification (hydrophobicity alteration) could strongly alter the energetics of peptide: bilayer binding by electrostatic fine-tuning.[4] Stronger binding affinity of arginine and arginine-containing peptides to the simple bilayer models relative to the lysine analogs attributed to the higher antimicrobial potency of the former. It is evident that molecular simulations of simple peptide: micelle/bilayer systems could successfully explain the experimental observations and play a vital role in the rational design of antimicrobial peptides.[5-12] The short cationic heptapeptide P4 served as an excellent template for systematic mutations to design AMPs with improved antimicrobial potency. Here, we employed alchemical free energy simulations to quantify the effect of amino acid substitution at the 3rd and the 4th residue of P4 on the bilayer binding affinity. We hypothesized that the cationic peptides with improved binding affinity to the bilayer would be more effective in their membranolytic activity. First, we performed molecular dynamics (MD) simulations of P4 and eight P4-mutants

(Figure 3.1) in the presence and absence of bilayer to identify the mutations that improve the stability of peptide: bilayer complex. Based on the calculated peptide: bilayer stability, the peptides were ranked and proceeded for experimental validation. All nine peptides were synthesized, characterized, and tested *in vitro* to assess the antimicrobial potency against three microbial strains (Gram-negative bacteria *Acinetobacter baumannii*, Gram-positive bacteria Methicillin-resistant *Staphylococcus aureus*, and fungus *Candida albicans*). We quantified the effect of tryptophan residue(s) at the 3rd and/or 4th position in stabilizing the peptide: bilayer complex and improving the antimicrobial potency by 2-5 folds. We showed that, as anticipated, the computationally designed new synthetic peptides exhibited enhanced antimicrobial activity. The results demonstrated an excellent correlation between membranolytic antimicrobial potency and peptide binding affinity to the simplest bacterial-membrane-mimetic-bilayer models. So far, this study is the first attempt at an alchemical simulation-based design of membrane-active short AMPs.

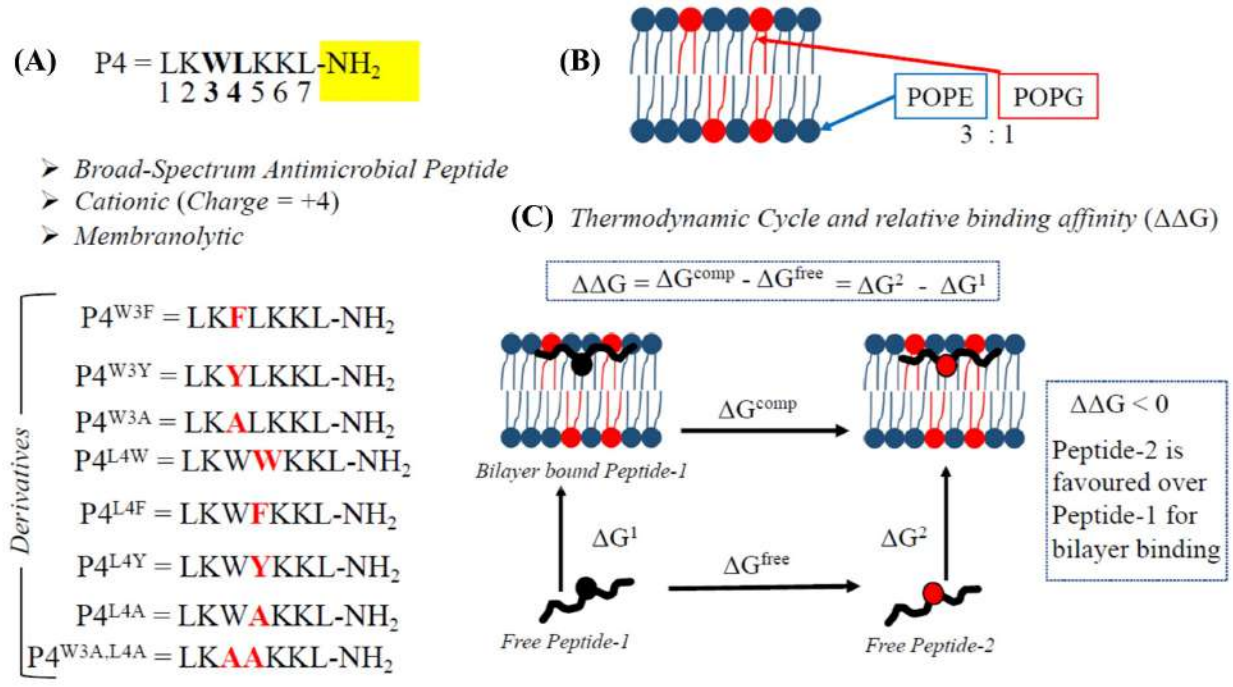

Figure 3.1. (A) Sequence of synthetic antimicrobial hepta-peptide P4 (template) and derivatives. Amine (-NH_2) capping in the C-terminal is highlighted in yellow. (B) Schematic diagram of the bacterial membrane-mimetic-bilayer model composed of 1-palmitoyl-2oleoyl-phosphatidylethanolamine (POPE) and 1-palmitoyl-2-oleoyl-phosphatidylglycerol (POPG) in 3:1 ratio. (C) Thermodynamic cycle used to calculate relative binding free energy (ΔΔG) between different peptides (peptide-1 and peptide-2) to the bilayer. In this work, peptide-1 and peptide-2

are P4-template and P4-derivative peptides, respectively. Horizontal legs correspond to the alchemical transformation of the amino-acid side chain (viz., W3 → F/Y/A or L4→W/F/Y/A or W3L4 →AA) of P4 in complex with the bilayer (upper leg) or free in water (lower leg). Alchemical simulations calculated the ΔG^{comp} and ΔG^{free} (horizontal legs), and their difference is the relative binding affinity ($\Delta\Delta G$).

3.2. Results

3.2.1. Peptide design based on the thermodynamics of peptide: bilayer stability

We performed alchemical free energy calculations to study the thermodynamics of peptide selectivity by the bacterial-membrane-mimetic-bilayer (Figure 3.1). The calculations computed the change in the bilayer binding affinity ($\Delta\Delta G$) upon W3→(F/Y/A) and L4→(F/Y/A) mutations in the 3rd and 4th position in the functional P4 heptapeptide. The objective was to quantitatively estimate the effect of the aromatic side-chain on the peptide: bilayer stability without altering the net charge of the peptide. Employing an appropriate thermodynamic cycle [Figure 3.1(C)], we calculated the alchemical free energies (ΔG^{comp} and ΔG^{free}, Table B1, Appendix B) to estimate $\Delta\Delta G$. The results [Figure 3.2(A)] revealed several noteworthy features. Firstly, the bilayer disfavoured the aromatic side-chain substitution at the 3rd position of P4 (i.e., W3→F3/Y3), indicating the importance of tryptophan (W3) for bilayer binding. Thus, the tryptophan containing antimicrobial P4 peptide was the most potent binder to the bilayer relative to its F3/Y3-aromatic analogs. Secondly, the aromatic side-chain at the 4th position of the P4 peptide (i.e., L4→W4/F4/Y4) improved the bilayer binding affinity, where L4→W4 was noticeable ($\Delta\Delta G$~ -4 kcal/mol). The tryptophan residue at the third position (W3) stabilize the aromatic residue at the fourth position of the peptide in the bilayer. Thirdly, W3→A3 and W3L4→A3A4 substitutions in the peptide were strongly disfavoured for bilayer binding ($\Delta\Delta G$~ +3 to +4 kcal/mol). However, the bilayer displayed weak discrimination between P4 and $P4^{L4A}$ mutants, marginally favouring the latter by < 1 kcal/mol. Based on the calculated relative bilayer binding affinities, we predicted tryptophan-rich ($P4^{L4W}$) and alanine-rich ($P4^{W3A}$ and $P4^{W3A,L4A}$) peptides as the most and least potent antibacterial peptides among the nine peptides studied in this work [Figure 3.2(A) & Table B1, Appendix B]. Next, we undertook a series of experiments to validate our computational predictions.

3.2.2. Antimicrobial activity of the peptides against A. baumannii, methicillin-resistant S. aureus, and C. albicans

All nine peptides, including the control P4, were synthesized, purified, and characterized (Figure B1-B27, Appendix B). The peptides were screened for their antimicrobial potency against Gram-negative bacteria (*A. baumannii*), Gram-positive bacteria (Methicillin-resistant *S. aureus*), and fungus (*C. albicans*) [Figure 3.2(B)]. The strength of antimicrobial activity [Figure 3.2(B) & Table B2, Appendix B] confirmed $P4^{L4W}$ as the most potent peptide, whereas $P4^{W3A}$ and $P4^{W3A,L4A}$ were inactive, corroborating the prediction from the calculated relative binding free affinities [ΔΔG of Figure 3.2(A)]. A five-fold improvement of the antimicrobial activity of $P4^{L4W}$ ($MIC_{90\%}$ = 40 μM) relative to the template peptide P4 ($MIC_{90\%}$ = 200 μM) against MRSA was noticeable. Similarly, L4→W4 substitution in the P4 peptide decreased the MIC by two/three-fold for *A. baumannii*/*C. albicans* [Figure 3.2(B) & Table B2, Appendix B]. $MIC_{90\%}$ for P4 and $P4^{L4W}$ against *A. baumannii*/*C. albicans* were estimated to be 80 μM and 40 μM/30 μM and 10 μM respectively. Loss of antimicrobial activity ($MIC_{90\%}$ > 200 μM) was observed in response to W3→A3/F3/Y3 substitution in the template peptide P4. Thus, tryptophan (W3) was crucial for antimicrobial potency, which was aligned with our computational claim. The antimicrobial potency was either or remained the same upon leucine to aromatic substitution (L4 → F4/Y4) in the peptide P4 [Figure 3.2(B)]. However, L4→A4 substitution in P4 severely compromised the antimicrobial activity [Figure 3.2(B) & Table B2, Appendix B].

In silico predicted $P4^{L4W}$ and $P4^{W3A \text{ or } W3A,L4A}$ were experimentally verified as the most potent and inactive peptides respectively relative to the template P4 against all three types of tested microorganisms. Thus, we considered double-tryptophan-containing ($P4^{L4W}$) and double-alanine-containing ($P4^{W3A,L4A}$) peptides for further experimental investigations to gain deeper insight into the mechanism of the antimicrobial activity.

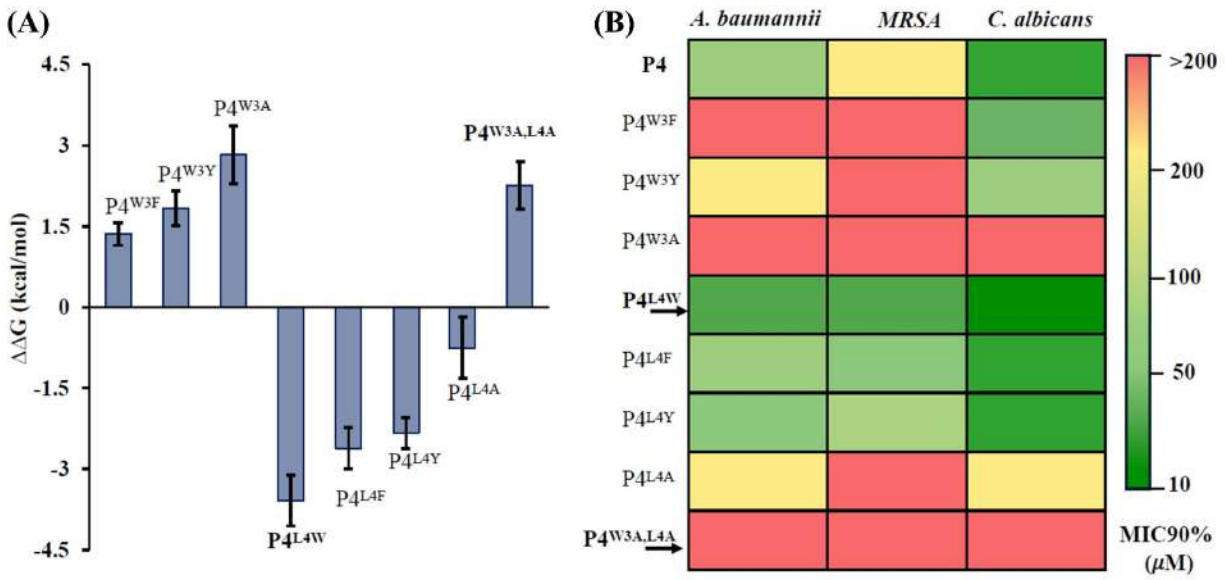

Figure 3.2. (A) Calculated energetics (ΔΔG) of the peptide selectivity in the bilayer. Bilayer binding free energies of the derivative peptides are given relative to the template P4 peptide. Error bars, 1 s.e.m. (B) Color-coded 2D heatmap representation of the minimum inhibitory concentration ($MIC_{90\%}$ in μM) of the nine peptides (P4 and derivatives) against Gram-negative *A. baumannii*, Gram-positive Methicillin-resistant *S. aureus* (MRSA) and fungus *C. albicans*. Dark green to red represents a high to low potency of the peptide.

3.2.3. Mode of antimicrobial activity

Our previous studies showed that the template peptide P4 adopted random-coil conformation (both in the presence and absence of lipid micelle) and was membranolytic against pathogenic bacteria.[1] As the P4-analog peptides retained the same positive charge (+4) and size (7 residues) as P4, they were also hypothesized to possess membranolytic properties. To exhibit membranolytic properties, the analog peptides must interact with the membranes. CD and tryptophan fluorescence experiments analysed the interaction between the peptide (P4, $P4^{L4W}$) and SDS micelles (the simplest microbial membrane mimic system) (Figure 3.3). The peptides were unstructured in water and in the presence of SDS micelles [Figure 3.3(A)]. The intrinsic fluorescence of the constituent tryptophan residues of $P4^{L4W}$ and its parent peptide P4 (20 μM each), were recorded and compared [Figure 3.3(B)] in the presence and absence of SDS micelles (30 mM). Both peptides exhibited a λmax at 359 nm in buffer, though the intensity of $P4^{L4W}$ was significantly higher due to the presence of two tryptophan residues in it, compared to that of one in P4. In the presence of the

SDS micelles, a blue shift of the emission maxima ($\Delta\lambda_{max}$) of approximately 13 nm was observed for both the peptides, indicating micelle binding. Moreover, the presence of a single fluorescence emission peak for $P4^{L4W}$, both in the presence (λ_{max} = 346 nm) and in the absence (λ_{max} = 359 nm) of micelles, indicated that both the tryptophan residues (W3 and W4) experienced a similar local environment [Figure 3.3(B)]. They were similarly hydrated in water, while in SDS micelles, they were buried in a comparable hydrophobic lipid environment.

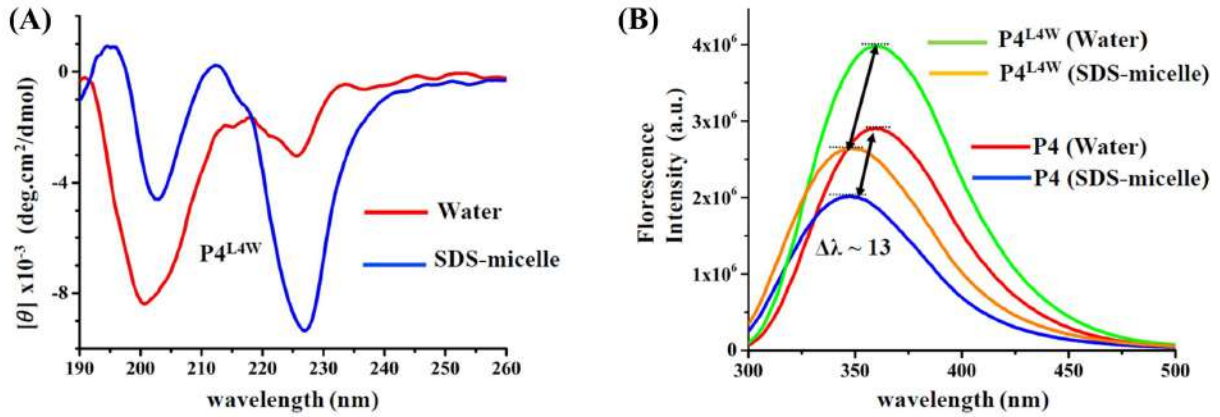

Figure 3.3. (A) CD spectra of $P4^{L4W}$ (100 µM) in water (red) and 30 mM SDS (blue). (B) Intrinsic tryptophan fluorescence emission spectra of P4 and $P4^{L4W}$ (20 µM) in the absence and presence of SDS-micelle (30 mM). A shift of emission maxima of ~13 nm is observed for tryptophan in the absence and presence of SDS-micelles for both peptides.

The propidium iodide (PI, a fluorophore) assay was employed to compare the inner membrane permeability of $P4^{L4W}$ and $P4^{W3A,L4A}$ with that of the template peptide P4 in *A. baumannii*, MRSA and *C. albicans* cells (Figure 3.4). PI generates a fluorescence signal upon intercalating with DNA bases, accessed through the compromised cell membranes. Thus the enhancement of PI fluorescence emission signal reflects AMP penetration through a compromised cell membrane, or its ability to permeabilize the inner membrane. Untreated cells (negative control) showed no enhancement in PI fluorescence. Both P4 and $P4^{L4W}$ exhibited increased PI fluorescence across all cell lines, demonstrating their ability to permeabilize microbial inner membranes. Of the two, $P4^{L4W}$ showed a higher increase in PI fluorescence intensity than P4, indicating the former's superior inner membrane permeability. The results corroborated the enhanced activity of $P4^{L4W}$ over P4 as seen in antimicrobial assays [$MIC_{90\%}$, Figure 3.2(B)] and ΔΔG values [Figure 3.2(A)].

In contrast, $P4^{W3A,L4A}$ did not induce any significant change in PI fluorescence, consistent with its lack of antimicrobial activity.

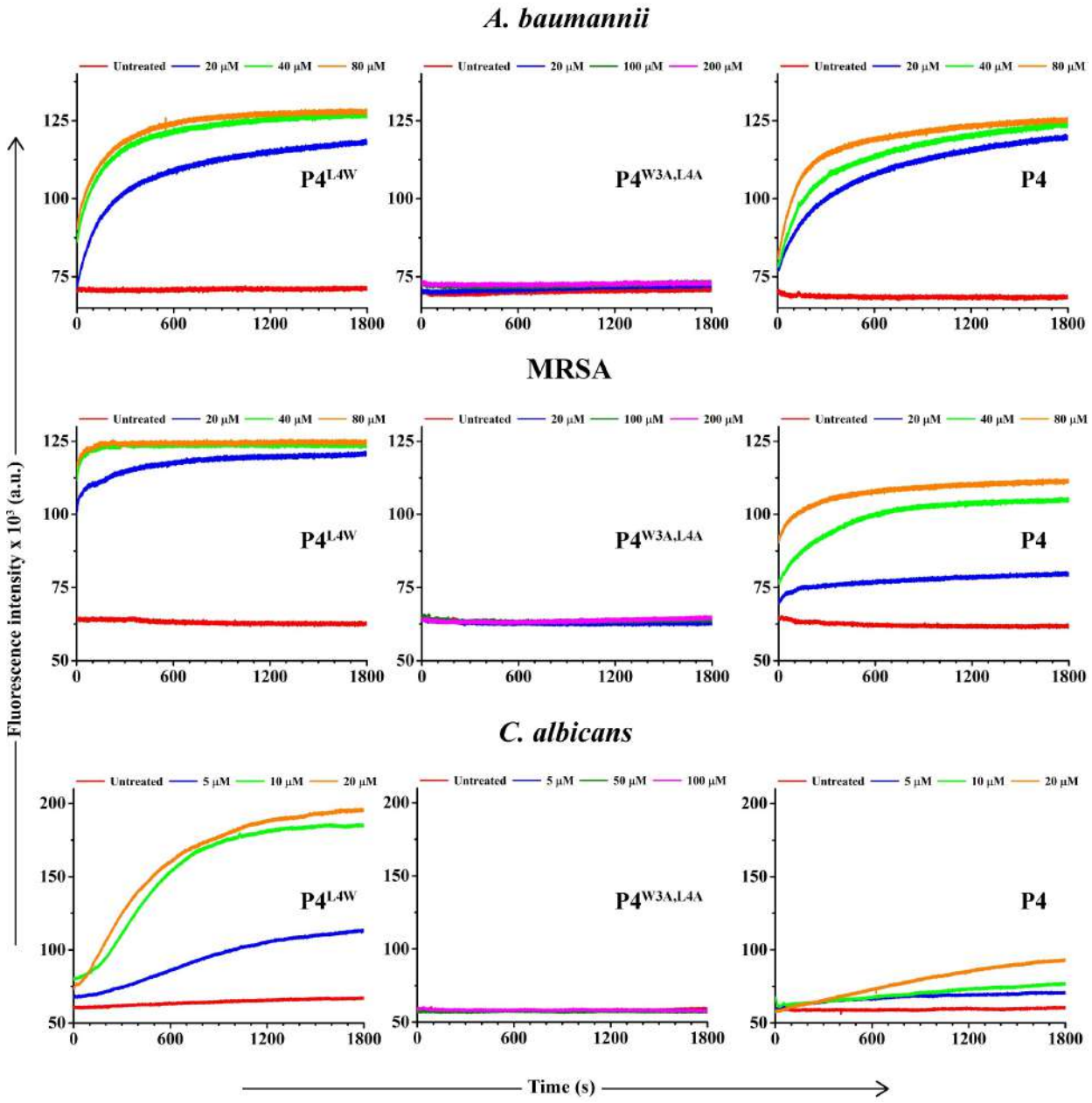

Figure 3.4. Inner membrane permeability assay of Gram-negative bacteria *A. baumannii,* Gram-positive bacteria MRSA, and fungus *C. albicans* in the presence of $P4^{L4W}$, $P4^{W3A,L4A}$ and P4. Fluorescence spectra of PI-incubated microbial cells were recorded upon addition of the $P4^{L4W}$ at its respective 0.5X, 1X, and 2X MIC concentrations against the individual microbes. To compare the potency of $P4^{L4W}$ with P4, fluorescence spectra were recorded for PI-incubated microbial cells treated with P4 at the same concentrations at which $P4^{L4W}$ was added against the individual

microbes. Fluorescence spectra were also recorded for PI incubated microbial cells, treated with different concentrations of $P4^{W3A,L4A}$ ranging from 0.5X MIC of $P4^{L4W}$ against the individual strains (for comparison) to as high as 200 µM. Untreated microbial cells were considered as the negative control.

FESEM studies visually confirmed the membranolytic mode of action of $P4^{L4W}$ on the membranes of *A. baumannii,* MRSA and *C. albicans* (Figure 3.5). Incubation of all the cells with $P4^{L4W}$ led to the deformation of the cellular morphology (damage of the membranes), and eventual lysis of the cells. The surface morphology, size, and shape of the microbial cells were more or less identical in the presence and absence of $P4^{W3A,L4A}$ (Figure 3.5), indicating the inactive nature of the peptide $P4^{W3A,L4A}$. The alchemical binding free energy difference [ΔΔG, Figure 3.2(A)] indicated poor stability of $P4^{W3A,L4A}$: bilayer complex, in line with the abolished activity of $P4^{W3A,L4A}$ observed in the experimental antimicrobial assay [Figure 3.2(B)].

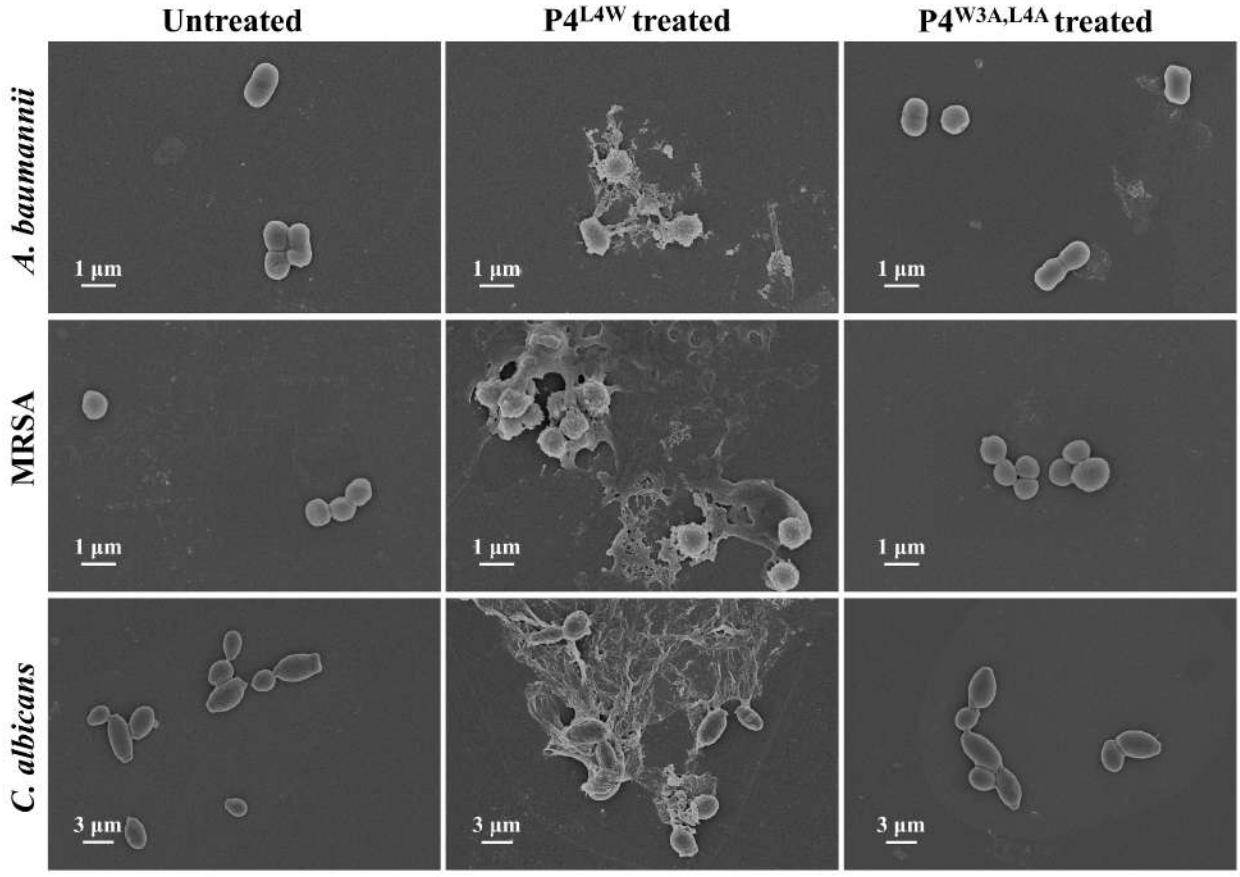

Figure 3.5. FESEM images of untreated, $P4^{L4W}$ (1X MIC) treated and $P4^{W3A,\ L4A}$ (200 µM: maximum limit of experimentally tested concentration) treated of *A. baumannii,* MRSA and *C.*

albicans cells. In contrast to the control untreated cells, $P4^{L4W}$ (1X MIC) treated cells showed cellular deformation, membrane damage, leaked-out intracellular material, cell lysis, and the presence of cellular debris, establishing the membranolytic mechanism of action of the AMP. Treatment with $P4^{W3A,L4A}$ did not bring about any visual change in the cellular morphology and membrane texture, indicating the inactivity of this peptide.

A real-time NMR experiment was performed (Figure 3.6) after by adding peptides ($P4^{L4W}$ and $P4^{W3A,L4A}$) to the living cells of *C. albicans* cells. Line width broadening associated with the signals from the $P4^{L4W}$ peptide was evident upon incubation with the cells, indicating an interaction between peptides and the live cells. Moreover, incubation of the cells with the peptides led to new peaks in the NMR spectra over time. The appearance of these new peaks was attributed to the metabolites that leaked from the damaged cells (lysed), further supporting the membranolytic mode of action of $P4^{L4W}$. In contrast, incubation of $P4^{W3A,L4A}$ with the live cells of *C. albicans* neither showed broadening of the peptide signals nor the appearance of new peaks in the spectra, corroborating its inability to interact with the microbial cells accounting for its inactivity.

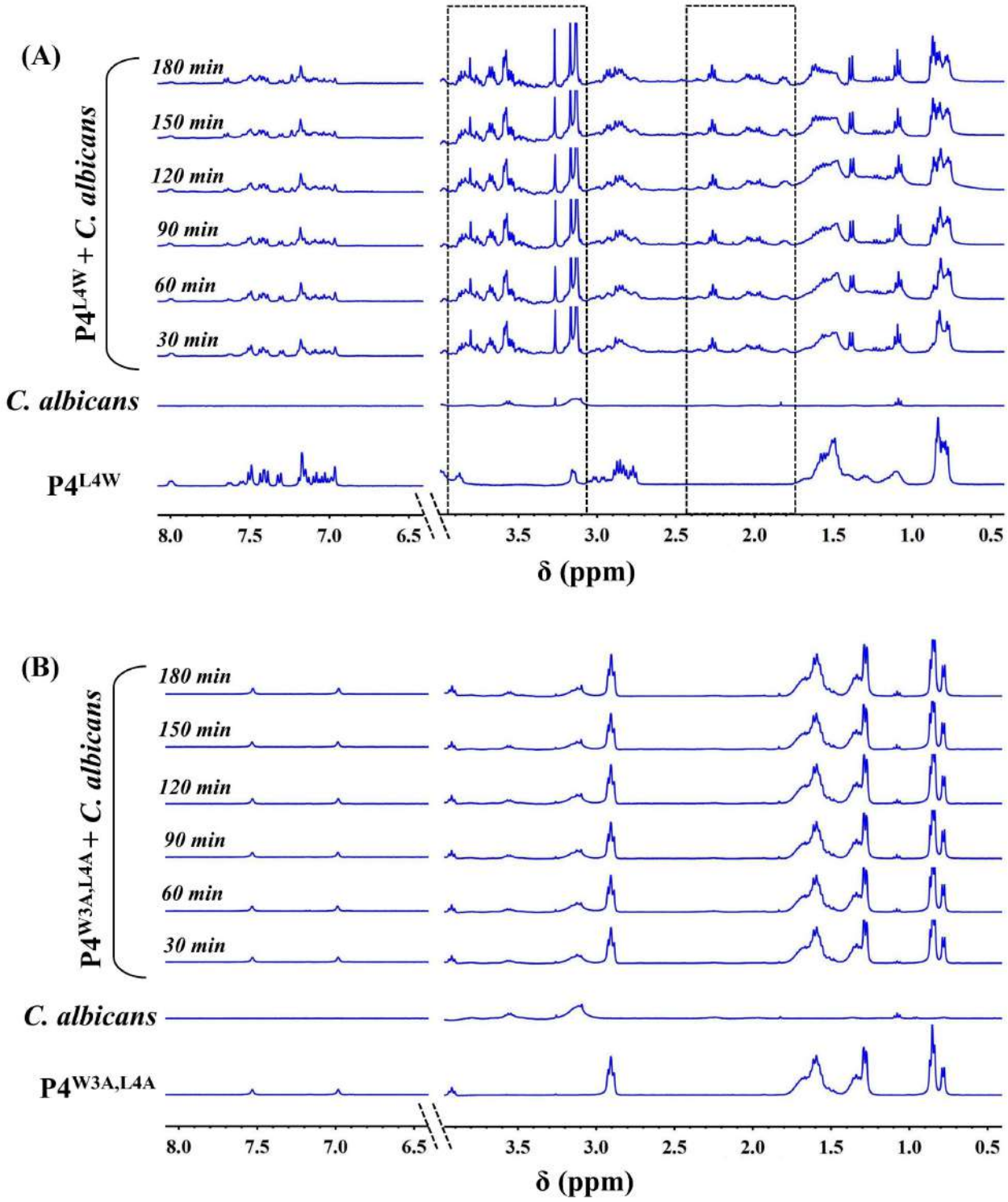

Figure 3.6. Live cell ^{1}H NMR experiment involving the peptides P4^{L4W} /P4^{W3A,L4A} and *C. albicans cells* (Final O.D. = 1) at 400 MHz and 25° C. *C. albicans* cells were added to (A) P4^{L4W} and (B) P4^{W3A,L4A} individually and the NMR spectra were recorded corresponding to different intervals of incubation period. NMR spectra of the untreated cells and peptides alone were recorded as

controls. Broadening of the $P4^{L4W}$ signals was observed upon incubation with *C. albicans* cells, accompanied by the appearance of new peaks in the spectra (highlighted by dotted boxes). No new peaks appeared in the spectra of $P4^{W3A,L4A}$.

3.2.4. Molecular basis of bilayer selectivity and correlation to antimicrobial activity

MD structures of the peptide: bacterial membrane mimetic bilayer complexes can provide insight into the early stage of membranolytic antimicrobial activity to some extent. Simulations showed that these short peptides (in water) were unstructured in the presence and absence of bacterial membrane mimetic bilayer. Circular dichroism (CD) spectrum of P4 and $P4^{L4W}$ [Figure 3.3(A)], in water and in simplest-bacterial-membrane-mimetic-system (SDS micelle), always contained a negative cotton effect peak at ~ 190-200 nm, suggesting that the peptides adopted a random coil conformation in both the free state and in the presence of membrane mimetic environment. The strong negative cotton effect peak at ~ 230 nm observed for $P4^{L4W}$ in the presence of SDS could be attributed to the interaction of the aromatic rings of Trp with the peptide backbone and stacking of the Trp rings.[13-16] As the peptides existed in random coil conformation in the presence of SDS micelles, they might be expected to exist as random coils even after binding to microbial cells. The folded secondary structure of short peptides is known to be thermodynamically disfavored.[17] The favourable enthalpy term is often insufficient to offset the unfavourable entropic term, hindering secondary structure formation in the case of short AMPs.

$P4^{L4W}$: bilayer MD structure (Figure 3.7) revealed that: (1) the peptide was unstructured on the bilayer surface, collaborating with the CD experiments [Figure 3.3(A)]. (2) Both W3 and W4 were buried in similar hydrophobic cores of the bilayer, in lines with a single observed shift in the "fluorescence emission maxima" of the tryptophan residues of the peptide [Figure 3.3(B)]. Intra peptide W3:W4 aromatic: aromatic edge-to-face stacking interaction was observed, supported by the observation of a strong negative CD band at 230 nm. Moreover, W3 and W4 were also engaged in hydrophobic interaction with the aliphatic chain of the lipid and L7, respectively. The intra-peptide interactions stabilized the $P4^{L4W}$: bilayer hydrophobic contact, thus stabilizing the complex. (3) Local deformation of the lipid-bilayer was indicated by larger peptide: bilayer interaction area (~49 Å2) and peptide penetration depth (~14.3 Å). (4) As expected, the positively charged side-chain and the polar backbone of the peptide either interacted with the bulk water molecules or formed a direct/water-mediated interaction with the phosphate oxygen atoms of the

lipid bilayer. Multiple independent MD runs confirmed the robustness of the above structural features (see Method). A stronger association of $P4^{L4W}$: bilayer relative to the P4: bilayer [ΔΔG ~ -4 kcal/mol, Figure 3.2(A)] was evident by large interaction area, deeper bilayer-penetration, and intra-peptide hydrophobic interactions [Figure 3.7(A) & Table B3, Appendix B].

Poor $P4^{W3A,L4A}$: bilayer association relative to P4:bilayer complex [ΔΔG ~ +4 kcal/mol, Figure 3.2(A)] was evident by the loss of interaction area and weaker bilayer penetration in response to side-chain substitution (W3 and L4 → A3 and A4) [Figure 3.7(B) & Table B3, Appendix B]. Simulations revealed that the A3 and A4 side-chains of $P4^{W3A,L4A}$ were on the opposite sides away from each other (relative to the peptide backbone) in the bilayer. A single alanine residue (A3 or A4) was exposed to water, compromising the peptide: bilayer hydrophobic interactions in the $P4^{W3A,L4A}$: bilayer complex [Figure 3.7(B)].

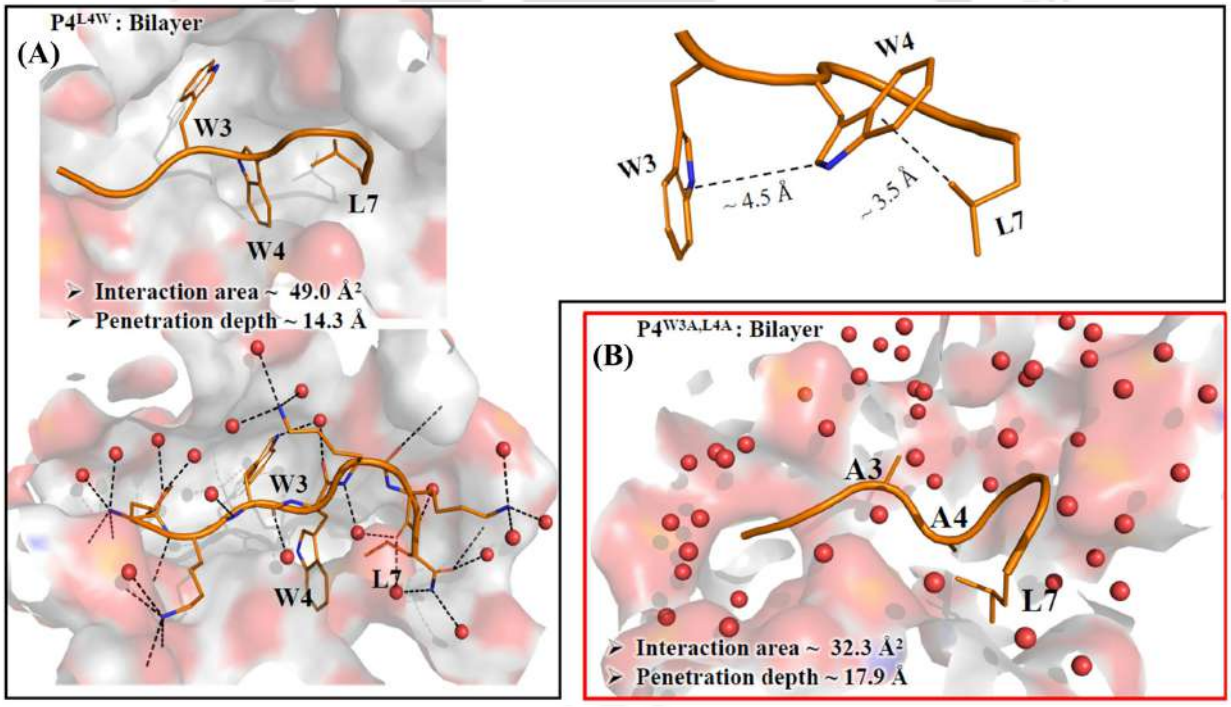

Figure 3.7. (A) Zoomed-in view of $P4^{L4W}$: Bilayer complex from MD simulation, where the characteristic intra-peptide hydrophobic interactions (Face-to-edge interaction involving tryptophan residues, proximity of leucine and tryptophan) are highlighted in the upper right corner. Peptide residues satisfy their hydrogen bonding requirement by interaction with the bilayer (direct or water-mediated) or with water bulk water molecules (lower left corner). (B) $P4^{W3A,L4A}$: Bilayer complex indicated loose association and higher solvent exposure (noticeable for A3) of the peptide.

The dashed line indicates interaction (heavy atom distance < 3.4Å), and the red sphere represents water molecules. Trajectory averaged hydrophobic surface area (formed by the aliphatic hydrocarbon of the lipid bilayer) around 3.4 Å of the peptide side chain was estimated and reported as an interaction area. Penetration depth is the distance between the center of the bilayer and the backbone (cα) of the fourth residue (middle) of the peptide, estimated from the last frame of the trajectory.

3.3. Discussion

The sequence, composition, and structure of the antimicrobial peptides are intimately linked to their membrane activity but is difficult to be summarized by a simple set of rules.[18] In this work, we attempted to use the energetics of peptide: bilayer binding affinity (ΔΔG, alchemical simulations) as an index to fine-tune the potency of broad-spectrum-membranolytic peptides. Heptapeptide P4, earlier studied in our laboratory, offered an excellent template to design a plethora of AMPs cost-effectively, including easy manipulation through sequence/backbone/side-chain/termini modifications.[1-2,19-20] In this study, we designed a library of P4 analogs to investigate the role of the aromatic tryptophan residue at the third position of P4, aiming to enhance its antimicrobial potency. Tryptophan residue with borderline hydrophobicity plays a crucial role in peptide(cationic): membrane interactions.[16] We designed P4 analogs where W3 was substituted to Phe, Tyr and Ala, L4 was substituted to Trp, Phe, Tyr and Ala, and W3/L4 were both substituted to Ala. We demonstrated that peptide: bilayer energetics varied drastically in response to the 3rd and 4th residue mutation in the P4 peptide. The underlying thermodynamics (ΔΔG) explained the origin of the antimicrobial potency of these membrane-active peptides. MD simulations predicted W3 mutant variants of P4 to lose their antimicrobial potency compared to the template peptide, while it predicted $P4^{L4W}$ to have the best antimicrobial activity. $P4^{W3A,L4A}$ was predicted to have the least activity from the theoretical calculations. We validated our theoretical predictions with experiments against Gram-negative bacteria *A. baumannii,* Gram-positive bacteria MRSA, and fungus *C. albicans*. We found the results to be completely corroborative of the theoretical predictions. $P4^{L4W}$ had improved activity over P4 [Figure 3.2(B) & Table B2, Appendix B], having a MIC of 40 μM, 40 μM and 10 μM in contrast to 80 μM, 200 μM, and 30 μM for P4, against *A. baumannii,* MRSA and *C. albicans* respectively. $P4^{L4W}$ had a considerable antifungal activity, given its small size and charge.[21] Thus, the alchemical peptide: bilayer binding free energy

difference (ΔΔG) could be a useful index for designing effective broad-spectrum membranolytic peptides. The principle of antimicrobial activity could be deduced by correlating the calculated free energy (ΔΔG) with the MD structures and experiments. Favourable tryptophan: lipid hydrophobic interaction (at 3rd and/ or 4th position) stabilized the peptide: bilayer complex, thus crucial for the antimicrobial activity. On the other hand, alanine substitution in the place of W3 or L4 destabilized the peptide: bilayer complex, due to the less peptide: bilayer hydrophobic interactions, resulting in loss of activity.

The present study considered designing of the short, cationic, unstructured, broad-spectrum, and membranolytic antimicrobial peptides, which can be argued to adopt a general mechanism for antimicrobial activity involving a non-specific target, like the disruption of cell membranes by binding to negatively charged membrane lipids, in contrast to targeting microbe-specific targets viz., receptors. The computationally intensive rigorous modelling of the microbe specific membranes might likely improve the accuracy of the estimated free energy difference (ΔΔG). Still, it would be challenging (sampling and convergence issues) due to their larger size. The adopted simulation approach was based on estimating the binding free energy difference (ΔΔG) of two different peptides to the simplest bilayer model. The anticipated substantial errors associated with the use of simple peptide: bilayer system (viz., use of fixed charged force-field, computational models) were expected to largely cancel, when we compared the free energy change in the lipid (ΔG^{comp}) to that in solution (ΔG^{free}). We showed that despite the possible uncertainty (due to force field, finite sampling, and simulation size), a fairly converged ΔΔG could be estimated, which facilitated the rational design of new peptides and could explain experimental observations.

3.4. Conclusion

In this study, we have demonstrated that quantitative estimation of the effect of peptide mutations on the peptide: bilayer stability (ΔΔG) through alchemical simulations might be a valuable tool to identify new membrane-active peptides. The adopted approach could establish a link between energetics, antimicrobial activity, and molecular interactions, potentially accelerating the discovery of new therapeutic membrane-active peptides.

3.5. Methods

3.5.1. Computational methodology

The protocol adopted for performing the conventional molecular dynamics simulation and alchemical free energy calculations has been discussed in detail in our previous work.[2]

3.5.2. Model of the peptides

Extended peptide (Figure 3.1) was modelled (using PyMOL software[22]) and placed at the center of an equilibrated water box of dimension $5 \times 5 \times 5$ nm^3. Negatively charged chloride ions were added to neutralize the solvated peptide system. The charge-neutral simulation box was then subjected to minimization followed by MD simulations. Simulations were carried out using GROMACS software,[23] and the standard CHARMM36m force field[24] was used to describe molecular interactions.

3.5.3. Model of bacterial membrane mimetic bilayer and peptide: bilayer binding

A simple bilayer was considered for mimicking bacterial membranes. The bilayer model comprised of two types of lipids (zwitterionic POPE and negatively charged POPG lipids, Figure 3.1) in a 3:1 ratio (Total of 96 lipid molecules: 72 POPE and 24 POPG). The POPE/POPG bilayer was solvated with a 2.5 nm water layer on both sides. Monovalent counterions (Na^+) were added to ensure the charge neutrality of the solvated bilayer system. The final MD structures (of the solvated bilayer) from various independent simulations were selected to study peptide binding to the bilayer. First, the peptide was placed at least 2 nm away and parallel to the surface of the equilibrated bilayer. Next, conventional MD simulations (for & 1 μs) were carried out to study the binding of the peptide to the bilayer. Each simulation setup was performed in triplicate, and the final peptide: bilayer complex, was subjected to alchemical simulation and relative binding affinity ($\Delta\Delta G$) estimation.

3.5.4. Alchemical simulations and estimation of peptide binding affinity difference (ΔG)

An appropriate thermodynamic cycle [Figure 3.1(C)] allowed estimation of the relative binding free energies ($\Delta\Delta G$). The final MD structure of the P4:POPE/POPG-bilayer complex from the standard molecular dynamics simulations was subjected to alchemical transformation [upper horizontal arm of Figure 3.1(C)]. Alchemical simulation slowly transformed the side chain(s) of the 3rd and 4th amino acids of P4, thus altering the peptide identity. The free energy charge (ΔG^{comp}) associated with the alchemical transformations of P4 in complex with the bilayer was

estimated using the popular Bennett acceptance ratio (BAR)[25] method implemented in GROMACS software. The alchemical simulation was repeated for the free peptide in water to calculate the ΔG^{free}. Single alchemical free energy simulations were conducted across 21 equally spaced λ windows, with 15 ns of sampling per window, resulting in a total simulation time of 21 × 15 = 315 ns. Free energies from three independent alchemical trials (3 x 315 = 945 ns MD) are averaged to estimate ΔG^{comp} and ΔG^{free} (Table B1, Appendix B). Good convergence and reasonable statistical error (less than 1.0 kcal/mol, Table B1, Appendix B) were assured by a total sampling of more than 15 μs. Free energies from various independent trajectories were averaged and reported as ΔG^{comp} and ΔG^{free} (where s.e.m. is the error). The errors associated with ΔG^{comp} and ΔG^{free} were propagated to assign the error of ΔΔG. The sign of $\Delta\Delta G = \Delta G^{comp} - \Delta G^{free}$ indicated the preference, whereas the magnitude indicated the strength of preference.

3.5.5. Materials

Rink amide resin, Fmoc protected amino acids: Fmoc-Leu-OH, Fmoc-Lys(Boc)-OH, Fmoc-Trp(Boc)-OH, Fmoc-Phe-OH, Fmoc-Tyr(tBu)-OH, Fmoc-Ala-OH and the coupling reagents: HBTU (Hexafluorophosphate Benzotriazole Tetramethyl Uronium) and HOBt (1-Hydroxybenzotriazole) were purchased from GL Biochem Ltd., Shanghai. N, N-dimethyl formamide (DMF), N, N-diisopropylethylamine (DIPEA), Piperidine, Pyridine, Trifluoroacetic acid (TFA), Monosodium phosphate (NaH_2PO_4) and Disodium phosphate (Na_2HPO_4) were purchased from Merck Life Science Pvt. Ltd., Mumbai, India. Acetic anhydride manufactured by SD Fine Chem Limited, Mumbai, India, was provided by the Department of chemistry, IIT Guwahati. Dichloromethane (DCM), HPLC grade acetonitrile, and Diethyl ether were purchased from Finar Limited, Ahmedabad, India. Nutrient broth, BHI broth, YPD broth were purchased from Himedia Laboratories Pvt. Ltd., Mumbai, India. Triisopropylsilane, Deuterium oxide (D_2O), α-Cyano-4-hydroxycinnamic acid (HCCA), Sodium dodecyl sulphate (SDS), Propidium Iodide (PI), and Glutaraldehyde were purchased from Sigma-Aldrich, St. Louis, USA.

3.5.6. Synthesis and characterization of the peptides

The peptides were synthesized by solid phase peptide synthesis strategy using Fmoc chemistry. To have C- terminal amidated peptides, rink amide resin was used for the loading of the amino acids. Rink amide resin corresponding to a loading capacity of 0.1 mmol, was weighed and swelled in DMF. Swelled resin was deprotected to remove the Fmoc-protection using 20% piperidine, and

linked to the first amino acid (starting from the C-terminus of the peptide sequence). Fmoc-protected amino acid (3 eqv. of the resin, 0.3 mmol), HBTU (3 eqv. of the resin, 0.3 mmol) and HOBt (3 eqv. of the resin, 0.3 mmol) dissolved together in DMF and mixed with DIPEA (6 eqv. of the resin, 0.6 mmol) were added to the deprotected resin for the coupling of the first amino acid. The first amino acid coupled resin was capped using a solution of DMF, acetic anhydride and pyridine (7:2:1) to block the unreacted amines from participating in further coupling. This cycle of Fmoc deprotection, coupling of the amino acids and capping of the resin was repeated till the full grown sequence of amino acids was assembled on the resin. The peptide was finally cleaved off from the resin and the side chains deprotected using a solution trifluoroacetic acid containing traces of triisopropylsilane and water. Cold diethyl ether was used for the precipitation of the peptides. The peptide precipitated in ether was allowed to settle, centrifuged and dried to obtain the crude peptide.

The synthesis of the peptides was confirmed from the MALDI analysis of the crude peptides. Peptides were purified using semi preparative HPLC (Thermo Scientific Ultimate 3000) using a C-18 reverse phase column [Luna 5 μm C18(2) 100 Å, LC Column 250 x 21.2 mm) and water-acetonitrile (each solvent acidified with 0.1% trifluoroacetic acid) as the solvent system. The purified peptides were characterized using MALDI spectroscopy (Instrument: Bruker autoflex speed), analytical HPLC [Instrument: Thermo Scientific Vanquish; column: Thermo Scientific, Biobasic-18, dimension: 150 x 4.6, particle size: 5 μ; Solvent: acetonitrile-water (5-100%) linear gradient over a period of 20 min] and ^{1}H-NMR spectra (Bruker Avance III 400 MHz NMR spectrometer, 5-8 mM in D_2O, RT).

3.5.7. Microbial strains

Acinetobacter baumannii (MTCC 1425) and *Candida albicans* (MTCC 1637) were purchased from Microbial Type Culture Collection and Gene Bank (MTCC), Chandigarh, India. Methicillin-resistant *Staphylococcus aureus* (MRSA 100) is a clinal isolate obtained from Prof. Benu Dhawan, All India Institute of Medical Science (AIIMS), New Delhi.

3.5.8. Determination of Minimum Inhibitory Concentration (MIC)

The minimum inhibitory concentration ($MIC_{90\%}$) of the peptides were determined against Gram-negative bacteria *Acinetobacter baumannii*, Gram-positive bacteria Methicillin-resistant *Staphylococcus aureus* (MRSA) and fungus *Candida albicans*. *Acinetobacter baumannii* was

grown in nutrient broth, MRSA was grown in BHI broth while *Candida albicans* was grown in YPD broth. The bacteria and fungi were grown at 37 °C and 28 °C respectively. Briefly, the microbes grown at their respective mid-log phase were pipetted out in microcentrifuge tubes and were centrifuged to discard the growth medium. The pelleted down cells were washed for three consecutive times with phosphate buffer (10 mM, pH -7.4) and finally suspended back in the same buffer. The washed cells were diluted serially to the order of 10^5 CFU/ml. 50 µL of this cell suspensions were added to 50 µL of peptide solutions diluted at different concentrations, and were incubated for a period of 4 h at 37 °C and 28 °C respectively for the bacteria and fungus. Untreated cells were maintained as the negative control while cells treated with Polymyxin B, Vancomycin and Amphotericin B were used as the positive controls against Gram-negative bacteria, Gram-positive bacteria and fungus respectively. Cells (both treated/ untreated) post incubation were added with another 100 µL of the respective media and incubated further overnight under continuous shaking, maintaining the respective growth temperatures. Finally, the OD values of the cells treated with the peptides at different concentrations were compared with those of the untreated cells and cells treated with the positive control to determine their percentage inhibition. The OD of the cells in all the cases were recorded at 600 nm. $MIC_{90\%}$ value for a peptide against a particular microbe was the concentration at which that peptide induced more than 90% inhibition of that microbe, considering the positive control to induce 100% inhibition.

3.5.9. Propidium iodide assay or inner membrane permeation assay

Bacterial cells (*A. baumannii* and MRSA) and fungal cells (*C. albicans*) grown at their respective mid-log phases were washed with phosphate buffer (10 mM, pH -7.4) and serially diluted to the order of 10^7 CFU/ml and 10^6 CFU/ml respectively. Propidium iodide at a final concentration of 10 µM was added to each of the cellular suspensions and were incubated for 30 min under uniform orbital shaking. The cellular suspensions in their untreated form were subjected to fluorescence intensity measurements over a period of 30 min using an excitation wavelength of 535 nm (slit width: 10 nm) and emission wavelength 617 nm (slit width: 10 nm). The enhancement in the fluorescence intensity of cellular suspensions upon addition of the peptide $P4^{L4W}$ at its 0.5X MIC, 1X MIC and 2X MIC concentrations against the respective strains was then monitored. For comparisons of PI intake between the peptides $P4^{L4W}$ and P4, fluorescence emission enhancements of the cellular suspensions upon addition of P4 at the same three concentrations at which $P4^{L4W}$ were added against each of the strain, was recorded. The fluorescence emission enhancement of

PI treated cells upon addition of $P4^{W3A,L4A}$ (at various concentrations upto 200 μM) was also monitored over the time.

3.5.10. FESEM imaging of the microbes treated with peptides

A. baumannii, MRSA and *C. albicans* grown at their respective mid-log phases, washed with phosphate buffer (10 mM, pH -7.4) and diluted to the order of 10^5 CFU/ml, were treated with the peptide $P4^{L4W}$ at its respective $MIC_{90\%}$ against the individual microbial strains, as well as 200 μM of the peptide $P4^{W3A, L4A}$ (highest concentration upto which the peptide were screened for their $MIC_{90\%}$ determination) and kept incubated under continuous orbital shaking for a period of 2 h. The peptide treated cells post incubation as well the untreated cells were fixed with a solution of 2.5% glutaraldehyde and were subsequently incubated for another hour. The glutaraldehyde fixed cells were finally washed with phosphate buffer, concentrated and casted on silicon wafers and allowed to dry in the laminar hood. The cells casted on silicon wafers after complete drying were washed with different grades of ethyl alcohol ranging from 30-90% and re-dried. The casted samples were coated and the images were acquired using a Field emission scanning electron microscope (Gemini 500, Zeiss).

3.5.11. Live cell NMR

Candida albicans grown till mid-log phase were washed with PB and diluted to a final O.D. =1 using a solution of PB acidified to pH 6.5, and added with 10% D_2O. The 400 MHz ^1H NMR spectra of the peptides (1 mM), untreated cells, and cells treated with peptides for different time intervals were acquired at RT in PB (pH 6.5) and 10% D_2O. ^1H-NMR spectra were acquired by suppressing the peak for water using zgpr pulse program and recording 128 scans each time.

3.5.12. CD spectra

CD spectra for peptide $P4^{L4W}$ at a final concentration of 100 μM in mili-Q water as well as in 30 mM SDS solution was acquired. A quartz cuvette of 350 μL volume having a pathlength of 1 mm was used for the purpose. Spectra were acquired over a wavelength of 260-190 nm, at a scanning rate of 100 nm/min, data pitch of 1 nm and band width of 1 nm. Spectra were acquired using a JASCO J-1500 CD spectrometer.

3.5.13. Blue shift experiment

Fluorescence spectra of P4 and $P4^{L4W}$ (20 μM) were acquired in water as well in 30 mM SDS. An excitation wavelength of 280 nm was used corresponding to the presence of tryptophan in both the peptides. The spectra were acquired over a wavelength of 300-500 nm.

References

1. Pandit, G.; Ilyas, H.; Ghosh, S.; Bidkar, A. P.; Mohid, S. A.; Bhunia, A.; Satpati, P.; Chatterjee, S. Insights into the Mechanism of Antimicrobial Activity of Seven-Residue Peptides. *J. Med. Chem.* **2018**, *61*, 7614-7629.

2. Ghosh, S.; Sarkar, T.; Chatterjee, S.; Satpati, P. Bridging Thermodynamics, Antimicrobial Activity, and PH Sensitivity of Cationic Membranolytic Heptapeptides- A Computational and Experimental Study. *J. Chem. Inf. Model.* **2023**, *63*, 2393-2408.

3. Ghosh, S.; Chatterjee, S.; Satpati, P. Effect of Leu/Val Mutation on the Energetics of Antimicrobial Peptide:Micelle Binding. *J. Phys. Chem. B* **2022**, *126*, 5262-5273.

4. Ghosh, S.; Chatterjee, S.; Satpati, P. Effect of Spacer Length Modification of the Cationic Side Chain on the Energetics of Antimicrobial Peptide Binding to Membrane-Mimetic Bilayers. *J. Chem. Inf. Model.* **2023**, *63*, 5823-5833.

5. Das, P.; Sercu, T.; Wadhawan, K.; Padhi, I.; Gehrmann, S.; Cipcigan, F.; Chenthamarakshan, V.; Strobelt, H.; Dos Santos, C.; Chen, P.Y.; Yang, Y.Y.; Tan, J.P.K.; Hedrick, J.; Crain, J.; Mojsilovic, A. Accelerated antimicrobial discovery via deep generative models and molecular dynamics simulations. *Nat. Biomed. Eng*. **2021**, *5*, 613-623.

6. Maccari, G.; Di Luca, M.; Nifosì, R. In silico design of antimicrobial peptides. *Methods Mol. Biol*. **2015**, *1268*, 195-219.

7. Agüero-Chapin, G.; Galpert-Cañizares, D.; Domínguez-Pérez, D.; Marrero-Ponce, Y.; Pérez-Machado, G.; Teijeira, M.; Antunes, A. Emerging Computational Approaches for Antimicrobial Peptide Discovery. *Antibiotics* **2022**, *11*, 936.

8. Al-Khdhairawi, A.; Sanuri, D.; Akbar, R.; Lam, S.D.; Sugumar, S.; Ibrahim, N.; Chieng, S.; Sairi, F. Machine learning and molecular simulation ascertain antimicrobial peptide against Klebsiella pneumoniae from public database. *Comput. Biol. Chem*. **2023**, *102*, 107800.

9. Palmer, N.; Maasch, J.R.M.A.; Torres, M.D.T.; de la Fuente-Nunez, C. Molecular Dynamics for Antimicrobial Peptide Discovery. *Infect. Immun.* **2021**, *89*, e00703-20.

10. Porto, W.F.; Irazazabal, L.; Alves, E.S.F.; Ribeiro, S.M.; Matos, C.O.; Pires, Á.S.; Fensterseifer, I.C.M.; Miranda, V.J.; Haney, E.F.; Humblot, V.; Torres, M.D.T.; Hancock, R.E.W.; Liao, L.M.; Ladram, A.; Lu, T.K.; de la Fuente-Nunez, C.; Franco, O.L. In silico optimization of a guava antimicrobial peptide enables combinatorial exploration for peptide design. *Nat. Commun*. **2018**, *9*, 1490.

11. Aronica, P.G.A.; Reid, L.M.; Desai, N.; Li, J.; Fox, S.J.; Yadahalli, S.; Essex, J.W.; Verma, C.S. Computational Methods and Tools in Antimicrobial Peptide Research. *J. Chem. Inf. Model.* **2021**, *61*, 3172-3196.

12. Chen, C.H.; Starr, C.G.; Troendle, E.; Wiedman, G.; Wimley, W.C.; Ulmschneider, J.P.; Ulmschneider, M.B. Simulation-Guided Rational de Novo Design of a Small Pore-Forming Antimicrobial Peptide. *J Am Chem Soc*. **2019**, *141*, 4839-4848.

13. Fossum, C.J.; Johnson, B.O.V.; Golde, S.T.; Kielman, A.J.; Finke, B.; Smith, M.A.; Lowater, H.R.; Laatsch, B.F.; Bhattacharyya, S.; Hati, S. Insights into the Mechanism of Tryptophan Fluorescence Quenching due to Synthetic Crowding Agents: A Combined Experimental and Computational Study. *ACS Omega* **2023**, *8*, 44820-44830.

14. Richaud, A.D.; Mandal, S.; Das, A.; Roche, S.P. Tunable CH/π Interactions within a Tryptophan Zipper Motif to Stabilize the Fold of Long β-Hairpin Peptides. *ACS Chem. Biol*. **2023**, *18*, 2555-2563.

15. Khemaissa, S.; Walrant, A.; Sagan, S. Tryptophan, more than just an interfacial amino acid in the membrane activity of cationic cell-penetrating and antimicrobial peptides. *Q. Rev. Biophys*. **2022**, *55*, e10.

16. Spencer, T.A.; Ditchfield, R. Tryptophan Stabilization of a Biochemical Carbocation Evaluated by Analysis of π Complexes of 3-Ethylindole with the *t*-Butyl Cation. *ACS Omega* **2023**, *8*, 26497-26507.

17. Bastida, A.; Zúñiga, J.; Requena, A.; Miguel, B.; Cerezo, J. On the Role of Entropy in the Stabilization of α-Helices. *J. Chem. Inf. Model*. **2020**, *60*, 6523-6531.

18. Straus, S.K. Tryptophan- and arginine-rich antimicrobial peptides: Anti-infectives with great potential. *Biochim. Biophys. Acta Biomembr*. **2024**, *1866*, 184260.

19. Pandit, G.; Sarkar, T.; S. R. V., Debnath, S.; Satpati, P.; Chatterjee, S. Delineating the Mechanism of Action of a Protease Resistant and Salt Tolerant Synthetic Antimicrobial Peptide against *Pseudomonas aeruginosa*. *ACS Omega* **2022**, *7*, 15951-15968.

20. Sarkar, T.; Ghosh, S.; Sundaravadivelu, P.K.; Pandit, G.; Debnath, S.; Thummer, R.P.; Satpati, P.; Chatterjee, S. Mechanism of Protease Resistance of D-Amino Acid Residue Containing Cationic Antimicrobial Heptapeptides. *ACS Infect. Dis*. **2024**, *10*, 562-581.

21. Perez-Rodriguez, A.; Eraso, E.; Quindós, G.; Mateo, E. Antimicrobial Peptides with Anti-*Candida* Activity. *Int. J. Mol. Sci.* **2022**, *23*, 9264.

22. Schrodinger, L.L.C. The PyMOL Molecular Graphics System, Version 2.4.0. **2010.**

23. Van Der Spoel, D.; Lindahl, E.; Hess, B.; Groenhof, G.; Mark, A.E.; Berendsen, H.J. GROMACS: fast, flexible, and free. *J. Comput. Chem*. **2005**, *26*, 1701-1718.

24. Huang, J.; Rauscher, S.; Nawrocki, G.; Ran, T.; Feig, M.; de Groot, B.L.; Grubmüller, H.; MacKerell, A.D. Jr. CHARMM36m: an improved force field for folded and intrinsically disordered proteins. *Nat. Methods*. **2017**, *14*, 71-73.

25. Bennett, C. H. Efficient Estimation of Free Energy Differences from Monte Carlo Data. *J. Comput. Phys.* **1976**, 245-268.

Chapter 4: Development of Protease Resistant and Non-cytotoxic Jelleine Analogs with Enhanced Broad-Spectrum Antimicrobial Efficacy

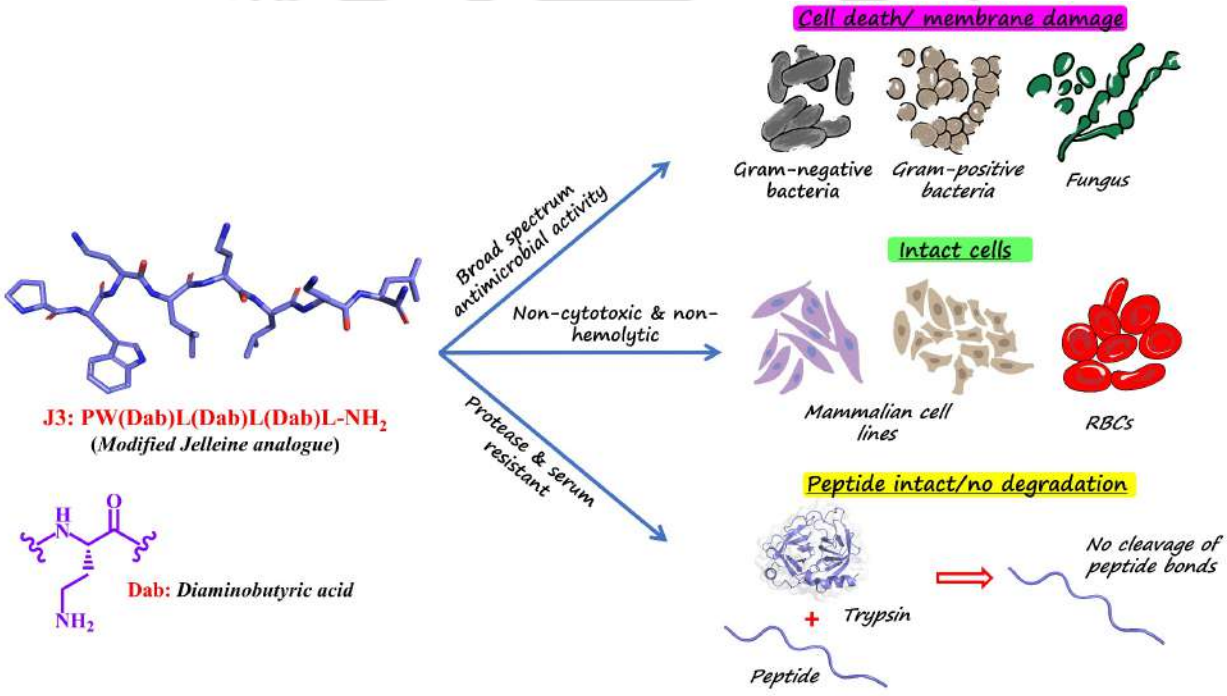

4.1. Introduction

In this chapter we tried to address two of the major limitations of the naturally occurring AMPs: their moderate activity[1] and protease susceptibility[2] through incorporation of unnatural amino acids in the sequence of a naturally occurring peptide jelleine-I. Jelleines are a class of AMPs obtained from the royal jelly of *apis mellifera.* These are typically 8-9 residues long and have broad a spectrum activity against a wide range of Gram-positive and Gram-negative bacteria and fungus.[3-4] Among the four jelleines reported jelliene- I was found to be most active of all.[3] We chose jelleine-I (Jc) as our template, and modified it, for developing analogs with enhanced activity and stability. We modified Jc to obtain analogs J1- J4, by incorporating amino acid residues with positive charge, enhanced membrane binding ability and unnatural amino acid residues. The designed peptides were investigated in details using both experimental approaches that involved various biological assays, biophysical tools, spectroscopic and microscopic techniques and molecular dynamics simulations. The investigations resulted in the development of a couple of economically viable, highly potent, non-cytotoxic, protease resistant and serum stable membranolytic broad spectrum AMPs.

4.2. Results

4.2.1. Design and synthesis of the peptides

Jelleine-I (Jc, PFKLSLHL-NH_2), is a short peptide obtained from *Apis mellifera* reported to have broad-spectrum antimicrobial activity[3-4] against a wide range of microbes. With an intension of developing novel and better antimicrobials, Jc was chosen as the primary template for the design and synthesis of a series of octapeptides J1-J4 **(**Figure 4.1 & Table 4.1**)**. Following modifications were introduced in the modified analogues: (1) Phenylalanine (F) was mutated to tryptophan (W) in all the four sequences namely J1-J4; (2) Lysine (K) was mutated to cationic unnatural amino acid residue, diaminobutyric acid (Dab) in J1 [PW(Dab) LSLHL-NH_2]; (3) Both lysine (K) and serine (S) were replaced with Dab in J2 [PW(Dab)L(Dab)LHL-NH_2]; (3) Lysine (K), serine (S), and histidine (H) were replaced with Dab in J3 [PW(Dab)L(Dab)L(Dab)L(Dab)L-NH_2]; and (4) Proline (P), lysine (K), serine (S), and histidine (H) were replaced with Dab in J4 [**(**Dab)W(Dab)L(Dab)L(Dab)L-NH_2]. Tryptophan is an amino acid widely encountered in the sequences of antimicrobial peptides[5-6] and due to its unique hydrophobicity is known to locate itself at the hydrocarbon-water interface of membrane bilayers.[7] Because of this unique characteristic of Trp, we mutated Phe of Jc to Trp, in the designed analogs J1-J4. With an intention

of imparting protease resistance to Jc, basic (K, H), polar (S) and proline residue(s) were progressively substituted by the unnatural amino acid residue Dab. Substitution of the polar or hydrophobic amino acid residue with a cationic Dab residue increased the overall charge of the peptides J2-J4. In addition to the intension of increasing the activity of the designed peptides with increasing charge, we were also curious to investigate the effect of the changing the hydrophobic-hydrophilic balance of the peptides on their activity.

Jc and its modified analogues J1-J4 were synthesized using Solid Phase Peptide synthesis strategy (SPPS) and purified using preparative HPLC (Table 4.1). Before using them further, peptides were thoroughly characterized using MALDI-MS (Figure C1-C5, Appendix C), analytical HPLC (Figure C6-C10, Appendix C) and ^{1}H NMR (Figure C11-C15, Appendix C).

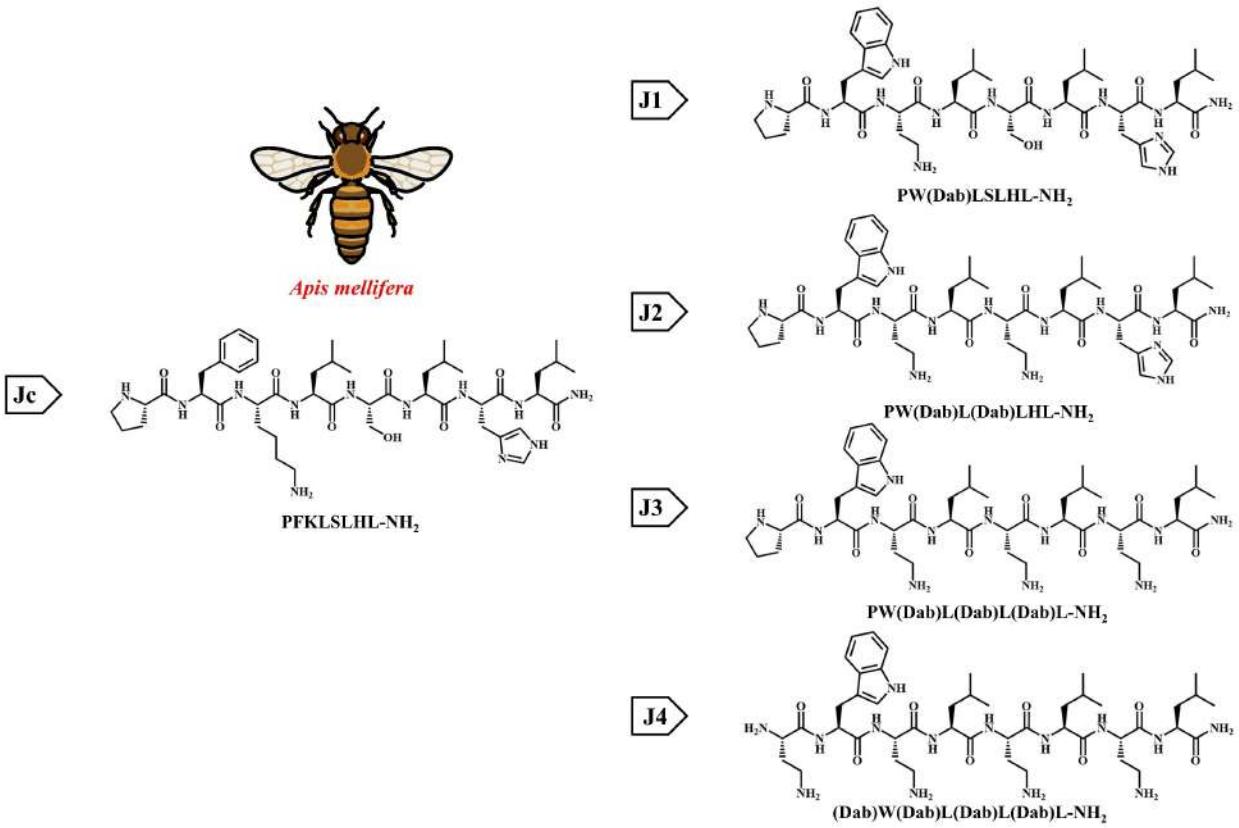

Figure 4.1. Chemical structures of jelleine-I (Jc) and the designed jelleine analogs J1-J4.

Table 4.1. Physicochemical properties of the peptides Jc and J1-J4.

Peptide Name	Sequence	Number of amino acid residues	Net charge (pH- 7.4)	Theoretical Molecular Weight (Da)	Retention time (min)
Jc	PFKLSLHL-NH_2	8	+2	953.19	8.63
J1	PW(Dab)LSLHL-NH_2	8	+2	964.18	8.54
J2	PW(Dab)L(Dab)LHL-NH_2	8	+3	977.22	8.53
J3	PW(Dab)L(Dab)L(Dab)L-NH_2	8	+4	940.20	8.45
J4	(Dab)W(Dab)L(Dab)L(Dab)L-NH_2	8	+5	943.20	8.25

4.2.2. Biological activity

Determination of Minimum Inhibitory Concentration ($MIC_{90\%}$)

Minimum Inhibitory Concentration or $MIC_{90\%}$ of the peptides were determined against Gram-negative bacteria *P. aeruginosa, K. pneumoniae* and Gram-positive bacteria *S. aureus* and Methicillin-resistant *S. aureus (MRSA)* and fungus *C. albicans* (Table 4.2 & Figure C16, Appendix C). Though there was a microbe specific variation, all the designed peptides other than J1 in general had an improved potency over Jc. Among all the designed analogs, J3 and J4 had the best activity against all the tested bacterial and fungal strains, most probably owing to their increased overall charge (+4 and +5 respectively). J3 and J4 particularly seemed most promising against *P. aeruginosa* and *C. albicans*.

Table 4.2. MIC values of the peptides Jc and J1-J4 against various ESKAPE pathogens and fungi *C. albicans*.

Peptides/ Strains	**$MIC_{90\%}$ (μM)**				
	P. aeruginosa	*K. pneumoniae*	*S. aureus*	*MRSA*	*C. albicans*
Jc	20	50	20	100	10
J1	20	40	30	100	20
J2	20	30	10	50	10
J3	5	10	10	30	5
J4	5	30	10	30	5

Determination of minimum inhibitory concentration (MIC) in the presence of salts

Further, MIC values of the peptides Jc and J1-J4 were determined in the presence of physiological concentration of salts (Phosphate buffer, pH- 7.4, strength- 10 mM containing 150 mM NaCl), against Gram-negative bacteria *P. aeruginosa*, Gram-positive bacteria *S. aureus* (Table 4.3 & Figure C17, Appendix C). All the peptides lost their activities to some extent in the presence salts (150 mM NaCl). Overall J3 was the best in retaining its antimicrobial activity in the presence of salts among all the designed peptides, acting as a moderate antimicrobial agent.

Table 4.3. MIC values of the peptides Jc and J1-J4, in PB containing physiological concentration (150 mM) of NaCl. The MIC values of the peptides against the respective bacterial strains in the absence of salts have also been presented in the table for comparison.

Peptides/ Strains	**$MIC_{90\%}$ (μM)**			
	P. aeruginosa		*S. aureus*	
	150 mM NaCl	Absence of salts	150 mM NaCl	Absence of salts
Jc	100	20	30	20
J1	100	20	40	30
J2	50	20	40	10
J3	50	5	30	10
J4	200	5	100	10

Cytotoxicity

As a successful therapeutic agent must be non-cytotoxic to the mammalian cells, the cytotoxicity of the designed peptides was evaluated against a normal cell line, Human Dermal Fibroblasts (HDF). To assess if these peptides possessed anticancer properties, cytotoxicity against HeLa, a cancer cell line, was also evaluated. Against HDF, all the peptides were more or less viable till a concentration of 160 μM [Figure 4.2(A)]. However, J3 appeared to be the most non-cytotoxic among all, displaying close to 100 % viability even at the highest concentration tested (160 μM). J4 was comparatively less viable at higher concentrations against HDF, though it was completely non-cytotoxic at its biologically relevant concentrations. Noticeably, the overall cytotoxicity of all the designed peptides were improved in comparison to Jc. All the peptides screened were non-

cytotoxic against HeLa cell lines [Figure 4.2(B)]. Thus, these AMPs did not have any anticancer properties.

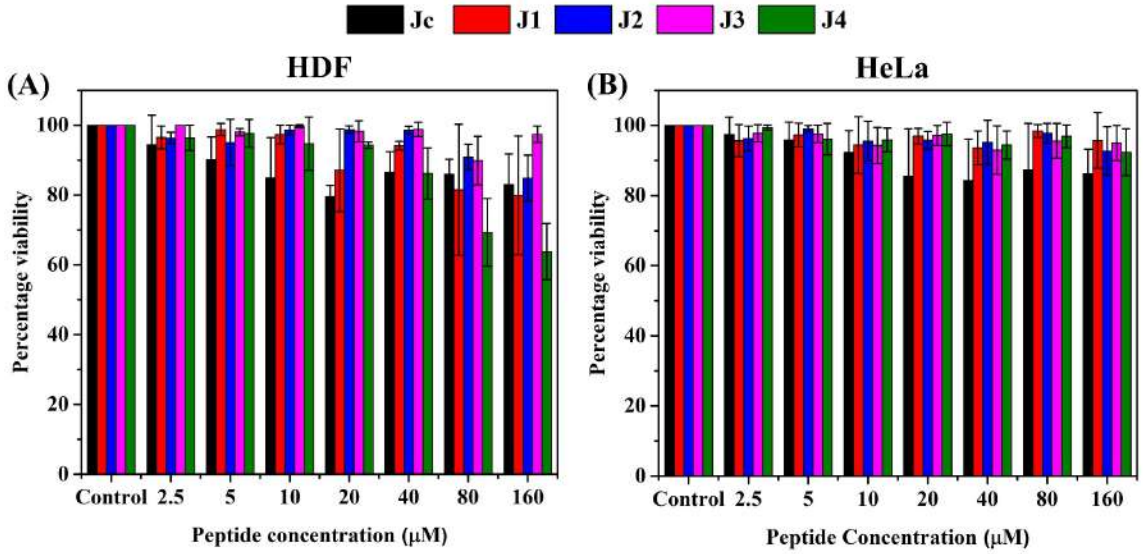

Figure 4.2. Cytotoxicity assay. Bar diagram depicting the viability of (A) HDF and (B) HeLa cell lines tested against different concentrations of the peptides Jc, J1, J2, J3 and J4.

Hemolytic activity

Hemolytic activities of the peptides were determined up to a concentration of 100 μM against 1 % human red blood cells.[8-9] None of the peptides displayed any significant hemolysis up to highest the tested concentration (Figure 4.3). The modified peptides as well as the control may therefore be considered safe to be employed in physiological systems for treating microbial infections.

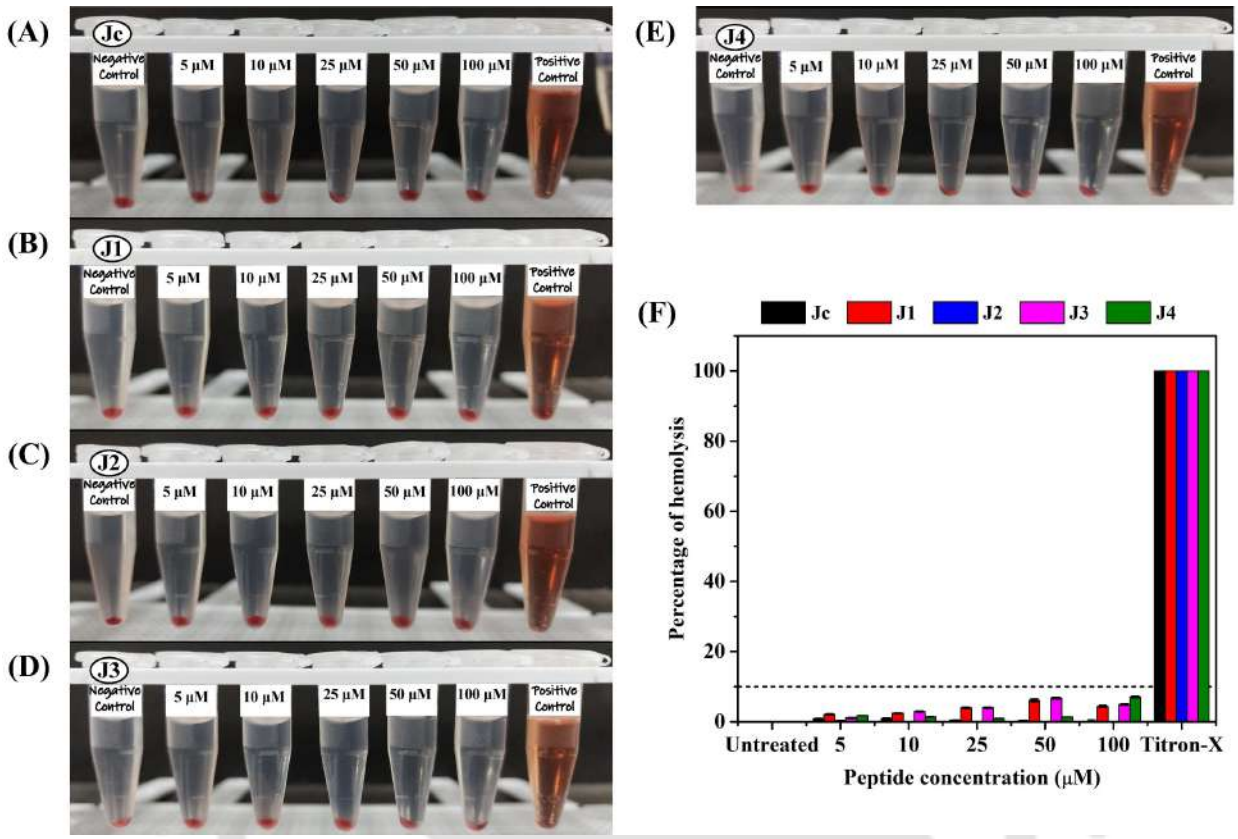

Figure 4.3. Hemolytic assay. Microcentrifuge tubes containing 1% RBCs in its untreated form as well as treated with different concentration of the peptides (A) Jc, (B) J1, (C) J2, (D) J3 and (E) J4 post incubation at 37 °C for 1 h. (F) Bar diagram depicting the percentage hemolysis induced by the peptides at different concentrations assuming 1% Triton-X 100 to induce 100% hemolysis.

Time kill kinetics

Time-kill kinetics assay was performed against *P. aeruginosa* to determine the time required for the two most potent peptides J3 and J4 to exhibit their bactericidal properties (Figure 4.4). *P. aeruginosa* cells were incubated with J3 and J4 at their respective MIC values, for different time intervals ranging from 2.5 to 90 min. It was found that J3 eliminated all the bacterial colonies completely within a period of 30 min [Figure 4.4(A) & (C)]. On the other hand, J4 took a little longer, displaying complete killing at 60 min [Figure 4.4(B) & (C)]. Thus, though both J3 and J4 has the same MIC against *P. aeruginosa*, J3 was a better antimicrobial in terms of faster killing when compared to J4.

The fact that J3 with a lower positive charge than J4, was a better antimicrobial agent in terms of potency (across various microbial strains), salt sensitivity of the antimicrobial potency, the kinetics

of antimicrobial activity and cytotoxicity suggested that optimum hydrophilic-hydrophobic balance was a more important factor driving the biological activity than the positive charge on the peptide.

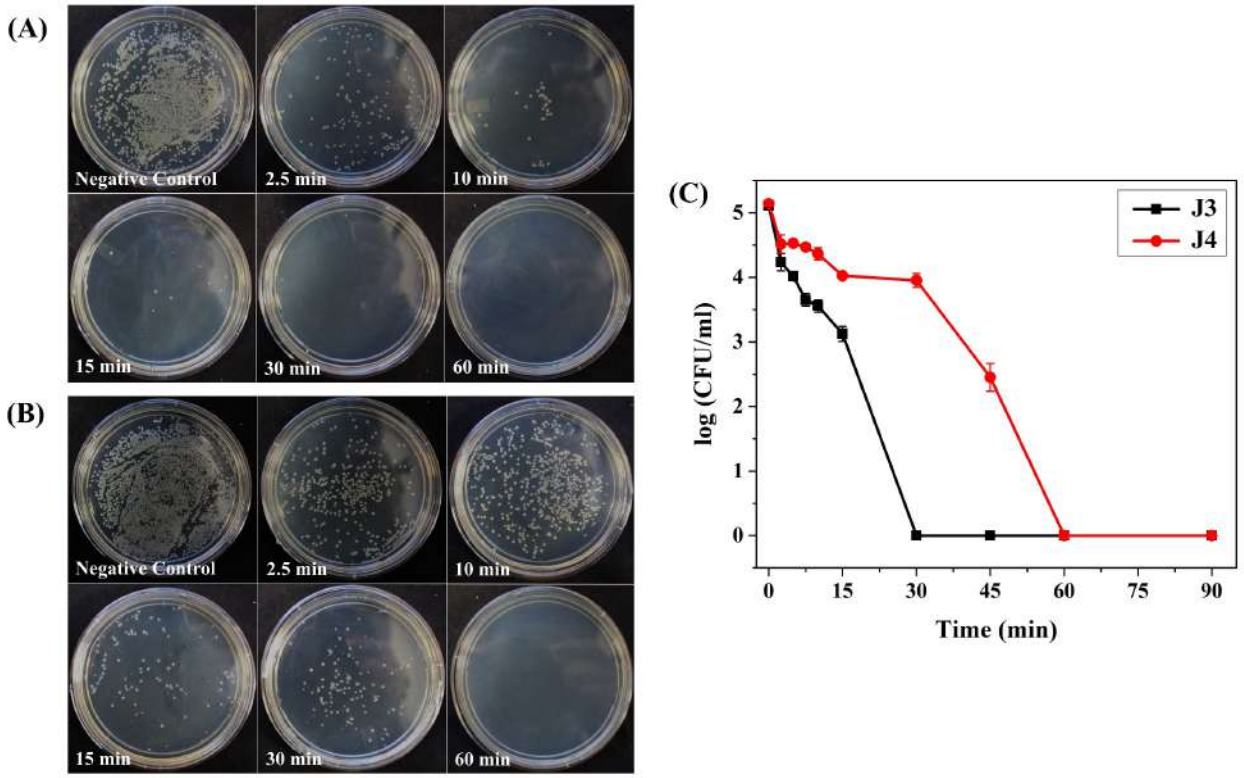

Figure 4.4. Time-kill kinetics assay. Photographs of the agar plates (representative of a set of triplicates) showing the growth of *P. aeruginosa* cells treated with MIC concentrations of the peptides (A) J3 and (B) J4 for different time intervals. (C) Graph representing elimination of the bacterial colonies as a function of log (CFU/mL) vs time (min).

Protease resistance

The stability of the control peptide Jc**,** and the most active designed analogs J3 and J4 were evaluated in the presence of trypsin (Figure 4.5). Trypsin is a proteolytic enzyme found in the small intestine that helps in digestion of proteins (or peptides) at the carboxylic ends of cationic residues like lysine or arginine.[10-12] Peptides Jc**,** J3 and J4 were incubated with trypsin for different time intervals up to a period of 24 h. Upon incubation of Jc with trypsin, >75 % of it got degraded after 1 h, and >90 % of it got degraded after 24 h of incubation [Figure 4.5(A) and (D)]. J3 and J4 were 100 % intact even after 24 h of incubation [Figure 4.5(B), (C) and (D)]. MALDI spectra of the trypsin treated peptides Jc**,** J3 and J4 were analysed, which proved the fragmentation of the peptide

Jc, in contrast to J3 and J4 (Figure C18-C20, Appendix C). Jc was a Lys containing peptide, and hence was susceptible to trypsin. J3 and J4 on the other hand containing Dab, the unnatural analog of Lys amino acid residue, gained resistance in the presence of trypsin.

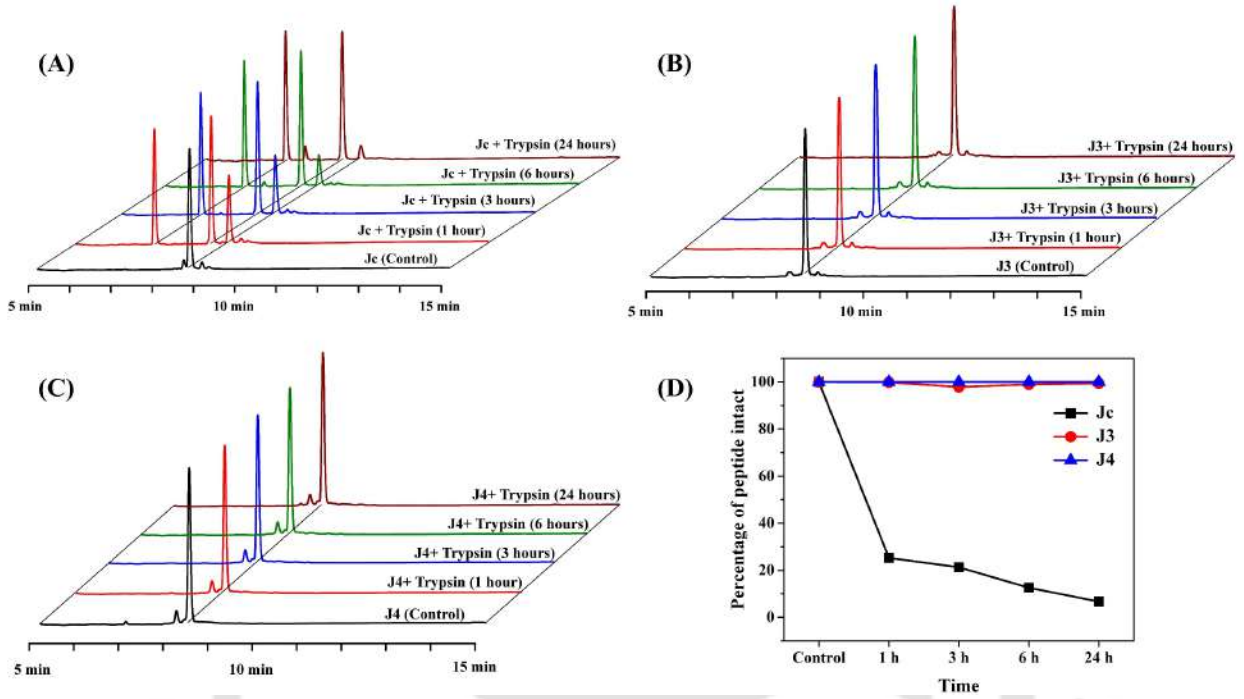

Figure 4.5. Proteolytic stability displayed by the peptides (A) Jc, (B) J3 and (C) J4 determined using analytic HPLC method. (D) Plot of intact peptides (%), post incubation with trypsin, as a function of time.

Serum stability

Human serum is a source of several proteolytic enzymes.[13] Most AMPs obtained from nature are susceptible to serum as they are hydrolysed by the enzymes present in it. In some cases, the susceptibility of the AMPs to the serum stems from the unspecific interactions with the other proteins that are present in the serum.[14-15] Thus, even though J3 and J4 were resistant to trypsin, we tested the serum stability of the peptides. Peptides Jc, J3 and J4 were incubated with serum for different time intervals. In line with the earlier experiment, J3 and J4 did not degrade even upon incubation with serum for 24 h [Figure 4.6(B), (C) and (D)]. Surprisingly, Jc composed of all natural amino acid residues, was resistant to serum degradation and retained its chemical integrity [Figure 4.6(A) and (D)]. MALDI spectra of the reaction mixtures of Jc, J3 and J4 incubated with serum, confirmed the serum stability of these peptides (Figure C21-C23, Appendix C).

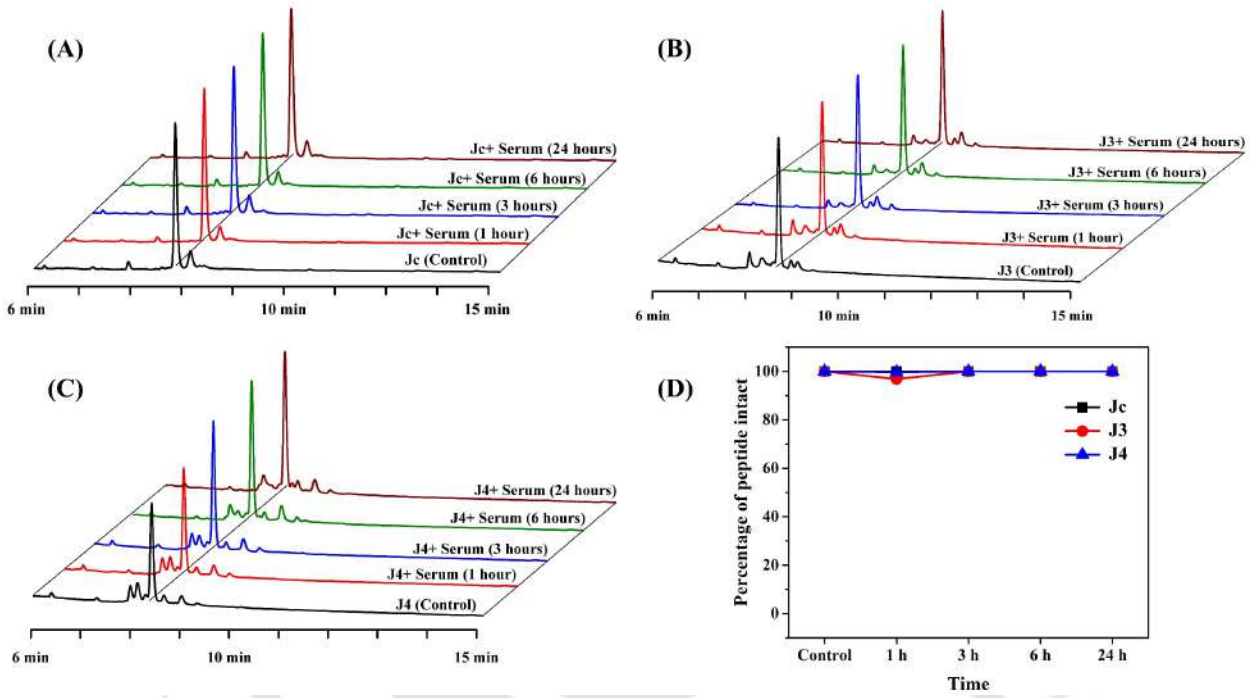

Figure 4.6. Serum stability displayed by the peptides (A) Jc, (B) J3 and (C) J4 determined using analytic HPLC method. (D) Plot of intact peptides (%), post incubation with serum, as a function of time.

Retention of biological activity in the presence of serum

To further investigate if the antimicrobial potency of the peptides were retained in the presence of serum, we determined the MIC values of the serum incubated peptides against *P. aeruginosa*. We incubated Jc, J3 and J4 with equal volume of serum for a period of 4 h. Serum incubated peptides were then used for the determination of the $MIC_{90\%}$ against *P. aeruginosa*. $MIC_{90\%}$ of all the tested peptides were found to remain unchanged (Figure 4.7). This conclusively proved that not only was the chemical integrity of Jc, J3 and J4 retained in the presence of serum, but even their antimicrobial potency remained unaltered.

Thus, from all of the above biological studies, it was concluded that J3 and J4 were the two promising Jelleine analogs developed in this study, with the former being a better candidate over the latter. As these peptides were most active against *P. aeruginosa*, the mechanistic investigations were studied only on these two AMPs against *P. aeruginosa*.

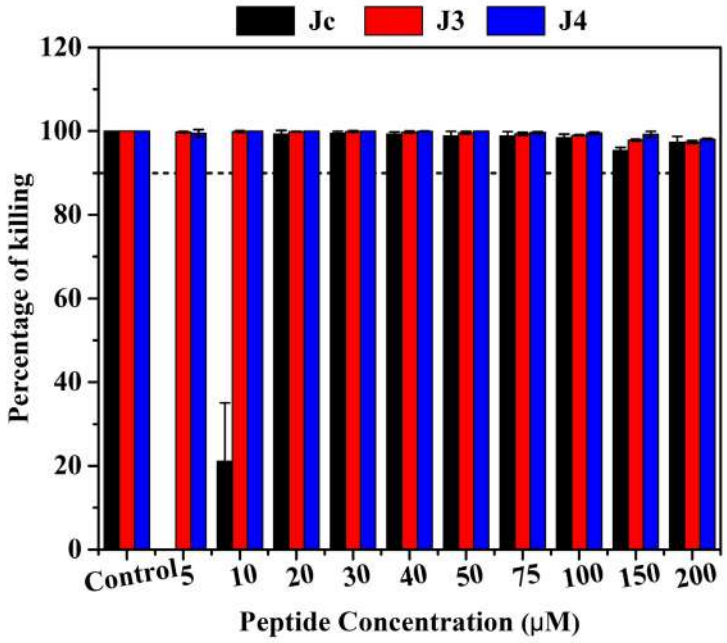

Figure 4.7. Determination of Minimum Inhibitory Concentration (MIC) of Jc, J3 and J4 pre-incubated with human serum against *P. aeruginosa*. Bar diagram depicts the percentage killing of *P. aeruginosa* cells treated with different concentrations of the peptides that were pre-incubated with human serum. $MIC_{90\%}$ values were the lowest concentrations at which > 90 % killings were observed.

4.2.3. Peptide membrane interactions

Blue shift of fluorescence emission maxima (λ_{max}) of Trp in presence of microbial membrane mimic SDS and live P. aeruginosa cells

Intrinsic fluorescence property of Trp was used to study the interaction of the peptides J3 and J4 with microbial membrane mimic D8PG and SDS, and mammalian membrane mimic DPC [Figure 4.8(A), (B) & C24, Appendix C]. J3 and J4 were titrated against an increasing concentration of D8PG, SDS and DPC, with ratios ranging from 1:0.25 to 1:10. J3 displayed a blue shift of the λ_{max} of Trp by 22 nm and 12 nm, when titrated against SDS (10×) and D8PG (10×) respectively, while no shift was observed when titrated against DPC. The shift values of J4 corresponding to titrations against 10× concentrations of SDS, D8PG and DPC were 22 nm, 11 nm and 0 nm respectively. Prominent blue shifting of the λ_{max} of Trp, indicated an interaction in between the peptides and the membrane mimics. Additionally, observation of blue shift selectively in the presence of bacterial

membrane mimics like SDS and D8PG suggested, selective interaction of the AMPs only with the microbial membranes over the mammalian membranes.

Interactions of the peptides J3 and J4 with living *P. aeruginosa* cells were also studied using fluorescence spectroscopy. Peptides J3 and J4 at their respective MIC values, were titrated against increasing volumes of *P. aeruginosa* cells. Upon increasing the volume of *P. aeruginosa* cells, a steady increase in the blue shift of the λ_{max} in the fluorescence emission of Trp was observed. Addition of 2×10^6 cells each time resulted in significant wavelength shifts in both the peptides, and after ten consecutive additions, both J3 and J4 displayed a λmax shift of 19 nm each [Figure 4.8(C) & C25, Appendix C], indicating the membrane interaction of J3 and J4 with the live *P. aeruginosa* cells.

Solvent accessibility of Trp in presence of membrane mimics

In order to understand the solvent exposure of Trp residue of J3 and J4 in the free state and when in complex with SDS (1:20) and DPC (1:20), acrylamide, a static quencher was titrated against the peptides in all three states up to a concentration of 200 mM. The extent of quenching in the fluorescence of Trp, in the free state as well as in the presence of SDS and DPC complexes were determined from the Stern-Volmer constant (K_{SV}). The K_{SV} values of J3 and J4 in the free state as well as in the presence of DPC were higher than when in complex with SDS, implying preferential interactions of the peptides with SDS [Figure 4.8(D) &(E)]. Burial of Trp residues in the SDS micelle led to lower accessibility of solvents, that eventually attributed to the lower K_{SV} values of the peptides in the presence of SDS. This experiment proved the selective interaction of AMPs J3 and J4 with SDS with respect to DPC micelles. Thus, the selective membrane interaction could be the plausible reason for their high antimicrobial potency and non-cytotoxicity**.**

CD in presence of live cells

Interaction of the peptides with the cells of *P. aeruginosa* was studied with the help of CD spectroscopy [Figure 4.8(F) &(G)]. CD spectra for untreated *P. aeruginosa* cells and peptides J3 and J4 (50 μM in water) were acquired at the beginning of the experiment. Cells were incubated with J3 and J4 (50 μM) for various time intervals and CD spectra of the reaction mixture of peptides and cells, were acquired at the end of these time intervals. A shift in the peak positions and the variation in the peak intensities of the cells in the CD spectra were observed upon incubation with the peptides, which became more prominent with time, implying interaction of the

peptides with the cells. Although a decrease in the peak intensity of the untreated control cells could be seen at the end of 2 h, no shift in the peak position was observed. On the other hand, cells treated with Polymyxin-B (antibiotic, positive control), also displayed a shift in the peak position and intensity, which was similar to those of the cells treated with J3 and J4 for 1 h. Thus, interaction of the peptides with the live *P. aeruginosa* cells could be clearly established from the CD experiment.

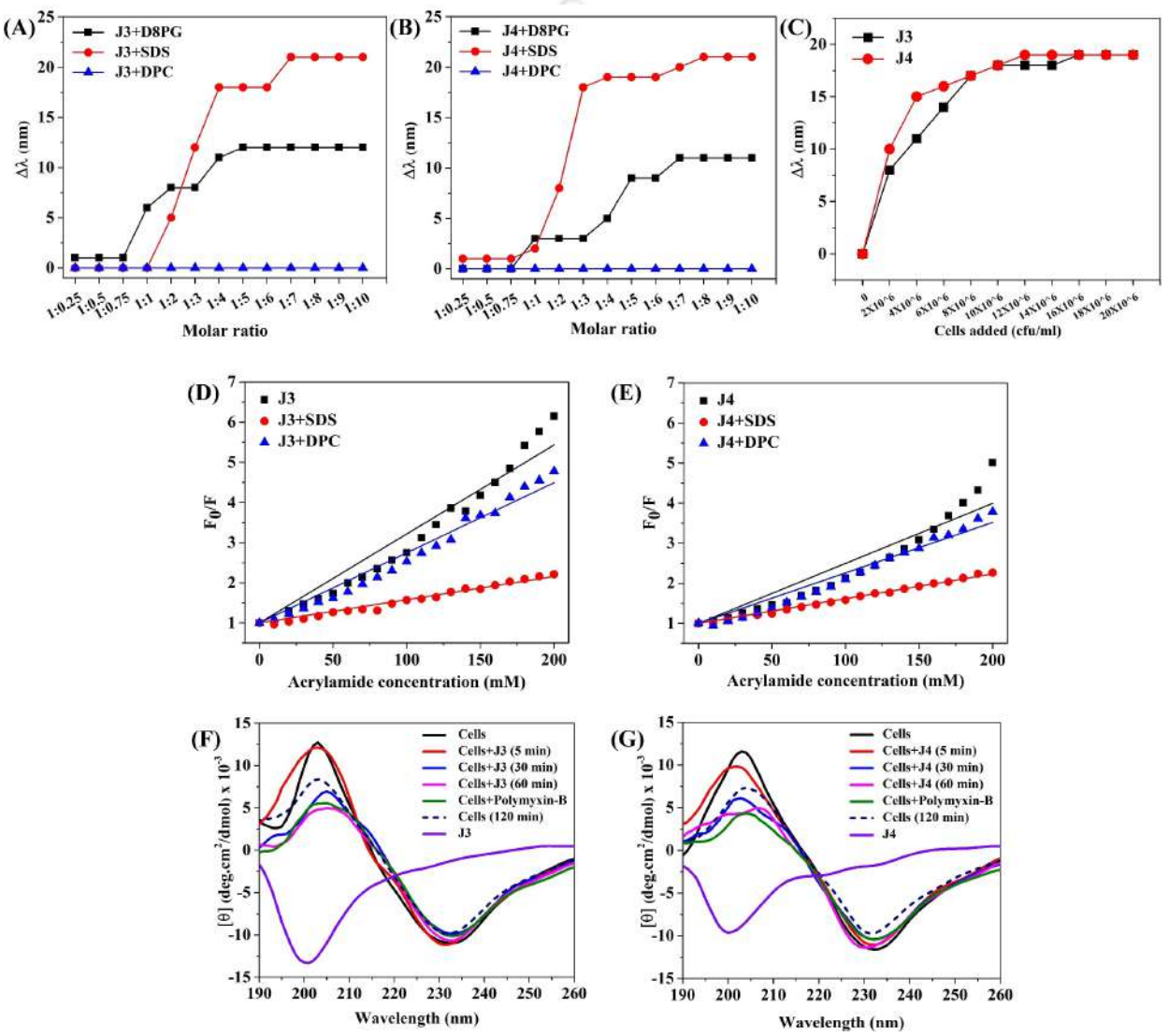

Figure 4.8. (A) and (B) Trp Blue Shift Experiments. λ_{max} shift of the Trp fluorescence of peptides J3 and J4 in presence of increasing concentrations of D8PG, SDS and DPC. (C) Live cell fluorescence experiment. λ_{max} shift of the Trp fluorescence of the peptides J3 and J4 corresponding to increasing cell volumes (*P. aeruginosa*). (D) and (E) Solvent accessibility experiment. Solvent

accessibility plot of J3 and J4. F_0/F plotted against increasing acrylamide (static quencher) concentration. Slope denotes the Stern-Volmer constant (K_{SV}). (F) and (G) Live cell CD spectra of untreated and J3/J4 treated *P. aeruginosa* cells.

Thermodynamics of peptide: membrane mimic interaction: isothermal titration calorimetry

The interactions of J3 and J4 with lipopolysaccharide obtained from *P. aeruginosa* was studied using isothermal titration calorimetry (ITC) (Figure 4.9). J3 and J4 were both found to interact with the *P. aeruginosa* LPS as evident from the ITC isotherms. J3 had a better binding affinity to the LPS compared to that of J4, as evident from their values of equilibrium dissociation constants (K_D) values of 20.92 μM and 43.10 μM respectively (Figure 4.9 & Table 4.4).

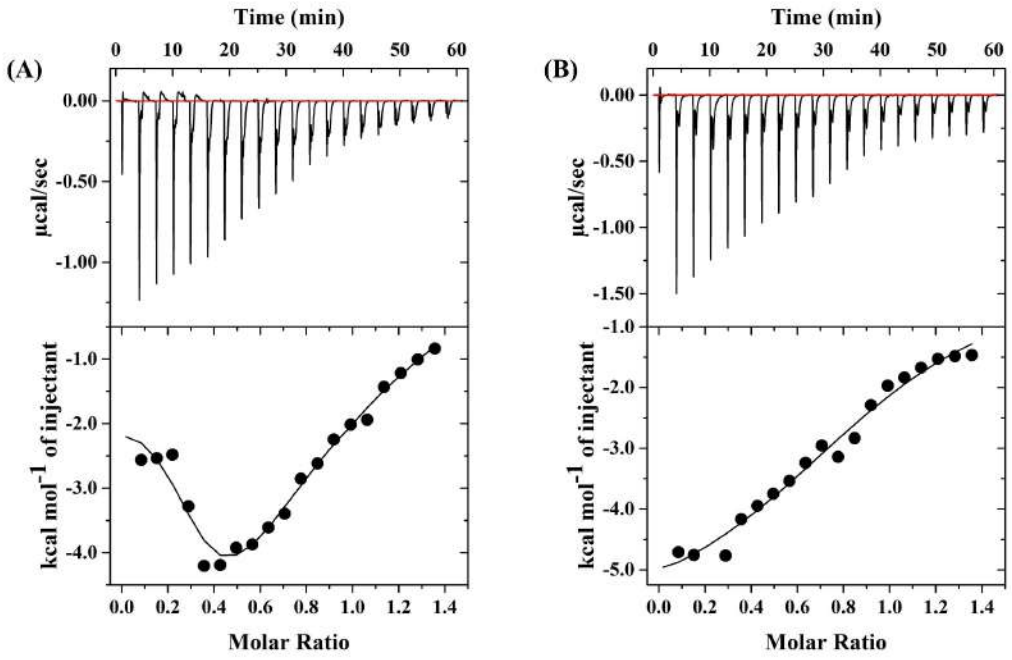

Figure 4.9. Isothermal titration calorimetry (ITC) isotherms showing the interactions between the peptides (A) J3 and (B) J4 with lipopolysaccharides (Origin: *P. aeruginosa*).

Table 4.4. Thermodynamic parameters for the interaction of *P. aeruginosa* Lipopolysaccharide (LPS) with J3 and J4**.**

Thermodynamic parameters	J3	J4
Model	One binding site	One binding site

Temperature	310 K (37 °C)	310 K (37 °C)
K_A (M^{-1})	$4.78x10^4$	$2.32x10^4$
N	1.290	0.923
ΔH (cal.mol^{-1})	-5064.0	-6139.0
ΔS (cal.mol^{-1}.deg^{-1})	5.14	0.176
TΔS (cal.mol^{-1})	1593.40	54.56
ΔG (cal.mol^{-1})	- 6657.40	-6193.56
K_D (μM)	20.92	43.10

Interaction of J3 and J4 with SDS was also studied using ITC (Figure 4.10 & Table 4.5). Isotherms for both the titrations were fitted using a one site binding model. Dissociation equilibrium constants (K_D) were evaluated to be 156.25 μM and 172.71 μM for J3 and J4 respectively, making J3 a marginally stronger binder than J4.

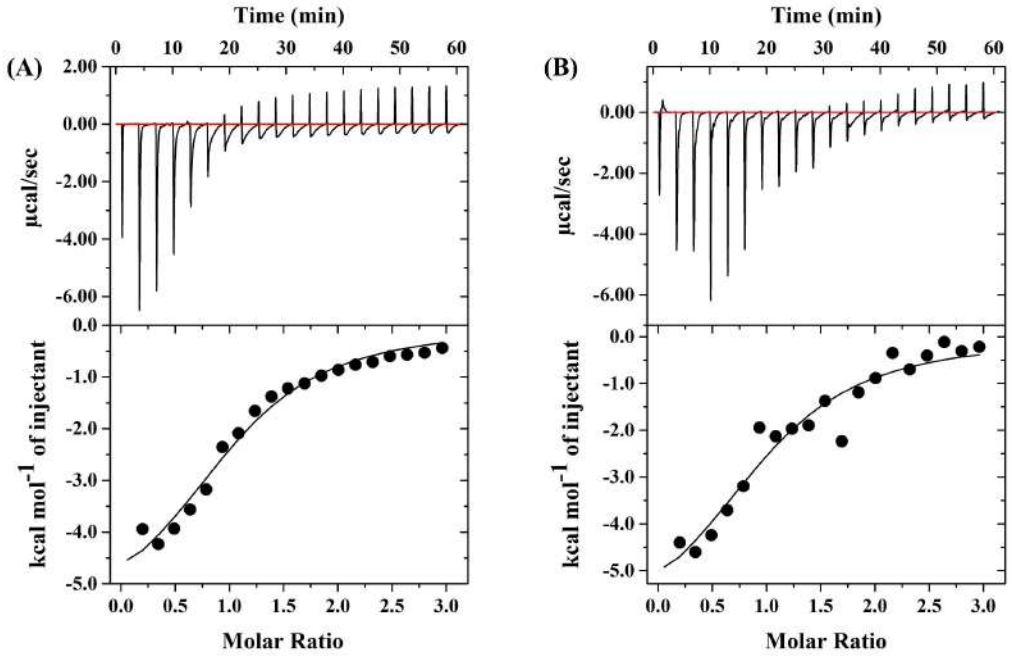

Figure 4.10. Isothermal titration calorimetry (ITC) isotherms showing the interactions between the peptides (A) J3 and (B) J4 with SDS (bacterial membrane mimic).

Table 4.5. Thermodynamic parameters for the interaction of J3 and J4 with SDS.

Thermodynamic parameters	J3	J4
Model	One binding site	One binding site
Temperature	310 K (37 °C)	310 K (37 °C)
K_A (M^{-1})	$6.40X10^3$	$5.79X10^3$
N	1.04	1.01
ΔH ($cal.mol^{-1}$)	-5967.0	-6677.0
ΔS ($cal.mol^{-1}.deg^{-1}$)	-1.83	-4.31
TΔS ($cal.mol^{-1}$)	- 567.3	-1336.1
ΔG ($cal.mol^{-1}$)	-5399.7	-5340.9
K_D (μM)	156.25	172.71

No interactions were observed in between the peptides and DPC (Figure 4.11). This experiment clearly proved the selective binding of the peptides for the LPS from *P. aeruginosa* and microbial membrane mimics over the mammalian membrane mimics, corroborating their high antimicrobial potency and non-cytotoxicity towards mammalian cells.

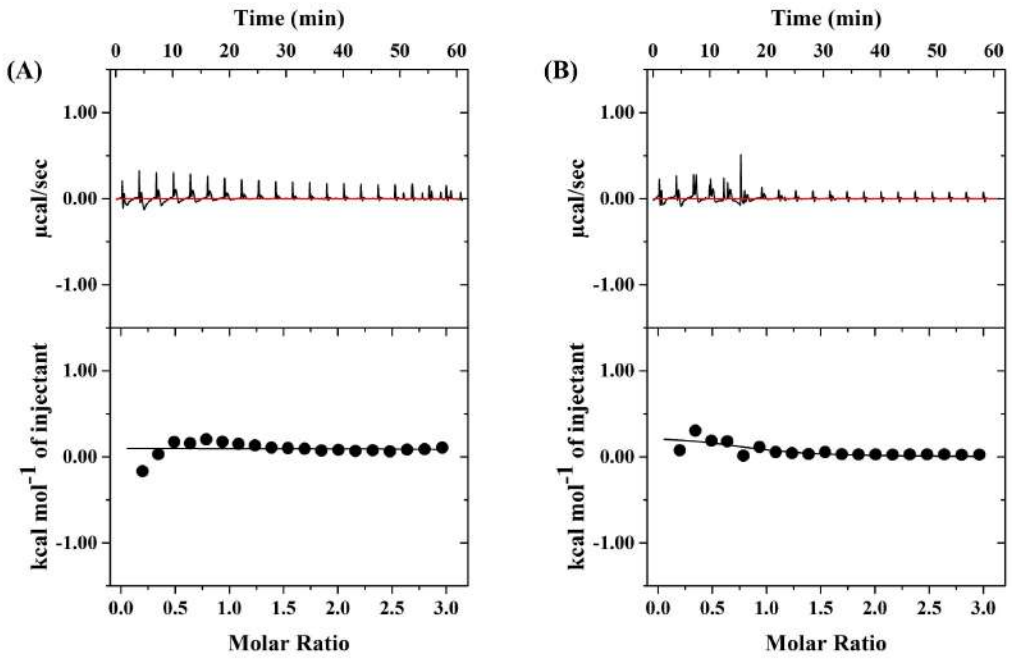

Figure 4.11. Isothermal titration calorimetry (ITC) isotherms showing the interactions between the peptides (A) J3 and (B) J4 with DPC (mammalian membrane mimic).

Studying the interaction in between the peptides and the membrane mimics by using CD Spectroscopy

The interaction of the peptides with the different membrane mimetics (SDS and DPC) were investigated using CD spectroscopy (Figure 4.12). We assumed that the interaction of the peptides with the membrane mimetics might induce change in the secondary structure of the peptides, which could be detected in the CD spectra. Analysis of CD spectra revealed that template peptide Jc, as well as all the designed analogs, namely J1-J4**,** mostly adopted random coil conformation in free state in water. Significant changes in the CD spectra of most of the peptides (mostly tending to be helical) could be seen in the presence of SDS, implying peptide-SDS interactions. In the presence of DPC, the changes in the spectra of the peptides compared to that in the water were negligible, suggesting no interaction of the peptides with the mammalian membrane mimic. Finally, in the presence of 50 % TFE, a solvent known for promoting helical conformation in peptides, the changes in the CD spectra were also quite significant. Thus, the membrane selectivity of the designed AMPs could clearly be established from their change in CD spectral patterns.

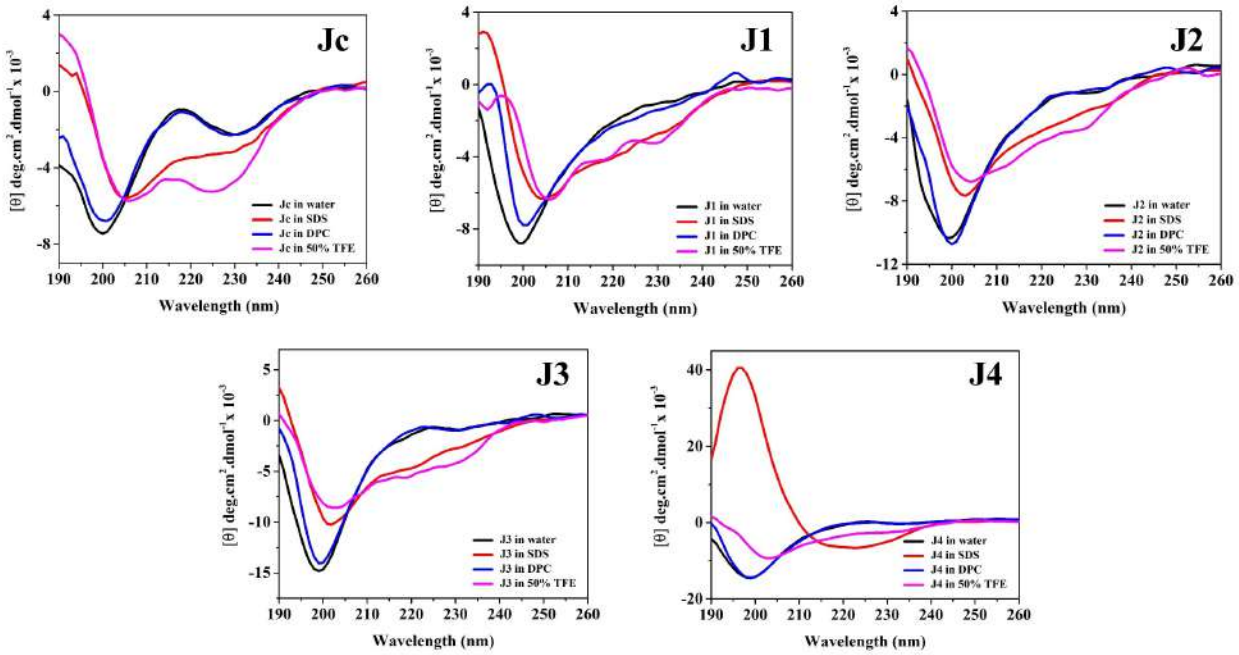

Figure 4.12. CD spectra of peptides Jc, J1, J2, J3 and J4 in the free state (water) as well as in the presence of bacterial membrane mimic SDS, mammalian membrane mimic DPC and 50% TFE (a helix promoter).

4.2.4. Modes of action

Inner and outer membrane permeation assay

Propidium iodide (PI) is a dye that shows an enhanced fluorescence upon binding to DNA molecules. This dye however is impermeable to the intact and living microbial membranes. Upon damage of the bacterial inner membrane, PI readily penetrates the membrane and binds to the genetic material exhibiting enhanced fluorescence. Thus, an enhancement of the PI fluorescence is a quantitative estimate of the inner membrane permeability of the cell. Incubation of *P. aeruginosa* cells with 0.5× MIC and 1× MIC of J3 led to 7 % and 60 % enhancement of fluorescence intensity, relative to the positive control, 10 μM of Polymyxin-B (estimated 100 % permeation) [Figure 4.13(A)]. J4 on the other hand, could induce an enhancement of fluorescence intensity by about 19 % and 73 % respectively at its 0.5× and 1× MIC concentrations [Figure 4.13(B)]. Enhancement of fluorescence intensity of PI in the presence of J3 and J4, established their inner membrane permeation ability. Greater permeation ability of J4 over J3 could be attributed to the greater positive charge in the former over the latter.

N-Phenyl 1-napthylamine (NPN) shows enhanced fluorescence upon binding to the membrane lipids. However, NPN cannot access the lipids in the intact membranes, and thus an increase in the NPN fluorescence is a marker of the membrane disruption. Upon incubation of the cells with 0.5× and 1× MIC of J3, a fluorescence enhancement of 57 % and 89 % was observed [Figure 4.13(C)]. while 0.5× and 1× MIC of J4 effected an increase of fluorescence intensity by 26 % and 97 % [Figure 4.13(D)]. All the estimates were normalized with reference to 10 µM polymyxin-B. Increase in the fluorescence intensity of NPN in the presence of J3 and J4, proved their outer membrane permeability, with the latter being more efficient at it owing to its higher charge.

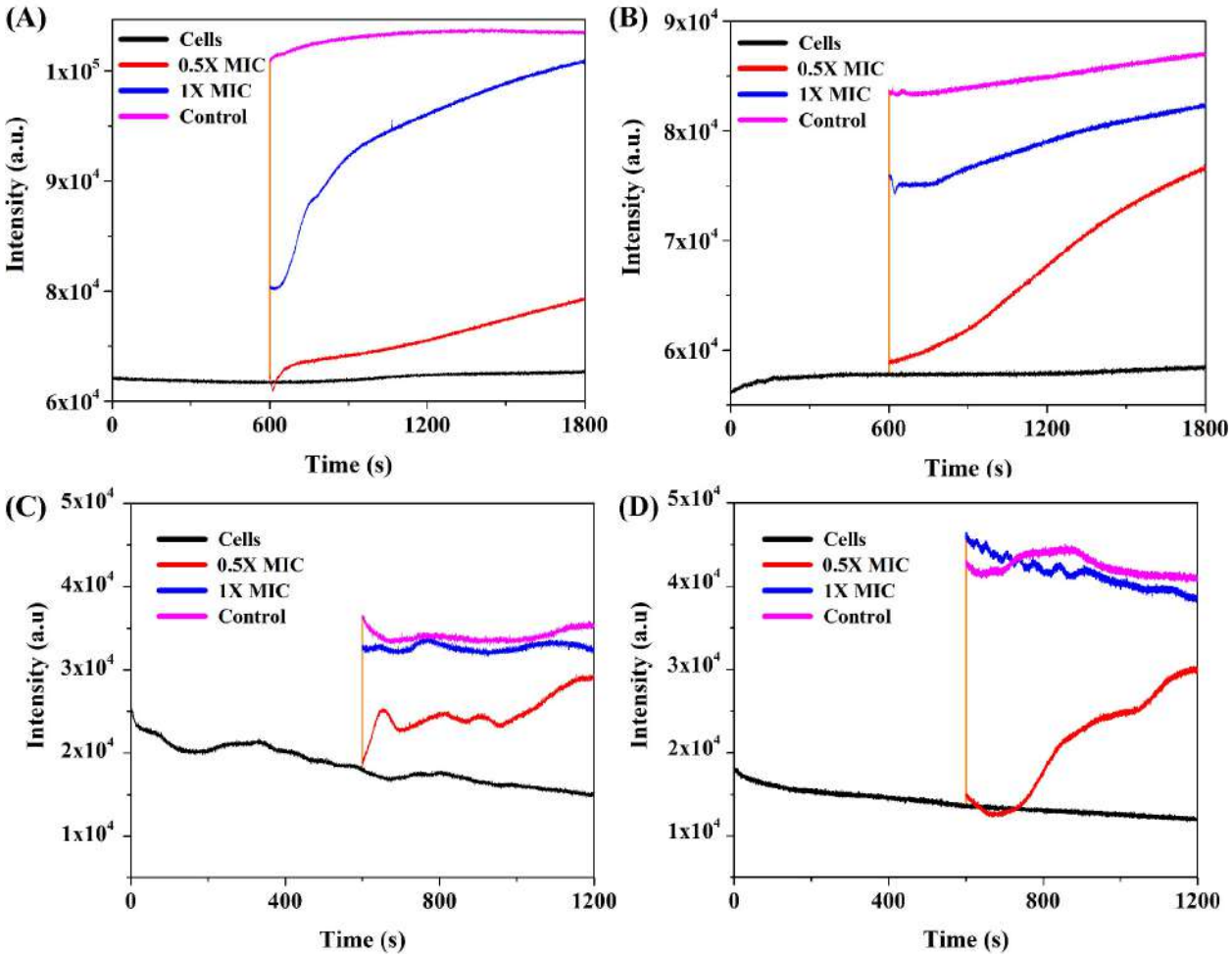

Figure. 4.13. Inner membrane permeation assay (PI uptake assay) and outer membrane permeation (NPN uptake assay). Fluorescence spectra *of P. aeruginosa* cells preincubated with PI treated with 0.5× MICs and 1× MICs of the peptides (A) J3 and (B) J4 as well as 10 µM of Polymyxin-B (positive control). (C) and (D) represent the fluorescence spectra *of P. aeruginosa* cells

preincubated with NPN treated with respectively 0.5× MICs, and 1× MICs of the peptides J3 and J4, as well as 10 μM of Polymyxin-B as the positive control.

Membrane leakage studies through live cell NMR

To investigate the membrane leakage ability of AMPs J3 and J4**,** live cell NMR was performed. *P. aeruginosa* cells were treated with J3 and J4 for various lengths of time and ^{1}H-1D NMR was recorded corresponding to each time interval. Freshly washed untreated cells did not show any prominent peaks in NMR spectra, while the peptides had their characteristic peaks observable in the spectra. Addition of the peptides to the cells led to broadening of its peaks, suggesting interaction in between the peptide and the cells [Figure 4.14(A) & (B)]. Appearance of new peaks, and intensifying of certain peaks were observed over the time. These might be attributed to the metabolites that leaked out of the *P. aeruginosa* cells, upon incubation of the peptides. Thus, in other words, appearance of new peaks demonstrated the membrane leakage ability of J3 and J4.

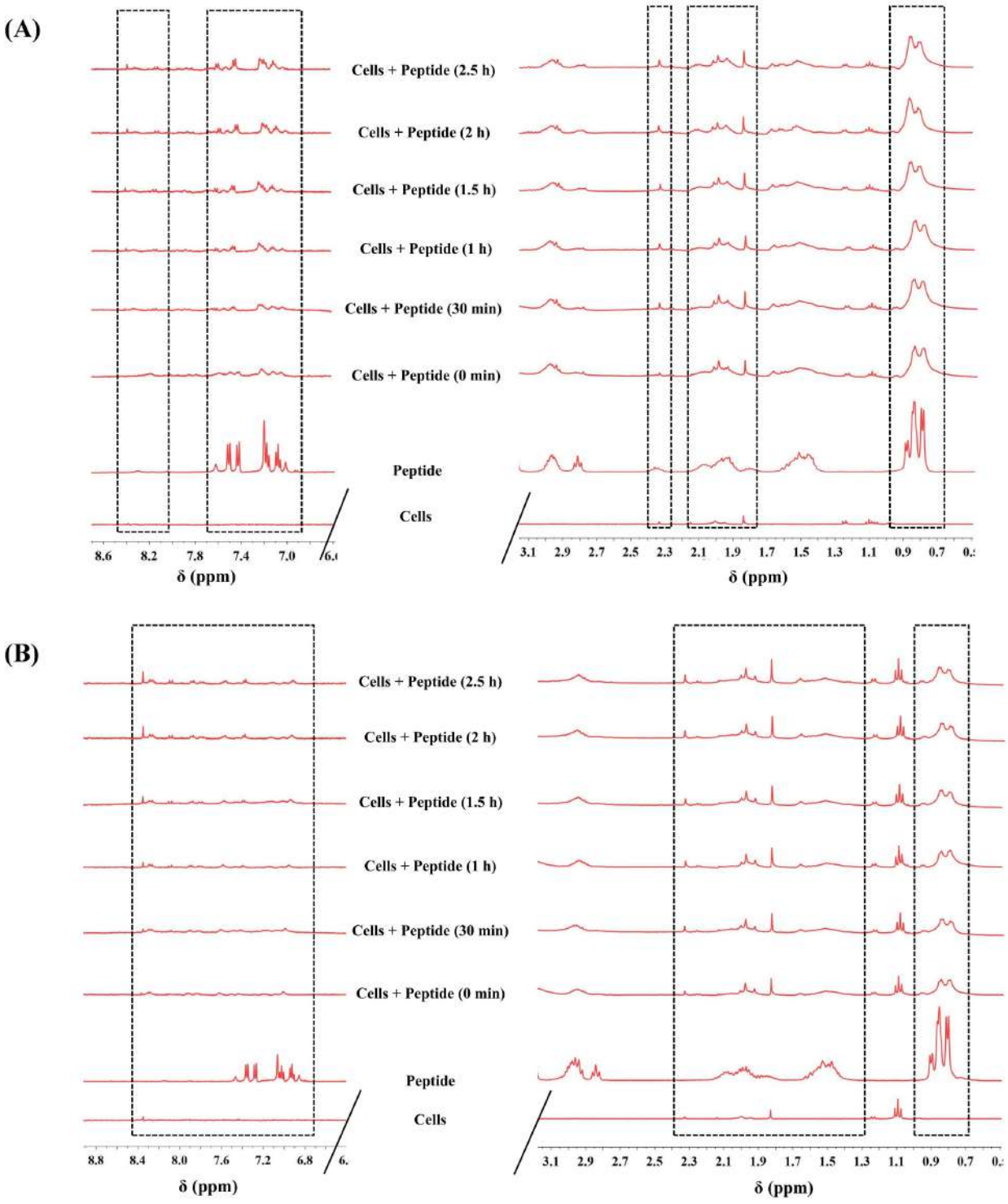

Figure. 4.14. Live Cell NMR experiment. ^{1}H-NMR spectra corresponding to (A) J3 and (B) J4 added with *P. aeruginosa* cells and kept incubated for different time intervals.

FESEM images of the peptide treated microbes

FESEM images of *P. aeruginosa* cells treated with 1× and 2× MIC concentrations of the peptides J3 and J4**,** were acquired to visualize the effect of the peptides on the bacterial membranes (Figure 4.15). Untreated cells were also imaged as the negative control. It was found that incubation of the bacterial cells with 1× MIC of both the peptides induced significant damage to the bacterial membranes. At 2× MIC, more fatal effects were visible, membrane lysis leading to severe cell membrane damages could be observed.

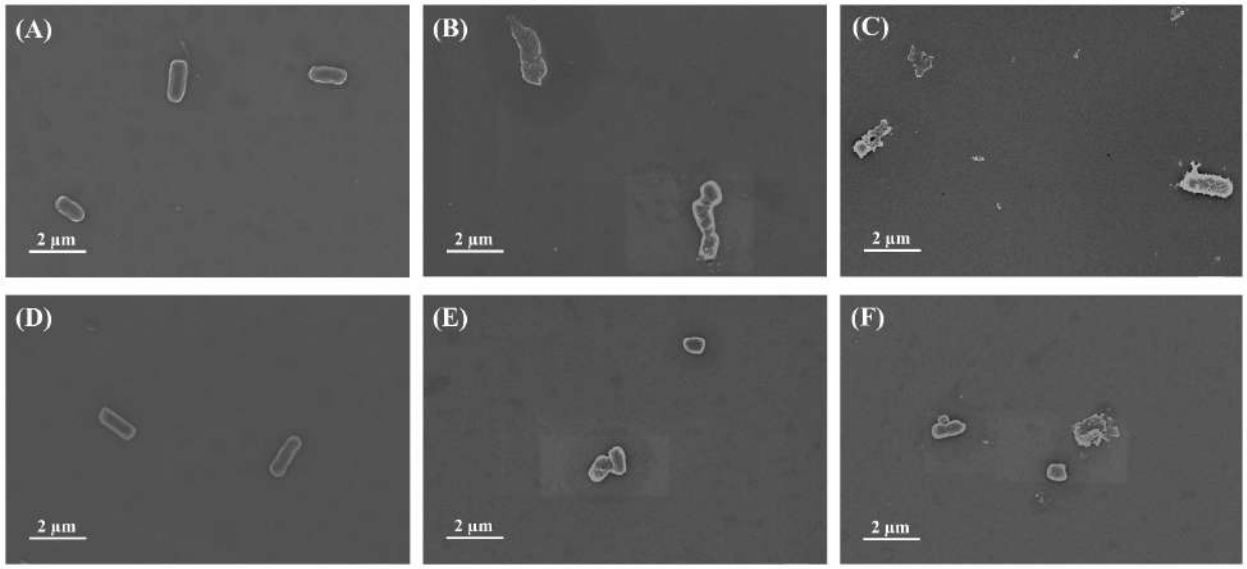

Figure 4.15. FESEM images of *P. aeruginosa* cells. (A) and (D) Untreated cells or negative control; *P. aeruginosa* cells treated with (B) 1× MIC of J3, (C) 2× MIC of J3, (E) 1× MIC of J4 and (F) 2× MIC of J4.

Live cell/dead cell assay

The membranolytic effects of the AMPs J3 and J4 were further established using live cell dead cell assay, studied using confocal microscopy (Figure 4.16). Acridine orange is a dye that can permeate through the cytoplasmic membrane of the living cells (cells with intact/ uncompromised cytoplasmic membrane) and emit green fluorescence upon binding with the cytoplasmic RNA (also the nuclear RNA).[16] Propidium iodide, PI as mentioned earlier, is impenetrable into healthy cells and shows enhanced red fluorescence upon intercalating with the DNA molecules,[17] only upon permeating through compromised membrane. As membrane compromise eventually leads to cell death, PI-stained cells indicate the dead cells. Acridine orange and propidium iodide were added to both untreated and J3/J4 treated *P. aeruginosa* cells. Untreated *P. aeruginosa* cells emitted

green signal upon incubation with acridine orange, but did not strain with PI being healthy and intact. Upon treatment with the peptides, the cells showed very weak green fluorescence of acridine orange, while it showed intense red staining of PI indicating cell death. This experiment corroborated with the live cell NMR and the FESEM studies, and conclusively established the membranolytic mode of action of the peptides.

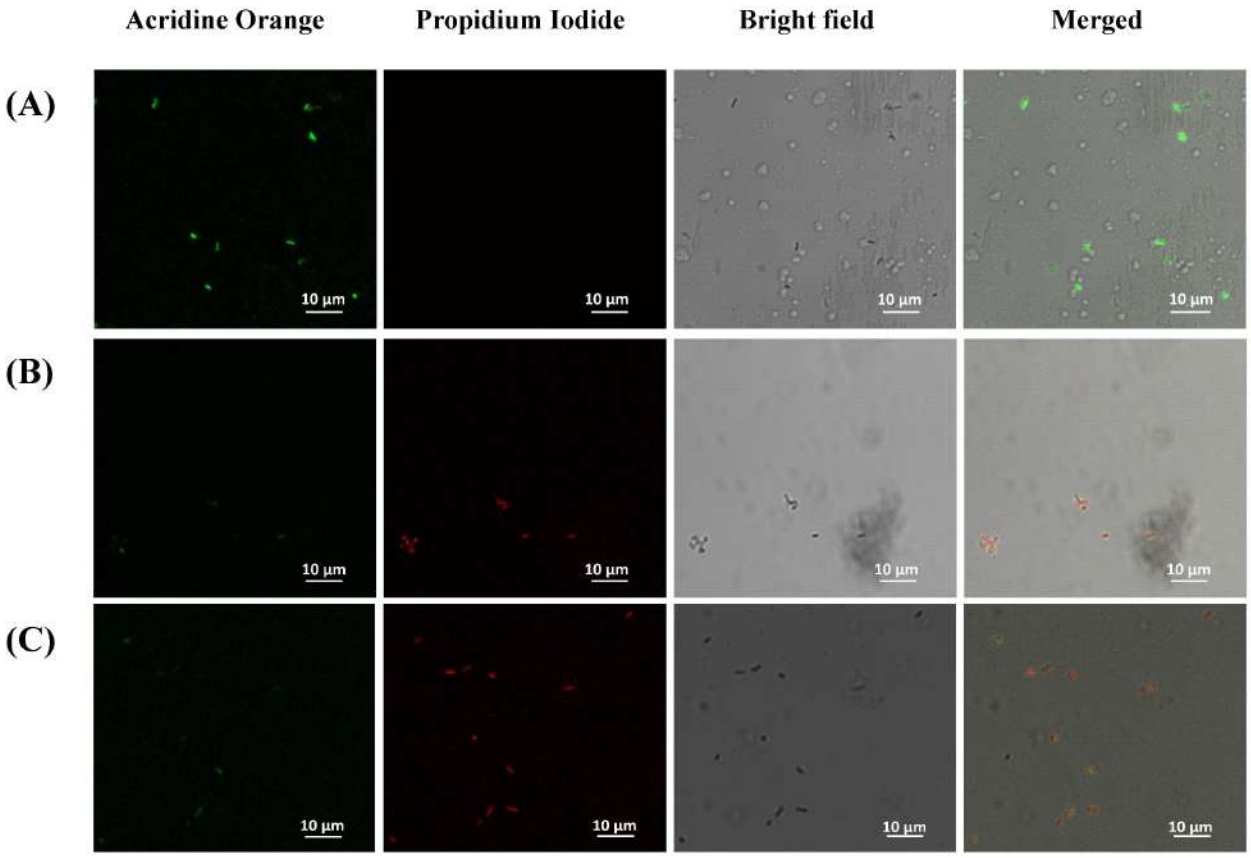

Figure 4.16. Live Cell Dead Cell assay using acridine orange and propidium iodide. (A) Untreated *P. aeruginosa* cells; *P. aeruginosa* cells treated with (B) J3 and (C) J4.

4.2.5. Structure and dynamics of the peptide in the presence and absence of bilayer: insights from MD simulations

MD simulations confirmed that the peptides (J3 and Jc) remained unstructured (containing bends and turns) in the presence or absence of the lipid bilayer, corroborating the CD experiments (Figure 4.17).

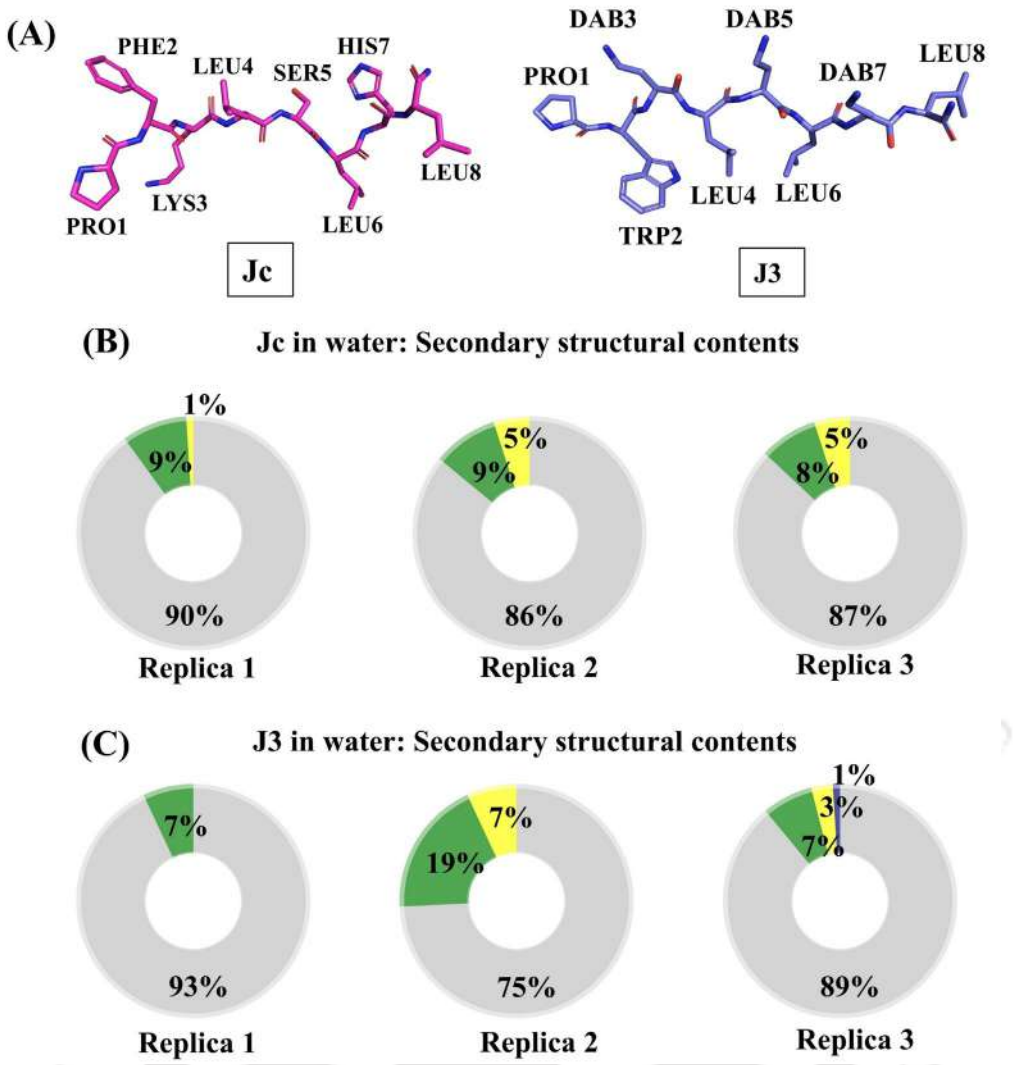

Figure 4.17. (A) Structure of Jc and J3 (in sticks) after 100 ns of MD simulations (free in water). Hydrogen atoms, water molecules, and chloride ions are not shown for clarity. Secondary structural content (in percentage) of the free peptide (in water) was estimated from three independent MD replicas, (B) Jc, (C) J3. (grey = random coil, green= bend and yellow= turn, blue = helix).

The plot of d_{COM} (relative distance between the center of mass of the peptide and the bilayer) as a function of time is shown in Figure 4.18. A plateau after 200 ns was evident (d_{COM} ~ 1.95 nm), indicating structural convergence of the peptide: bilayer complex.

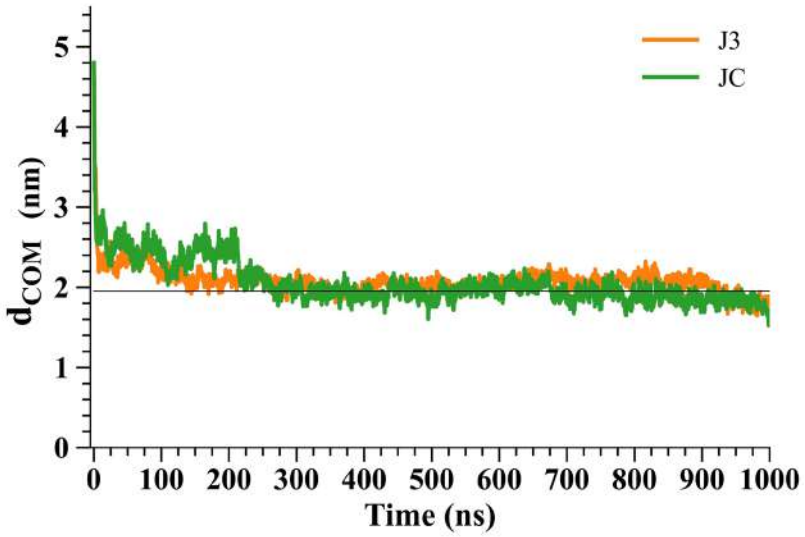

Figure 4.18. Peptide: bilayer distance as a function of time. d_{COM} is the distance between the center of mass of the peptide (J3, Jc) and the center of mass of the bilayer. The black horizontal line (dCOM ~ 1.95 nm) was the averaged d_{COM} obtained from the last 500 ns of the 1000 ns trajectory that corresponds to stable peptide: membrane complex.

The peptide: bilayer binding was irreversible as the dissociation event was not observed in the time-scale of the simulation. J3-bilayer binding was driven by electrostatic interactions (negatively charged phosphates of the Lipid A of the bilayer and positively charged $-NH_3^+$ tips of DAB) followed by placement of the hydrophobic side-chain of the peptide (TRP2, LEU4, LEU6, and LEU8) in the aliphatic core of the bilayer as well as forming additional favourable electrostatic contacts [Figure 4.19(A)]. The bonding requirement of the peptide is satisfied by either forming direct interactions with the bilayer phosphate charges [Figure 4.19(A)] or forming hydrogen bonds with the water molecules [Figure 4.19(B)]. The tryptophan residue (TRP2) was buried in the hydrophobic aliphatic core of the bilayer [Figure 4.19(A)], corroborating the tryptophan fluorescence calculating the peptide heavy-atoms root mean square fluctuation (RMSF) in the absence and presence of a bilayer. As expected, the RMSF plot confirmed the reduction of peptide flexibility in response to bilayer binding [Figure 4.19(E)]. Estimation of solvent-accessible surface area (SASA) provides insight into the solvent accessibility of the peptide residues in the presence of a bilayer [Figure 4.19(D)].

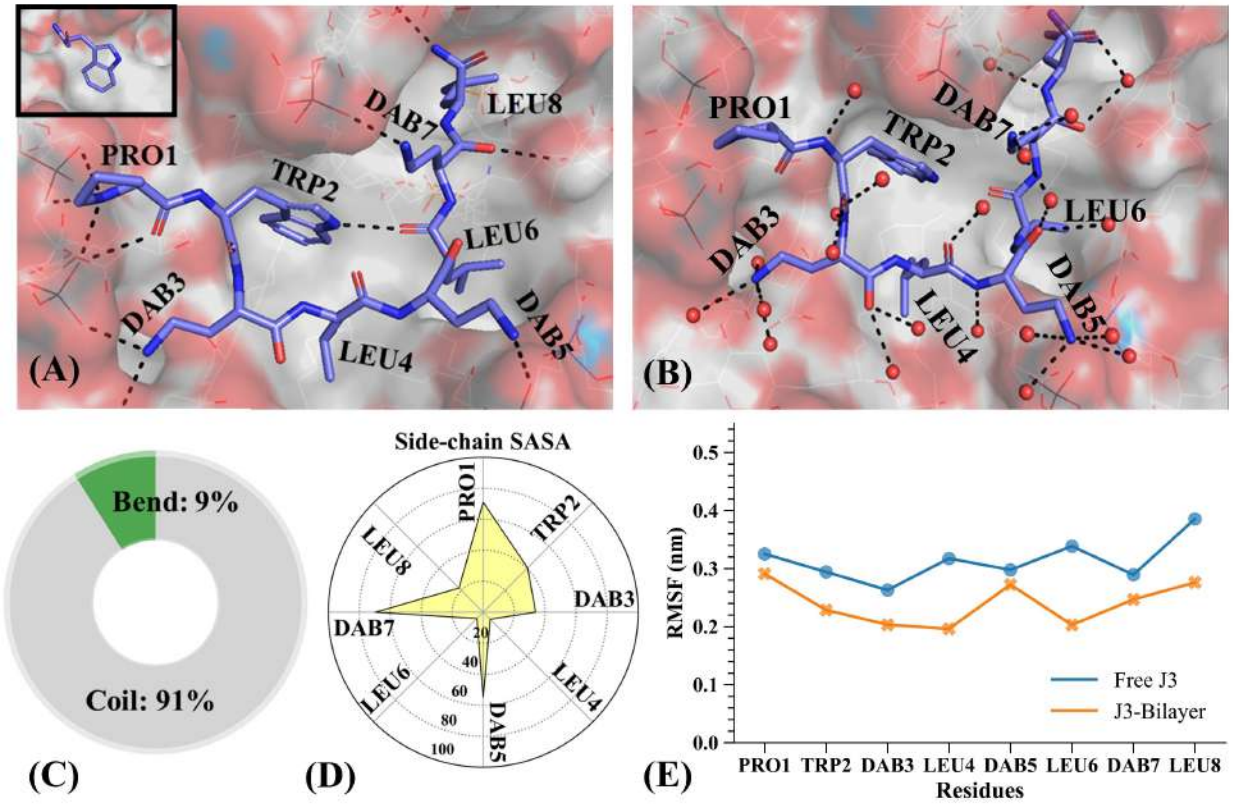

Figure 4.19. The structure of the complex after binding of J3 to the bilayer (*P. aeruginosa* outer membrane mimic) after 1000 ns of MD. Peptide J3 in violet sticks (nitrogen, blue; oxygen, red) and the bilayer in surface (red-blue-oxygen) representation. The dashed black line indicated the electrostatic interaction network (heavy atom distances ≤0.34 nm). (A) Peptide: bilayer electrostatic contact in broken line. Tryptophan residue (TRP2) is buried in the desolvated dry hydrophobic pocket in the bilayer (shown explicitly in the solid box). TRP2 satisfies the hydrogen bonding requirement by forming an H-bond with the main chain of LEU6. Hydrophobic side chains (LEU4, LEU6, and LEU8) were positioned in the hydrophobic core of the bilayer. (B) Peptide water electrostatic contact. (C) Secondary structural content of the J3 peptide (grey = random coil, green = bend). (D) Residue-wise trajectory averaged percent solvent exposure of the side-chain of J3 is shown in the yellow net plot with contours of constant percent exposure. Solvent exposer is estimated as: (SASA of amino acid residue in J3:bilayer complex/SASA of the amino acid residue in J3) × 100. (E) Residue-wise root mean square fluctuation (RMSF) of the heavy atoms of J3 in the absence (blue) and presence of bilayer (red). The data from the last 500 ns of the 1000 ns MD trajectory has been averaged and reported in (C), (D), and (E).

Peptide binding to the bilayer strongly alters the density of the upper leaflet (negatively charged Lipid A, the surface that binds to the peptide) as well as the distribution of the positively charged counter ions relative to the upper leaflet side (Figure 4.20).

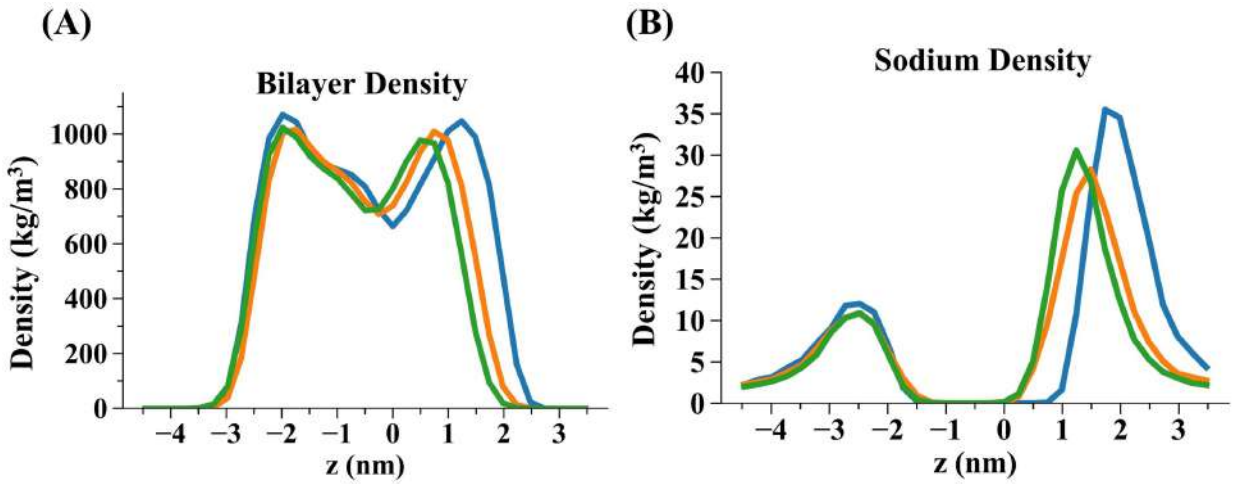

Figure 4.20. MD trajectory averaged (a) Bilayer density and (B) Sodium density. Blue, orange, and green corresponds to the peptide-free bilayer, J3: bilayer, and Jc: bilayer, respectively. "z" denotes the bilayer thickness centered at 0.

4.3. Discussion

Increase in the charge of the cationic synthetic AMPs is usually considered as an easy mean of increasing their antimicrobial potency, as it facilitates the electrostatic interaction in between the AMPs and the negatively charged microbial membranes.[18-20] However, increasing the charge of the AMPs is often accompanied by the increase in the cytotoxicity of the peptides.[21-22] In other studies, it has been established that it is the optimum hydrophobic-hydrophilic balance of the AMPs that is more important than the charge alone.[23-29] In this study, we designed modified analogs of naturally occurring peptide Jelleine with an aim of increasing its salt tolerant antimicrobial potency and protease resistance. We also aimed to retain the non-cytotoxicity of the Jelleines while making the modifications. We increased the charge of the designed peptides J1-J4 systematically from +2 to +5, while incorporating non-standard cationic amino acid Dab (analog of Lys) for inducing the protease resistance to the designed peptides. With the replacement of polar and hydrophobic amino acid residues with cationic Dab residue along the series of J1-J4 peptides, the hydrophobic-hydrophilic balance of the peptides has also been diminished systematically. J3 and J4 were the most active, among the designed peptides against both Gram-positive and Gram-

negative microbes. J3 and J4 also showed very good activity against the fungus *C. albicans*. However, J3 was a clearly better antimicrobial than J4 in the presence of physiological concentration of salts (150 mM NaCl), though the latter had a higher charge over the former. The greater loss in activity of J4 could plausibly be attributed to the inactivation caused by the counter ions of the salt owing to its higher charge density in comparison to J3. J3 also possessed a faster killing kinetics with respect to J4. J3 and J4 were equally protease trypsin and serum resistant and retained their activity upon being incubated with serum. Though both J3 and J4 were non-cytotoxic towards the mammalian cell lines at their physiologically relevant concentrations, upon increasing the concentration considerably, J4 developed partial cytotoxicity faster than J3. The inner and outer cell permeability of J4 was slightly greater than that of J3, owing to its larger charge and the fact that the experiments were carried out in the absence of physiological concentrations of salt. These cationic peptides were too small to adopt any specific secondary structure as proved earlier[30-32] and even in this study through CD and MD simulations (considering SDS micelle earlier or membrane bilayer model now). The antimicrobial potency of the small cationic peptides was independent of any secondary structural requirements, and mostly governed by the electrostatic interaction in between the AMPs and the negatively charged microbial membranes. Membrane interaction, permeation followed by leakage of the intracellular materials led to subsequent membranolysis and eventual cell death. Thus, summarizing the studies, it may be concluded that J3 with a lower positive charge than J4, was a better AMP compared to the latter. It may also be concluded that the optimum hydrophobic-hydrophilic balance is a very important feature to be considered while designing synthetic AMPs.

4.4. Conclusions

In this study we have developed AMP J3, which is a synthetic analog of the naturally occurring AMP jelleine I, isolated from the royal jelley of honeybee. J3 has considerably improved activity, salt tolerance of its antimicrobial potency, protease resistance in comparison to the natural analogue, while retaining the non-cytotoxicity and non-hemolytic abilities of its parent peptide. We have established with several experiments and MD simulations that though increased charge is a major way of enhancement of the activity of the peptides, maintenance of the optimum hydrophobic-hydrophilic balance remains the most crucial parameter. Such fundamental

understanding of the design principles of the synthetic AMPs is vital and can be extended to development of better therapeutics in the future.

4.5. Methods

4.5.1. Materials

Rink amide resin, Fmoc protected amino acids: Fmoc-Pro-OH, Fmoc-Phe-OH, Fmoc-Lys(Boc)-OH, Fmoc-Leu-OH, Fmoc-Ser(tBu)-OH, Fmoc-His(trt)-OH, Fmoc-Trp(Boc)-OH, Fmoc-Dab(Boc)-OH, coupling reagents HBTU [2-(1H-benzotriazol-1-yl)-1,1,3,3-tetramethyluronium hexafluorophosphate, Hexafluorophosphate Benzotriazole Tetramethyl Uronium] and HOBt (1-Hydroxybenzotriazole) were purchased from GL Biochem Ltd., Shanghai, China. N,N-diisopropylethylamine (DIPEA), N,N-dimethyl formamide (DMF), piperidine, pyridine, trifluoroacetic acid (TFA) were purchased from Merck Life Science Pvt. Ltd., Mumbai, India. Acetic anhydride was obtained from the department of chemistry, IIT Guwahati and was manufactured by SD Fine Chem Limited, Mumbai, India. Dichloromethane (DCM), HPLC grade acetonitrile and diethyl ether were purchased from Finar Limited, Ahmedabad, India. Monosodium phosphate (NaH_2PO_4), disodium phosphate (Na_2HPO_4), monopotassium phosphate (KH_2PO_4), sodium Chloride (NaCl), potassium Chloride (KCl) were purchased from Merck Life Science Pvt. Ltd., Mumbai, India. Nutrient broth, BHI broth, YPD broth, and trypsin were purchased from Himedia Laboratories Pvt. Ltd., Mumbai, India. 1,2-Dioctanoyl-sn-glycero-3-phospho-(1'-rac-glycerol) (sodium salt) (D8PG), n-dodecylphosphocholine (DPC) were purchased from Avanti Polar Lipids, Inc., USA. Sodium dodecyl sulfate (SDS), N-phenyl 1-napthylamine (NPN), propidium iodide (PI), 2,2,2-trifluoroethanol (TFE), lipopolysaccharide extracted from *P. aeruginosa*, acrylamide, glutaraldehyde, deuterium oxide (D_2O), α-Cyano-4-hydroxycinnamic acid, trypsin (porcine pancreas) were purchased from Sigma-Aldrich, St. Louis, USA.

4.5.2. Bacterial and fungal strains

Pseudomonas aeruginosa (MTCC 2488), *Klebsiella pneumoniae* (MTCC 432), *Staphylococcus aureus* (MTCC 96), *Candida albicans* (MTCC 1637) were procured from Microbial Type Culture Collection and Gene Bank (MTCC), Chandigarh, India. MRSA (MRSA-100) strain used for the study was clinically isolated from a patient in AIIMS, New Delhi and was obtained from Prof. Benu Dhawan, AIIMS, New Delhi.

4.5.3. Synthesis and purification of the peptides

All the peptides designed for the study were amidated at the C-terminus, so rink amide resin was chosen for the synthesis of these peptides. Rink amide resin corresponding to 0.1 mM peptide was weighed and swelled using DMF. After the resin was swelled properly the Fmoc-protection of the resin was removed using a solution of 20% piperidine in DMF. To the Fmoc deprotected resin Fmoc-protected amino acid (3 eqv of the resin, 0.3 mM) at the C-terminus, coupling reagents HBTU (3 eqv of the resin, 0.3 mM), HOBt (3 eqv of the resin, 0.3 mM), and base DIPEA (6 eqv of the resin, 0.6 mM) were added and allowed to couple for 6-8 h. Resin coupled to the first amino acid was washed using DMF (3 times) and DCM (3 times) and was subjected to capping (DMF: Acetic anhydride: Pyridine = 7:2:1). The resin capped for 1 h was further washed with DMF and DCM and proceeded for the next deprotection followed by the coupling of the next amino acid. The amino acids were linked to the resin one by one until the sequence was completed and finally cleaved off from the resin using a solution of trifluoroacetic acid (TFA) containing traces of triisopropylsilane (TIS) and water. The cleaved resin was precipitated in diethyl ether and centrifuged and dried to obtain the crude peptide.

The crude peptide was dissolved in water and purified using high performance liquid chromatography (HPLC) [Thermo Scientific Ultimate 3000]. A C-18 column (Luna 5µm C18(2) 100 Å, size: 250 x 21.2mm) was used and a multistep gradient involving two solvents water and acetonitrile (both containing 0.1% TFA) was programmed for the purification process.

4.5.4. Characterization of the peptides

The peptides synthesized and purified were characterized using MALDI-TOF spectroscopy, analytic HPLC traces and ^{1}H-NMR spectroscopy.

MALDI samples were prepared by dissolving peptide solutions in equal volume of HCCA matrix and the spectra were acquired using a Bruker Autoflex Speed MALDI-TOF mass spectrometer (Bruker).

HPLC traces of the peptides were acquired by injecting 20 µL of each of the peptides (1 mM) into a C-18 analytic HPLC column (Agilent Eclipse Plus C-18, 5 µm, 4.6x250 mm) using a HPLC analytic machine (Themo Scientific Vanquish). A linear gradient of increasing acetonitrile percentage (decreasing water percentage) was used for acquiring the traces at 214 nm.

NMR samples were prepared by dissolving 4-5 mg of the purified peptides in 500 µL of D_2O. ^1H-NMR spectra of the peptides were acquired using a Bruker Avance Neo 500 MHz FT NMR spectrometer.

4.5.5. Determination of Minimum Inhibitory Concentration (MIC)

The minimum inhibitory concentration or $MIC_{90\%}$ of the peptides were determined against Gram-negative bacteria: *Pseudomonas aeruginosa, Klebsiella pneumoniae*; Gram-positive bacteria: *Staphylococcus aureus* and Methicillin-resistant *Staphylococcus aureus (MRSA)* and a fungus *Candida albicans*. The Gram-negative bacteria were grown in nutrient broth, Gram-positive bacteria were grown in BHI broth and the fungus was grown in YPD broth. The bacteria were grown at 37 °C and the fungus was grown at 28 °C under continuous orbital shaking. At their mid-log phases, the bacteria and fungus were centrifuged to discard the media and the pelleted cells were washed using phosphate buffer of strength 10 mM and pH- 7.4. The cells after three consecutive washes were suspended back again in the phosphate buffer solution and the OD values of the washed cells were determined at 600 nm. The cells were then serially diluted to the order of 10^5 cfu/ml. 50 µL of each of these cell suspensions (10^5 cfu/ml) were mixed with another 50 µL of different concentrations of the peptides and kept incubated for 4 h under constant orbital shaking and requisite temperature. Cells treated with Polymyxin-B[33-37] (bacteria) and Amphotericin-B[38-39] (fungus) were the positive control for the experiments whereas untreated cells were the negative control for the experiments. After 4 h of incubation, the cells peptide mixtures were treated with 100 µL of the respective media and kept incubated overnight. The OD values of the wells corresponding to the cells treated with different concentrations of the peptides, untreated cells and that of the cells treated with the positive control were read at 600 nm and the $MIC_{90\%}$ of the peptides were determined with reference to the positive and negative controls. The experiments were performed in triplicates and repeated at least twice.

4.5.6. Determination of Minimum Inhibitory Concentration (MIC) in the presence of salts

$MIC_{90\%}$ of the peptides were further determined in the presence of phosphate buffer (pH- 7.4 and strength 10 mM) containing 150 mM NaCl. The method followed the same protocol as described in the previous section. Here Phosphate buffer (pH- 7.4 and strength 10 mM) was replaced with phosphate buffer (pH- 7.4 and strength 10 mM) containing 150 mM NaCl.

4.5.7. Determination of Minimum Inhibitory Concentration (MIC) in the presence of serum

Jc, J3 and J4 were mixed with an equal volume of serum (obtained as the supernatant from the centrifugation of blood) and were incubated at 37 °C under continuous orbital shaking for 4 h. The peptide serum mixture was then quenched with 10% of $HClO_4$ solution at the end of the incubation period and the final concentration of the peptides were diluted to 1 mM. 50 µL of *P. aeruginosa* cells of the order 10^5 cfu/ml suspended in phosphate buffer (pH- 7.4, strength- 10 mM) were mixed with another 50 µL of the serum incubated peptides diluted to different concentrations and kept incubated under continuous orbital shaking at 37 °C. Polymyxin-B treated cells and untreated cells were the positive and negative controls respectively. After 4 h, 100 µL of the nutrient broth media was added to each of the wells and the cell peptide mixtures nourished with media was kept incubated further overnight. The OD values of the individual wells were read at 600 nm and the $MIC_{90\%}$ values of the peptides incubated with serum were calculated with respect to the positive and negative controls.

4.5.8. Cytotoxicity

Human dermal fibroblasts (HDF) and HeLa cells were used as the mammalian cell lines for determination of cytotoxicity of the peptides. Peptides Jc, J1, J2, J3 and J4 at different concentrations ranging from 2.5 µM to 160 µM in quadruplicates were added to HDF and HeLa cells respectively at a density of 2000 and 5000 cells/well in a 96 well plate. At the end of incubation after 24 h, cells were treated with 0.25 mg/ml of MTT [3-(4,5-Dimethylthiazol-2-yl)-2,5-Diphenyltetrazolium Bromide] and were further incubated for 2 h. Addition of MTT resulted in the formation of formazan crystals which were dissolved in DMSO and the readings were taken at 570 nm with 650 nm as the reference. Percentage viability of the cells was calculated in reference to the untreated cells. Experiments were repeated at least twice.

4.5.9. Hemolytic activity

2 ml of human blood collected in an EDTA vial was transferred 1 ml each in two separate microcentrifuge tubes and were centrifuged at 5000 rpm for 10 min. The supernatant obtained (serum) was carefully removed to obtained red blood cells (RBCs) settled at the bottom. RBCs obtained were washed with phosphate buffer (pH- 7.4 and strength 10 mM) for three consecutive times and finally were suspended back in the same buffer solution to a final volume of 1 ml. 10 µL of this RBCs suspended in buffer were added to 990 µL of different concentrations of the

peptides, only buffer (negative control) and buffer containing 1% of Triton X 100 (positive control) and were incubated for 1 h at 37 °C under constant orbital shaking. Post incubation, the red blood cells treated with peptides of different concentrations, untreated red blood cells and blood cells treated with 1% Triton X-100 were centrifuged, photographed and the OD values of the supernatant were measured at 540 nm and percentage hemolysis of the peptides at different concentrations were determined in reference to the positive and negative controls.

4.5.10. Time-kill kinetics

P. aeruginosa cells grown to mid-log phase were washed and serially diluted to the order of 10^5 cfu/ml using phosphate buffer (pH- 7.4, strength- 10 mM). 50 µL of this cell suspension were mixed with another 50 µL of the peptides (J3 and J4) at their respective MIC concentrations and were incubated at 37 °C under continuous orbital shaking. Corresponding to different time intervals the cells treated with the peptides were taken out and 10 µL of the sample corresponding to each time interval were casted on a petri dish containing agar-nutrient broth mixture (1:1) and spread uniformly over its surface with the help of a cell spreader. The agar plates were incubated overnight at 37 °C. Post incubation, the colonies corresponding to the cells treated with the peptides for different time intervals were counted. The experiments were performed in triplicates and the mean of the log(cfu/ml) vs time was plotted to determine the killing kinetics of the peptides.

4.5.11. Blue shift experiments

Peptides J3 and J4 at their respective MICs (lowest MIC value determined i.e. against *P. aeruginosa*) were titrated against increasing concentrations of D8PG, SDS and DPC ranging from 0.25 to 10 times the concentration of the peptides. Peptides J3 and J4 both having tryptophan present in them were excited by an excitation wavelength of 280 nm using a slit width of 10 nm. The spectra of the peptides at their respective MICs as well as on increasing the concentrations of the titrants (D8PG, SDS and DPC) at each step were acquired over a range of 300-450 nm, using a Fluoromax Spectrofluorometer (Horiba scientific). The wavelength shifts ($\Delta\lambda$) associated with each addition of the titrants in reference to the free peptides were calculated and plotted against increasing titrant (D8PG/SDS/DPC) concentrations.

4.5.12. Solvent accessibility

Peptide J3 and J4 at their respective MICs (lowest MIC value determined i.e. against *P. aeruginosa*), J3-SDS complex (1:20), J4-SDS complex (1:20), J3-DPC complex (1:20) and J4-

DPC complex (1:20) were titrated against an increasing concentration of a static quencher acrylamide varying from 10 mM to 200 mM. The spectra of the peptides or the peptide complexes were acquired before and after every single addition of acrylamide and the changes in their fluorescence intensities were monitored. The changes in the fluorescence intensities (F_0/F) of the peptides as well as the peptide complexes were plotted against the increasing concentration of acrylamide and fitted to a linear plot following Stern-Volmer equation. The fluorescence spectra were acquired over a range of 300-450 nm, using an excitation wavelength of 280 nm and 10 nm slit width using a Fluoromax Spectrofluorometer (Horiba scientific).

4.5.13. Live cell blue shift

P. aeruginosa cells were washed using phosphate buffer (pH- 7.4, Strength- 10 mM) and concentrated to a final concentration of 10^8 cfu/ml. Cells amounting to $2x10^6$ cfu/ml were added to 1 ml of the peptides J3 and J4 at their respective MICs for 10 consecutive times and the fluorescence spectra of the untreated peptides and peptide treated with increasing concentrations of the cells after each addition were measured. The wavelength shift associated with the intrinsic tryptophan fluorescence of the peptides upon addition of the increasing concentration of the cells were determined.

4.5.14. Circular dichroism

CD spectra of the peptides in the free state (50 µM in dd water), in the presence of bacterial membrane mimic (50 µM of the peptides in 30 mM of SDS), mammalian membrane mimic (50 µM of the peptides in 10 mM of DPC) and helix promoter (50 µM of the peptides in 50% TFE) were acquired. 300 µL of the peptides (in the free state or in the presence of SDS/DPC/TFE) were placed in a 350 µL CD cuvette of path length 1 mm. Spectra were acquired over a wavelength of 190-260 nm range maintaining a scanning rate of 100 nm/min, data pitch of 1nm, D.I.T. 4 s and bandwidth of 1 nm, using a JASCO J-1500 CD spectrometer.

4.5.15. Live cell CD

P. aeruginosa cells were centrifuged, washed, and resuspended in phosphate buffer (pH- 7.4 and strength 10 mM) to obtain a final stock solution of 10^8 cfu/ml. Peptide J3 and J4 amounting to a final concentration of 50 µM were added to *P. aeruginosa* and kept incubated at room temperature for different time intervals. Only peptides at a concentration of 50 µM, untreated cells, cells treated with J3 and J4 for different time intervals, and cells treated with Polymyxin B were recorded using

a CD cuvette of 1mm path length. Spectra were acquired over a range of 260-190 nm using a JASCO J-1500 CD spectrometer with parameters set at 100 nm/min scanning speed, 1 nm bandwidth, D.I.T. 4s, 1.0 nm data pitch data taken over 5 accumulations.

4.5.16. FESEM images of the peptide treated bacteria

P. aeruginosa cells at their mid-logarithmic phase post washing were diluted to a final strength 10^5 cfu/ml. Cells were then incubated with the 1X MICs and 2X MICs of the peptides J3 and J4. Untreated cells were maintained as the negative control. After two h of incubation, cells samples were treated with 2.5 percent glutaraldehyde and reincubated for one more h. Glutaraldehyde fixed cells were washed again with phosphate buffer and finally after suspending the cells back in buffer, they were casted on silicon wafers. The bacterial samples casted on the wafers were allowed to dry followed by serial washings of the samples with 30-90% of ethanol. Ethanol washed samples were dried again and finally gold coated to obtain FESEM images.

4.5.17. Inner membrane permeation assay

P. aeruginosa cells obtained at their mid-logarithmic phase were diluted to the order of 10^6 cfu/ml. Propidium iodide was added to the cell suspension at a final concentration of 10 µM and kept incubated at 37 °C for 30 min under continuous shaking. Fluorescence spectra of the PI containing cell suspension (untreated) was acquired over a period of 30 min as the negative control. Spectra of the cell suspensions treated with 0.5X MICs and 1X MICs of the peptides were also acquired over the same time period one after the other. Finally, the fluorescence spectra of the cell suspension treated with 10 µM Polymyxin-B was acquired as the positive control. PI was excited using a wavelength of 535 nm and 10 nm slit width while the emission wavelength was set at 617 nm having a slit width of 10 nm. All the spectra were acquired using a Fluoromax Spectrofluorometer (Horiba scientific). The percentage of inner membrane permeation induced by the peptides at their MIC and sub-MIC concentrations were calculated from their respective spectra obtained in reference to that of what obtained from the negative and positive controls.

4.5.18. Outer membrane permeation assay

Cells of *P. aeruginosa* at their mid-log phase washed with phosphate buffer for three consecutive times and resuspended in the same buffer followed by dilution of the cells to the order of 10^6 cfu/ml. To the cells, N-Phenyl 1-napthylamine (NPN) dye at a final concentration of 10 µM was added and kept incubated for 1 h under continuous shaking at 37 °C. Fluorescence of the cells in

the untreated condition (negative control), followed by addition of peptides to the cells at the concentrations of 0.5X MICs, 1X MICs and 10 µM Polymyxin-B were recorded over a period of 20 min. The excitation wavelength for the dye was set at 350 nm (slit width: 5 nm) and the emission wavelength was set at 410 nm (slit width: 5 nm). The spectra were acquired using a Fluoromax Spectrofluorometer (Horiba scientific).

4.5.19. Isothermal Titration Calorimetry 9ITC)

Interactions of the peptides J3 and J4 against lipopolysaccharide (LPS) obtained from *P. aeruginosa*, against bacterial membrane mimic SDS and against mammalian membrane mimic DPC were studied using isothermal titration calorimetry.

280 µL of LPS (200 µM, above the concentration of critical micellar concentration) was placed in the cell and it was titrated against 1.5 µL of 2.5 mM of the peptide (J3 or J4) loaded in the syringe for 20 consecutive injections. The temperature of the reaction was set at 37 °C, while the stirring speed was fixed at 400 rpm. The reaction isotherms for both J3 and J4 was fitted using a one site binding model.

280 µL of the peptide (J3 or J4) of concentration 0.5 mM placed at the cell and was titrated against SDS solution of 10 mM concentration, 2 µL of SDS being injected each time for 20 times. The stirring speed was maintained at 350 rpm and the temperature was fixed at 37 °C. Isotherms for the peptides J3 and J4 titrated against SDS were fitted using a one binding site model.

Similarly, 0.5 mM of the peptide (J3 or J4) placed at the cell was titrated against DPC of 10 mM concentration for 20 consecutive times, each injection being of 2 µL volume. The isotherms for the reactions involving J3 and J4 vs DPC were fitted using a one binding site model.

4.5.20. Serum stability

Human blood collected in an EDTA vial was pipetted out in a microcentrifuge tube. The blood sample was centrifuged and the supernatant separated was gently removed. The supernatant isolated is human serum rich in several proteolytic enzymes. 50 µL of this serum was mixed with another 50 µL of 4 mM of the peptides (Jc, J3 and J4) prepared using phosphate buffer saline or PBS (pH- 10 mM, strength- 7.4) and were incubated for different time intervals (1 h, 3 h, 6 h, and 24 h) under continuous orbital shaking at 37 °C. At the end of each incubation period, peptide serum mixtures were quenched with an equal volume of 10% $HClO_4$ solution. Addition of 10%

$HClO_4$ solution resulted in an instantaneous precipitation in the peptide serum mixtures. The curdy white mass precipitated was removed from the samples using centrifugation at low temperature. The supernatants obtained are the source of intact peptides/peptide fragments. 20 µL of this solution corresponding to different peptides treated with serum for different time intervals were then injected into a C-18 analytic column (Agilent Eclipse Plus C-18, 5 µm, 4.6x250 mm). A linear gradient involving 5-100% acetonitrile-water was programmed for 15 min to obtain the HPLC analytic traces, at 214 nm, using a HPLC analytic machine (Themo Scientific Vanquish). Traces were also acquired for peptides serum mixtures quenched at 0 min as the control.

4.5.21. Protease resistance

Peptides Jc, J3 and J4 at a final concentration of 2 mM were treated with trypsin (1 mg/ml, source: bovine) and the samples were incubated corresponding to different time intervals: 1 h, 3 h, 6 h, and 24 h maintaining a temperature of 37 °C under constant shaking. At the end of each incubation period, the activity of the enzyme was quenched with an equal volume of acetonitrile-water mixture containing 1% TFA. HPLC analytic traces of the untreated peptides (Jc, J3 and J4) as well as for the peptides treated with the enzyme corresponding to different time intervals were acquired. 20 µL of the samples were injected into a C-18 analytic column (Agilent Eclipse Plus C-18, 5 µm, 4.6x250 mm). A linear gradient of 5-100% acetonitrile-water was programmed for the process using a HPLC analytic machine (Themo Scientific Vanquish). All the traces were acquired at 214 nm.

4.5.22. Live cell NMR

P. aeruginosa cells at their mid-log phase were washed using phosphate buffer (10 mM, pH- 7.4) and after three consecutive washes the pelleted down cells were concentrated to a final OD of 1.0 using phosphate buffer of strength 10 mM and pH- 6.5 containing 10% D_2O. ^{1}H-NMR of the untreated cells, cells treated with the peptides and of only peptides at concentrations same as that added to the cells were acquired. A total number of 128 scans were acquired in each of the cases, water suppression was performed using pre-saturation zgpr pulse program. Spectra were acquired using a Bruker Avance 400 NMR spectrometer at room temperature.

4.5.23. Live cell dead cell assay using confocal microscope

A culture of *P. aeruginosa* at its mid-log phase was washed and serially diluted to the order of 10^6 cfu/ml. To these cells were added J3 and J4 at their respective MICs, cells without peptide was the

control for the experiment. To the peptide treated as well as the untreated cells acridine orange (capable of staining both live and dead cells) and propidium iodide (capable of staining only dead cells or cells compromised of their membrane integrity) were further added. Cells were then kept incubated for half an hour before they casted on glass slides to acquire the images. A confocal microscope (Leica TCS SP8) was used to acquire the fluorescent images corresponding to acridine orange and propidium iodide using an excitation wavelength of 488 nm and emission wavelength of 530 nm, and that of for propidium iodide using excitation wavelength of 535 nm and emission wavelength of 617 nm respectively along with the bright field image.

4.5.24. Models of the peptides (Jc and J3) in water

The linear models of the peptides (Jc and J3) were generated using PyMOL software.[40] The peptides' N- and C- termini were modelled as $-NH_2^+$ (as proline was the N-terminal residue) and $-CONH_2$ respectively. The overall charge on the peptides Jc and J3 were +2 and +4 respectively. The peptides (Jc or J3) were placed at the centre and a water box of dimension 50 × 50 × 50 $Å^3$. Chloride ions were added to the solvated simulation box to ensure charge neutrality. The resulting simulation box (consisting of ~14,000 atoms) was subjected to MD simulations.

4.5.25. Bilayer model as bacterial membrane-mimetic system

We have modelled a bilayer that mimicked the outer membrane of *P. aeruginosa*[41] using CHARMM-GUI Membrane Builder.[42-43] The adopted bilayer model included Lipid A (*P. aeruginosa*) in the outer layer, whereas the inner layer comprised of phosphatidylethanolamine (PE), phosphatidylglycerol (PG), and cardiolipin (CL) (Figure C26, Appendix C). The bilayer composition is given in Table C1 (Appendix C). The bilayer was kept at the center and solvated with a water box of dimensions 73 × 73 × 115 $Å^3$ (X, Y, Z). The width or thickness of the bilayers was along the Z direction. Presence of monovalent counter ions (viz., Na^+ or K^+) are reported to reasonably reproduce the experimental membrane properties in the molecular simulations of membrane mimetic bilayer models. Hence, a total of 80 Na^+ ions were added to ensure the charge neutrality of the simulation box. A total of ~52800 atoms were considered for MD simulations of the solvated bilayer models. The final structure of the solvated bilayer from the production MD simulation was used to investigate peptide: bilayer binding event.

4.5.26. Setup for studying peptide: bilayer binding

The final structure of the free peptide in water was selected from the production dynamics, and the center of mass of that peptide (J3 or Jc) was positioned ~50 Å away from the center of mass of the equilibrated bilayer. Another 15 Å water padding was added along the thickness of the membrane to ensure sufficient solvation of the peptide. The dimension of the initial simulation setup (peptide away from the bilayer) was 67.5 × 67.5 × 130 $Å^3$. A total of ~62500 atoms were subjected to MD simulation to study peptide: bilayer binding. The results were found to be more or less independent of the initial setup (Figure C27 & Table C2, Appendix C), thus indicating convergence.

4.5.27. MD simulation and parameters

All-atom explicit-solvent classical molecular dynamics (MD) simulations were carried out using GROMACS v2019 software.[44-45] Standard CHARMM36 (version July 2022)[46-49] force field was used to describe the biomolecular interactions. The TIP3P water model[50] was used to describe water molecules. The simulation box was subjected to energy minimization using the steepest descent algorithm (step size = 0.1 Å, 50000 steps). The energy-minimized simulation box was then subjected to 200 ps equilibration. The initial 100 ps equilibration was considered an NVT ensemble in which the peptide and bilayer were restrained, whereas the next 100 ps equilibration was performed using an NPT ensemble without restraint. After equilibration, the production run for 1000 ns (NTP ensemble without restraint) was performed, and the last 500 ns was considered for analysis. The simulation parameters adopted for this work are given in Table C3 (Appendix C). Coordinates were saved and analysed at every 10 ps from the MD trajectories.

4.5.28. Trajectory analysis

Root mean square deviation (RMSD), Root mean square fluctuation (RMSF), solvent accessible surface area (SASA), and secondary structural analysis (DSSP) of the peptides have been performed. Bilayer properties (viz., density, thickness, etc.) have been estimated. SASA was calculated using *gmx sa*[51-52] with a probe radius of 1.4 Å. Secondary structural analysis for the peptide was performed using *the gmx dssp*[53] tool. Structural variations of the membrane were assessed using *gmx density*. The distance between the centre of mass of the bilayer and the peptide was estimated from the MD trajectories using the *gmx distance*. Plots from the computational analysis were generated using in-house Python scripts, and images were rendered using PyMOL visualization software.

References

1. Sarkar, T.; Chetia, M.; Chatterjee, S. Antimicrobial Peptides and Proteins: From Nature's Reservoir to the Laboratory and Beyond. *Front. Chem*. **2021**, *9*, 691532.

2. Chen, C.H.; Lu, T.K. Development and Challenges of Antimicrobial Peptides for Therapeutic Applications. *Antibiotics (Basel)* **2020**, *9*, 24.

3. Fontana, R.; Mendes, M.A.; de Souza, B.M.; Konno, K.; César, L.M.; Malaspina, O.; Palma, M.S. Jelleines: a family of antimicrobial peptides from the Royal Jelly of honeybees (Apis mellifera). *Peptides* **2004**, *25*, 919-928.

4. Jia, F.; Wang, J.; Peng, J.; Zhao, P.; Kong, Z.; Wang, K.; Yan, W.; Wang, R. The in vitro, in vivo antifungal activity and the action mode of Jelleine-I against Candida species. *Amino Acids* **2018**, *50*, 229-239.

5. Bi, X.; Wang, C.; Ma, L.; Sun, Y.; Shang, D. Investigation of the role of tryptophan residues in cationic antimicrobial peptides to determine the mechanism of antimicrobial action. *J. Appl. Microbiol.* **2013**, *115*, 663-672.

6. Mishra, A.K.; Choi, J.; Moon, E.; Baek, K.H. Tryptophan-Rich and Proline-Rich Antimicrobial Peptides. *Molecules* **2018**, *23*, 815.

7. de Planque, M.R.; Bonev, B.B.; Demmers, J.A.; Greathouse, D.V.; Koeppe, R.E. 2nd; Separovic, F.; Watts, A.; Killian, J.A. Interfacial anchor properties of tryptophan residues in transmembrane peptides can dominate over hydrophobic matching effects in peptide-lipid interactions. *Biochemistry* **2003**, *42*, 5341-5348.

8. Baral, A.; Roy, S.; Ghosh, S.; Hermida-Merino, D.; Hamley, I.W.; Banerjee, A. A Peptide-Based Mechano-sensitive, Proteolytically Stable Hydrogel with Remarkable Antibacterial Properties. *Langmuir* **2016**, *32*, 1836-1845.

9. Ma, Z.; Liu, X.; Nie, J.; Zhao, H.; Li, W. Nano-Antimicrobial Peptides Based on Constitutional Isomerism-Dictated Self-Assembly. *Biomacromolecules* **2022**, *23*, 1302-1313.

10. Rawlings, N.D.; Barrett, A.J. Families of serine peptidases. *Methods Enzymol*. **1994**, *244*, 19-61.

11. Polgár L. The catalytic triad of serine peptidases. *Cell Mol. Life Sci*. **2005**, *62*, 2161-2172.

12. Koshikawa, N.; Hasegawa, S.; Nagashima, Y.; Mitsuhashi, K.; Tsubota, Y.; Miyata, S.; Miyagi, Y.; Yasumitsu, H.; Miyazaki, K. Expression of trypsin by epithelial cells of various tissues, leukocytes, and neurons in human and mouse. *Am. J. Pathol*. **1998**, *153*, 937-944.

13. Sasaki, M.; Yamamoto, H.; Iida, S. Interaction of human serum proteinase inhibitors with proteolytic enzymes of animal, plant, and bacterial origin. *J. Biochem*. **1974**, *75*, 171-177.

14. Sivertsen, A.; Isaksson, J.; Leiros, H.K.; Svenson, J.; Svendsen, J.S.; Brandsdal, B.O. Synthetic cationic antimicrobial peptides bind with their hydrophobic parts to drug site II of human serum albumin. *BMC Struct. Biol*. **2014**, *14*, 4.

15. Li, J.; Koh, J.J.; Liu, S.; Lakshminarayanan, R.; Verma, C.S.; Beuerman, R.W. Membrane Active Antimicrobial Peptides: Translating Mechanistic Insights to Design. *Front. Neurosci*. **2017**, *11*, 73.

16. Byvaltsev, V.A.; Bardonova, L.A.; Onaka, N.R.; Polkin, R.A.; Ochkal, S.V.; Shepelev, V.V.; Aliyev, M.A.; Potapov, A.A. Acridine Orange: A Review of Novel Applications for Surgical Cancer Imaging and Therapy. *Front. Oncol*. **2019**, *9*, 925.

17. Arndt-Jovin, D.J.; Jovin, T.M. Fluorescence labeling and microscopy of DNA. *Methods Cell Biol*. **1989**, *30*, 417-448.

18. Dathe, M.; Nikolenko, H.; Meyer, J.; Beyermann, M.; Bienert, M. Optimization of the antimicrobial activity of magainin peptides by modification of charge. *FEBS Lett*. **2001**, *501*, 146-150.

19. Matsuzaki, K. Control of cell selectivity of antimicrobial peptides. *Biochim. Biophys. Acta* **2009**, *1788*, 1687-1692.

20. Islam, M.M.; Asif, F.; Zaman, S.U.; Arnab, M.K.H.; Rahman, M.M.; Hasan, M. Effect of charge on the antimicrobial activity of alpha-helical amphibian antimicrobial peptide. *Curr. Res. Microb. Sci.* **2023**, *4*, 100182.

21. Sosiangdi, S.; Taemaitree, L.; Tankrathok, A.; Daduang, S.; Boonlue, S.; Klaynongsruang, S.; Jangpromma, N. Rational design and characterization of cell-selective antimicrobial peptides based on a bioactive peptide from Crocodylus siamensis hemoglobin. *Sci. Rep*. **2023**, *13*, 16096.

22. Du, K.; Yang, Z.R.; Qin, H.; Ma, T.; Tang, J.; Xia, J.; Zhou, Z.; Jiang, H.; Zhu, J. Optimized Charge/Hydrophobicity Balance of Antimicrobial Peptides Against Polymicrobial Abdominal Infections. *Macromol. Biosci*. **2024**, *24*, e2300451.

23. Yin, L.M.; Edwards, M.A.; Li, J.; Yip, C.M.; Deber, C.M. Roles of hydrophobicity and charge distribution of cationic antimicrobial peptides in peptide-membrane interactions. *J. Biol. Chem.* **2012**, *287*, 7738-7745.

24. Edwards, I.A.; Elliott, A.G.; Kavanagh, A.M.; Zuegg, J.; Blaskovich, M.A.; Cooper, M.A. Contribution of Amphipathicity and Hydrophobicity to the Antimicrobial Activity and Cytotoxicity of β-Hairpin Peptides. *ACS Infect. Dis*. **2016**, *2*, 442-450.

25. Sharma, P.; Sharma, S.; Joshi, S.; Barman, P.; Bhatt, A.; Maan, M.; Singla, N.; Rishi, P.; Ali. M.E.; Preet, S.; Saini, A. Design, characterization and structure-function analysis of novel antimicrobial peptides based on the N-terminal CATH-2 fragment. *Sci. Rep*. **2022**, *12*, 12058.

26. Tang, Z.; Jiang, W.; Li, S.; Huang, X.; Yang, Y.; Chen, X.; Qiu, J.; Xiao, C.; Xie, Y.; Zhang, X.; Li, J.; Verma, C.S.; He, Y.; Yang, A. Design and evaluation of tadpole-like conformational antimicrobial peptides. *Commun. Biol*. **2023**, *6*, 1177.

27. Lin, B.; Hung, A.; Singleton, W.; Darmawan, K.K.; Moses, R.; Yao, B.; Wu, H.; Barlow, A.; Sani, M.A.; Sloan, A.J.; Hossain, M.A.; Wade, J.D.; Hong, Y.; O'Brien-Simpson, N.M.; Li, W. The effect of tailing lipidation on the bioactivity of antimicrobial peptides and their aggregation tendency. *Aggregate* **2023**, *4*, e329.

28. Grimsey, E.; Collis, D.W.P.; Mikut, R.; Hilpert, K. The effect of lipidation and glycosylation on short cationic antimicrobial peptides. *Biochim. Biophys. Acta Biomembr*. **2020**, *1862*, 183195.

29. Armas, F.; Di Stasi, A.; Mardirossian, M.; Romani, A.A.; Benincasa, M.; Scocchi, M. Effects of Lipidation on a Proline-Rich Antibacterial Peptide. *Int. J. Mol. Sci*. **2021**, *22*, 7959.

30. Pandit, G.; Ilyas, H.; Ghosh, S.; Bidkar, A.P.; Mohid, S.A.; Bhunia, A.; Satpati, P.; Chatterjee, S. Insights into the Mechanism of Antimicrobial Activity of Seven-Residue Peptides. *J. Med. Chem*. **2018**, *61*, 7614-7629.

31. Seo, M.D.; Won, H.S.; Kim, J.H.; Mishig-Ochir, T.; Lee, B.J. Antimicrobial peptides for therapeutic applications: a review. *Molecules* **2012**, *17*, 12276-12286.

32. Kang, S.J.; Nam, S.H.; Lee, B.J. Engineering Approaches for the Development of Antimicrobial Peptide-Based Antibiotics. *Antibiotics (Basel)* **2022**, *11*, 1338.

33. Zavascki, A.P.; Goldani, L.Z.; Li, J.; Nation, R.L. Polymyxin B for the treatment of multidrug-resistant pathogens: a critical review. *J. Antimicrob. Chemother*. **2007**, *60*, 1206-1215.

34. Ledger, E.V.K.; Sabnis, A.; Edwards, A.M. Polymyxin and lipopeptide antibiotics: membrane-targeting drugs of last resort. *Microbiology (Reading)* **2022**, *168*, 001136.

35. Poirel, L.; Jayol, A.; Nordmann, P. Polymyxins: Antibacterial Activity, Susceptibility Testing, and Resistance Mechanisms Encoded by Plasmids or Chromosomes. *Clin. Microbiol. Rev*. **2017**, *30*, 557-596.

36. Yoshida, T.; Hiramatsu, K. Potent in vitro bactericidal activity of polymyxin B against methicillin-resistant Staphylococcus aureus (MRSA). *Microbiol. Immunol*. **1993**, *37*, 853-859.

37. Boyen, F.; Verstappen, K.M.; De Bock, M.; Duim, B.; Weese, J.S.; Schwarz, S.; Haesebrouck, F.; Wagenaar, J.A. In vitro antimicrobial activity of miconazole and polymyxin B against canine meticillin-resistant Staphylococcus aureus and meticillin-resistant Staphylococcus pseudintermedius isolates. *Vet. Dermatol*. **2012**, *23*, 381-e70.

38. de Aquino Lemos, J.; Costa, C.R.; de Araújo, C.R.; Souza, L.K.; Silva Mdo, R. Susceptibility testing of Candida albicans isolated from oropharyngeal mucosa of HIV(+) patients to fluconazole, amphotericin B and Caspofungin. killing kinetics of caspofungin and amphotericin B against fluconazole resistant and susceptible isolates. *Braz. J. Microbiol*. **2009**, *40*, 163-169.

39. Cordeiro, R.A.; Teixeira, C.E.; Brilhante, R.S.; Castelo-Branco, D.S.; Paiva, M.A.; Giffoni Leite, J.J.; Lima, D.T.; Monteiro, A.J.; Sidrim, J.J.; Rocha, M.F. Minimum inhibitory concentrations of amphotericin B, azoles and caspofungin against Candida species are reduced by farnesol. *Med. Mycol*. **2013**, *51*, 53-59.

40. Schrödinger, L.L.C. The PyMOL Molecular Graphics System, Version 2.0.

41. Pogozheva, I.D.; Armstrong, G.A.; Kong, L.; Hartnagel, T.J.; Carpino, C.A.; Gee, S.E.; Picarello, D.M.; Rubin, A.S.; Lee, J.; Park, S.; Lomize, A.L.; Im, W. Comparative Molecular Dynamics Simulation Studies of Realistic Eukaryotic, Prokaryotic, and Archaeal Membranes. *J. Chem. Inf. Model.* **2022**, *62*, 1036-1051.

42. Jo, S.; Kim, T.; Iyer, V.G.; Im, W. CHARMM-GUI: a web-based graphical user interface for CHARMM. *J. Comput. Chem*. **2008**, *29*, 1859-1865.

43. Wu, E.L.; Cheng, X.; Jo, S.; Rui, H.; Song, K.C.; Dávila-Contreras, E.M.; Qi, Y.; Lee, J.; Monje-Galvan, V.; Venable, R.M.; Klauda, J.B.; Im, W. CHARMM-GUI Membrane Builder toward realistic biological membrane simulations. *J. Comput. Chem*. **2014**, *35*, 1997-2004.

44. Van Der Spoel, D.; Lindahl, E.; Hess, B.; Groenhof, G.; Mark, A.E.; Berendsen, H.J. GROMACS: fast, flexible, and free. *J. Comput. Chem*. **2005**, *26*, 1701-1718.

45. Abraham, M.J.; van der Spoel, D.; Lindahi, E.; Hess, B. GROMACS Development Team, GROMACS User Manual Version. **2018**, 2016.5, 2019.

46. Brooks, B.R.; Brooks, C.L. 3rd; Mackerell, A.D. Jr.; Nilsson, L.; Petrella, R.J.; Roux, B.; Won, Y.; Archontis, G.; Bartels, C.; Boresch, S.; Caflisch, A.; Caves, L.; Cui, Q.; Dinner, A.R.; Feig, M.; Fischer, S.; Gao, J.; Hodoscek, M.; Im, W.; Kuczera, K.; Lazaridis, T.; Ma, J.; Ovchinnikov, V.; Paci, E.; Pastor, R.W.; Post, C.B.; Pu, J.Z.; Schaefer, M.; Tidor, B.; Venable, R.M.; Woodcock, H.L.; Wu, X.; Yang, W.; York, D.M.; Karplus, M. CHARMM: the biomolecular simulation program. *J. Comput. Chem*. **2009**, *30*, 1545-1614.

47. Rice, A.; Rooney, M.T.; Greenwood, A.I.; Cotton, M.L.; Wereszczynski, J. Lipopolysaccharide Simulations Are Sensitive to Phosphate Charge and Ion Parameterization. *J. Chem. Theory Comput*. **2020**, *16*, 1806-1815.

48. Huang, J.; Rauscher, S.; Nawrocki, G.; Ran, T.; Feig, M.; de Groot, B.L.; Grubmüller, H.; MacKerell, A.D. Jr. CHARMM36m: an improved force field for folded and intrinsically disordered proteins. *Nat. Methods*. **2017**, *14*, 71-73.

49. Croitoru, A.; Park, S.J.; Kumar, A.; Lee, J.; Im, W.; MacKerell, A.D. Jr.; Aleksandrov, A. Additive CHARMM36 Force Field for Nonstandard Amino Acids. *J. Chem. Theory Comput*. **2021**, *17*, 3554-3570.

50. Jorgensen, W.L.; Chandrasekhar, J.; Madura, J.D.; Impey, R.W.; Klein, M.L. Comparison of simple potential functions for simulating liquid water, *J. Chem. Phys*. **1983**, *79*, 926-935.

51. Eisenhaber, F.; Lijnzaad, P.; Argos, P.; Sander, C.; Scharf, M. The double cubic lattice method: efficient approaches to numerical integration of surface area and volume and to dot surface contouring of molecular assemblies, *J. Comput. Chem*. **1995**, *16*, 273-284.

52. Bondi, A. van der Waals volumes and radii. *J. Phys. Chem*. **1964**, *68*, 441-451.

53. Kabsch, W.; Sander, C. Dictionary of protein secondary structure: pattern recognition of hydrogen-bonded and geometrical features. *Biopolymers* **1983**, *22*, 2577-2637.

Chapter 5: *De Novo* Design of Tryptophan Containing Broad-Spectrum Cationic Antimicrobial Octapeptides

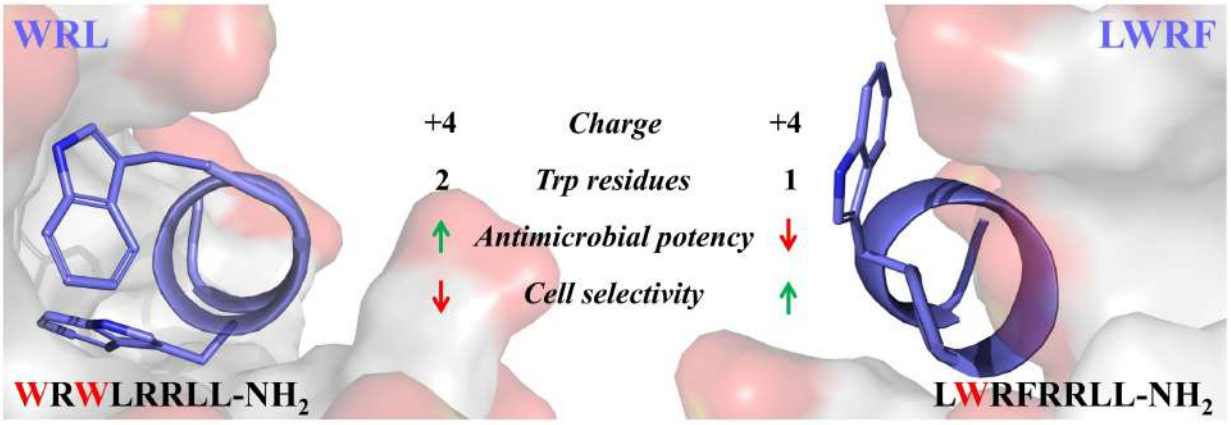

5.1. Introduction

Here in this chapter, we have reported two cationic octapeptides WRL and LWRF using arginine and tryptophan residues in combination with other hydrophobic amino acid residues like leucine and phenylalanine. Arginine and tryptophan are two commonly encountered amino acid residues in many of the natural and synthetic antimicrobial peptides.[1-4] Arginine having strong cationic properties along with its unique hydrogen bonding abilities, in association with the complex properties of tryptophan like intermediate hydrophobicity and superior membrane binding, seem to deliver excellently for the objective of antimicrobial peptides. While the cationic charge of arginine facilitates electrostatic interactions of the peptides to the target anionic microbial membranes, its excellent hydrogen bonding ability assists its interaction with the negatively charged lipopolysaccharides, teichoic acids, or phospholipid headgroups present on the membranes.[1,5-6] Preference of the tryptophan residue towards the interfacial region of lipid bilayers owing to its borderline hydrophobicity, is well known.[7-10] Tryptophan can also be involved in cation- π interactions with positively charged choline headgroups of the phospholipids.[11] Hence inclusion of these two amino acids promote excellent antimicrobial activity even in very short sequences of peptides.[12-15]

Though the overall charge in both the designed peptides WRL and LWRF were kept identical, the number of tryptophan residues and the hydrophobic-hydrophilic landscape at their N-terminus were varied, to study their effect on the peptides' activities. In earlier studies from the group, we have established that cationic peptides interact with the membranes through initial interaction with the N-terminus.[16-17] In this study, the antimicrobial potency of the peptides was assessed in the absence and presence of physiological salt concentrations against a wide variety of microbes: Gram-positive and Gram-negative bacteria and fungi. Peptides were screened for their selectivity towards microbial/mammalian cells. Mechanism of action of the peptides were established using different spectroscopic and biophysical experiments involving both bacterial cells or membrane mimetics. An attempt was also made to understand the structure activity relationship of the peptides both experimentally as well as from molecular dynamics simulations. Peptide membrane interactions at the atomistic levels were also assessed through MD simulations.

5.2. Results

5.2.1. Design, synthesis and characterization of the peptides

Peptides WRL and LWRF designed from *de novo* principles, were rich in arginine and tryptophan (Figure 5.1). Peptides containing these two amino acids, have been reported in the literature to possess high potency against several microbial strains.[1-2,12-14] Amphipathic helical AMPs have also been reported to have high activity through facilitated membrane binding.[18-22] Previous studies have reported that small synthetic peptides adopted a partial helical conformation in the presence of microbial membrane mimetics.[23] The primary sequences of the WRL and LWRF peptides were derived from the helical wheel projections (Figure 5.1), such that in case they adopted helical conformation, they would generate amphipathicity essential for antimicrobial activity.[24-27] Reports in the literature revealed that the positioning of the tryptophan residue at the interface of the hydrophobic and hydrophilic faces of the amphipathic helix, proved beneficial in attaining potency. In WRL we have strategically positioned the two tryptophan residues at the hydrophobic-hydrophilic interfaces. In the second peptide LWRF, one of the tryptophan residues have been substituted by a Phe residue (Figure 5.1).

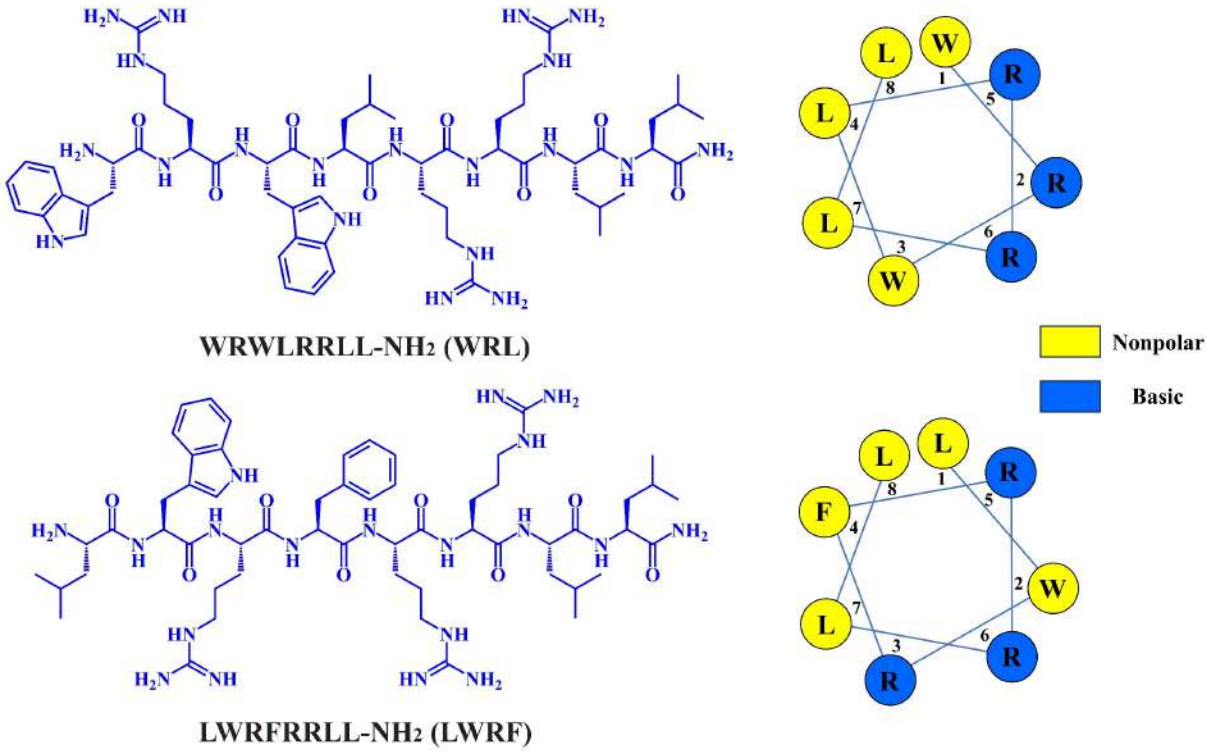

Figure 5.1. Chemical structures of the peptides WRL and LWRF and their helical wheel projections.

The designed peptides were synthesized, purified and characterized using HRMS (Figures D1-D2, Appendix D), analytical HPLC (Figures D3-D4, Appendix D) and ^{1}H NMR (Figures D5-D6, Appendix D). Both the peptides were found to be > 95% pure from the HPLC traces.

Table 5.1. Physicochemical properties of the WRL and LWRF.

Peptide Name	Sequence	Number of amino acid residues	Net charge	Theoretical Molecular Weight (Da)	Retention time (min)
WRL	WRWLRRLL -NH_2	8	+4	1197.5060	8.03
LWRF	LWRFRRLL -NH_2	8	+4	1158. 4690	7.45

5.2.2. Antimicrobial potency of WRL and LWRF

Determination of Minimum Inhibitory Concentration (MIC) values

Minimum Inhibitory concentration ($MIC_{90\%}$) of peptides WRL and LWRF were determined against three Gram-negative bacterial strains *Pseudomonas aeruginosa, Escherichia coli, Klebsiella pneumonia,* two Gram-positive bacterial strains *Staphylococcus aureus* and Methicillin-resistant *Staphylococcus aureus* (*MRSA*) and a fungal strain *Candida albicans* (Table 5.2 & Figure D7, Appendix D). Both WRL ($MIC_{90\%}$: 5 µM) and LWRF ($MIC_{90\%}$: 7.5 µM) were found to display excellent antimicrobial activity against the Gram-negative *P. aeruginosa*. WRL also exhibited good antimicrobial activity against Gram-negative *K. pneumoniae* ($MIC_{90\%}$: 15 µM) and *E. coli* ($MIC_{90\%}$:15 µM). LWRF on the other hand, displayed a moderate $MIC_{90\%}$ value of 50 µM against each of *K. pneumoniae* and *E. coli*. WRL showed an $MIC_{90\%}$ value of 4 µM and 7.5 µM respectively against Gram-positive *S. aureus* and MRSA, LWRF too was considerably active against both *S. aureus* ($MIC_{90\%}$: 15 µM) and *MRSA* ($MIC_{90\%}$: 20 µM). Both the peptides appeared to display significant antifungal activity, with WRL and LWRF having a $MIC_{90\%}$ of 5 µM and 15 µM respectively against *C. albicans*. Thus, in general WRL displayed better antimicrobial activity against all the microbial strains in comparison to that of LWRF (Table 5.2 & Figure D7, Appendix D). As both the peptides had the same net positive charge of +4 at a physiological pH of 7.4, the greater efficacy of WRL in comparison to LWRF originated due to differences in the number and position of the tryptophan residues in their sequences.[28-30] Antimicrobial peptides containing tryptophan in many cases were found to be more potent than those containing phenylalanine.[31] Additionally, the presence of tryptophan residue at the N-terminus of WRL might have contributed

further to its better antimicrobial activity over LWRF, as the placement of tryptophan at the N-terminus was reported to be associated with increased peptide-membrane interactions in the literature.[32-33] However, in spite of reduced activity of LWRF than WRL, both the peptides displayed strong antimicrobial potencies.

Table 5.2. $MIC_{90\%}$ values of the peptides WRL and LWRF.

Strains/ Peptides	**$MIC_{90\%}$ (µM)**					
	Gram-negative			Gram-positive		Fungus
	P. aeruginosa	*K. pneumoniae*	*E. coli*	*S. aureus*	*MRSA*	*C. albicans*
WRL	5	15	15	4	7.5	5
LWRF	7.5	50	50	15	20	15

Determination of Minimum Inhibitory Concentration (MIC) values in the presence of physiological concentrations of different salts

Biological systems are characterized with presence of different metallic salts. Presence of physiological concentrations of salts have shown to impact antimicrobial activity of many of the peptides significantly.[34-35] We checked the salt tolerance of the antimicrobial activity of WRL and LWRF by determining their MIC values against all the Gram-positive, Gram-negative and fungal strains used in this study, in the presence of phosphate buffer saline or PBS (pH 7.4, 10 mM) (Table 5.3 & Figures D8-D10, Appendix D). The osmolarity and ionic concentrations of PBS (pH 7.4, 10 mM) used was similar to that of the human system.[36-37] WRL completely retained its activity against *E. coli* ($MIC_{90\%}$: 15 µM), lost its activity marginally against *P. aeruginosa* ($MIC_{90\%}$ 10 µM), *S. aureus* ($MIC_{90\%}$: 10 µM), MRSA ($MIC_{90\%}$: 20 µM) and *C. albicans* ($MIC_{90\%}$: 15 µM), and lost its activity moderately against *K. pneumoniae* ($MIC_{90\%}$: 50 µM) in PBS. LWRF on the other hand, could assert its antimicrobial activity against *P. aeruginosa*, *S. aureus* and *C. albicans* at a relatively higher concentration ($MIC_{90\%}$: 50 µM) in PBS. LWRF lost its activity significantly against *E. coli*, *K. pneumoniae* and *MRSA* having $MIC_{90\%}$ values well above 50 µM in each of the cases.

Table 5.3. $MIC_{90\%}$ values of peptides in the presence of PBS.

Peptides/ Strains	**$MIC_{90\%}$ (µM)**					
	P. aeruginosa	*K. pneumoniae*	*E. coli*	*S. aureus*	*MRSA*	*C. albicans*
WRL	10	50	15	10	20	15

LWRF	50	> 50	> 50	50	> 50	50

$MIC_{90\%}$ values for the peptides were also determined against *P. aeruginosa* and *S. aureus* in the presence of physiological concentrations of different salts: Na^+ (150 mM), Ca^{2+} (1.25 mM), Mg^{2+} (1 mM), Zn^{2+} (8 µM), Fe^{3+} (4 µM) (Table 5.4 & Figures D8-D9, Appendix D). WRL had little to no reduction its activity in the presence of these salts against both *P. aeruginosa* and *S. aureus*. Loss of activity of LWRF in the presence of these salts was less pronounced against *P. aeruginosa* except in the presence of Na^+ ions. LWRF lost its activity significantly against *S. aureus* in the presence of Na^+, Ca^{2+} and Mg^{2+}, but retained its activity in the presence of Zn^{2+} and Fe^{3+} ions. Overall, WRL was found to be significantly more salt tolerant than LWRF in its antimicrobial potency, in the presence of physiological concentrations of different salts. It can also be concluded that salts at higher concentration had more significant effect on the activity of the peptides that the salts at lower concentration. PBS (pH 7.4, 10 mM containing 150 mM NaCl) and 150 mM NaCl had more prominent effect on the antimicrobial activity of the peptides than that of 1.25 mM $CaCl_2$ and 1 mM $MgCl_2$. $ZnCl_2$ (8 µM), $FeCl_3$ (4 µM) had almost negligible to no effect on the activity of the peptides. Thus, the salt tolerance of the AMPs was found to be dependent on the nature of the peptide, the microbial strain in question and the concentration and nature of the salts, with WRL being more salt tolerant than LWRF in general.

Table 5.4. $MIC_{90\%}$ values of WRL and LWRF in the presence of physiological concentrations of various salts.

Peptides/ Strains		**$MIC_{90\%}$ (µM)**				
		150 mM Na^+	1.25 mM Ca^{2+}	1 mM Mg^{2+}	8 µM Zn^{2+}	4 µM Fe^{3+}
WRL	*P. aeruginosa*	7.5	5	7.5	5	5
	S. aureus	10	10	7.5	5	5
LWRF	*P. aeruginosa*	50	15	20	10	7.5
	S. aureus	50	50	50	15	15

5.2.3. Cytotoxicity

Applications of peptides for therapeutic purposes requires them to be non-cytotoxic towards mammalian cells. We screened the peptides against two mammalian cell lines: Human Dermal Fibroblasts (HDF) and HeLa, a cancer cell line [Figure 5.2(A) & (B)]. WRL was almost non-cytotoxic (cell viability ~ 90%) upto a concentration of 80 µM and 40 µM respectively against the HDF and HeLa cell lines. WRL became substantially toxic to the HDF cells at 160 µM, a concentration much above its bactericidal/ fungicidal concentrations (which is in the range 5-50 µM) both in the presence and in the absence of salts. WRL became cytotoxic to HeLa cells at the concentration of 80 µM and eradicated it almost completely at 160 µM indicating its anticancer property at higher concentrations, being preferentially viable to normal cells. LWRF was completely non-cytotoxic against both the cell lines even at high concentrations (160 µM). Both the peptides were therefore quite suitable for therapeutic purposes.

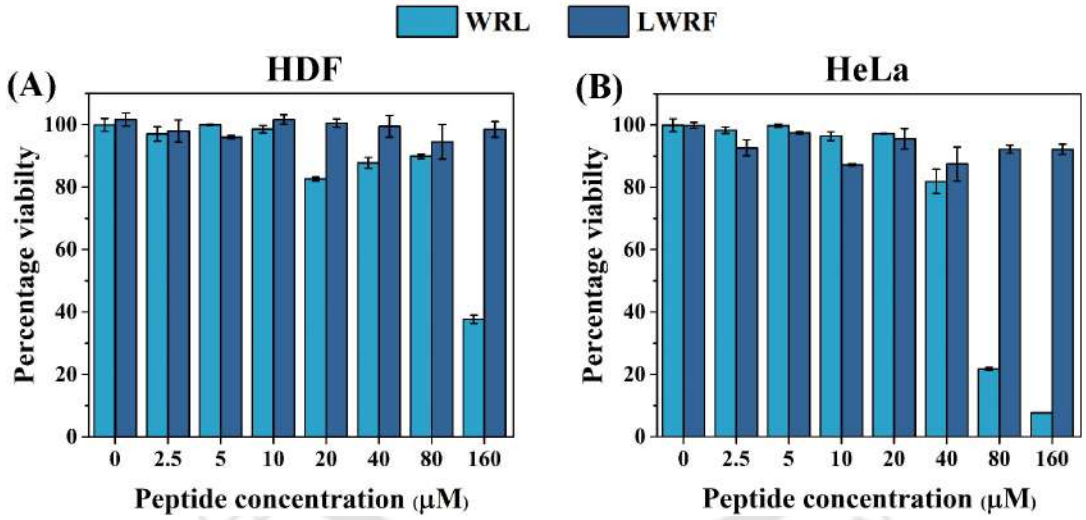

Figure 5.2. Evaluation of cytotoxicity of the peptides. Bar diagram depicting the viability of (A) Human Dermal Fibroblast (HDF) and (B) HeLa cell lines tested against different concentrations of the peptides WRL and LWRF.

5.2.4. Hemolytic activity

Viability of the red blood cells in the presence of the peptides is an equally important attribute of therapeutic peptides. Hemolytic activity of the peptides was determined against human red blood cells (Figure 5.3). WRL displayed no significant hemolysis upto a concentration of 50 µM (well within the range of its antimicrobial activity against all the microbes tested in this work, both in

the presence and in the absence of the salts). LWRF was also almost completely non-hemolytic till 200 μM, the highest tested concentration in this study.

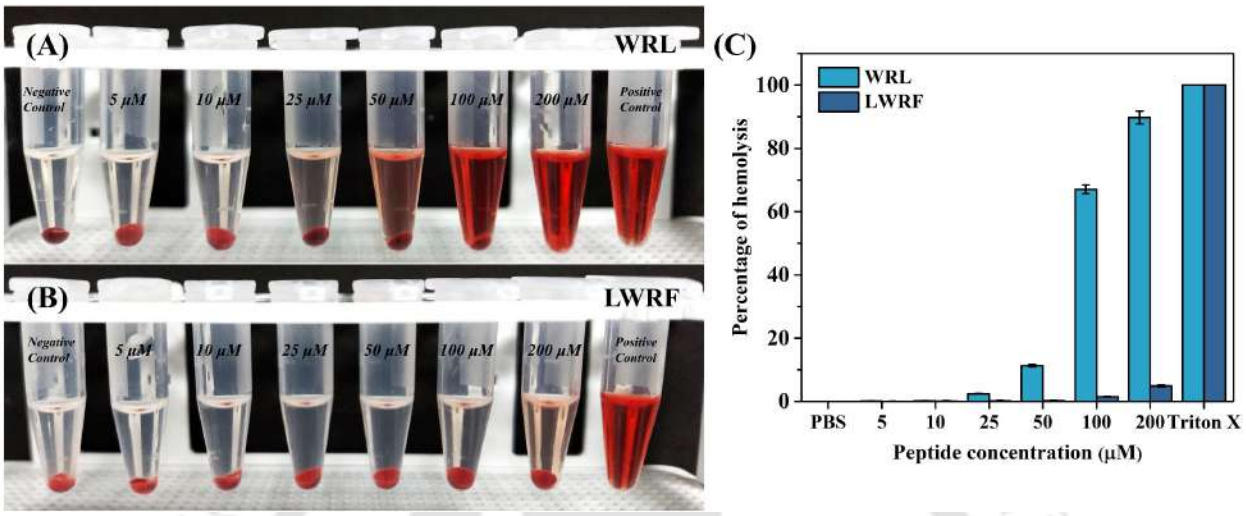

Figure 5.3. Determination of hemolytic activity of the peptides. (A) Photographs of red blood cells (RBCs) centrifuged post incubation for 1 h at 37 °C: untreated (negative control)/ treated with different concentrations of WRL and LWRF and with 1% of Triton X-100 (positive control). (B) Bar diagrams representing percentage of hemolysis induced by the peptides at different concentrations.

5.2.5. Time-kill kinetics

Bactericidal kinetics of the peptides were determined next

(Figure 5.4). WRL at its MIC concentration eradicated 10^5 CFU/ml of the *P. aeruginosa* cells within 10 min of its incubation time. LWRF at its MIC took 60 min against *P. aeruginosa* for its complete neutralization. WRL and LWRF at their respective MICs displayed complete bactericidal activity against *S. aureus* at 10 min and 15 min respectively. WRL appeared superior to LWRF by displaying faster bactericidal abilities.

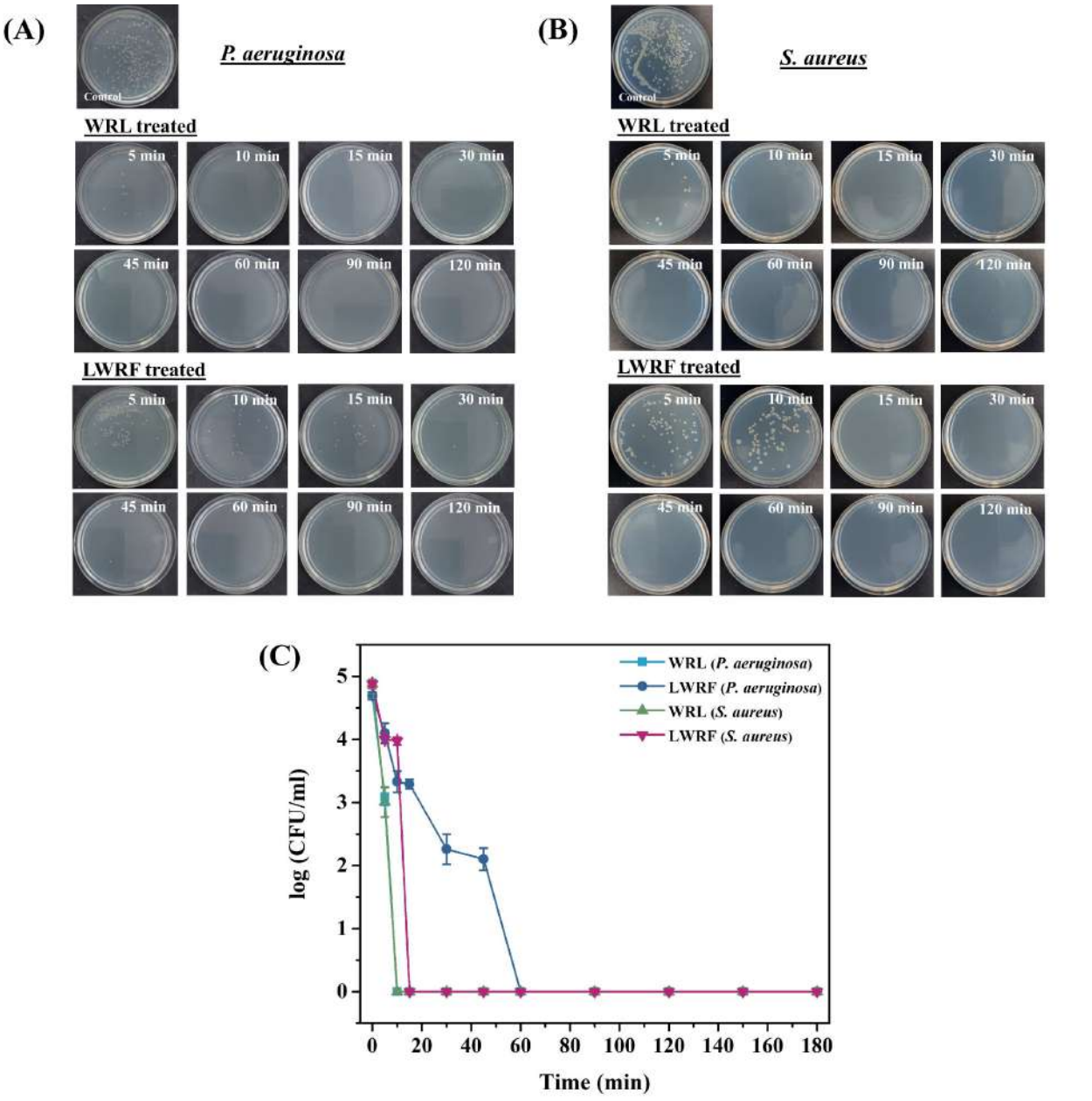

Figure 5.4. Time-kill kinetics assay. Photographs of colonies formed on agar plates corresponding to the bacterial cells of (A) *P. aeruginosa* and (B) *S. aureus* treated with WRL and LWRF at their respective MICs incubated for different time intervals. Each plate represents one set of the triplicates maintained corresponding to each time point of incubation. (C) Log (CFU/ml) plotted as a function of time to determine the time required for WRL and LWRF to eradicate *P. aeruginosa* and *S. aureus* completely at their respective MIC values against the individual microbes.

5.2.6. Structure of the AMPs studied by circular dichroism

Secondary structures of the peptides were determined using CD spectroscopy. CD spectra of the peptides (Figure 5.5) were acquired in the free state (water), in the presence of bacterial membrane mimic sodium dodecyl sulfate or SDS (30 mM, above CMC value), mammalian membrane mimic dodecylphosphocholine or DPC (10 mM) and 50% 2,2,2-trifluoroethanol or TFE (helix promoting solvent). Analysis of the CD spectra revealed both the peptides assumed random coil structures in water. In the presence of bacterial membrane mimic SDS as well as helix promoting TFE, peptides WRL and LWRF were found to assume some extent of alpha helical structures (Table 5.5). Helix formations were marginally more prominent for WRL than for LWRF. Peptides also assumed helices to some extent in DPC although in percentages much less compared to that formed in SDS or TFE.

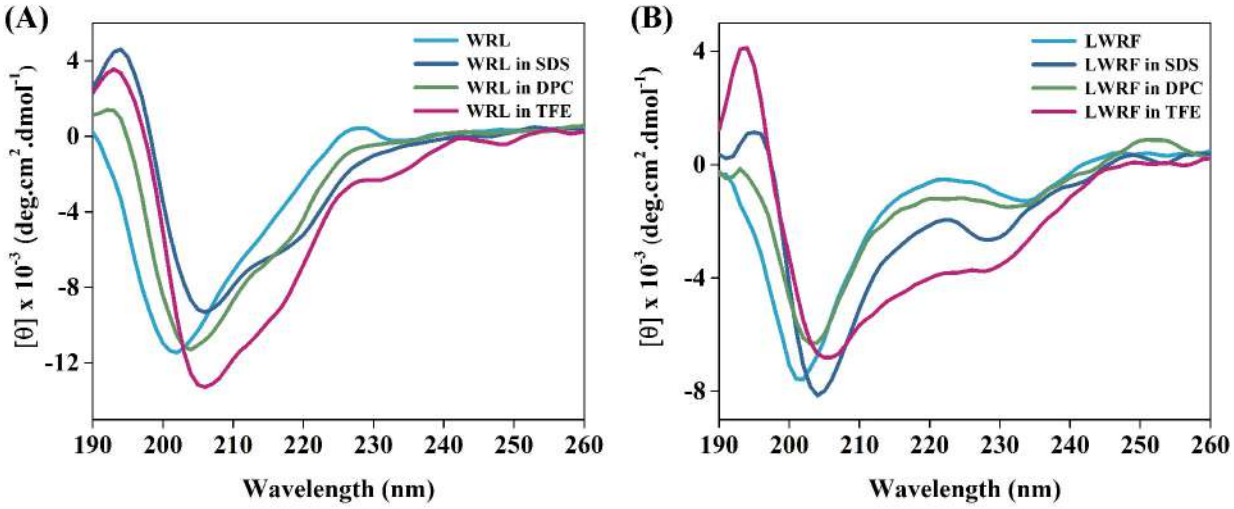

Figure 5.5. CD spectra of peptides (A) WRL and (B) LWRF in the free state as well as in the presence of bacterial membrane mimic SDS, mammalian membrane mimic DPC and helix promoting 50% TFE.

Table 5.5. Percentages of various secondary structures adopted by the peptides WRL and LWRF in water, 30 mM SDS (bacterial membrane mimic), 10 mM DPC (mammalian membrane mimic), and 50 % TFE (helix promoter) determined from CD spectroscopy analyzed using BeStSel software.[38]

Percentages of secondary structures		
Peptides	**WRL**	**LWRF**

Medium/ Secondary structures	Water	SDS	DPC	TFE	Water	SDS	DPC	TFE
Helices	3.1	37.4	14.1	59.8	11.6	29.7	18.9	39.1
β-strand	26.9	10.6	18.0	25.9	25.1	22.7	18.2	18.6
Turn	5.7	0.0	0.0	0.0	24.5	13.8	17.0	11.0
Others	64.3	52.0	67.9	14.3	38.8	33.8	45.9	31.3

5.2.7. AMP-membrane mimic/membrane interactions

Fluorescence blue shift experiments

Interactions of the peptides WRL and LWRF with bacterial membrane mimic D8PG[39] and mammalian membrane mimic DPC[40] were studied using intrinsic fluorescence of tryptophan present in the peptides [Figure 5.6(A) & D11, Appendix D]. Interaction of the peptides with the membrane mimetics changes the microenvironment of tryptophan to more hydrophobic, thus resulting in the shift of the λ_{max} values of tryptophan. Both the peptides (10 μM) were titrated against increasing concentrations of D8PG and DPC, each upto a ratio 20 times the concentration of the peptides. Both WRL and LWRF showed a consistent shift in the λ_{max} values with increasing concentrations of D8PG, WRL and LWRF achieving a $\Delta\lambda_{max}$ values of 13 nm and 11 nm respectively when titrated against 200 μM (or 20 times the concentration of the peptides) of D8PG. Thus, in general, the λ_{max} blue shift of WRL was greater than LWRF, suggesting a stronger interaction in between WRL and the microbial membrane mimics than the LWRF. The higher shifting of the λ_{max} in the case of WRL compared to that of LWRF can be accounted on the basis of the number as well as the position of the tryptophan residues present their sequences. This experiment also demonstrated the role of tryptophan residue in peptide-membrane interaction and hence in the activity of the AMPs. No shift in the λ_{max} ($\Delta\lambda$ max = 0 nm) value was observed for both the peptides titrated against DPC upto concentrations 20 times that of the peptides. Thus, both the peptides interacted selectively with the negatively charged phospholipid D8PG but were unable to interact with zwitterionic phospholipid DPC. This experiment corroborated the selectivity of the peptides for the microbial cells over the mammalian cells that was earlier seen in the biological activity assays and suggested that the interaction in between the peptides and the microbial membrane was primarily of electrostatic origin.

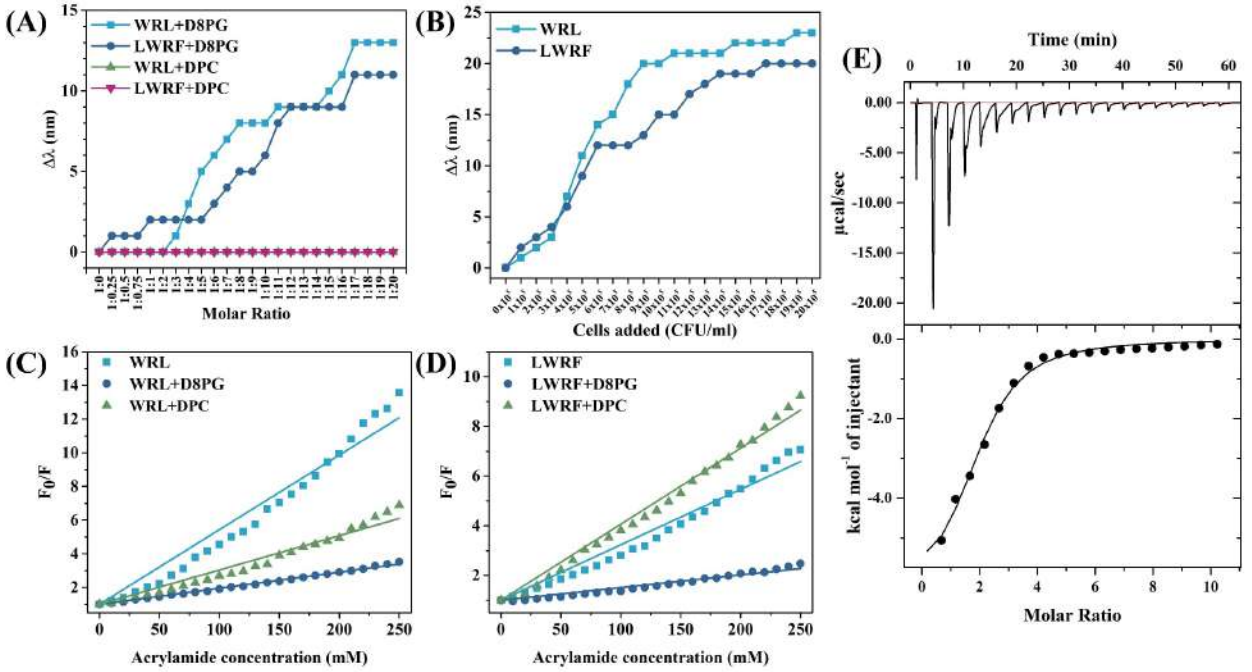

Figure 5.6. (A, B) Blue Shift Experiments. Wavelength shift of the peptides WRL and LWRF corresponding to increasing concentrations of (A) D8PG (bacterial membrane mimic) and DPC (mammalian membrane mimic) (B) living *P. aeruginosa* cells. (C, D) Solvent accessibility experiment. Solvent accessibility plot of (C) WRL and (D) LWRF. F_0/F plotted against acrylamide concentration (mM). Slope denotes the Stern-Volmer constant (K_{SV}). (E) Isothermal Titration Calorimetry (ITC). Determination of binding abilities of the peptide WRL to microbial membrane mimic SDS.

Live cell fluorescence

Interactions of WRL and LWRF with living *P. aeruginosa* and *S. aureus* cells were studied in the similar way as above using the intrinsic fluorescence of tryptophan present in the peptides. WRL ($MIC_{90\%}$: 5 µM) and LWRF ($MIC_{90\%}$: 7.5 µM) at their respective MICs displayed a final shift value ($\Delta\lambda_{max}$) of 23 nm and 20 nm respectively when titrated against an increasing concentration of *P. aeruginosa* cells upto a final concentration of $2x10^6$ CFU/ml in each case [Figure 5.6(B) & D12, Appendix D]. WRL ($MIC_{90\%}$: 4 µM) displayed a $\Delta\lambda_{max}$ shift value of 16 nm against $2x10^6$ CFU/ml of *S. aureus* cells, while LWRF ($MIC_{90\%}$: 15 µM) displayed a wavelength shift of 15 nm against 10^7 CFU/ml of *S. aureus* cells (Figure D13, Appendix D). High shift in the λ_{max} values of the peptides on being titrated against increasing concentrations of the bacterial cells implied

considerable abilities of the peptides to interact with both the Gram-positive as well Gram-negative bacterial membranes.

Solvent accessibility experiment

Peptides in their free form (10 μM), and in the presence of D8PG and DPC (each 20 times the molar ratio of the peptides) were quenched with increasing concentrations of acrylamide, a static quencher to understand the accessibility of the peptides in the free state and in the presence of membrane mimics ([Figure 5.6(C) & (D)]. Fluorescence intensities in the presence of increasing amounts of acrylamide (10-250 mM), were fitted using Stern-Volmer equation $F_0/F = 1+K_{SV}[Q]$, F_0 representing initial fluorescence intensity, F denoting fluorescence intensity at each quenching concentration, Q denoting molarity and K_{SV} denoting the Stern-Volmer quenching constant. Peptides in their free state displayed high Ksv value, suggesting higher solvent accessibility than in the presence of bacterial membrane mimic D8PG. Reduced accessibility of solvents in D8PG environment implied significant peptide-lipid interactions. On the other hand, WRL in DPC environment displayed comparatively lower Ksv compared to that of the peptide in the free state but higher than that of the peptide in D8PG. This implied that there might be slight interactions between the peptide and DPC, that was comparatively lower than that with D8PG. Ksv of LWRF in DPC was found to be higher than that of the peptide in free state implying no peptide-lipid interactions. Solvent accessibility experiment also explained preferential bactericidal but non-cytotoxic nature of the designed peptides, LWRF being relatively more non-cytotoxic amongst the two.

Isothermal Titration Calorimetry (ITC)

Interactions between the peptide WRL and bacterial membrane mimic SDS were studied using isothermal titration calorimetry (ITC). Peptide WRL was found to efficiently interact with SDS as evident from the ITC interaction patterns and thermodynamic parameters [Figure 5.6(E) & Table 5.6].

Table 5.6. Thermodynamic parameters for the interaction of WRL with SDS determined using ITC.

Thermodynamic parameters	WRL vs SDS
Model	One binding site
Temperature (T)	310 K (37 °C)

K_A (M^{-1})	$2.51x10^3$
N	1.91
ΔH ($cal.mol^{-1}$)	-6538.0
ΔS ($cal.mol^{-1}.deg^{-1}$)	-5.53
TΔS ($cal.mol^{-1}$)	- 1714.3
ΔG ($cal.mol^{-1}$)	-4823.7
K_D (μM)	398.41

5.2.8. Membrane permeation of the designed AMPs

Inner membrane permeation

Propidium iodide (PI) added to the cells of *P. aeruginosa* at their untreated form showed a steady fluorescence signal over a period of time. Significant enhancement in the fluorescence intensities were observed upon addition of 0.5X MIC and 1X MICs of the peptides [Figure 5.7(A) & (B)]. As enhancement of the fluorescence intensity of PI could occur upon intercalation of the peptide to the DNA, which was only possible when the inner membrane of the cell was permeabilized,[41] the enhancement of its fluorescence intensity of PI upon addition of the peptides to the cells, indicated the inner membrane permeabilizing abilities of the peptides. Polymyxin B (10 μM), added as the positive control, to the cell suspension containing PI induced comparable fluorescence enhancements as induced by the peptides at their respective MICs.

Outer membrane permeation

N-Phenyl-1-naphthylamine or NPN is a weak fluorescent probe in aqueous environment which manifests significant fluorescent properties upon binding with the membrane lipids.[42] However, interaction of NPN with the membrane lipids is not possible in the healthy cells and occurs only upon permeation of the outer membrane.[43] NPN showed a weak fluorescence in the suspensions of untreated cells but its fluorescence significantly enhanced upon addition of peptides (0.5X and 1X MIC) to the cells [Figure 5.7(C) & (D)]. This enhancement of NPN fluorescence intensity proved the outer membrane permeation ability of the cells. Polymyxin B (10 μM) added as the positive control, was found to induce comparable NPN fluorescence enhancements to the peptides at their MIC concentrations. This suggested outer membrane permeation ability of the peptides in line with the commercially available antibiotics (Polymyxin B).

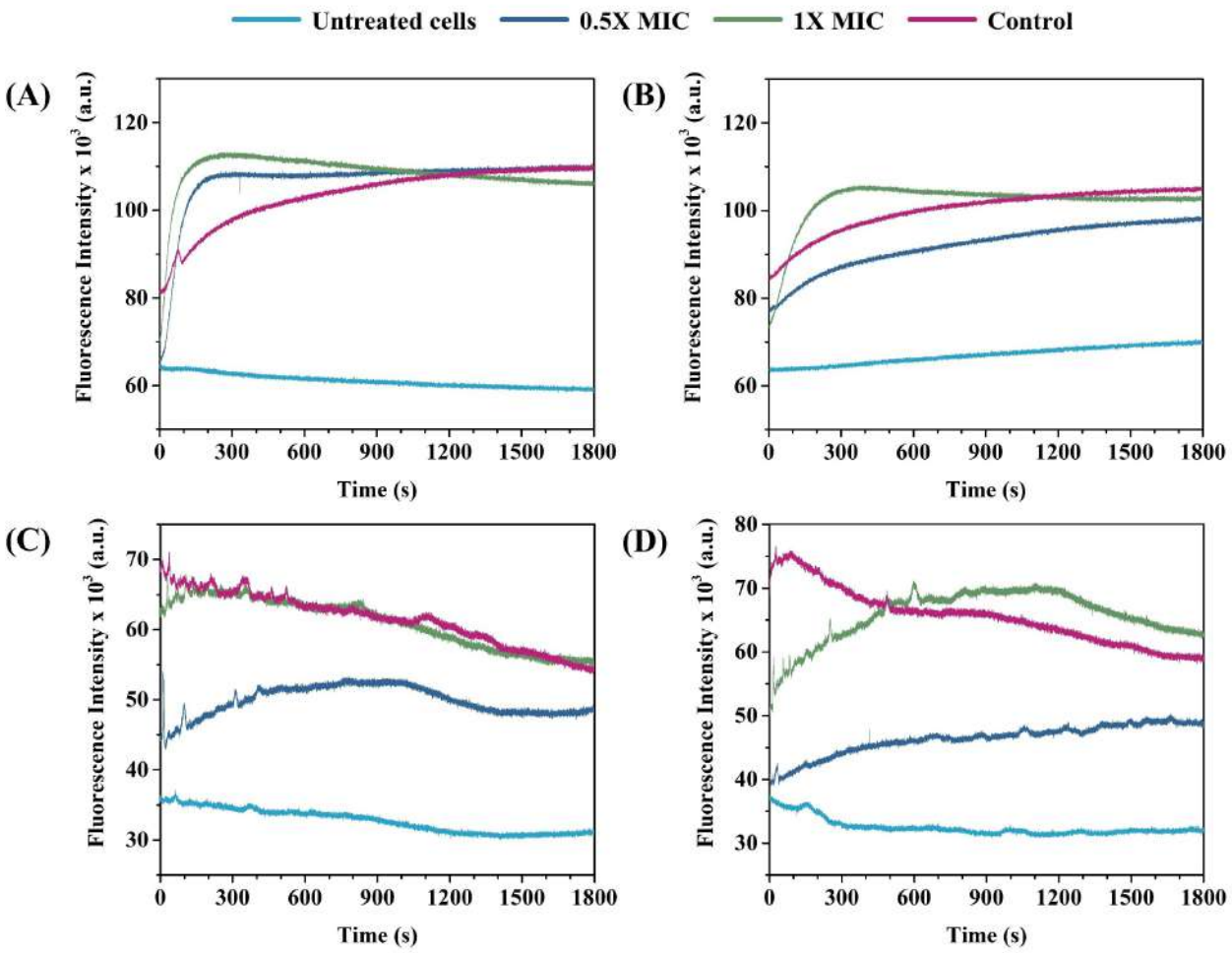

Figure 5.7. (A, B) Inner membrane permeation assay or Propidium iodide (PI) assay. Fluorescence spectra *of P. aeruginosa* cells preincubated with PI treated with 0.5X MICs, 1X MICs of the peptides (A) WRL and (B) LWRF as well as 10 µM Polymyxin-B used as the positive control. (C, D**)** Outer membrane permeation assay or NPN assay. Fluorescence spectra *of P. aeruginosa* cells preincubated with NPN treated with 0.5X MICs, 1X MICs of the peptides (C) WRL and (D) LWRF as well as 10 µM Polymyxin-B used as the positive control.

5.2.9. Membranolytic action of the peptides

Live cell NMR experiment

Interaction of WRL with the membrane of *S. aureus* was further studied using ^{1}H-NMR spectroscopy (Figure 5.8). ^{1}H-NMR spectra of WRL and that of the untreated cells, in 10% added D_2O were acquired first. Peptide was added to the cells and the spectra of the peptide treated cells were acquired at different time intervals. *S. aureus* cells induced broadening of peptide peaks with

progression of time, signifying peptide-membrane association. Also, leakage of metabolites was evident from the appearance of new peaks in the cell-peptide mixtures with increasing incubation time, establishing the membranolytic mode of action of WRL.

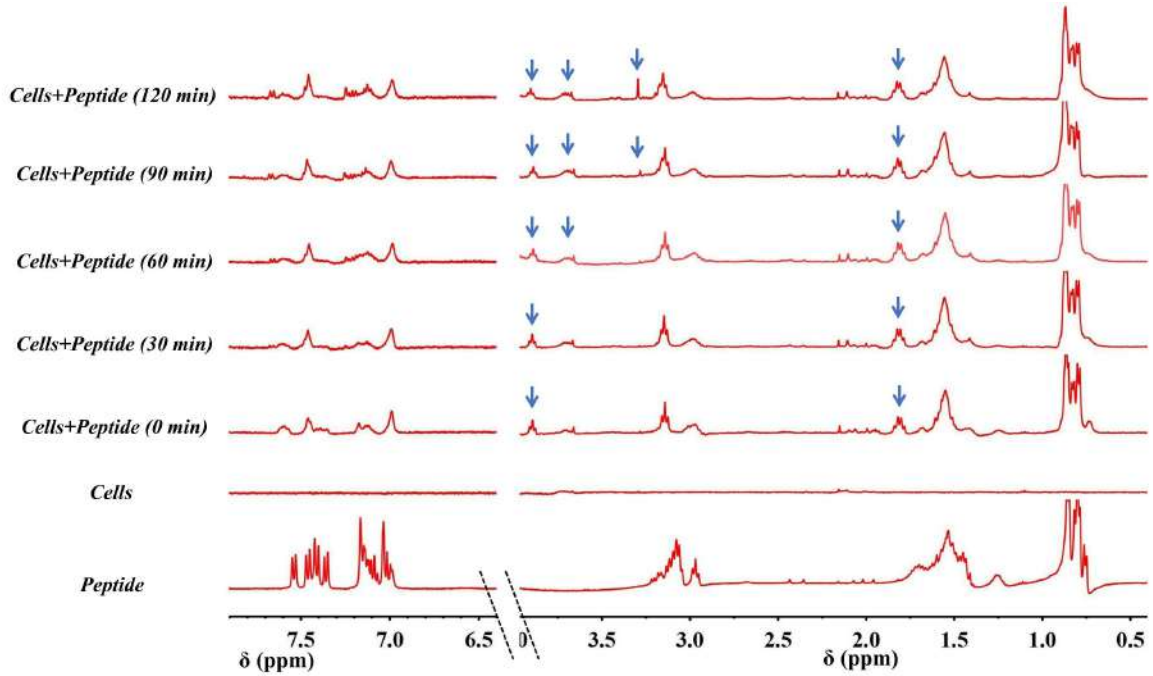

Figure 5.8. Live Cell NMR experiment. 400 MHz ^{1}H NMR spectra of *S. aureus* cells (10^{8} CFU/ml) treated with WRL (1 mM) for different time intervals. The blue lines indicate appearance of new peaks as a result of leakage leading to the release of metabolites or cellular matrix from the lysed cells. Peak broadening can be seen though out the spectra indication of peptide membrane association.

FESEM and FETEM images of peptide treated bacterial cells

Effect of the peptides on *P. aeruginosa* and *S. aureus* membranes were visualized by using electron microscopy. FESEM images revealed serious deformation of the bacterial membranes, distortion of shapes and complete disintegration of bacterial cells treated with 1X and 2X MICs of the respective peptides [Figure 5.9(A) I-V & (B) I-V]. FETEM imaging also revealed distortion of bacterial cells on being treated with the peptides [Figure 5.9(A) VI-VIII and (B) VI-VIII].

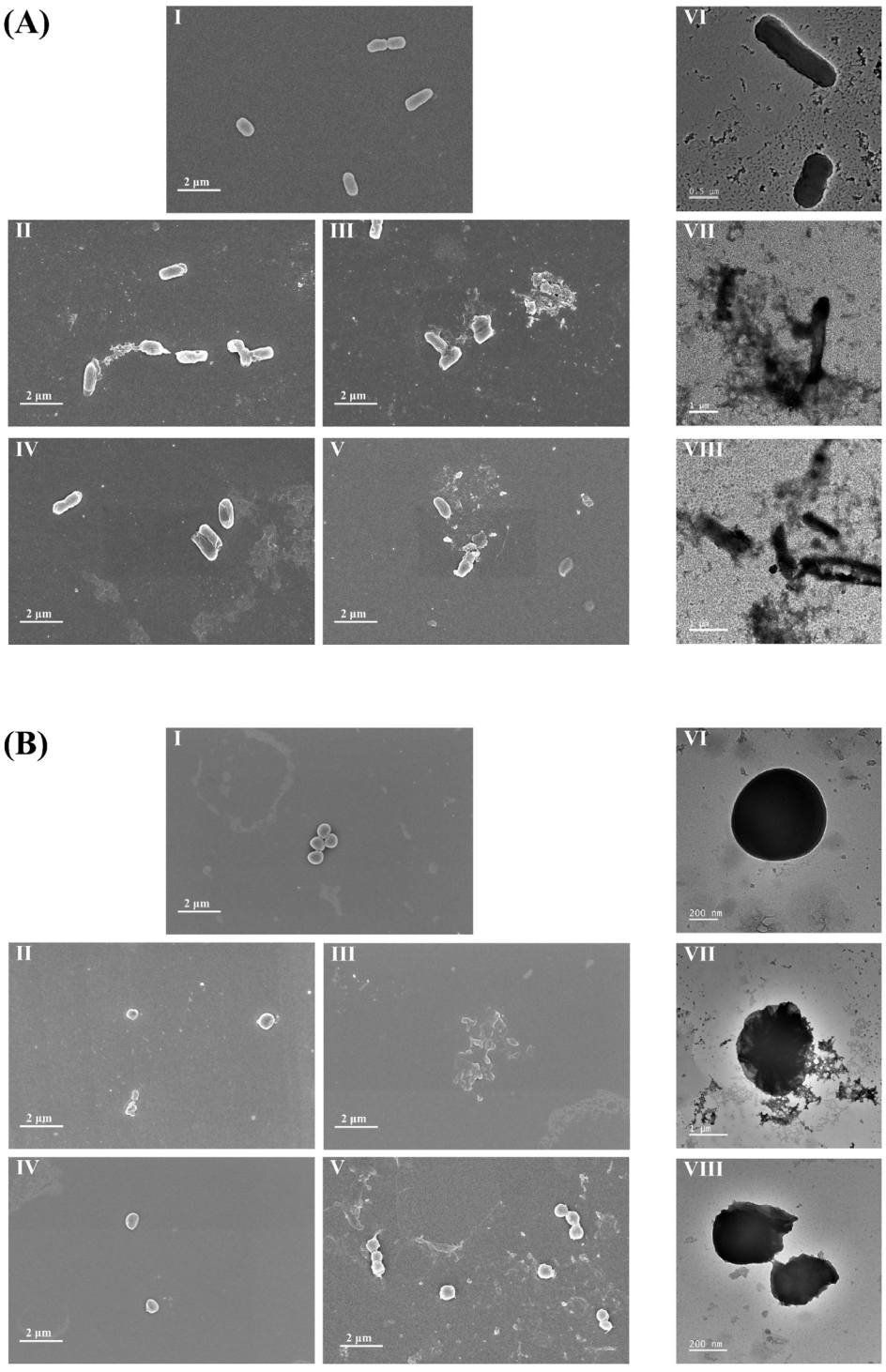

Figure 5.9. (A) FESEM and FETEM images of *P. aeruginosa* cells. FESEM images of (I) untreated *P. aeruginosa* cells, cells treated with (II) 1X and (III) 2X MIC of WRL, and cells treated with (IV) 1X and (V) 2X MIC of LWRF. FETEM images of (VI) untreated *P. aeruginosa*, and *P. aeruginosa* cells treated with 1X MIC of (VII) WRL and (VIII) LWRF. (B) FESEM and FETEM

images of *S. aureus* cells. FESEM images of (I) untreated *S. aureus* cells, *S. aureus* cells treated with (II) 1X and (III) 2X MIC of WRL, and with (IV) 1X and (V) 2X MIC of LWRF. FETEM images of (VI) untreated *S. aureus* cells, *S. aureus* cells treated with 1X MIC of (VII) WRL and (VIII) LWRF.

Flow assisted cell sorting

Flow assisted cell sorting technique was further utilized to ascertain the membranolytic and bactericidal properties of the peptides. PI was added to the untreated as well as the peptide treated (WRL and LWRF at their respective 1X and 2X MICs) *P. aeruginosa* cells [Figure 5.10(A) & (B)]. Dead cells stained with PI were sorted out from a population of certain cells based on their enhanced PI fluorescence. Untreated cells, used as control only had 7.9% PI-stained cells, corresponding to the percentage of dead cells in the healthy bacterial cell culture. 1X MIC and 2X MIC of WRL killed 75.4 % and 86.8% of the cells while 1X and 2X MIC of LWRF killed 79.9% and 89.0% of the cells respectively. Cells suspensions corresponding to a final optical density of 0.1 was used for this assay.

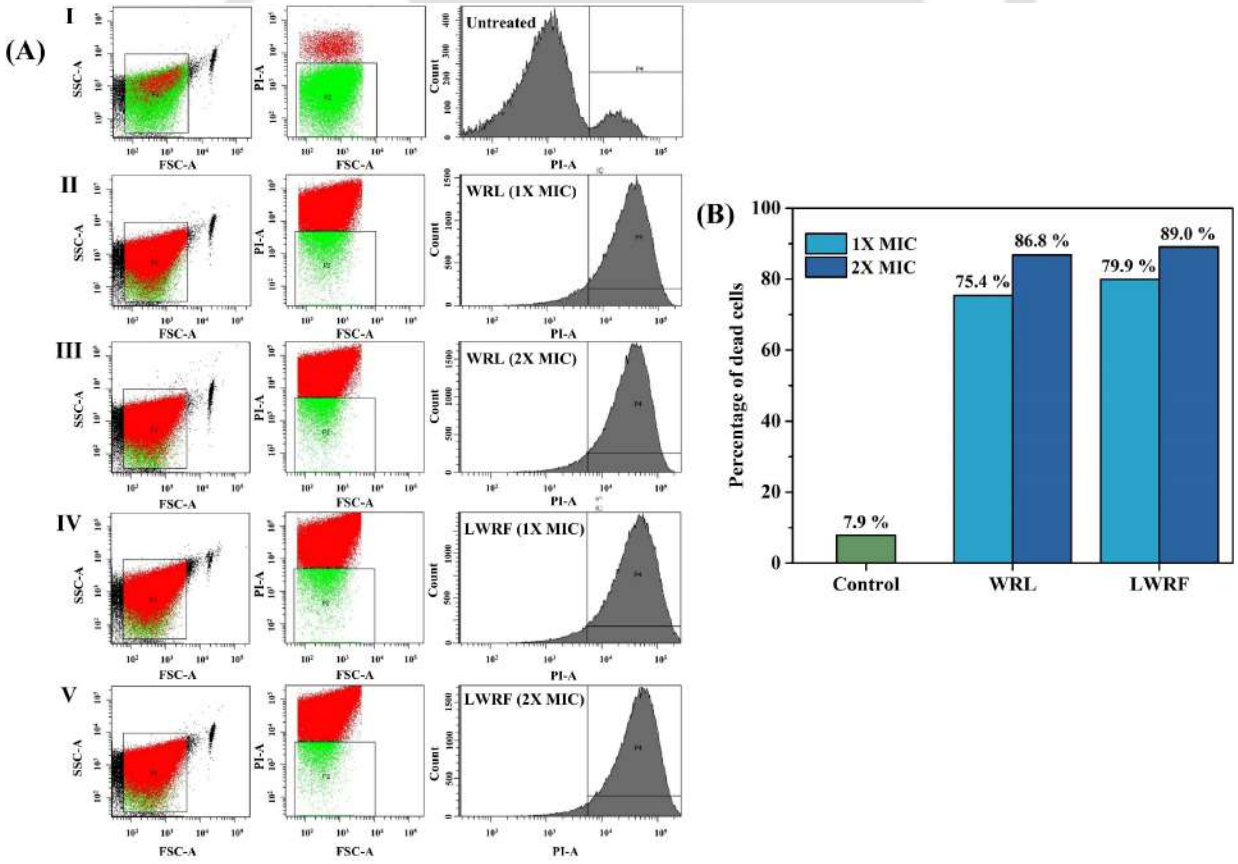

Figure 5.10. (A) FACS histograms showing the permeability of PI in the (I) untreated, (II-III)

1X, 2X MIC of WRL treated, and (IV-V) 1X, 2X MIC of LWRF treated *P. aeruginosa* cells respectively. (B) Bar diagram showing the percentage killing of *P. aeruginosa* cells incubated with 1X and 2X MICs of WRL and LWRF respectively.

Live cell/ dead cell assay

Bactericidal effect of the AMPs was visualized in the live cell/ dead cell assay with the help of confocal microscopy. Acridine orange[44] is a dye capable of penetrating through cells with intact bacterial membrane and hence stains living cells (also capable of staining dead cells). PI on the other hand as discussed previously is unable to penetrate intact membranes and are capable of staining only dead cells. *P. aeruginosa* cells were incubated with acridine orange and propidium iodide followed by treatment with MIC concentrations of the peptides. As expected, confocal images of the untreated cells showed signals corresponding to acridine orange or the living cells and no signals from propidium iodide (Figure 5.11). Cells treated with the peptides on the other hand showed prominent signals arising from propidium iodide and weak signals arising from acridine orange. Addition of peptides to the cells induced rupture in the membrane or generated holes in them allowing PI molecules to migrate inside the cells and bind with the nucleic acids generating prominent signals.

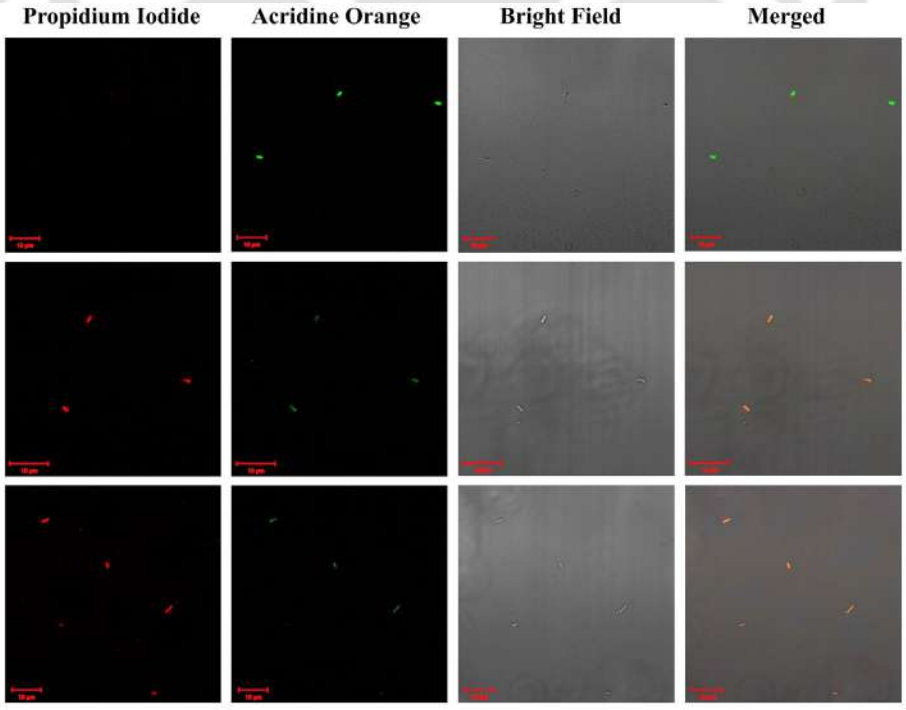

Figure 5.11. Live Cell Dead Cell assay using acridine orange and propidium iodide. (I) untreated; (II) WRL treated and (III) LWRF treated *P. aeruginosa* cells.

5.2.10. MD simulations: structure and dynamics of the peptide in the presence and absence of micelle/ bilayer complexes

MD simulations of the peptides (WRL or LWRF) in the presence and absence of membrane mimetic model (viz., SDS micelle) indicated unstructured random-coil peptide conformations [Figure 5.12(A)]. However, CD experiments indicated that the peptide underwent partial conformational change (random-coil → helix) in response to SDS-micelle binding (Figure 5.5). Although the MD structure of the peptide-coil: micelle complex provided insight into the initial peptide: micelle complex, it could not capture the micelle-induced peptide conformational change. Thus, we obtained the MD structure of the peptide-helix: micelle complex by placing the helical peptide ~26.5 Å away from the micelle and subjecting the resulting initial model to MD simulations.

MD structure of peptide-helix: micelle complex and the calculated solvent-accessible surface area (SASA) of the peptide residues indicated that both the tryptophan residues of WRL peptide (W1 and W3) were buried in the desolvated hydrophobic core of the SDS-micelle [Figure 5.12(B)]. The local environment around the tryptophan residues was more or less identical. In the fluorescence experiment, a blue shift (~8 nm, λ_{max}: 359 nm→351 nm) was observed for WRL [Figure D14(A), Appendix D] in response to SDS micelle (30 mM). The presence of a single blue-shifted peak indicated that two tryptophan residues (W1 and W3) of WRL were in a similar environment in the presence or absence of micelle. The magnitude of the blue shift indicated an increase in non-polar environments around the tryptophan residues (aqueous to aliphatic core). Thus, the fluorescence data was in line with the MD structure of the WRL^{helix}: micelle complex. On the contrary, the MD structure of the $LWRF^{helix}$:micelle complex showed that the tryptophan residue (W2) of the LWRF was mostly exposed to water [Figure 5.12(B)]. A relatively small blue shift (~2 nm) for the LWRF peptide (Figure [Figure D14(B), Appendix D] in the SDS miceller environment indicated that W2 was likely to be relatively more exposed to water, thus supporting the predicted $LWRF^{helix}$: micelle MD structure and the calculated SASA data.

(A) Peptide Secondary Structural analysis		Coil	Bend	Turn	Helix	Sheet
Free  *Peptide*	WRL	0.84±0.05	0.11±0.04	0.05±0.02	0.0	0.0
	LWRF	0.98±0.03	0.02±0.03	0.00±0.00	0.0	0.0
Complex 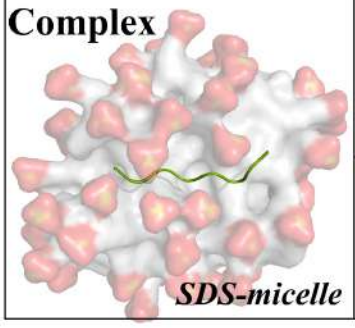 *SDS-micelle*	WRL	0.80±0.01	0.12±0.02	0.01±0.01	0.0	0.0
	LWRF	0.90±0.04	0.10±0.01	0.00±0.00	0.0	0.0

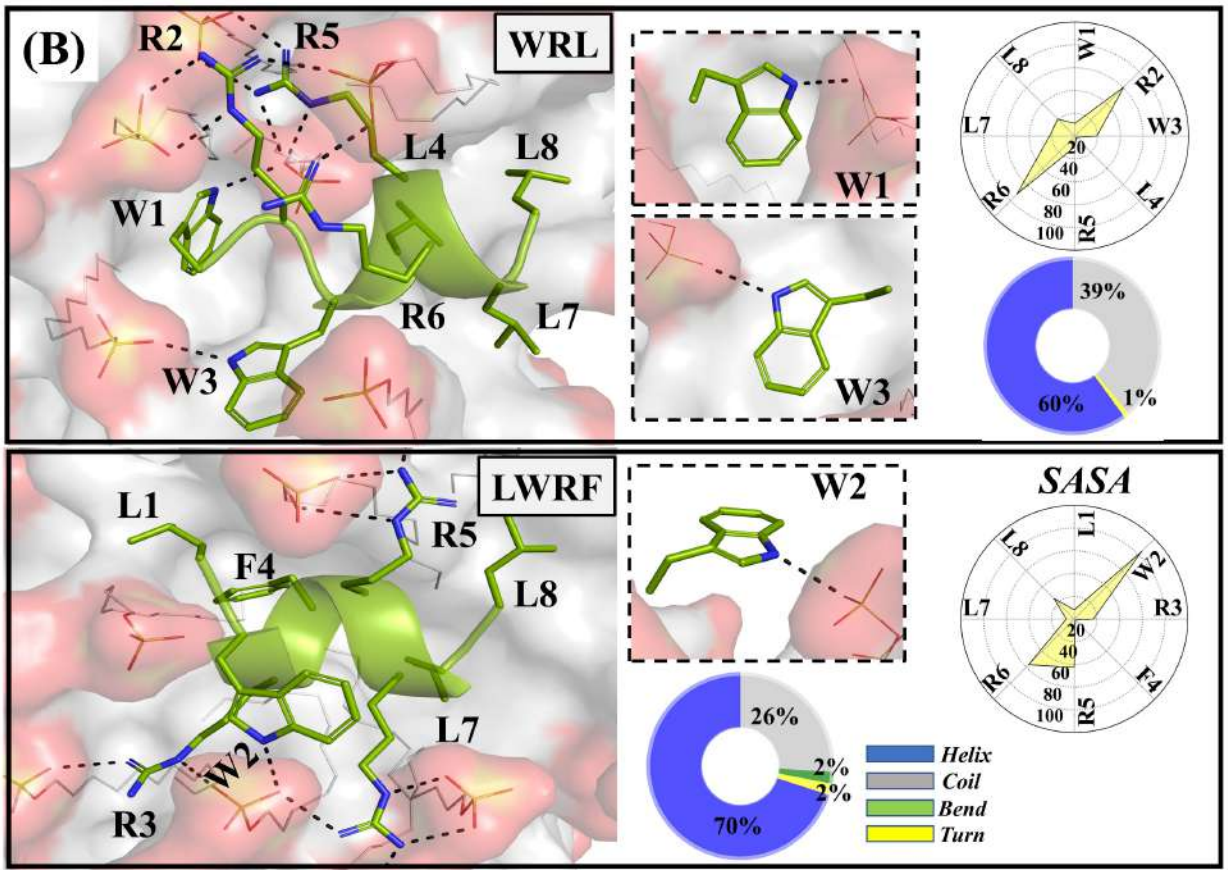

Figure 5.12. (A) Secondary structural analysis of the peptide in the presence and absence of micelle. (B) Trajectory averaged solvent accessible surface area (SASA; net-plot where the

contours of constant solvent exposure are shown) and the secondary structural features (helix, coil, bend, and turn) of the helical peptides in the Peptide^{helix}: micelle complex.

Irrespective of the secondary structure of the peptides (random-coil or helix), MD simulations could capture some robust features of peptide: micelle binding event. The center-of-mass distance (d_{COM}) between the peptides and bilayer during the MD trajectory was plotted (Figure 5.13). The plateau in the d_{COM} versus time plot indicated the structural convergence of the peptide: micelle complex. Peptide: micelle dissociation was not observed during the course of the simulation, indicating the irreversible nature of the binding. Electrostatic interactions (positively charged peptide and negatively charged micelle surface) drove the initial peptide: micelle contact. Subsequently, the favorable van der Waals interactions facilitated the settlement of the peptide on the micelle by placing the hydrophobic peptide side-chains in the micelle core. Direct or water-mediated peptide: micelle contact or interaction with the bulk water molecules fulfilled the H-bonding requirements of the peptides.

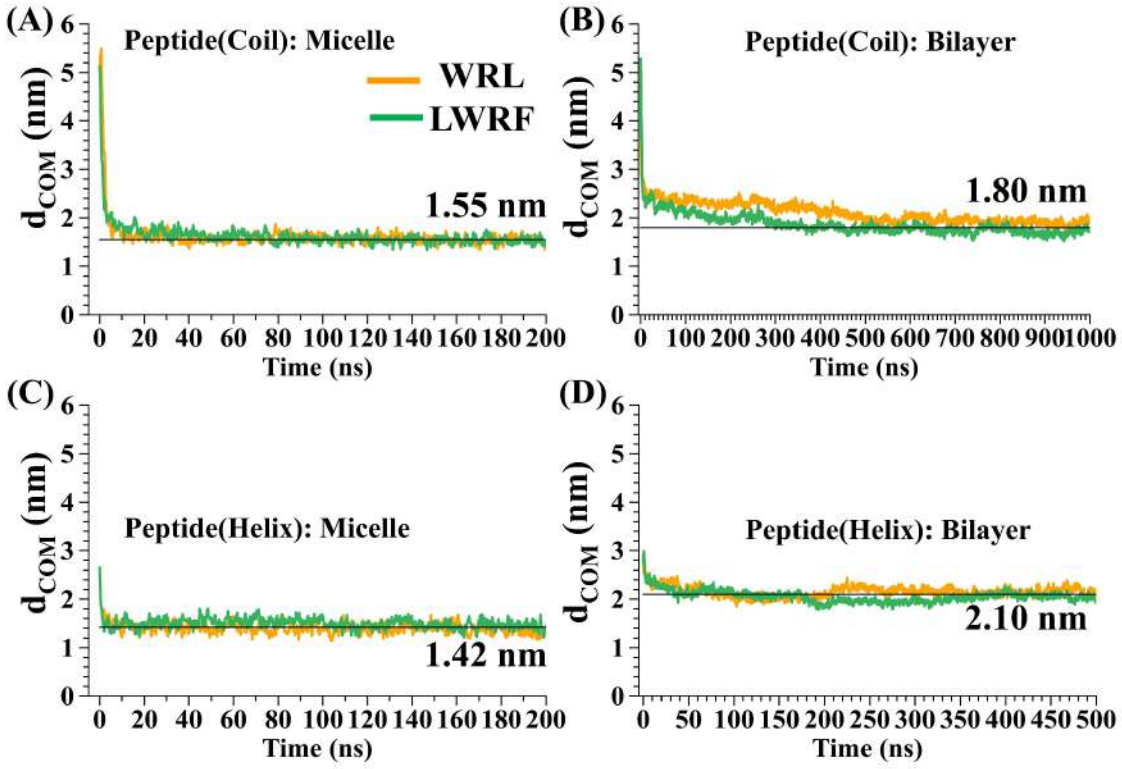

Figure 5.13. Peptide: micelle/bilayer distance as a function of time. d_{COM} is the distance between the center of mass of the peptide (WRL or LWRF) and the center of mass of the micelle/bilayer. The black horizontal line was the trajectory averaged d_{COM} (last 150 ns).

As expected, the reduced flexibility of the peptide upon micelle binding was evident from the RMSF data (Figure D15-D16, Appendix D). Similar observations were observed in the case of peptide: bilayer binding (Figure 5.14).

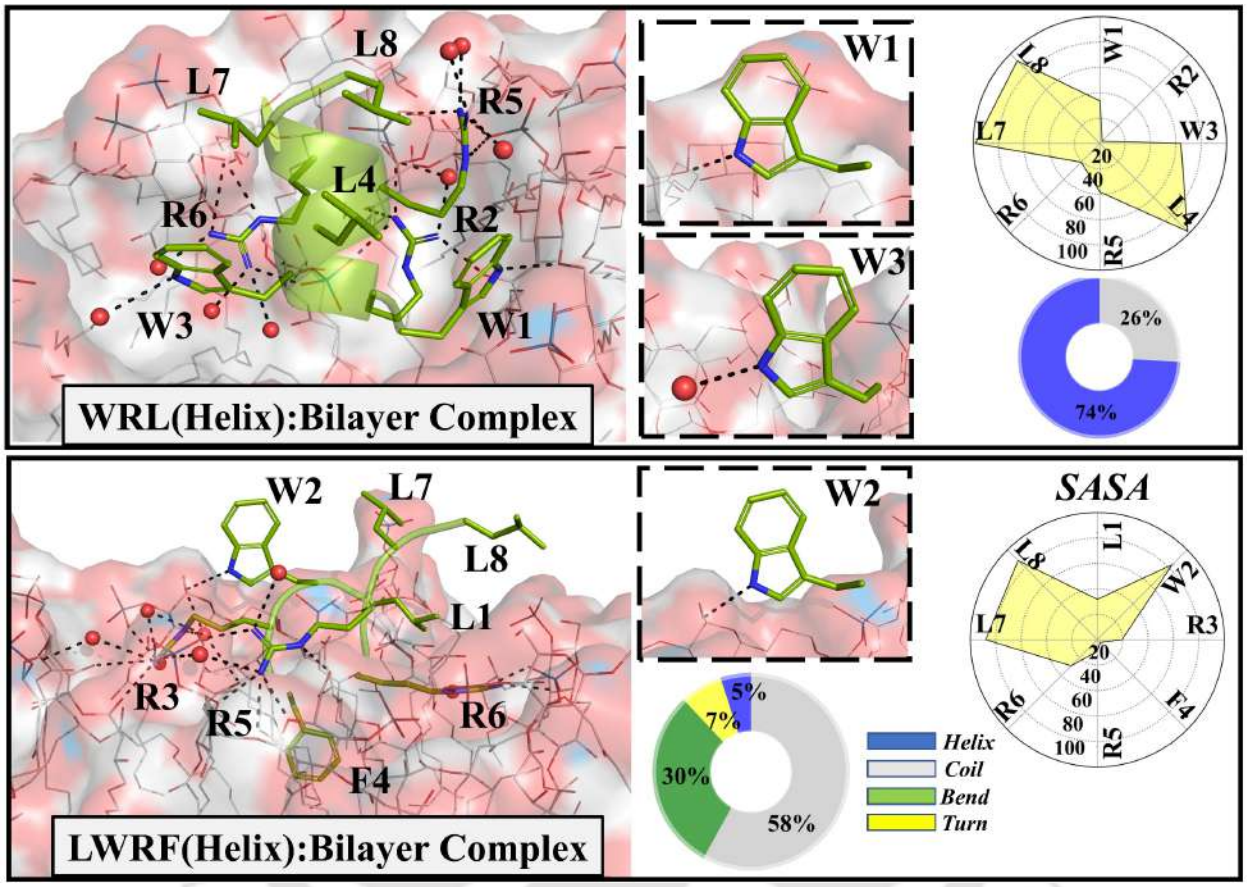

Figure 5.14. Secondary structural analysis of the peptides WRL and LWRF in the presence of bilayer. Trajectory averaged solvent accessible surface area (SASA; net-plot where the contours of constant solvent exposure is shown) and the secondary structural features (helix, coil, bend, and turn) of the helical peptide in the Peptide^{helix}: bilayer complex.

5.3. Discussion

Two broad-spectrum cationic octapeptides rich in arginine and tryptophan were designed and developed in this study. AMP WRL had greater potency over LWRF against all the microbial strains that were tested. In addition, WRL had faster killing kinetics and better salt tolerance of its antimicrobial potency over LWRF. The enhanced efficacy of the WRL was most probably attributed to the presence of two tryptophan residues in WRL, one of them being at the N-terminus, over the only non-terminal tryptophan residue in LWRF. The position of the two tryptophan

residues of WRL at the interface of the hydrophobic/hydrophilic surfaces of the helix that was formed in the presence of the membrane mimetics, might also contribute to the enhanced activity of WRL. Due to the borderline hydrophobicity of tryptophan, it is known to induce membrane binding better.[7] Terminal tryptophan residues are also known to enhance the activity of the AMPs.[32-33] Both the peptides adopted random coil like conformation in free state in water and a partial helical conformation in the presence of membrane mimetics. In an attempt to understand the membrane mimic: peptide interaction, we performed MD simulations where in the case of WRL, both the tryptophan residues were found to be properly anchored inside hydrophobic pockets of the membrane bilayer in contrast to LWRF, where the sole tryptophan was pointing towards the water. This led to better peptide membrane interaction for WRL compared to LWRF. Both the cationic peptides were membranolytic in their mechanism of action as was clearly established through several spectroscopic, microscopic and biophysical experiments. The peptide membrane interaction was primarily driven by the electrostatic interactions as seen from the MD simulations. Despite of having the exact same charge, WRL and LWRF varied greatly in their antimicrobial efficacy owing to better membrane peptide interactions of the former. Though both the peptides were selective towards microbial membrane mimics over the mammalian membrane mimics at their biologically relevant concentration, LWRF had a better selectivity than WRL towards microbial membranes over the mammalian membranes, as seen from the cytotoxicity assays. This might be a result of better membrane binding ability of WRL over LWRF, making it indiscriminate in binding to different membranes, leading to low selectivity. This study conclusively demonstrated that for cationic peptides of similar charge, number and the position of the tryptophan residues played a crucial role in determining the efficacy of the AMPs owing to the critical role played by tryptophan in the initial peptide membrane interactions. However, one must also be aware that selectivity towards membrane binding decreased with the increase in the number of tryptophan residues. Hence, selecting an optimum number of tryptophan residues is crucial in striking a balance between high antimicrobial potency and membrane selectivity.

5.4. Conclusion

In this work we have developed two cationic non-cytotoxic octapeptides WRL and LWRF with broad spectrum antimicrobial activity against several Gram-positive and Gram-negative bacteria belonging to the ESKAPE pathogen group and the fungus *Candida albicans*. WRL was a better

antimicrobial agent both in the absence and the presence of salts with a faster killing kinetics due to the presence of greater number and favourable position of tryptophan residues which helped in better membrane interaction of the peptide. However, better membrane associating potential due to greater number of tryptophans in WRL also led to lesser selectivity of membrane binding. Thus, in cationic peptides which work via membrane association, damage and subsequent death, tryptophan residues that promote membrane interactions play a critical role. An optimum number of tryptophan residues would ensure both high antimicrobial potency and selectivity. Such fundamental understanding of the design principles of AMPs would lead to the design of more effective AMPs in the future to expand the existing toolbox of antimicrobial therapeutics.

5.5. Methods

5.5.1. Materials

Rink amide resin, Fmoc protected amino acids: Fmoc-Leu-OH, Fmoc-Arg(Pbf)-OH, Fmoc-Trp(Boc)-OH, Fmoc-Phe-OH, Hexafluorophosphate Benzotriazole Tetramethyl Uronium (HBTU), 1-Hydroxybenzotriazole (HOBt) were purchased from GL Biochem Ltd., Shanghai, China. N, N-dimethyl formamide (DMF), N, N-diisopropylethylamine (DIPEA), Piperidine, Pyridine, Trifluoroacetic acid (TFA) were purchased from Merck Life Science Pvt. Ltd., Mumbai, India. Acetic anhydride was obtained from the department of chemistry, IIT Guwahati and was manufactured by SD Fine Chem Limited, Mumbai, India. Dichloromethane (DCM), HPLC grade acetonitrile and Diethyl ether were purchased from Finar Limited, Ahmedabad, India. Monosodium phosphate (NaH_2PO_4), Disodium phosphate (Na_2HPO_4), Monopotassium phosphate (KH_2PO_4), Sodium Chloride (NaCl), Potassium Chloride (KCl), Calcium chloride ($CaCl_2$), Magnesium chloride ($MgCl_2$), Zinc Chloride ($ZnCl_2$) and Ferric chloride ($FeCl_3$) were purchased from Merck Life Science Pvt. Ltd., Mumbai, India. Nutrient broth, BHI broth, YPD broth were purchased from Himedia Laboratories Pvt. Ltd., Mumbai, India. Deuterium oxide (D_2O), α-Cyano-4-hydroxycinnamic acid (HCCA), Triton X-100, 2,2,2-trifluoro ethanol (TFE), Sodium dodecyl sulphate (SDS), Acrylamide, Propidium Iodide (PI), N-Phenyl 1-napthylamine (NPN) and Glutaraldehyde were purchased from Sigma-Aldrich, St. Louis, USA. 1,2-dioctanoyl-sn-glycero-3-phospho-(1'-rac-glycerol) (sodium salt) (D8PG) and n-Dodecylphosphocholine (DPC) were purchased from Avanti Polar Lipids, Inc., USA. Acridine orange dye was purchased from Himedia Laboratories Pvt. Ltd., Mumbai, India.

5.5.2. Synthesis, purification and characterization of the peptides

Peptides were synthesized using solid phase peptide synthesis using standard Fmoc chemistry. Briefly rink amide resin corresponding to 0.1 mM of loading capacity was weighed, swelled and deprotected using 20% piperidine in DMF to link the first amino acid (peptide was synthesized starting from the C-terminus to the N-terminus, so the amino acid placed at the C-terminus of the peptide sequence was linked as the first amino acid). 3 equiv. of the Fmoc-protected amino acids (0.3 mM), 3 equiv. of the coupling reagents HBTU (0.3 mM) and 3 equiv. of HOBt (0.3 mM) were mixed with 6 equiv. of the base DIPEA in DMF and added to the resin in order to link the amino acids. Coupling reaction was followed by capping the unreacted amino acid terminals using a solution of 7:2:1 DMF: acetic anhydride: pyridine. Amino acids were linked one after the other following the same protocol to complete the primary sequence of the peptides starting from the C-terminus to end at the N-terminus. Finally, the full-grown peptides were cleaved off the resin using a cocktail of TFA (TFA: TIS: H_2O 96: 2.5: 1.5) and precipitated using cold diethyl ether. Crude peptides were purified through preparative HPLC [Thermo Scientific Ultimate 3000] using a multigradient solvent program of acetonitrile and water. Peptides were characterized using MALDI spectroscopy (Bruker Autoflex Speed MALDI-TOF mass spectrometer), ^{1}H-NMR (Bruker Avance Neo 500 MHz FT NMR spectrometer) and analytic HPLC traces (Thermo Scientific Vanquish). Both the purified peptides were > 95% pure.

5.5.3. Microbial strains

Pseudomonas aeruginosa (MTCC 2488), *Klebsiella pneumoniae* (MTCC 432), *Escherichia coli* (MTCC 433), *Staphylococcus aureus* (MTCC 96) and *Candida albicans* (MTCC 1637) were acquired from Microbial Type Culture Collection and Gene Bank (MTCC), Chandigarh, India. Methicillin resistant *Staphylococcus aureus* (MRSA 100) strain used in this study was clinically isolated from the wound of a patient and was obtained from Prof. Benu Dhawan, AIIMS, New Delhi.

5.5.4. Determination of Minimum Inhibitory Concentration (MIC)

Minimum Inhibitory Concentration or MIC of the peptides were determined against three Gram-negative bacteria (*P. aeruginosa*, *K. pneumoniae* and *E. coli*), two Gram-positive bacterial strains (*S. aureus* and MRSA) and one fungus (*C. albicans*). Gram-negative bacteria were grown in nutrient broth, Gram-positive bacteria were grown in BHI broth both at 37 °C while the fungus

was grown in YPD both at 25 °C. Bacteria or fungus obtained at their mid-log phase were centrifuged to discard the media, followed by washing of the cells pelleted down with phosphate buffer (PB, pH 7.4, 10 mM) and finally diluted to 10^5 CFU/ml in the same buffer used for washing. 50 µl of these cell suspensions were treated with another 50 µl of the peptides diluted at different concentrations in PB (pH 7.4, 10 mM) and were incubated at a uniform shaking speed and temperature (37 °C for bacteria and 28 °C for fungus) for 4 h. Untreated cells (negative control) and cells treated with Polymyxin-B (Gram-negative bacteria)/ Vancomycin (Gram-positive bacteria)/ Amphotericin-B (fungus) [positive control] were also incubated along with the cells treated with different concentration of the peptides. Cells post incubation were added with 100 µl of the respective media and kept incubated overnight again. Killing percentages of the peptides at different concentrations were determined from their respective OD values upon comparing them with the OD values of the untreated cells (negative control) and that of the cells treated with Polymyxin-B/ Vancomycin/ Amphotericin-B (positive control). $MIC_{90\%}$ of a peptide is the lowest concentration at which it killed 90% of the cells or inhibited the growth of 90% of the cells with respect to the positive control (Polymyxin-B/ Vancomycin/ Amphotericin-B).

5.5.5. Determination of Minimum Inhibitory Concentration (MIC) in the presence of PBS

Minimum Inhibitory Concentration or $MIC_{90\%}$ of the peptides were also determined against *P. aeruginosa*, *K. pneumoniae* and *E. coli*, *S. aureus*, *MRSA* and *C. albicans* in the phosphate buffer saline (PBS, pH 7.4, 10 mM). The method was same as for the determination of MIC in PB, except for the use of PBS instead of PB in the previous assay.

5.5.6. Determination of Minimum Inhibitory Concentration (MIC) in the presence of different salts

Minimum Inhibitory Concentration or $MIC_{90\%}$ of the peptides against Gram-negative *P. aeruginosa* and Gram-positive *S. aureus* were determined in the presence of physiological concentrations of different salts: Na^+ (150 mM), Ca^{2+} (1.25 mM), Mg^{2+} (1 mM), Zn^{2+} (8 µM) and Fe^{3+} (4 µM). Weighed amounts of NaCl, $CaCl_2$, $MgCl_2$, $ZnCl_2$ and $FeCl_3$ at their respective physiological concentrations were added to PB (pH 7.4, 10 mM). MIC values were determined following the same protocol as described above but here the buffer solution containing physiological concentrations of the respective salts were used for the assay.

5.5.7. Cytotoxicity

Cytotoxicity of the peptides were determined against Human dermal fibroblasts (HDF) and HeLa cells. HDF and HeLa cells seeded at a density of 2000 and 5000 cells/well respectively were treated with different concentrations of the peptides in quadruplicates and were incubated for a period of 24 h. Cells were then treated with 0.25 mg/ml of MTT and were further kept incubated for another 2 h. Formazan crystals formed due to the addition of MTT were dissolved in DMSO and OD values were read at 570 nm with 650 nm as the reference. Percentage viability of the cells was calculated with reference to the untreated cells. Experiments were repeated at least twice.

5.5.8. Hemolytic activity

Human blood was collected from a healthy individual after taking his due consent. Human blood was centrifuged to discard the serum obtained as supernatant. The pelleted down red blood cells were washed with PBS (pH 7.4, 10 mM) for three times and was finally suspended in the same buffer. 10% of this RBC suspensions was then added to the peptide solutions diluted at different concentrations in PBS and were incubated for a period of 2 h at 37 °C under continuous shaking conditions. 10% of the untreated RBC suspensions were maintained as the negative control, while that treated with 1% of Triton X-100 were maintained as the positive control. Post incubation, microcentrifuge tubes were centrifuged and photographed. OD values of the supernatant of the cells treated with peptides of different concentrations, cells treated with 1% of Triton X-100 and that of the untreated cells were read at 540 nm. The percentage hemolysis corresponding to different concentrations of the peptides were determined from the OD values with respect to that of the positive control and negative control.

5.5.9. Time-kill kinetics assay

The bactericidal kinetics of the peptides were determined against Gram-negative *P. aeruginosa* and Gram-positive *S. aureus.* Cells obtained at their mid-log phase were washed and diluted to the order of 10^5 CFU/ml in PB (pH 7.4, 10 mM). These cell suspensions of the order 10^5 CFU/ml were added to the peptides at their respective MICs against the individual bacterial strains and kept incubated for different time intervals. Cells kept treated with the peptides corresponding to each time interval were withdrawn and spread uniformly on the agar plates containing media with help of cell spreaders. Plates corresponding to the untreated cells were also maintained. Agar plates were incubated at 37 °C overnight to allow the formation of visible colonies on the plates. The

colonies were counted and the plates were photographed. Experiments were performed in triplicates. Plot of log (CFU/ml) as a function of time (min) was reported.

5.5.10. Circular Dichroism

CD spectra of the peptides were acquired at a final concentration of 100 µM in water, SDS (30 mM), DPC (10 mM) and in 50% TFE. A 350 µl cuvette of 1 mm path length was used and the spectra were acquired over a range of 190-260 nm, at a scanning rate of 100 nm/min, data pitch of 1nm and bandwidth fixed at 1 nm. JASCO J-1500 CD spectrometer was used for acquiring all the spectra.

5.5.11. Blue shift experiment

Peptides at a final concentration of 10 µM were titrated against increasing concentrations of D8PG and DPC. 10 mM stock solutions of D8PG and DPC were prepared and were added to peptides at different ratios ranging from 0.25 to 20 times the concentration of the peptides. Taking the advantage of intrinsic fluorescence properties of tryptophan present in the peptides, the changes in the λ_{max} ($\Delta\lambda$) values of the peptides were monitored upon each addition of the titrants D8PG or DPC. Peptide solutions were excited using an excitation wavelength of 280 nm and slit width 10 nm. The fluorescence spectra were acquired at a wavelength of 300-500 nm using a Fluoromax Spectrofluorometer (Horiba scientific). The shift in the maxima ($\Delta\lambda$) of the spectra corresponding to the addition of different ratios of D8PG and DPC were determined.

5.5.12. Live cell blue shift

P. aeruginosa and *S. aureus* cells were concentrated to the order of 10^8 CFU/ml suspended in PB (pH 7.4, 10 mM). Peptides at their respective MIC values against each microbe were titrated against an increasing volume of the cells. Spectra were acquired over a wavelength of 300-500 nm using an excitation wavelength of 280 nm. The wavelength shift ($\Delta\lambda$) associated with the increasing volume of the cells were determined.

5.6.13. Solvent accessibility

Peptides at a final concentration of 10 µM in their free state, in the presence of D8PG (20X the concentration of the peptides), in the presence of DPC (20X the concentration of the peptides) were titrated against increasing concentrations of acrylamide (10 mM-250 mM). The fluorescence spectra were acquired over a wavelength of 300-500 nm using an excitation wavelength of 280

nm. The ratio of changes in the fluorescence intensities (F_0/F) were determined and plotted against the increasing acrylamide concentrations fitted using a linear curve to determine the Stern-Volmer constant.

5.5.14. Isothermal Titration Calorimetry

Interaction of the peptide WRL with bacterial membrane mimic SDS was studied using isothermal titration calorimetry. Peptide WRL at a final concentration of 1 mM in PB (pH 7.4, 10 mM) was placed in the cell and was titrated against 2 µL of 50 mM SDS loaded in the syringe each time for 20 consecutive times. The reaction was set at 37 °C and a uniform stirring speed of 350 rpm was maintained throughout. The spacing between the two injections was set at 180 s, each injection duration being of 4 s.

5.5.15. Inner membrane permeation assay

P. aeruginosa cells grown till mid-log phase were washed and diluted to the order of 10^6 CFU/ml. Propidium iodide at a final concentration of 10 µM were added to these cell suspensions and were incubated for 30 min at 37 °C under continuous shaking conditions. Fluorescence spectra of the PI containing cells in its untreated form as well as for the cells treated with 0.5X and 1X MICs of the respective peptides were acquired for over a period of 30 min using an excitation wavelength of 535 nm and emission wavelength of 617 nm having a slit width of 10 nm in both the cases. Spectra for the PI incubated *P. aeruginosa* cells treated with 10 µM Polymyxin B was also acquired as the positive control. All the spectra were acquired using a Fluoromax Spectrofluorometer (Horiba scientific).

5.5.16. Outer membrane permeation assay

Cells of *P. aeruginosa* obtained at their mid-log phase were diluted to the order of 10^6 CFU/ml followed by addition of N-Phenyl 1-napthylamine (NPN) dye to a final concentration of 10 µM and were incubated for 1 h at 37 °C under continuous orbital shaking. Fluorescence spectra of the untreated cells and that of cells treated with 0.5X and 1X MICs of the peptides were acquired for a period of 30 min using an excitation wavelength of 350 nm (slit width: 5 nm) and the emission wavelength of 410 nm (slit width: 5 nm). NPN incubated cells treated with 10 µM Polymyxin B was used as the positive control for the experiment. The spectra were acquired using a Fluoromax Spectrofluorometer (Horiba scientific).

5.5.17. Live cell NMR

P. aeruginosa and *S. aureus* cells at their mid-log phase were washed and were concentrated to the order of 10^8 CFU/ml using phosphate buffer (10 mM) acidified at pH 6.5 and added with 10% D_2O. ^{1}H-NMR spectra of the cells in their untreated form, cells treated with the peptide (final concentration of 1 mM) for different time intervals and that of the peptide alone [in same solvent 10% D_2O-90% PB (pH 6.5) and at the same concentration as added to the cells] were also acquired. All the ^{1}H-NMR spectra were acquired suppressing the peak for water using a Bruker Avance 400 NMR spectrometer.

5.5.18. FESEM images

P. aeruginosa and *S. aureus* grown till mid-log phase were washed and diluted to the order of 10^5 CFU/ml. Cells were then treated with the peptides at their respective 1X and 2X MICs and kept incubated for a period of 2 h. Post incubation, the peptide incubated cells were fixed with 2.5% glutaraldehyde solution for further 1 h. Untreated cells (negative control) were also fixed along with the peptide treated cells. Fixed cells were finally washed, resuspended and casted on silicon wafers, and allowed to dry under a laminar flow. Cells casted on the silicon wafers were further washed using different grades of alcohol (30%, 50%, 70% and 90%) and dried. Wafers were gold coated and images were acquired using a Field Emission Scanning Electron Microscope (Gemini 300).

5.5.19. FETEM images

P. aeruginosa and *S. aureus* cells in their untreated form as well as the cells treated with 1X MICs of the peptides were fixed with glutaraldehyde, followed by washing and resuspension of the cells. Resuspended cells (treated/ untreated) were casted on TEM grids followed by staining with 1% of uranyl acetate solution. FETEM images were captured using a Field Emission Transmission Electron Microscope (JOEL, Model: 2100 F).

5.5.20 Live cell/ dead cell assay using confocal microscope

P. aeruginosa cells obtained at its mid-log phase were washed and finally diluted to the order of 10^6 CFU/ml. PI and acridine orange were added to cell suspensions and allowed to incubate for 1 h under continuous shaking conditions at 37 °C. Confocal images were acquired for the untreated cells as well as for the cells treated with peptides at their respective MICs for 10 min using a Zeiss LSM880 microscope.

5.5.21. Fluorescence Assisted Cell Sorting (FACS)

P. aeruginosa cells were washed and diluted to a final optical density of 0.1 in PB (10 mM, pH 7.4). Cells were added with PI at a final concentration of 10 μM and were kept incubated with 1X and 2X MICs of the peptides for 45 min under shaking conditions. Untreated cells were also added with PI at the same strength and was subjected to incubation for the same period. BD LSRFortessa flow cytometry analyzer was used for the cell sorting. One hundred thousand events were recorded for each sample and the live dead cell percentages were analyzed using the BD FACSDiva software.

5.5.22. Modelling peptides in water

Peptide models (WRL and LWRF, where -N/-C terminal was $-NH^{+}_{3}$/$-CONH_2$) were generated in PyMOL software[45] and placed at the center of a water box (dimension $50 \times 50 \times 50$ Å^3). Four chloride ions were added to ensure charge neutrality, and the resulting solvated peptide was considered for MD simulations.

5.5.23. Membrane mimetic models: micelle or bilayer in water

Two different types of models (SDS-micelle and Bilayer mimicking the outer membrane of *P. aeruginosa*) were considered as membrane mimetic models for computational analysis. Models were generated using CHARMM-GUI Membrane Builder.[46-47]

SDS micelle consisted of 60 SDS molecules, a popular choice for simulation study.[48-52] Keeping the micelle at the center, a box of water ($100 \times 100 \times 100$ Å^3) was overlaid, and a total of 60 Na^+ were added. The resulting model of solvated SDS micelle in water was subjected to MD simulations.

The bilayer model consists of (1) Lipid A of *P. aeruginosa* in the outer layer and (2) phosphatidylethanolamine (PE), phosphatidylglycerol (PG), and cardiolipin (CL) in the inner layer. The bilayer was overlaid with a box of water ($73 \times 73 \times 115$ Å^3, thickness along the longest dimension) and neutralized by adding monovalent counter ions (80 Na^+). The neutralized solvated bilayer box was subjected to equilibration and production MD simulation. The final snapshot from the production dynamics of micelle/bilayer in water was selected to study peptide binding.

5.5.24. Setup for peptide: micelle/bilayer binding

The final structure of the free peptide (WRL or LWRF) in water was selected and placed ~50 Å away from the center of mass of the micelle/bilayer. An extra 15 Å water solvation was included along the bilayer thickness or outer shell of the micelle to ensure adequate solvation. The initial structural model of the peptide placed away from the bilayer was of dimension $67.5 \times 67.5 \times 130$ Å^3. MD simulation was performed to study the peptide: micelle/bilayer binding.

5.5.25. Molecular Dynamics simulations

Molecular dynamics (MD) simulations were performed using GROMACS software.[53] CHARMM36m[54] force field described biomolecular interaction potential energy. CHARMM-modified TIP3P water model[55] described the water molecules. The solvated simulation box was energy minimized (steepest descent algorithm, 50000 steps, step-size = 0.1 Å) followed by 200 ps equilibration (first and second half of equilibration considered NVT and NTP ensemble respectively). Harmonic restraint was applied (to the solute-heavy atoms) during equilibration. A minimum of 200 ns to a maximum of 1000 ns of production dynamics was performed after equilibration. Unretained NTP production dynamics were considered for analysis. The MD parameters and bilayer composition adopted in this work were described previously.[56] Structures at every ten ps from the production MD trajectories were selected and analyzed. Multiple independent MD replicas were performed (Table D1) and the averaged data was reported in the result section.

References

1. Chan, D.I.; Prenner, E.J.; Vogel, H.J. Tryptophan- and arginine-rich antimicrobial peptides: structures and mechanisms of action. *Biochim. Biophys. Acta* **2006**, *1758*, 1184-1202.

2. Clark, S.; Jowitt, T.A.; Harris, L.K.; Knight, C.G.; Dobson, C.B. The lexicon of antimicrobial peptides: a complete set of arginine and tryptophan sequences. *Commun. Biol*. **2021**, *4*, 605.

3. Mishra, A.K.; Choi, J.; Moon, E.; Baek, K.H. Tryptophan-Rich and Proline-Rich Antimicrobial Peptides. *Molecules* **2018**, *23*, 815.

4. Khemaissa, S.; Sagan, S.; Walrant, A. Tryptophan, an Amino-Acid Endowed with Unique Properties and Its Many Roles in Membrane Proteins. *Crystals* **2021**, *11*, 1032.

5. Hristova, K.; Wimley, W.C. A look at arginine in membranes. *J. Membr. Biol*. **2011**, *239*, 49-56.

6. Cutrona, K.J.; Kaufman, B.A.; Figueroa, D.M.; Elmore, D.E. Role of arginine and lysine in the antimicrobial mechanism of histone-derived antimicrobial peptides. *FEBS Lett*. **2015**, *589*, 3915-3920.

7. Yau, W.M.; Wimley, W.C.; Gawrisch, K.; White, S.H. The preference of tryptophan for membrane interfaces. *Biochemistry* **1998**, *37*, 14713-14718.

8. Persson, S.; Killian, J.A.; Lindblom, G. Molecular ordering of interfacially localized tryptophan analogs in ester- and ether-lipid bilayers studied by 2H-NMR. *Biophys. J*. **1998**, *75*, 1365-1371.

9. Killian, J.A.; Salemink, I.; de Planque, M.R.; Lindblom, G.; Koeppe, R.E. 2nd; Greathouse, D.V. Induction of nonbilayer structures in diacylphosphatidylcholine model membranes by transmembrane alpha-helical peptides: importance of hydrophobic mismatch and proposed role of tryptophans. *Biochemistry* **1996**, *35*, 1037-1045.

10. Khemaissa, S.; Walrant, A.; Sagan, S. Tryptophan, more than just an interfacial amino acid in the membrane activity of cationic cell-penetrating and antimicrobial peptides. *Q Rev. Biophys*. **2022**, *55*, e10.

11. Aliste, M.P.; MacCallum, J.L.; Tieleman, D.P. Molecular dynamics simulations of pentapeptides at interfaces: salt bridge and cation-pi interactions. *Biochemistry* **2003**, *42*, 8976-8987.

12. Deslouches, B.; Steckbeck, J.D.; Craigo, J.K.; Doi, Y.; Mietzner, T.A.; Montelaro, R.C. Rational design of engineered cationic antimicrobial peptides consisting exclusively of arginine and tryptophan, and their activity against multidrug-resistant pathogens. *Antimicrob. Agents Chemother.* **2013**, *57*, 2511-2521.

13. Bacalum, M.; Dragulescu, E.C.; Necula, G.; Codita, I.; Radu, M. Short tryptophan- and arginine-rich peptide shows efficacy against clinical methicillin-resistant Staphylococcus aureus strains isolated from skin and soft tissue infections. *Sci. Rep*. **2019**, *9*, 17176.

14. Necula, G.; Bacalum, M.; Radu, M. Interaction of Tryptophan- and Arginine-Rich Antimicrobial Peptide with *E. coli* Outer Membrane-A Molecular Simulation Approach. *Int. J. Mol. Sci.* **2023**, *24*, 2005.

15. Marimuthu, S.K.; Nagarajan, K.; Perumal, S.K.; Palanisamy, S.; Subbiah, L. Structural stability of antimicrobial peptides rich in tryptophan, proline and arginine: a computational study. *J. Biomol. Struct. Dyn*. **2022**, *40*, 3551-3559.

16. Pandit, G.; Ilyas, H.; Ghosh, S.; Bidkar, A.P.; Mohid, S.A.; Bhunia, A.; Satpati, P.; Chatterjee, S. Insights into the Mechanism of Antimicrobial Activity of Seven-Residue Peptides. *J. Med. Chem*. **2018**, *61*, 7614-7629.

17. Pandit, G.; Sarkar, T.; S. R. V.; Debnath, S.; Satpati, P.; Chatterjee, S. Delineating the Mechanism of Action of a Protease Resistant and Salt Tolerant Synthetic Antimicrobial Peptide against *Pseudomonas aeruginosa*. *ACS Omega* **2022**, *7*, 15951-15968.

18. Giangaspero, A.; Sandri, L.; Tossi, A. Amphipathic alpha helical antimicrobial peptides. *Eur. J. Biochem.* **2001**, *268*, 5589-5600.

19. Juretić, D.; Vukičević, D.; Tossi, A. Tools for Designing Amphipathic Helical Antimicrobial Peptides. *Methods Mol. Biol*. **2017**, *1548*, 23-34.

20. Huang, Y.; Huang, J.; Chen, Y. Alpha-helical cationic antimicrobial peptides: relationships of structure and function. *Protein Cell* **2010**, *1*, 143-152.

21. Zelezetsky, I.; Tossi, A. Alpha-helical antimicrobial peptides--using a sequence template to guide structure-activity relationship studies. *Biochim. Biophys. Acta* **2006**, *1758*, 1436-1449.

22. Yang, C.H.; Chen, Y.C.; Peng, S.Y.; Tsai, A.P.; Lee, T.J.; Yen, J.H.; Liou, J.W. An engineered arginine-rich α-helical antimicrobial peptide exhibits broad-spectrum bactericidal activity against pathogenic bacteria and reduces bacterial infections in mice. *Sci. Rep*. **2018**, *8*, 14602.

23. Pandit, G.; Chowdhury, N.; Abdul Mohid, S.; Bidkar, A.P.; Bhunia, A.; Chatterjee, S. Effect of Secondary Structure and Side Chain Length of Hydrophobic Amino Acid Residues on the Antimicrobial Activity and Toxicity of 14-Residue-Long de novo AMPs. *ChemMedChem*. **2021**, *16*, 355-367.

24. Liu, C.B.; Shan, B.; Bai, H.M.; Tang, J.; Yan, L.Z.; Ma, Y.B. Hydrophilic/hydrophobic characters of antimicrobial peptides derived from animals and their effects on multidrug resistant clinical isolates. *Dongwuxue Yanjiu* **2015**, *36*, 41-47.

25. Du, K.; Yang, Z.R.; Qin, H.; Ma, T.; Tang, J.; Xia, J.; Zhou, Z.; Jiang, H.; Zhu, J. Optimized Charge/Hydrophobicity Balance of Antimicrobial Peptides Against Polymicrobial Abdominal Infections. *Macromol. Biosci*. **2024**, *24*, e2300451.

26. Kiyota, T.; Lee, S.; Sugihara, G. Design and synthesis of amphiphilic alpha-helical model peptides with systematically varied hydrophobic-hydrophilic balance and their interaction with lipid- and bio-membranes. *Biochemistry* **1996**, *35*, 13196-13204.

27. Edwards, I.A.; Elliott, A.G.; Kavanagh, A.M.; Zuegg, J.; Blaskovich, M.A.; Cooper, M.A. Contribution of Amphipathicity and Hydrophobicity to the Antimicrobial Activity and Cytotoxicity of β-Hairpin Peptides. *ACS Infect. Dis*. **2016**, *2*, 442-450.

28. Bi, X.; Wang, C.; Dong, W.; Zhu, W.; Shang, D. Antimicrobial properties and interaction of two Trp-substituted cationic antimicrobial peptides with a lipid bilayer. *J. Antibiot (Tokyo)* **2014**, *67*, 361-368.

29. Zhu, X.; Ma, Z.; Wang, J.; Chou, S.; Shan, A. Importance of Tryptophan in Transforming an Amphipathic Peptide into a Pseudomonas aeruginosa-Targeted Antimicrobial Peptide. *PLoS One* **2014**, *9*, e114605.

30. Bi, X.; Wang, C.; Ma, L.; Sun, Y,; Shang, D. Investigation of the role of tryptophan residues in cationic antimicrobial peptides to determine the mechanism of antimicrobial action. *J. Appl. Microbiol.* **2013**, *115*, 663-672.

31. Midura-Nowaczek, K.; Markowska, A. Antimicrobial peptides and their analogs: searching for new potential therapeutics. *Perspect. Medicin. Chem*. **2014**, *6*, 73-80.

32. Ferreira, A.R.; Teixeira, C.; Sousa, C.F.; Bessa, L.J.; Gomes, P.; Gameiro, P. How Insertion of a Single Tryptophan in the N-Terminus of a Cecropin A-Melittin Hybrid Peptide Changes Its Antimicrobial and Biophysical Profile. *Membranes (Basel)* **2021**, *11*, 48.

33. Singh, S.; Datta, A.; Schmidtchen, A.; Bhunia, A.; Malmsten, M. Tryptophan end-tagging for promoted lipopolysaccharide interactions and anti-inflammatory effects. *Sci. Rep*. **2017**, *7*, 212.

34. Kandasamy, S.K.; Larson, R.G. Effect of salt on the interactions of antimicrobial peptides with zwitterionic lipid bilayers. *Biochim. Biophys. Acta* **2006**, *1758*, 1274-1284.

35. Goldman, M.J.; Anderson, G.M.; Stolzenberg, E.D.; Kari, U.P.; Zasloff, M.; Wilson, J.M. Human beta-defensin-1 is a salt-sensitive antibiotic in lung that is inactivated in cystic fibrosis. *Cell* **1997**, *88*, 553-560.

36. Son, M.; Lee, Y.S.; Lee, M.J.; Park, Y.; Bae, H.R.; Lee, S.Y.; Shin, M.G.; Yang, S. Effects of osmolality and solutes on the morphology of red blood cells according to three-dimensional refractive index tomography. *PLoS One* **2021**, *16*, e0262106.

37. Martin, N.C.; Pirie, A.A.; Ford, L.V.; Callaghan, C.L.; McTurk, K.; Lucy, D.; Scrimger, D.G. The use of phosphate buffered saline for the recovery of cells and spermatozoa from swabs. *Sci. Justice* **2006**, *46*, 179-184.

38. Micsonai, A.; Wien, F.; Kernya, L.; Lee, Y.H.; Goto, Y.; Réfrégiers, M.; Kardos, J. Accurate secondary structure prediction and fold recognition for circular dichroism spectroscopy. *Proc. Natl. Acad. Sci. USA.* **2015**, *112*, E3095-E3103.

39. Wang, G. Determination of solution structure and lipid micelle location of an engineered membrane peptide by using one NMR experiment and one sample. *Biochim. Biophys. Acta* **2007**, *1768*, 3271-3281.

40. Warschawski, D.E.; Arnold, A.A.; Beaugrand, M.; Gravel, A.; Chartrand, É.; Marcotte, I. Choosing membrane mimetics for NMR structural studies of transmembrane proteins. *Biochim. Biophys. Acta* **2011**, *1808*, 1957-1974.

41. Boulos, L.; Prévost, M.; Barbeau, B.; Coallier, J.; Desjardins, R. LIVE/DEAD BacLight : application of a new rapid staining method for direct enumeration of viable and total bacteria in drinking water. *J. Microbiol. Methods* **1999**, *37*, 77-86.

42. Mäntsälä. Binding of the Fluorescent probes 1-anilinonaphthalene-8-sulfonate and N-phenyl-1-naphthylamine to bacteria. *Acta Chem. Scand. B* **1975**, *29*, 733-740.

43. Loh, B.; Grant, C.; Hancock, R.E.W. Use of the fluorescent probe 1-N-phenylnaphthylamine to study the interactions of aminoglycoside antibiotics with the outer membrane of Pseudomonas aeruginosa. *Antimicrob. Agents Chemother*. **1984**, *26*, 546-551.

44. Dallas, S.D.; Harrington, A. *Clinical Microbiology Procedures Handbook, 5th Edition*, ASM Press, Washington, DC. **2023**.

45. Schrödinger, L.L.C. The PyMOL Molecular Graphics System, Version 2.0.

46. Jo, S.; Kim, T.; Iyer, V.G.; Im, W. CHARMM-GUI: a web-based graphical user interface for CHARMM. *J. Comput. Chem*. **2008**, *29*, 1859-1865.

47. Wu, E.L.; Cheng, X.; Jo, S.; Rui, H.; Song, K.C.; Dávila-Contreras, E.M.; Qi, Y.; Lee, J.; Monje-Galvan, V.; Venable, R.M.; Klauda, J.B.; Im, W. CHARMM-GUI Membrane Builder toward realistic biological membrane simulations. *J. Comput. Chem*. **2014**, *35*, 1997-2004.

48. MacKerell, A. D., Jr. Molecular dynamics simulation analysis of a sodium dodecyl sulfate micelle in aqueous solution: Decreased fluidity of the micelle hydrocarbon interior. *J. Phys. Chem.* **1995**, *99*, 1846-1855.

49. Rakitin, A. R.; Pack, G. R. Molecular Dynamics Simulations of Ionic Interactions with Dodecyl Sulfate Micelles. *J. Phys. Chem. B.* **2004**, *108*, 2712-2716.

50. Wang, Q.; Hong, G.; Johnson, G.R.; Pachter, R.; Cheung, M.S. Biophysical properties of membrane-active peptides based on micelle modeling: a case study of cell-penetrating and antimicrobial peptides. *J. Phys. Chem. B*. **2010**, *114*, 13726-13735.

51. Lebecque, S.; Crowet, J.M.; Nasir, M.N.; Deleu, M.; Lins, L. Molecular dynamics study of micelles properties according to their size. *J. Mol. Graph. Model*. **2017**, *72*, 6-15.

52. Ghosh, S.; Chatterjee, S.; Satpati, P. Effect of Leu/Val Mutation on the Energetics of Antimicrobial Peptide:Micelle Binding. *J. Phys. Chem. B*. **2022**, *126*, 5262-5273.

53. Spoel, D.V.D.; Lindahl, E.; Hess, B.; Groenhof, G.; Mark, A.E.; Berendsen, H.J. GROMACS: fast, flexible, and free. *J. Comput. Chem*. **2005**, *26*, 1701-1718.

54. Huang, J.; Rauscher, S.; Nawrocki, G.; Ran, T.; Feig, M.; de Groot, B.L.; Grubmüller, H.; MacKerell, A.D. Jr. CHARMM36m: an improved force field for folded and intrinsically disordered proteins. *Nat. Methods* **2017**, *14*, 71-73.

55. Jorgensen, W.L.; Chandrasekhar, J.; Madura, J.D.; Impey, R.W.; Klein, W.L. Comparison of simple potential functions for simulating liquid water. *J. Chem. Phys.* **1983**, *79*, 926-935.

56. Sarkar, T.; Vignesh, S.R.; Sehgal, T.; Ronima, K.R.; Thummer, R.P.; Satpati, P.; Chatterjee, S. Development of protease resistant and non-cytotoxic Jelleine analogs with enhanced broad spectrum antimicrobial efficacy. *Biochim. Biophys. Acta Biomembr*. **2024**, *1866*, 184336.

Chapter 6: *De novo* Design of Alpha Helical AMPs and their Mechanistic Studies

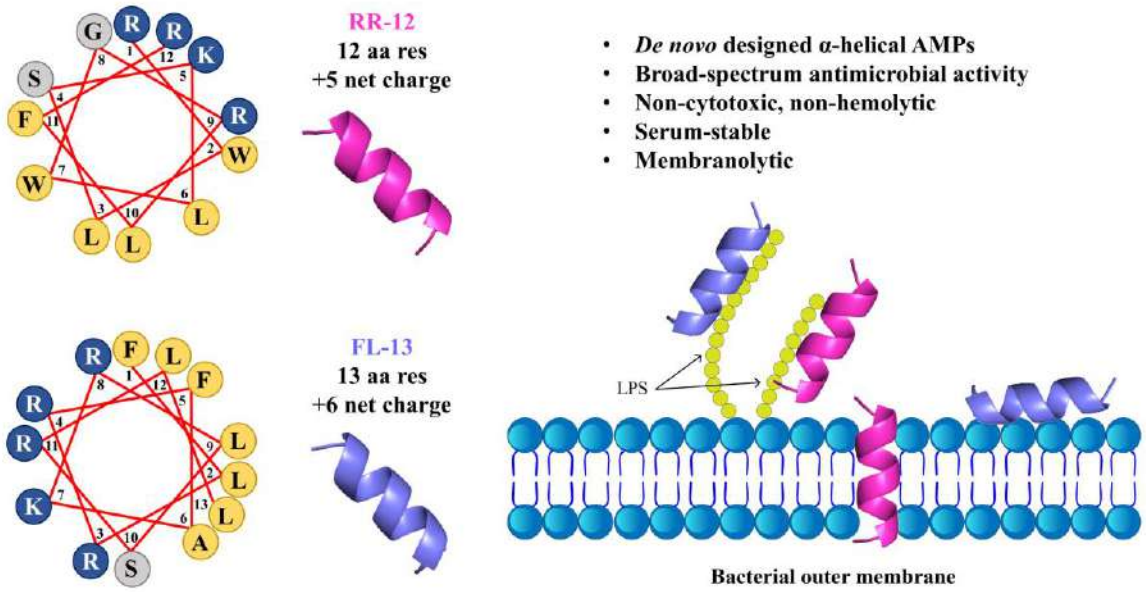

6.1. Introduction

Secondary structures of the AMPs are found to play an important role in their activity.[1-3] Amphipathic α-helical peptides represent one such class of peptides. These peptides adopt helical conformation in contact with the microbial surfaces as their positive charges (originating from the basic amino acids like lysine or arginine in the sequences) tend to interact with the negatively charged microbial surfaces.[4-8] Antimicrobial peptides with alpha helical structures are commonly expressed in all domains of life forms starting from insects, invertebrates, amphibians to mammals.[9]

In this work, taking inspiration from the nature, we have *de novo* designed[10-11] two amphipathic short cationic peptides RR-12 and FL-13, based on the helical wheel projections. Both the peptides displayed broad spectrum antimicrobial activity screened against a number ESKAPE pathogens, including MRSA, as well as fungus *Candida albicans* with low $MIC_{90\%}$ values (2-7.5 μM). The antimicrobial potency of the peptides was considerably retained in the presence of physiological salt concentrations and human serum. Designed AMPs were non-cytotoxic and non-hemolytic within the range of their bactericidal concentrations, capable of displaying very fast bactericidal/fungicidal activities and membranolytic in their mode of action. The mechanism of action of the AMPs were established using rigorous biophysical, spectroscopic and microscopic experimental techniques in addition to *in silico* studies using MD simulations.

6.2. Results

6.2.1. De novo design of peptides

One of the critical parameters for a helical peptide to display antimicrobial activity is its amphipathicity. In a typical antimicrobial peptide with an α-helical secondary structure, the hydrophilic region constituted by the cationic residues are positioned at one of the sides of the helix, while the hydrophobic regions that are composed of non-polar amino acids are placed at the other side of the helix.[12] Based on these attributes, we designed two peptides RR-12 and FL-13 using helical wheel projections, assuming them to adopt helical conformations in the presence of the microbial membranes or in the presence of microbial membrane mimics. In both the peptides, cationic amino acid residues arginine and lysine, and polar uncharged residue serine formed the hydrophilic face, while the hydrophobic residues like leucine, alanine, phenylalanine or tryptophan

formed the opposite hydrophobic face of the helix. RR-12 [Figure 6.1(A)] with a sequence RWLSKLWGRLFR-NH_2, contained a total of 12 aa residues, bearing net charge of +5. FL-13 [Figure 6.1(B)] was constructed with a total of 13 aa residues with a sequence FLRRFAKRLSRLL-NH_2, bearing net charge of +6. Both the peptides were amidated at the C-terminus, RR-12 contained a total of three aromatic residues, two being tryptophan and the other being phenylalanine, while FL-13 had a total of two aromatic residues in its sequence both being phenylalanine. Peptides were synthesized using solid phase peptide synthesis strategies, purified using reverse phase HPLC and were characterized using MALDI MS (Figure E1-E2, Appendix E) and NMR spectroscopy (Figure E3-E4, Appendix E). The purity of the peptides (> 95% in each case) was assessed through reverse phase analytic HPLC traces (Figure E5-E6, Appendix E).

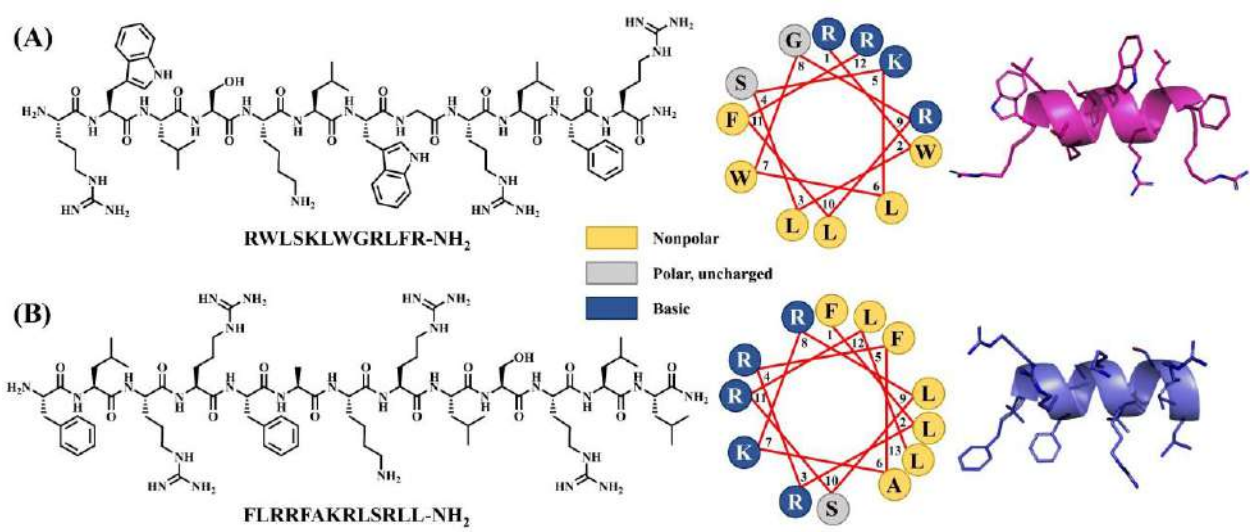

Figure 6.1. Chemical structures of the peptides (A) RR-12 and (B) FL-13, their respective helical wheel projections and estimated 3D helical structures created using PyMol molecular modelling software.

6.2.2. Screening of antimicrobial activity

The antimicrobial activity of the peptides was evaluated through determination of their $MIC_{90\%}$ values. Peptides were screened for their antimicrobial activity against several pathogens majority of them belonging to the ESKAPE group, namely Gram-negative pathogens: *Escherichia coli*, *Klebsiella pneumoniae*, *Acinetobacter baumannii* and *Pseudomonas aeruginosa*, and Gram-positive pathogens: *Staphylococcus aureus* and Methicillin-resistant *Staphylococcus aureus*. Antifungal efficacy of the peptides was tested against fungus *Candida albicans*. Both the peptides

displayed very good antimicrobial activity with low $MIC_{90\%}$ values (≤ 7.5 μM) against all the strains. RR-12 displayed $MIC_{90\%}$ values at concentrations as low as 3 μM against *E. coli*, *P. aeruginosa* and *C. albicans*, while for FL-13 $MIC_{90\%}$ values were as low as 2 μM against *S. aureus* and *C. albicans*. $MIC_{90\%}$ values for RR-12 were relatively higher at concentrations of 7.5 μM against *K. pneumoniae and* methicillin-resistant *S. aureus*. For FL-13, $MIC_{90\%}$ values did not exceed over 5 μM tested against any of the microbes. Hence, overall FL-13 displayed antimicrobial activity superior to that of RR-12. Better antimicrobial activity of FL-13 compared to that of RR-12 could be traced to its higher net positive charge compared to that of the later. The $MIC_{90\%}$ values of the peptides (Figure E7-E8, Appendix E) are provided in Table 6.1.

Biological systems are characterized with the presence of physiological concentrations of different salts and the salt-sensitivity of antimicrobial peptides is quite well known.[13-15] Hence, to study the effect of salts on the activity of our designed peptides, we screened these peptides further against all the stains in phosphate buffer saline (pH- 7.4, 10 mM) (E9-E10, Appendix E & Table 6.1), a solution with effective salt concentrations similar to that of the physiological systems.[16-17] Effect of PBS on the $MIC_{90\%}$ values were almost negligible for *P. aeruginosa*, *S. aureus* and MRSA, marginal against *E. coli* and *A. baumannii*, and somewhat significant against *K. pneumoniae* and *C. albicans*.

Table 6.1. $MIC_{90\%}$ values of the RR-12 and FL-13 in the absence (PB) and in the presence of salts (PBS) against different bacteria (Gram-negative and Gram-positive) and fungus *Candida albicans*.

	E. coli	***K. pneumoniae***	***A. baumannii***	***P. aeruginosa***	***S. aureus***	***MRSA***	***C. albicans***
RR-12	3	7.5	5	3	5	7.5	3
RR-12 (PBS)	7.5	20	7.5	4	7.5	7.5	15
FL-13	3	5	3	3	2	5	2
FL-13 (PBS)	7.5	50	7.5	4	2	5	15

6.2.3. Safety assessment of the peptides against the mammalian host cells

Cytotoxicity evaluation of the peptides

For an antimicrobial agent to be an effective therapeutic, it should be non-cytotoxic towards the hosts' cells at its bactericidal concentrations. We studied the effect of the peptides on mammalian cell lines human derma fibroblasts (HDF) and HeLa for their safety evaluation. Both the peptides remained completely non-cytotoxic towards HDF, a normal cell line, upto a concentration of 40 μM, a concentration 5-20 times greater than the $MIC_{90\%}$ values of the peptides [Figure 6.2(A)]. The peptides displayed higher cytotoxicity towards HeLa cells, which were cancerous in nature. The peptides remained non-cytotoxic towards the HeLa cells till a concentration of 20 μM, still higher above the average MICs of the peptides [Figure 6.2(B)]. Overexpression of negatively charged phospholipids like phosphatidylserine in the cancer cell membranes[18-19] make them more susceptible to the positively charged AMPs compared to that of the normal cells[20] and this explains the lesser viability of the HeLa cells compared to that of the healthy HDF cells. Since, both the cells were viable within the bactericidal concentrations of the peptides, they can be considered safe for therapeutic administrations.

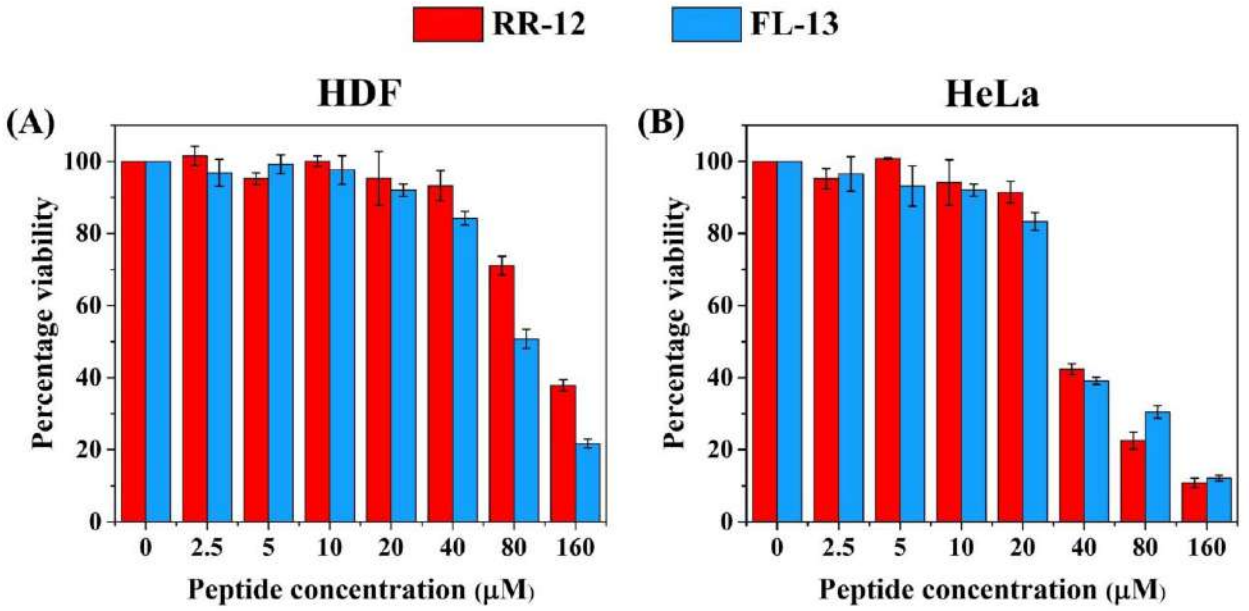

Figure 6.2. Cytotoxicity assay. Bar diagrams representing the percentage viability of (A) HDF cell lines and (B) HeLa cell lines treated with increasing concentrations of the peptides.

Hemolytic activity of the peptides

The viability of red blood cells too was tested against different concentrations of the peptides [Figure 6.3(A), (B) & (C)]. The peptides induced no hemolysis at lower concentrations close to

the MIC values of the peptides. Significant hemolysis was evident only at concentrations of 100 μM or above, further validating the safety of the peptides.

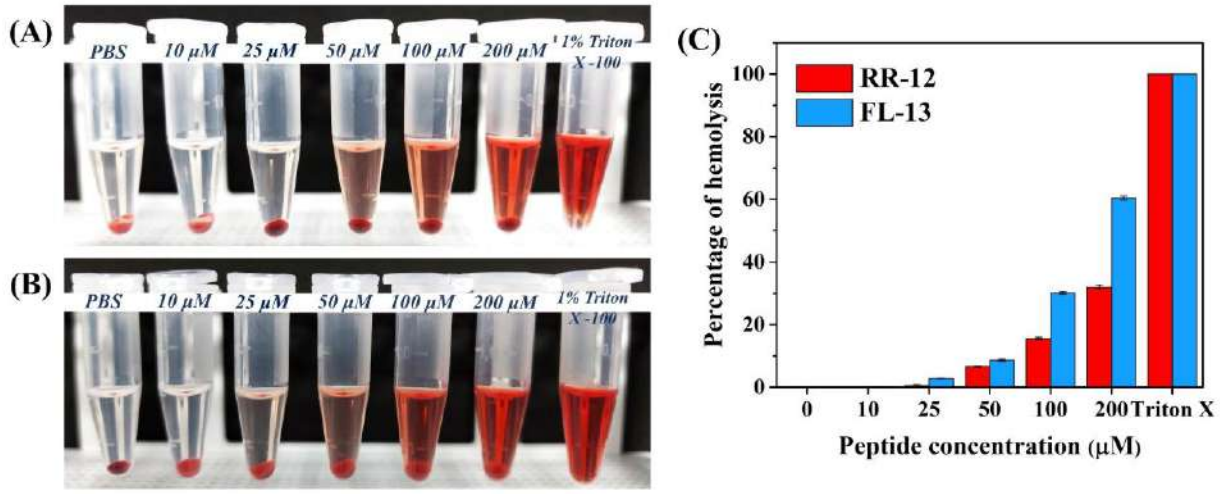

Figure 6.3. Hemolytic activity. Photographs of the microcentrifuge tubes depicting the extent of hemolysis induced by (A) RR-12 and (B) FL-13 at different concentrations incubated for an hour. (C) Percentage of hemolysis induced by the peptides at different concentrations.

Selectivity Index (SI)

The selectivity of the peptides was assessed through their selectivity index (SI) calculations. Selectivity index is a parameter that measures how effective an antimicrobial agent is, against the microbial cells without being toxic to the hosts' cells. Mathematically, selectivity index (SI) = (IC_{50} or HC_{50}) /MIC_{90}, where IC_{50} is defined as the minimum concentration of a compound displaying 50% cytotoxicity against mammalian cells and HC_{50} being the minimum concentration of the compound that causes 50% hemolysis to the red blood cells. MIC_{90} is the minimum inhibitory concentration of that particular compound against a particular microbe or the geometric mean value of the MICs of the compound against a number of microbes.

Higher the selectivity index, more partial is a peptide in asserting its antimicrobial activity while remaining non-toxic to the hosts' cells. Alternatively, higher the SI value, wider is the therapeutic window.

The selectivity indexes of the peptides RR-12 and FL-13 for HDF and HeLa cell lines, as well as human red blood cells were obtained by comparing their IC_{50}/HC_{50} values to that of their mean of the $MIC_{90\%}$ values against all the microbes (Table 6.2). The peptides displayed significantly high

selectivity values against the normal cell line HDF as well the RBCs signifying their high therapeutic potentials. The selectivity indexes of the peptides were comparatively lower against the cancer cell line HeLa.

Table 6.2. Selectivity index of the peptides RR-12 and FL-13 for HDF, Hela and RBC cell lines.

Peptide	IC_{50} (HDF) μM	IC_{50} (HeLa) μM	HC_{50} (RBC) μM	Mean $MIC_{90\%}$ μM	Selectivity Index (SI)		
					HDF	HeLa	RBC
RR-12	160	40	200	4.51	35.47	8.87	44.35
FL-13	160	40	>200	3.09	51.77	12.94	>44.35

6.2.4. Time-kill kinetics

The bactericidal/fungicidal kinetics of the peptides were determined against both bacteria as well as fungus. *P. aeruginosa* cells and *C. albicans* cells, both at strengths ~10^5 cfu/ml, were treated with the peptides RR-12 and FL-13 at their respective MIC concentrations and kept incubated for different time intervals. Both RR-12 and FL-13 displayed very fast microbial neutralization, at their respective MICs, eliminating *P. aeruginosa* cells (~10^5 cfu/ml) completely within 5 min of their incubation time [Figure 6.4(A)]. RR-12 and FL-13 also neutralized *C. albicans* colonies within 5 min and 7.5 min of the incubation time respectively [Figure 6.4(B)].

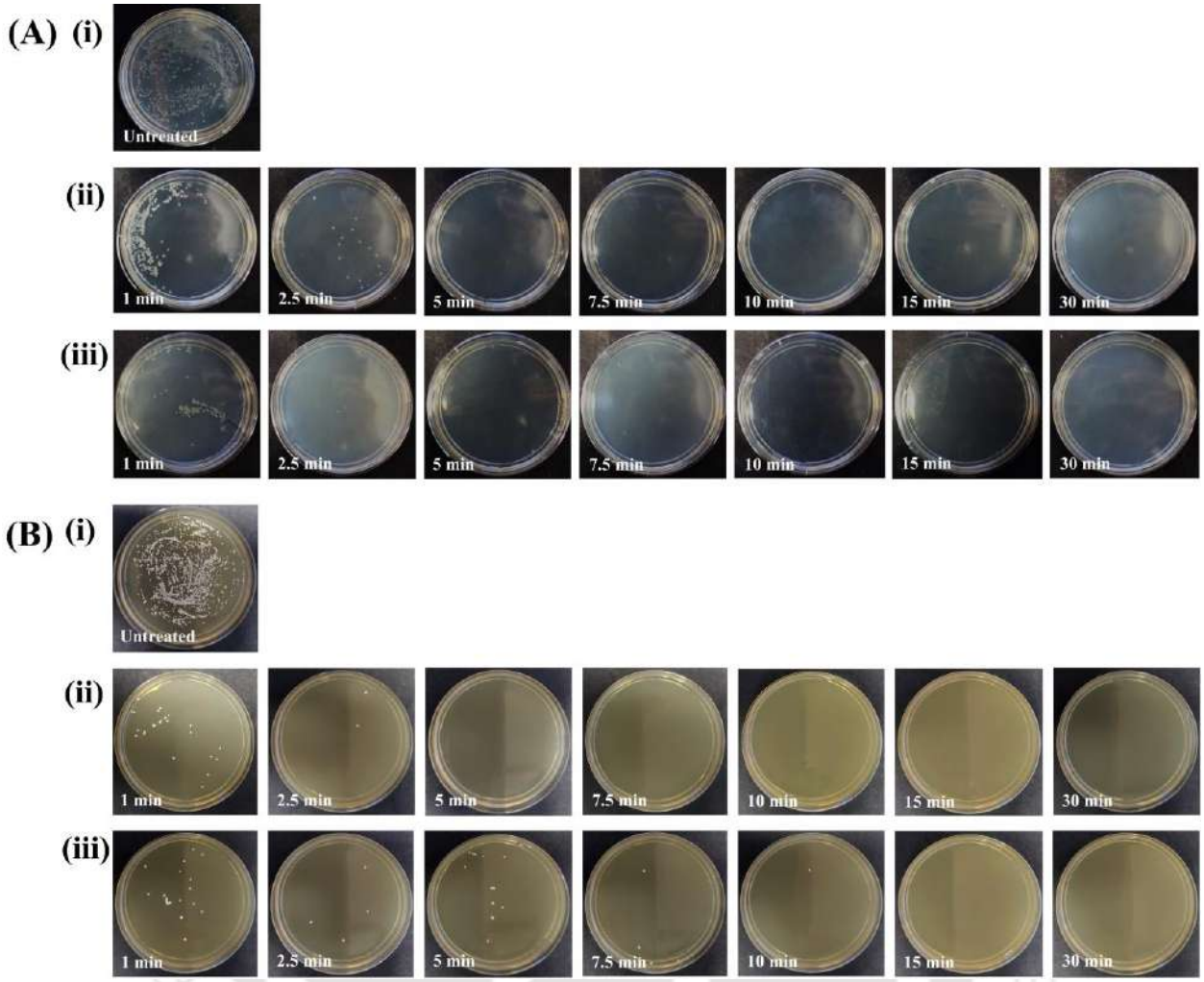

Figure 6.4. Time-kill kinetics assay. Plates showing the growth of colonies of (A) *P. aeruginosa* cells and (B) *C. albicans* cells respectively in their (i) untreated form and upon being incubated with respective MIC concentrations of the peptide (ii) RR-12 and (iii) FL-13 for different time intervals. Each of the plate is a representative of a set of the triplicates maintained corresponding to each incubation time.

6.2.5. Serum stability of the peptides and their antimicrobial efficacy in the presence of serum

We evaluated the stability of the peptides in human serum. Human serum is a source of a number of proteolytic enzymes[21-22] capable of targeting proteins or peptides and cleaving them into smaller fragments.[23-24] Serum proteins also bind to AMPs non-specifically rendering them ineffective.[25-26] Hence, efficacy of peptide molecules intended as therapeutics may get affected in the presence of serum. Both the peptides RR-12 and FL-13 were incubated with human serum for different time

intervals ranging between 30 min to 24 h. The stability of the peptides incubated with serum corresponding to each time intervals were assessed through analytic HPLC traces [Figure 6.5(A), (B)]. It is evident from the HPLC traces that the peptides remained almost unfragmented in the initial periods of incubations, cleaved marginally on being incubated for 6-12 h and underwent proteolytic fragmentation to some considerable extent only on being incubated with serum for 24 h (Figure 6.5). This observation was consistent with the MALDI spectra (Figure E11-E14, Appendix E) of RR-12 and FL-13 kept incubated with serum for 1 h and 24 h. Peaks corresponding to different fragments of RR-12 and FL-13 appeared in the MALDI spectra of (RR-12+serum)/ (FL-13+serum) incubated for 24 h (Figure E12 & E14, Appendix E). However, no peaks corresponding to any probable fragments appeared in the MALDI spectra of (RR-12+serum)/ (FL-13+serum) incubated for 1 h (Figure E11 & E13, Appendix E). The extent of cleavage for RR-12 was found to be higher than that of FL-13 [Figure 6.5(C)].

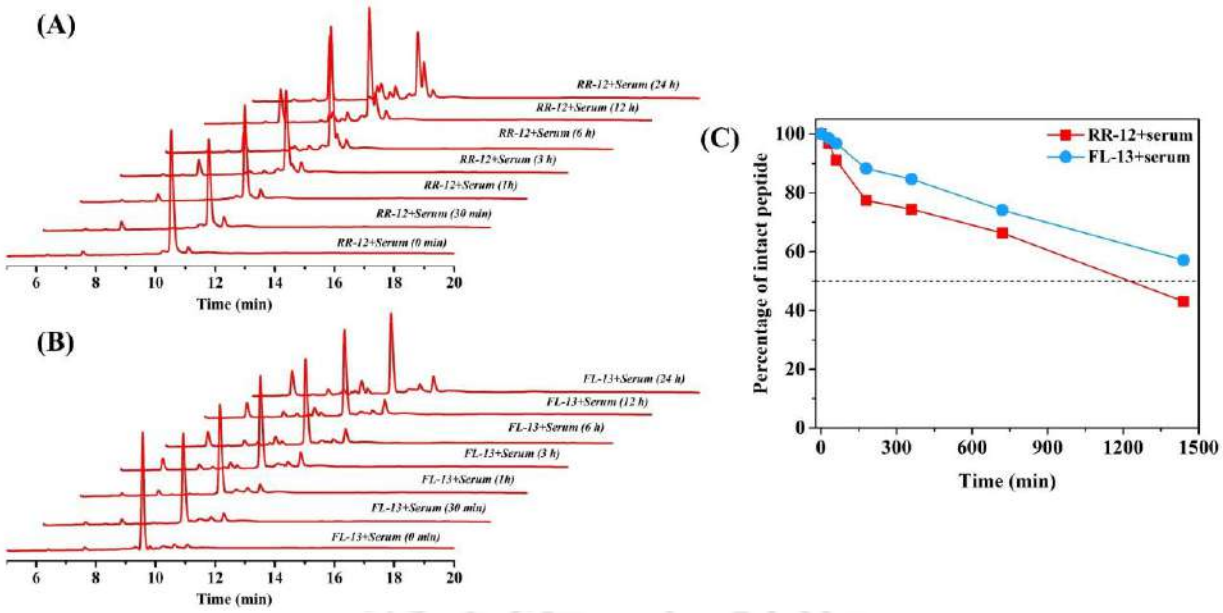

Figure 6.5. Analytical HPLC traces of the peptides (A) RR-12 and (B) FL-13 treated with human serum for different time intervals. (C) Percentage of the peptides that remained intact upon incubation with serum for different time intervals.

Effect of serum in the antimicrobial activity of the peptides were determined next. *P. aeruginosa*, against which the peptides had lowest MIC values, and that against which the peptides displayed best salt-resistance of antimicrobial potency was chosen for this purpose. Peptide RR-12 lost its activity considerably in the presence of 25% serum against *P. aeruginosa* with a drop in $MIC_{90\%}$

from 3 μM to 20 μM (Figure 6.6). $MIC_{90\%}$ of peptide FL-13 was affected to a smaller extent from 3 μM in the absence of the serum to 5 μM in the presence of 25% serum (Figure 6.6). Thus, even though the potencies were compromised partially, both the AMPs retained considerable activity, with FL-13 being the better of the two.

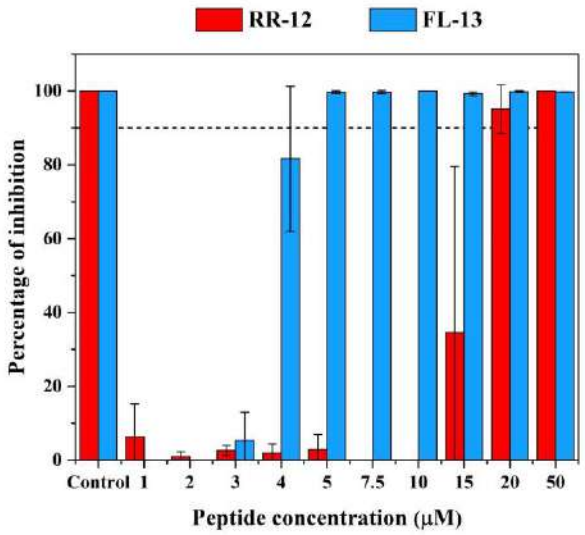

Figure 6.6. Bar diagrams representing the percentage of growth inhibition induced by the peptides RR-12 and FL-13 against *P. aeruginosa* in the presence of 25% serum. $MIC_{90\%}$ was determined to be the lowest concentration at which the peptides inhibited growth of 90% or more of the microbes.

6.2.6. Secondary structures of the peptides

As our design principle was based on helical wheel projections, hypothesizing that the peptides would adopt α-helices in the presence of negatively charged microbial surfaces, we resorted to CD spectroscopy to investigate the secondary structures adopted by RR-12 and FL-13. The CD spectra of the peptides were determined in water, microbial membrane mimicking SDS micelles (30 mM), mammalian membrane mimicking DPC (10 mM) and helix promoting solvent TFE (50%) (Figure 6.7 & Table E1, Appendix E). Analysis of the CD spectra of the peptides revealed that the peptides were completely unstructured in water but adopted α-helices almost exclusively in SDS. Peptide RR-12 assumed considerable percentages of α-helices in 50% TFE, while FL-13, almost exclusively formed α-helices in it. Both the peptides also adopted some extent of helices in the presence of DPC micelles, although in percentages negligible compared to that formed in SDS micelles. Hence, CD establishes formation of α-helical structures in the presence of microbial membranes mimic SDS linking structure-activity relationship of the peptides.

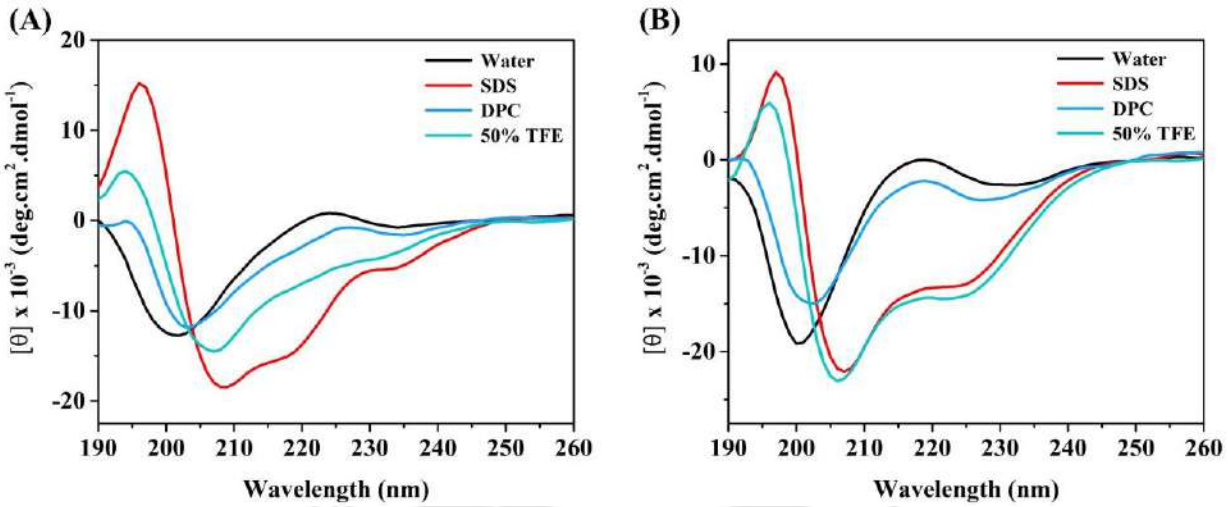

Figure 6.7. CD spectra of the peptides (A) RR-12 (100 μM) and (B) FL-13 (100 μM) in the free state in water, as well as in the presence of bacterial membrane mimic (30 Mm SDS), mammalian membrane mimic DPC (10 mM DPC) and helix promoting solvent TFE (50% in water).

The peptides also assumed considerable percentages of α-helices in the presence of lipopolysaccharides of *P. aeruginosa*. The helical percentages of the peptides were determined against different ratios of LPS (Peptide: LPS = 0.5, 1 and 2). Helicity of the peptides increased with increase in the ratio of LPS from 0.5 to 1, but remained the same on further increasing the ratio upto 2 (Figure 6.8 & Table E2, Appendix E).

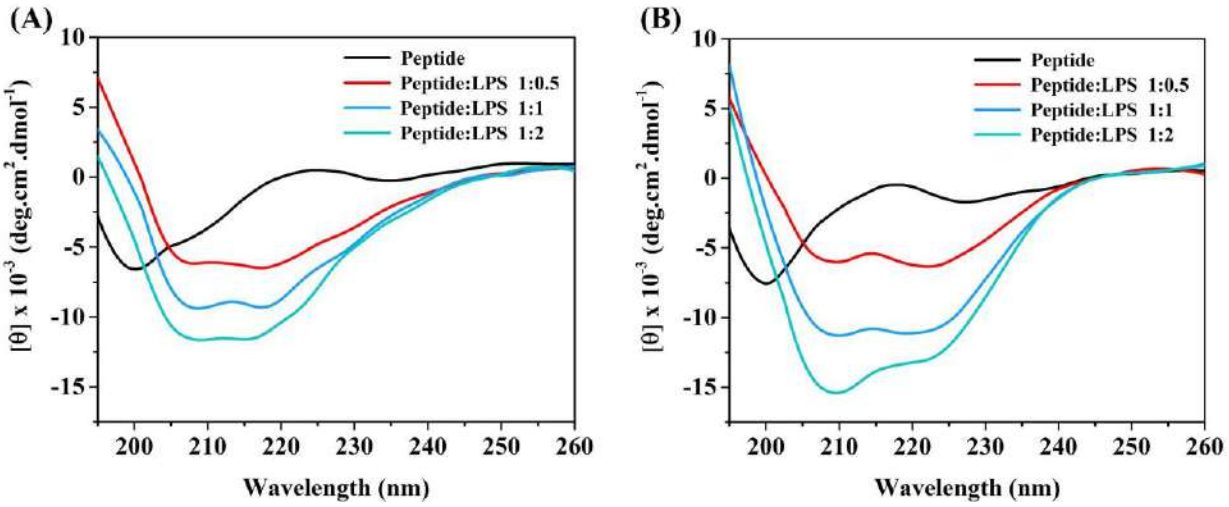

Figure 6.8. CD spectra of the peptides (A) RR-12 (50 μM) and (B) FL-13 (50 μM) in their free states as well as in different ratios of Lipopolysaccharides.

6.2.7. Peptide-membrane interactions

Using the intrinsic fluorescence of tryptophan residues present in the peptide RR-12, the interaction of the peptide with different membrane mimics D8PG, SDS and DPC were studied. RR-12 titrated against an increasing concentration of bacterial membrane mimics D8PG [Figure 6.9(A)] and SDS [Figure 6.9(B)] upto a ratio ten times that of the peptide, showed a significant blue shift in the λ_{max} value [Figure 6.9(D)] of the peptide, amounting to 12 nm and 17 nm respectively indicating peptide-bacterial membrane interactions. No such shifts were evident on titrating the peptide against an increasing concentration of mammalian membrane mimic DPC [Figure 6.9 (C) & (D)], explaining the non-cytotoxic nature of the peptides.

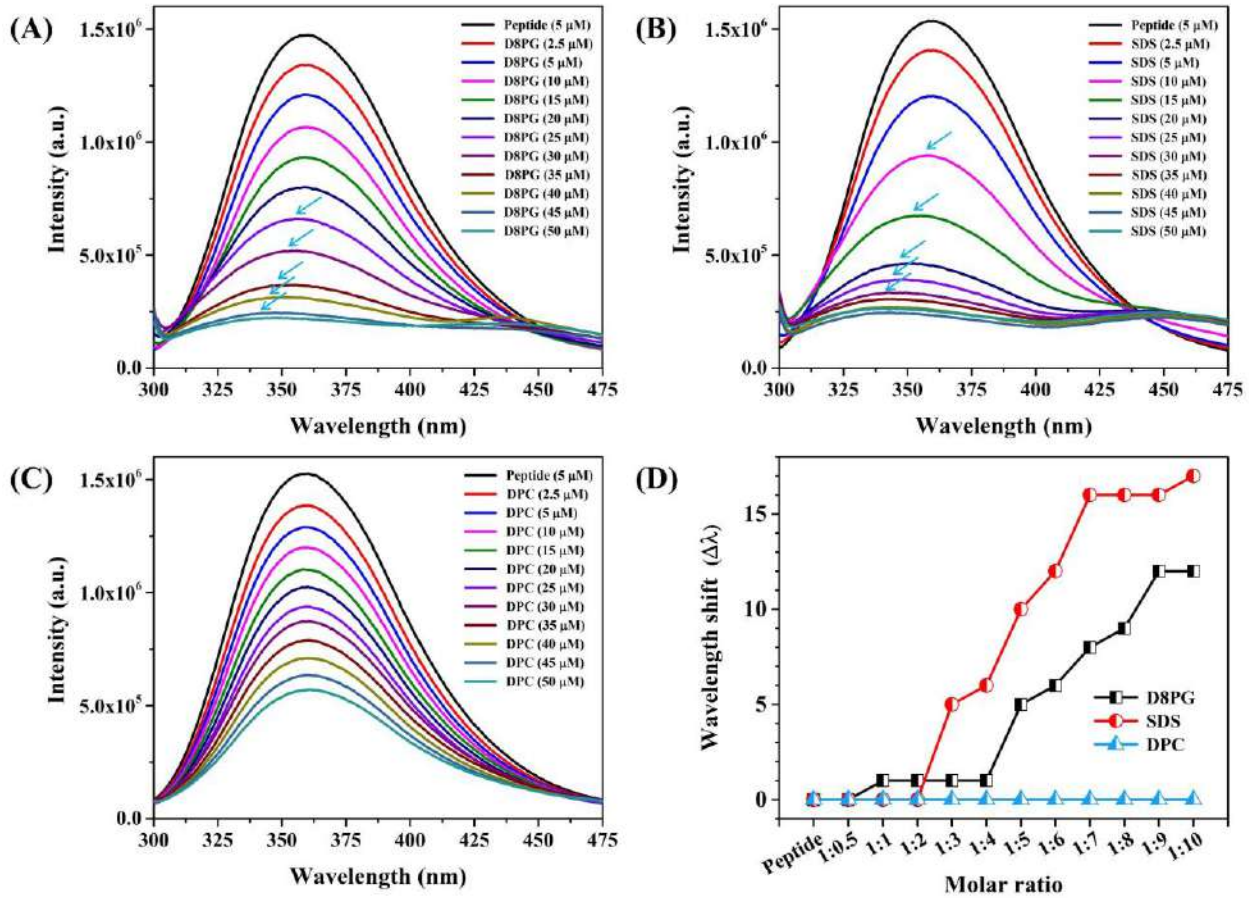

Figure 6.9. Fluorescence spectra of the peptide RR-12 (5 μM) titrated against increasing concentration of (A) D8PG (bacterial membrane mimic) (B) SDS (bacterial membrane mimic) and (C) DPC (mammalian membrane mimic) at ratios 1 to 10 times the concentration of the peptide (5 μM). (D) Blue shift ($\Delta\lambda_{max}$) values observed corresponding to addition of different ratios of the titrants to the peptide.

Interactions of the peptides RR-12 and FL-13 with bacterial membrane mimic SDS as indicated by CD and fluorescence experiments were further confirmed by ITC experiments. ITC isotherms indicated strong interactions between the peptides and bacterial membrane mimicking SDS [Figure 6.10(A), (B)]. K_D value of 147.28 μM corresponding to interactions of RR-12 with SDS, against that of FL-13's 60.97 μM (Table 6.3) clearly indicated better membrane binding abilities of the later. Enhanced membrane binding of FL-13 could be attributed to the presence of higher positive charge in it and was in the line with its overall better antimicrobial efficacy (lower MIC values) over RR-12.

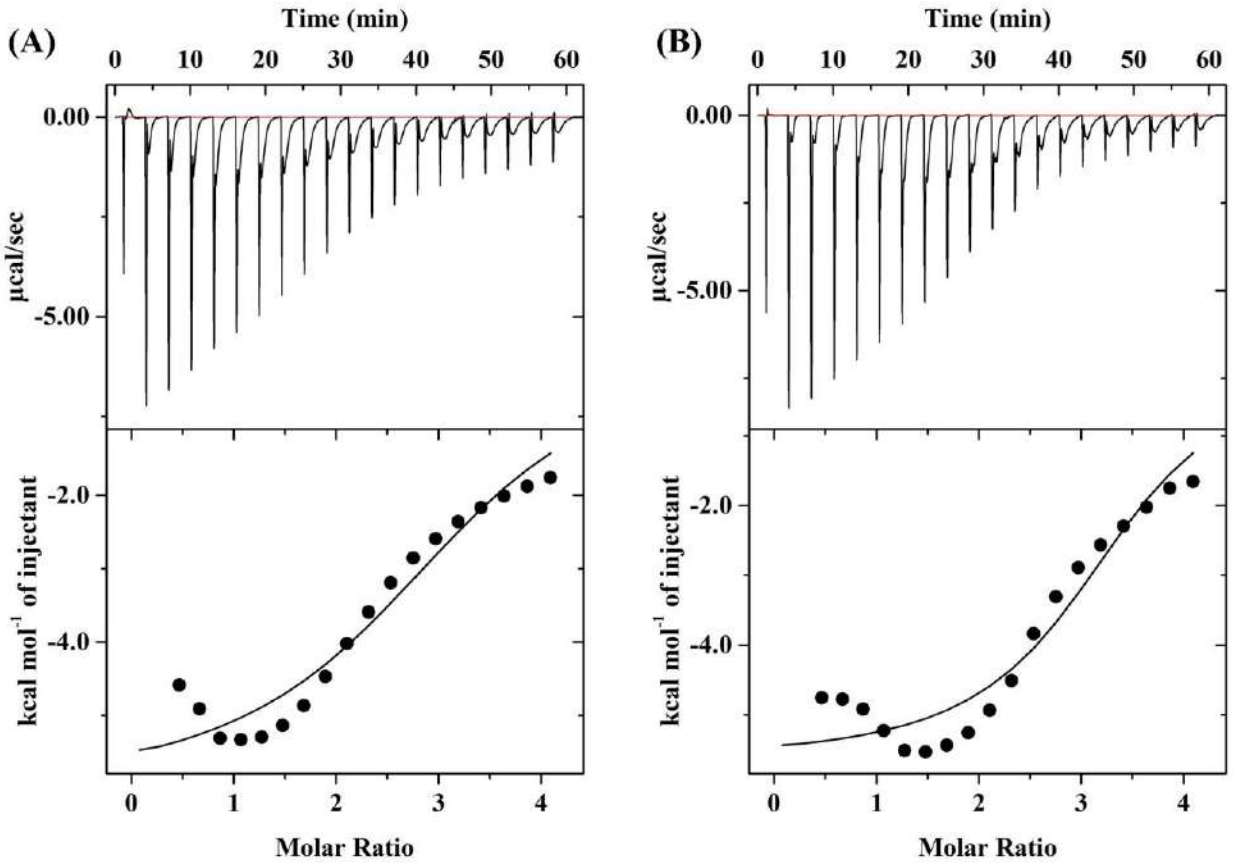

Figure 6.10. Isothermal titration calorimetry (ITC) isotherms of (A) RR-12 and (B) FL-13 titrated against SDS.

Table 6.3. Thermodynamic parameters involving peptide-SDS interactions determined using ITC.

Thermodynamic parameters	**RR-12**	**FL-13**
Model	One binding site	One binding site
Temperature	310 K (37 °C)	310 K (37 °C)
K_A (M^{-1})	$6.79X10^3$	$1.64X10^4$
N	3.16	3.26
ΔH ($cal.mol^{-1}$)	-5997.0	-5645.0
ΔS ($cal.mol^{-1}.deg^{-1}$)	-1.80	1.08
TΔS ($cal.mol^{-1}$)	-558.0	334.8
ΔG ($cal.mol^{-1}$)	-5439.0	-5979.8
K_D (μM)	147.28	60.98

6.2.8. Fluorescence assays using dyes to understand the mode of action of the peptides

To investigate mode of action of the peptides several assays were performed. Bacterial *P. aeruginosa* cells and fungal *C. albicans* cells were chosen for the purpose.

Inner-membrane permeation assay

Propidium iodide[27] was incubated with *P. aeruginosa* and *C. albicans* cells, and added with the peptides RR-12 and FL-13. This resulted in enhancement in the fluorescence signals of the dye [Figure 6.11(A)-(D)]. PI fluorescence is known to increase on binding DNA. As PI was impermeable to the healthy cells, steady fluorescence signals were observed for the untreated cells incubated with PI. However, increase in the fluorescence intensity upon addition of the peptides, suggested the compromise of the inner membranes induced by the peptides, allowing PI molecules to migrate inside of the cells and bind the DNA molecules. The enhancements were more rapid on increasing the peptide concentrations.

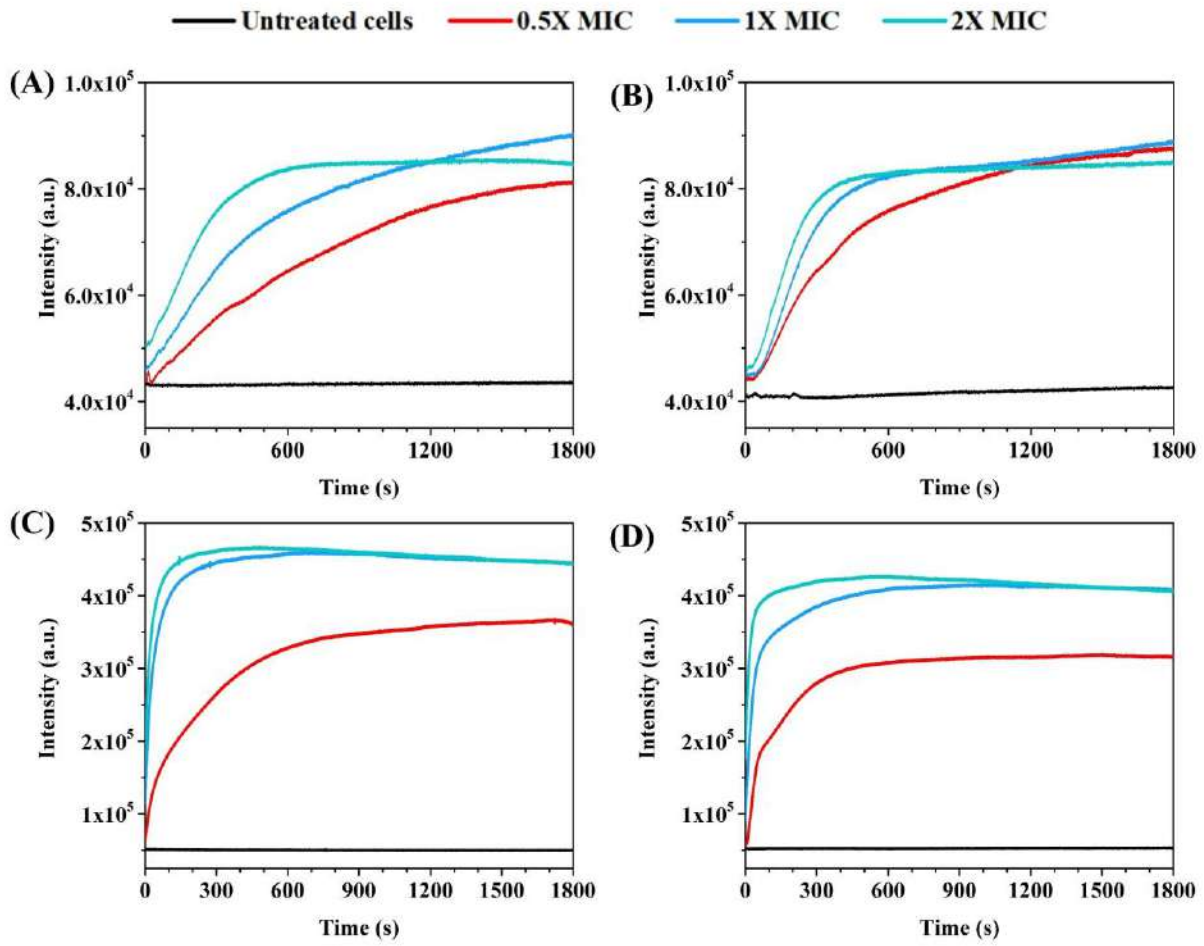

Figure 6.11. Inner membrane permeation assay or propidium iodide assay. *P. aeruginosa* cells preincubated treated with PI and treated with the peptides (A) RR-12 and (B) FL-13 at their respective 0.5X, 1X and 2X MIC concentrations. (C) RR-12 and (D) FL-13 at their 0.5X, 1X and 2X concentrations added to suspensions of *C. albicans* preincubated with PI.

Outer-membrane permeation assay

Next, NPN incubated *P. aeruginosa* and *C. albicans cells* were treated with the peptides to probe their outer membrane permeation capabilities. NPN is associated with fluorescence enhancements on exposure to hydrophobic surfaces like lipid tails of the phospholipids that constitute the bacterial membranes.[28-29] Enhancements in the fluorescence intensity of NPN was noticed upon addition of peptides to the cells of *P. aeruginosa* [Figure 6.12(A), (B)] but no appreciable enhancements were observed against *C. albicans* [Figure E15(A), (B), Appendix E]. Presence of an outer membrane constituted by lipids[30] that get exposed on membrane rupture upon addition of

the peptides, explains for the NPN fluorescence enhancements in *P. aeruginosa*. Fungus cell envelopes are devoid of such outer membrane with hydrophobic lipids. Instead, they are composed of thick layers of mannoproteins, peptidoglycans and chitins,[31] and hence even upon outer membrane disruption by AMPs in this case, NPN may not find hydrophobic surfaces to bind to that might increase its fluorescence. This explained for the lack of NPN fluorescence enhancements in *C. albicans*, upon addition of the peptides.

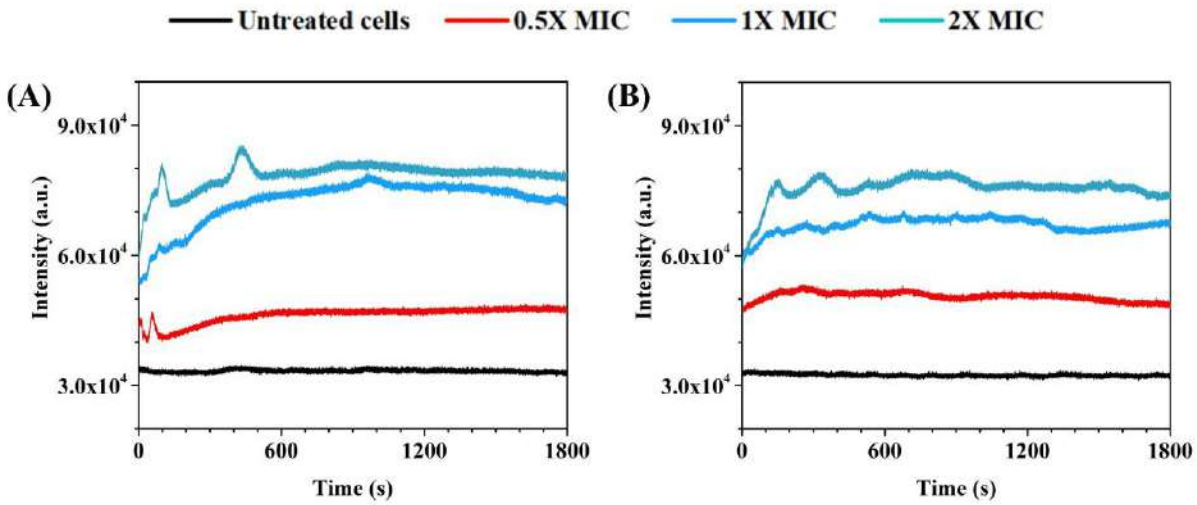

Figure 6.12. Outer membrane permeation assay or NPN assay. Fluorescence enhancements in the signals of the dye NPN preincubated with *P. aeruginosa* cells added with the peptides (A) RR-12 and (B) FL-13 at their respective 0.5X, 1X and 2X MIC concentrations.

Membrane depolarization assay

DiSC3(5) (3,3′-dipropylthiadicarbocyanine iodide) is a fluorescent dye that accumulates on the microbial membranes when their membrane is polarized (intact) and remains in the quenched state.[32] Depolarization of the microbial membrane effected upon addition of an antimicrobial agent is accompanied by an increase in fluorescence intensity emitted by the dye with its release from the membranes. Hence, an increase in the fluorescence intensity of DiSC3(5) signals is an indication of membrane depolarization induced by the added antimicrobial agent.[33] Peptides RR-12 and FL-13 added to the suspensions of *P. aeruginosa* [Figure E16(A), (B), Appendix E] induced no enhancements in the fluorescence intensity of DiSC3(5), ruling out the possibility of membrane depolarization in inducing membrane damage. DiSC3(5) enhancements were however observable

upon their addition to *C. albicans* Figure [6.13(A) & (B)] suggesting that the peptides induced membrane damage via depolarization of membranes in this case.

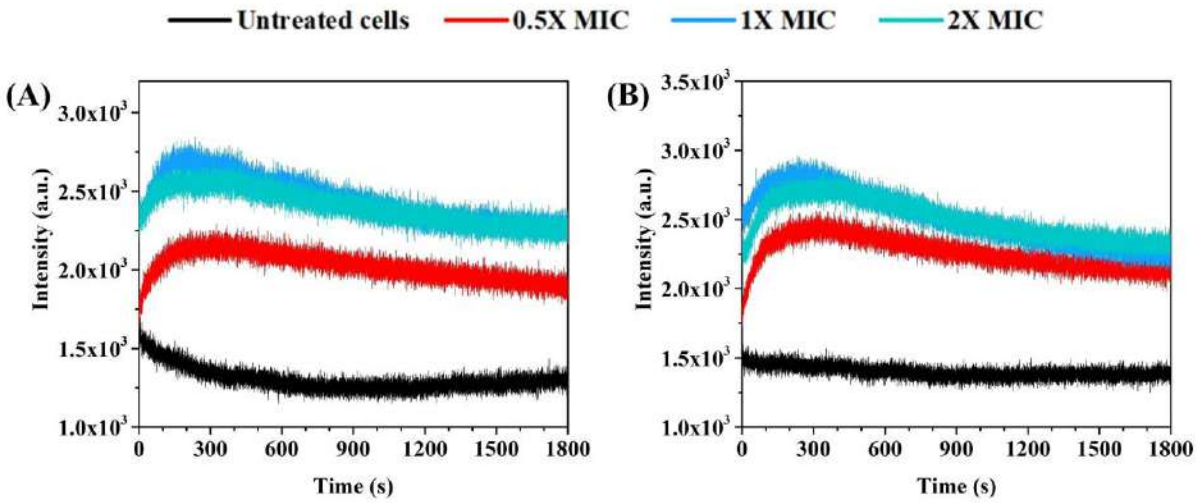

Figure 6.13. Membrane depolarization assay or DiSC3(5) assay. Fluorescence enhancements observed upon addition of the peptides (A) RR-12 and (B) FL-13 to the cells of *C. albicans* preincubated with DiSC3(5) dye.

In summary, fluorometric assays using different dyes gave us an insight into the mechanism of action of the peptides.[34] PI assay established inner membrane disruptive ability for both the peptides, against both bacterial *P. aeruginosa* and fungal *C. albicans*. NPN assay implied that the peptides induced rupture of the outer membrane in Gram-negative bacteria which in turn should have initiated through the binding of the peptides to lipopolysaccharides. DiSC3(5) assay on the other hand reveled membrane depolarization to be underlying cause of membrane disruption in the case of fungus *C. albicans*. Hence, our study revealed that same peptides may act in slightly different mechanistic pathways in inducing membrane damage against different microbes.

6.2.9. Electron microscopic images to probe the mechanism of action

Effect of the peptides RR-12 and FL-13 on the membranes of *P. aeruginosa* cells and *C. albicans* cells were further studied using FESEM (Figure 6.14) and FETEM (Figure 6.15) imaging. Severe deformations can be seen on the membranes of *P. aeruginosa* and *C. albicans* cells treated with the peptides further concluding the membranolytic mode of action of the peptides.

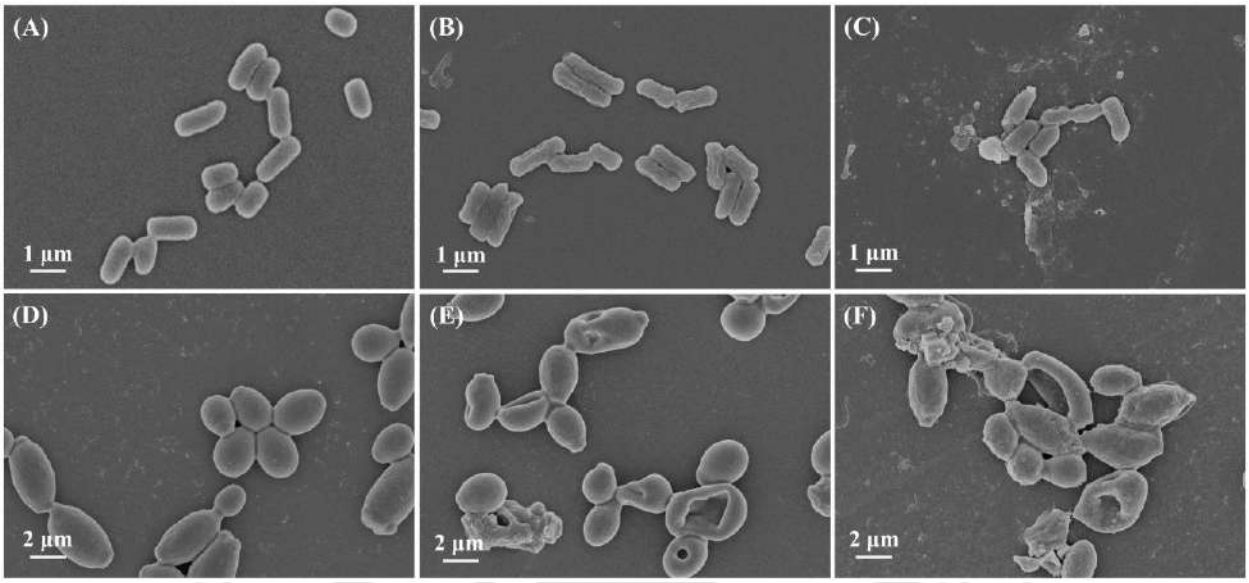

Figure 6.14. FESEM images of *P. aeruginosa* cells: (A) untreated, (B) treated with RR-12 (1X MIC), (C) treated with FL-13 (1X MIC) and that of *C. albicans* cells: (D) untreated, (E) treated with RR-12 (1X MIC), (F) treated with FL-13 (1X MIC).

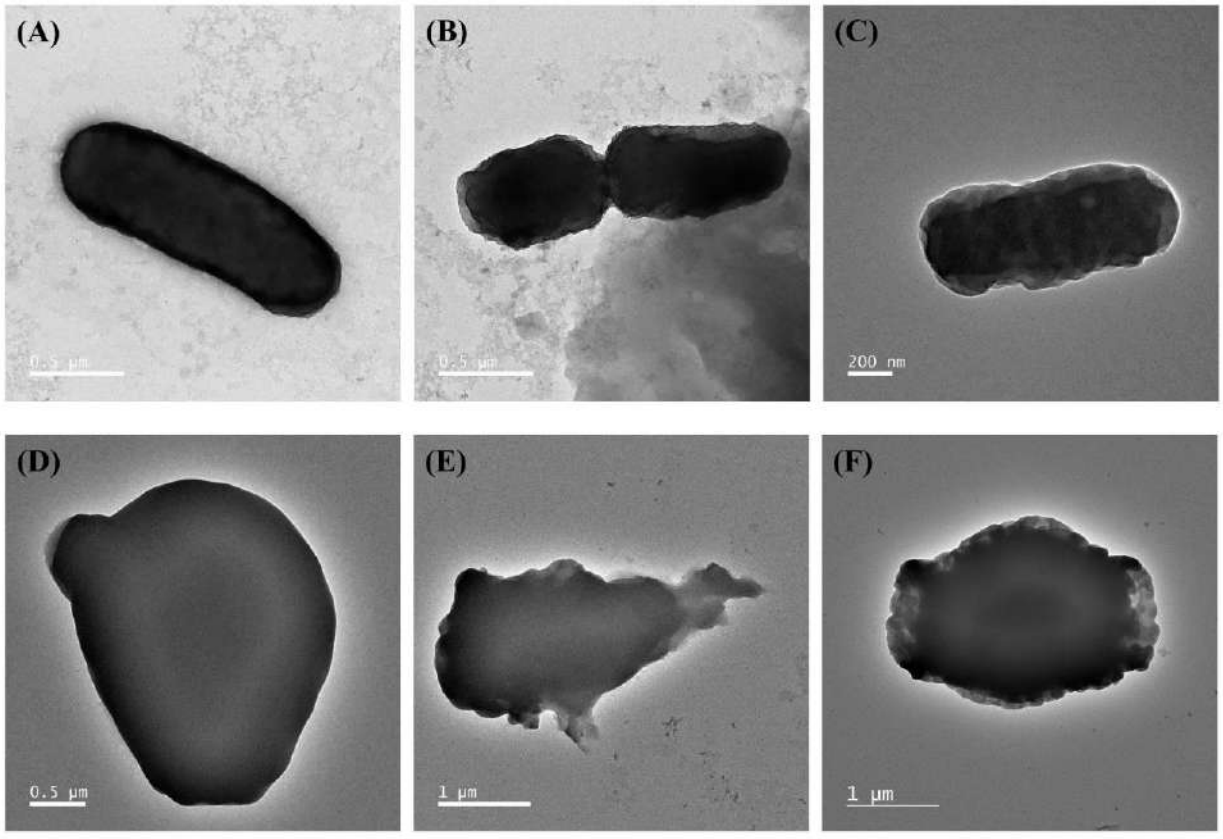

Figure 6.15. FETEM images of *P. aeruginosa* cells: (A) untreated, (B) treated with RR-12 (1X

MIC), (C) treated with FL-13 (1X MIC) and that of *C. albicans* cells: (D) untreated, (E) treated with RR-12 (1X MIC), (F) treated with FL-13 (1X MIC).

6.2.10. Confocal imaging of the peptide treated bacterial cells

P. aeruginosa cells co-incubated with a mixture of two dyes acridine orange[35] and propidium iodide[36] were imaged in their untreated form as well as after being treated with the peptides RR-12 and FL-13 using confocal imaging. Acridine orange is capable of staining intact/living cells while PI can stain only dead cells.[37] Untreated cells showed strong signals arising from the acridine orange and very poor to almost no signals due to propidium iodide [Figure 6.16(A)]. But upon addition of the peptides to the cells, strong fluorescence due to PI could be detected emitting out of the cells [Figure 6.16(B), (C)], implying that the peptides induced pore in the membranes allowing PI to migrate inside, bind DNA, and display enhanced fluorescence. This experiment also established the membranolytic mode of action displayed by the peptides.

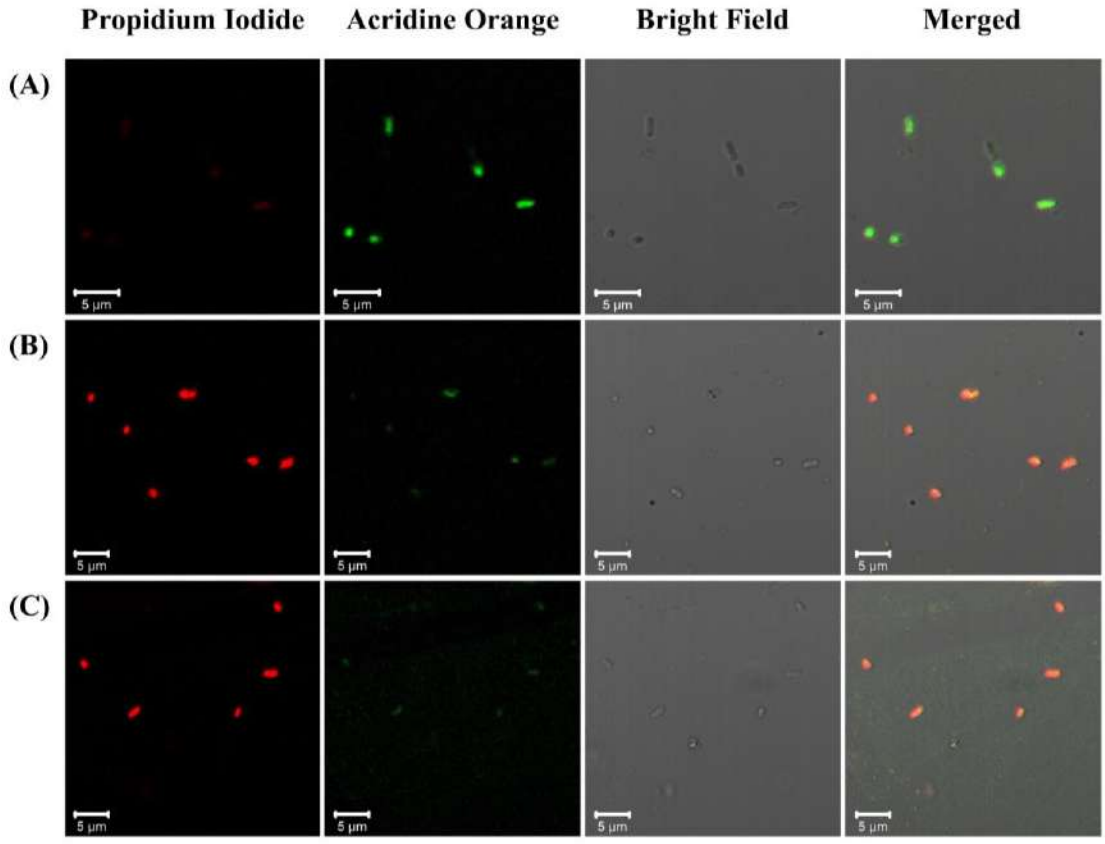

Figure 6.16. Live cell/dead cell assay studied using acridine orange (AO) and propidium iodide (PI). Confocal images of *P. aeruginosa* cells incubated with AO and PI: (A) untreated, treated with (B) RR-12 and (C) FL-13.

Confocal images were also acquired for the microbes (*P. aeruginosa*) treated with the peptides tagged with carboxyfluorescein. Carboxyfluorescein tagged peptides Cf-RR-12 and Cf-FL-13 were synthesized (E17-E18, Appendix E) and added to the cells. Cells incubated with the Cf-tagged peptides for a very short duration were found to emit signals corresponding to the carboxyfluorescein (Figure 6.17) suggesting accumulation of the peptides on the bacterial membranes, which is supposedly driven by the electrostatic interactions between the cationic charges on the peptides and negatively charged bacterial surfaces.

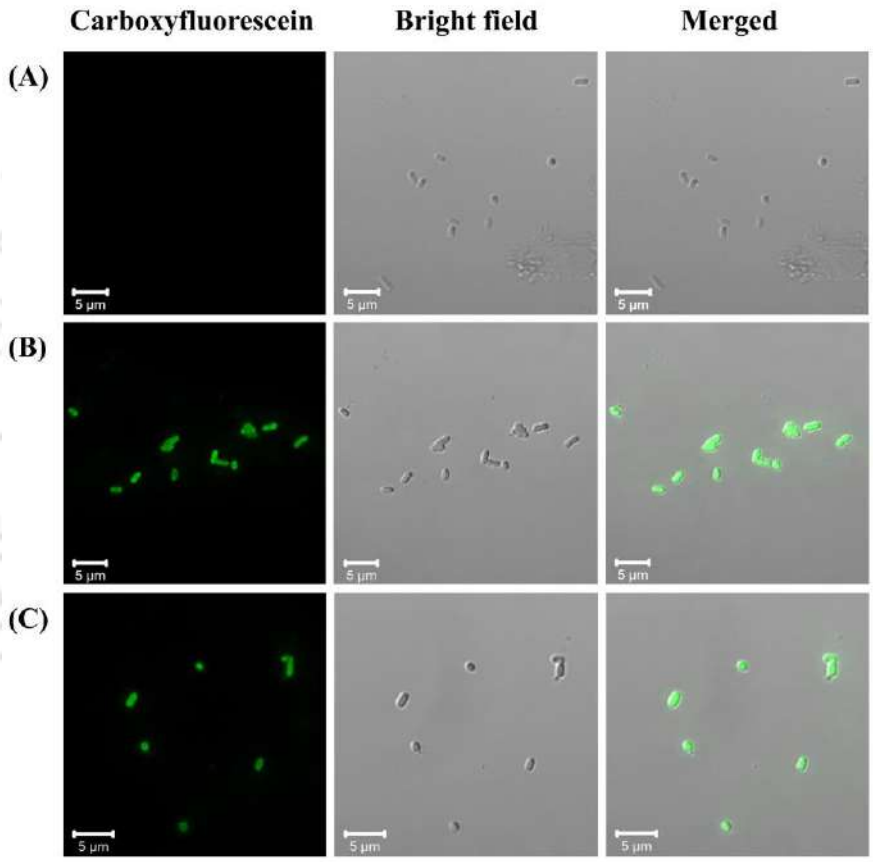

Figure 6.17. Confocal images of *P. aeruginosa cells*: (A) untreated, and treated with (B) Cf-RR-12 and (C) Cf-FL-13.

6.2.11. Live cell NMR

Membranolytic effect of the peptides was also established through the live cell NMR experiments. ^{1}H-NMR spectra of the peptides in their untreated form and that after addition of *C. albicans/ P. aeruginosa* cells were acquired over a period of time to study the effect of the peptides on microbial membranes or vice-versa. Broadening in the peaks of the peptides over the entire range of the

spectra (both in the aliphatic as well as aromatic region) were observed in each of the cases, corroborating probable peptide-membrane interactions [Figure 6.18 & Figure 6.19]. New peaks were also observed in the spectra of the peptide-cells mixtures. This indicated to the lysis of the cellular membranes leading to the release of different cellular contents or metabolites, which showed up as new peaks. New peaks were much more eminent in the spectra of *C. albicans* cells treated with the peptides RR-12 and FL-13 [Figure 6.18(A), (B)], compared those of *P. aeruginosa* cells treated with the peptides [Figure 6.19(A), (B)].

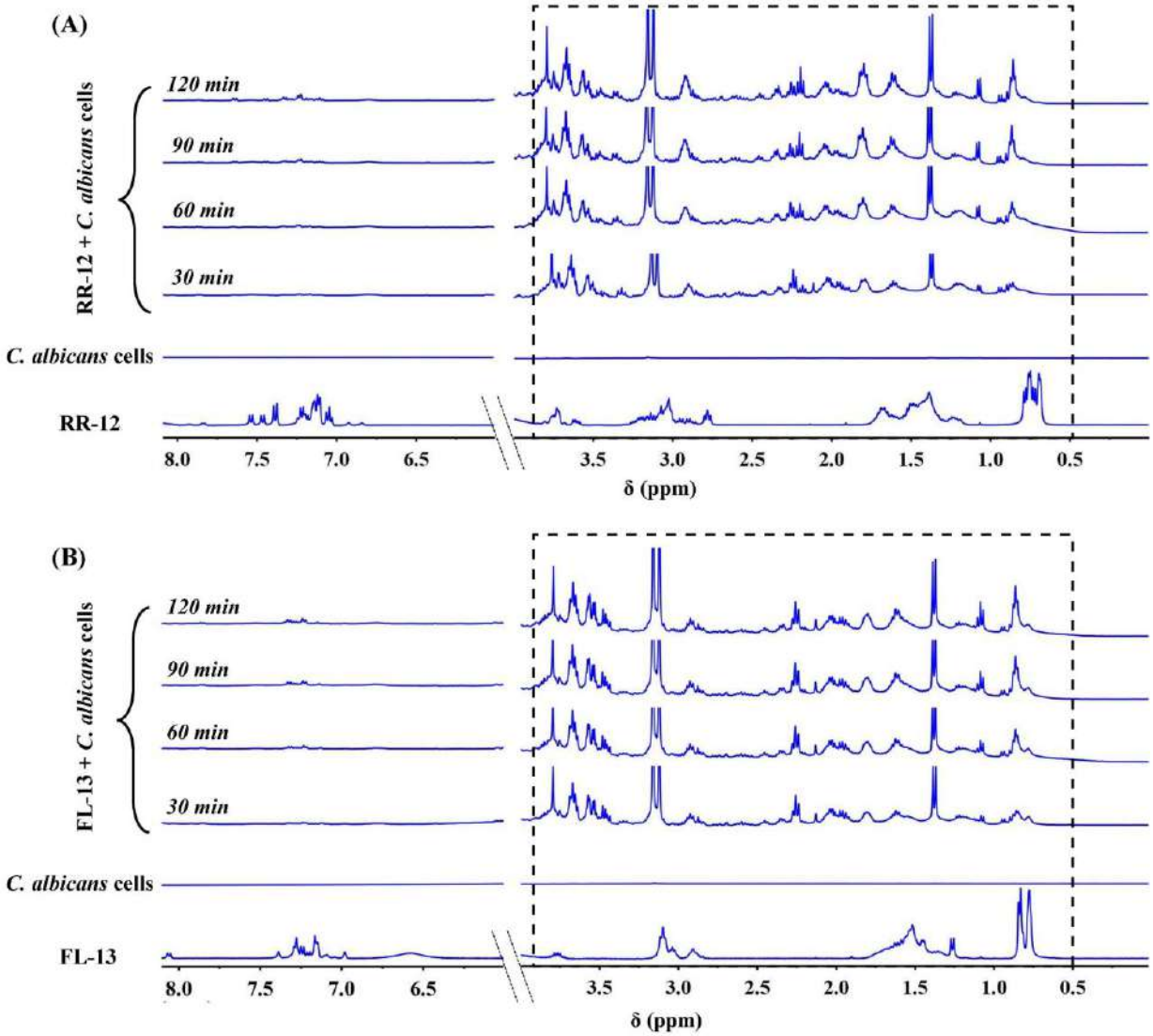

Figure 6.18. Live cell NMR experiments involving the peptides (A) RR-12 and (B) FL-13 and *C. albicans*. Stacked plots of ^{1}H NMR (400 MHz) spectra of the peptides (untreated, 1 mM), *C. albicans* cells (OD =1) and the mixtures of the peptides and cells incubated for various time

intervals. Broadening of signals and change in the chemical shifts of signals indicate peptide membrane interactions. A large number of new peaks appeared in the spectra of the mixture of peptide and cells (marked by dotted boxes). These might be from the metabolites leaking out of the cells upon treatment with the peptides, suggesting the membranolytic nature of the peptides.

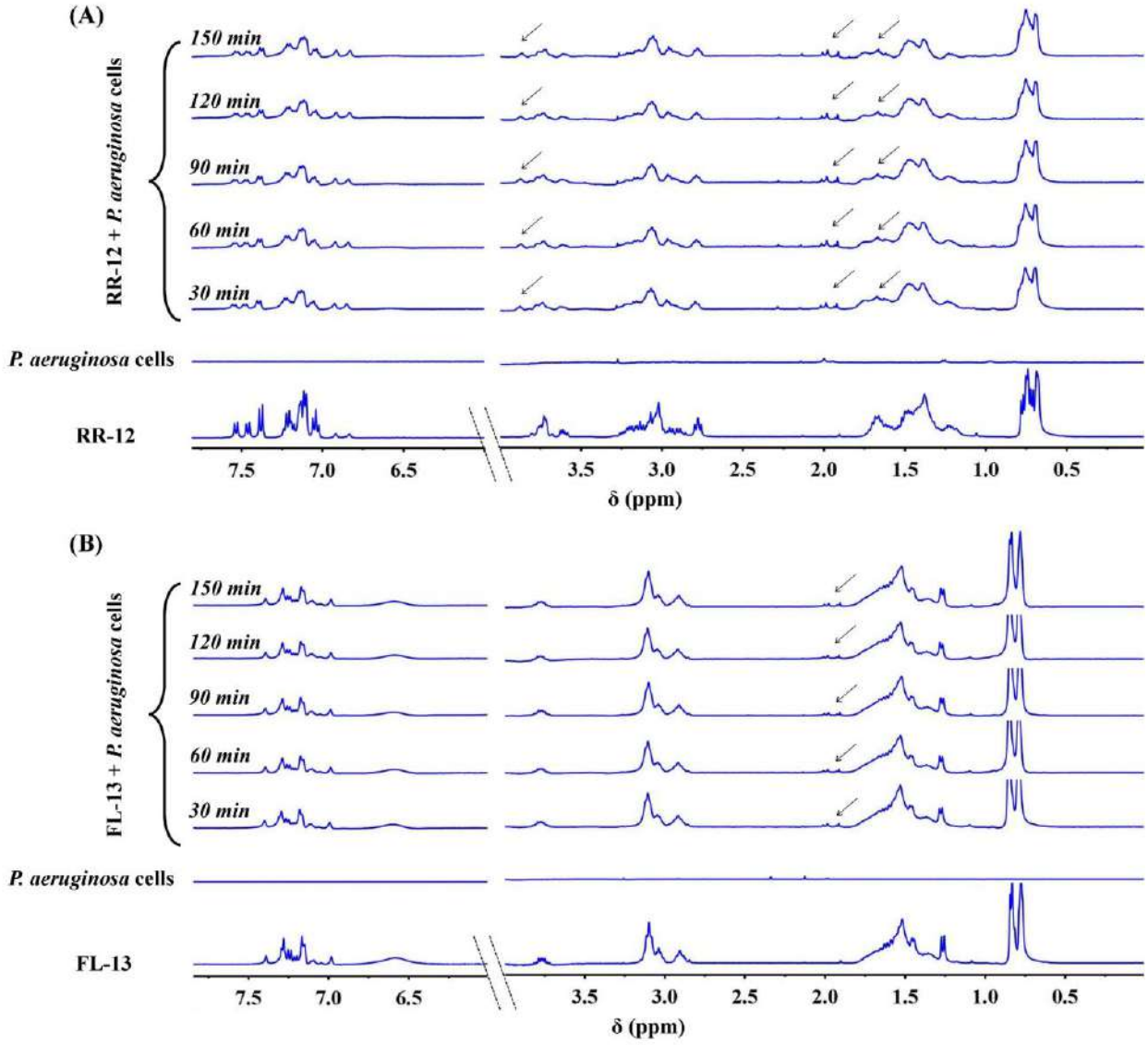

Figure 6.19. Live cell NMR experiments involving the peptides (A) RR-12 and (B) FL-13 and *P. aeruginosa* cells. Stacked ^{1}H NMR (400 MHz) spectra of the peptides (untreated, 1 mM), untreated *P. aeruginosa cells* (OD = 1) and the mixtures of the peptides and cells incubated for various time intervals. New peaks (indicated by arrows) appeared in the spectra of the peptide incubated cells, corresponding to the leakage of cellular contents or metabolites as result of membrane disruption.

6.2.12. Insights from MD simulations

The MD structure of the peptides (RR-12, FL-13) in complex with an SDS micelle (illustrated in Figure 6.20) provides insights into the interaction network and conformation of the peptides. The peptides meet their hydrogen bonding requirements through direct and water-mediated interactions with the sulfate groups of the micelle [Figure 6.20(A)]. Notably, both tryptophan residues in RR-12 are situated within the hydrophobic pocket of the micelle, as evidenced by their reduced solvent exposure, measured through solvent-accessible surface area (SASA) [Figure 6.20(B)]. All the hydrophobic side chain residues of the peptides are placed in the lipid core of the micelle, except for F11 of RR-12. Trajectory analysis reveals that the peptides predominantly adopt a helical conformation, with over 70-80% of their structures exhibiting helical characteristics, though some melting is observed at the terminal ends. This observed helical conformation of the peptides corroborates the circular dichroism experiments (Figure 6.7 & 6.8). Note that the helical content of FL-13 is marginally higher relative to RR-12 in the complex with the micelle. The trajectory-averaged root mean square fluctuation (RMSF) of the side-chain heavy atoms demonstrates a significant reduction in the flexibility of the peptides in response to micelle binding [Figure 6.20(B)].

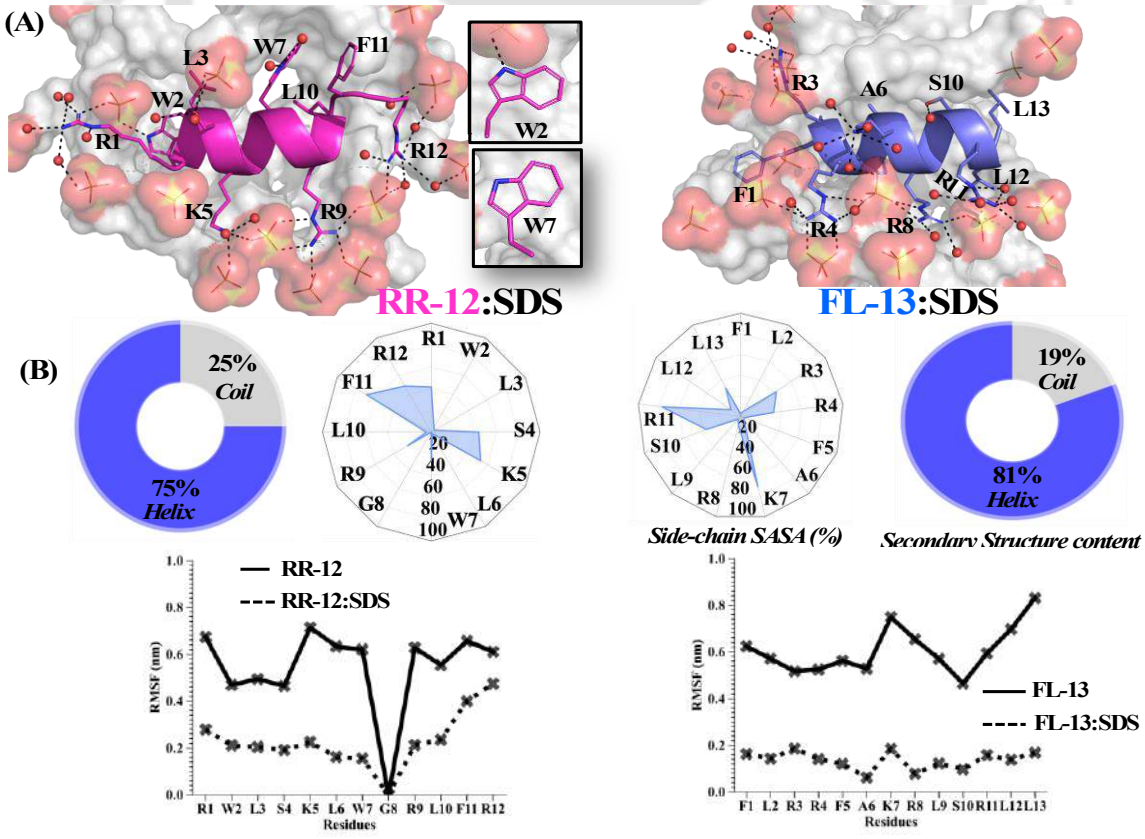

Figure 6.20. (A) The molecular dynamics (MD) structure of the RR-12 peptide (on the left) and the FL-13 peptide (on the right), both in complex with an SDS micelle, is presented. A zoomed-in view (highlighted with a black border) reveals the tryptophan residues (W3, W7 of RR-12) situated within the hydrophobic core of the micelle. Interactions amongst the residues are indicated by broken black lines, while water molecules are depicted as red spheres. (B) The trajectory-averaged residue-wise solvent accessibility (SASA) of the side chains is represented as a net plot with contours that indicate constant exposure percentages. Trajectory averaged secondary structure content of the peptides (helix, coil) is shown. The RMSF plots demonstrate a notable reduction in peptide flexibility in response to micelle binding.

Supplementary calculations performed using a bilayer model confirmed the reliability of these findings (Figure 6.21).

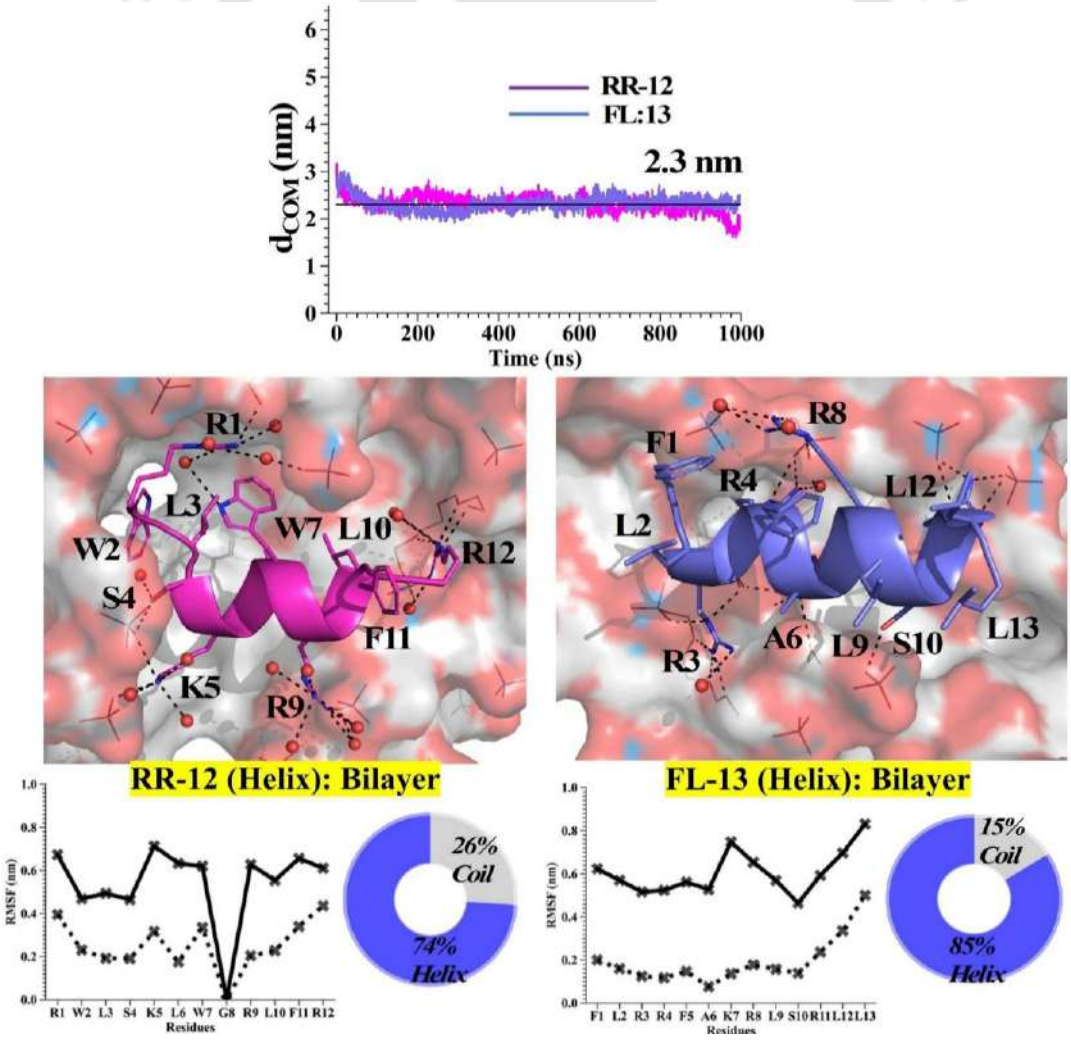

Figure 6.21. The distance between the centre of mass of the peptides and the bilayer (d_{COM}) varies over time, exhibiting a plateau at approximately 2.3 nm. The molecular dynamics (MD) structure of the peptide in its helix form, complexed with the bilayer, is presented with a zoomed-in view. In this view, interactions are illustrated with dotted lines, while water molecules are represented with spheres. The trajectory averaged residue-wise root mean square fluctuation (RMSF) of the peptide in the presence and absence of the bilayer and percentage of helices adopted by the peptides in complex with the membranes has also been presented.

6.3. Discussion

Reports of several α-helical AMPs obtained from natural sources or developed synthetically prompted us to use the secondary structural element in enhancing the antimicrobial potency in our *de novo* designed AMPs. It is known that that inducing secondary structural effect in small peptides is challenging without the use of constrained unnatural amino acid residues or structural confinements like stapling. In this work, our objective was to develop small, cationic, highly potent AMPs with high alpha-helical conformational propensity from linear, non-constrained peptides made of all alpha amino acid residues.

To achieve our goals, we designed two peptide sequences using the helical wheel projection and used natural amino acid residues that are known to have moderate to high helical propensity. Extensive studies from our group had earlier established that small cationic AMPs failed to adopt any canonical secondary structures in free and membrane bound state.[38-39] We had shown that increasing the length of the peptides had started inducing secondary structures in our peptides along with improving their activity.[40-41] In our present study, the primary sequence of the peptides were designed to have a clear segregation of the hydrophilic and hydrophobic faces in the helix, that we hypothesized our designed peptides would adopt.

The peptides RR-12 and FL-13 were highly potent ($MIC_{90\%} \leq 7.5\mu m$) against several ESKAPE pathogens and fungus *C. albicans*, FL-13 being more potent of the two. This could be attributed to the higher overall charge of the peptide FL-13 in comparison to RR-12. Both the peptides also had very good salt tolerance of their antimicrobial activity having $MIC_{90\%}$ values in PBS within 2-3 folds of their $MIC_{90\%}$ in the absence of the salts, against most of the tested strains. The peptides however had weaker salt sensitivity against *K. Pneumoniae* and *C. albicans*. These strain specific

variations in the activity could be attributed to the differences in the individual membrane compositions. RR-12 and FL-13 were non-cytotoxic towards the healthy mammalian cell lines HDF and RBCs till far above their active bactericidal concentrations. Both the peptides had high selectivity index towards healthy mammalian cell lines (HDF and RBC) while a relatively smaller selectivity index for the cancer cell line HeLa. Both the peptides manifested their bactericidal effects within 5-7.5 min and were found to be completely serum stable till 1 h. Beyond an hour, both RR-12 and FL-13 are partially degraded. The antibacterial potency of both the AMPs were considerably retained in the presence of serum, with FL-13 having < 2 folds increase in its $MIC_{90\%}$. As the average human systemic blood circulation time is approximately < 20 seconds, these AMPs very well qualify as potential therapeutic that can be applied intravenously.

The high potency of the peptides was most probably owing to the high positive charge content in addition to their ability to adopt helical structures while interacting with the microbial membranes as was proved through the structure determination using CD experiments in the presence of microbial membrane mimetic environments and bacterial LPS. ITC studies showed effective membrane binding of the peptides with bacterial membrane mimic SDS, with FL-13 being the better binder of the two. This also is in line with the better antimicrobial potency of the FL-13 over RR-12 seen earlier. MD simulation studies proved effective binding of the helical peptides to the SDS micelles.

The AMPs could induce inner membrane permeabilization in both gram-negative bacterial strain *P. aeruginosa*, as well as the fungal strain *C. albicans*. The outer membrane permeabilization effected by the AMPs in *P. aeruginosa* could be proved through the enhancement of the NPN fluorescence. However, the difference in the composition of the outer membrane in the *C. albicans*, led to failed binding of NPN dye, resulting in no enhancement in its fluorescence intensity and failure to prove the outer membrane permeabilization. However, the permeabilization of the inner membrane of *C. albicans*, suggested access of the AMPs to the inner membrane, and served as an indirect proof of the permeabilization of its outer membrane. The AMPs could affect membrane depolarization in fungus *C. albicans*, while it could not do so in gram negative *P. aeruginosa*. This selective ability of the AMPs in effecting the membrane depolarization could be attributed to the difference in their membrane composition.[42-43] Interestingly, live cell NMR studies established the leakage of the intracellular materials from both the fungus *C. albicans* and gram-negative bacteria

P. aeruginosa, with more pronounced effect in the former than the later. FESEM/ FETEM studies showed the membrane deformation, disruption, cell lysis and the formation of cellular debris in both the *C. albicans* and *P aeruginosa* cells effected by the peptides. Thus, it can be concluded that though the AMPs might have microbicidal effect against different pathogens with an overall membranolytic mechanisms of action, there might be smaller variations in the detailed mechanisms of action due to the difference in the membrane composition of the different species.

6.4. Conclusion

We have designed two highly potent broad-spectrum cationic alpha helical antimicrobial peptides, RR-12 and FL-13 in this study. These antimicrobials circumvent several existing drawbacks of the AMPs that limit their success for commercialization. Of the two designed AMPs, FL-13 was more promising, owing to its higher overall charge. Along with the salt tolerance of their antimicrobial activity, the developed AMPs were non-cytotoxic towards mammalian cells and RBCs, showed very fast bactericidal kinetics and considerable retention of activity in the presence of human serum. We established that though the overall mechanism of action of these membrane active peptides was membranolytic across the microbial spectrum that were studied, there were subtle differences in their mechanism depending on the composition of the different microbes in question. A combination of positive charge, balanced hydrophobicity-hydrophilicity, ability to adopt helical conformation, efficient and selective binding to the microbial membranes remained the major attributes for the high performance of these designed peptides. These molecules are important additions to the repertoire of antimicrobial therapeutics, efficient in combating microbial infections.

6.5. Methods

6.5.1. Materials

Rink amide resin, Fmoc protected amino acids: Fmoc-Arg(Pbf)-OH, Fmoc-Trp(Boc)-OH, Fmoc-Phe-OH, Fmoc-Leu-OH, Fmoc-Ser(tBu)-OH, Fmoc-Lys(Boc)-OH, Fmoc-Gly-OH, Fmoc-Ala-OH, coupling reagents: HBTU and HOBt were purchased from GL Biochem, Shanghai. N,N-Dimethylformamide (DMF), Piperidine, Pyridine, Trifluoroacetic acid (TFA) were purchased from Merck Life Science Private Limited, Mumbai, India. Acetic anhydride was manufactured by SD Fine Chem Limited and was supplied by the department of chemistry, IIT Guwahati. Dichrolomethane (DCM), HPLC grade acetonitrile and Diethyl ether were purchased from Finar

Chemicals, Gujarat, India. N,N-Diisopropylethylamine (DIPEA) was purchased from Spectrochem Private Limited, Mumbai, India. Nutrient broth, BHI broth, YPD broth, Monosodium phosphate (NaH_2PO_4), Disodium phosphate (Na_2HPO_4), Monopotassium phosphate (KH_2PO_4), Sodium chloride (NaCl), Potassium chloride (KCl), Acridine orange were purchased from Himedia Laboratories, Mumbai, India. D8PG [1,2-dioctanoyl-sn-glycero-3-phospho-(1'-rac-glycerol) (sodium salt)] and Dodecylphosphorylcholine (DPC) were purchased from Avanti Polar Lipids, USA. Deuterium oxide (D_2O), α-Cyano-4-hydroxycinnamic acid (HCCA), Triton X-100, Sodium dodecyl sulphate (SDS), 2,2,2-trifluoroethanol (TFE), Lipopolysaccharide (*Pseudomonas aeruginosa*), Propidium Iodide (PI), N-Phenyl 1-napthylamine (NPN), DiSC 3(5) [3,3'-Dipropylthiadicarbocyanine iodide], Glutaraldehyde and 5(6)-Carboxyfluorescein were purchased from Sigma-Aldrich, St. Louis, USA.

6.5.2. Solid phase peptide synthesis

The peptides were synthesized using solid phase peptide synthesis using Fmoc-chemistry. Briefly rink amide resins corresponding to 0.1 mmol scale was weighed and swelled in a solvent mixture containing DCM-DMF. The swelled resins were deprotected with 20% piperidine in DMF to link the first amino acids. 3 equivalents of the Fmoc protected amino acids (0.3 mmol), 3 equivalents of each of HBTU (0.3 mmol) and HOBt (0.3 mmol), 6 equivalents of DIPEA (0.6 mmol) were weighed, mixed in DMF and added to the deprotected rink amide resins. The resulting mixtures were then allowed to rock in the resins for at least 6-8 h, for effective linking of the amino acids to the resins. This was followed by the washing of the resins coupled with the amino acids using DMF (3 times) and DCM (3 times), and then subjected to capping using a solution containing pyridine: acetic anhydride: DMF (1:2:7) for a period of 1 h. All the amino acids in the sequences were then linked to resins, one after the other following the same protocol as followed for the linking of the first amino acids to the resins. Once, finished the peptide grown on the resins were cleaved off from the resins using a cocktail TFA: TIS: H_2O (96:2.5:1.5) and was precipitated on cold dry diethyl ether.

6.5.3. Purification

The peptides were purified using reversed phase high performance liquid performance chromatography (HPLC) using a Thermo Scientific Ultimate 3000 HPLC instrument. Water and acetonitrile each acidified with 0.1% TFA were used as the solvents for peptide purification. A

multigradient programme with increasing percentage of acetonitrile (5-100%) was set to purify the peptides. Flow rate of the solvent was kept steady at 10 ml/min. A C-18 reverse phase column (Luna 5 μm C18(2) 100 Å, size: 250 × 21.2 mm) was used for the process of purification.

6.5.4. Characterisation of the peptides

Peptides synthesised were characterised using MALDI-TOF mass spectrometry (acquired using Autoflex speed, Bruker), and ^{1}H-NMR spectroscopy (acquired using 600 MHz Bruker Avance III HD NMR spectrometer). The purity of the peptides was evaluated using analytic HPLC traces acquired using a Themo Scientific Vanquish HPLC instrument fitted with a reverse phase C-18 column (Agilent Eclipse Plus C-18, 5 μm, 4.6 × 250 mm).

6.5.5. Microbial strains

Escherichia coli (MTCC 433), *Klebsiella pneumoniae* (MTCC 432), *Acinetobacter baumannii* (ATCC 1425), *Pseudomonas aeruginosa* (MTCC 2488), *Staphylococcus aureus* (MTCC 96) and *Candida albicans* (MTCC 1637) were acquired from Microbial Type Culture Collection and Gene Bank (MTCC), Chandigarh, India. Methicillin resistant *Staphylococcus aureus* (MRSA 100) strain used in this study was clinically isolated from the wound of a patient and was obtained from Prof. Benu Dhawan, AIIMS, New Delhi.

6.5.6. Determination of Minimum Inhibitory Concentration (MIC)

Gram negative *E. coli, K. pneumoniae, A. baumannii, P. aeruginosa* were grown in nutrient broth, Gram-positive *S. aureus* and MRSA were grown in BHI broth while the fungus *C. albicans* was grown in YPD broth. Each of the microbes grown at their respective mid-log phases were pipetted out and centrifuged. The pelleted down cells obtained after centrifugation were washed with phosphate buffer (10 mM, pH -7.4) for three consecutive times. Post washing, the cells were suspended in the same phosphate buffer solution and were serially diluted to the order of 10^5 cfu/ml. 50 µL of these diluted cell suspensions were added with 50 µL of the peptides diluted at different concentrations. Untreated cells as the negative control while polymyxin-B treated cells against the Gram-negative microbes, vancomycin treated cells against the Gram-positive microbes and amphotericin-B treated cells against the fungus as the positive controls were also maintained alongside with the peptide treated cells. These peptide-cell mixtures (also the untreated cells or positive-control treated cells) were kept incubated at 37 °C for the bacterial microbes and at 28 °C

for the fungal microbe under a continuous orbital shaking for a period of 4 h. After 4 h of incubation, respective media were added to the treated/ untreated cells and were incubated further overnight at the respective temperatures. Finally, post overnight incubation, cells were subjected to optical density measurements at 600 nm and minimum inhibitory concentration (MIC) values were determined by comparing the optical densities recorded for that of the positive control as well as for the negative control. $MIC_{90\%}$ for a compound was reported to be the lowest concentration of a peptide at which it inhibited the growth of 90% or more of a particular microbe assuming the positive control to inhibit the growth that particular microbe by 100%.

6.5.7. Determination of Minimum Inhibitory Concentration (MIC) in the presence of salts

Further, the minimum inhibitory concentrations of the peptides were determined in the presence of salts. Phosphate buffer saline of strength 10 mM and pH- 7.4 was used for the purpose. The method followed was same as for the determination of $MIC_{90\%}$ described in section above. Only the difference in this case was that the phosphate buffer of pH-7.4 was replaced by phosphate buffer saline of pH-7.4 in all the cases where buffer was used.

6.5.8. Cytotoxicity assay

Cytotoxicity of the peptides were evaluated against HDF and HeLa cells lines. Peptides at different concentrations ranging from 2.5 µM to 160 µM in quadruplicates were treated with HDF and HeLa cells respectively at a density of 2000 and 5000 cells/well in a 96 well plate. At the end of incubation after 24 h, cells were treated with MTT and were further incubated for 2 h. Addition of MTT resulted in the formation of formazan crystals which were dissolved in DMSO and the readings were taken at 570 nm with 650 nm as the reference. Percentage viability of the cells was calculated in reference to the untreated cells. Experiments were repeated at least twice.

6.5.9. Hemolytic activity

Human blood was collected in an EDTA vial withdrawn from a healthy volunteer with consent. Blood was centrifuged to discard the supernatant. The red blood cells settled at the bottom were washed using phosphate buffer saline of pH- 7.4 and strength 10 mM for three consecutive times and finally were suspended in the same buffer. The resuspended blood suspensions diluted at 10% were then treated with the peptides at different concentrations as well as with 1% Triton-X added as the positive control and kept incubated for 1 h under continuous shaking at 37 °C. 10% of the

untreated cells as the negative control for the experiment was also maintained alongside with the treated RBC suspensions. Post incubation period, the cells were centrifuged again and the OD values of the supernatant were recorded at 540 nm. The percentage hemolysis induced by a peptide at particular concentration was determined by comparing the OD values of the supernatant obtained corresponding to that concentration with those of the cells kept untreated (negative control, assuming 0% hemolysis) and treated with 1% Triton-X (positive control, assuming 100% hemolysis).

6.5.10. Time-kill kinetics

P. aeruginosa and *C. albicans* grown at their respective mid-log phases were washed and serially diluted to the order of 10^5 cfu/ml. These cell suspensions were then treated with the peptides at their respective MIC concentrations and incubated corresponding to different time intervals, at temperatures of 37 °C and 28 °C respectively for the bacteria and fungus. The peptide treated cells corresponding to different time intervals were withdrawn with the help of a micropipette and spread uniformly on agar plates containing the respective growth media for the microbes i.e. nutrient broth for *P. aeruginosa* and YPD broth for *C. albicans*.

6.5.11. Determination of the serum stability of the peptides

Peptides at a final concentration of 2 mM, was added with equal volumes of the serum (centrifuged out of human blood as the supernatant) and kept incubated under shaking conditions for different time intervals (30 min, 1 h, 3 h, 6 h, 12 h and 24 h) at a temperature of 37 °C. The peptide-enzyme interactions at the end corresponding to each incubation periods were quenched using a solution of acetonitrile-methanol-water (8:1:1) added to the peptide-serum mixtures at equal volumes. The serum precipitated out of the solution after of addition of the quenching solution, and was centrifuged out of the solution. The solution obtained as the supernatant was separated carefully to analyse the peptides or peptide fragments contained in it, using reverse phase analytic HPLC traces (instrument: Thermo Scientific Ultimate 3000 HPLC / column: Luna 5 μm C18(2) 100 Å, size:250 × 21.2 mm). A control data corresponding to the peptide-serum mixtures quenched at 0 min was also acquired using HPLC. MALDI spectra for the serum-peptide mixtures incubated for 1 h and 24 h were acquired to confirm the peptide fragmentations.

6.5.12. MIC in the presence of serum

50 µL of *P. aeruginosa* cells diluted to the order of 10^5 cfu/ml in buffer (pH- 7.4, 10 mM strength) was added to 25 µL of the peptide solution, diluted at different concentrations in the same buffer, and another 25 µL serum (obtained as the supernatant after centrifugation of blood). This mixture was allowed to incubate under shaking conditions at 37 °C for a period of 4 h, followed by addition of media and subsequent incubation under similar conditions overnight. Untreated cells, cells treated with polymyxin-B both of which containing a final volume of 25% serum were set as the respective negative and positive controls for the experiment. The $MIC_{90\%}$ (serum) values were determined to the lowest concentrations of the individual peptides at which 90% or more inhibitions were observed based on the OD values compared to that of the negative (assuming 0% inhibition) and positive (assuming 100% inhibition) controls.

6.5.13. Determination of secondary structures: circular dichroism spectrometry

Secondary structures of the peptides were determined using CD spectroscopy. CD Spectra for 100 µL of each of the peptides in deionized water, 30 mM SDS, 10 mM DPC and 50% TFE were acquired. A Jasco J-815 spectropolarimeter was used for the same. The spectra were measured using a cuvette of pathlength 1 mm, acquired over a wavelength of 260 nm to 190 nm, 100 nm/ min scanning rate, 1 nm data pitch, bandwidth of 1 nm and a D.I.T value of 1 second. Five scans were acquired for each of the samples.

For the CD spectra in LPS, peptide concentrations at a final strength of 50 µM was used. Peptides in the free state (50 µM) as well as in LPS at ratios 0.5X (25 µM), 1X (50 µM) and 2X (100 µM) to that of the peptides were subjected to CD measurements using the same parameters as mentioned above.

6.5.14. Blue shift experiments

Using the intrinsic fluorescence of tryptophan residues present in the peptide RR-12, the interactions of the peptide with the membrane mimics namely D8PG and SDS (bacterial membrane mimic) as well as DPC (mammalian membrane mimic) were studied. RR-12 at a concentration of 5 µL was titrated against D8PG, SDS and DPC individually at increasing concentration ratios ranging from 0.5X to 10X the concentration of the peptide. The changes in the λ_{max} values in the

fluorescence spectra of the peptides were monitored upon each addition of the titrants. The spectra were acquired in the range 300-500 nm excited at a wavelength of 280 nm.

6.5.15. Isothermal Titrations Calorimetry

The interactions between the peptides and SDS were studied with the help of isothermal titration calorimetry. Peptides at a concentration of 500 μM (0.5 mM) were placed in the cell and were titrated against SDS solution of 10 mM concentration placed in syringe for 20 consecutive times, each time injected with a volume of 2 μL. The reaction was set at 37 °C, with a stirring speed of 350 rpm, each injection being of 3 seconds and with a spacing of 180 seconds maintained between each injection. Reactions for both the peptides against SDS were fitted through a one binding site model.

6.5.16. Propidium iodide assay

P. aeruginosa and C. albicans cells obtained at their respective mid-log phases were washed and serially diluted to the order of 10^6 cfu/ml in phosphate buffer (pH- 7.4, strength-10 mM). Propidium iodide at a final concentration of 10 μM was added to the cell suspensions and kept incubated for a minimum of 30 min at 37 °C and 28 °C respectively for bacteria and the fungus. Fluorescence measurements were acquired for the untreated cells and that of the cells treated with the respective 0.5X, 1X and 2X MIC concentrations of the peptides over a period of 30 min in each of the cases. The fluorescence was monitored at the room temperature using an excitation wavelength of 535 nm (slit width: 10 nm) and an emission wavelength of 617 nm (slit width: 10 nm) using a Fluoromax 4 spectrophotometer (Horiba scientific).

6.5.17. NPN assay

NPN dye at a final concentration of 10 μM was added to a suspension of *P. aeruginosa and C. albicans* cells obtained at their respective mid-log phases and diluted to the order of 10^6 cfu/ml in phosphate buffer (pH- 7.4, strength-10 mM), and kept incubated for at least 1 h. The untreated cells as well as the cells treated with different concentrations of the peptides ranging from 0.5X to 2X of their respective MIC values against the individual microbes were subjected to fluorescence kinetics measurements over a period of 30 min, at room temperature. Excitation and emission wavelengths were set at 350 nm (slit width: 5 nm) and 410 nm (slit width: 5 nm) respectively for acquiring the fluorescence. The fluorescence kinetics spectra were acquired using a Fluoromax 4 spectrophotometer (Horiba scientific).

6.5.18. Membrane depolarization assay or DiSC 3(5) assay

P. aeruginosa and *C. albicans* obtained at their respective mid-log phases were washed, diluted to the order of 10^6 cfu/ml in phosphate buffer (pH- 7.4, strength-10 mM) and were added with DiSC 3(5) dye at a final concentration of 1 μM. The resulting suspension was kept incubated under shaking conditions at 37 °C for a period of at least 1 h or more. Both the types of microbial cells at their untreated form as well as treated with the respective 0.5X to 2X MIC concentrations of the peptides against the individual microbes were subjected to fluorescence measurements over a period of 30 min in each of the cases. A Fluoromax 4 spectrophotometer (Horiba scientific) was used for acquiring the fluorescence kinetics using an excitation wavelength of 622 nm (slit width: 10 nm) and an emission wavelength of 670 nm (slit width: 5 nm).

6.5.19. FESEM and FETEM imaging of the microbial cells treated with the peptides

P. aeruginosa as well *C. albicans* cells obtained in their mid-logarithmic phases and diluted to the order of 10^5 cfu/ml were treated with respective MIC concentrations of the peptides against each of the individual microbes and kept incubated for a period of 1 h. Post incubation period, the peptide-treated cells as well as the untreated cells (negative control) were fixed with 2.5% glutaraldehyde and were subjected to incubation further for 1 h. The glutaraldehyde-fixed cells were washed, concentrated and drop casted on silicon wafers for the purpose of FESEM imaging and on TEM grids for the purpose of FETEM imaging.

The cells casted on the silicon wafers were allowed to dry, and the dried samples were washed with different grades of ethanol (30%,50%, 70% and 90%) followed by further drying. Samples were gold coated and FESEM images were acquired using a Zeiss Gemini 300 Field emission scanning electron microscope.

FETEM samples casted on TEM grids were stained with 1% uranyl acetate solution and allowed to dry. Images were acquired on a JEOL 2100F Field emission transmission electron microscope.

6.5.20. Confocal imaging of the peptide treated bacterial cells

Acridine orange and propidium iodide dyes were added to the washed cells of *P. aeruginosa* diluted to the order of 10^5-10^6 cfu/ml and kept incubated for some time. Confocal images of the untreated cells and those of the cells treated with the peptides were acquired irradiated with excitation

wavelengths corresponding to each of the acridine orange dye as well as the propidium iodide dye. A bright field image was also acquired corresponding to each of the confocal images acquired.

5(6)-Caboxyfluorescein was tagged to each of the peptides and were synthesized by linking of carboxyfluorscein moiety at the N-terminus of the full peptide sequences grown on the resins using the same coupling reagents HBTU and HOBt and base DIPEA as used for coupling amino acids, followed by cleaving off of the carboxyfluorescein tagged peptides from the resin using TFA. The Carboxyfluoscein tagged peptides Cf-RR-12 and Cf-FL-13 were characterized using MALDI spectroscopy (Figure E17-E18, Appendix E). Confocal images of *P. aeruginosa* cells untreated as well treated with Cf-RR-12 and Cf-FL-13 were acquired irradiated with excitation wavelength corresponding to that of the FITC dye. Bright field images corresponding to that of the confocal images were also acquired likewise. A confocal microscope of model JSM-7610F (Zeiss) was used for the purpose of confocal imaging in both the cases.

6.5.21. Live cell NMR

P. aeruginosa cells as well as *C. albicans* cells both were washed and concentrated/ diluted to a final OD = 1 in a solution of phosphate buffer of 10 mM strength, acidified to a pH of 6.5, and added with 10% D_2O. ^{1}H-NMR spectra of the peptides at a final concentration of 1 mM dissolved in the same solvent system as used for the suspensions of the cells [90% phosphate buffer (10 mM, pH- 6.5)+10% D_2O], that of the untreated cells and also of the cells treated with the peptides (1 mM) corresponding to different time points of incubation were acquired. 256 scans were acquired corresponding to each of the spectra, water suppression was carried out using a pulse program of zgpr.

6.5.22. Modelling peptides and membrane mimetic systems in water

Models of the RR-12 peptide (charge: +5) and the FL-13 peptide (charge: +6), featuring -NH_3^+ at the N-terminus and -$CONH_2$ at the C-terminus, were designed using PyMOL software.[44] The peptides were positioned at the centre of an equilibrated water box measuring 70 × 70 × 70 Å^3. Chloride ions were added to neutralise the system, after which it was subjected to molecular dynamics (MD) simulations.

Two bacterial membrane-mimetic models were employed to investigate peptide interactions: a micelle model (SDS: sodium dodecyl sulfate) and a bilayer model mimicking the outer membrane of *Pseudomonas aeruginosa*. The CHARMM-GUI micelle builder[45] and membrane builder[46]

facilitated the generation of the micelle and bilayer models, respectively. Negatively charged SDS micelles represent a simplified model of bacterial membranes.[47] The experimentally determined aggregation number of SDS molecules is approximately 60, leading to the inclusion of 60 SDS molecules in the micelle model, which was solvated with a water box of dimensions 100 × 100 × 100 Å^3. Neutralisation was achieved by adding 60 Na^+ ions, following which the simulation system underwent MD simulations.

The bilayer model was developed to provide a more sophisticated representation of the outer membrane by mimicking the outer membrane lipids of *Pseudomonas aeruginosa*. The outer layer consisted of Lipid A, while the asymmetric inner layer was composed of a mixture of phosphatidylethanolamine (PE), phosphatidylglycerol (PG), and cardiolipin (CL).[48] This bilayer model was solvated in a water box measuring 67.5 × 67.5 × 110 Å^3 and neutralised by adding 80 Na^+ ions. The adopted model has been shown to replicate experimentally determined membrane properties accurately.[49]

6.5.23. Setup for peptide: micelle/bilayer binding

The final structure of the free linear peptide (RR-12 or FL-13) in an aqueous solution was positioned at a distance of 50 Å from the centre of mass of the equilibrated micelle. Following the placement of the peptide, an additional 40 Å of water padding was incorporated along the outer shell of the micelle to ensure adequate solvation. The resulting model was subjected to MD simulations. The distance (d_{COM}) between the peptide and micelle centre of mass was plotted over time (Figure E19, Appendix E). The plateau in the d_{COM} versus time plot (~ 1.55 nm) indicated peptide settlement on the micelle. The peptide was in random coil conformation in complex with the micelle (Figure E19, Appendix E). The conformational change (random coil → helix) was not captured during the time scale of the simulations. To gain insight into the helical-peptide: micelle complex, we modelled the helical peptide and initially placed the peptide at least 30 Å away from the micelle surface. The simulations resulted in the helical-peptide: micelle complex. The simulations were repeated with the peptide positioned 50 Å from the bilayer's centre of mass, producing results similar to those from the micelle (Figure 6.21). We performed a comprehensive sampling duration of 15.2 μs, encompassing a series of independent replicas. Each replica was uniquely configured, differing in initial velocities, orientations, and the presence or absence of salt (Table E3, Appendix E).

6.5.24. Molecular Dynamics simulations

All-atom classical molecular dynamics (MD) simulations were carried out using the GROMACS package (version 2023).[50] To model the interactions and characteristics of the biomolecular systems, the CHARMM36m force field was employed.[51] The TIP3P water model[52] was utilised to depict the solvent environment surrounding the biomolecules.

The solvated simulation box initially underwent an energy minimisation (50000 steps with a step size of 0.1 Å) using the steepest descent algorithm to attain a stable conformation before the dynamic simulations commenced. Following energy minimisation, an equilibration phase took place over a duration of 200 ps, divided into two segments: the first half was conducted under the NVT ensemble, which maintains constant particle number, volume, and temperature, while the second half transitioned to the NPT ensemble, where particle number, pressure (1 bar), and temperature (310 K) remain constant. The production run of the simulations was executed for varying lengths, with a minimum duration of 200 ns (for peptide binding micelle) and a maximum of 1000 ns (for peptide binding to bilayer). Production dynamics considered NPT ensemble to ensure the system accurately reflects realistic physiological conditions. Coordinates from the production dynamics were recorded at intervals of every ten picoseconds (ps) and analysed.

6.5.25. Trajectory analysis

The analyses conducted included root mean square fluctuation (RMSF), secondary structural assessment (using DSSP), solvent accessible surface area (SASA), and the distance between the centre of mass of the peptide and the micelle/bilayer (d_{COM}).

Residual fluctuations were evaluated through trajectory averaging with the "*gmx rmsf*" implemented in GROMACS. The secondary structure of the peptide was analysed in both free and bound states using "*gmx dssp*". We calculated the solvent exposure of amino acid side chains by calculating SASA using "*gmx sasa*", by employing a probe radius of 1.4 Å. The distance between the centre of mass was determined as a function of simulation time using the "*gmx distance*" command. Lastly, images were rendered with the PyMOL visualisation tool (version 3.1.1).

References

1. Li, S.; Wang, Y.; Xue, Z.; Jia, Y.; Li, R.; He, C.; Chen, H. The structure-mechanism relationship and mode of actions of antimicrobial peptides: A review. *Trends Food Sci. Technol.* **2021**, *109*, 103-115.

2. Liang, Y.; Zhang, X.; Yuan, Y.; Bao, Y.; Xiong, M. Role and modulation of the secondary structure of antimicrobial peptides to improve selectivity. *Biomater. Sci*. **2020**, *8*, 6858-6866.

3. Ciulla, M.G.; Gelain, F. Structure-activity relationships of antibacterial peptides. *Microb. Biotechnol*. **2023**, *16*, 757-777.

4. Dathe, M.; Wieprecht, T. Structural features of helical antimicrobial peptides: their potential to modulate activity on model membranes and biological cells. *Biochim. Biophys. Acta* **1999**, *1462*, 71-87.

5. Dennison, S.R.; Wallace, J.; Harris, F.; Phoenix, D.A. Amphiphilic alpha-helical antimicrobial peptides and their structure/function relationships. *Protein Pept. Lett*. **2005**, *12*, 31-39.

6. Huang, Y.; Huang, J.; Chen. Y. Alpha-helical cationic antimicrobial peptides: relationships of structure and function. *Protein Cell* **2010**, *1*, 143-152.

7. McKay, M.J.; Afrose, F.; Koeppe, R.E. 2nd; Greathouse, D.V. Helix formation and stability in membranes. *Biochim. Biophys. Acta Biomembr*. **2018**, *1860*, 2108-2117.

8. Islam, M.M.; Asif, F.; Zaman, S.U.; Arnab, M.K.H.; Rahman, M.M.; Hasan, M. Effect of charge on the antimicrobial activity of alpha-helical amphibian antimicrobial peptide. *Curr. Res. Microb. Sci*. **2023**, *4*, 100182.

9. Tossi, A.; Sandri, L.; Giangaspero, A. Amphipathic, alpha-helical antimicrobial peptides. *Biopolymers* **2000**, *55*, 4-30.

10. Zelezetsky, I.; Tossi, A. Alpha-helical antimicrobial peptides - Using a sequence template to guide structure-activity relationship studies. *Biochim. Biophys. Acta* **2006**, *1758*, 1436-1449.

11. Beevers, A.J.; Dixon A.M. Helical membrane peptides to modulate cell function. *Chem. Soc. Rev*. **2010**, *39*, 2146-2157.

12. Phuong, H.B.T.; Ngan, H.D.; Huy, B.L.; Dinh, H.V.; Xuan, H.L. The amphipathic design in helical antimicrobial peptides. *ChemMedChem* **2024**, *19*, e202300480.

13. Goldman, M.J.; Anderson, G.M.; Stolzenberg, E.D.; Kari, U.P.; Zasloff, M.; Wilson, J.M. Human beta-defensin-1 is a salt-sensitive antibiotic in lung that is inactivated in cystic fibrosis. *Cell* **1997**, *88*, 553-560.

14. Lee, I.H.; Cho, Y.; Lehrer, R.I. Effects of pH and salinity on the antimicrobial properties of clavanins. *Infect. Immun*. **1997**, *65*, 2898-2903.

15. Kandasamy, S.K.; Larson, R.G. Effect of salt on the interactions of antimicrobial peptides with zwitterionic lipid bilayers. *Biochim. Biophys. Acta* **2006**, *1758*, 1274-1284.

16. Strazzullo, P.; Leclercq, C. Sodium. *Adv. Nutr*. **2014**, *5*, 188-190.

17. Son, M.; Lee, Y.S.; Lee, M.J.; Park, Y.; Bae, H.R.; Lee, S.Y.; Shin, M.G.; Yang, S. Effects of osmolality and solutes on the morphology of red blood cells according to three-dimensional refractive index tomography. *PLoS One* **2021**, *16*, e0262106.

18. Vishwakarma, M.; Agrawal, P.; Soni, S.; Tomar, S.; Haider, T.; Kashaw, S.K.; Soni, V. Cationic nanocarriers: A potential approach for targeting negatively charged cancer cell. *Adv. Colloid Interface Sci*. **2024**, *327*, 103160.

19. Szlasa, W.; Zendran, I.; Zalesińska, A.; Tarek, M.; Kulbacka, J. Lipid composition of the cancer cell membrane. *J. Bioenerg. Biomembr*. **2020**, *52*, 321-342.

20. Tornesello, A.L.; Borrelli, A.; Buonaguro, L.; Buonaguro, F.M.; Tornesello, M.L. Antimicrobial Peptides as Anticancer Agents: Functional Properties and Biological Activities. *Molecules* **2020**, *25*, 2850.

21. Jambunathan, K.; Galande, A.K. Sample collection in clinical proteomics-proteolytic activity profile of serum and plasma. *Proteomics Clin. Appl*. **2014**, *8*, 299-307.

22. Koutedakis, Y.; Raafat, A.; Sharp, N.C.; Rosmarin, M.N.; Beard, M.J.; Robbins, S.W. Serum enzyme activities in individuals with different levels of physical fitness. *J. Sports Med. Phys. Fitness* **1993**, *33*, 252-257.

23. Sandín, D.; Valle, J.; Chaves-Arquero, B.; Prats-Ejarque, G.; Larrosa, M.N.; González-López, J.J.; Jiménez, M.Á.; Boix, E.; Andreu, D.; Torrent, M. Rationally Modified Antimicrobial Peptides from the N-Terminal Domain of Human RNase 3 Show Exceptional Serum Stability. *J. Med. Chem*. **2021**, *64*, 11472-11482.

24. Knappe, D.; Henklein, P.; Hoffmann, R.; Hilpert, K. Easy strategy to protect antimicrobial peptides from fast degradation in serum. *Antimicrob. Agents Chemother*. **2010**, *54*, 4003-4005.

25. Caporale, A.; Adorinni, S.; Lamba, D.; Saviano, M. Peptide-Protein Interactions: From Drug Design to Supramolecular Biomaterials. *Molecules* **2021**, *26*, 1219.

26. Kotynia, A.; Marciniak, A.; Kamysz, W.; Neubauer, D.; Krzyżak, E. Interaction of Positively Charged Oligopeptides with Blood Plasma Proteins. *Int J. Mol. Sci*. **2023**, *24*, 2836.

27. Boulos, L.; Prévost, M.; Barbeau, B.; Coallier, J.; Desjardins, R. LIVE/DEAD BacLight: application of a new rapid staining method for direct enumeration of viable and total bacteria in drinking water. *J. Microbiol. Methods*. **1999**, *37*, 77-86.

28. Helander, I.M.; Mattila-Sandholm, T. Fluorometric assessment of gram-negative bacterial permeabilization. *J. Appl. Microbiol*. **2000**, *88*, 213-219.

29. Helander, I.M.; Mattila-Sandholm, T. Permeability barrier of the gram-negative bacterial outer membrane with special reference to nisin. *Int. J. Food Microbiol*. **2000**, *60*, 153-161.

30. Sun, J.; Rutherford, S.T.; Silhavy, T.J.; Huang, K.C. Physical properties of the bacterial outer membrane. *Nat. Rev. Microbiol*. **2022**, *20*, 236-248.

31. Garcia-Rubio, R.; de Oliveira, H.C.; Rivera, J.; Trevijano-Contador, N. The Fungal Cell Wall: *Candida*, *Cryptococcus*, and *Aspergillus* Species. *Front. Microbiol*. **2020**, *10*, 2993.

32. Winkel, J.D.T.; Gray, D.A.; Seistrup, K.H.; Hamoen, L.W.; Strahl, H. Analysis of Antimicrobial-Triggered Membrane Depolarization Using Voltage Sensitive Dyes. *Front. Cell Dev. Biol*. **2016**, *4*, 9.

33. Cheng, M.; Huang, J.X.; Ramu, S.; Butler, M.S.; Cooper, M.A. Ramoplanin at bactericidal concentrations induces bacterial membrane depolarization in Staphylococcus aureus. *Antimicrob. Agents Chemother*. **2014**, *58*, 6819-6827.

34. Benfield, A.H.; Henriques, S.T. Mode-of-Action of Antimicrobial Peptides: Membrane Disruption vs. Intracellular Mechanisms. *Front. Med. Technol*. **2020**, *2*, 610997.

35. Plemel, J.R.; Caprariello, A.V.; Keough, M.B.; Henry, T.J.; Tsutsui, S.; Chu, T.H.; Schenk, G.J.; Klaver, R.; Yong, V.W.; Stys, P.K. Unique spectral signatures of the nucleic acid dye acridine orange can distinguish cell death by apoptosis and necroptosis. *J. Cell Biol*. **2017**, *216*, 1163-1181.

36. Crowley, L.C.; Scott, A.P.; Marfell, B.J.; Boughaba, J.A.; Chojnowski, G.; Waterhouse, N.J. Measuring Cell Death by Propidium Iodide Uptake and Flow Cytometry. *Cold Spring Harb. Protoc.* **2016**, *2016*.

37. Hussain, H.; L., R.S., Ahmad, S.; Razak, M.F.A., Wan Mohamud, W. N.W., Bakar, J.; Ghazali, H.M.; Yildiz, F. Determination of cell viability using acridine orange/propidium iodide dual-spectrofluorometry assay. *Cogent Food & Agriculture* **2019**, *5*, 1582398.

38. Pandit, G.; Ilyas, H.; Ghosh, S.; Bidkar, A.P.; Mohid, S.A.; Bhunia, A.; Satpati, P.; Chatterjee, S. Insights into the Mechanism of Antimicrobial Activity of Seven-Residue Peptides. *J. Med. Chem.* **2018**, *61*, 7614-7629.

39. Pandit, G.; Sarkar, T.; S., R. V.; Debnath, S.; Satpati, P.; Chatterjee, S. Delineating the Mechanism of Action of a Protease Resistant and Salt Tolerant Synthetic Antimicrobial Peptide against *Pseudomonas aeruginosa*. *ACS Omega* **2022**, *7*, 15951-15968.

40. Pandit, G.; Biswas, K.; Ghosh, S.; Debnath, S.; Bidkar, A.P.; Satpati, P.; Bhunia, A.; Chatterjee, S. Rationally designed antimicrobial peptides: Insight into the mechanism of eleven residue peptides against microbial infections. *Biochim. Biophys. Acta Biomembr*. **2020**, *1862*, 183177.

41. Pandit, G.; Chowdhury, N.; Mohid, S.A.; Bidkar, A.P.; Bhunia, A.; Chatterjee, S. Effect of Secondary Structure and Side Chain Length of Hydrophobic Amino Acid Residues on the Antimicrobial Activity and Toxicity of 14-Residue-Long de novo AMPs. *ChemMedChem*. **2021**, *16*, 355-367.

42. Sohlenkamp, C.; Geiger, O. Bacterial membrane lipids: diversity in structures and pathways. *FEMS Microbiol. Rev*. **2016**, *40*, 133-159.

43. Gow, N.A.R.; Latge, J.P.; Munro, C.A. The Fungal Cell Wall: Structure, Biosynthesis, and Function. *Microbiol. Spectr*. **2017**, *5*.

44. Schrödinger, L.L.C. The PyMOL Molecular Graphics System, Version 3.1.

45. Cheng, X.; Jo, S.; Lee, H.S.; Klauda, J.B.; Im, W. CHARMM-GUI micelle builder for pure/mixed micelle and protein/micelle complex systems. *J. Chem. Inf. Model*. **2013**, *53*, 2171-2180.

46. Wu, E.L.; Cheng, X.; Jo, S.; Rui, H.; Song, K.C.; Dávila-Contreras, E.M.; Qi, Y.; Lee, J.; Monje-Galvan, V.; Venable, R.M.; Klauda, J.B.; Im, W. CHARMM-GUI Membrane Builder toward realistic biological membrane simulations. *J. Comput. Chem*. **2014**, *35*, 1997-2004.

47. Wang, Q.; Hong, G.; Johnson, G.R.; Pachter, R.; Cheung, M.S. Biophysical properties of membrane-active peptides based on micelle modeling: a case study of cell-penetrating and antimicrobial peptides. *J. Phys. Chem. B*. **2010**, *114*, 13726-13735.

48. Pogozheva, I.D.; Armstrong, G.A.; Kong, L.; Hartnagel, T.J.; Carpino, C.A.; Gee, S.E.; Picarello, D.M.; Rubin, A.S.; Lee, J.; Park, S.; Lomize, A.L.; Im, W. Comparative Molecular Dynamics Simulation Studies of Realistic Eukaryotic, Prokaryotic, and Archaeal Membranes. *J. Chem. Inf. Model*. **2022**, *62*, 1036-1051.

49. Rice, A.; Rooney, M.T.; Greenwood, A.I.; Cotton, M.L.; Wereszczynski, J. Lipopolysaccharide Simulations Are Sensitive to Phosphate Charge and Ion Parameterization. *J. Chem. Theory Comput*. **2020**, *16*, 1806-1815.

50. Spoel, D.V.D.; Lindahl, E.; Hess, B.; Groenhof, G.; Mark, A.E.; Berendsen, H.J. GROMACS: fast, flexible, and free. *J. Comput. Chem*. **2005**, *26*, 1701-1718.

51. Huang, J.; Rauscher, S.; Nawrocki, G.; Ran, T.; Feig, M.; de Groot, B.L.; Grubmüller, H.; MacKerell, A.D. Jr.; CHARMM36m: an improved force field for folded and intrinsically disordered proteins. *Nat. Methods*. **2017**, *14*, 71-73.

52. Jorgensen, W.L.; Chandrasekhar, J.; Madura, J.D.; Impey, R.W.; Klein, W.L. Comparison of simple potential functions for simulating liquid water. *J. Chem. Phys.* **1983**, *79*, 926-935.

Chapter 7: Future Prospects

Several drawbacks of the naturally occurring antimicrobial peptides (AMPs) have been addressed through the development of the synthetic AMPs reported in this thesis, like that of protease susceptibility, serum instability, salt-sensitivity, cytotoxicity, hemolytic activity and high costs of production. Protease susceptibility and serum instability of the peptides were addressed through the design of peptides with D-amino acids and unnatural amino acids as the building blocks. The designed peptides that have been reported in all the chapters were non-cytotoxic and non-hemolytic within their microbicidal concentrations and displayed good salt-resistance. The economic viability of the peptides was considered through design of short or ultra-short peptides. Though we have been able to develop a host of potential AMPs in this thesis, a substantial amount of work needs to be done in the future for being able to translate these molecules to commercial applications.

Following are a few areas which remains to be investigated in the future:

- Although, we have screened the designed AMPs against the drug-resistant strain of methicillin-resistant *Staphylococcus aureus* (MRSA), these peptides should be screened against other drug-/multidrug-resistant strains like Vancomycin-resistant Enterococci (VRE), Carbapenem-resistant Enterobacteriaceae (CRE), Carbapenem-resistant *Pseudomonas aeruginosa* (CRPA), Multidrug-resistant *Mycobacterium tuberculosis* (MDR-TB) etc.
- The rate of resistance development against these peptides in different microbial strains should be studied in details in the future.
- Although, the designed AMPs screened in our studies were highly active *in vitro*, their *in vivo* efficiency in clearing pathogenic infections and safety against the hosts' cells should be evaluated thoroughly using animal model studies e.g., in mouse models of infections.
- Also, their pharmacokinetics and clearance from the animal system should be investigated thoroughly.
- The mode of administration of these peptides (tropical, oral, intravenous or direct administration at the site) should be evaluated using animal model studies.
- Indirect mode of action of these peptides (if any) should be investigated in the future studies, through study of their immunomodulatory effects like that of cytokines production, immune cell activation etc.

Appendix

Appendix A (for Chapter 2)

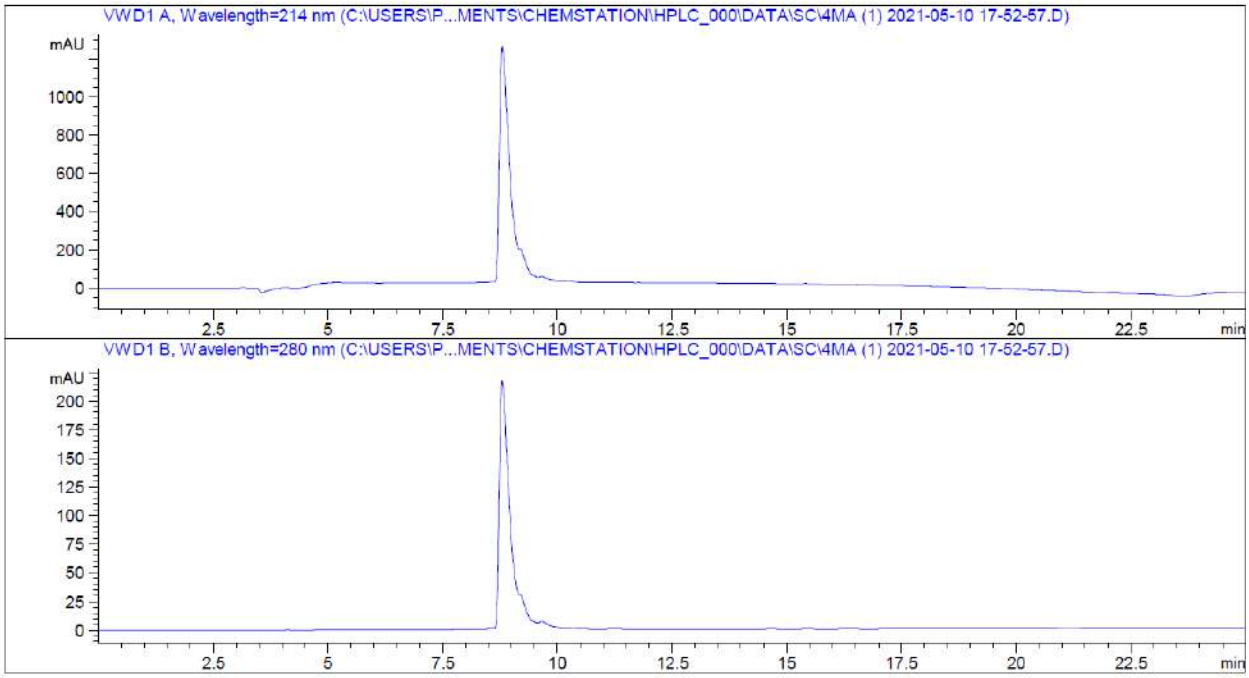

Figure A1. HPLC chromatogram of **P4A** at 214 nm and 280 nm. Retention time: 8.78 min. Percentage purity: 98.44 %.

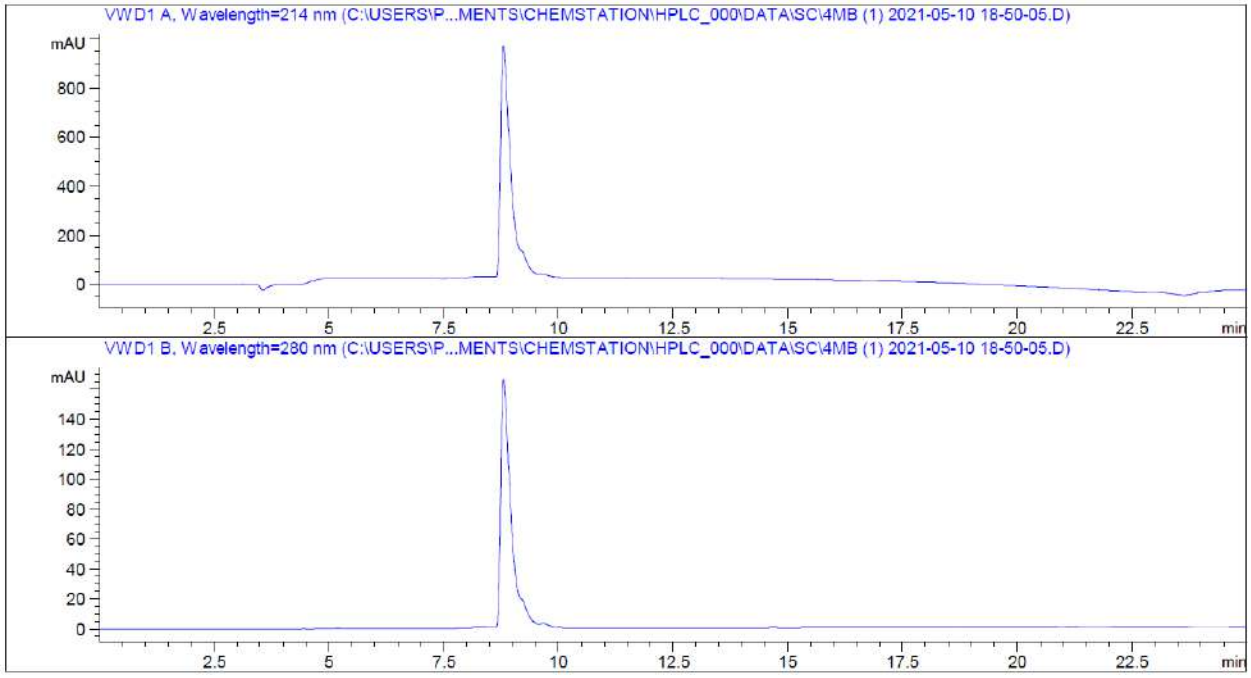

Figure A2. HPLC chromatogram of **P4B** at 214 nm and 280 nm. Retention time: 8.80 min. Percentage purity: 97.60%.

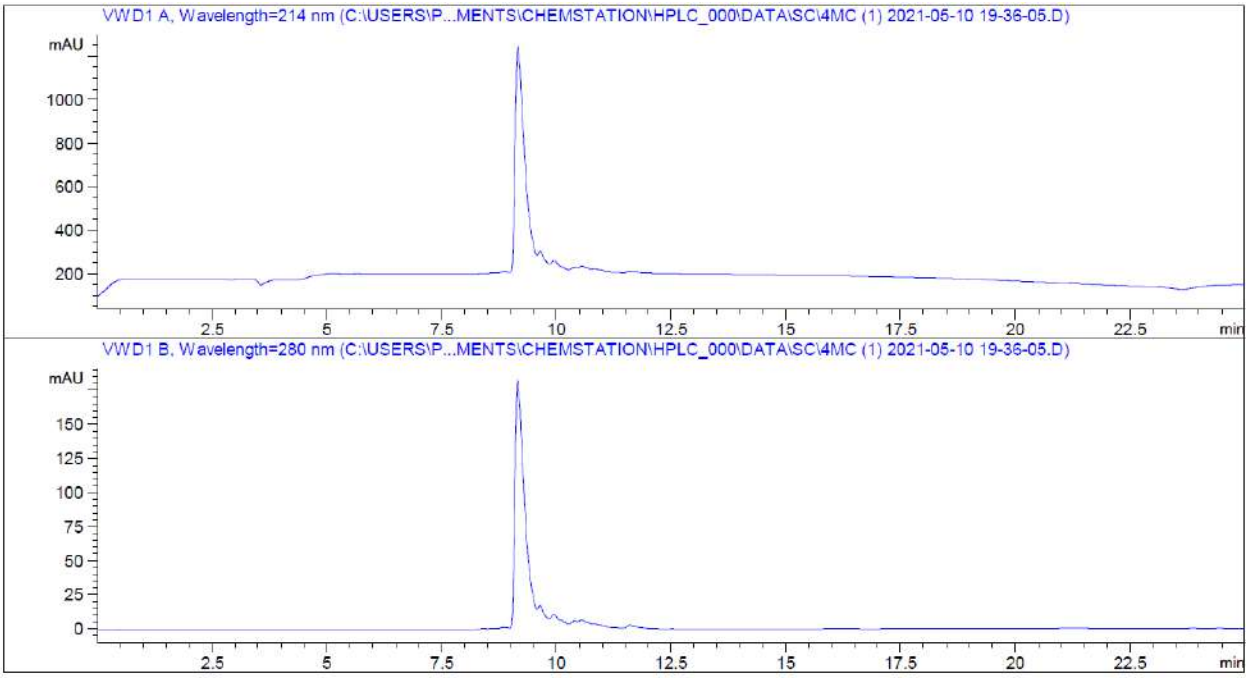

Figure A3. HPLC chromatogram of **P4C** at 214 nm and 280 nm. Retention time: 9.17 min. Percentage purity: 96.32%.

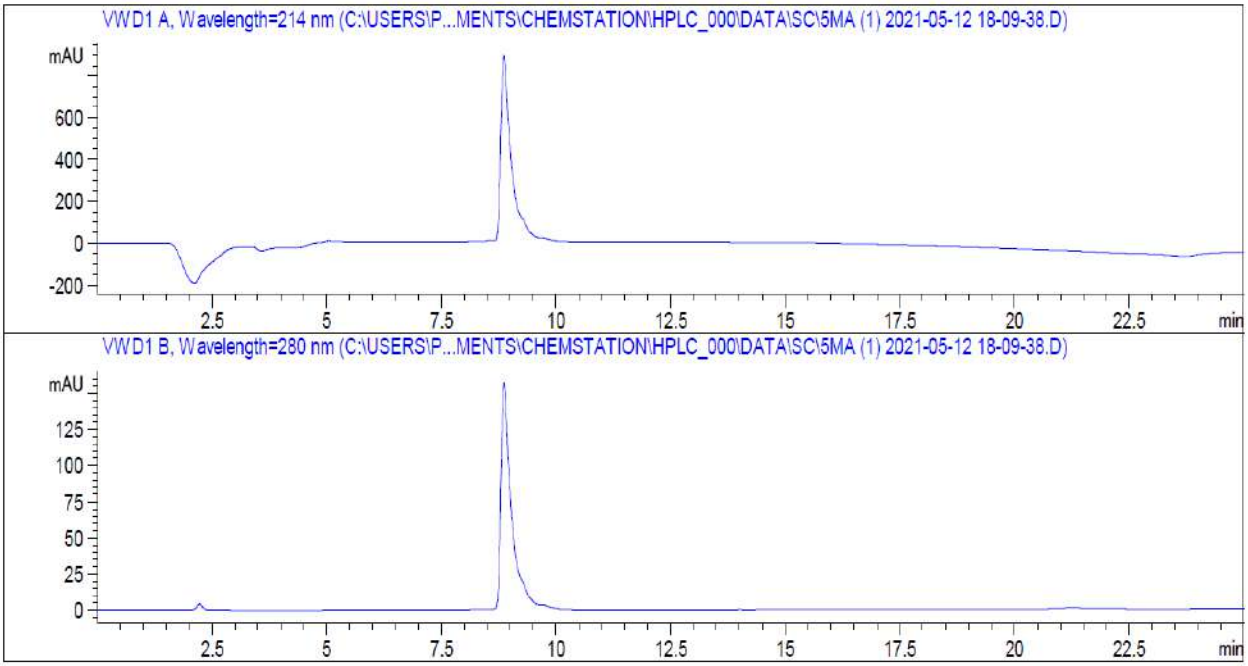

Figure A4. HPLC chromatogram of **P5A** at 214 nm and 280 nm. Retention time: 8.86 min. Percentage purity: 99.12%.

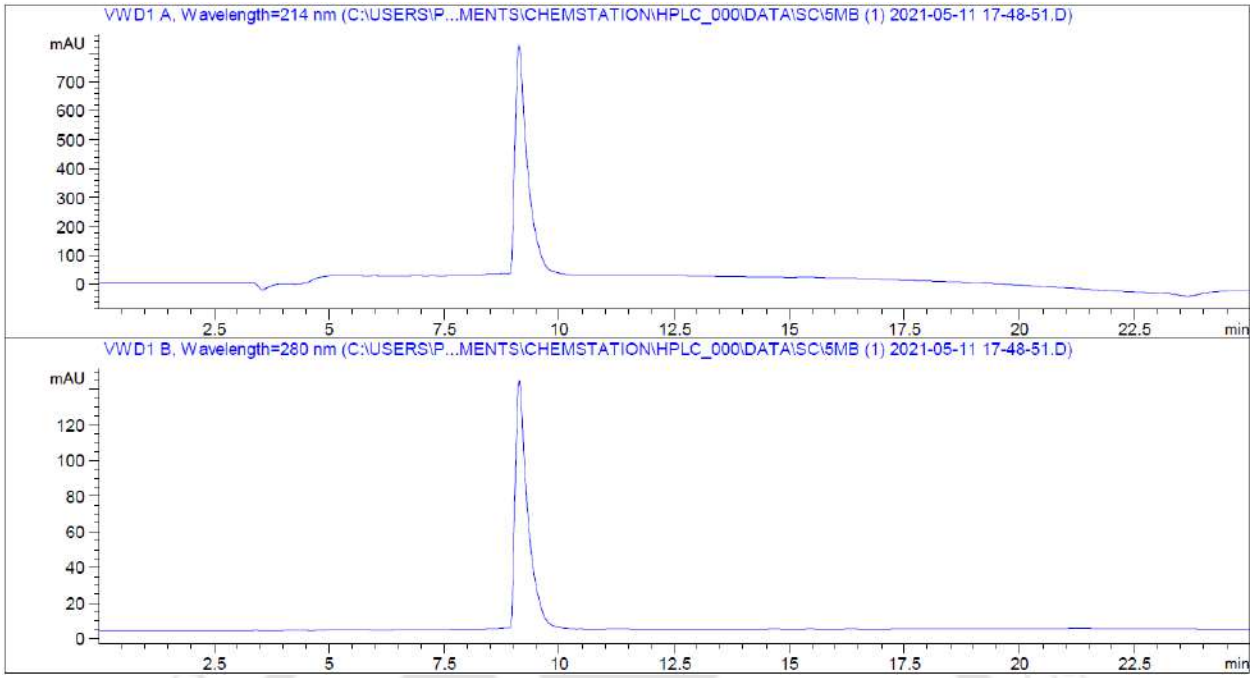

Figure A5. HPLC chromatogram of **P5B** at 214 nm and 280 nm. Retention time: 9.13 min. Percentage purity: 98.28%.

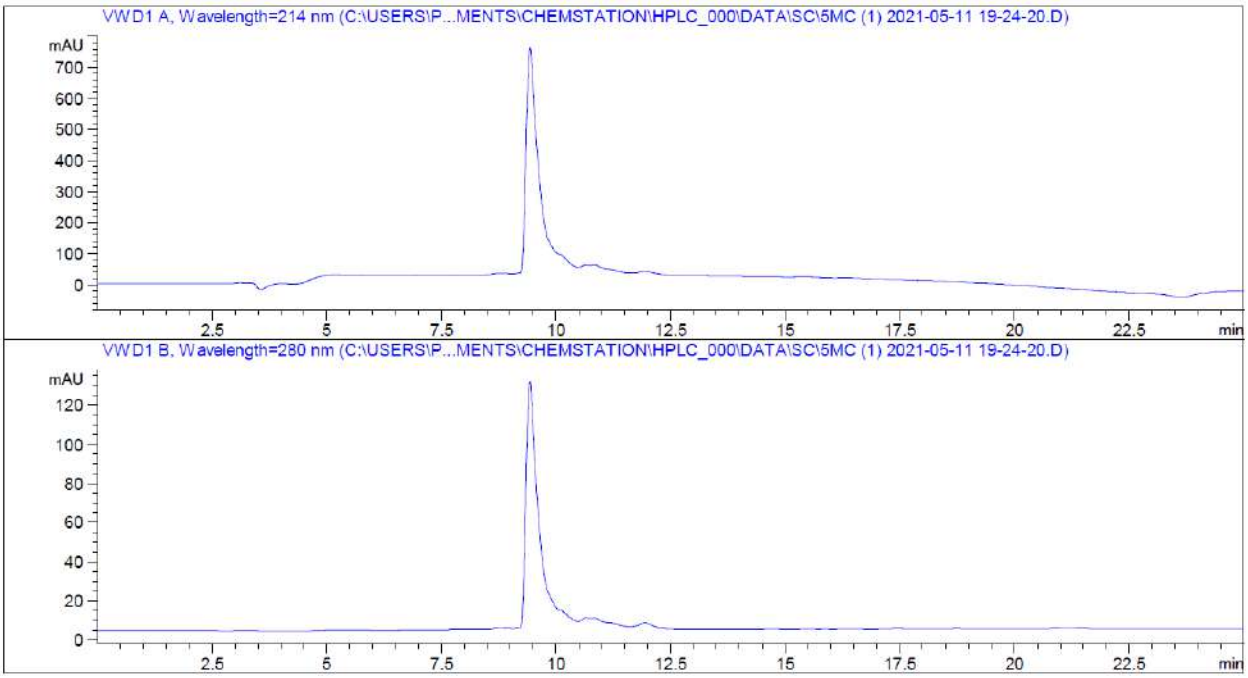

Figure A6. HPLC chromatogram of **P5C** at 214 nm and 280 nm. Retention time: 9.43 min. Percentage purity: 97.73%.

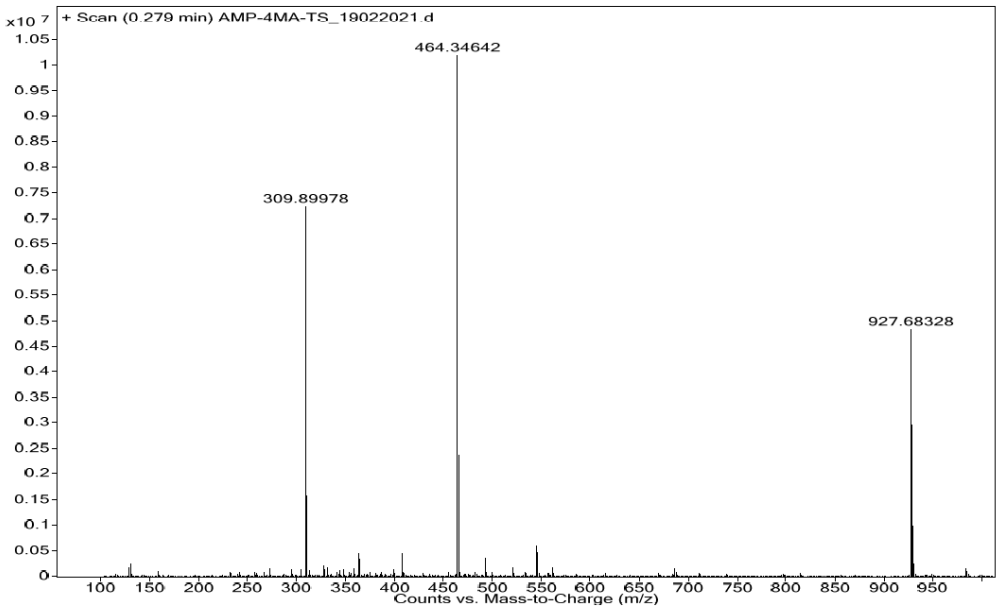

Figure A7. ESI-mass spectra of **P4A**. Expected mass $[M+H]^+$: 927.6502 Da; 927.6832 Da corresponds to $[M+H]^+$; 464.3464 Da corresponds to $[M+2H]^{2+}$; 309.8997 Da corresponds to $[M+3H]^{3+}$.

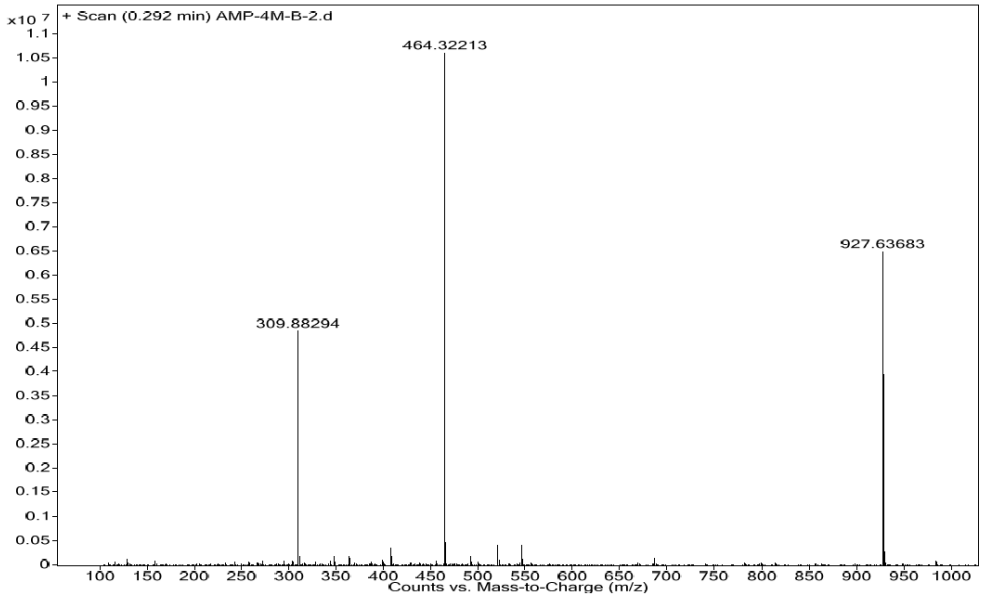

Figure A8. ESI-mass spectra of **P4B**. Expected mass $[M+H]^+$: 927.6502 Da; 927.6368 Da corresponds to $[M+H]^+$; 464.3221 Da corresponds to $[M+2H]^{2+}$; 309.8829 Da corresponds to $[M+3H]^{3+}$.

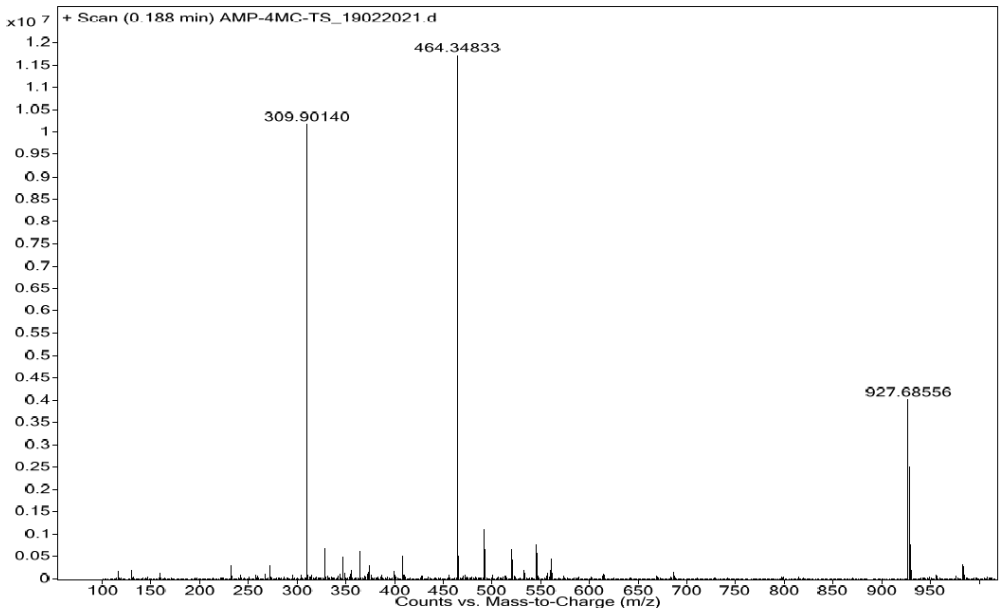

Figure A9. ESI-mass spectra of **P4C**. Expected mass $[M+H]^+$: 927.6502 Da; 927.6855 Da corresponds to $[M+H]^+$; 464.3483 Da corresponds to $[M+2H]^{2+}$; 309.9014 Da corresponds to $[M+3H]^{3+}$.

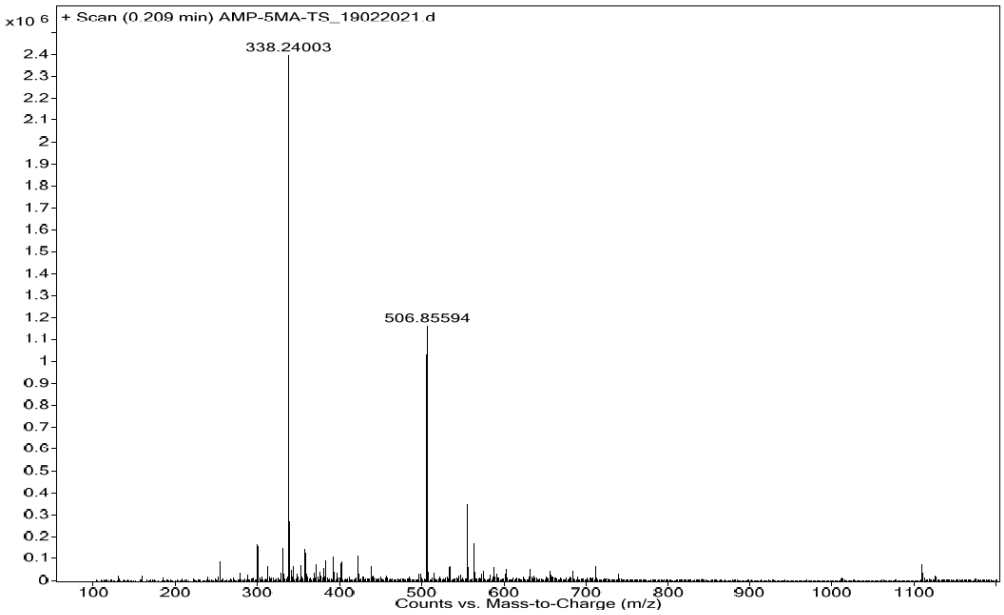

Figure A10. ESI-mass spectra of **P5A**. Expected mass $[M+H]^+$: 1011.6687 Da; 506.8559 Da corresponds to $[M+2H]^{2+}$; 338.2400 Da corresponds to $[M+3H]^{3+}$.

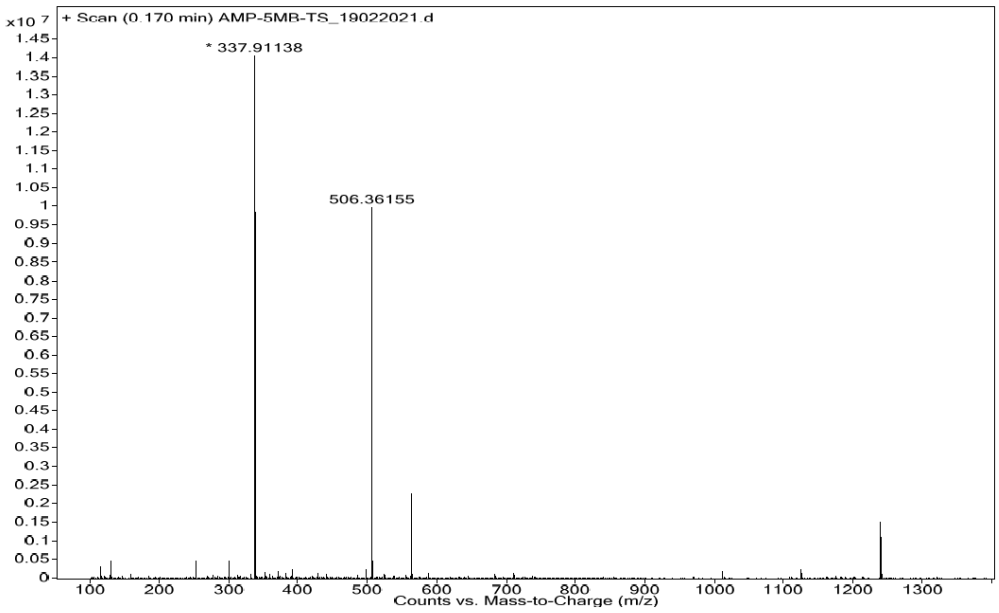

Figure A11. ESI-mass spectra of **P5B**. Expected mass $[M+H]^+$: 1011.6687 Da; 506.3615 Da corresponds to $[M+2H]^{2+}$; 337.9113 Da corresponds to $[M+3H]^{3+}$.

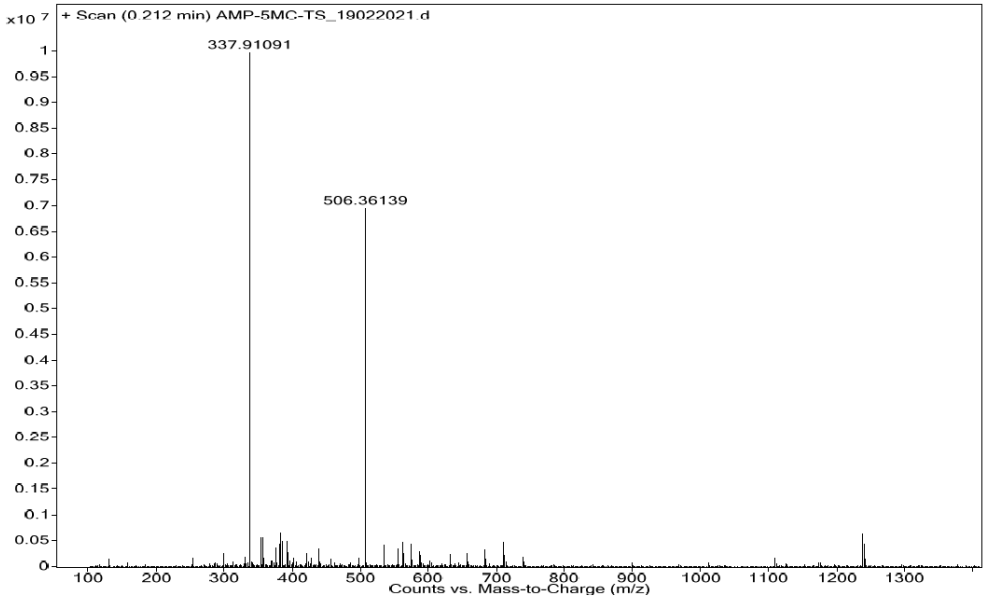

Figure A12. ESI-mass spectra of **P5C**. Expected mass $[M+H]^+$: 1011.6687 Da; 506.3613 Da corresponds to $[M+2H]^{2+}$; 337.9109 Da corresponds to $[M+3H]^{3+}$.

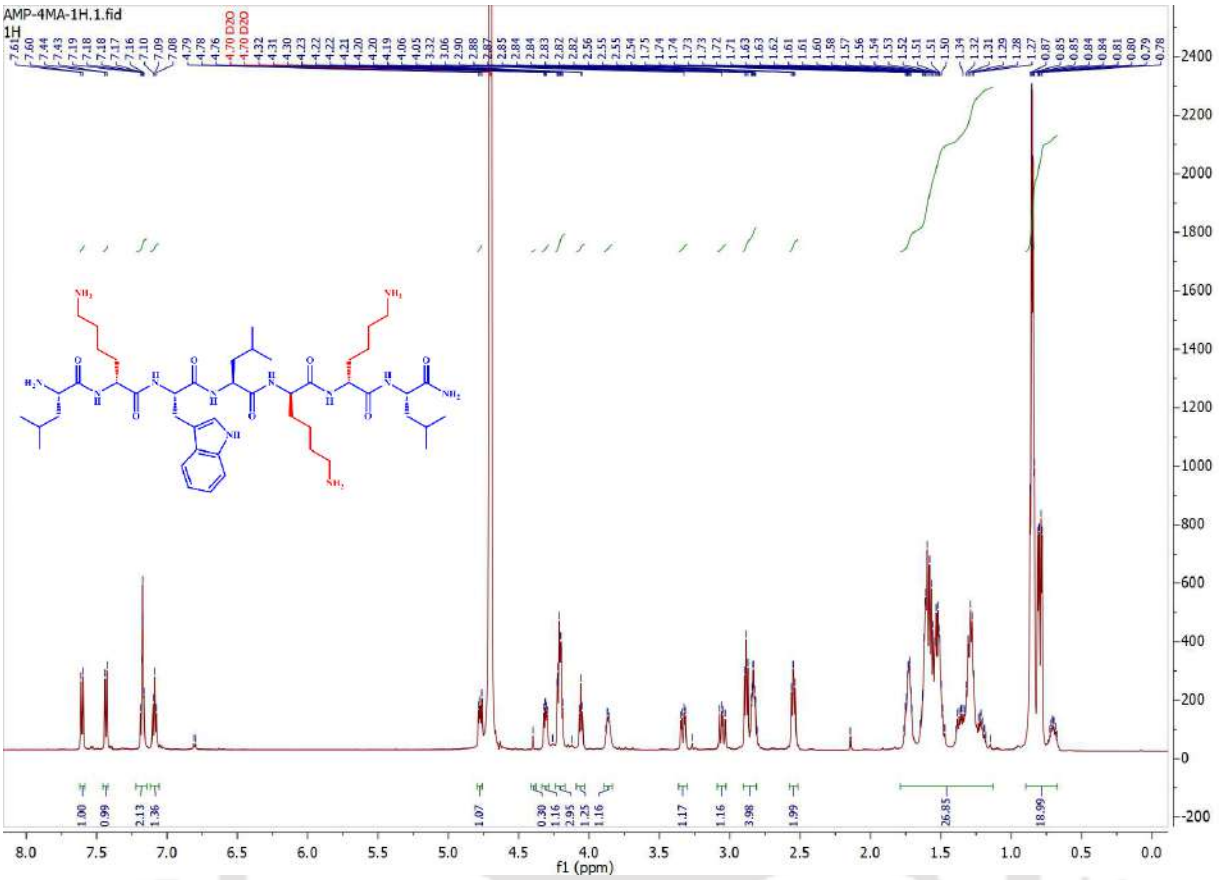

Figure A13. ^{1}H NMR spectra of **P4A** at a concentration of 10 mM at room temperature in D_2O. ^{1}H NMR (600 MHz, D_2O) δ 0.67-0.90 (m, 18H, Leucine), δ 1.14-1.79 (m, 27H, Leucine and Lysine), δ 2.53-3.38 (m, 8H, Lysine and Tryptophan), δ 3.84-4.80 (7 αH), 7.11-7.63 (5H, Tryptophan).

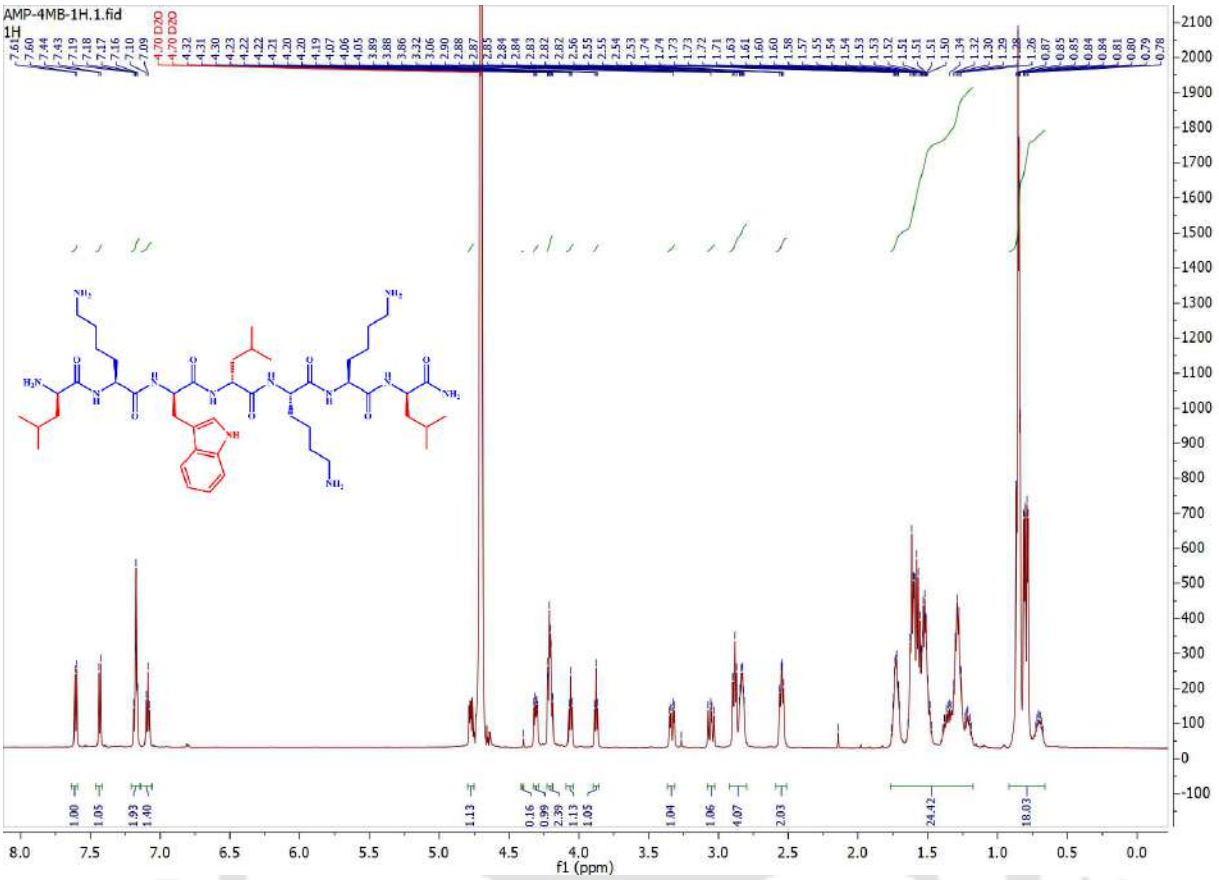

Figure A14. ^{1}H NMR spectra of **P4B** at a concentration of 10 mM at room temperature in D_2O. ^{1}H NMR (600 MHz, D_2O) δ 0.67-0.91 (m, 18H, Leucine), δ 1.18-1.78 (m, 27H, Leucine and Lysine), δ 2.50-3.38 (m, 8H, Lysine and Tryptophan), δ 3.86-4.80 (7 αH), 7.07-7.63 (5H, Tryptophan).

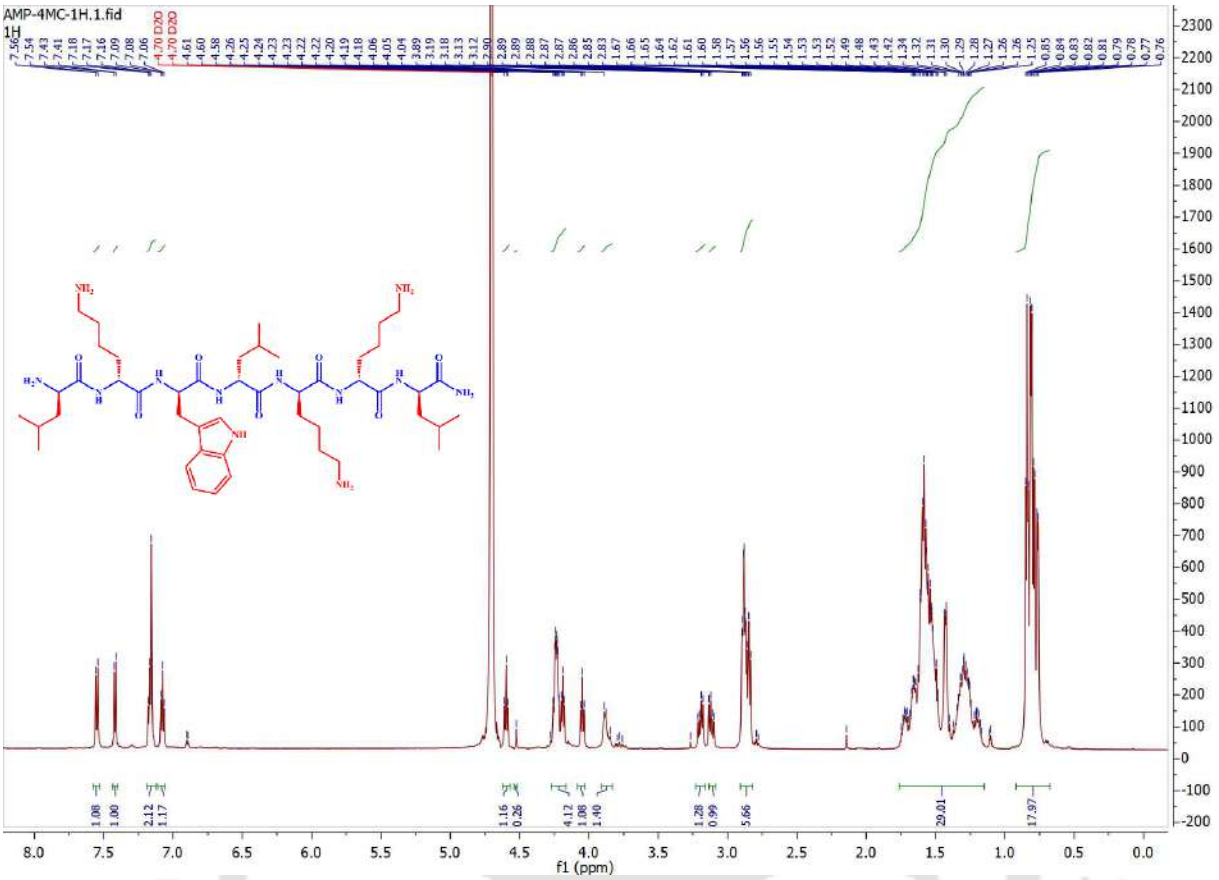

Figure A15. ^{1}H NMR spectra of **P4C** at a concentration of 10 mM at room temperature in D_2O. ^{1}H NMR (600 MHz, D_2O) δ 0.68-0.92 (m, 18H, Leucine), δ 1.15-1.76 (m, 27H, Leucine and Lysine), δ 2.82-3.23 (m, 8H, Lysine and Tryptophan), δ 3.84-4.62 (7 αH), 7.06-7.58 (5H, Tryptophan).

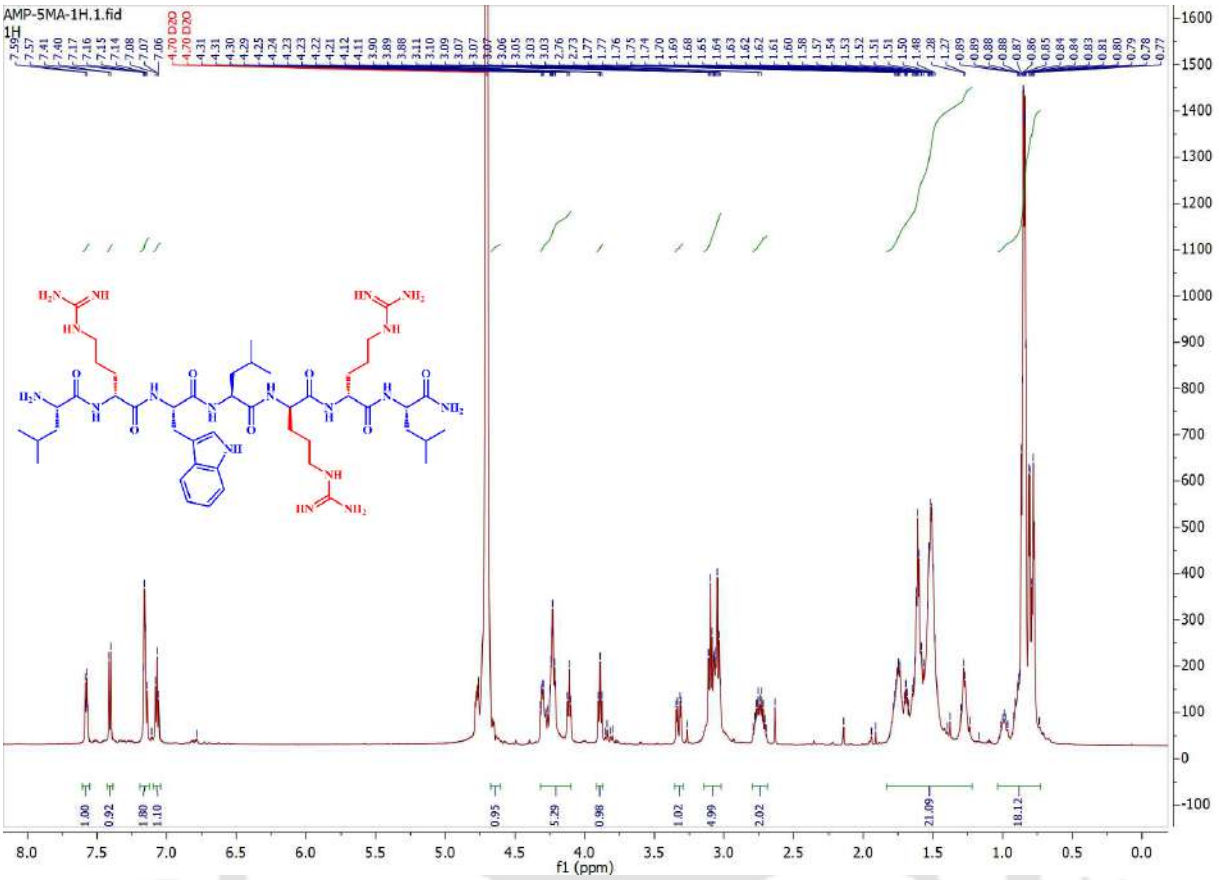

Figure A16. ^{1}H NMR spectra of **P5A** at a concentration of 10 mM at room temperature in D_2O. ^{1}H NMR (600 MHz, D_2O) δ 0.73-1.03 (m, 18H, Leucine), δ 1.23-1.82 (m, 21H, Leucine and Arginine), δ 2.68-3.34 (m, 8H, Arginine and Tryptophan), δ 3.86-4.67 (7 αH), 7.05-7.60 (5H, Tryptophan).

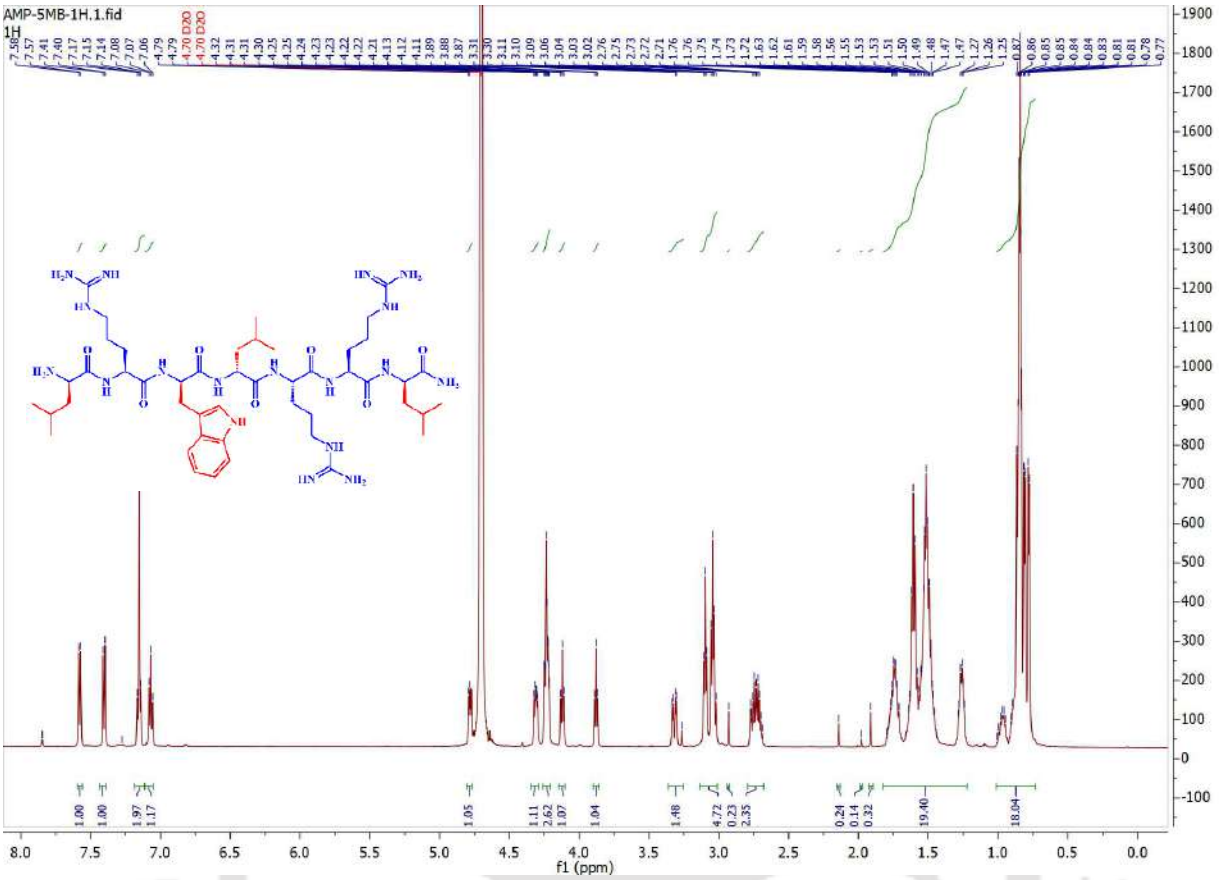

Figure A17. ^{1}H NMR spectra of **P5B** at a concentration of 10 mM at room temperature in D_2O. ^{1}H NMR (600 MHz, D_2O) δ 0.72-1.01 (m, 18H, Leucine), δ 1.22-1.83 (m, 21H, Leucine and Arginine), δ 2.68-3.36 (m, 8H, Arginine and Tryptophan), δ 3.86-4.81 (7 αH), 7.08-7.59 (5H, Tryptophan).

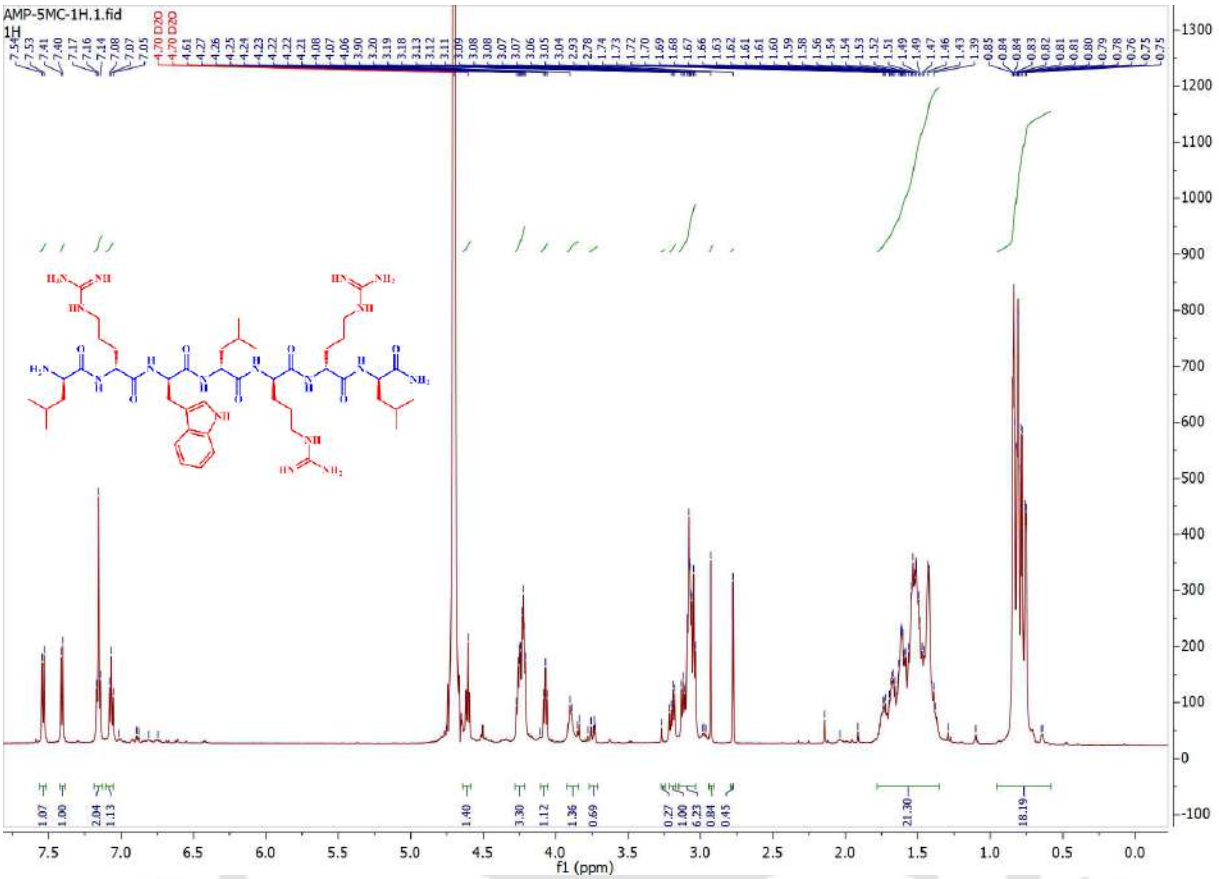

Figure A18. ^{1}H NMR spectra of **P5C** at a concentration of 10 mM at room temperature in D_2O. ^{1}H NMR (600 MHz, D_2O) δ 0.58-0.96 (m, 18H, Leucine), δ 1.35-1.78 (m, 21H, Leucine and Arginine), δ 2.77-3.27 (m, 8H, Arginine and Tryptophan), δ 3.71-4.65 (7 αH), 7.06-7.58 (5H, Tryptophan).

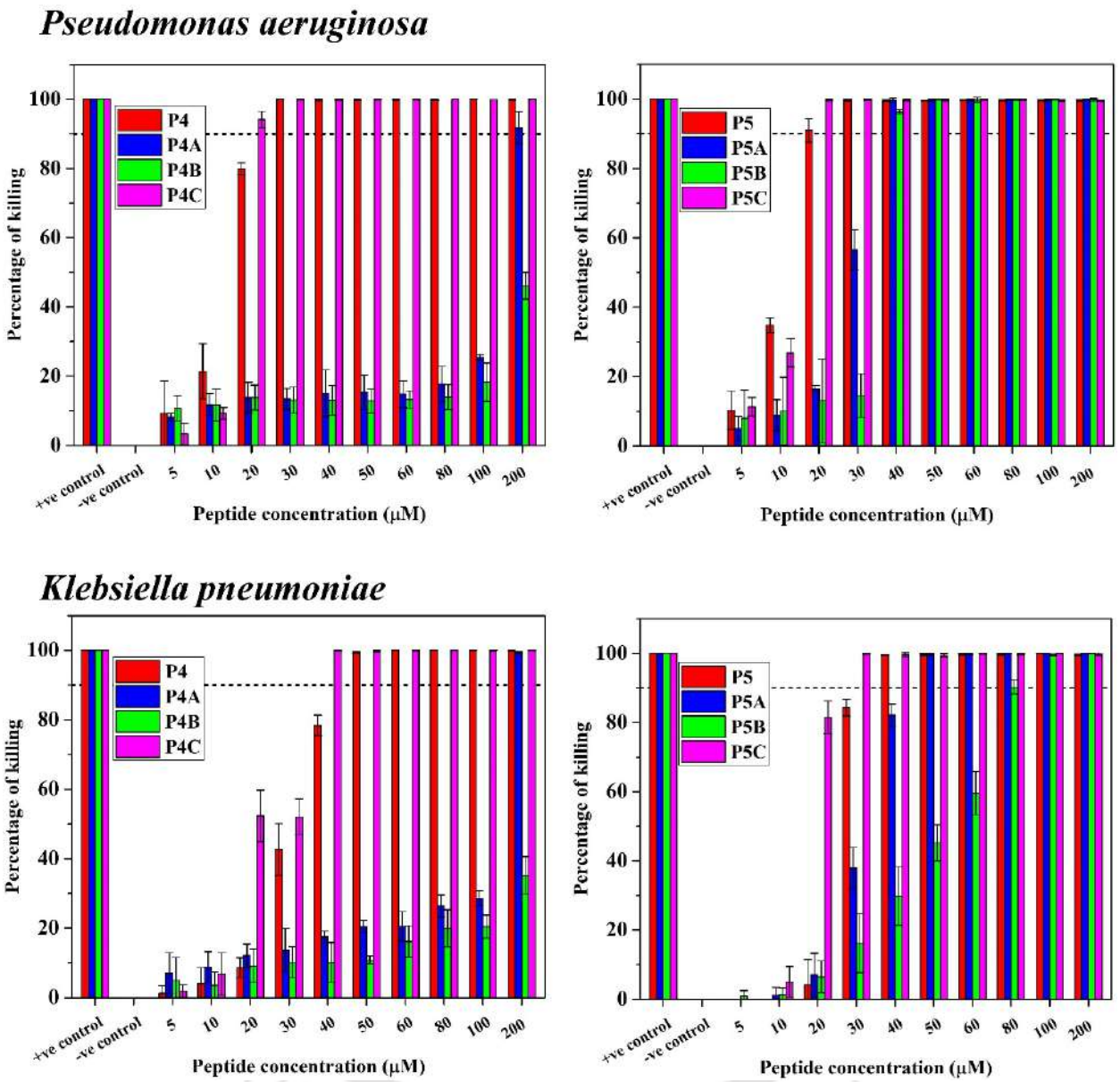

Figure A19. MIC of the peptides **P4**, **P4A**, **P4B**, **P4C**, **P5**, **P5A**, **P5B**, **P5C** against *P. aeruginosa* and *K. pneumoniae*. 90% killing of the microbes is denoted by a broken dashed line.

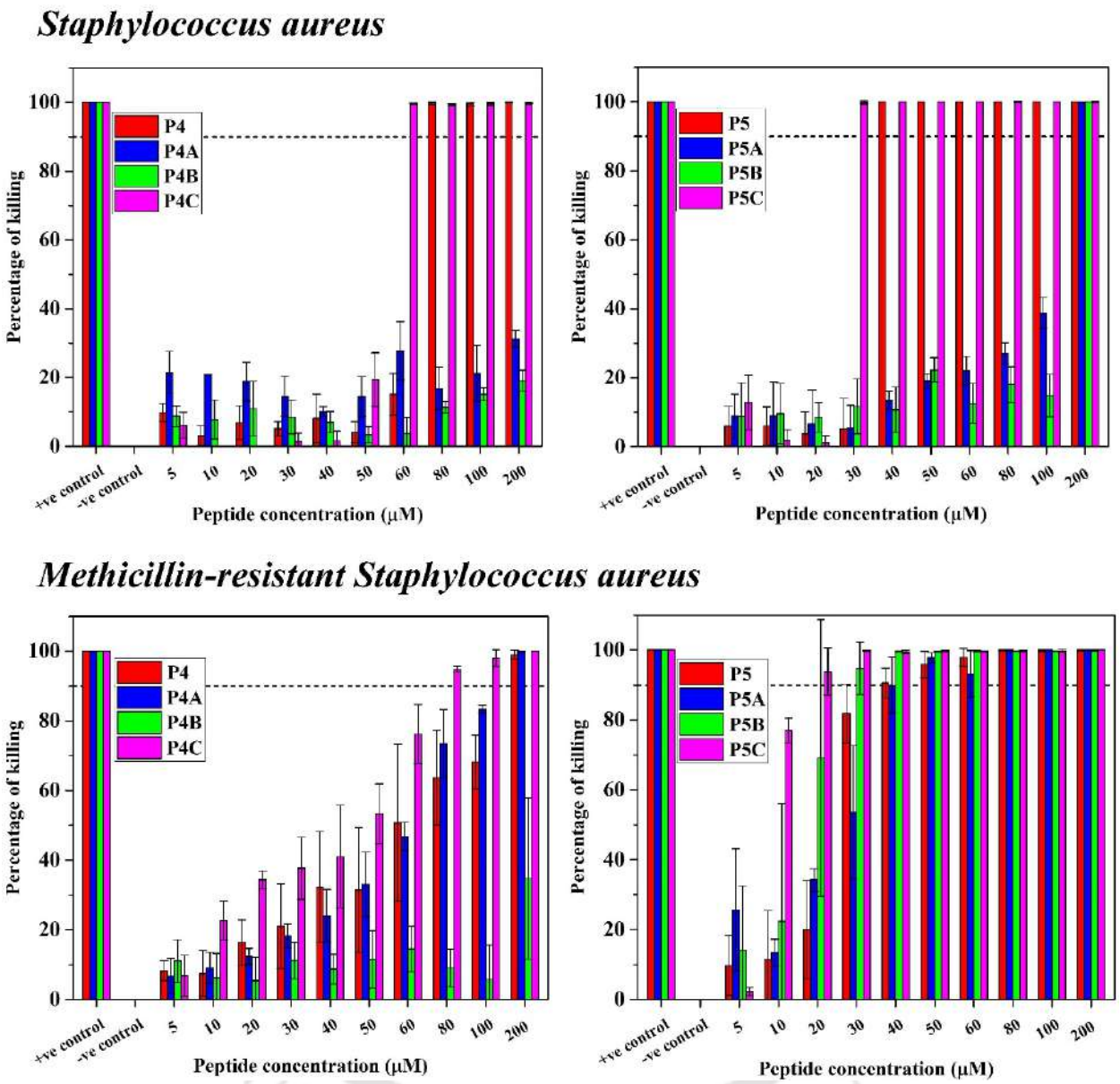

Figure A20. MIC of the peptides **P4**, **P4A**, **P4B**, **P4C**, **P5**, **P5A**, **P5B**, **P5C** against *S. aureus* and *Methicillin-resistant S. aureus.* 90% killing of the microbes is denoted by a broken dashed line.

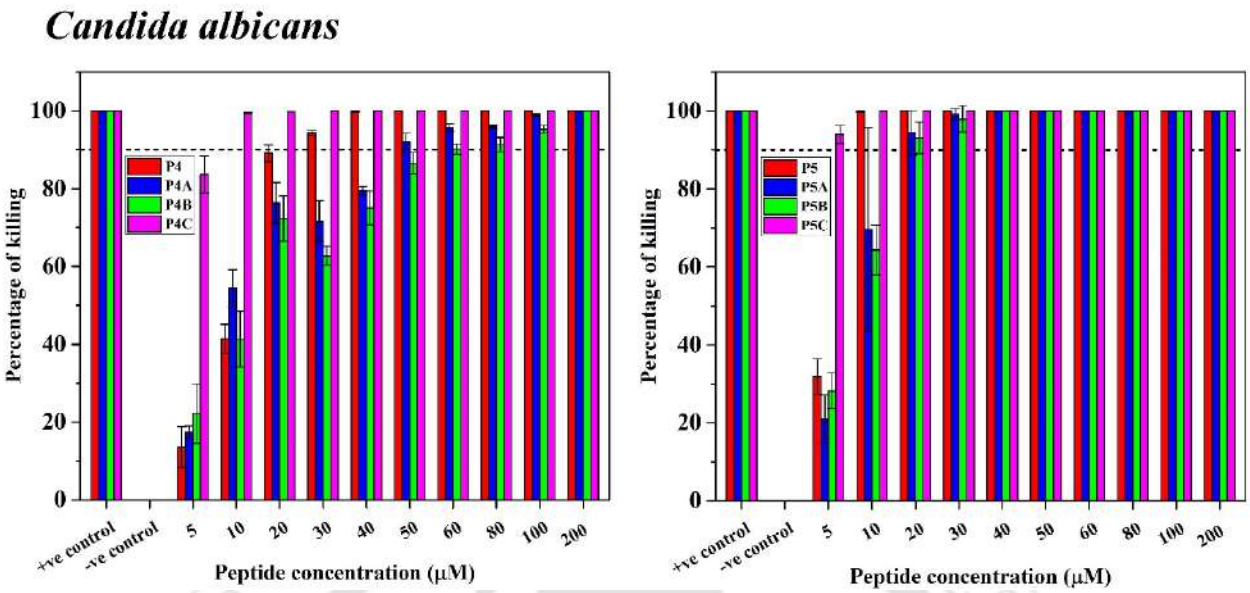

Figure A21. MIC of the peptides **P4**, **P4A**, **P4B**, **P4C**, **P5**, **P5A**, **P5B**, **P5C** against *C. albicans*. 90% killing of the microbes is denoted by a broken dashed line.

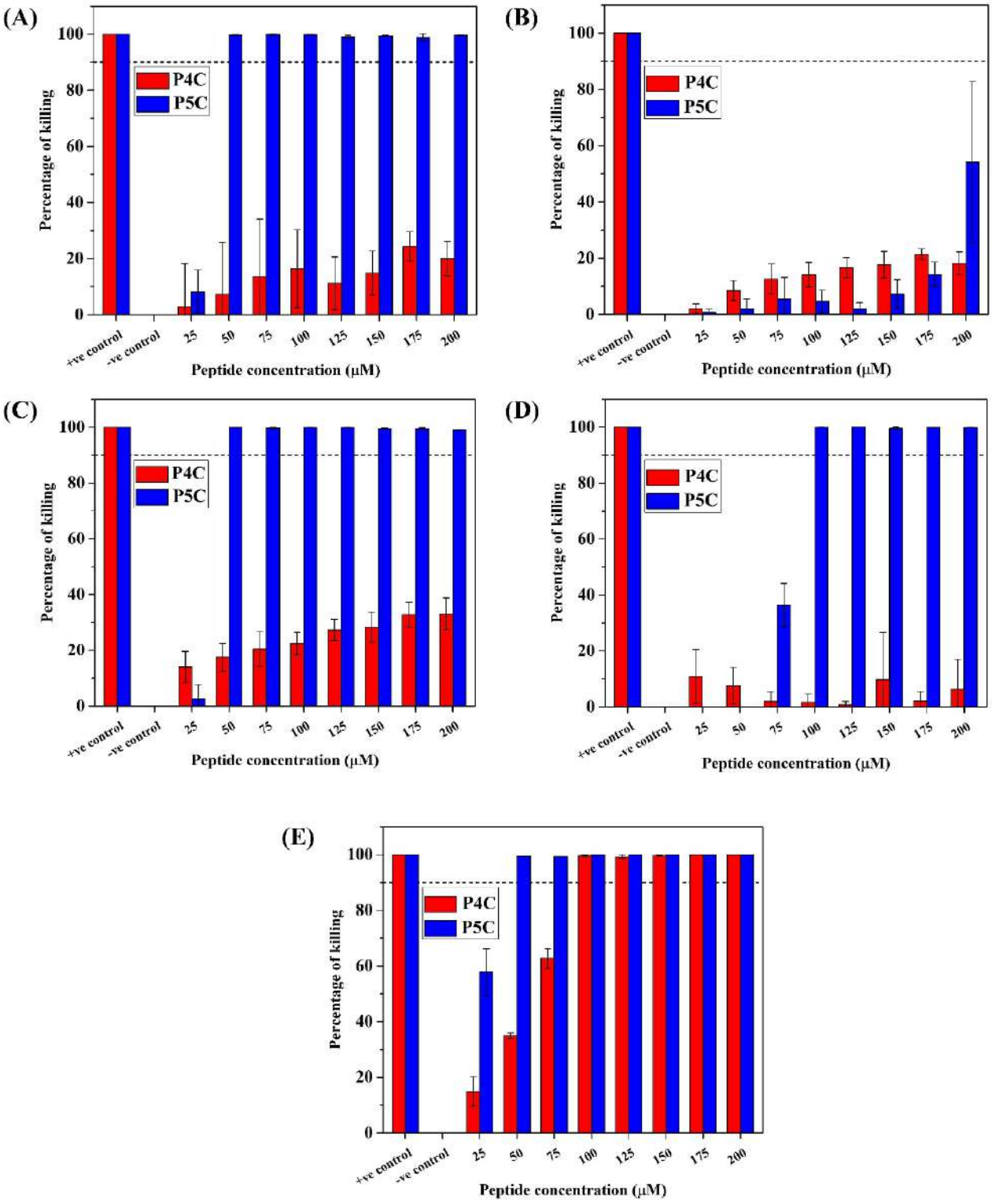

Figure A22. MIC of the peptides **P4C** and **P5C** against (A) *P. aeruginosa*, (B) *K. pneumoniae* and (C) *S. aureus* (D) *Methicillin-resistant S. aureus* (E) *C. albicans* in phosphate buffer saline (pH 7.4).

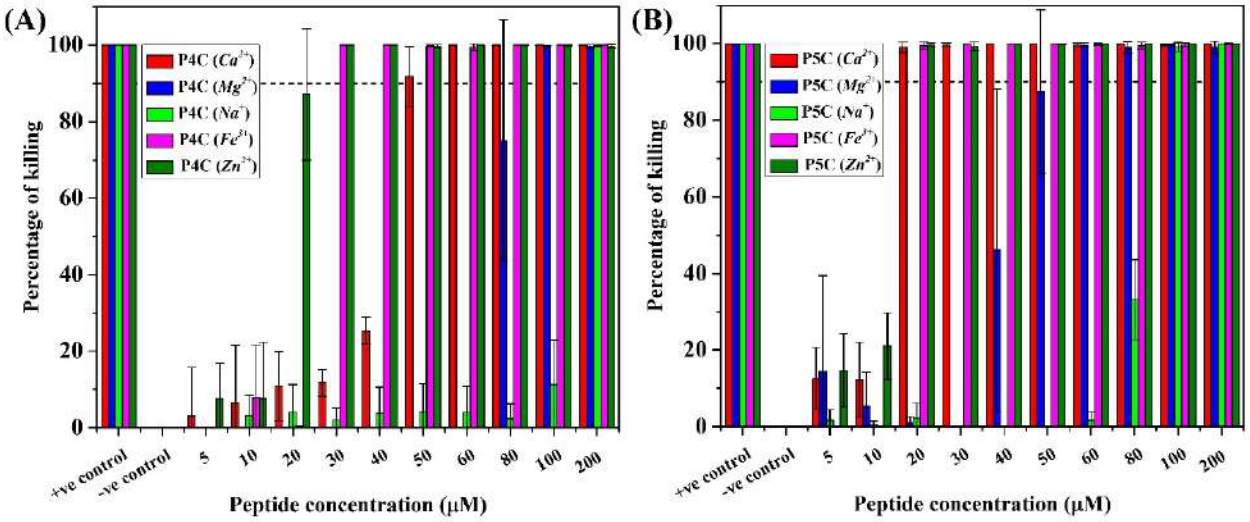

Figure A23. MIC of the peptides (A) **P4C** and (B) **P5C** against *P. aeruginosa* in the presence of various salts of different physiological concentrations. 90% killing of the microbes is denoted by a broken dashed line.

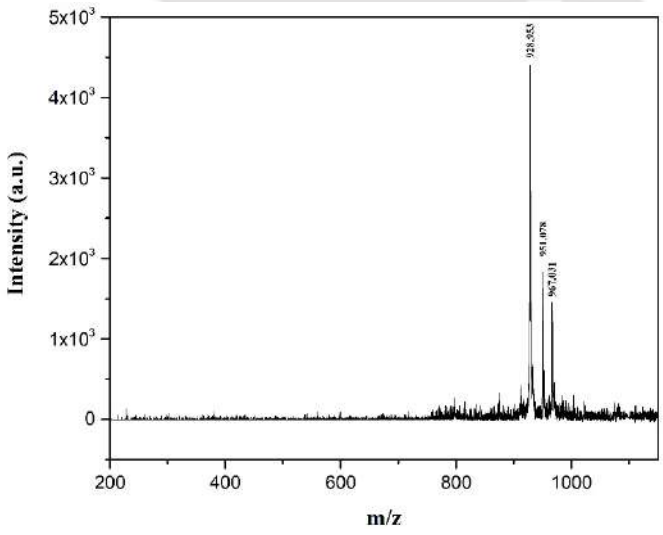

Figure A24. MALDI spectra of **P4: LKWLKKL-NH_2 (Untreated).** Expected mass of unfragmented P4, $[LKWLKKL\text{-}NH_2+H]^+$: 927.650 Da; 928.953 Da corresponds to $[LKWLKKL\text{-}NH_2+H]^+$; 951.078 Da corresponds to $[LKWLKKL\text{-}NH_2+Na]^+$; 967.031 Da corresponds to $[LKWLKKL\text{-}NH_2+K]^+$.

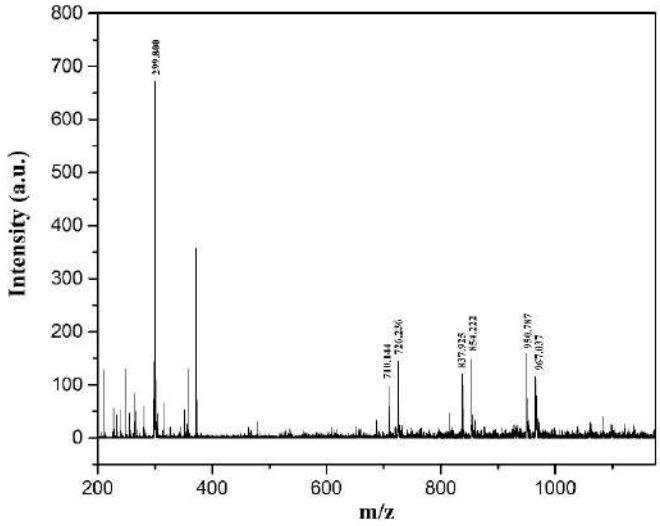

Figure A25. MALDI spectra of **P4+Chy+ProK+Trp (30 min).** Expected mass of unfragmented P4, $[LKWLKKL\text{-}NH_2+H]^+$: 927.650 Da; 299.800 Da corresponds to the fragment $[KL\text{-}NH_2+K]^+$; 710.144 Da corresponds to $[LKWLK\text{-}OH+Na]^+$; 726.236 Da corresponds to $[LKWLK\text{-}OH+K]^+$; 837.925 Da corresponds to $[LKWLKK\text{-}OH+Na]^+$; 854.222 Da corresponds to $[LKWLKK\text{-}OH+K]^+$; 950.787 Da corresponds to $[LKWLKKL\text{-}NH_2+Na]^+$; 967.037 Da corresponds to $[LKWLKKL\text{-}NH_2+K]^+$.

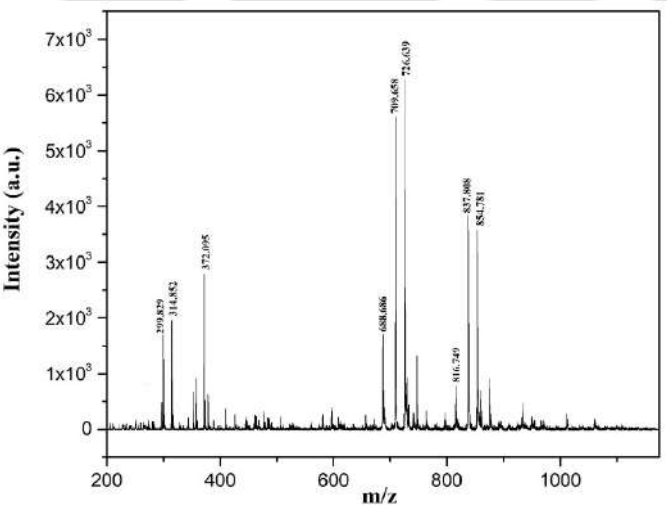

Figure A26. MALDI spectra of **P4+Chy+ProK+Trp (6 h).** Expected mass of unfragmented P4, $[LKWLKKL\text{-}NH_2+H]^+$: 927.650 Da; 299.829 Da corresponds to the fragment $[KL\text{-}NH_2+K]^+$; 688.686 Da corresponds to $[LKWLK\text{-}OH+H]^+$; 709.658 Da corresponds to $[LKWLK\text{-}OH+Na]^+$; 726.639 Da corresponds to $[LKWLK\text{-}OH\text{-}+K]^+$; 816.749 Da corresponds to $[LKWLKK\text{-}OH+H]^+$;

837.808 Da corresponds to [LKWLKK-OH+Na]$^+$; 854.781 Da corresponds to [LKWLKK-OH+K]$^+$.

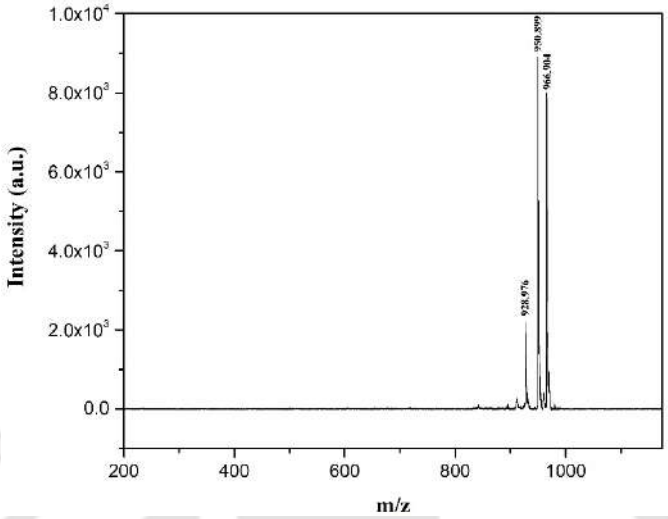

Figure A27. MALDI spectra of **P4C: lkwlkkl-NH$_2$ (Untreated).** Expected mass of unfragmented P4C, [lkwlkkl-NH$_2$+H]$^+$: 927.650 Da; 928.976 Da corresponds to [lkwlkkl-NH$_2$+H]$^+$; 950.899 Da corresponds to [lkwlkkl-NH$_2$+Na]$^+$; 966.904 Da corresponds to [lkwlkkl-NH$_2$+K]$^+$.

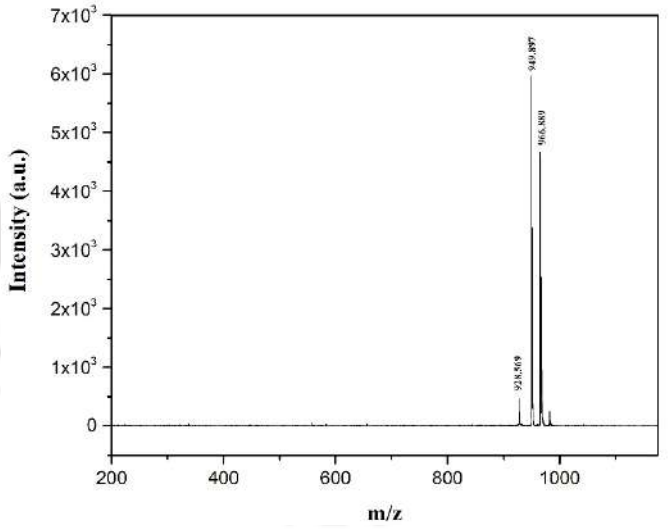

Figure A28. MALDI spectra of **P4C+Chy+ProK+Trp (30 min).** Expected mass of unfragmented P4C, [lkwlkkl-NH$_2$+H]$^+$: 927.650 Da; 928.569 Da corresponds to [lkwlkkl-NH$_2$+H]$^+$; 949.897 Da corresponds to [lkwlkkl-NH$_2$+Na]$^+$; 966.889 Da corresponds to [lkwlkkl-NH$_2$+K]$^+$.

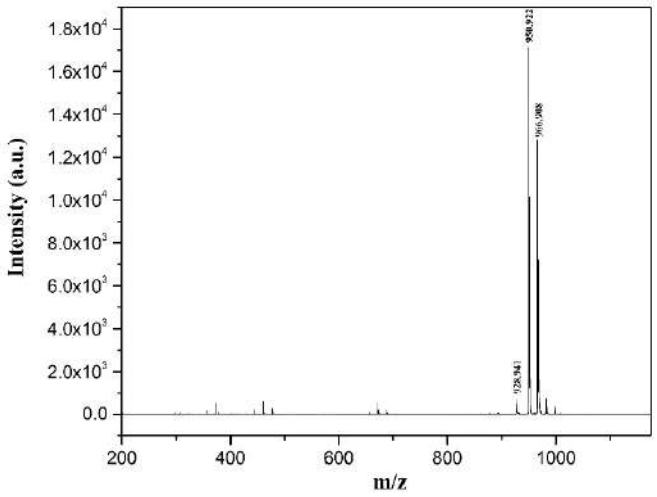

Figure A29. MALDI spectra of **P4C+Chy+ProK+Trp (6 h).** Expected mass of unfragmented P4C, [lkwlkkl-NH_2+H]$^+$: 927.650 Da; 928.941 Da corresponds to [lkwlkkl-NH_2+H]$^+$; 950.922 Da corresponds to [lkwlkkl-NH_2+Na]$^+$; 966.908 Da corresponds to [lkwlkkl-NH_2+K]$^+$.

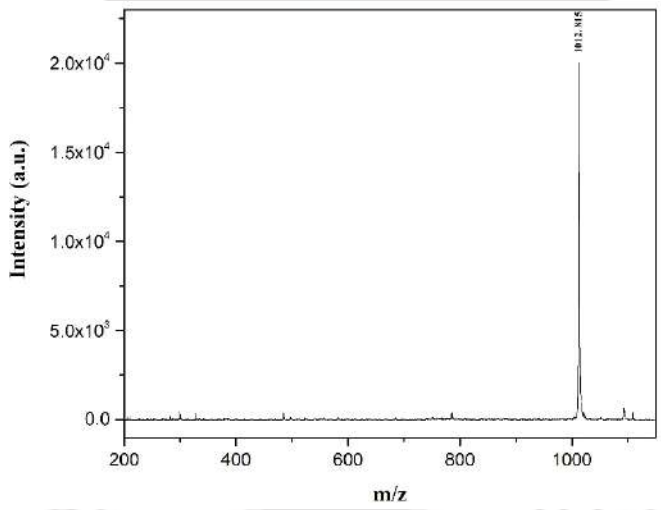

Figure A30. MALDI spectra of **P5: LRWLRRL-NH_2 (Untreated).** Expected mass of unfragmented P5, [LRWLRRL-NH_2+H]$^+$: 1011.669 Da; 1012.815 Da corresponds to [LRWLRRL-NH_2 +H]$^+$.

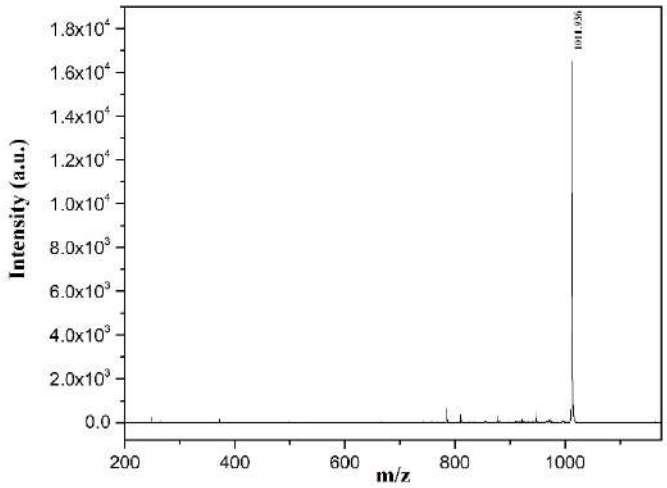

Figure A31. MALDI spectra of **P5+Chy+ProK+Trp (30 min).** Expected mass of unfragmented P5, $[LRWLRRL\text{-}NH_2+H]^+$: 1011.669 Da; 1011.936 Da corresponds to $[LRWLRRL\text{-}NH_2+H]^+$.

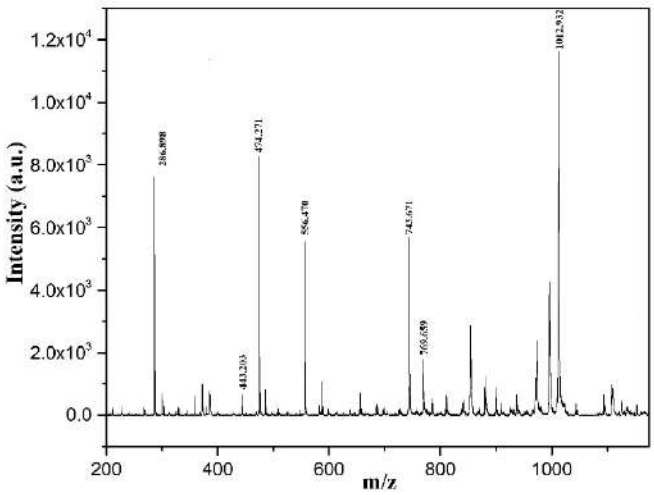

Figure A32. MALDI spectra of **P5+Chy+ProK+Trp (6 h).** Expected mass of unfragmented P5, $[LRWLRRL\text{-}NH_2+H]^+$: 1011.669 Da; 286.898 Da corresponds to $[RL\text{-}NH_2+H]^+$; 443.203 Da corresponds to $[RRL\text{-}NH_2+H]^+$; 474.271 Da corresponds to to $[LRW\text{-}OH+H]^+$; 556.470 Da corresponds to $[LRRL\text{-}NH_2+H]^+$; 743.671 Da corresponds to to $[LRWLR\text{-}OH+H]^+$; 1012.932 Da corresponds to $[LRWLRRL\text{-}NH_2+H]^+$.

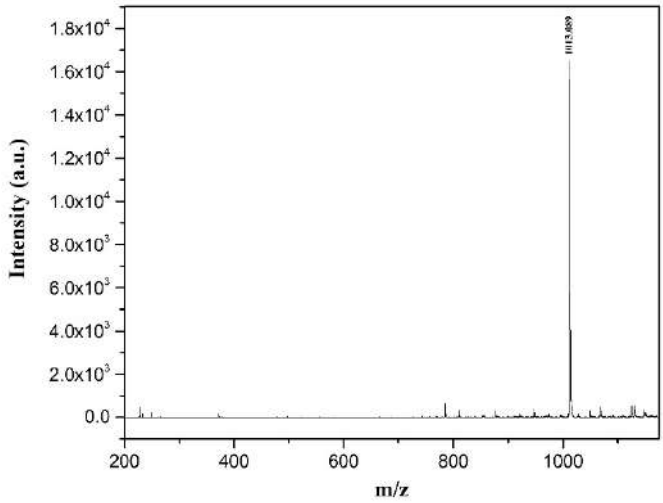

Figure A33. MALDI spectra of **P5C: lrwlrrl-NH_2 (Untreated).** Expected mass of unfragmented P5C, [lrwlrrl-NH_2+H]$^+$: 1011.669 Da; 1013.089 Da corresponds to [lrwlrrl-NH_2 +H]$^+$.

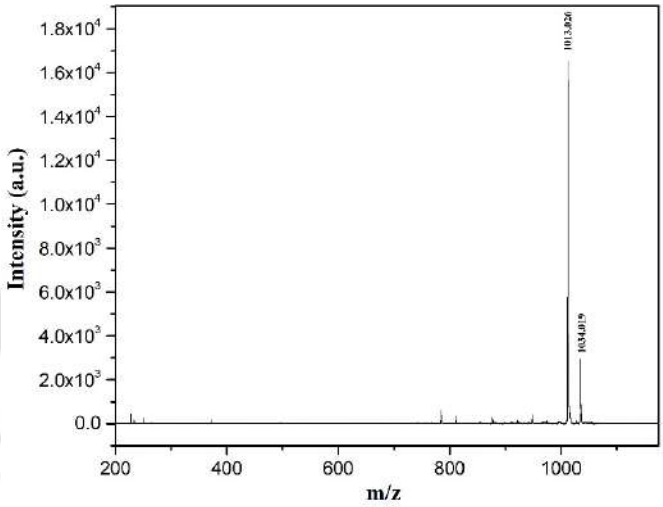

Figure A34. MALDI spectra of **P5C+Chy+ProK+Trp (30 min).** Expected mass of unfragmented P5C, [lrwlrrl-NH_2+H]$^+$: 1011.669 Da; 1013.026 Da corresponds to [lrwlrrl-NH_2 +H]$^+$; 1034.019 Da corresponds to [lrwlrrl-NH_2 +Na]$^+$.

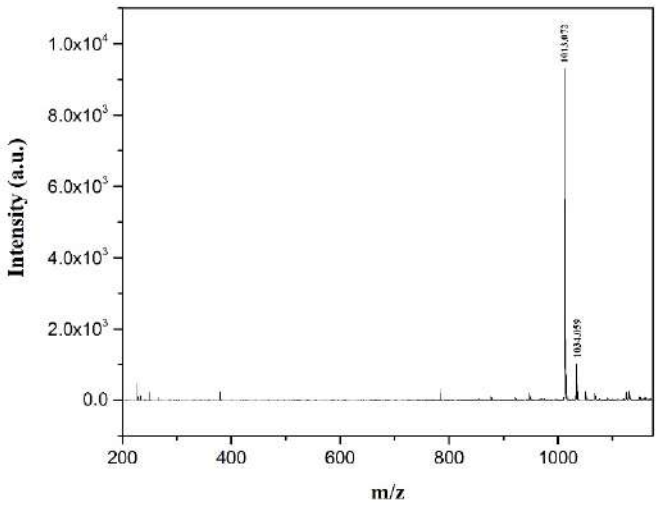

Figure A35. MALDI spectra of **P5C+Chy+ProK+Trp (6 h).** Expected mass of unfragmented P5C, $[lrwlrrl\text{-}NH_2+H]^+$: 1011.669 Da; 1013.072 Da corresponds to $[lrwlrrl\text{-}NH_2+H]^+$; 1034.059 Da corresponds to $[lrwlrrl\text{-}NH_2+Na]^+$.

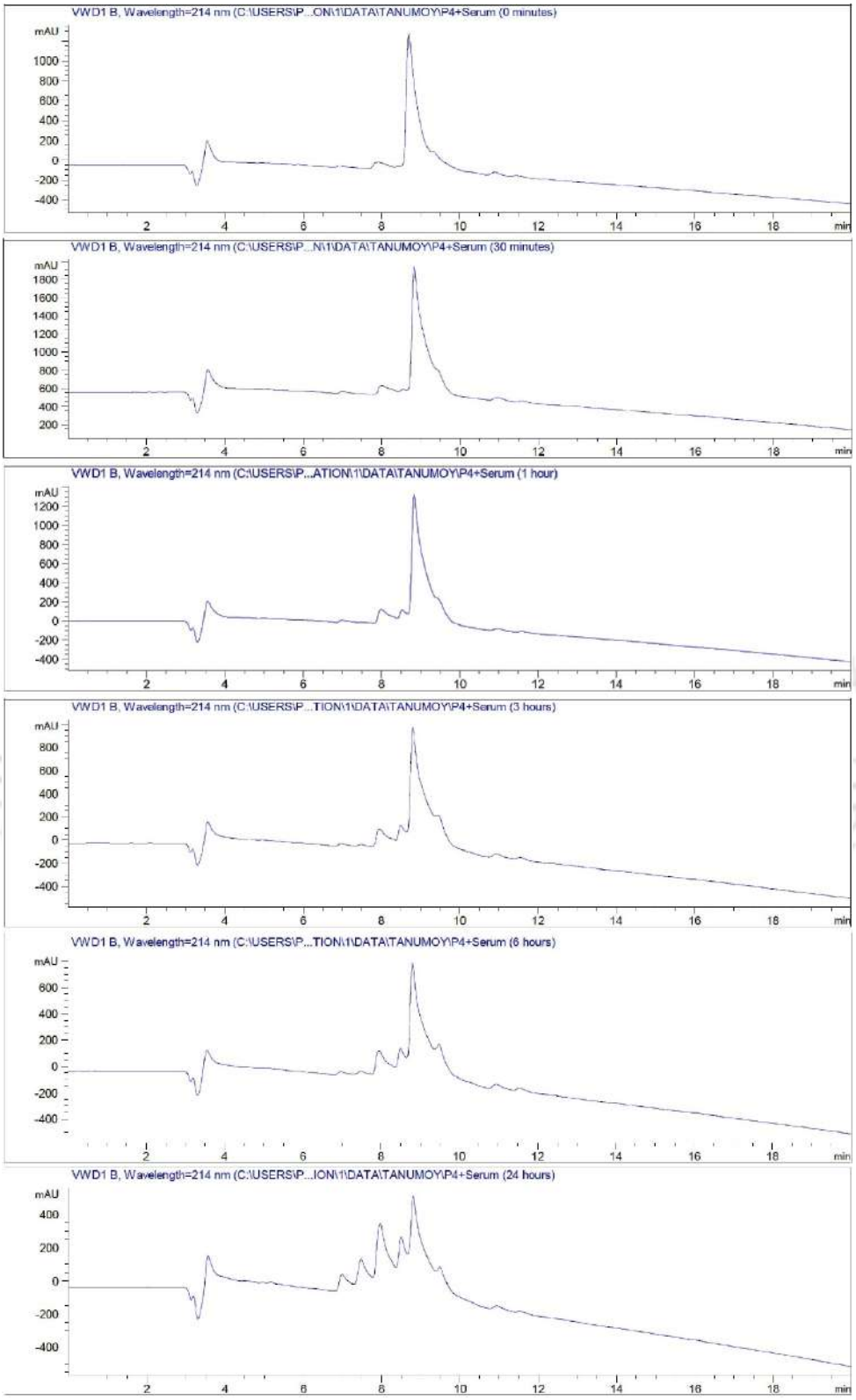

Figure A36. HPLC analytic traces of the peptide **P4** incubated with human blood serum for various time intervals (30 min, 1 h, 3 h, 6 h, 24 h).

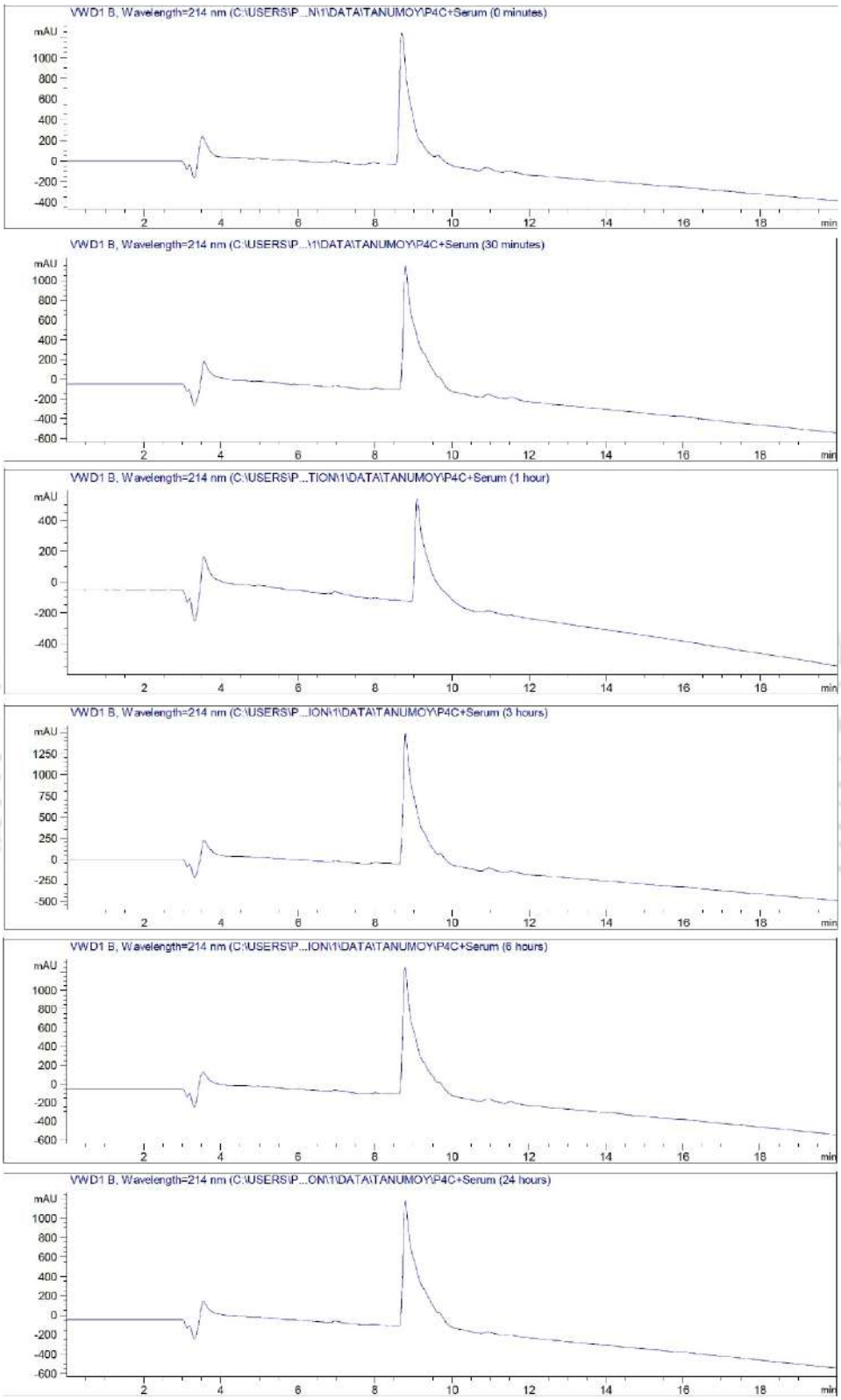

Figure A37. HPLC analytic traces of the peptide **P4C** incubated with human blood serum for various time intervals (30 min, 1 h, 3 h, 6 h, 24 h).

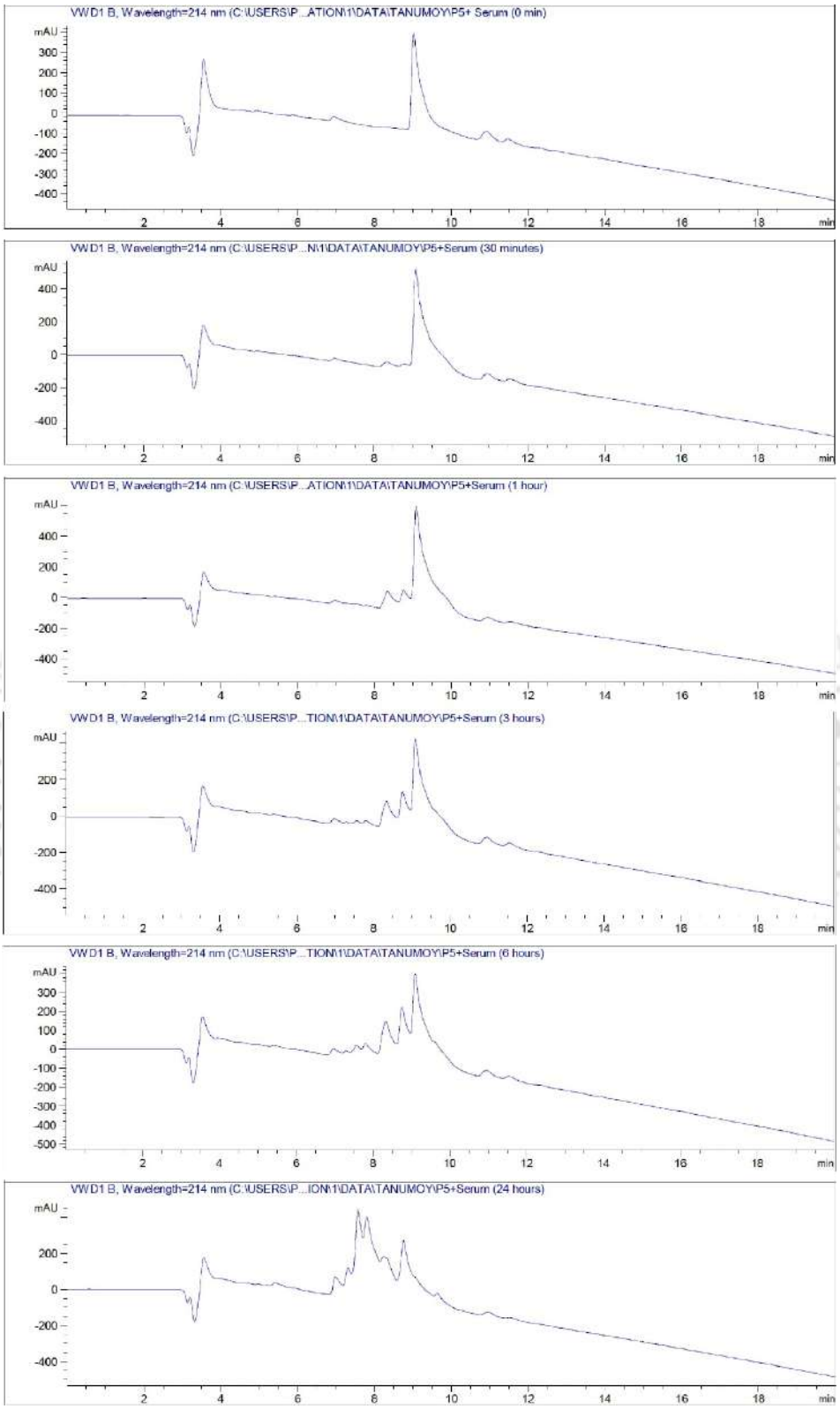

Figure A38. HPLC analytic traces of the peptide **P5** incubated with human blood serum for various time intervals (30 min, 1 h, 3 h, 6 h, 24 h).

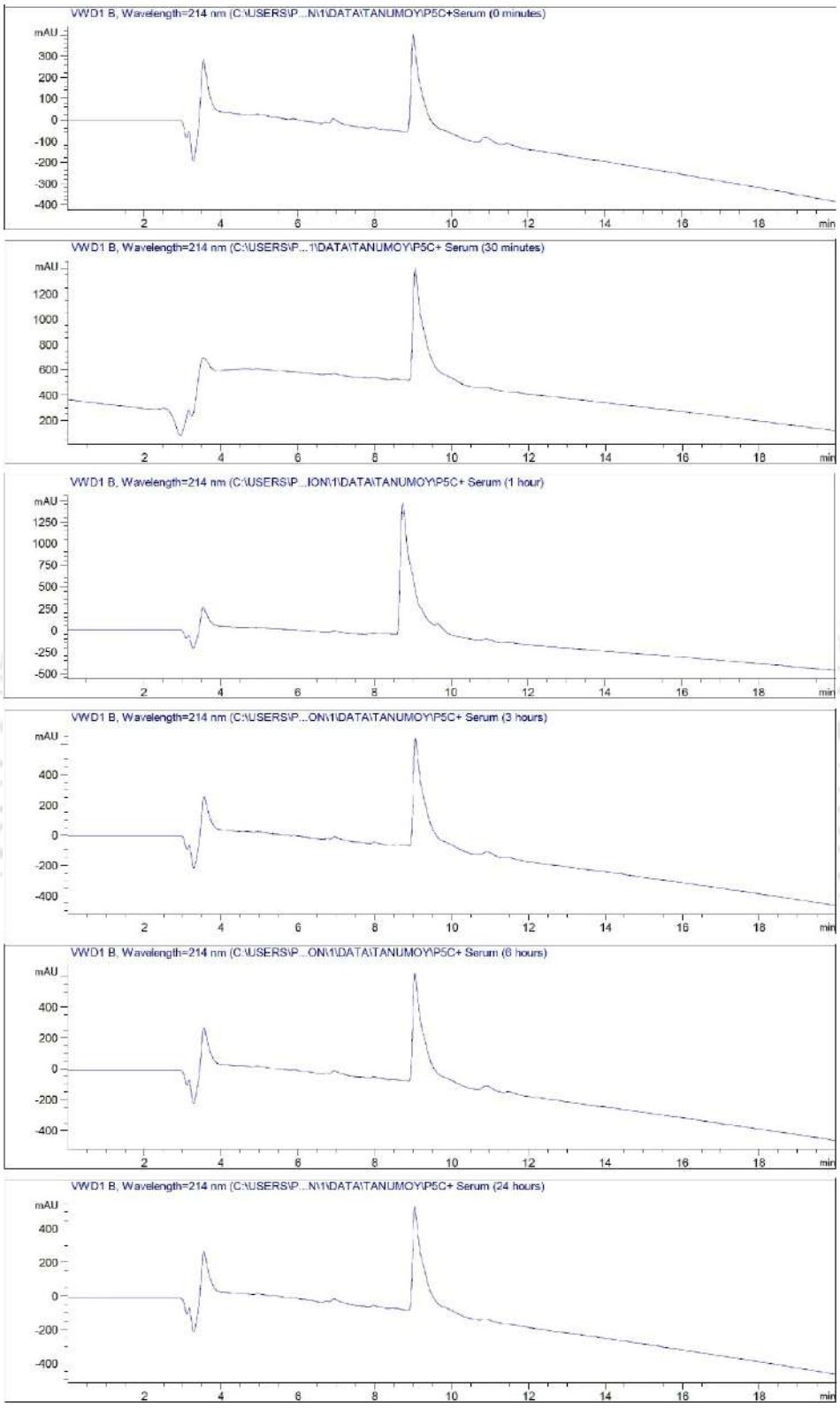

Figure A39. HPLC analytic traces of the peptide **P5C** incubated with human blood serum for various time intervals (30 min, 1 h, 3 h, 6 h, 24 h).

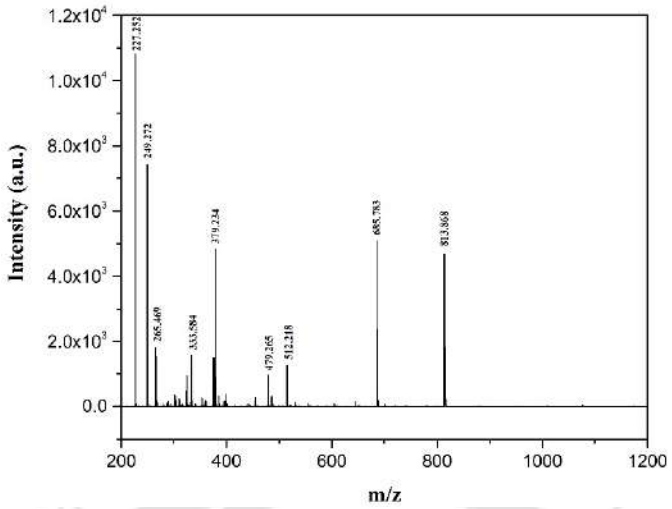

Figure A40. MALDI spectra of **P4+Serum (24 h).** Expected mass of unfragmented P4, $[LKWLKKL\text{-}NH_2+H]^+$: 927.650 Da; 685.783 Da corresponds to $[LKWLK\text{-}OH+H]^+$; 813.868 Da corresponds to $[LKWLKK\text{-}OH+H]^+$.

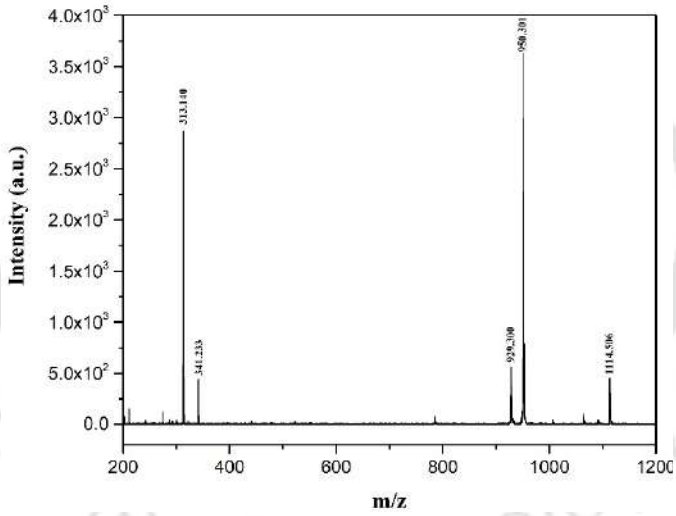

Figure A41. MALDI spectra of **P4C+Serum (24 h).** Expected mass of unfragmented P4C, $[lkwlkkl\text{-}NH_2+H]^+$: 927.650 Da; 929.300 Da corresponds to $[lkwlkkl\text{-}NH_2+H]^+$; 950.301 Da corresponds to $[lkwlkkl\text{-}NH_2+Na]^+$.

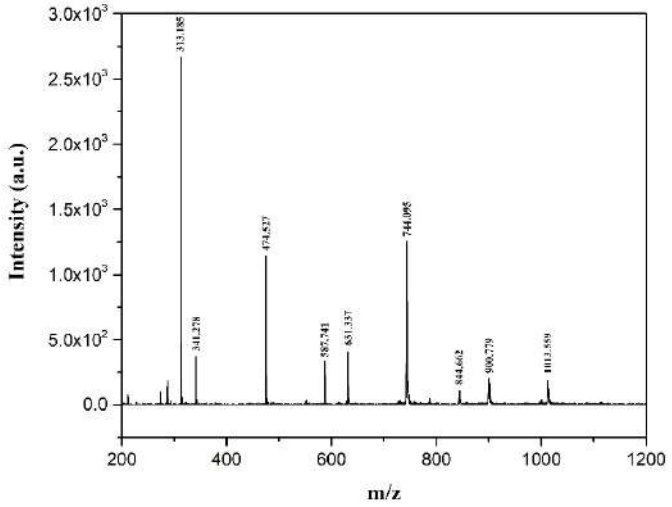

Figure A42. MALDI spectra of **P5+Serum (24 h).** Expected mass of unfragmented P5, $[LRWLRRL\text{-}NH_2+H]^+$: 1011.669 Da; 474.527 Da corresponds to to $[LRW\text{-}OH+H]^+$; 744.095 Da corresponds to to $[LRWLR\text{-}OH+H]^+$; 1013.559 Da corresponds to $[LRWLRRL\text{-}NH_2+H]^+$.

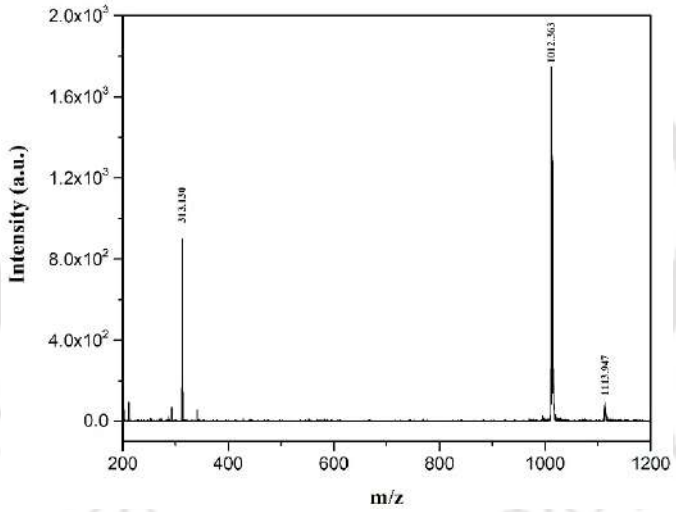

Figure A43. MALDI spectra of **P5C+Serum (24 h).** Expected mass of unfragmented P5C, $[lrwlrrl\text{-}NH_2+H]^+$: 1011.669; 1012.363 corresponds to $[lrwlrrl\text{-}NH_2+H]^+$.

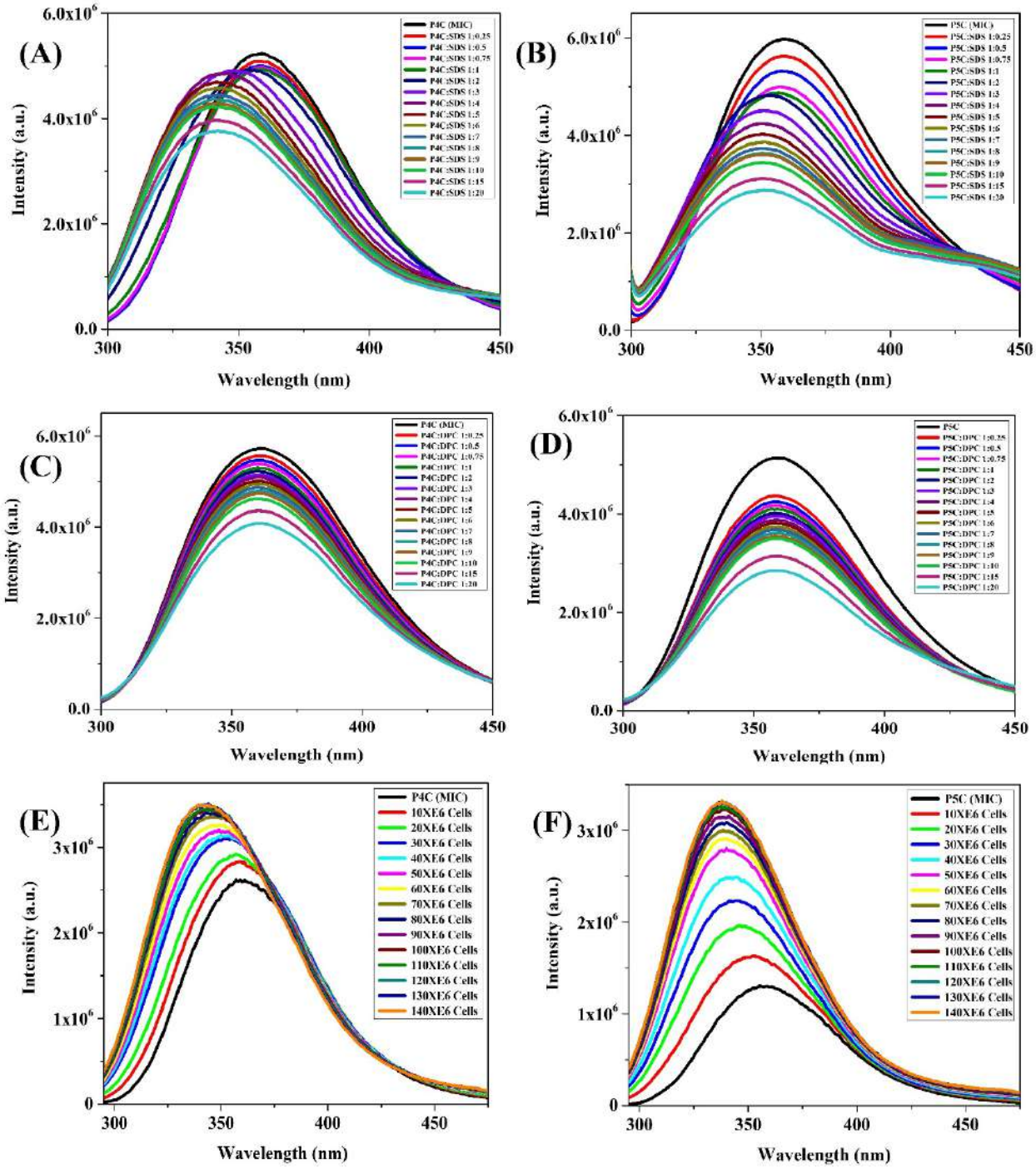

Figure A44. Blue shift experiments using intrinsic fluorescence of tryptophan present in **P4C** and **P5C**. (A) **P4C** and (B) **P5C** titrated against SDS at various ratios ranging from 0.25 to 20. (C) **P4C** and (D) **P5C** titrated against DPC at various ratios ranging from 0.25 to 20. (E) **P4C** and (F) **P5C** at their respective MICs titrated against the live cells of *P. aeruginosa.*

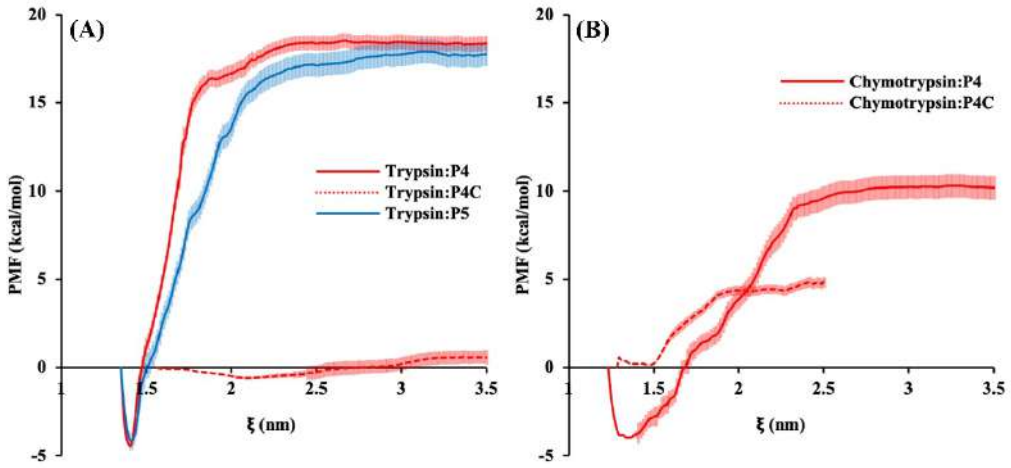

Figure A45. The potential of mean force (PMF) as a function of the COM pulling coordinate "ξ". Bootstrapping errors (100 cycles) are shown as vertical transparent bars. (A, B) Peptide dissociation from serine protease (Trypsin and Chymotrypsin).

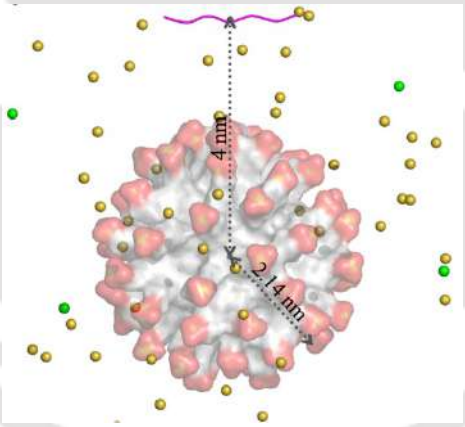

Figure A46. A graphical representation of peptide-micelle simulation setup. The extended peptide (magenta, cartoon) is placed above the micelle surface (center of mass of the peptide to center of the SDS micelle distance ~4 nm). The micelle comprises 60 SDS molecules (surface representation, micelle radius = 2.14 nm). Water molecules and hydrogen atoms are not shown for clarity, ions (spheres; Na^+ = yellow and Cl^- = green). The resulting setup was subjected to minimization, equilibration, and production MD (in NPT ensemble) at 310K and 1 bar.

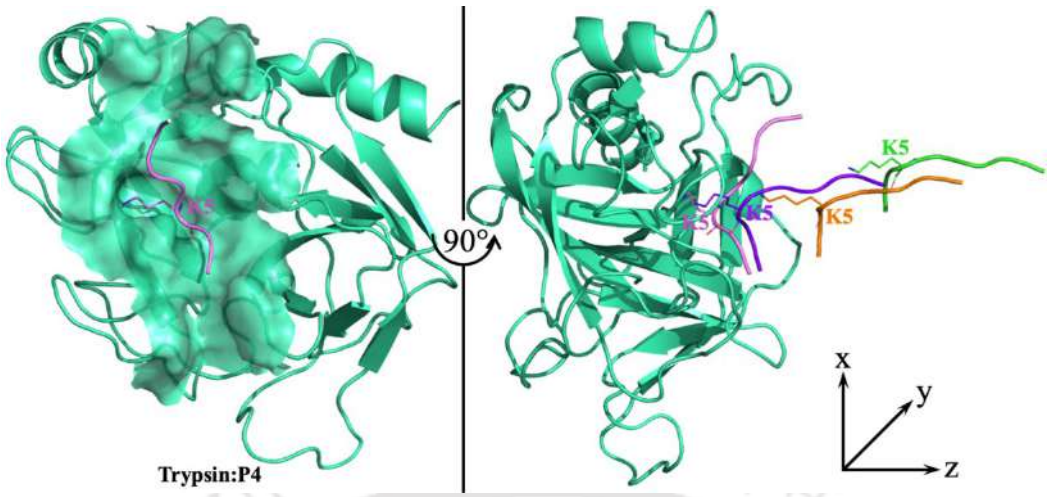

Figure A47. Steered molecular dynamics setup. Left: Final structure of trypsin: P4 complex after production dynamics (peptide P4: magenta, Trypsin: teal green surface). Right: The peptide is rotated to the z-axis, and four representative frames (out of 21) are generated after the center of mass pulling (Peptides relative to trypsin are highlighted: magenta → violet → orange → green).

Table A1. Simulation details (Total simulation time ~6.6 μs).

	Box dimension (nm^3)	**No of waters/Na/ Cl**	**Total no of atoms**	**Simulation Length (ns) (Equilibration/ Production Run)**	**No of trials**
P4C	5 × 5 × 5	4003/0/4	12165	0.20/200	3
P5C	5 × 5 × 5	3998/0/4	12156	0.20/200	3
P4C:SDS	8 × 8 × 8	14993/60/4	47670	0.50/200	3
P5C:SDS	8 × 8 × 8	14995/60/4	47721	0.50/200	3
Trypsin:P4	7.5 × 7.5 × 7.5	12539/0/10	41001	0.50/100	3
Trypsin:P5	7.5 × 7.5 × 7.5	12534/0/10	40991	0.50/100	3

Trypsin:P4C	7.5 × 7.5 × 7.5	12552/0/10	41039	0.50/500	3
Trypsin:P5C	7.5 × 7.5 × 7.5	12550/0/10	41036	0.50/500	3
Chymotrypsin :P4	7.5 × 7.5 × 7.5	12119/0/7	39990	0.50/100	3
Chymotrypsin :P4C	7.5 × 7.5 × 7.5	12079/0/7	39854	0.50/100	3

Table A2. Binding affinity (ΔG) estimated from umbrella sampling (Total simulation time ~15.8μs). Error calculated using Bootstrap Analysis (100 cycles). They averaged from three independent MD trials. Standard error of the mean (s.e.m) after ±.

Complex	**Replicas**	**Simulation length of Umbrella Sampling**	**ΔG (kcal/mol)**	**ΔG^{Avg} (kcal/mol)**
Trypsin:P4	Trial 1	21 windows × 50 ns = 1050 ns	-21.95 ± 0.38	**-22.79 ± 0.42**
	Trial 2	21 windows × 50 ns = 1050 ns	-22.99 ± 0.43	
	Trial 3	21 windows × 50 ns = 1050 ns	-23.42 ± 0.46	
Trypsin:P4C	Trial 1	21 windows × 50 ns = 1050 ns	-1.69 ± 0.39	**-1.24 ± 0.38**
	Trial 2	21 windows × 50 ns = 1050 ns	-0.95 ± 0.4	
	Trial 3	21 windows × 50 ns = 1050 ns	-1.09 ± 0.34	
Trypsin:P5	Trial 1	21 windows × 50 ns = 1050 ns	-21.73 ± 1.02	**-21.98 ± 0.98**
	Trial 2	21 windows × 50 ns = 1050 ns	-22.87 ± 0.94	

	Trial 3	21 windows × 50 ns = 1050 ns	-21.35 ± 0.97	
Chymorypsin:P4	Trial 1	21 windows × 50 ns = 1050 ns	-14.71 ± 0.67	**-14.34 ± 0.67**
	Trial 2	21 windows × 50 ns = 1050 ns	-15.13 ± 0.54	
	Trial 3	21 windows × 50 ns = 1050 ns	-13.17 ± 0.81	
Chymotrypsin:P4 C	Trial 1	21 windows × 50 ns = 1050 ns	-4.25 ± 0.39	**-4.86 ± 0.35**
	Trial 2	21 windows × 50 ns = 1050 ns	-5.29 ± 0.31	
	Trial 3	21 windows × 50 ns = 1050 ns	-5.03 ± 0.36	

Strains used for the study

Pseudomonas aeruginosa (MTCC 2488)

Klebsiella pneumoniae (MTCC 432)

Staphylococcus aureus (MTCC 96)

Methicillin-resistant Staphylococcus aureus (MRSA 100)

Candida albicans (MTCC 1637)

Appendix B (for Chapter 3)

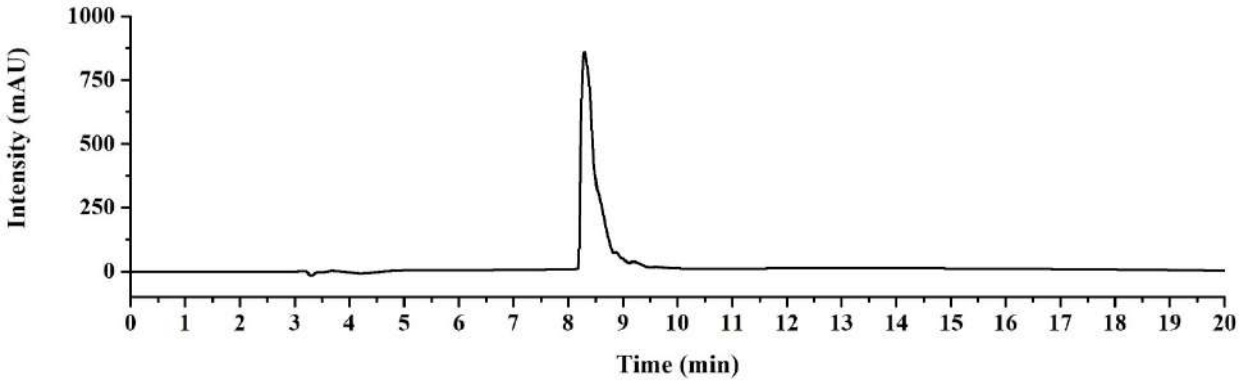

Figure B1. Analytic HPLC trace of LKWLKKL-NH_2 **(P4)**. Retention time: 8.29 min.

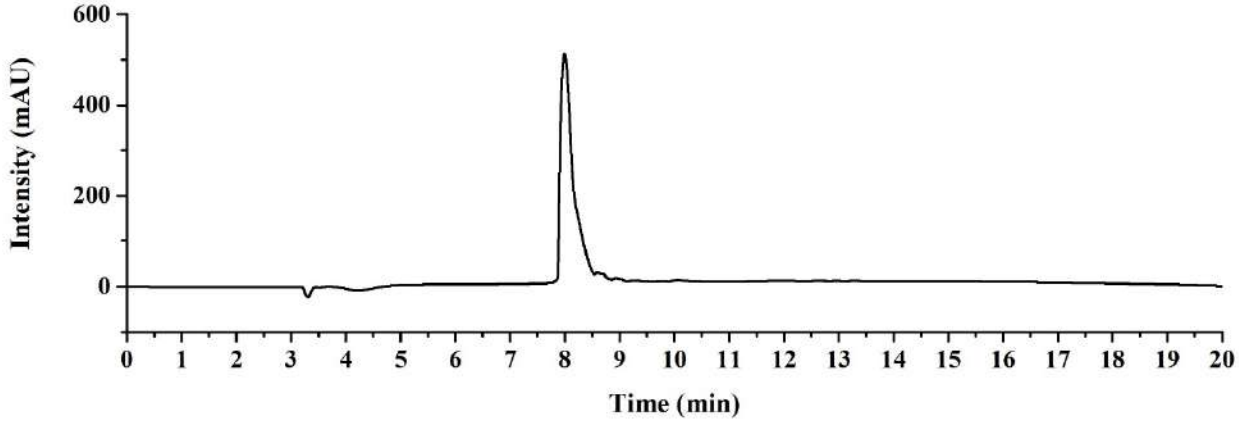

Figure B2. Analytic HPLC trace of LKFLKKL-NH_2 **($P4^{W3F}$)**. Retention time: 8.00 min.

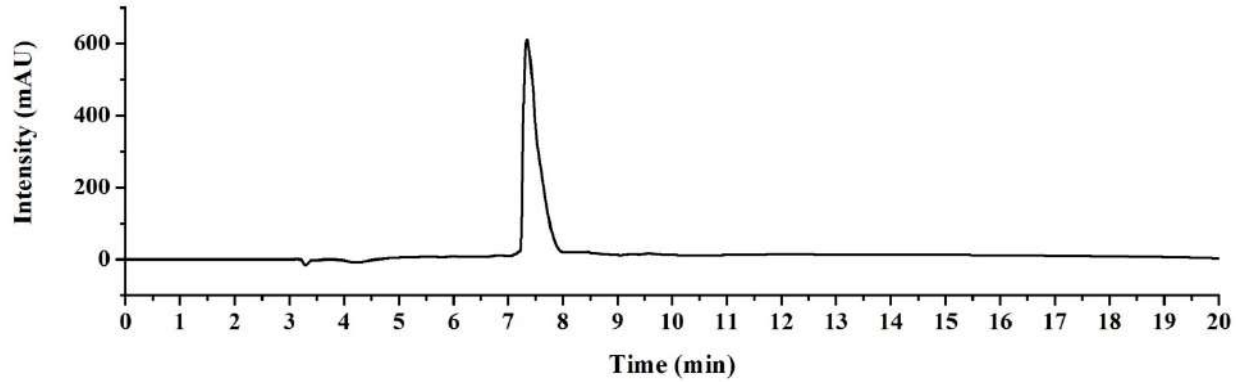

Figure B3. Analytic HPLC trace of LKYLKKL-NH_2 **($P4^{W3Y}$)**. Retention time: 7.35 min.

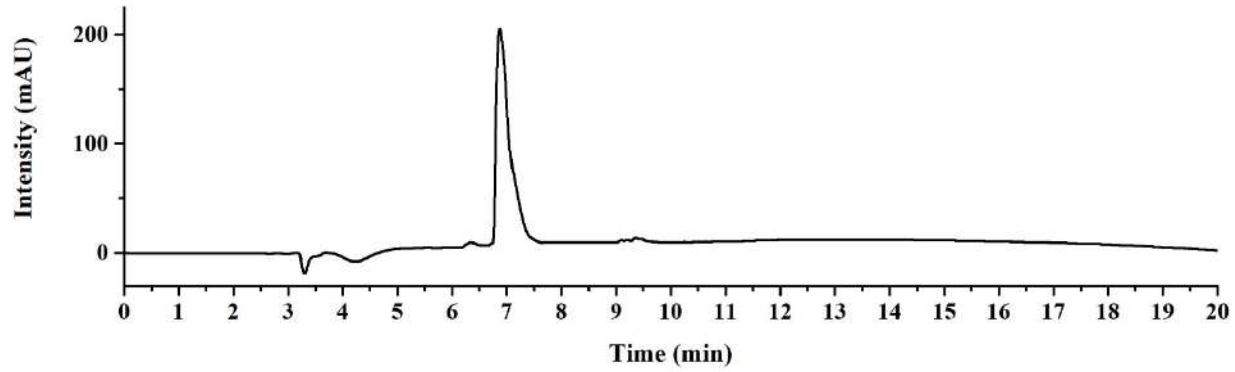

Figure B4. Analytic HPLC trace of LKALKKL-NH_2 **($P4^{W3A}$)**. Retention time: 6.88 min.

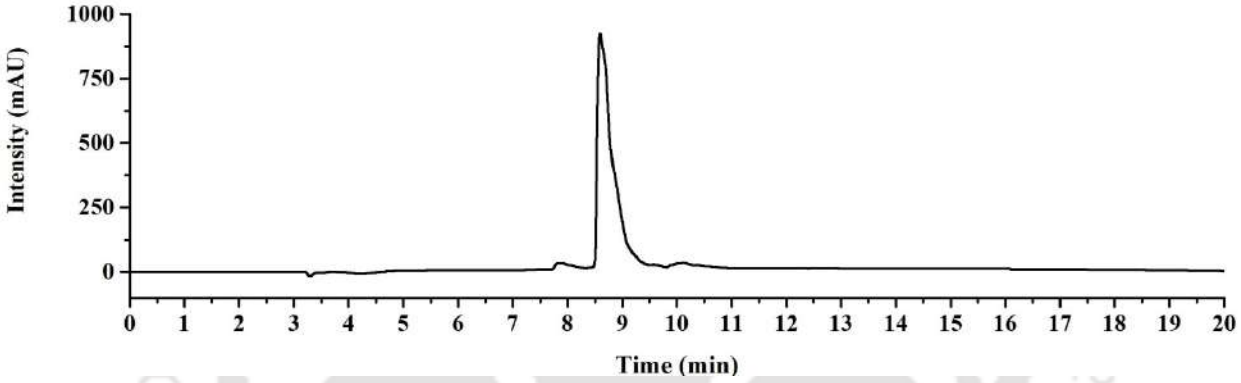

Figure B5. Analytic HPLC trace of LKWWKKL-NH_2 **($P4^{L4W}$)**. Retention time: 8.60 min.

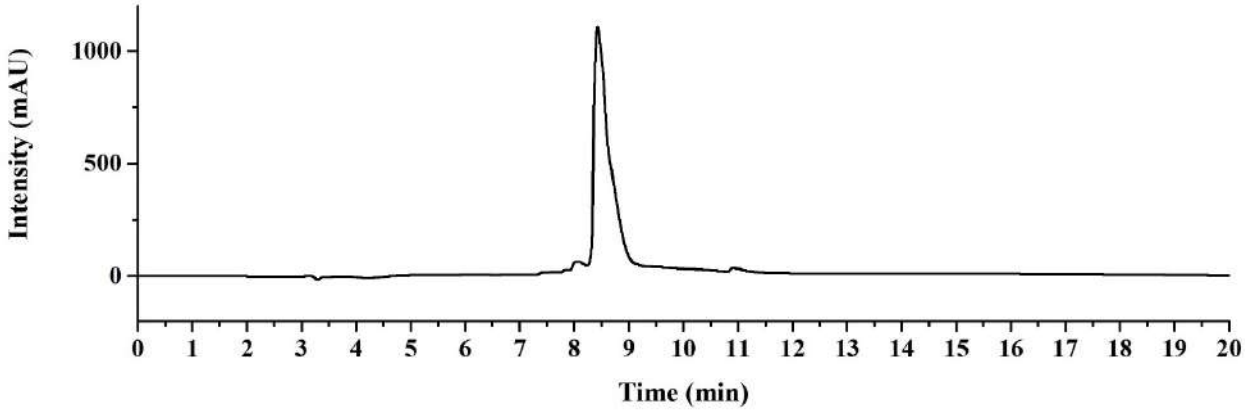

Figure B6. Analytic HPLC trace of **LKWFKKL-NH_2 ($P4^{L4F}$)**. Retention time: 8.43 min.

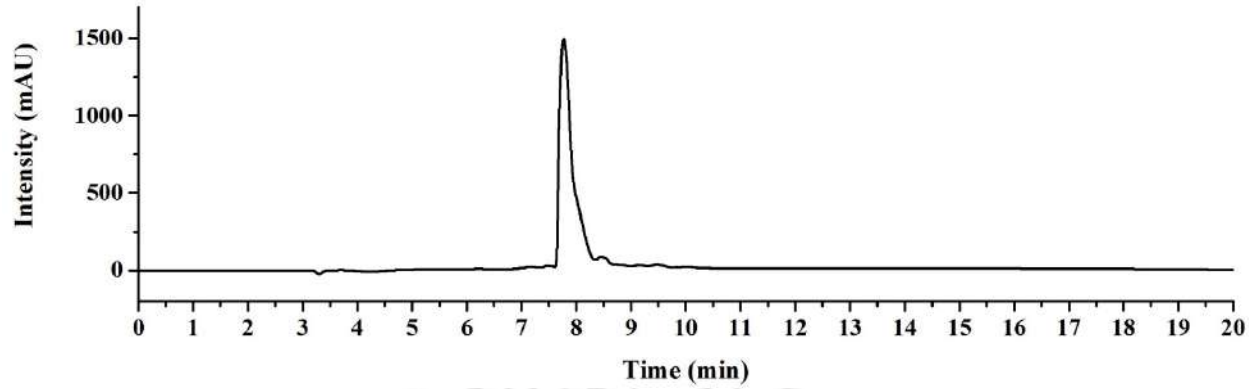

Figure B7. Analytic HPLC trace of **LKWYKKL-NH_2 ($P4^{L4Y}$)**. Retention time: 7.77 min.

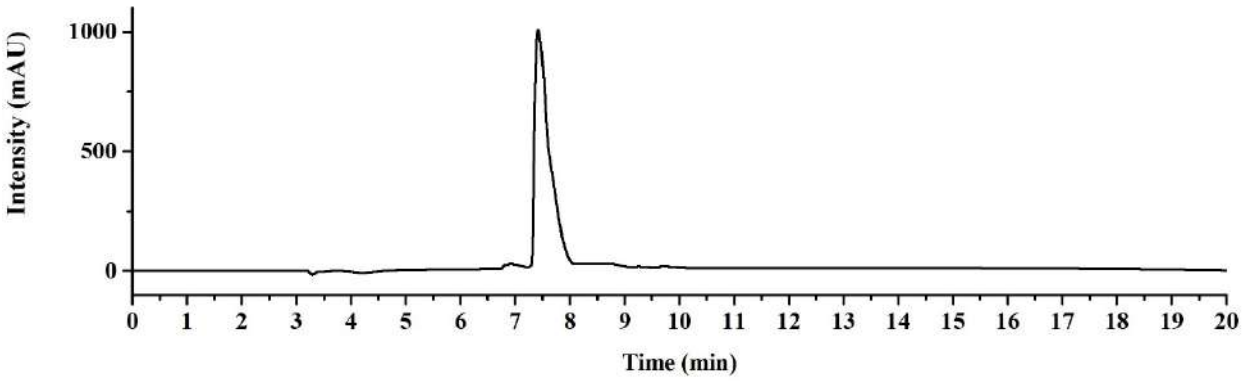

Figure B8. Analytic HPLC trace of **LKWAKKL-NH_2 ($P4^{L4A}$)**. Retention time: 7.43 min.

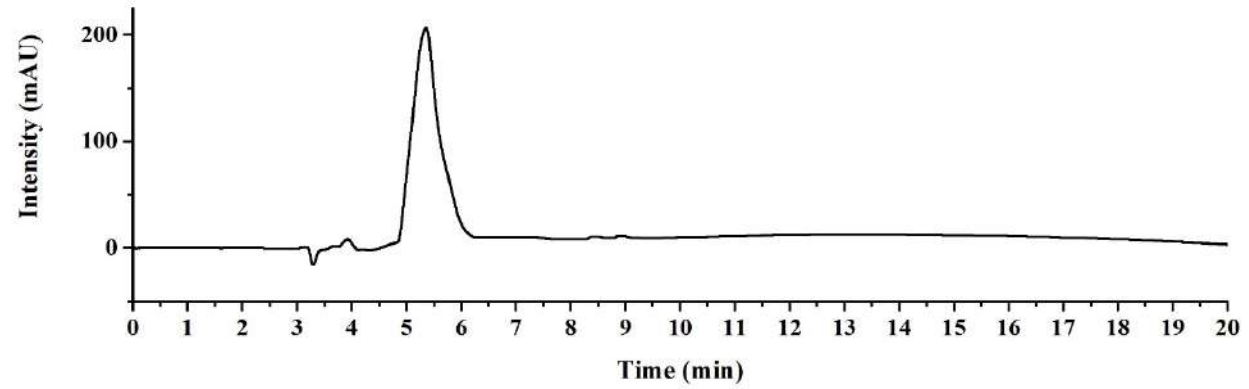

Figure B9. Analytic HPLC trace of **LKAAKKL-NH_2 ($P4^{W3A, L4A}$)**. Retention time: 5.36 min.

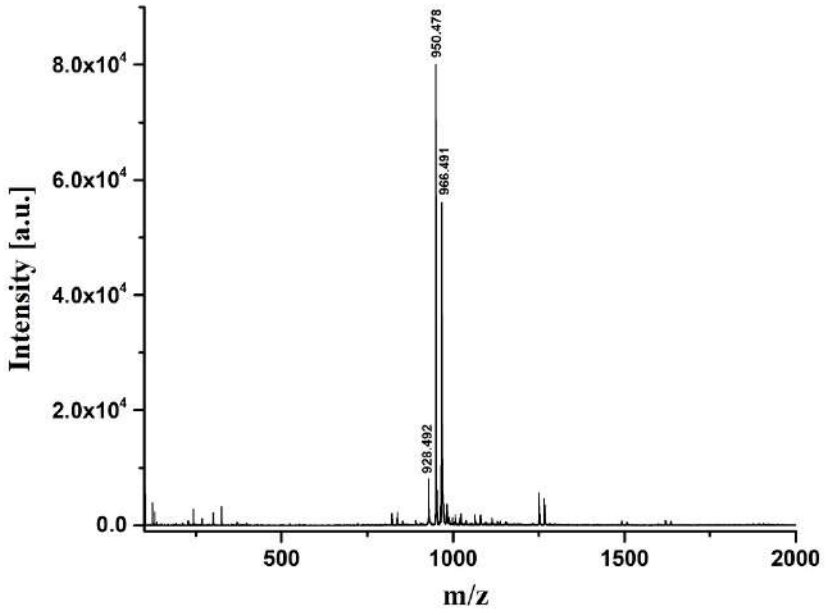

Figure B10. MALDI spectra of LKWLKKL-NH_2 **(P4)**. Expected $[M+H]^+$: 927.650; Observed $[M+H]^+$: 928.492; Observed $[M+Na]^+$: 950.478; Observed $[M+K]^+$: 966.491.

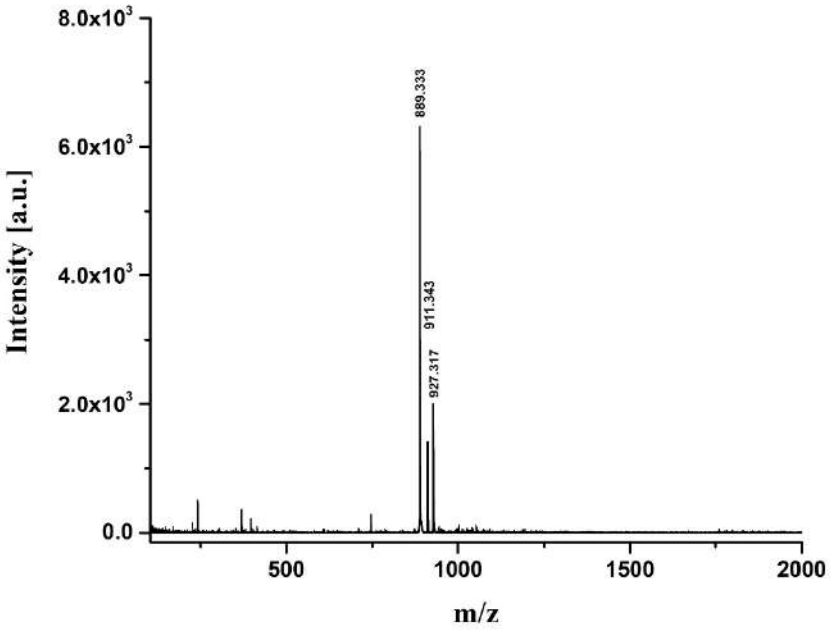

Figure B11. MALDI spectra of LKFLKKL-NH_2 **($P4^{W3F}$)**. Expected $[M+H]^+$: 888.639; Observed $[M+H]^+$: 889.333; Observed $[M+Na]^+$: 911.343; Observed $[M+K]^+$: 927.317.

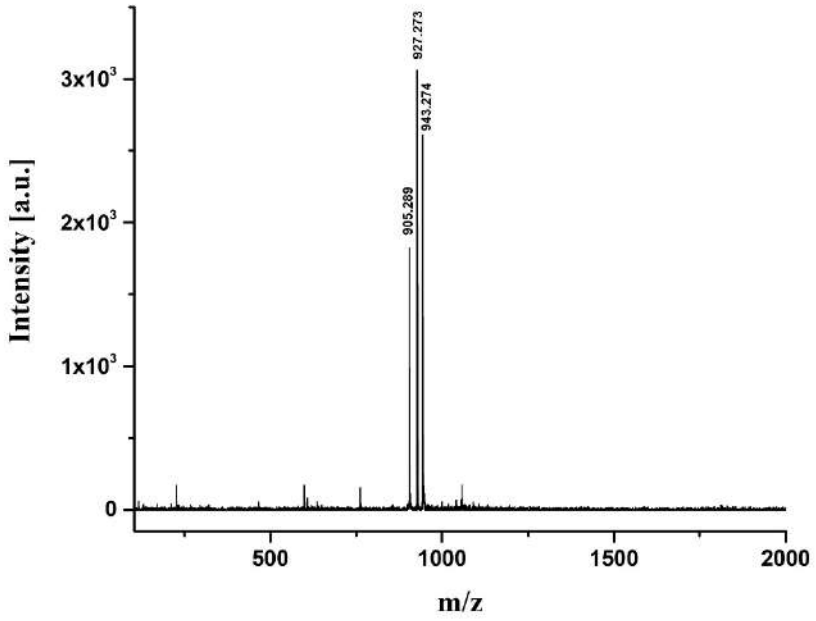

Figure B12. MALDI spectra of LKYLKKL-NH_2 **($P4^{W3Y}$)**. Expected $[M+H]^+$: 904.634; Observed $[M+H]^+$: 905.289; Observed $[M+Na]^+$: 927.273; Observed $[M+K]^+$: 943.274.

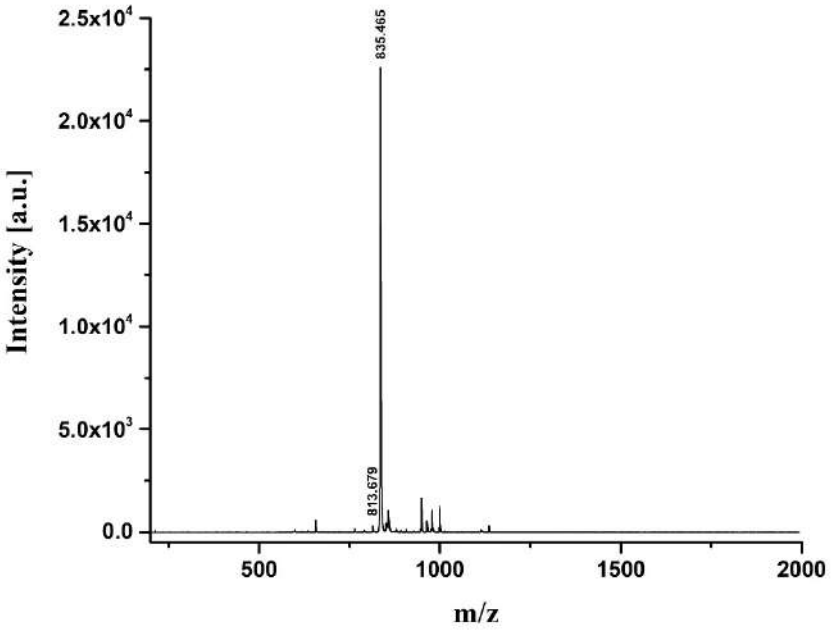

Figure B13. MALDI spectra of LKALKKL-NH_2 **($P4^{W3A}$)**. Expected $[M+H]^+$: 813.592; Observed $[M+H]^+$: 813.679; Observed $[M+Na]^+$: 835.465.

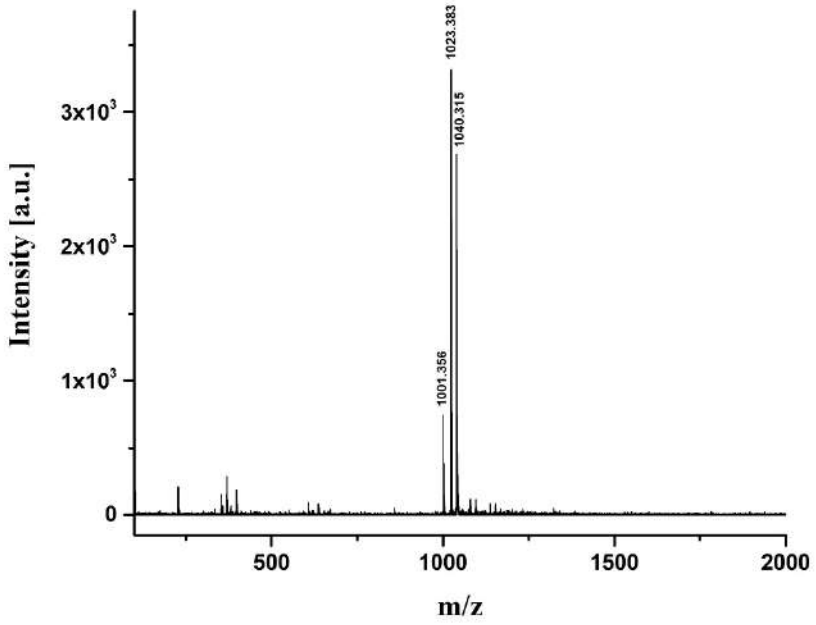

Figure B14. MALDI spectra of **LKWWKKL-NH$_2$ (P4^{L4W})**. Expected $[M+H]^+$: 1000.645; Observed $[M+H]^+$: 1001.356; Observed $[M+Na]^+$: 1023.383 ; Observed $[M+K]^+$: 1040.315.

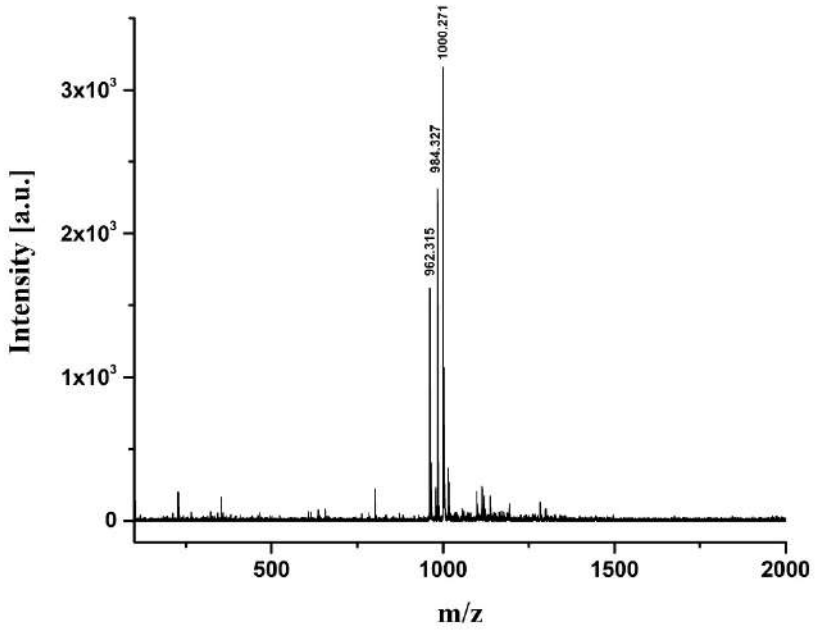

Figure B15. MALDI spectra of LKWFKKL-NH$_2$ **(P4^{L4F})**. Expected $[M+H]^+$: 961.634; Observed $[M+H]^+$: 962.315; Observed $[M+Na]^+$: 984.327; Observed $[M+K]^+$: 1000.271.

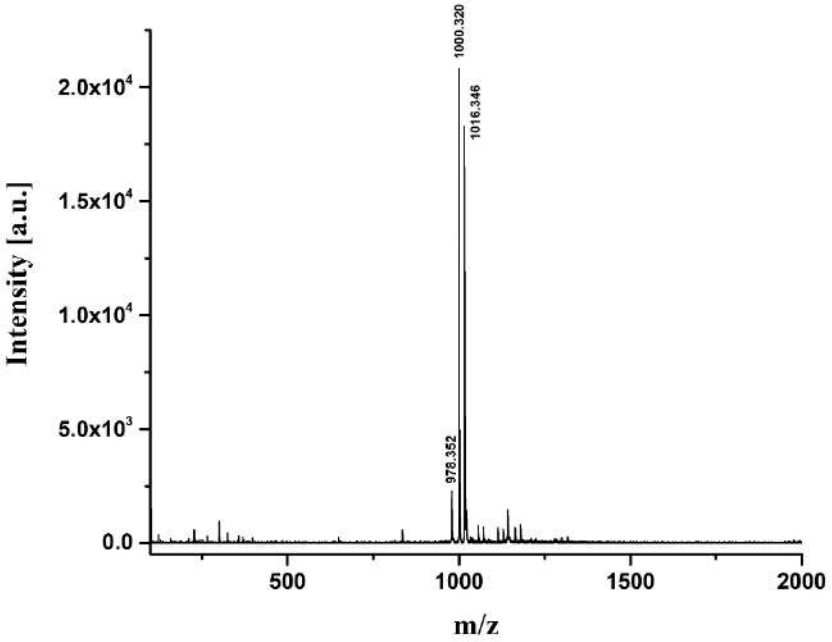

Figure B16. MALDI spectra of LKWYKKL-NH_2 **($P4^{L4Y}$)**. Expected $[M+H]^+$: 977.629; Observed $[M+H]^+$: 978.352; Observed $[M+Na]^+$: 1000.320; Observed $[M+K]^+$: 1016.346.

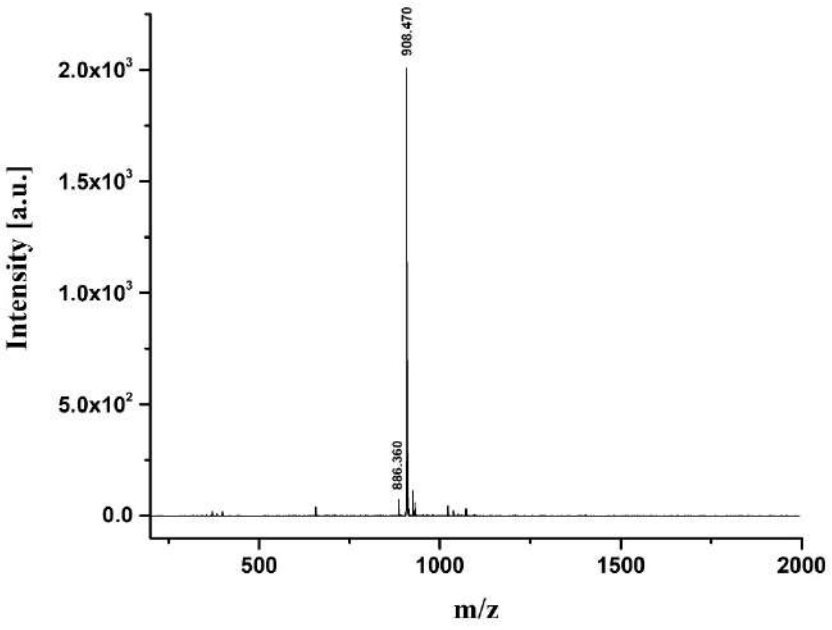

Figure B17. MALDI spectra of LKWAKKL-NH_2 **($P4^{L4A}$)**. Expected $[M+H]^+$: 885.603; Observed $[M+H]^+$: 886.360; Observed $[M+Na]^+$: 908.470.

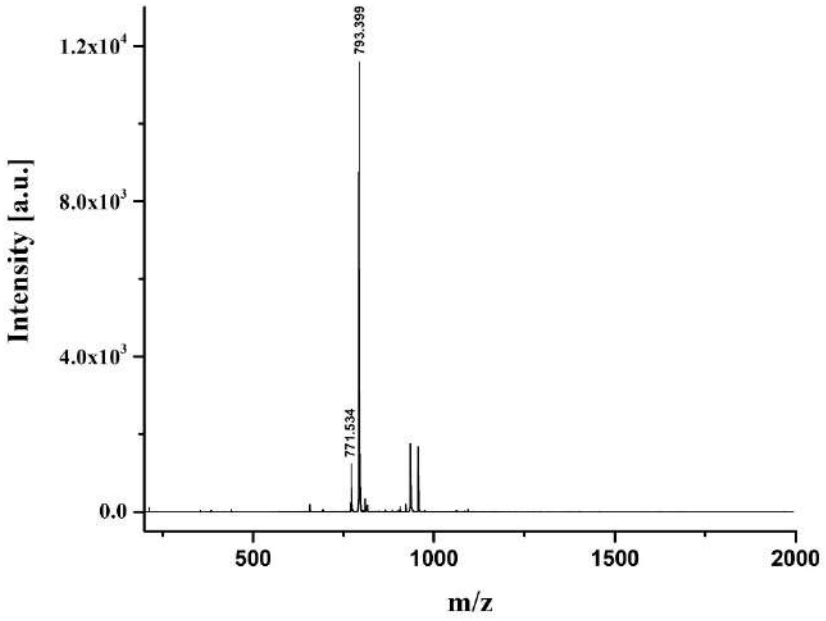

Figure B18. MALDI spectra of LKAAKKL-NH_2 **($P4^{W3A, L4A}$)**. Expected mass $[M+H]^+$: 770.561; Observed $[M+H]^+$: 771.534; Observed $[M+Na]^+$: 793.399.

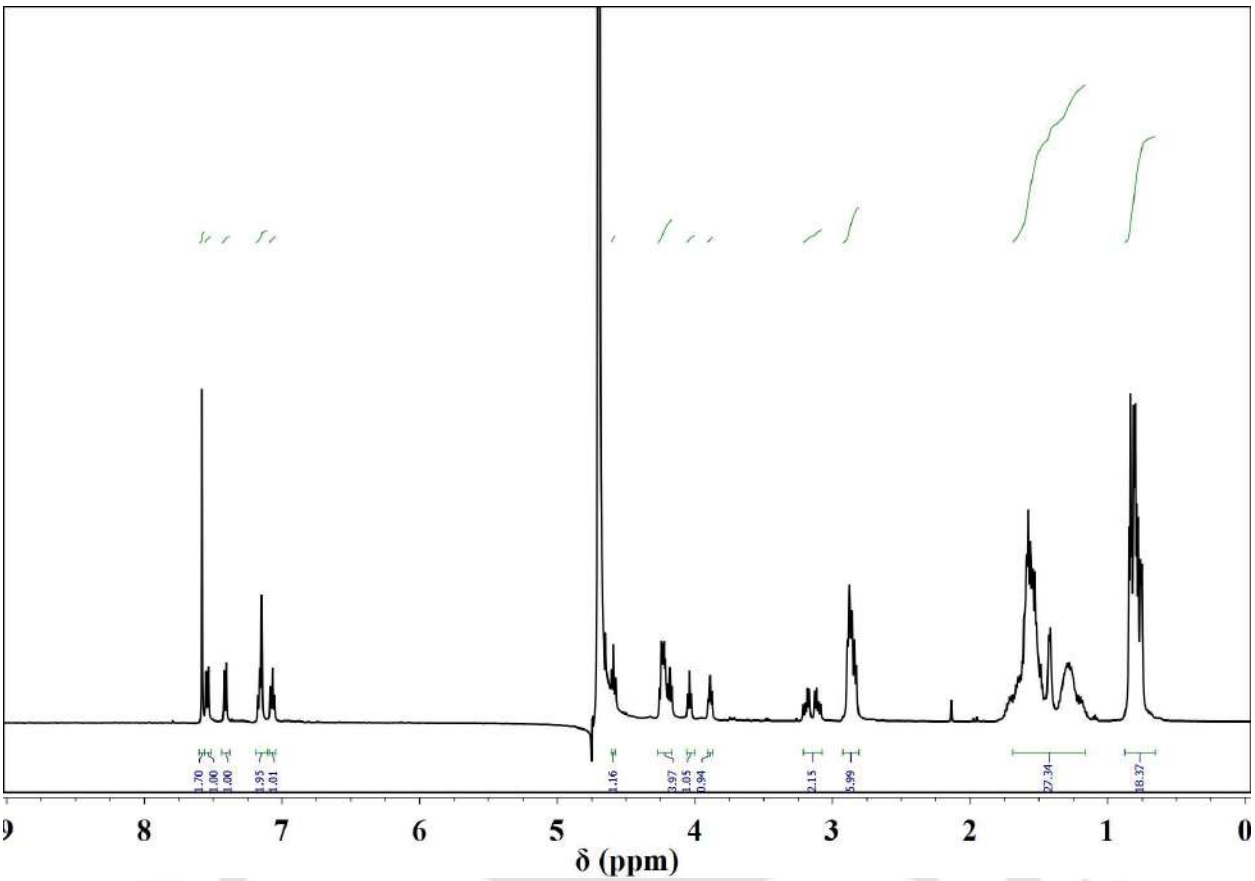

Figure B19. ^{1}H NMR spectra of LKWLKKL-NH_2 **(P4)** at room temperature in D_2O. ^{1}H NMR (500 MHz, D_2O) δ 0.65-0.88 (18H, Leucine), δ 1.16-1.69 (27H, Leucine and Lysine), δ 2.81-3.21 (8H, Lysine and Tryptophan), δ 3.87-4.60 (7 αH), δ 7.05-7.56 (5H, Tryptophan), δ 7.57-7.60 (2H, amide protons).

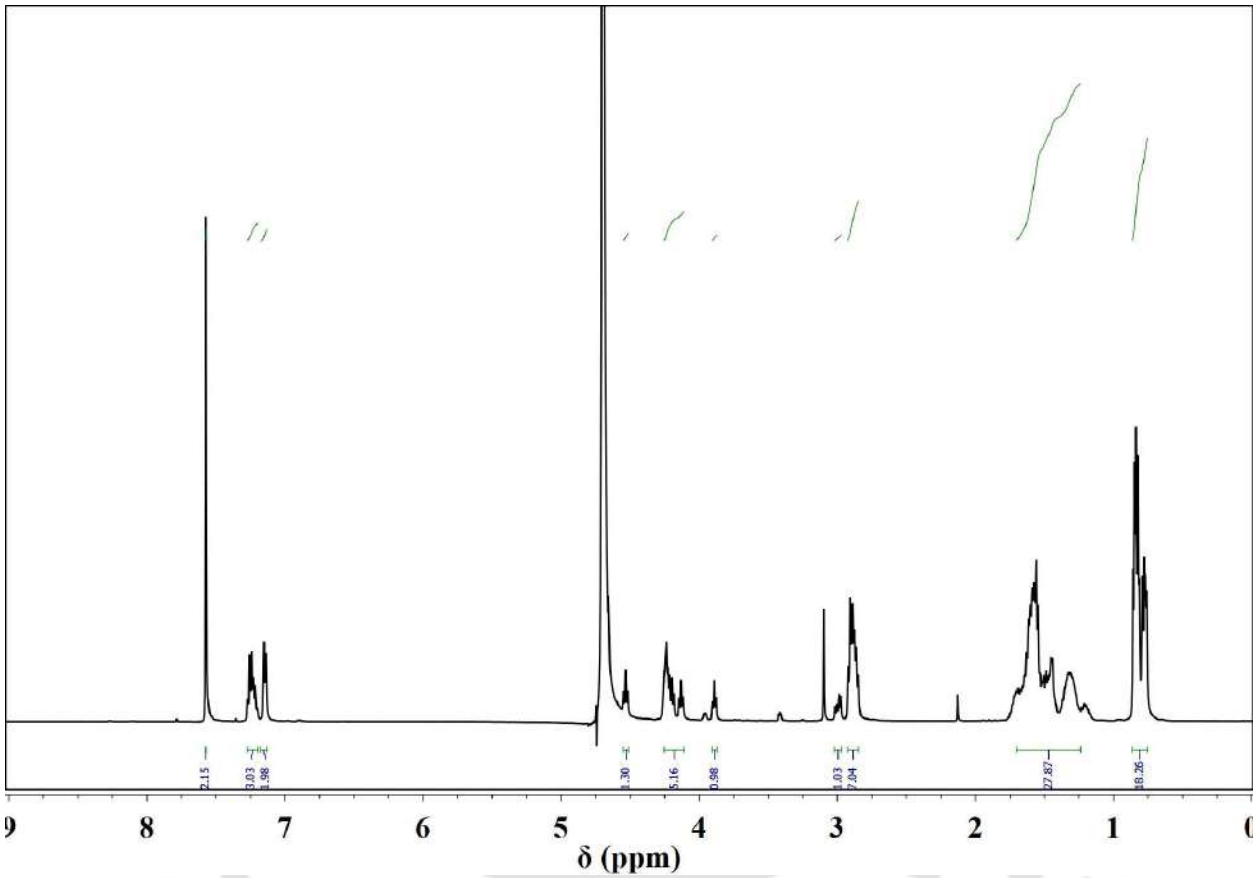

Figure B20. ^{1}H NMR spectra of LKFLKKL-NH_2 **(P4^{W3F})** at room temperature in D_2O. ^{1}H NMR (500 MHz, D_2O) δ 0.75-0.86 (18H, Leucine), δ 1.24-1.70 (27H, Leucine and Lysine), δ 2.85-3.02 (8H, Lysine and Phenylalanine), δ 3.87-4.55 (7 αH), δ 7.13-7.28 (5H, Phenylalanine), δ 7.56-7.58 (2H, amide protons).

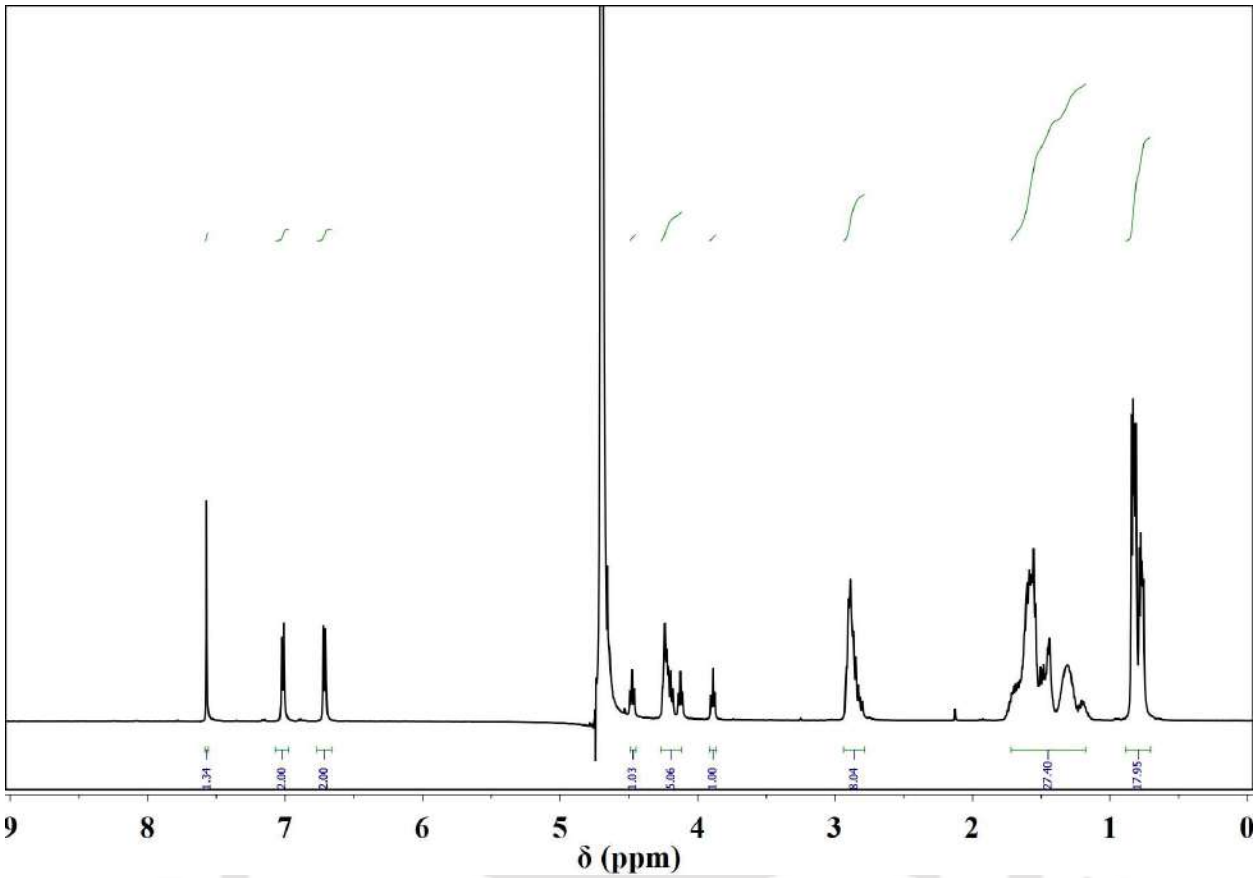

Figure B21. ^{1}H NMR spectra of LKYLKKL-NH_2 **(P4^{W3Y})** at room temperature in D_2O. ^{1}H NMR (500 MHz, D_2O) δ 0.70-0.88 (18H, Leucine), δ 1.18-1.72 (27H, Leucine and Lysine), δ 2.78-2.94 (8H, Lysine and Tyrosine), δ 3.86-4.49 (7 αH), δ 6.66-7.07 (4H, Tyrosine), δ 7.56-7.58 (2H, amide protons).

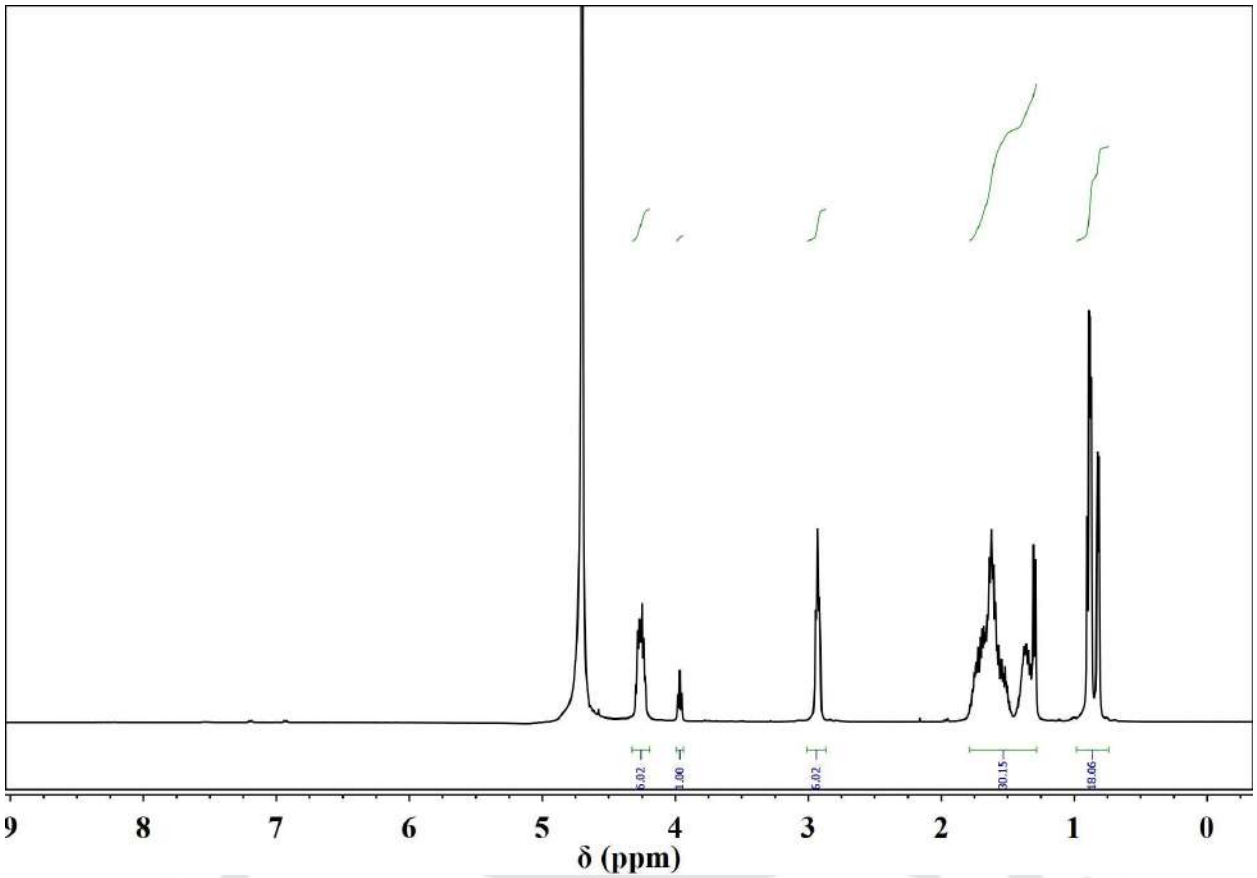

Figure B22. ^{1}H NMR spectra of LKALKKL-NH_2 **(P4^{W3A})** at room temperature in D_2O. ^{1}H NMR (500 MHz, D_2O) δ 0.74-0.98 (18H, Leucine), δ 1.28-1.79 (30H, Leucine, Lysine and Alanine), δ 2.87-3.01 (6H, Lysine), δ 3.94-4.32 (7 αH).

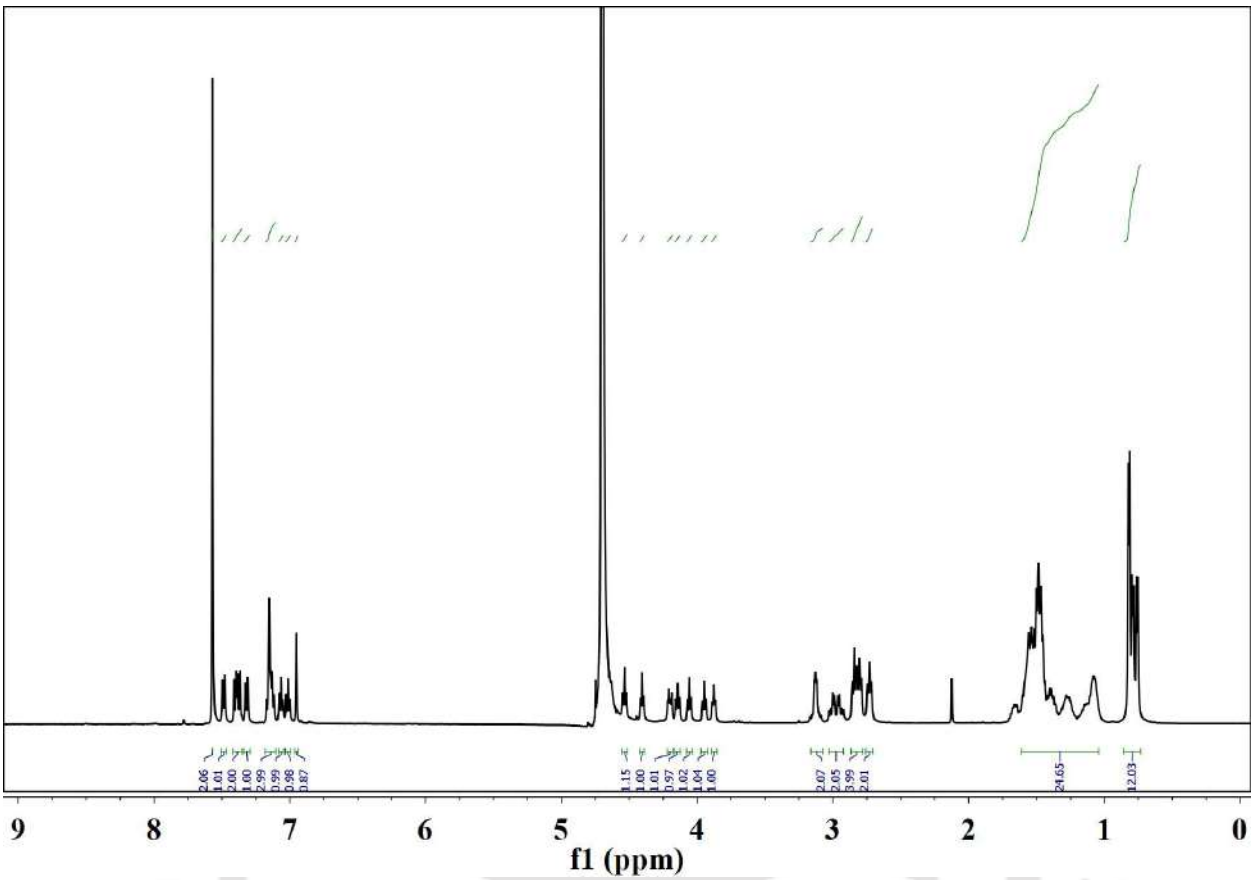

Figure B23. ^{1}H NMR spectra of LKWWKKL-NH_2 **(P4^{L4W})** at room temperature in D_2O. ^{1}H NMR (500 MHz, D_2O) δ 0.73-0.85 (12H, Leucine), δ 1.04-1.61 (24H, Leucine and Lysine), δ 2.70-3.16 (10H, Lysine and Tryptophan), δ 3.85-4.55 (7 αH), δ 6.94-7.50 (10H, Tryptophan), δ 7.56-7.58 (2H, amide protons).

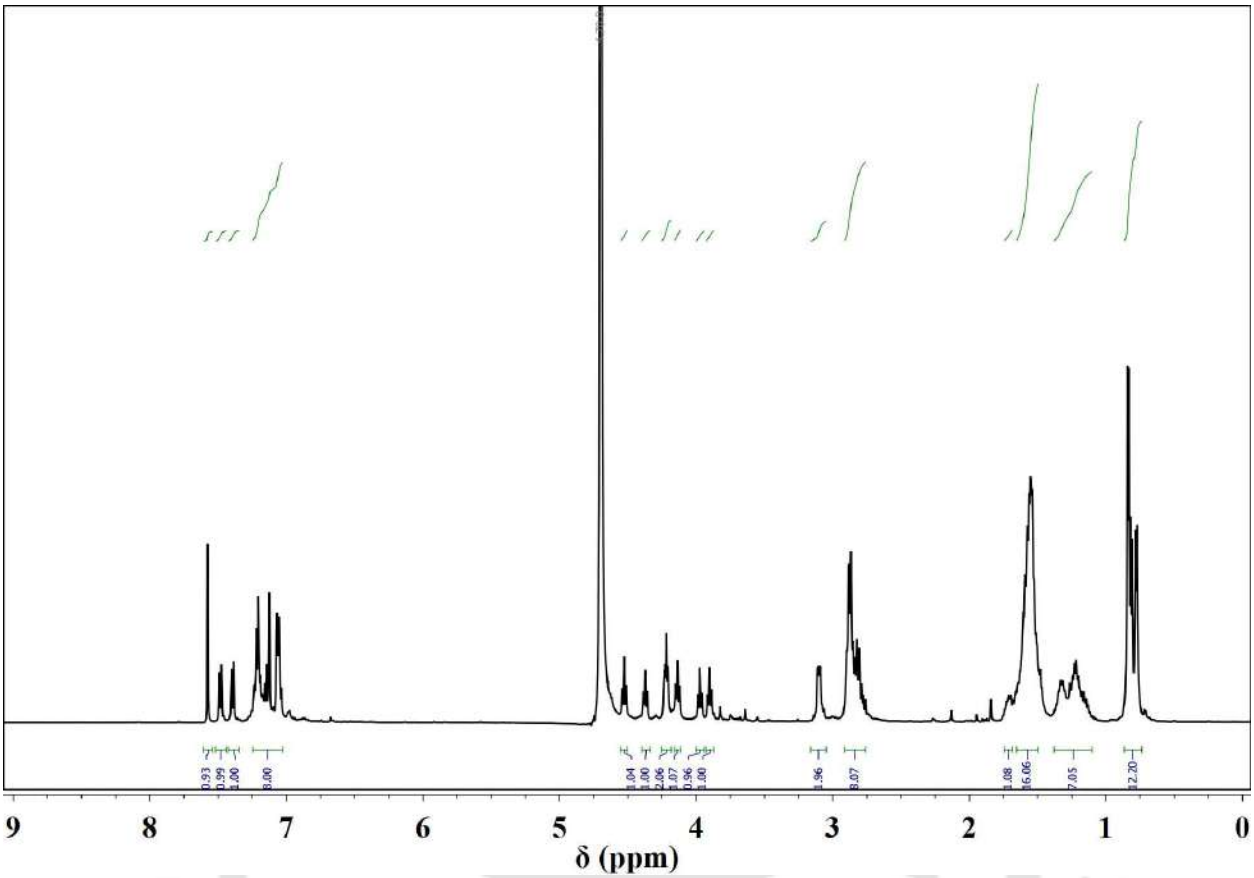

Figure B24. ^{1}H NMR spectra of LKWFKKL-NH_2 **($P4^{L4F}$)** at room temperature in D_2O. ^{1}H NMR (500 MHz, D_2O) δ 0.73-0.86 (12H, Leucine), δ 1.10-1.75 (24H, Leucine and Lysine), δ 2.76-3.16 (10H, Lysine, Tryptophan and Phenylalanine), δ 3.87-4.55 (7 αH), δ 7.04-7.52 (10H, Tryptophan and Phenylalanine), δ 7.55-7.59 (2H, amide protons).

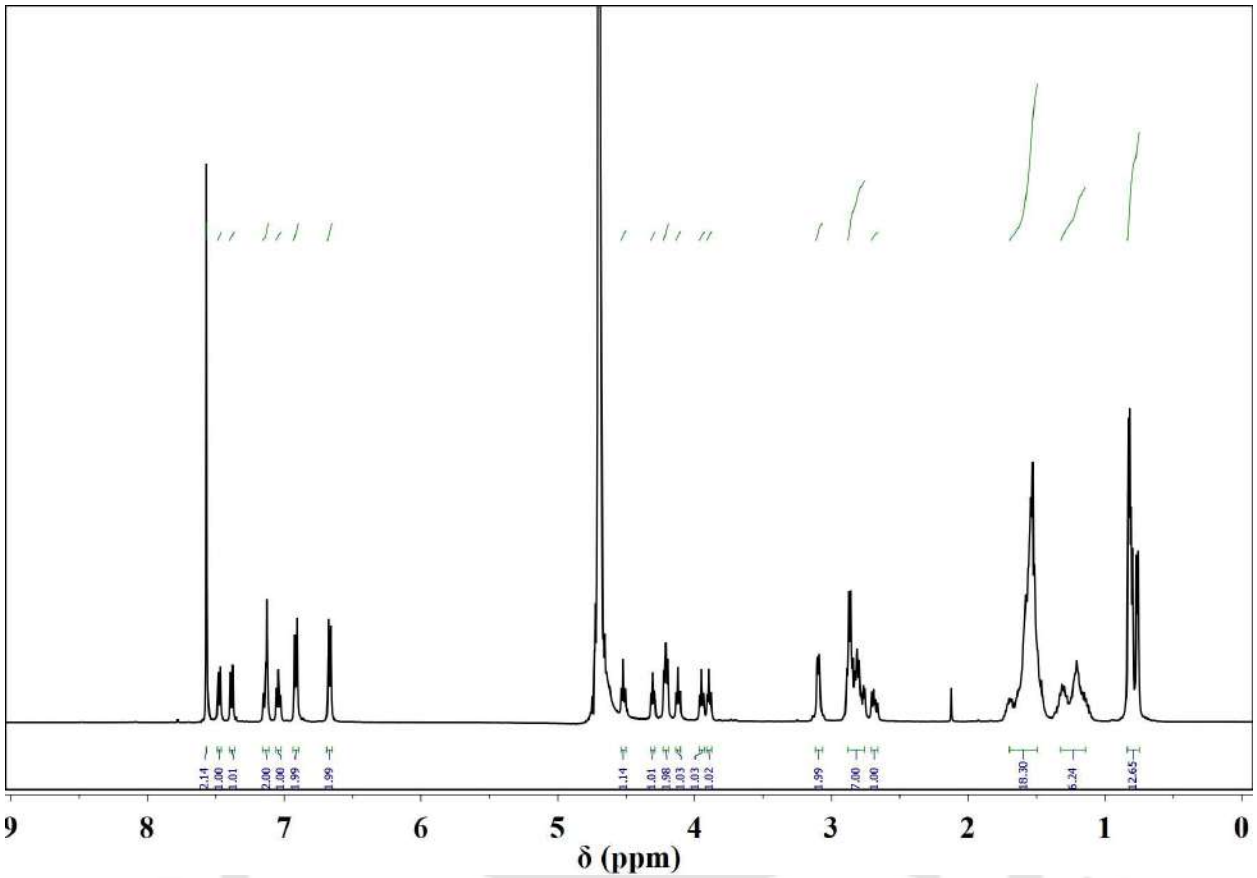

Figure B25. ^{1}H NMR spectra of LKWYKKL-NH_2 **(P4^{L4Y})** at room temperature in D_2O. ^{1}H NMR (500 MHz, D_2O) δ 0.75-0.84 (12H, Leucine), δ 1.15-1.71 (24H, Leucine and Lysine), δ 2.66-3.12 (10H, Lysine, Tryptophan and Tyrosine), δ 3.87-4.54 (7 αH), δ 6.64-7.50 (9H, Tryptophan and Tyrosine), δ 7.56-7.58 (2H, amide protons).

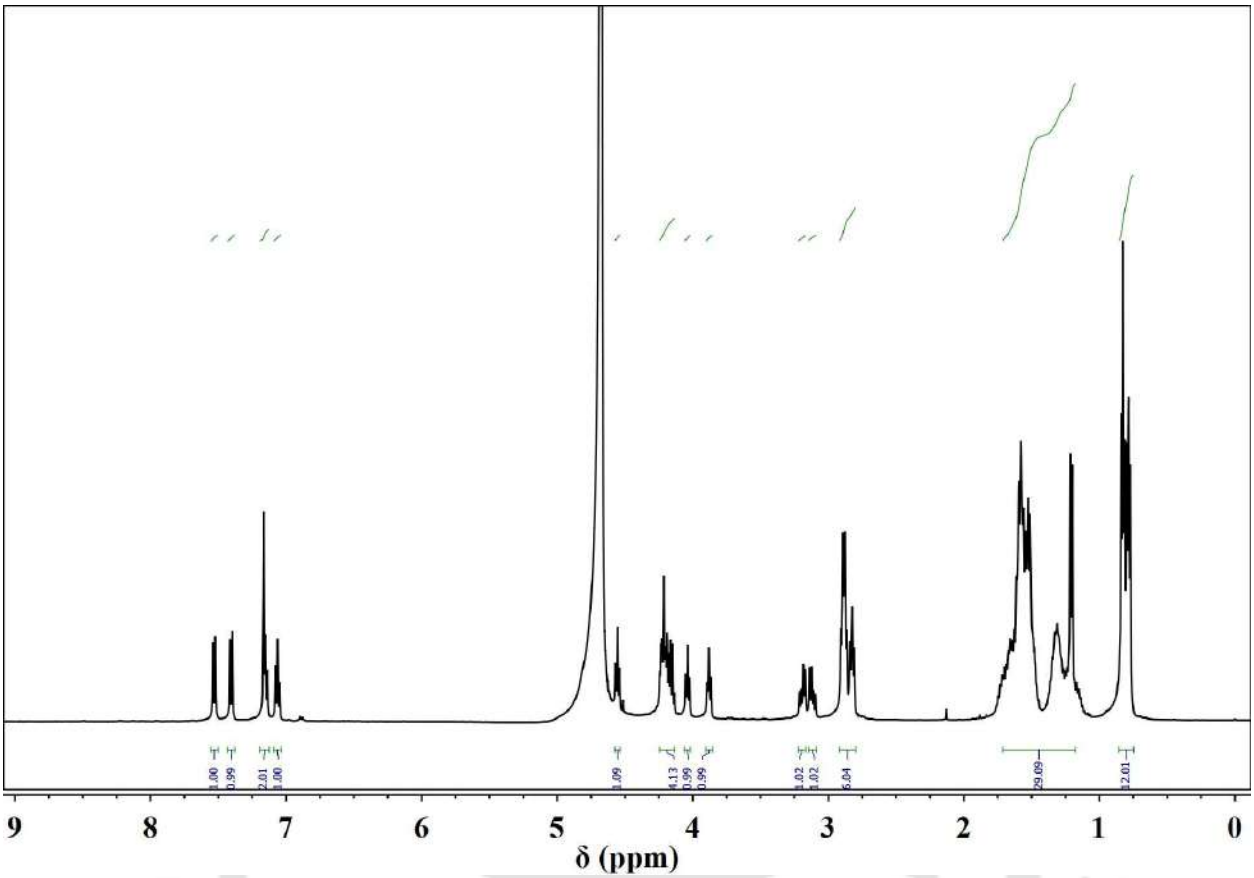

Figure B26. ^{1}H NMR spectra of LKWAKKL-NH_2 **(P4^{L4A})** at room temperature in D_2O. ^{1}H NMR (500 MHz, D_2O) δ 0.75-0.87 (12H, Leucine), δ 1.18-1.72 (27H, Leucine, Lysine and alanine), δ 2.79-2.91 (6H, Lysine), δ 3.09-3.23 (2H, Tryptophan), δ 3.85-4.57 (7 αH), δ 7.04-7.56 (5H, Tryptophan).

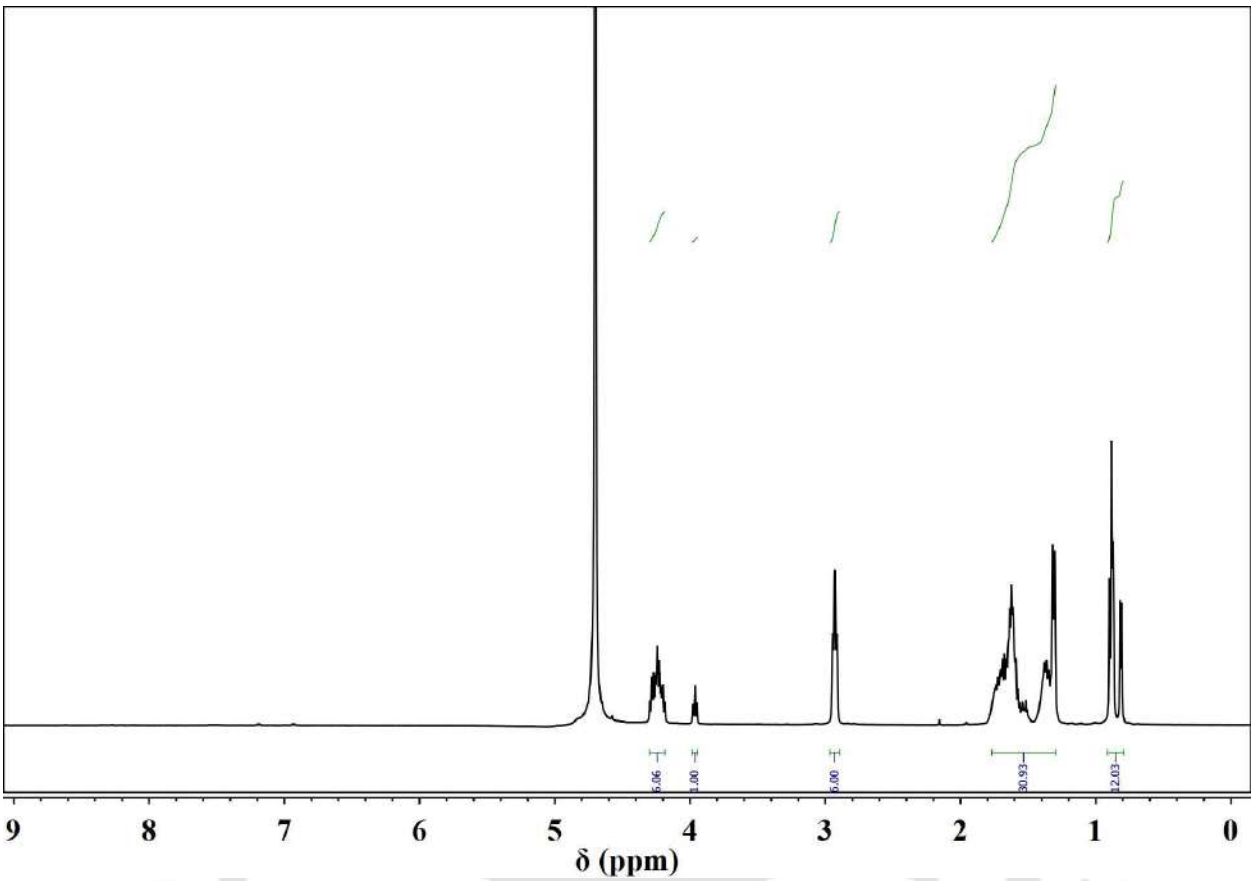

Figure B27. ^{1}H NMR spectra of LKAAKKL-NH_2 **(P4$^{W3A, L4A}$)** at room temperature in D_2O. ^{1}H NMR (500 MHz, D_2O) δ 0.79-0.91 (12H, Leucine), δ 1.29-1.77 (30H, Leucine, Lysine and Alanine), δ 2.89-2.87 (6H, Lysine), δ 3.94-4.30 (7 αH).

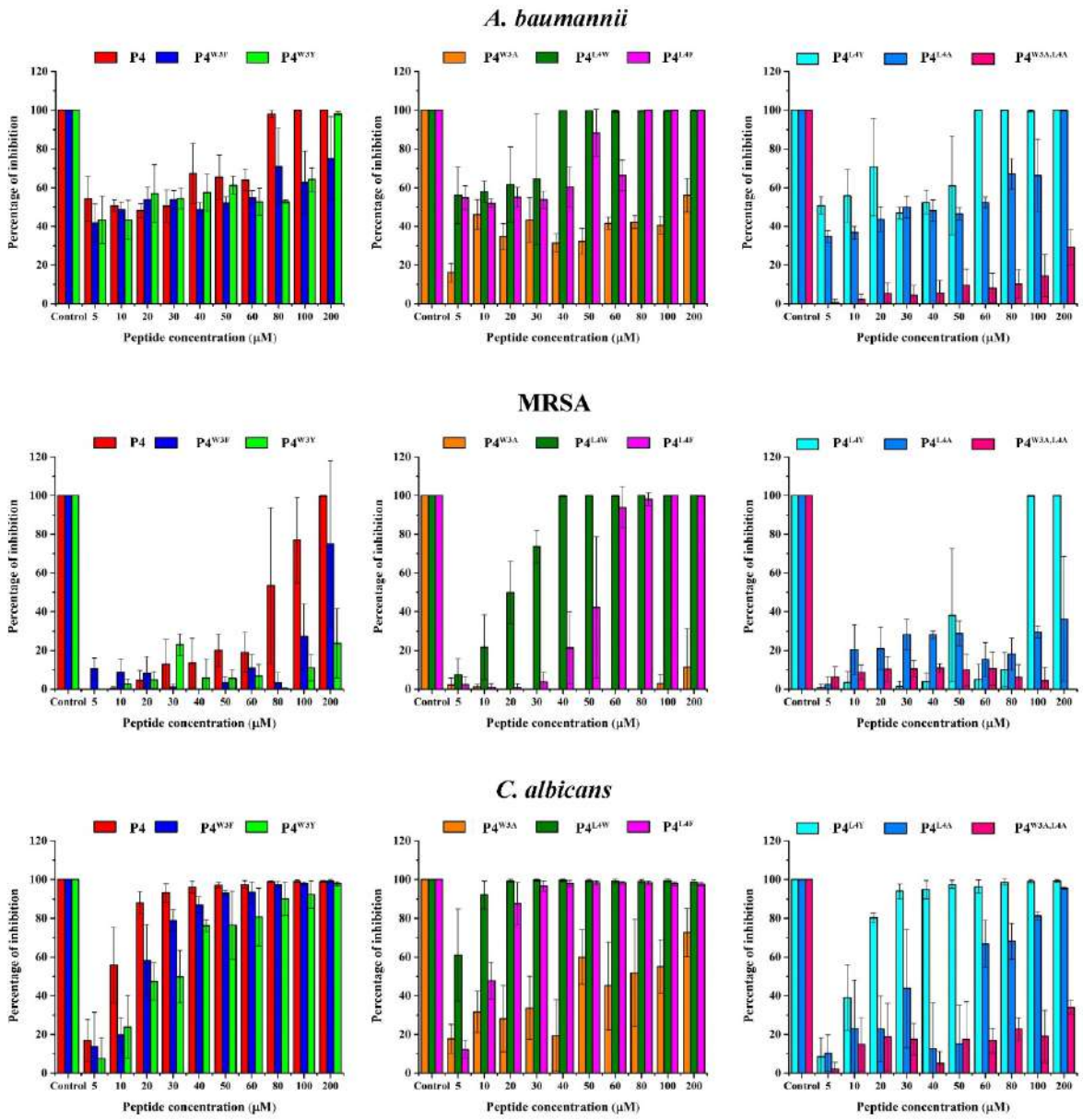

Figure B28. Bar diagrams for determination of minimum inhibitory concentration or $MIC_{90\%}$. Bar diagrams represent the percentage inhibition of the microbes *A. baumannii*, MRSA and *C. albicans* corresponding to different concentrations of the peptides used.

Table B1. Alchemical free energies (Kcal/mol). Standard error given after '±'.

	Free peptide in water (ΔG^{free})			
Alchemical transformation	Trial 1	Trial 2	Trial 3	Averaged ΔG^{free}
P4 → $P4^{W3F}$	-12.23 ± 0.04	-12.42 ± 0.05	-12.39 ± 0.05	-12.35 ± 0.05
P4 → $P4^{W3Y}$	-29.71 ± 0.03	-29.78 ± 0.08	-29.84 ± 0.07	-29.78 ± 0.06
P4 → $P4^{W3A}$	-21.32 ± 0.10	-21.25 ± 0.08	-21.29 ± 0.11	-21.29 ± 0.10
P4 → $P4^{L4W}$	36.12 ± 0.06	36.08 ± 0.09	36.17 ± 0.07	36.12 ± 0.07
P4 → $P4^{L4F}$	23.82 ± 0.11	23.77 ± 0.09	23.69 ± 0.11	23.76 ± 0.10
P4 → $P4^{L4Y}$	6.21 ± 0.04	6.29 ± 0.08	6.33 ± 0.05	6.28 ± 0.06
P4 → $P4^{L4A}$	15.31 ± 0.06	15.39 ± 0.09	15.28 ± 0.07	15.33 ± 0.07
P4 → $P4^{W3A,L4A}$	-6.53 ± 0.08	-6.49 ± 0.08	-6.43 ± 0.10	-6.48 ± 0.09
	Peptide bound to POPE/POPG-bilayer (ΔG^{comp})			
	Trial 1	Trial 2	Trial 3	Average ΔG^{comp}
P4 → $P4^{W3F}$	-10.75 ± 0.04	-11.18 ± 0.11	-11.02 ± 0.08	-10.98 ± 0.08
P4 → $P4^{W3Y}$	-28.11 ± 0.12	-27.65 ± 0.14	-28.04 ± 0.11	-27.93 ± 0.12
P4 → $P4^{W3A}$	-18.39 ± 0.10	-18.84 ± 0.08	-18.15 ± 0.07	-18.46 ± 0.08
P4 → $P4^{L4W}$	32.17 ± 0.08	32.59 ± 0.09	32.88 ± 0.14	32.55 ± 0.10
P4 → $P4^{L4F}$	21.48 ± 0.11	21.07 ± 0.09	20.89 ± 0.08	21.15 ± 0.09
P4 → $P4^{L4Y}$	4.08 ± 0.04	3.91 ± 0.06	3.86 ± 0.06	3.95 ± 0.05
P4 → $P4^{L4A}$	14.12 ± 0.06	14.58 ± 0.07	15.02 ± 0.04	14.57 ± 0.06
P4 → $P4^{W3A,L4A}$	-4.51 ± 0.08	-4.19 ± 0.09	-3.98 ± 0.07	-4.23 ± 0.08

	$\Delta\Delta G = \Delta G^{comp} - \Delta G^{free}$
P4 → $P4^{W3F}$	**1.36 ± 0.12**
P4 → $P4^{W3Y}$	**1.84 ± 0.27**
P4 → $P4^{W3A}$	**2.83 ± 0.37**
P4 → $P4^{L4W}$	**-3.58 ± 0.34**
P4 → $P4^{L4F}$	**-2.61 ± 0.24**
P4 → $P4^{L4Y}$	**-2.33 ± 0.18**
P4 → $P4^{L4A}$	**-0.75 ± 0.47**
P4 → $P4^{W3A,L4A}$	**2.26 ± 0.22**

Table B2. Minimal inhibitory concentration (MIC) of P4 and its analogues (> 200 = not detectable) against *Acinetobacter baumannii*, Methicillin-resistant *Staphylococcus aureus* (MRSA), and *Candida albicans*. $MIC_{90\%}$ is the minimum concentration of a peptide that inhibits the growth of 90% of a particular microbe.

Peptides	**Minimum Inhibitory Concentration ($MIC_{90\%}$)**		
	A. baumannii	MRSA	*C. albicans*
P4	**80**	**200**	**30**
$P4^{W3F}$	>200	>200	50
$P4^{W3Y}$	200	>200	80
$P4^{W3A}$	>200	>200	>200
$P4^{L4W}$	**40**	**40**	**10**
$P4^{L4F}$	80	60	30
$P4^{L4Y}$	60	100	30
$P4^{L4A}$	200	>200	200
$P4^{W3A,L4A}$	**>200**	**>200**	**>200**

Table B3. Trajectory averaged hydrophobic surface area (formed by the aliphatic hydrocarbon of lipid bilayer) around 3.4 Å of the peptide side chain was estimated and reported as "interaction area". Penetration depth is the distance between the centre of the bilayer and the backbone (c_α) of the fourth residue (middle) of the peptide, estimated from the last frame of the trajectory.

Complex	Interaction area ± Std. dev ($Å^2$)	Penetration depth (Å)
P4	**43.827 ± 1.236**	**15.7**
$P4^{W3F}$	41.421 ± 1.116	15.9
$P4^{W3Y}$	40.933 ± 0.988	16.1
$P4^{W3A}$	37.646 ± 1.729	17.2
$P4^{L4W}$	**48.996 ± 0.971**	**14.3**
$P4^{L4F}$	45.824 ± 1.052	14.9
$P4^{L4Y}$	44.973 ± 1.038	15.1
$P4^{W3A,L4A}$	**32.262 ± 1.985**	**17.9**

Appendix C (for Chapter 4)

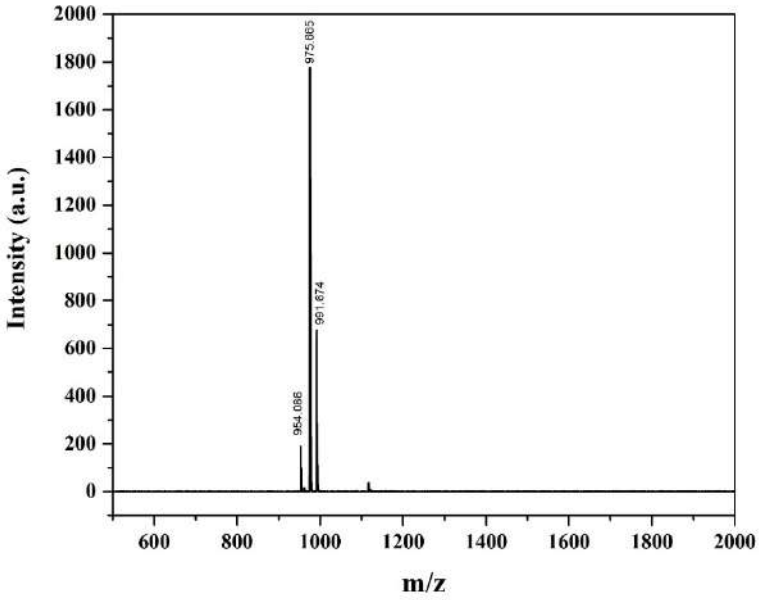

Figure C1. MALDI-TOF spectra of **Jc**. Calc. $(M+H)^+$ for Jc = 953.593 Da; Obs. $(M+H)^+$ = 954.086 Da, Obs. $(M+Na)^+$ = 975.665 Da, Obs. $(M+K)^+$ = 991.674 Da.

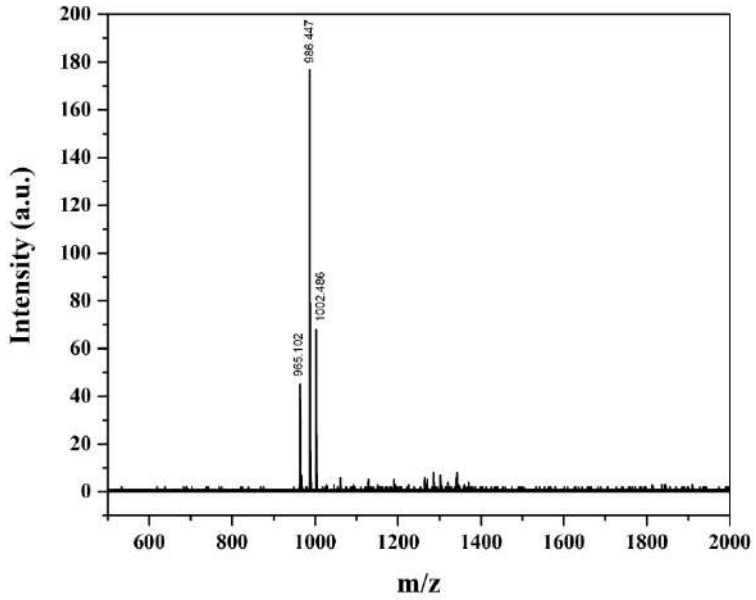

Figure C2. MALDI-TOF spectra of **J1**. Calc. $(M+H)^+$ for J1 = 964.573 Da; Obs. $(M+H)^+$ = 965.102 Da, Obs. $(M+Na)^+$ = 986.447 Da, Obs. $(M+K)^+$ = 1002.486 Da.

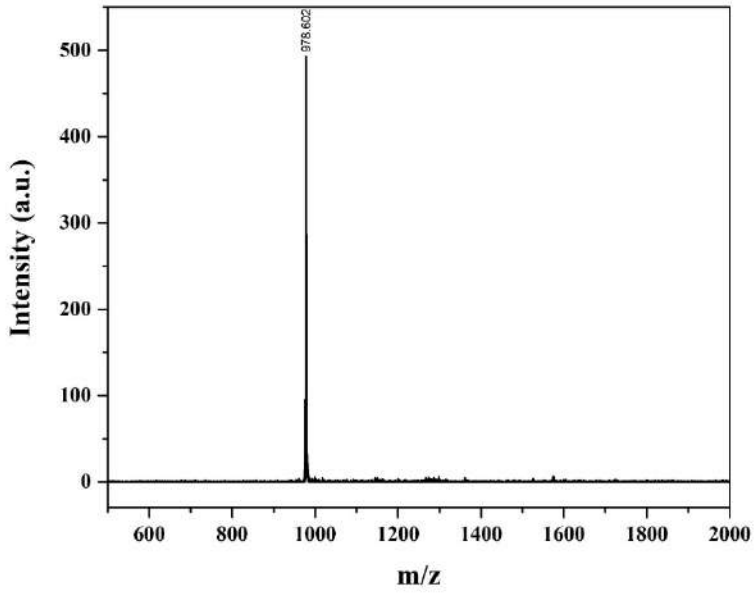

Figure C3. MALDI-TOF spectra of **J2**. Calc. $(M+H)^+$ for J2 = 977.604 Da; Obs. $(M+H)^+$ = 978.602 Da.

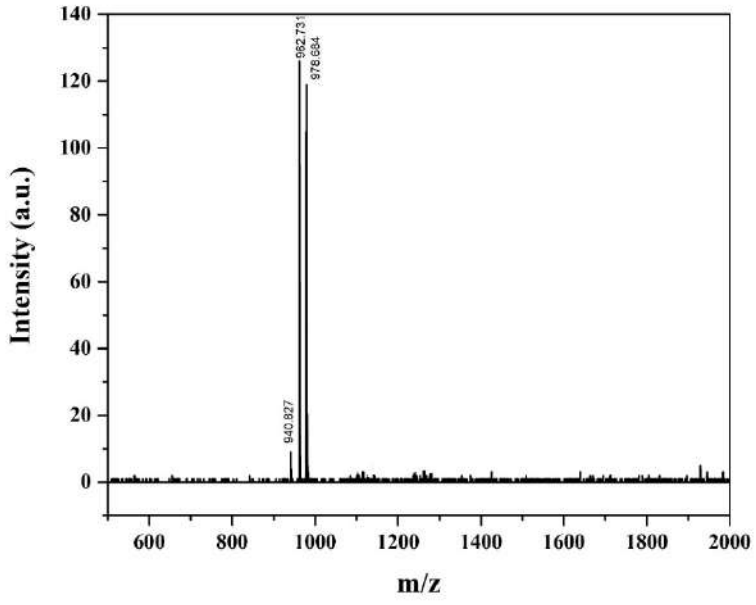

Figure C4. MALDI-TOF spectra of **J3**. Calc. $(M+H)^+$ for J3 = 940.609 Da; Obs. $(M+H)^+$ = 940.827 Da, Obs. $(M+Na)^+$ = 962.731 Da, Obs. $(M+K)^+$ = 978.684 Da.

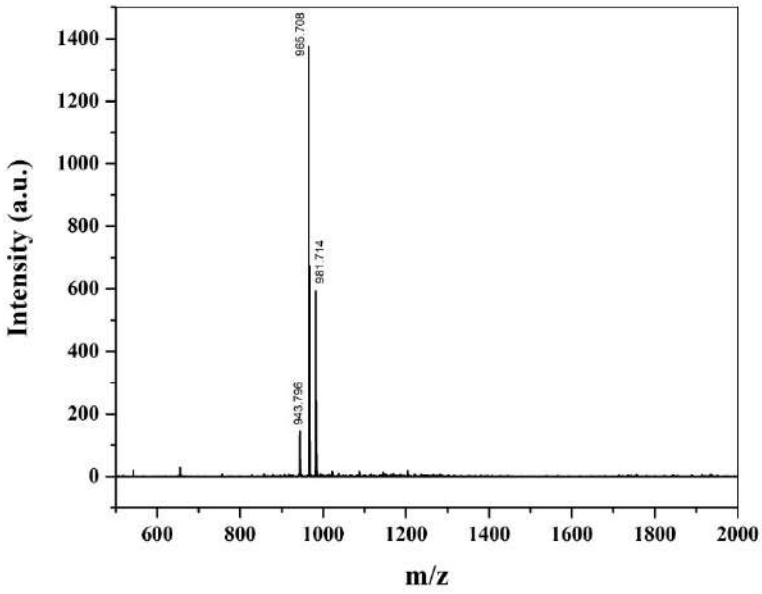

Figure C5. MALDI-TOF spectra of **J4**. Calc. $(M+H)^+$ for J4 = 943.620 Da; Obs. $(M+H)^+$ = 943.796 Da, Obs. $(M+Na)^+$ = 965.708 Da, Obs. $(M+K)^+$ = 981.714 Da.

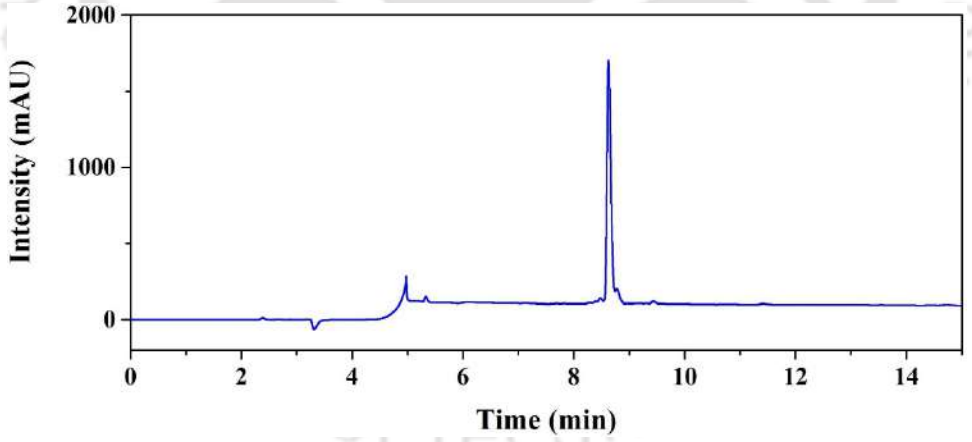

Figure C6. Analytic HPLC trace of **Jc** at 214 nm. Retention time: 8.63 min.

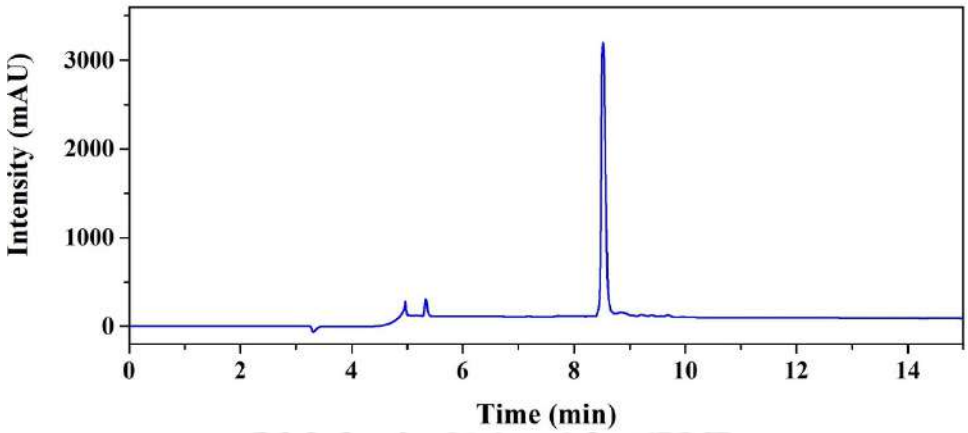

Figure C7. Analytic HPLC trace of **J1** at 214 nm. Retention time: 8.54 min.

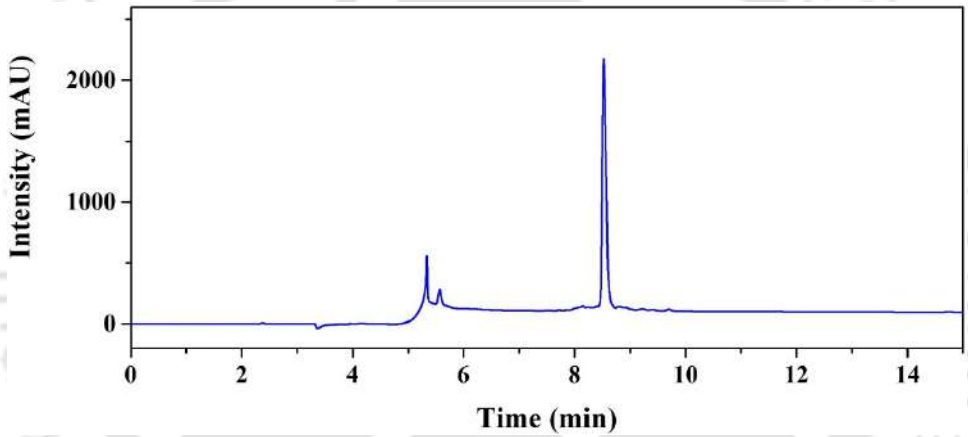

Figure C8. Analytic HPLC trace of **J2** at 214 nm. Retention time: 8.53 min.

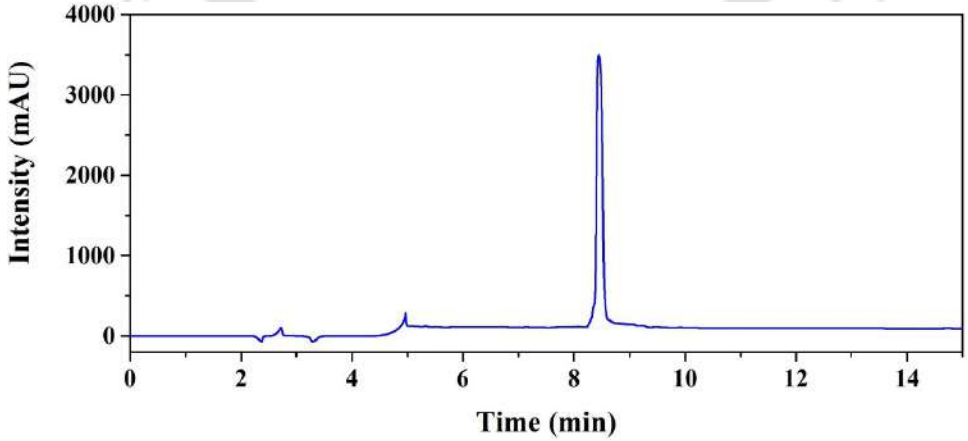

Figure C9. Analytic HPLC trace of **J3** at 214 nm. Retention time: 8.45 min.

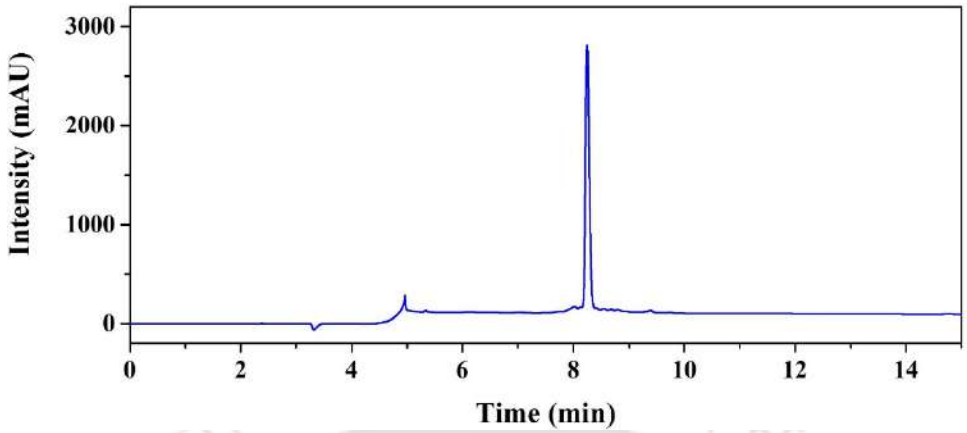

Figure C10. Analytic HPLC trace of **J4** at 214 nm. Retention time: 8.25 min.

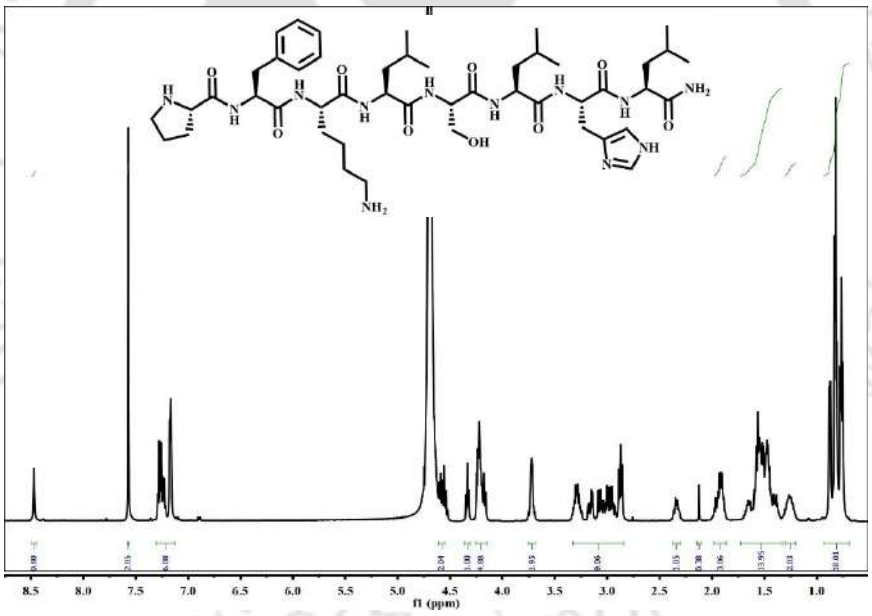

Figure C11. ^{1}H NMR spectra of **Jc** at room temperature in D_2O. ^{1}H NMR (500 MHz, D_2O) δ 0.69-0.94 (18H, Leucine), δ 1.20-1.98 (19H, Leucine, Lysine and Proline), δ 2.30-2.36 (1H, NH proton of Proline), δ 2.84-3.76 (11 H, Proline, Phenylalanine, Lysine, Serine, Histidine), δ 4.14-4.60 (8 αH), δ 7.12-7.31 (6H, 5 aromatic protons of Phenylalanine; 1 aromatic proton of Histidine), δ 7.12-7.31 (amide protons), δ 8.46-8.49 (1H, aromatic proton of Histidine).

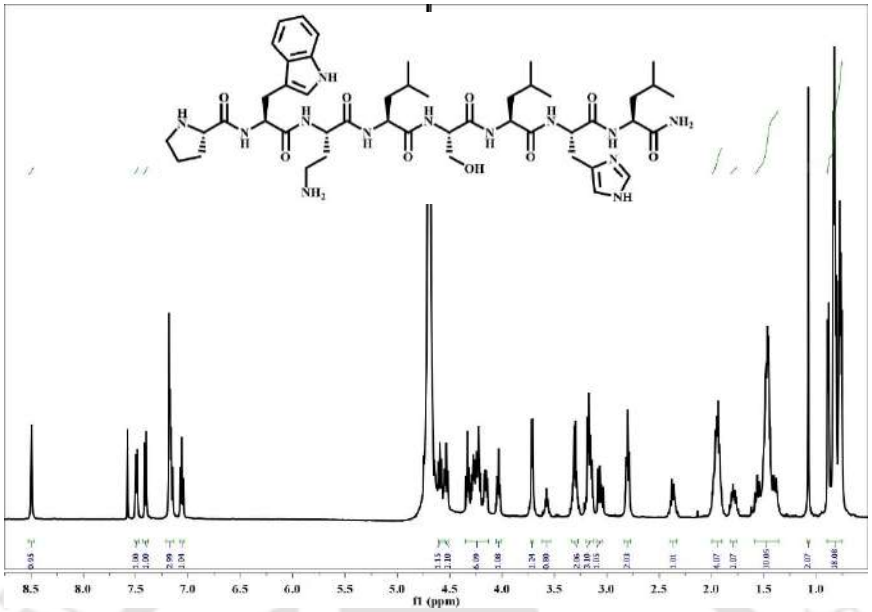

Figure C12. ^{1}H NMR spectra of **J1** at room temperature in D_2O. ^{1}H NMR (500 MHz, D_2O) δ 0.75-0.89 (18H, Leucine), δ 1.06-1.99 (15H, Leucine, Diaminobutyric acid and Proline), δ 2.33-2.39 (1H, amine of Proline), δ 2.77-4.06 (11 H, Proline, Tryptophan, Diaminobutyric acid, Serine, Histidine), δ 4.13-4.61 (8 αH), 7.03-7.51 (5H, aromatic protons of Tryptophan; 1H, aromatic proton of Histidine), 8.48-8.51 (1H, aromatic proton of Histidine).

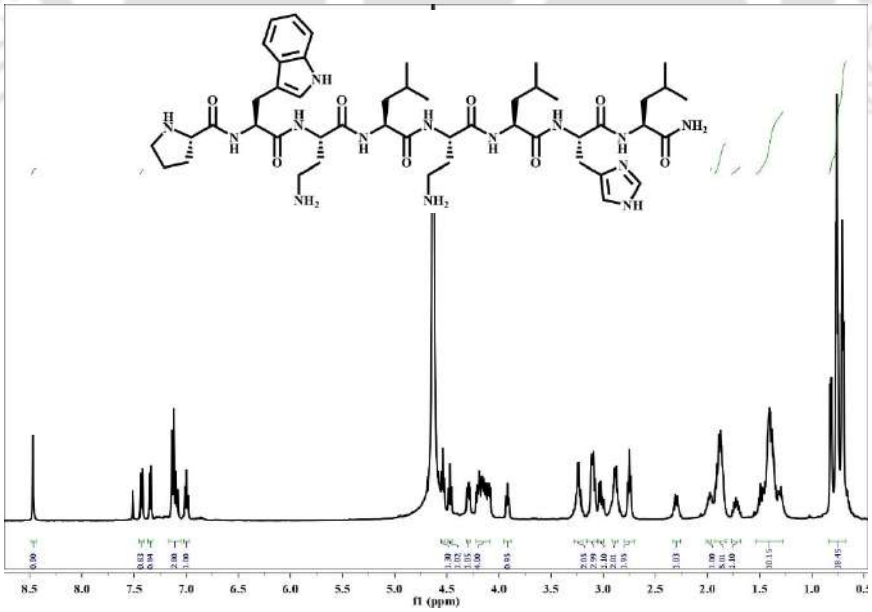

Figure C13. ^{1}H NMR spectra of **J2** at room temperature in D_2O. ^{1}H NMR (500 MHz, D_2O) δ 0.67-0.83 (18H, Leucine), δ 1.28-2.01 (17H, Leucine, Diaminobutyric acid and Proline), δ 2.26-

2.34 (1H, amine of Proline), δ 2.70-3.95 (11 H, Proline, Tryptophan, Diaminobutyric acid, Histidine), δ 4.09-4.56 (8 αH), 6.97-7.44 (5H, aromatic protons of Tryptophan; 1H, aromatic proton of Histidine), 8.44-8.48 (1H, aromatic proton of Histidine).

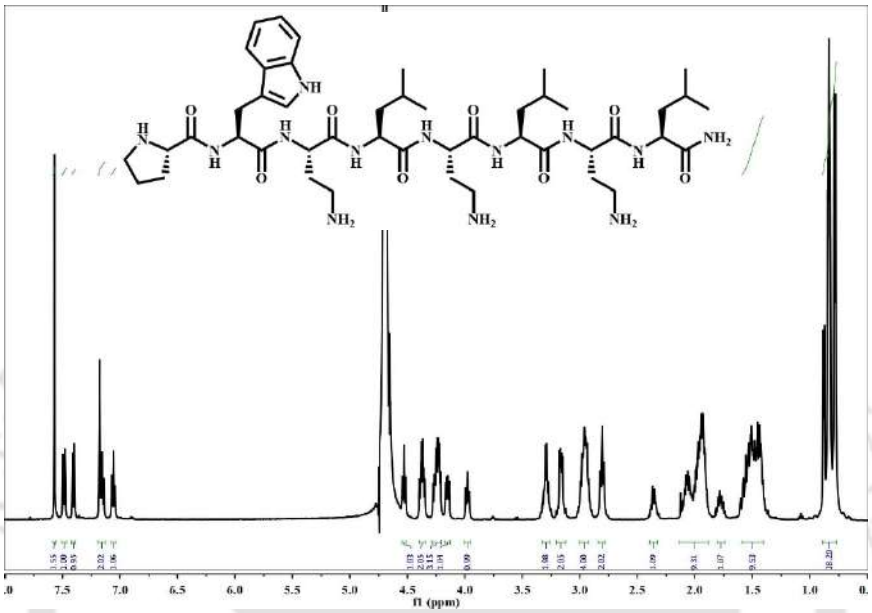

Figure C14. ^{1}H NMR spectra of **J3** at room temperature in D_2O. ^{1}H NMR (500 MHz, D_2O) δ 0.77-0.90 (18H, Leucine), δ 1.40-2.14 (19H, Leucine, Diaminobutyric acid and Proline), δ 2.33-2.39 (1H, amine of Proline), δ 2.77-4.01 (11 H, Proline, Tryptophan, Diaminobutyric acid), δ 4.13-4.55 (8 αH), 7.04-7.50 (5H, aromatic protons of Tryptophan).

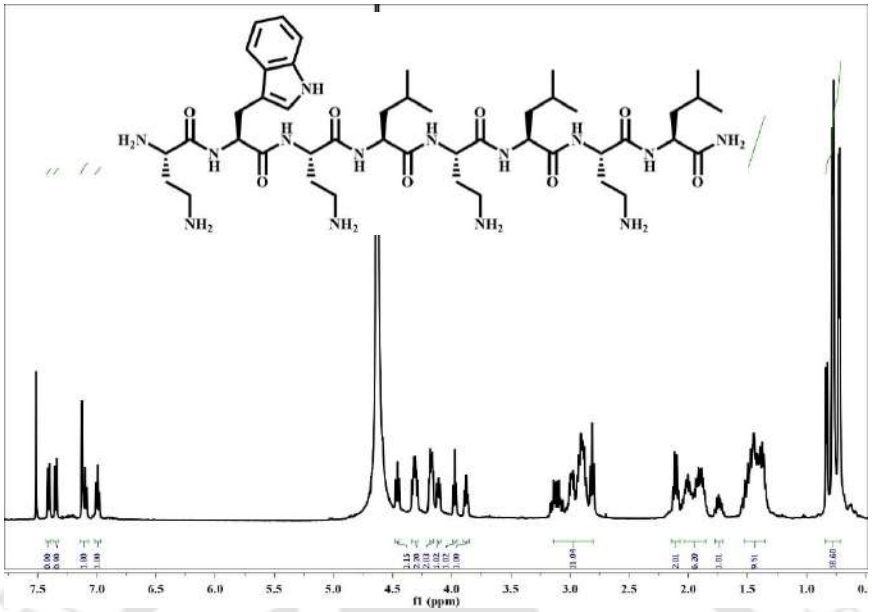

Figure C15. ^{1}H NMR spectra of **J4** at room temperature in D_2O. ^{1}H NMR (500 MHz, D_2O) δ 0.71-0.84 (18H, Leucine), δ 1.36-2.13 (17 H, Leucine, Diaminobutyric acid), δ 2.79-3.15 (11 H, Diaminobutyric acid, Tryptophan), δ 3.86-4.48 (8 αH), 6.96-7.43 (5H, aromatic protons of Tryptophan).

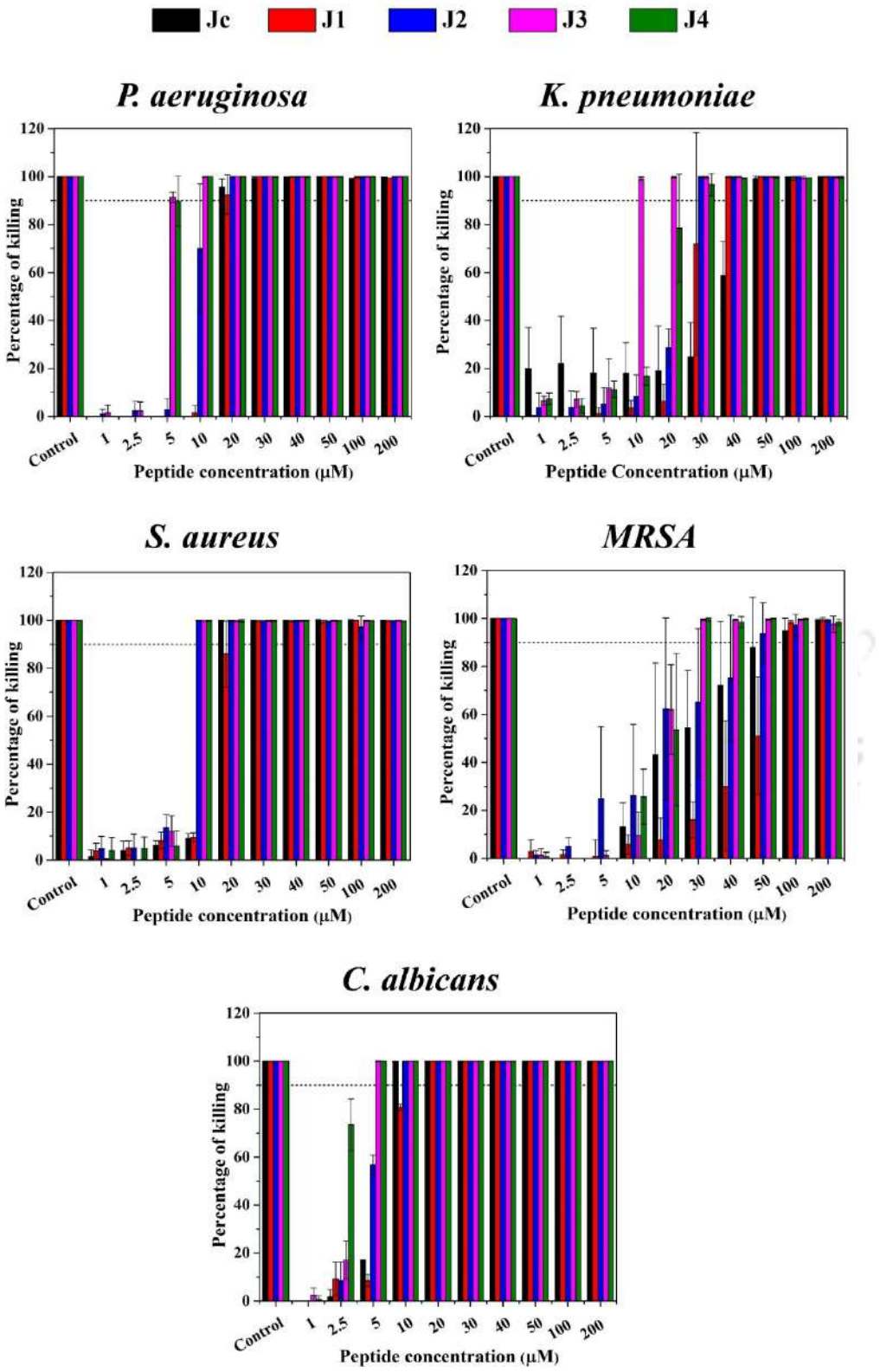

Figure C16. Determination of Minimum Inhibitory Concentration (MIC). Bar diagram representation depicting percentage killing of the microbes corresponding to different

concentrations. $MIC_{90\%}$ values were the lowest concentrations at which more than 90% killings were observed respectively for *P. aeruginosa, K. pneumoniae, S. aureus,* Methicillin Resistant *Staphylococcus aureus (MRSA)* and *C. albicans*.

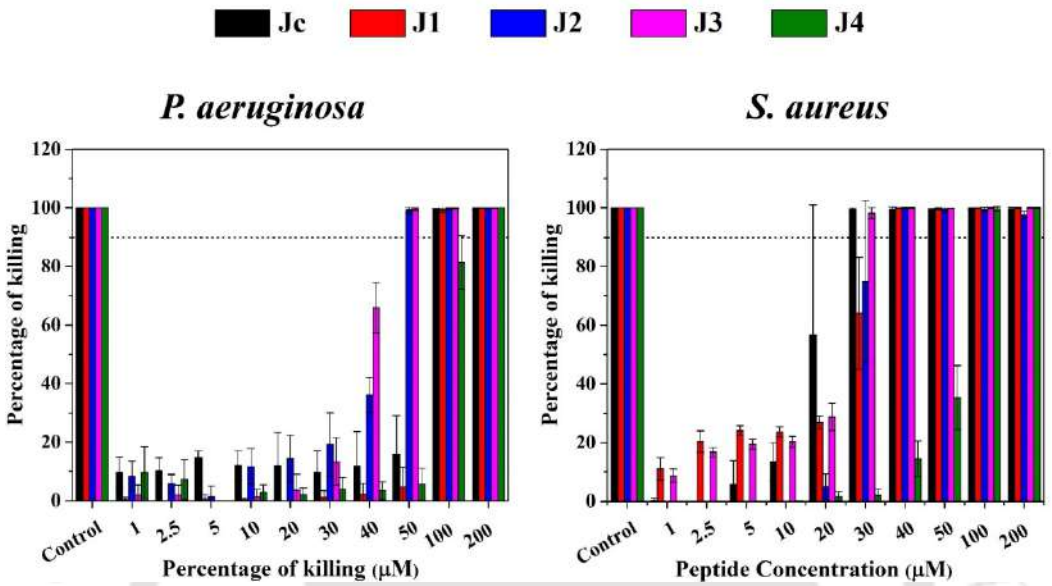

Figure C17. Determination of Minimum Inhibitory Concentration (MIC) in the presence of 150 mM NaCl. Bar diagram representation depicting percentage killing of *P. aeruginosa* and *S. aureus,* in the presence of 150 mM NaCl. $MIC_{90\%}$ values were the lowest concentrations at which more than 90% killings were observed.

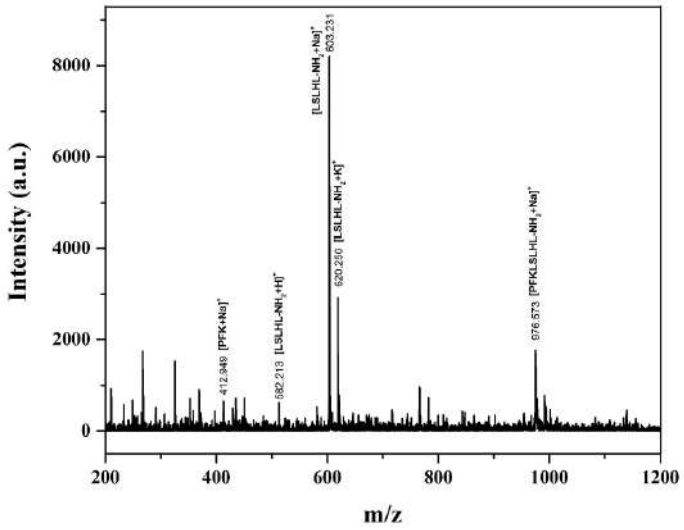

Figure C18. MALDI-TOF spectra of **Jc** (incubated with trypsin for 24 h). 412.949 Da corresponds to mass due to the fragment $[PFK+Na]^+$ (expected mass of PFK: 390.227 Da); 582.213 Da

corresponds to mass due to the fragment $[LSLHL\text{-}NH_2+H]^+$, 603.231 Da corresponds to mass due to the fragment $[LSLHL\text{-}NH_2+Na]^+$, 620.250 Da corresponds to mass due to the fragment $[LSLHL\text{-}NH_2+K]^+$ (expected mass of $LSLHL\text{-}NH_2$: 580.367 Da); 976.573 Da corresponds to $[PFKLSLHL\text{-}NH_2+Na]^+$ (expected mass of $PFKLSLHL\text{-}NH_2$: 952.586 Da). Therefore, MALDI spectra supports the cleavage of the peptide via the K-L bond fragmenting the peptides into two fragments PFK and $LSLHL\text{-}NH_2$.

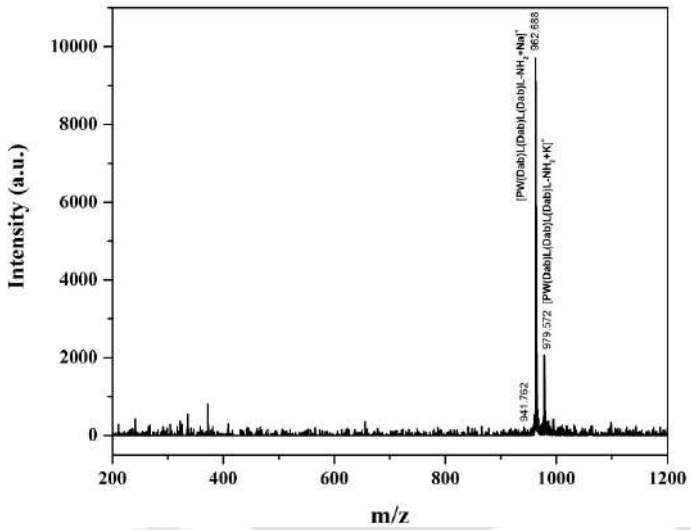

Figure C19. MALDI-TOF spectra of **J3** (incubated with trypsin for 24 h). 962.688 Da corresponds to $[PW(Dab)L(Dab)L(Dab)L\text{-}NH_2+Na]^+$, 979.572 Da corresponds to $[PW(Dab)L(Dab)L(Dab)L\text{-}NH_2+K]^+$ (expected mass: 939.602 Da) . Therefore, trypsin had no effect on the peptide J3 studied upto 24 h.

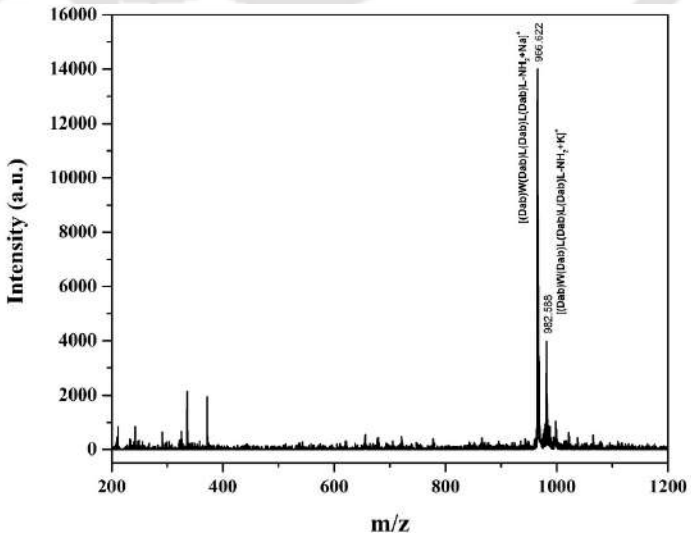

Figure C20. MALDI-TOF spectra of **J4** (incubated with trypsin for 24 h). 966.622 Da corresponds to $[(Dab)W(Dab)L(Dab)L(Dab)L\text{-}NH_2+Na]^+$, 982.588 Da corresponds to $[(Dab)W(Dab)L(Dab)L(Dab)L\text{-}NH_2+K]^+$ (expected mass: 942.613 Da) . No other peaks other than those for the unfragmented peptide proves trypsin had no cleaving effect on the peptide J4 studied upto 24 h.

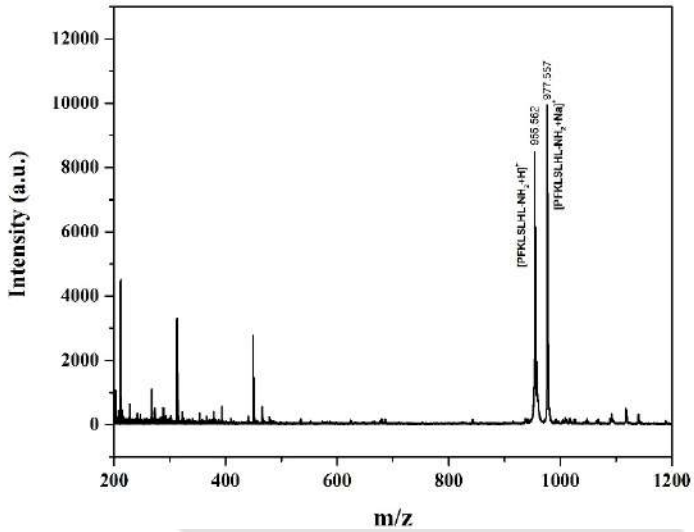

Figure C21. MALDI-TOF spectra of **Jc** (incubated with serum for 24 h). 955.562 Da corresponds to $[PFKLSLHL\text{-}NH_2+H]^+$, 977.557 Da corresponds to $[PFKLSLHL\text{-}NH_2+Na]^+$ (expected mass of $PFKLSLHL\text{-}NH_2$: 952.586 Da). Serum incubated with the peptide Jc had no effect on it upto 24 h indicating serum stability of the peptide.

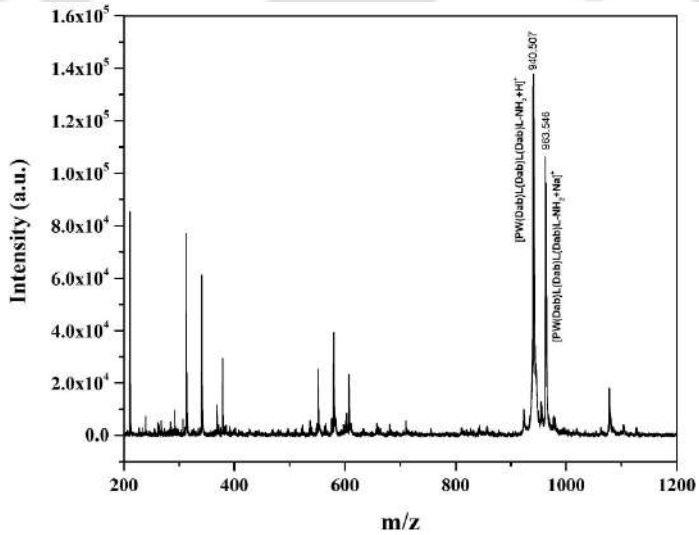

Figure C22. MALDI-TOF spectra of **J3** (incubated with serum for 24 h). 940.507 Da corresponds to $[PW(Dab)L(Dab)L(Dab)L\text{-}NH_2+H]^+$, 963.546 Da corresponds to $[PW(Dab)L(Dab)L(Dab)L\text{-}NH_2+ Na]^+$ (expected mass: 939.602 Da) . Therefore, serum had no effect on the peptide J3 studied upto 24 h.

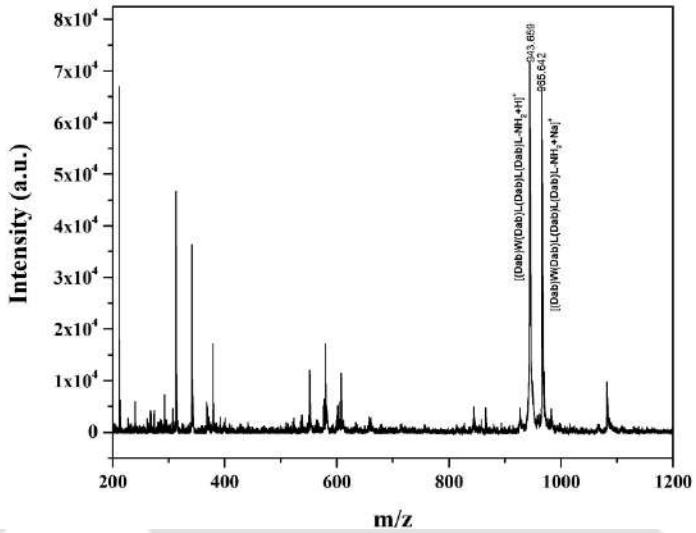

Figure C23. MALDI-TOF spectra of **J4** (incubated with serum for 24 h). 943.659 Da corresponds to $[(Dab)W(Dab)L(Dab)L(Dab)L\text{-}NH_2+H]^+$, 965.642 Da corresponds to $[(Dab)W(Dab)L(Dab)L(Dab)L\text{-}NH_2+ Na]^+$ (expected mass: 942.613 Da) . Thus, the peptide J4 was unaffected in the presence of serum upto 24 h.

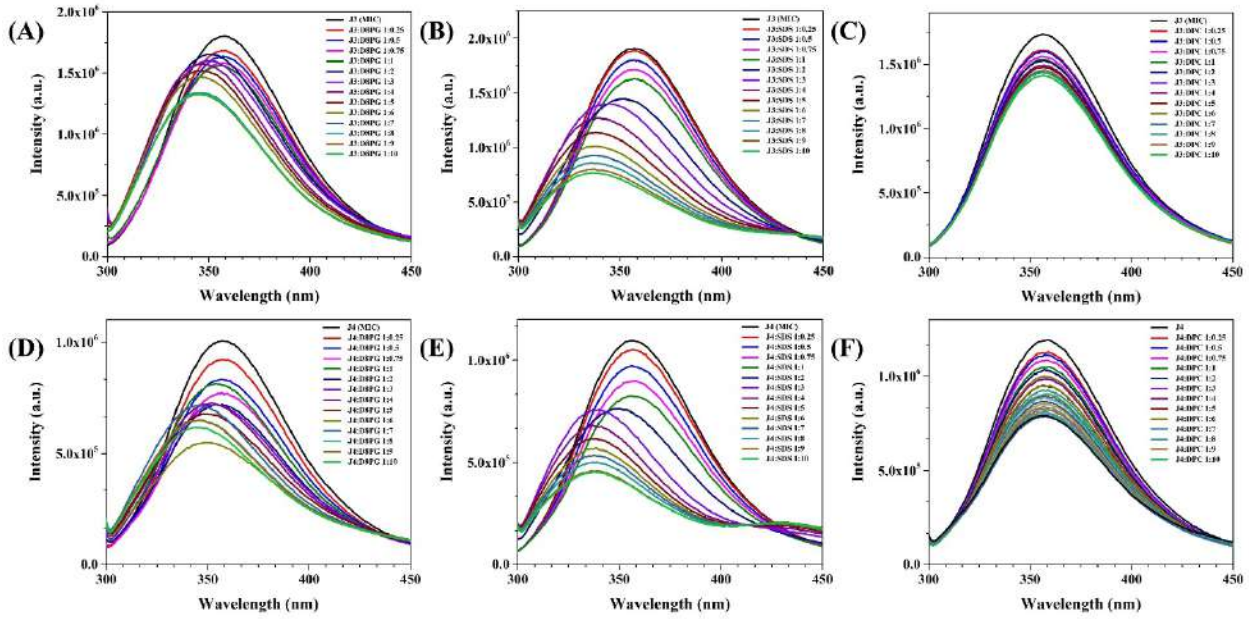

Figure C24. Blue Shift experiments. Fluorescence spectra of **J3** titrated against different ratios of (A) D8PG, (B) SDS and (C) DPC and that of **J4** titrated against different ratios of (D) D8PG, (E) SDS and (F) DPC.

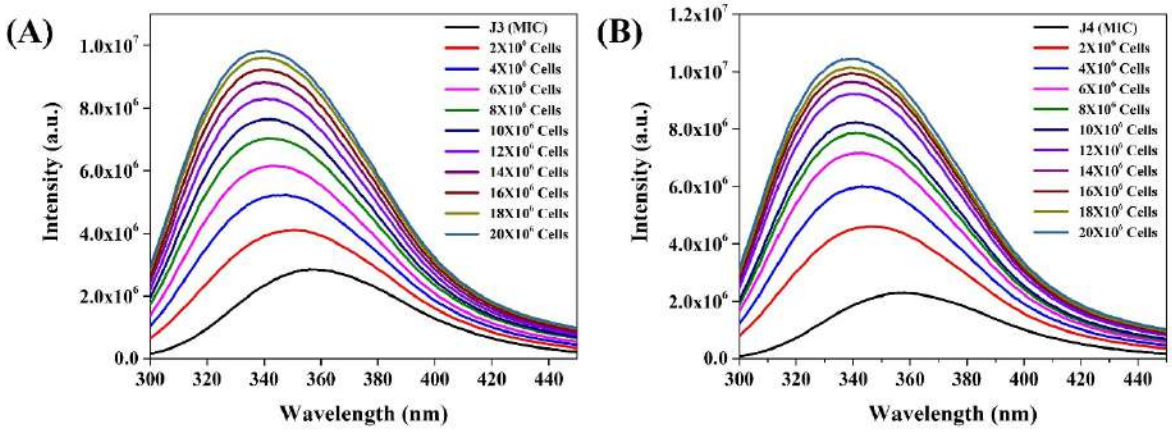

Figure C25. Live cell fluorescence experiment. Shift in the fluorescence spectra of (A) **J3** and (B) **J4** upon increasing concentrations of *P. aeruginosa* cells.

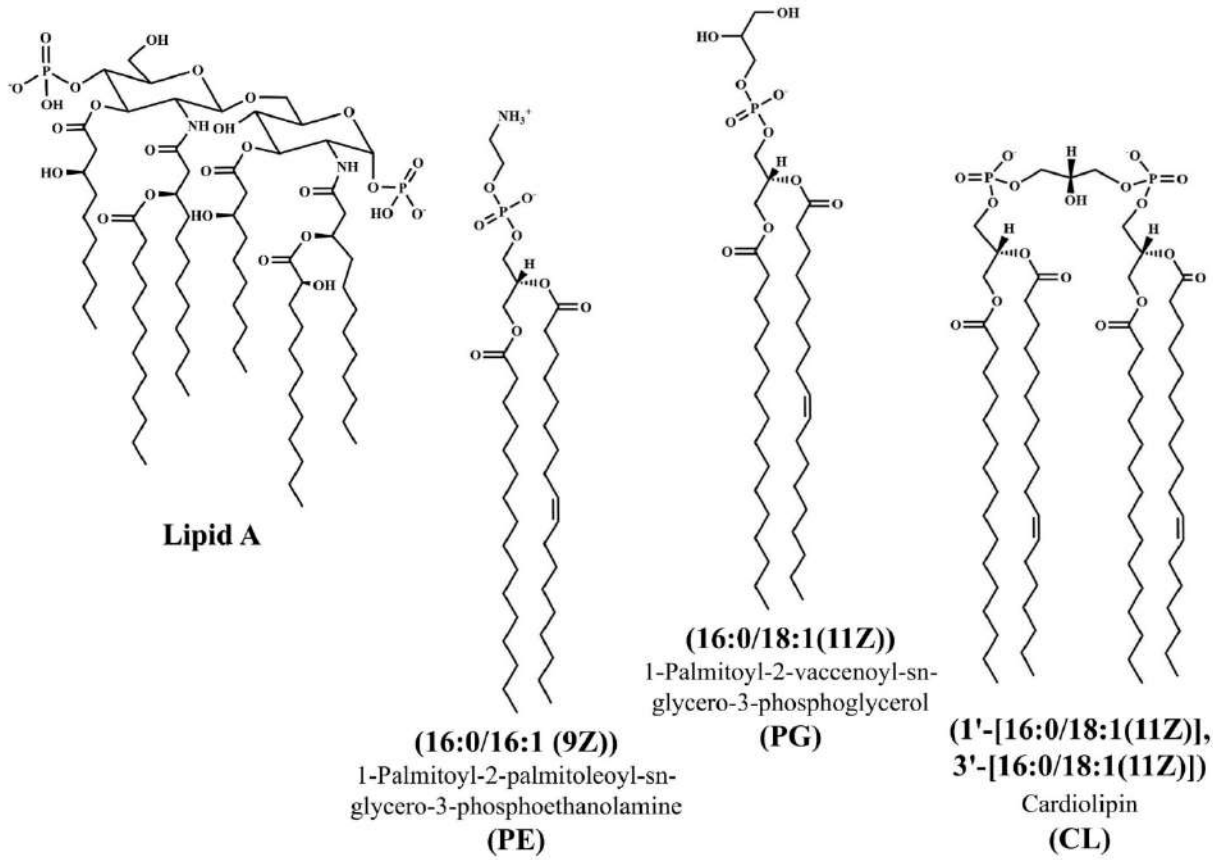

Figure C26. Structure of the lipid molecules used in model of the bilayer.

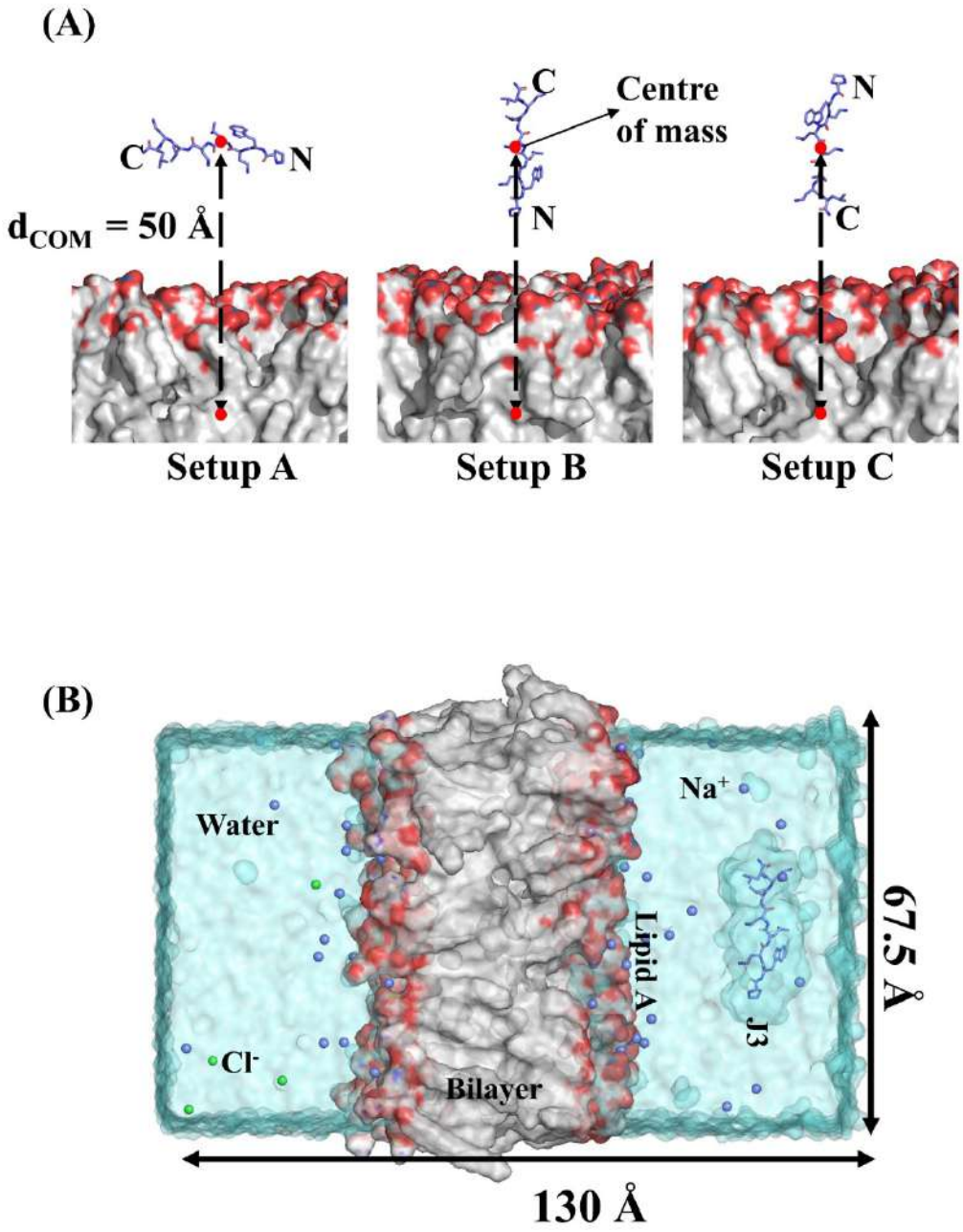

Figure C27. (A) Three initial models (Setup A, Setup B, and Setup C) for the MD simulation differ in the relative peptide bilayer orientation. The center of mass of the peptide (red circle) and the N-/C- terminals are highlighted. A broken double-headed arrow indicates the distance between the center of mass of the peptide and the bilayer. (B) The peptide bilayer system is overlaid with an equilibrated box of water (dimension 67.5×67.5×130 Å3). Bilayer = red-blue-white surface, J3-peptide =sticks, Na+ =violet sphere, Cl- =green sphere, and water in aquamarine transparent surface.

Table C1. Lipid composition of the bilayer model that mimics the outer membrane of *P aeruginosa*.

Bilayer Composition	# Number of Lipid molecules		Charge
	Outer Leaflet	Inner Leaflets	
Lipid A (of *P. aeruginosa*)	28	-	-56
PE	-	60	0
PG	-	16	-16
CL	-	4	-8
		Total Charge	**-80**

Table C2. Peptide (Jc, J3) in the presence and absence of bilayer as considered for MD simulations. The size of the solvated simulation box, composition, and MD run-length are given. Total sampling ~ 7.1 μs. The "bilayer" is composed of 108 lipid molecules (Lipid A, PE, PG, CL). SOD = Sodium, CLA = Chlorine, SOL = Water molecule.

S. No	Simulation Systems	No. of replicas	Box Size (Å^3)	No. of molecules	Simulation Time (ns)
1	Free bilayer in water	1	73 × 73 × 115	Lipid A – 28 PE – 60 PG – 16 CL – 4 SOD – 80 SOL – 11582	500
2	Free Jc in water	3	5 × 5× 5	Peptide – 1 CLA – 2 SOL - 4516	300 (100×3)
3	Free J3 in water	3	5 × 5× 5	Peptide – 1 CLA – 4 SOL – 4518	300 (100×3)
4	Jc-bilayer (Setup A)	1	67.5×67.5×130	Peptide – 1 Bilayer – 108 SOD – 80 CLA – 2 SOL- 13460	1000
5	Jc-bilayer (Setup B)	1			1000
6	Jc-bilayer	1			1000

	(Setup C)				
7	J3-bilayer (Setup A)	1	67.5×67.5×130	Peptide – 1 Bilayer – 108 SOD – 80 CLA – 4 SOL- 13458	1000
8	J3-bilayer (Setup B)	1			1000
9	J3-bilayer (Setup C)	1			1000

Table C3. Parameters used for MD simulation.

Molecular Dynamics Parameters (NPT ensemble)	
Integrator, time step	Leap-frog algorithm, 2 fs
Hydrogen Bonds Constraint Algorithm	LINCS[1]
Long range electrostatics, short range electrostatic cut-off	Particle Mesh Ewald (PME)[2], 12 Å
Short range van der Waals cut-off	12 Å
Boundary Conditions	Periodic Boundary condition
Temperature control, coupling constant	Nosé-Hoover algorithm[3-4], 1.0 ps
Pressure control, coupling constant	Parrinello-Rahman algorithm[5], 5.0 ps
Temperature	310 K
Pressure	1 bar

Appendix D (for Chapter 5)

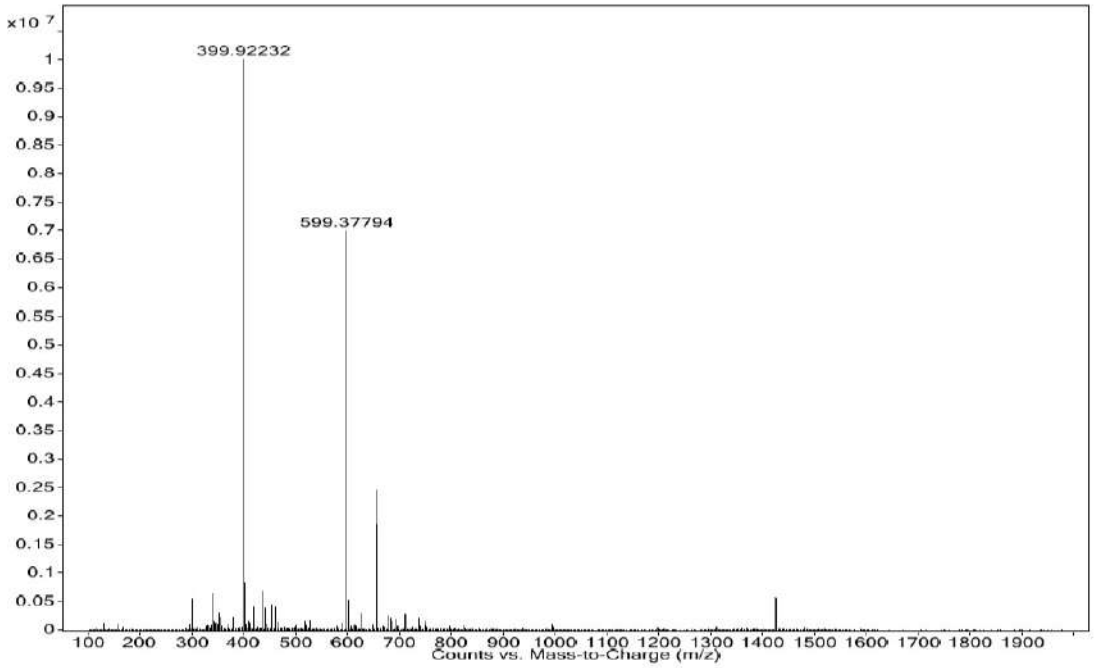

Figure D1. ESI-HRMS spectra of **WRL**. Calc. $[M+H]^{+}$ for WRL = 1197.7480 Da; Obs. $[M+2H]^{2+}$ = 599.3779 Da; Obs. $[M+3H]^{3+}$ = 399.9223 Da.

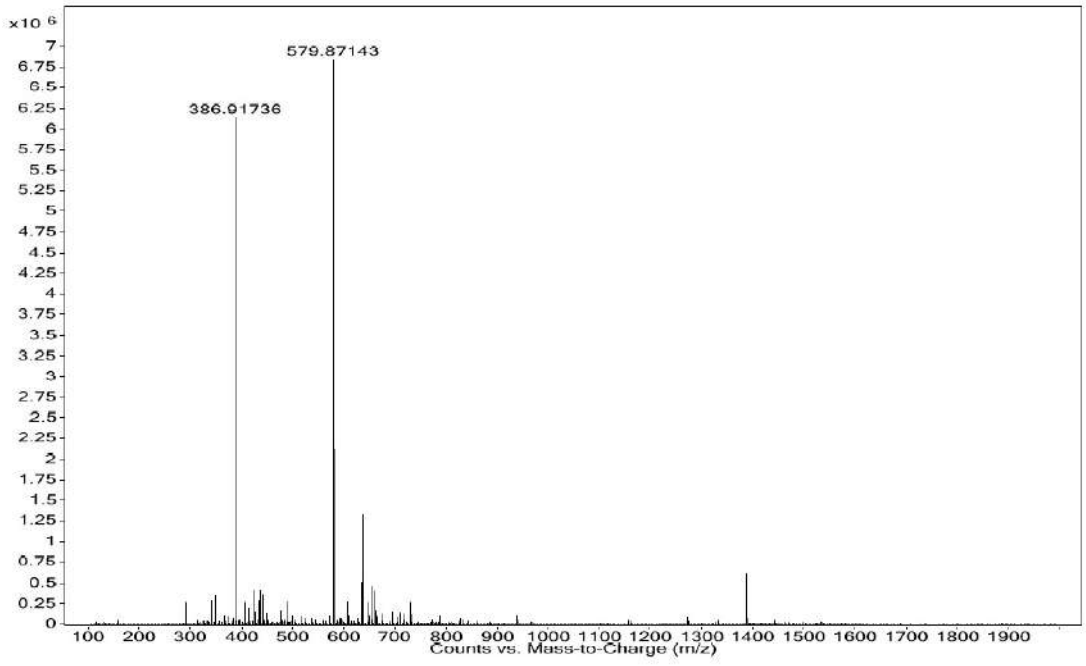

Figure D2. ESI-HRMS spectra of **LWRF**. Calc. $[M+H]^{+}$ for LWRF = 1158.7371 Da; Obs. $[M+2H]^{2+}$ = 579.8714 Da; Obs. $[M+3H]^{3+}$ = 386.9173 Da.

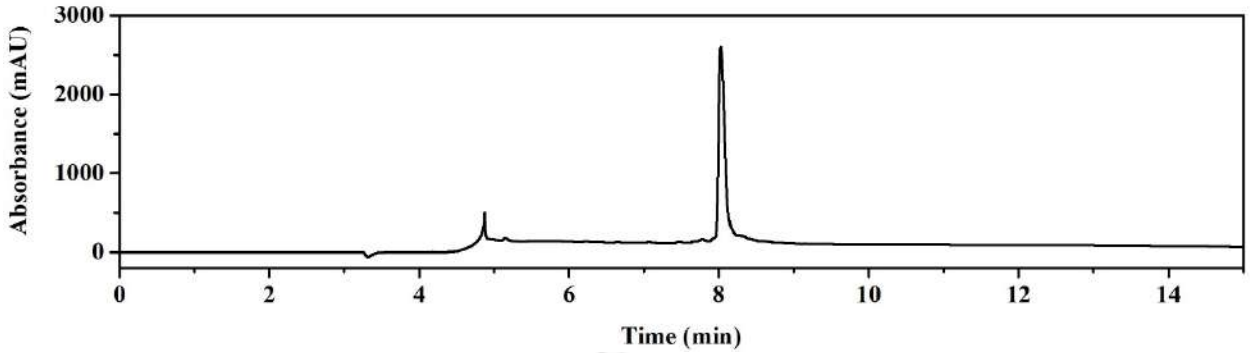

Figure D3. Analytic HPLC trace of **WRL** at 214 nm. Retention time: 8.03 min.

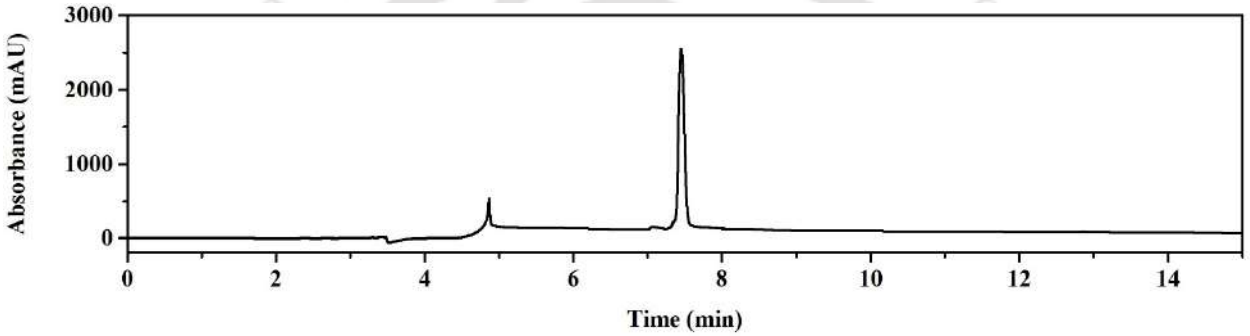

Figure D4. Analytic HPLC trace of **LWRF** at 214 nm. Retention time: 7.45 min.

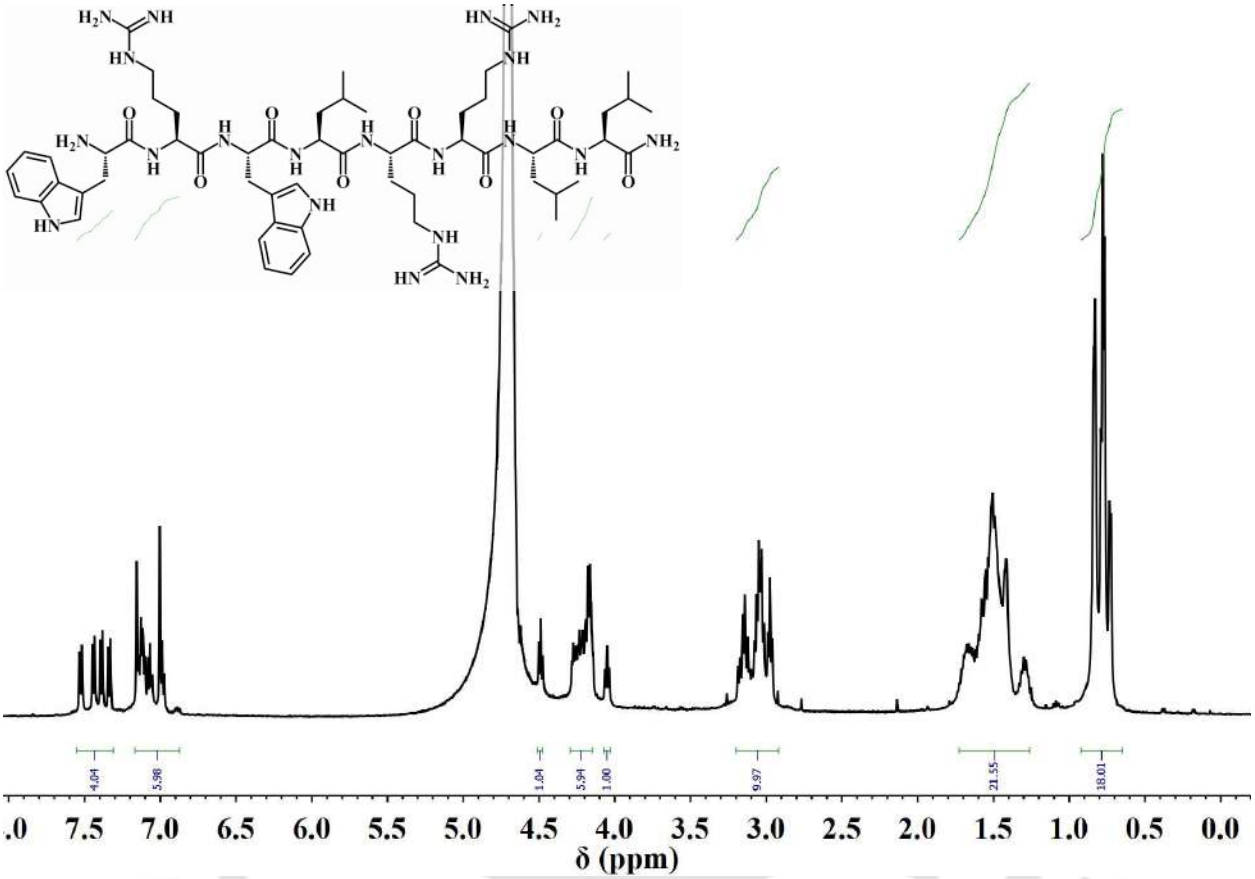

Figure D5. ^{1}H NMR spectra of **WRL** at room temperature in D_2O. ^{1}H NMR (500 MHz, D_2O): δ 0.65-0.92 (m, 18H, Leucine), δ 1.26-1.72 (m, 21H, Leucine and Arginine), δ 2.92-3.20 (m, 10H, Tryptophan and Arginine), δ 4.03-4.51 (8 αH), 6.87-7.55 (m, 10H, Tryptophan).

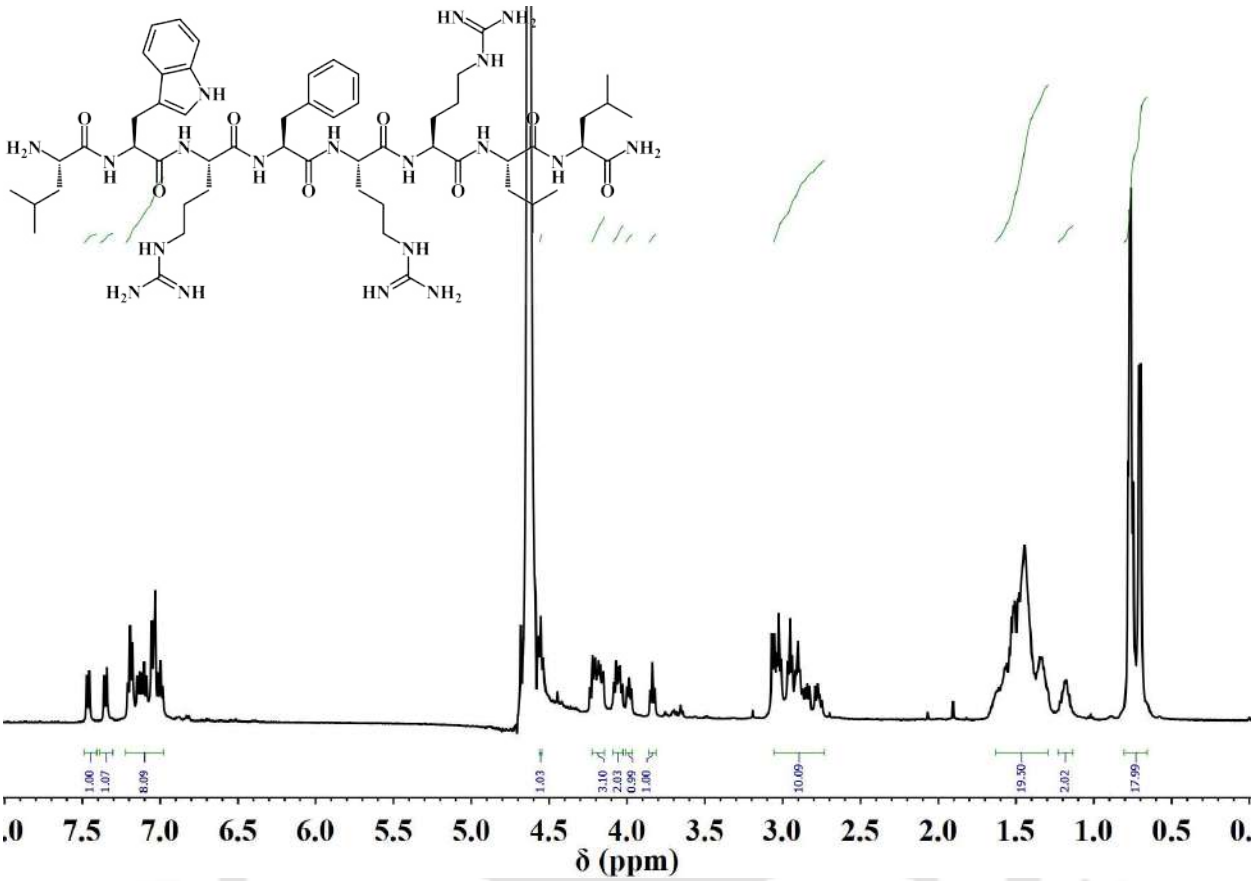

Figure D6. ^{1}H NMR spectra of **LWRF** at room temperature in D_2O. ^{1}H NMR (500 MHz, D_2O): δ 0.66-0.81 (m, 18H, Leucine), δ 1.14-1.64 (m, 21H, Leucine and Arginine), δ 2.75-3.07 (m, 10H, Tryptophan, Arginine and Phenylalanine), δ 3.82-4.56 (8 αH), 6.98-7.49 (m, 10H, Tryptophan and Phenylalanine).

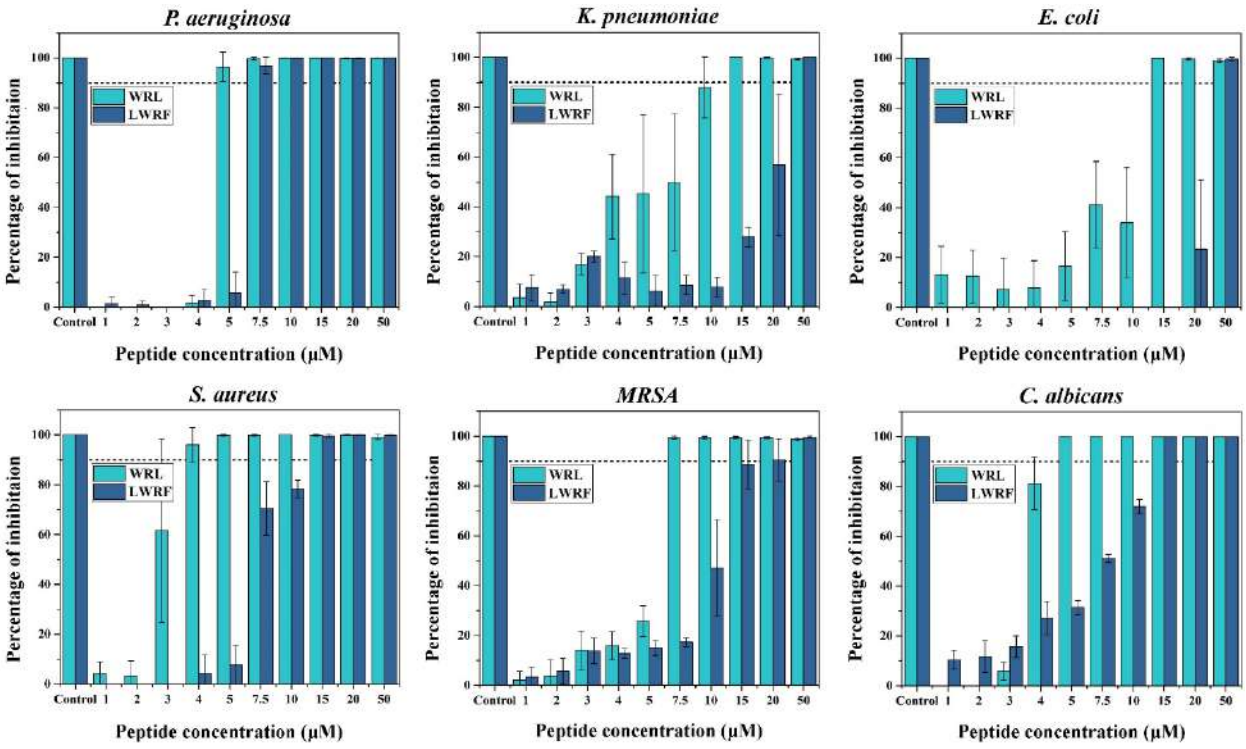

Figure D7. Determination of Minimum Inhibitory Concentration (MIC). Bar diagram representation depicting percentage of inhibition of the microbes corresponding to different concentrations of the peptides **WRL** and **LWRF**. $MIC_{90\%}$ values were the lowest concentrations at which 90% or more inhibitions were observed respectively against *P. aeruginosa, K. pneumoniae, E. coli, S. aureus,* Methicillin-resistant *Staphylococcus aureus* (MRSA) and C. *albicans*.

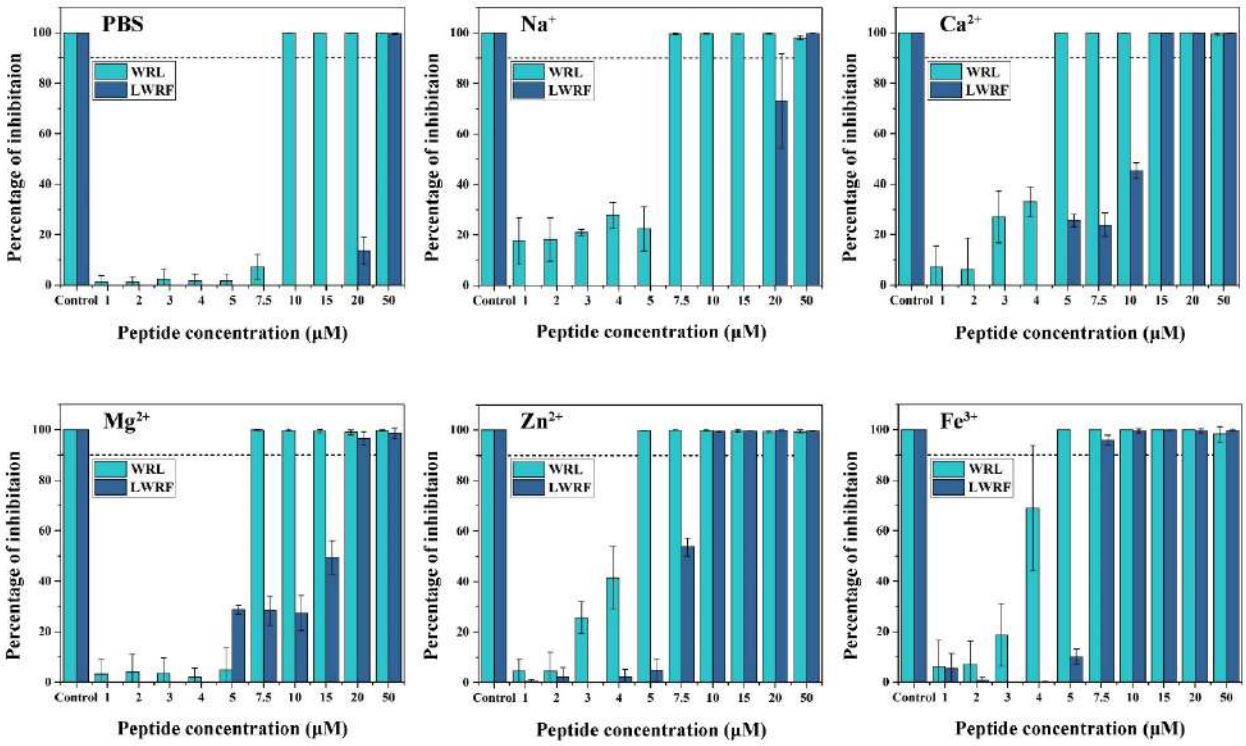

Figure D8. Determination of Minimum Inhibitory Concentration (MIC) of the peptides **WRL** and **LWRF** against *P. aeruginosa* in the presence of physiological concentrations of different salts. Bar diagram representation depicting percentage of inhibition of *P. aeruginosa* in the presence of PBS (10 mM), NaCl (150 mM), $CaCl_2$ (1.25 mM), $MgCl_2$ (1 mM), $ZnCl_2$ (8 μM) and $FeCl_3$ (4 μM) corresponding to different concentrations of the peptides. $MIC_{90\%}$ values were the lowest concentrations at which 90% or more inhibitions were observed against *P. aeruginosa* in the presence of PBS (10 mM), NaCl (150 mM), $CaCl_2$ (1.25 mM), $MgCl_2$ (1 mM), $ZnCl_2$ (8 μM) and $FeCl_3$ (4 μM).

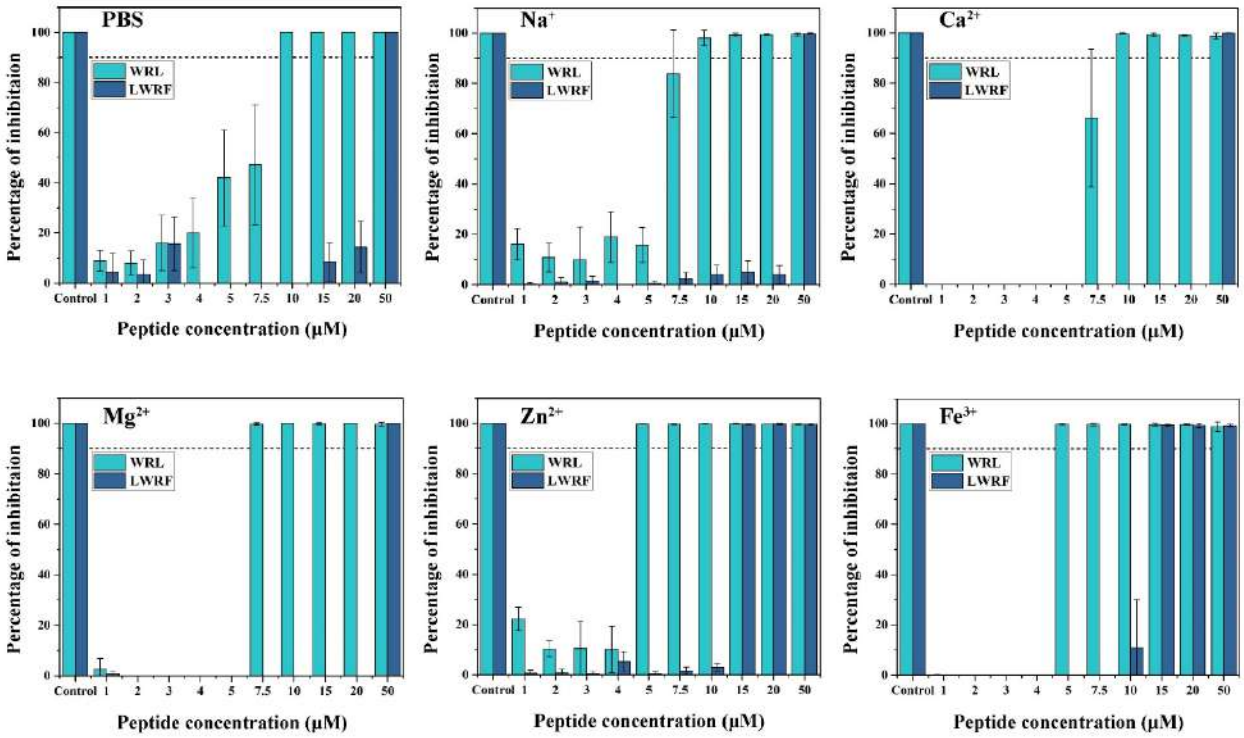

Figure D9. Determination of Minimum Inhibitory Concentration (MIC) of the peptides **WRL** and **LWRF** against *S. aureus* in the presence of physiological concentrations of different salts. Bar diagram representation depicting percentage of inhibition of *S. aureus* in the presence of PBS (10 mM), NaCl (150 mM), $CaCl_2$ (1.25 mM), $MgCl_2$ (1 mM), $ZnCl_2$ (8 μM) and $FeCl_3$ (4 μM) corresponding to different concentrations of the peptides. $MIC_{90\%}$ values were the lowest concentrations at which 90% or more inhibitions were observed against *S. aureus* in the presence of PBS (10 mM), NaCl (150 mM), $CaCl_2$ (1.25 mM), $MgCl_2$ (1 mM), $ZnCl_2$ (8 μM) and $FeCl_3$ (4 μM).

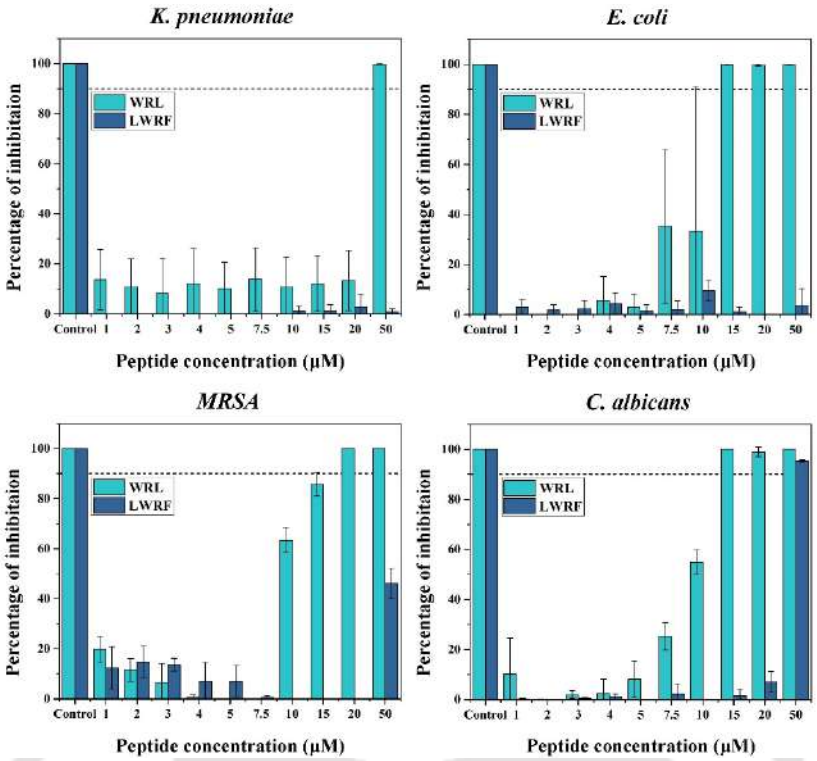

Figure D10. Determination of Minimum Inhibitory Concentration (MIC) of the peptides **WRL** and **LWRF** against *K. pneumoniae, E. coli,* Methicillin-resistant *Staphylococcus aureus* (MRSA*)* and C. *albicans* in PBS (10 mM). Bar diagram depicting percentage of inhibition of the microbes corresponding to different concentrations of the peptides in the presence of PBS. $MIC_{90\%}$ values were the lowest concentrations at which 90% or more inhibitions were observed against each of the individual microbes in the presence of PBS.

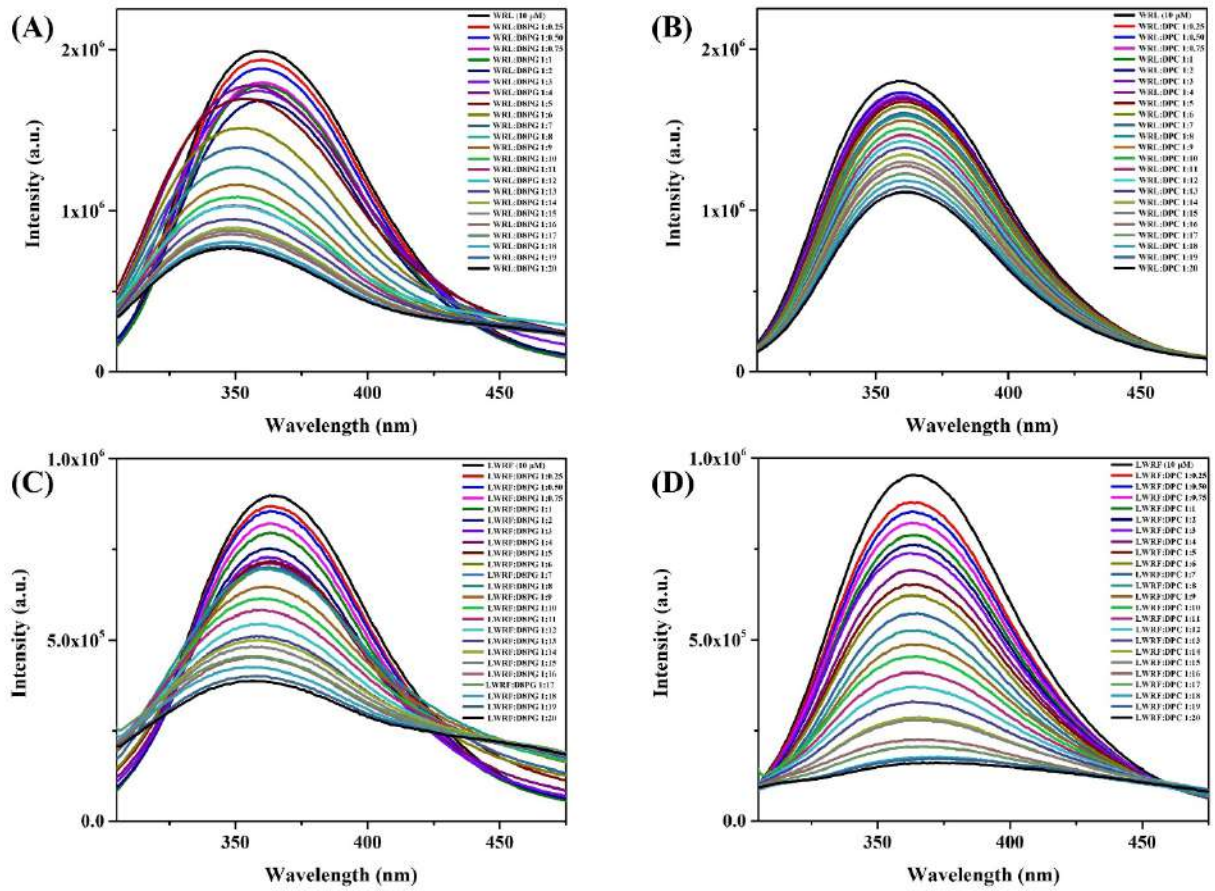

Figure D11. Blue Shift experiments. Fluorescence spectra of **WRL** titrated against different ratios of (A) D8PG, (B) DPC and **LWRF** titrated against different ratios of (C) D8PG, (D) DPC.

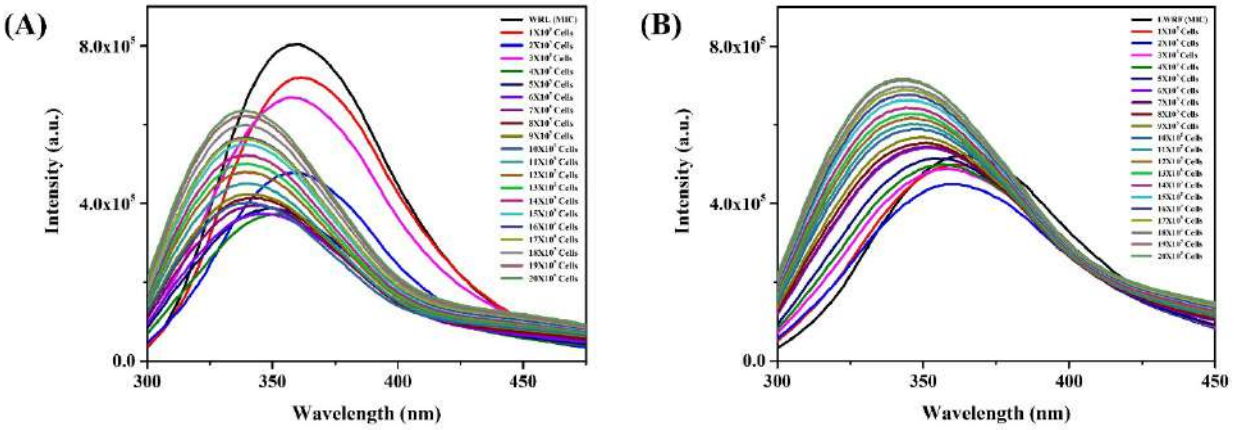

Figure D12. Live cell fluorescence experiment. Fluorescence spectra of (A) **WRL** and (B) **LWRF** at their respective MIC concentrations titrated against *P. aeruginosa* treated with increasing volumes of *P. aeruginosa* cells.

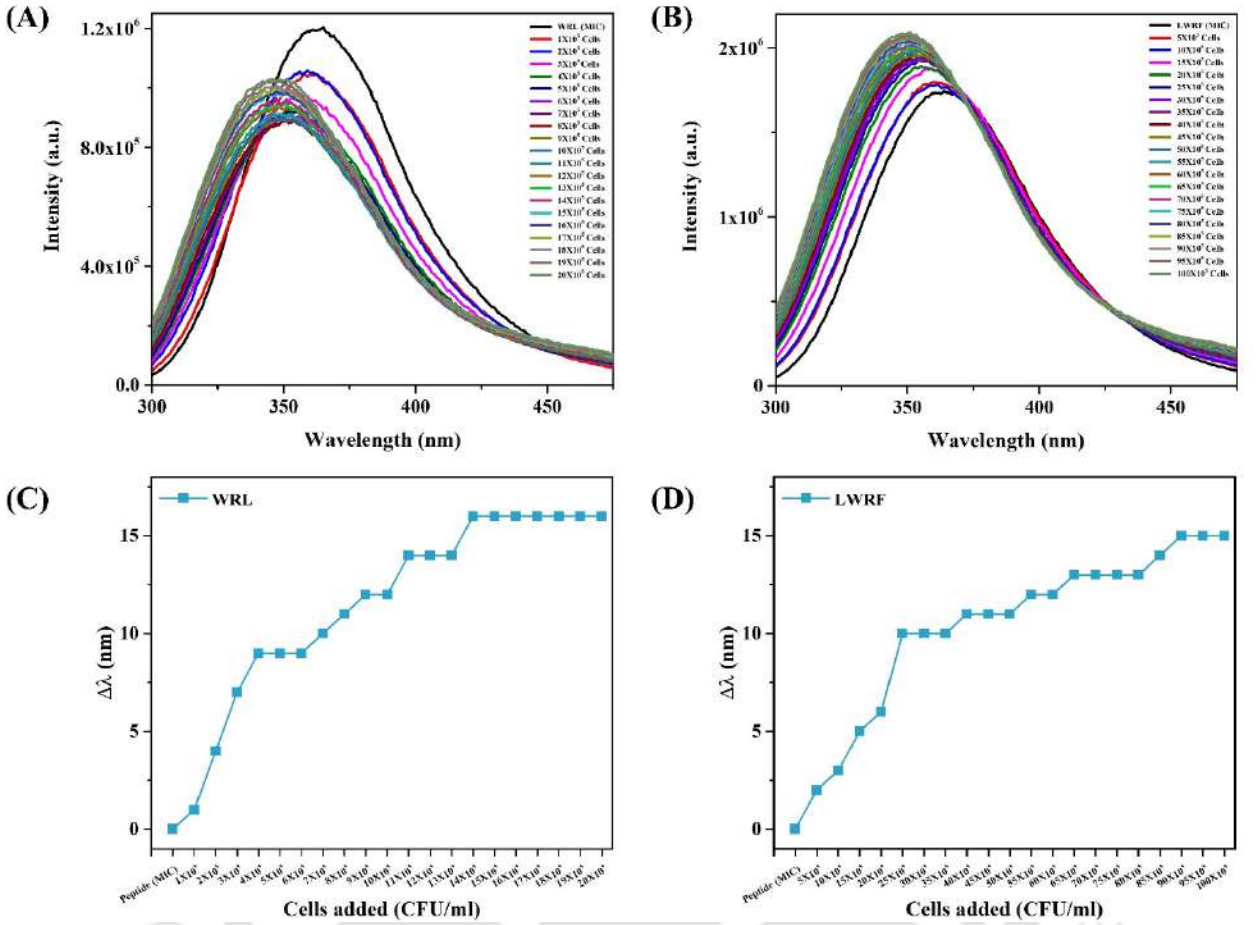

Figure D13. Live cell fluorescence experiment. Fluorescence spectra of (A) **WRL** and (B) **LWRF** at their respective MIC concentrations against *S. aureus* treated with increasing volumes of *S. aureus* cells. Wavelength shift (Δλ) shift associated with (C) **WRL** and (D) **LWRF** corresponding to the increasing concentrations of the cells.

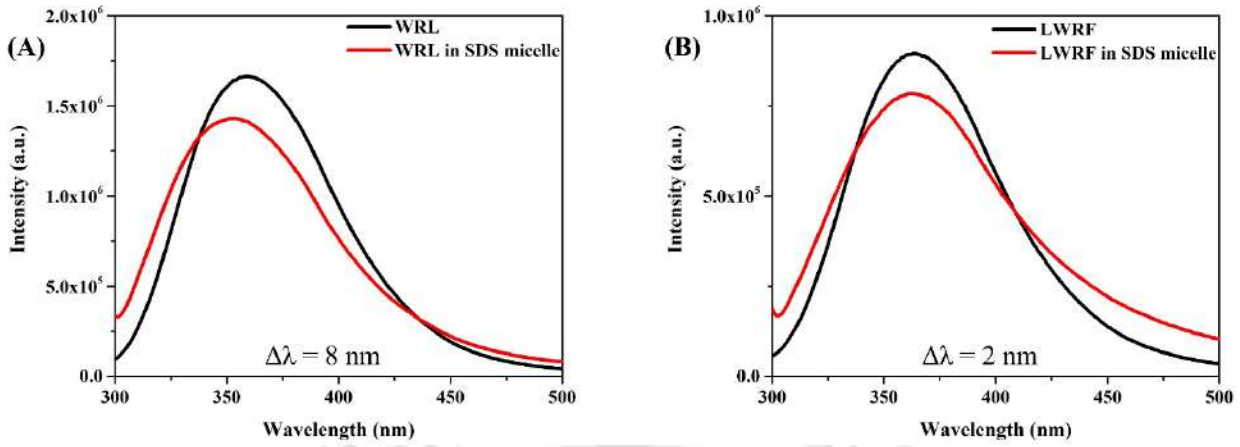

Figure D14. Fluorescence spectra of the peptides (A) **WRL** (10 μM) and (B) **LWRF** (10 μM) in the absence and in the presence of SDS micelles (30 mM).

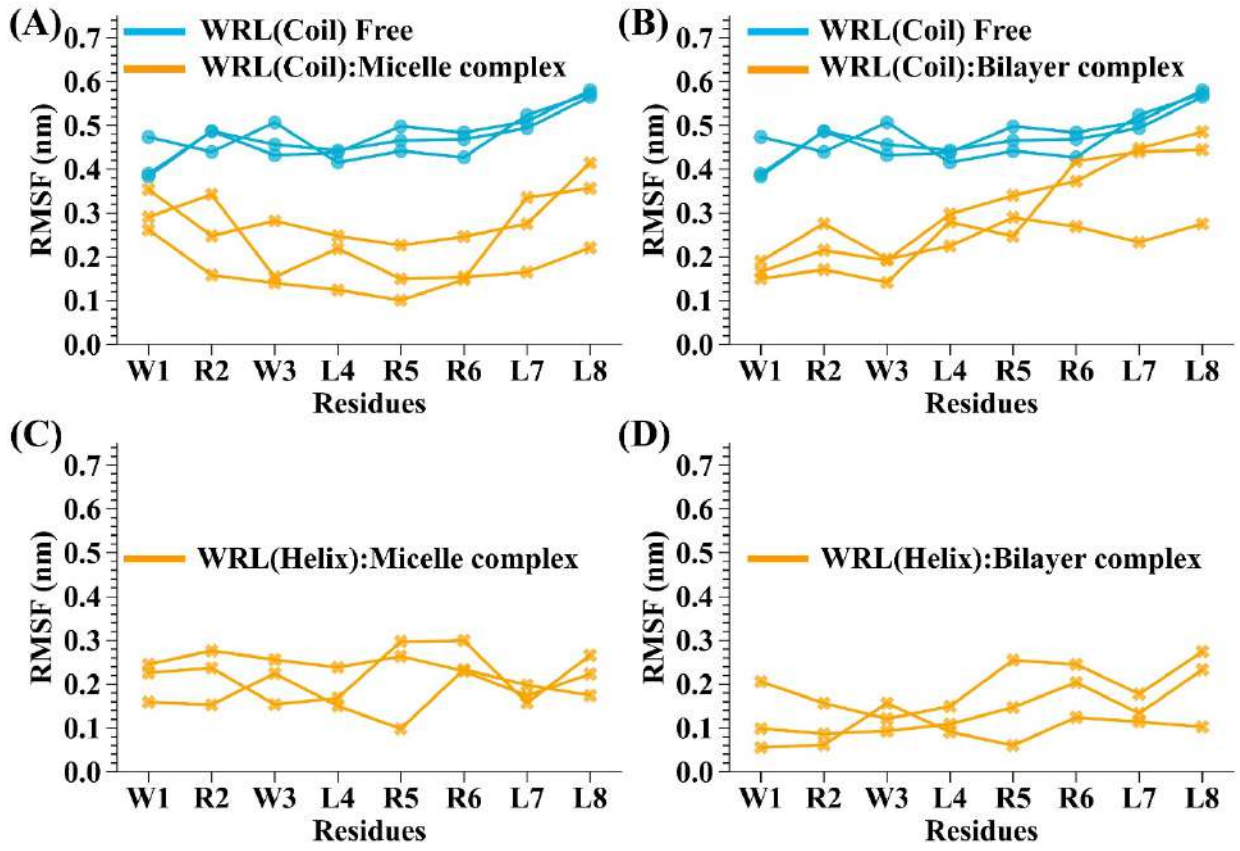

Figure D15: Residue-wise root mean square fluctuations (RMSF). (A) **WRL(Coil)** in the presence (orange) and absence (blue) of the SDS micelle. (B) **WRL(Coil)** in the presence (orange) and absence (blue) of the bilayer. (C) **WRL(Helix)** in the presence (orange) of the SDS micelle. (D)

WRL(Helix) in the presence (orange) of the bilayer. Data from three independent simulations are given.

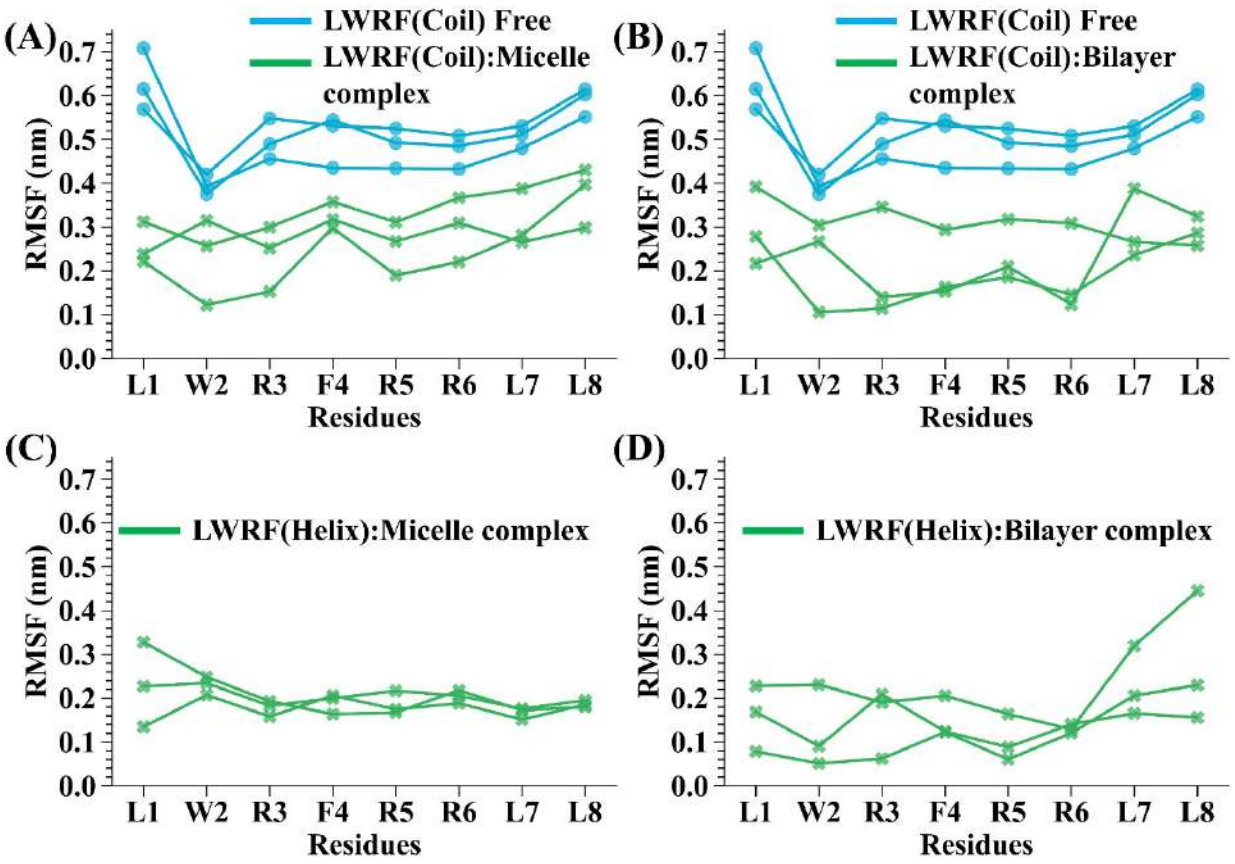

Figure D16: Residue-wise root mean square fluctuations (RMSF). (A) **LWRF(Coil)** in the presence (green) and absence (blue) of the SDS micelle. (B) **LWRF(Coil)** in the presence (green) and absence (blue) of the bilayer. (C) **LWRF(Helix)** in the presence (green) of the SDS micelle. (D) **LWRF(Helix)** in the presence (green) of the bilayer. Data from three independent simulations are given.

Table D1. Simulation setup for peptide (WRL or LWRF) in the presence and absence of the membrane mimics (Micelle/Bilayer). Total production run: 12.6 µs.

S. No	System	Replicas	Box Size ($Å^3$)	Number of molecules	Sampling (ns)
	Coil				
1	Free WRL	3	55×55×55	Peptide: 1 Chloride: 4 Solvent: 5690	600 (200×3)
2	Free LWRF	3	55×55×55	Peptide: 1 Chloride: 4 Solvent: 5689	600 (200×3)
3	WRL: SDS	3	100×100×140	Peptide: 1 SDS: 60 Sodium: 60 Chloride: 4 Solvent: 47401	600 (200×3)
4	LWRF: SDS	3	100×100×140	Peptide: 1 SDS: 60 Sodium: 60 Chloride: 4 Solvent: 47401	600 (200×3)
5	WRL: Bilayer Setup A Setup B Setup C	1 1 1	67.5×67.5×135	Peptide: 1 Lipids: 108 Sodium: 80 Chloride: 4 Solvent: 15613	1000 1000 1000
6	LWRF: Bilayer Setup A Setup B Setup C	1 1 1	67.5×67.5×135	Peptide: 1 Lipids: 108 Sodium: 80 Chloride: 4	1000 1000 1000

				Solvent: 15759	
	Helix				
7	WRL: SDS	3	100×100×100	Peptide: 1 SDS: 60 Sodium: 60 Chloride: 4 Solvent: 31699	600 (200×3)
8	LWRF: SDS	3	100×100×100	Peptide: 1 SDS: 60 Sodium: 60 Chloride: 4 Solvent: 31716	600 (200×3)
9	WRL: Bilayer	3	67.5×67.5×110	Peptide: 1 Lipids: 108 Sodium: 80 Chloride: 4 Solvent: 11612	1500 (500×3)
10	LWRF: Bilayer	3	67.5×67.5×110	Peptide: 1 Lipids: 108 Sodium: 80 Chloride: 4 Solvent: 11621	1500 (500×3)

Appendix E (for Chapter 6)

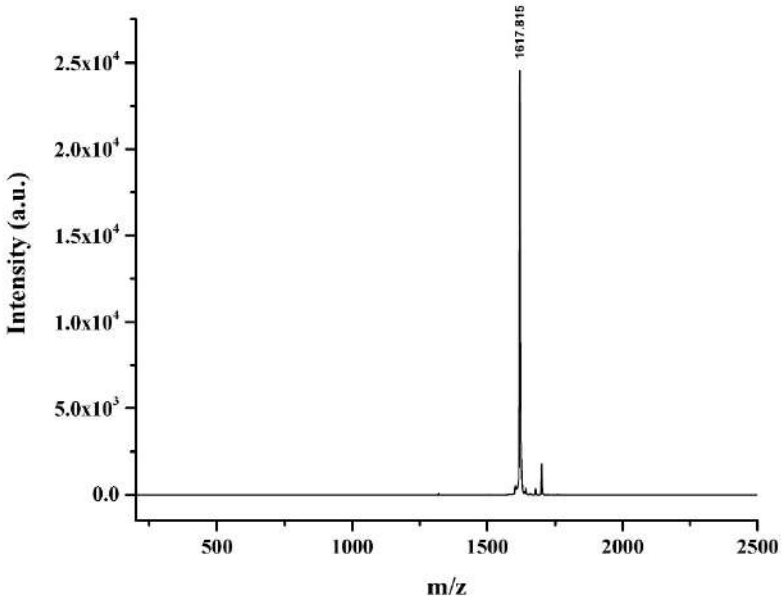

Figure E1. MALDI spectra of **RR-12**. Calculated $[M+H]^+$: 1616.965 Da; Observed $[M+H]^+$: 1617.815 Da.

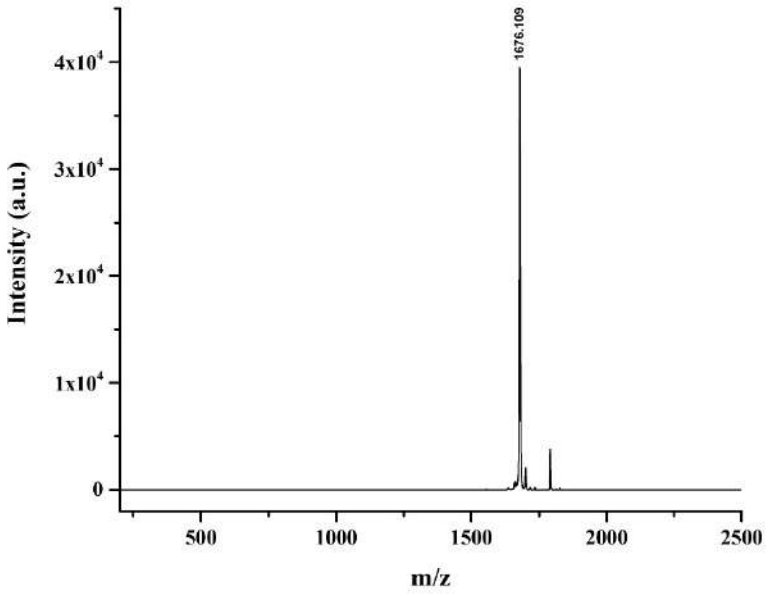

Figure E2. MALDI spectra of **FL-13**. Calculated $[M+H]^+$: 1675.075 Da; Observed $[M+H]^+$: 1676.109 Da.

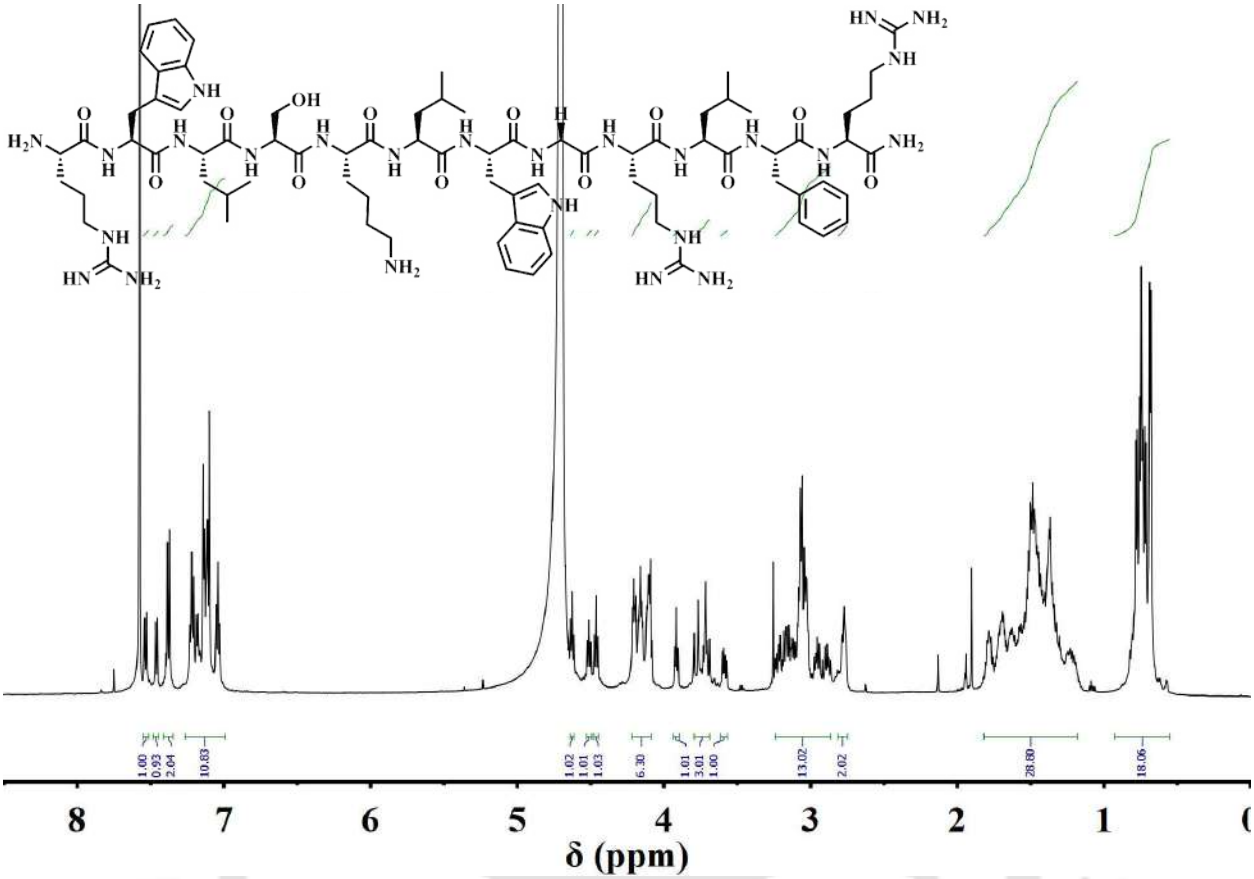

Figure E3. ^{1}H NMR spectra of **RR-12** at room temperature in D_2O. ^{1}H NMR (600 MHz, D_2O) δ 0.55-0.93 (18H: δ of 3 Leucine), δ 1.18-1.82 (27H: 6H from γ of 3 Arginine; 3H from γ of 3 Leucine; 2H from γ of 1 Lysine; 2H from δ of 1 Lysine; 6H from β of 3 Arginine; 6H from β of3 Leucine and 2H from β of 1 Lysine), δ 2.75-2.82 (2H: ε of 1 Lysine), δ 2.88-3.24 (13H: 6H from δ of 3 Arginine; 6H from β of 2 Tryptophan and 1 Phenylalanine, 1H from the α-H at the N-terminal), δ 3.57-3.80 (4H: 2H from β of 1 Serine; 2H from α of 1 Glycine), δ 4,09-4.64 (10H: 1 α-H from each of the amino acids other the one at the N-terminus and the 2 α-H originating from the Glycine), δ 6.99-7.27 (11H: 6H from the aromatic protons of 2 Tryptophan; 5H from the aromatic protons of 1 Phenylalanine), δ 7.34-7.55 (4H: aromatic protons of 2 Tryptophan).

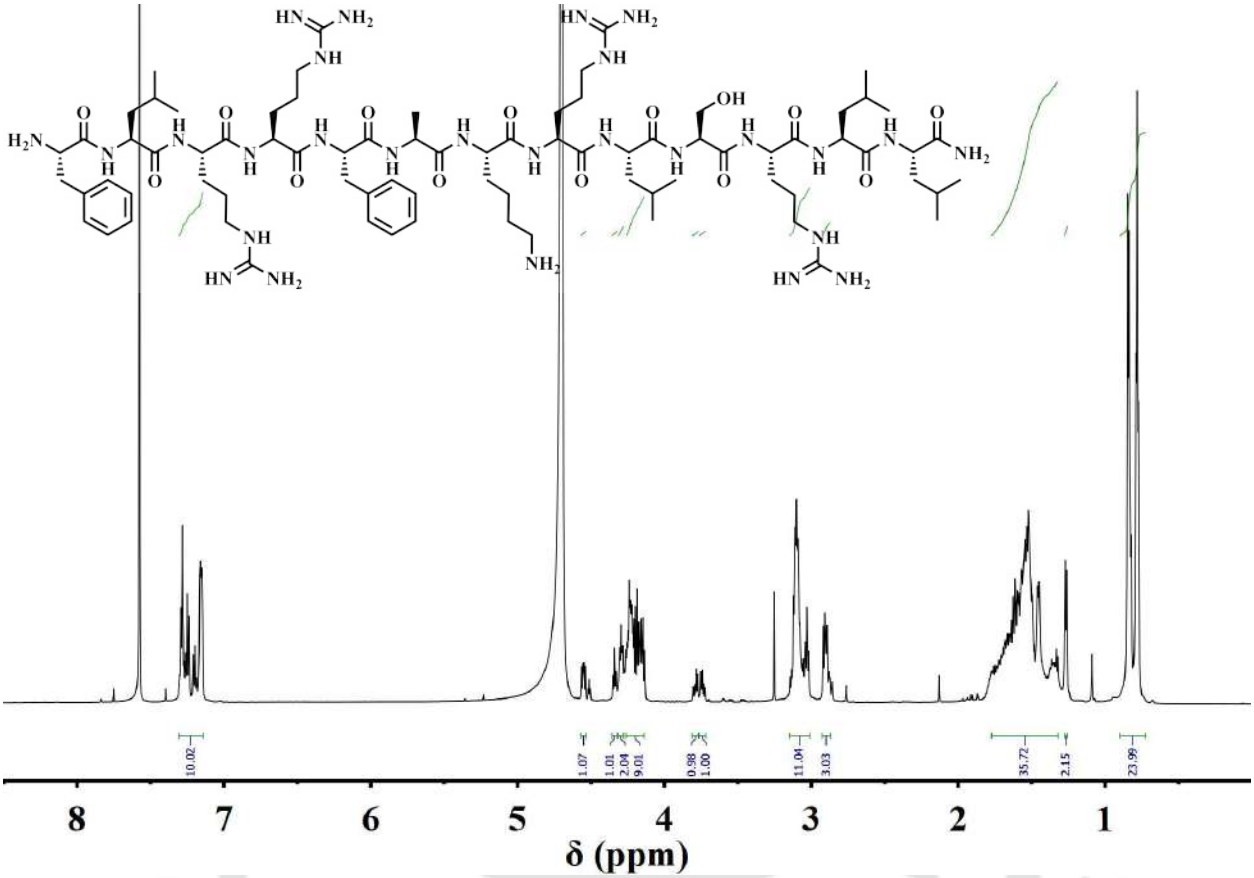

Figure E4. ^{1}H NMR spectra of **FL-13** at room temperature in D_2O. ^{1}H NMR (600 MHz, D_2O) δ 0.72-0.90 (24H, δ of 4 Leucine), δ 1.26-1.28 (2H: γ of 1 Lysine), δ 1.32-1.77 (35H: 4H from γ of 4 Leucine; 8H from γ of 4 Arginine; 3H from β of 3 Alanine; 2H from δ of 1 Lysine;8H from the β of 4 Leucine; 8H from the Arginine and 2H from the β of 1 Lysine), δ 2.87-3.15 (14H: 4H from β of 2 Phenylalanine; 8H from δ of 4 Arginine; 2H from ε of 1 Lysine), δ 2.72-3.81 (2H: 2H from β of Serine), δ 4.13-4.57 (13H, 1H each from α-H of each amino acid), δ 7.14-7.31 (10H, aromatic protons of 2 Phenylalanine).

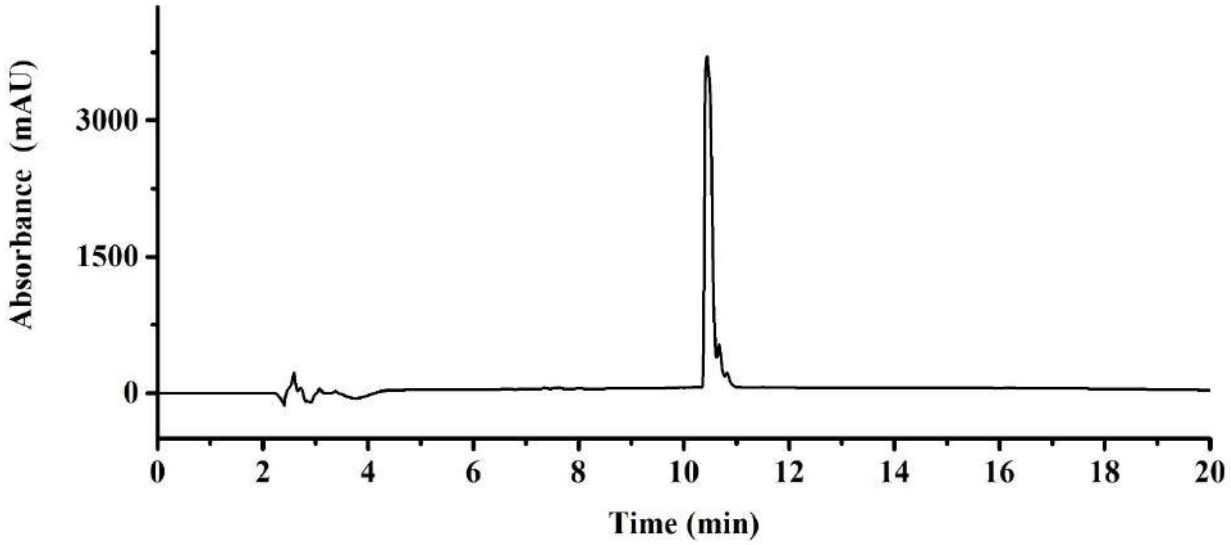

Figure E5. Analytic HPLC trace of **RR-12** at 214 nm. Retention time: 10.44 min.

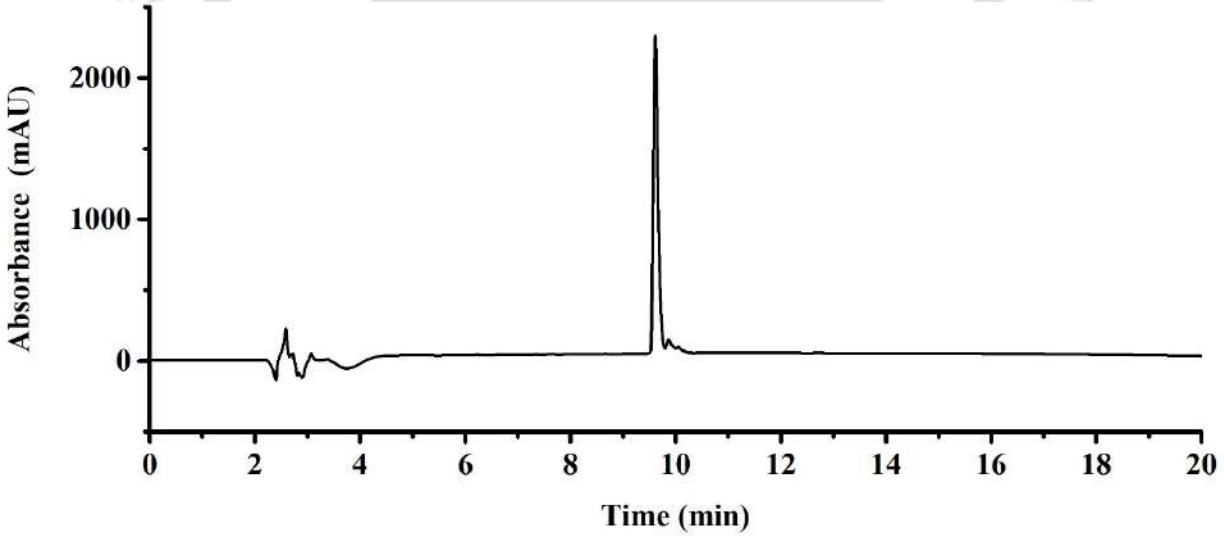

Figure E6. Analytic HPLC trace of **FL-13** at 214 nm. Retention time: 9.61 min.

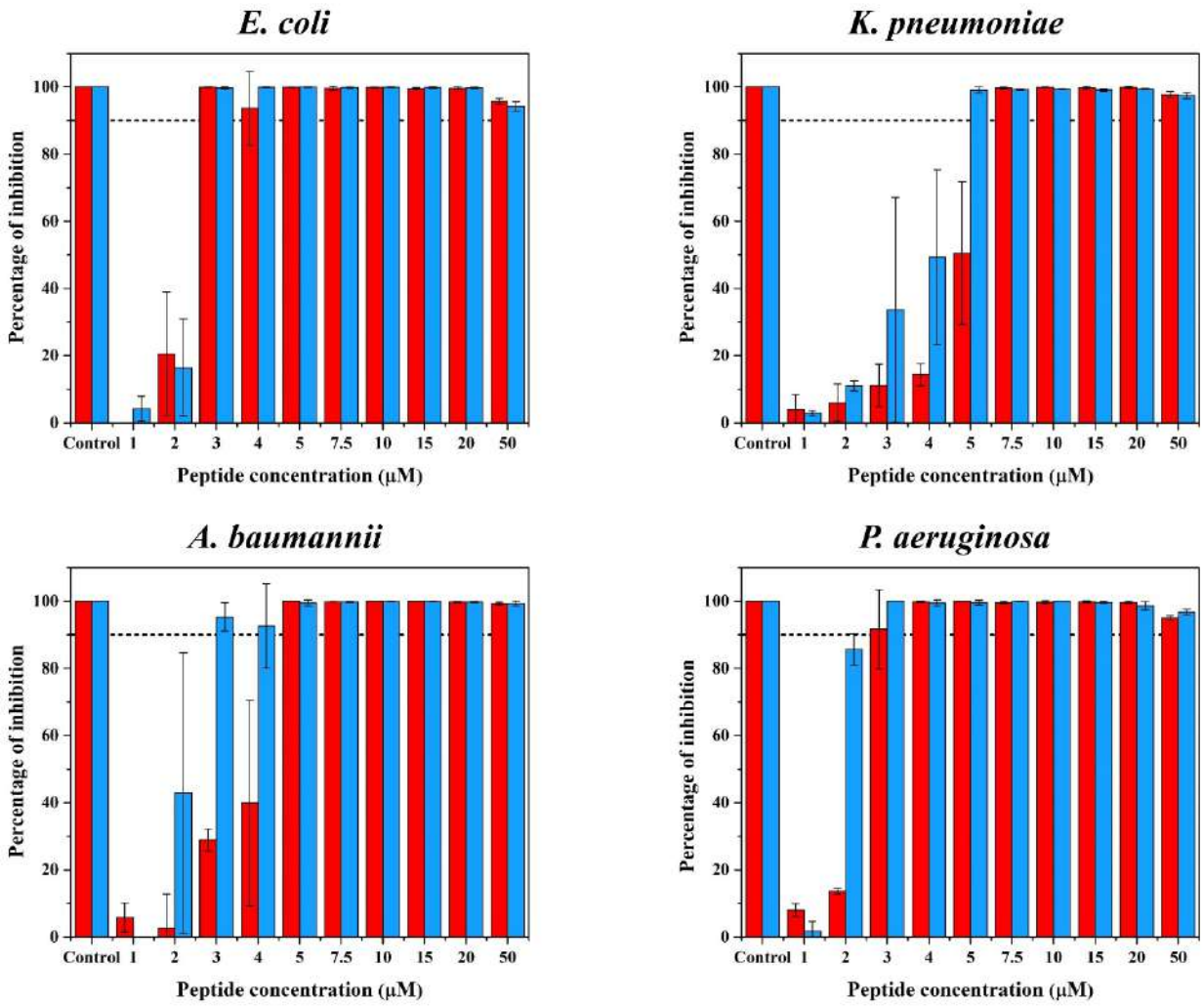

Figure E7. Bar diagrams representing the percentage of growth inhibition of different Gram-negative bacteria induced by the peptides **RR-12 (red)** and **FL-13 (blue)**. $MIC_{90\%}$ values were the lowest concentrations at which the peptides inhibited the growth of 90% or more of the microbes.

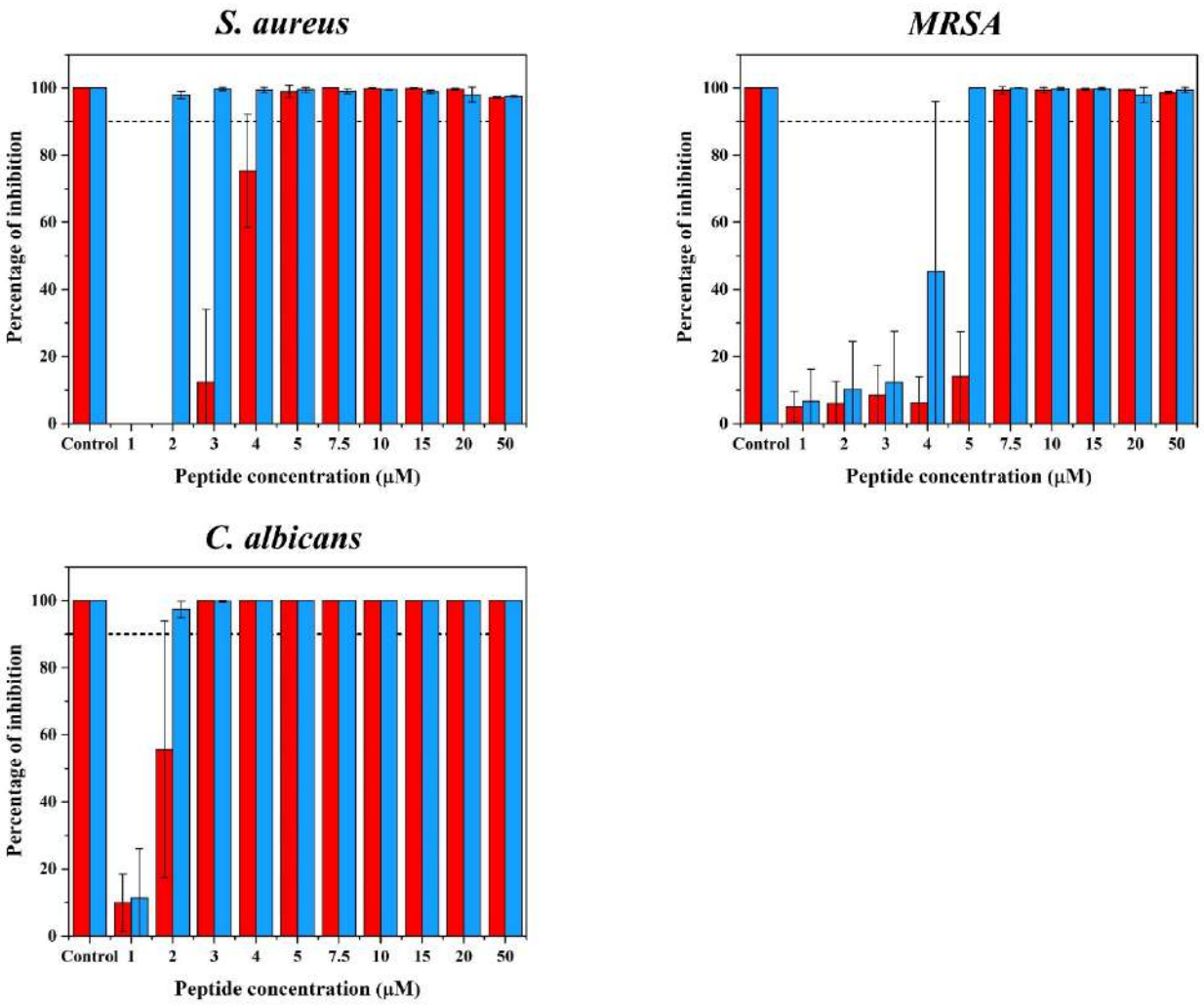

Figure E8. Bar diagrams representing the percentage of growth inhibition of two Gram-positive bacteria and fungus induced by the peptides **RR-12 (red)** and **FL-13 (blue)**. $MIC_{90\%}$ values were the lowest concentrations at which the peptides inhibited the growth of 90% or more of the microbes.

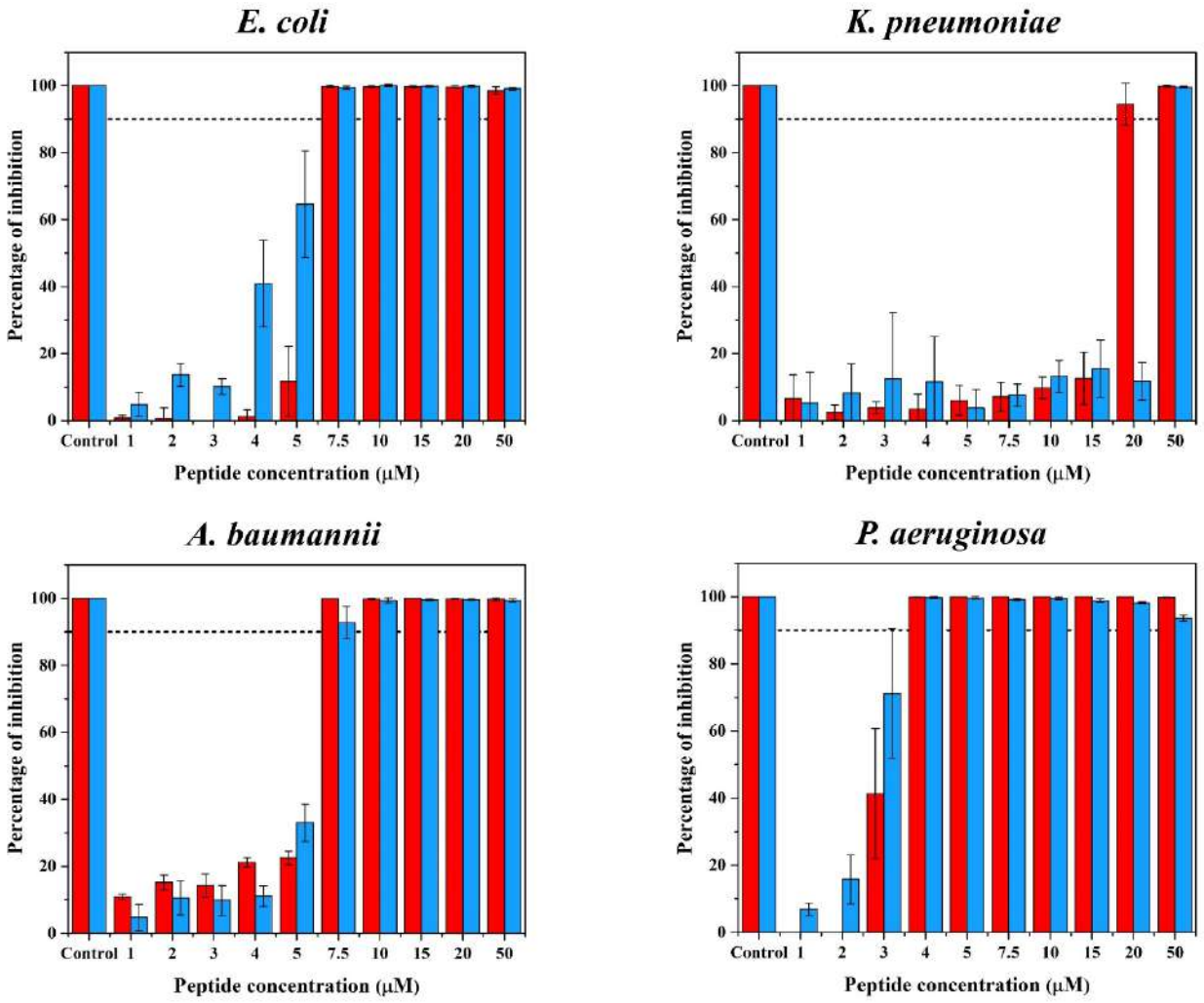

Figure E9. Bar diagrams representing the percentage of growth inhibition of different Gram-negative bacteria induced by the peptides **RR-12 (red)** and **FL-13 (blue)** in the presence of PBS. $MIC_{90\%}$ values were the lowest concentrations at which the peptides inhibited the growth of 90% or more of the microbes.

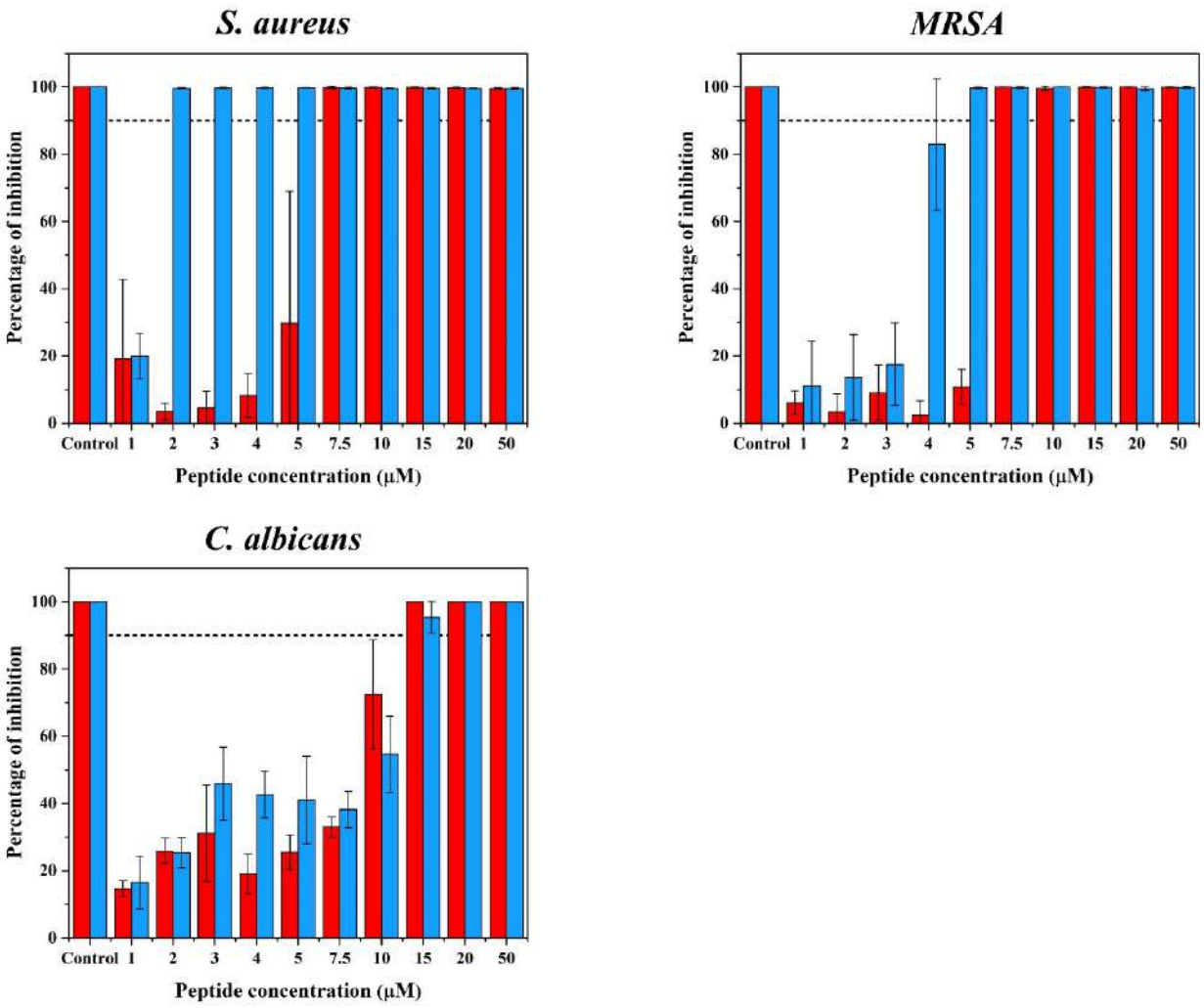

Figure E10. Bar diagrams representing the percentage of growth inhibition of two Gram-positive bacteria and fungus induced by the peptides **RR-12 (red)** and **FL-13 (blue)** in the presence of PBS. $MIC_{90\%}$ values were the lowest concentrations at which the peptides inhibited the growth of 90% or more of the microbes.

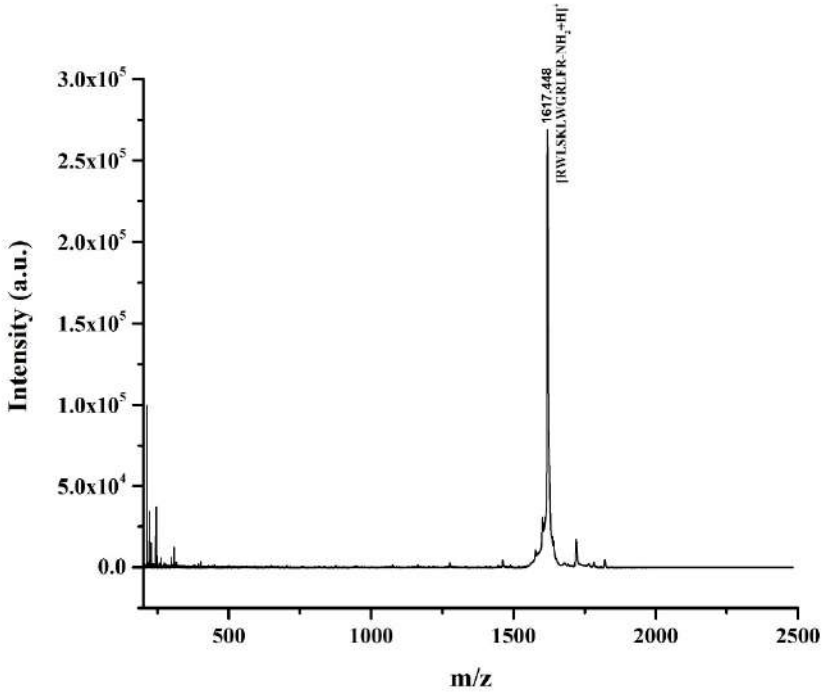

Figure E11. MALDI spectra of **RR-12** incubated with serum for 1 h. Peak at m/z 1617.448 Da corresponds to the unfragmented $[RWLSKLWGRLFR\text{-}NH_2+H]^+$. No other peaks corresponding to any probable fragmentations of the peptide were observed.

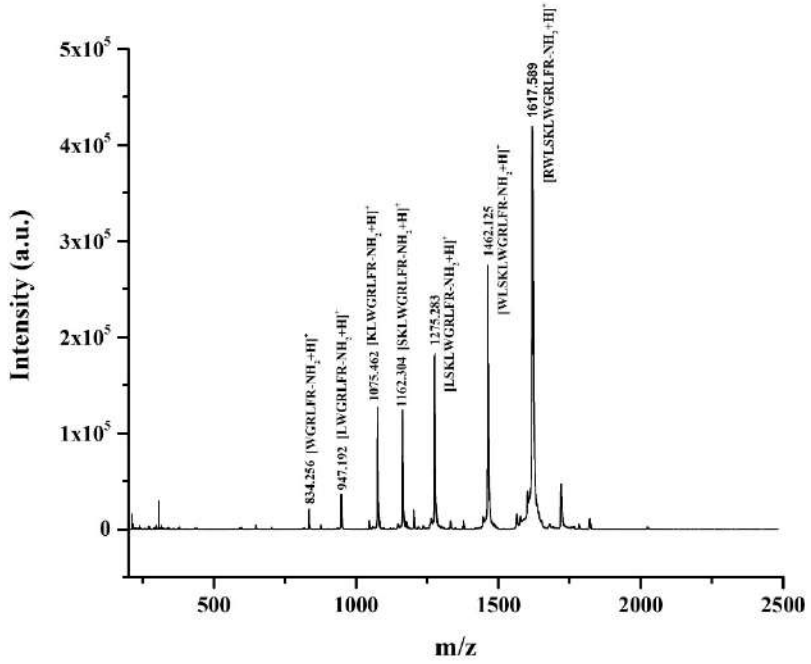

Figure E12. MALDI spectra of **RR-12** incubated with serum for 24 hours. Peak at m/z = 1617.589 Da corresponds to unfragmented [RWLSKLWGRLFR-NH_2+H]$^+$; Peaks at m/z = 1462.125 Da corresponds to [WLSKLWGRLFR-NH_2+H]$^+$, m/z = 1275.283 Da corresponds to [LSKLWGRLFR-NH_2+H]$^+$, m/z = 1162.304 Da corresponds to [SKLWGRLFR-NH_2+H]$^+$, m/z = 1075.462 Da corresponds to [KLWGRLFR-NH_2+H]$^+$, m/z = 947.192 Da corresponds to [LWGRLFR-NH_2+H]$^+$, and m/z = 834.256 Da corresponds to [WGRLFR-NH_2+H]$^+$. Hence, RR-12 incubated with serum for 24 h produces a large number peaks indicating proteolytic fragmentation effected by serum at different cleavage sites.

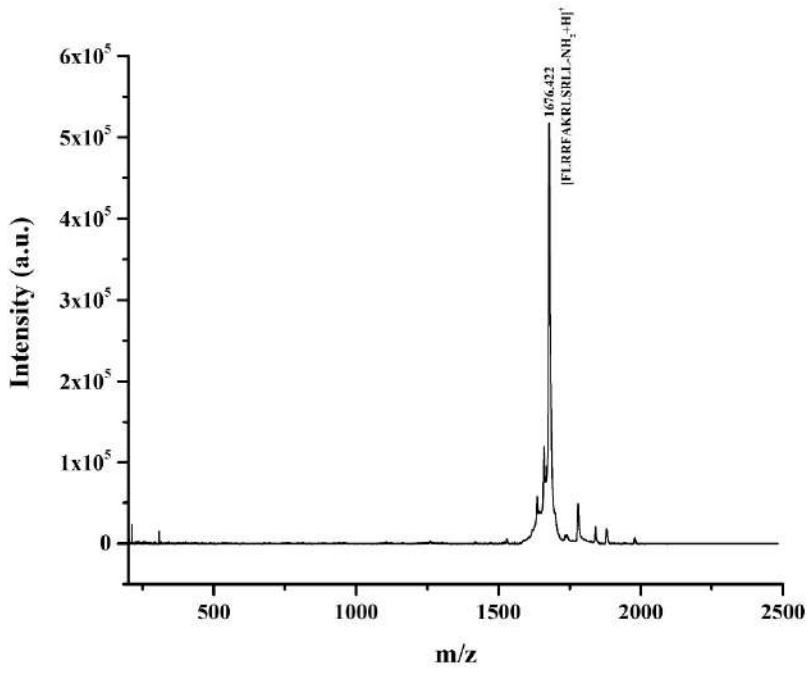

Figure E13. MALDI spectra of **FL-13** incubated with serum for 1 h. Peak at m/z = 1676.422 Da corresponds to unfragmented [FLRRFAKRLSRLL-NH_2+H]$^+$. No other peaks corresponding to any probable fragmentations of the peptide were observed.

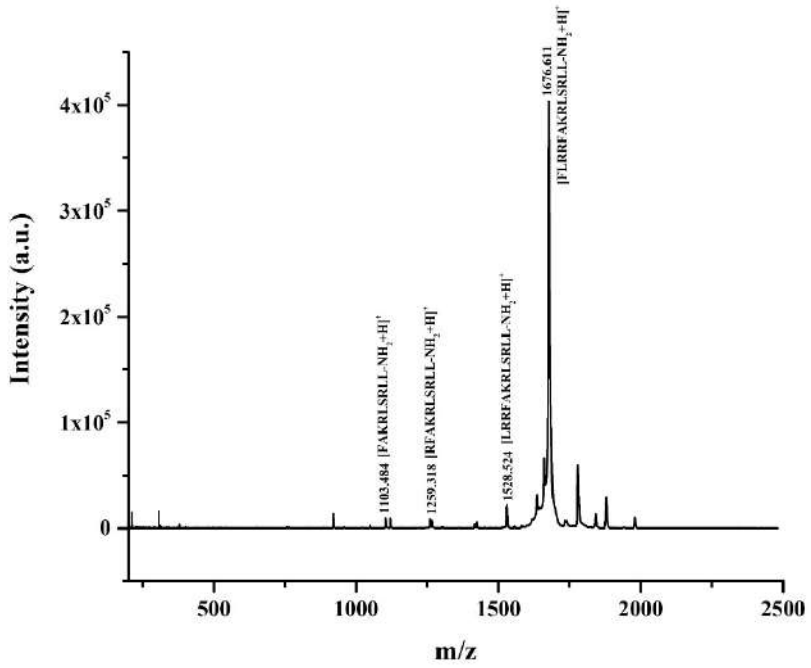

Figure E14. MALDI spectra of **FL-13** incubated with serum for 24 h. Peak at m/z = 1676.611 Da corresponds to unfragmented $[FLRRFAKRLSRLL\text{-}NH_2+H]^+$; Peaks at m/z = 1528.524 Da corresponds to $[LRRFAKRLSRLL\text{-}NH_2+H]^+$, m/z = 1259.318 Da corresponds to $[RFAKRLSRLL\text{-}NH_2+H]^+$, and m/z = 1103.484 Da corresponds to $[FAKRLSRLL\text{-}NH_2+H]^+$. Hence, FL-13 incubated with serum for 24 h produces a number peaks other than from unfragmented FL-13, indicating proteolytic fragmentation effected by serum at different cleavage sites.

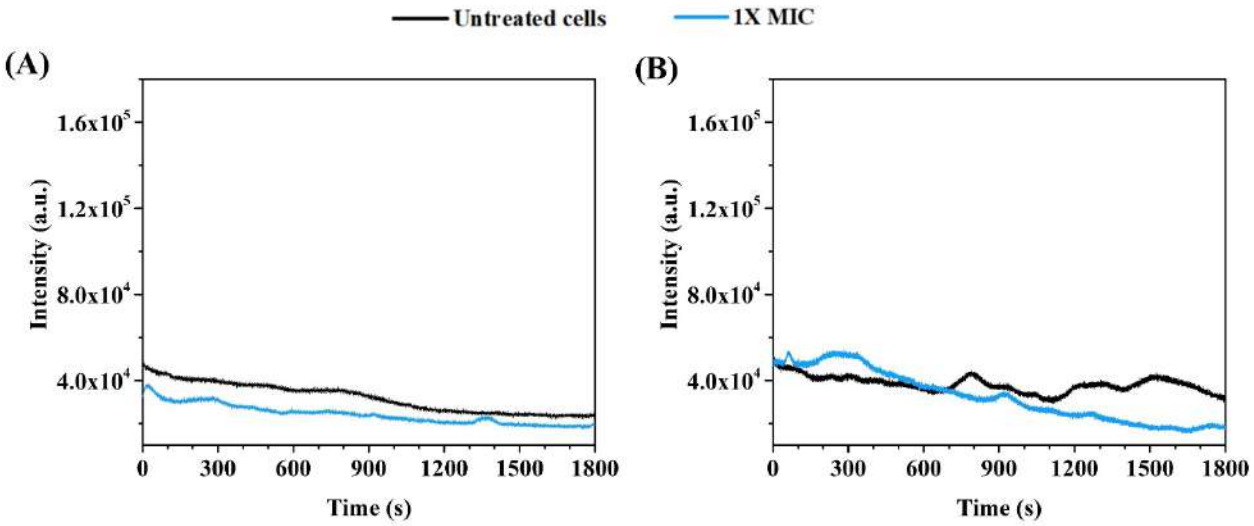

Figure E15. NPN preincubated with *C. albicans* cells treated with the peptides (A) **RR-12** and (B) **FL-13** showed almost no enhancements in the fluorescence intensities.

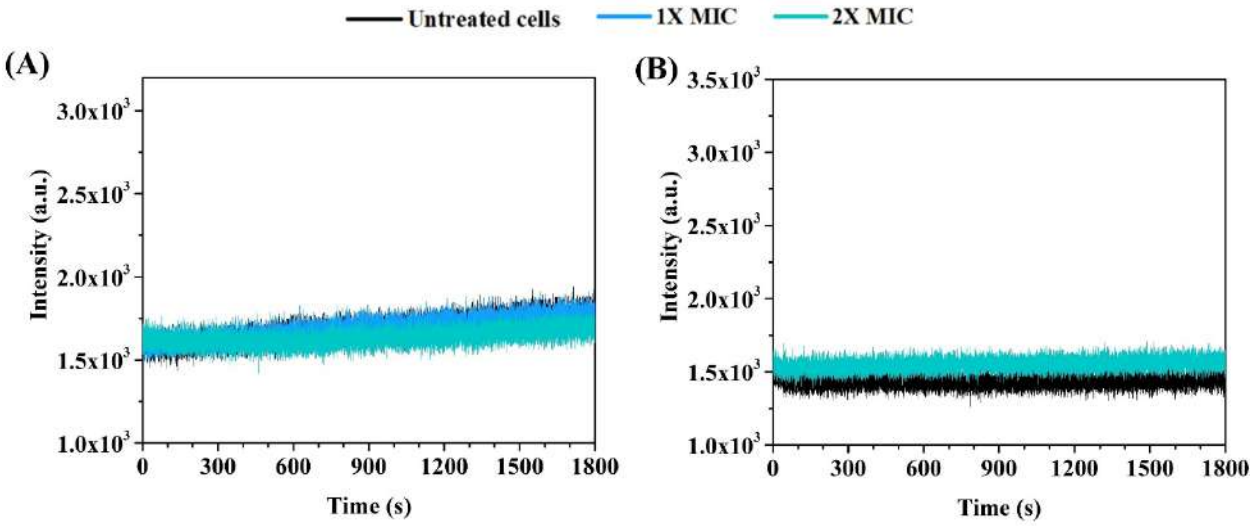

Figure E16. No enhancements in DiSC3(5) fluorescence signals were observed upon addition of the peptides (A) **RR-12** and (B) **FL-13** to *P. aeruginosa* cells.

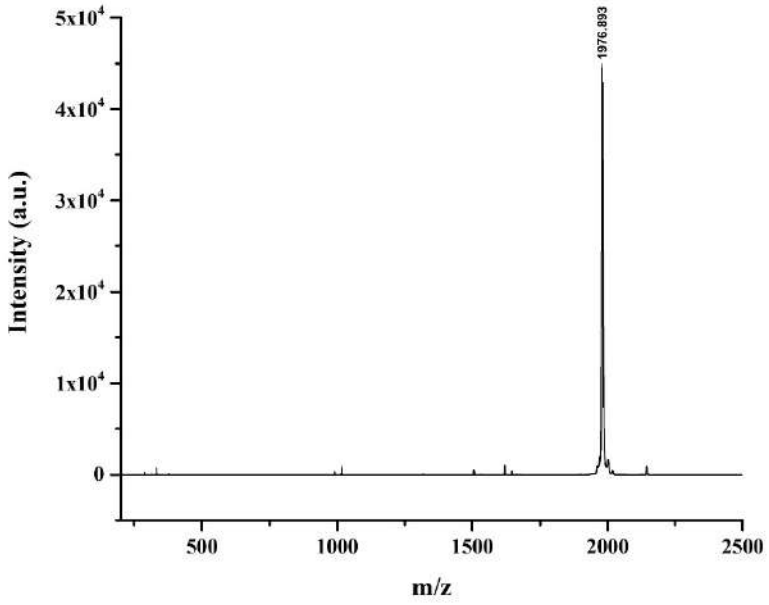

Figure E17. MALDI spectra of **Cf-RR-12**. Calculated $[M+H]^+$: 1976.016 Da; Observed $[M+H]^+$: 1676.893 Da.

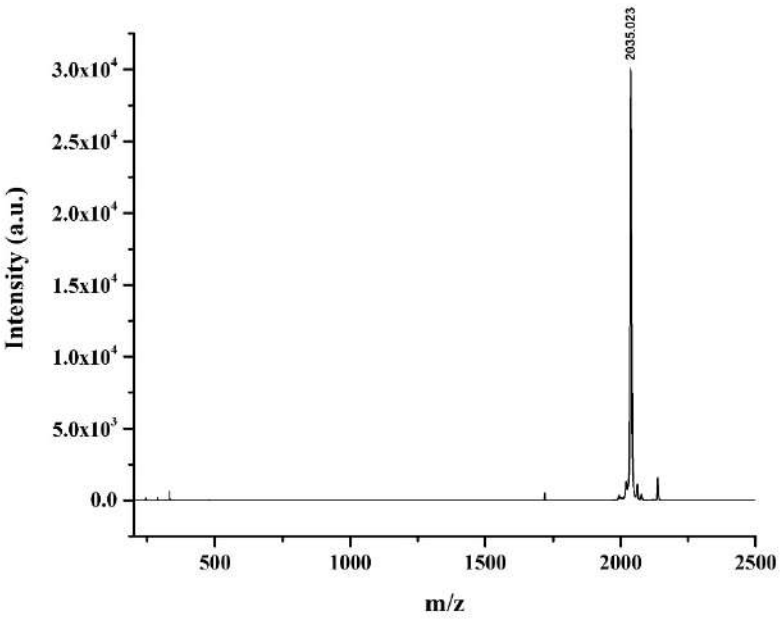

Figure E18. MALDI spectra of **Cf-FL-13**. Calculated $[M+H]^+$: 2034.127 Da; Observed $[M+H]^+$: 2035.023 Da.

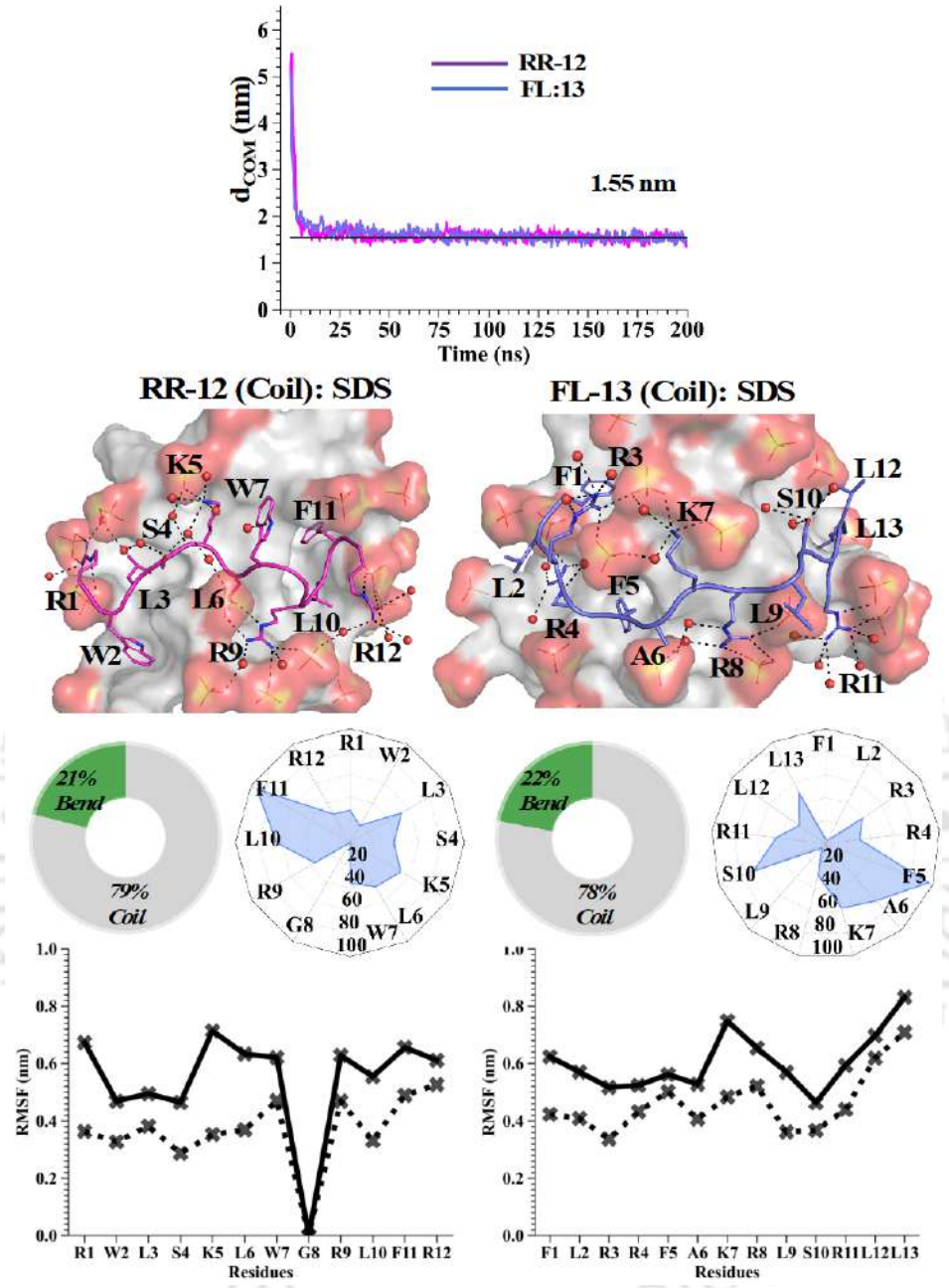

Figure E19. The distance between the centre of mass of the peptides and the micelle (d_{COM}) varies over time, exhibiting a plateau at approximately 1.55 nm. The molecular dynamics (MD) structure of the peptide in its coil form, complexed with the micelle, is presented with a zoomed-in view. In this view, interactions are illustrated with dotted lines, while water molecules are represented with spheres. The secondary structure content of the peptide within the micelle complex is highlighted. The solvent accessibility of the peptide's side-chain residues is depicted in a net plot (constant

contour in percentage). The trajectory averaged residue-wise root mean square fluctuation (RMSF) of the peptide in the presence and absence of the micelle.

Table E1. Percentages of various secondary structures adopted by the peptides in water, SDS (30 mM), DPC (10 mM) and 50% TFE analyzed using BeStSel software.

Peptides	Percentages of different secondary structures adopted			
	Helices	**β-strand**	**Turn**	**Others**
RR-12 in water	0.0	35.5	12.1	52.4
RR-12 in SDS	98.2	1.8	0.0	0.0
RR-12 in DPC	22.7	35.8	5.1	36.4
RR-12 in TFE	71.5	28.5	0	0.0
FL-13 in water	0.0	71.1	21.9	7.0
FL-13 in SDS	85.9	14.1	0.0	0.0
FL-13 in DPC	23.7	50.0	9.0	17.3
FL-13 in TFE	85.9	14.1	0.0	0.0

Table E2. Percentages of various secondary structures adopted by the peptides in water, LPS (1:0.5), LPS (1:1) and LPS (1:2) analyzed using BeStSel software.

Peptides	Percentages of different secondary structures adopted			
	Helices	**β-strand**	**Turn**	**Others**
RR-12 in water	0.0	31.3	9.0	59.7
RR-12 in LPS (1:0.5)	38.5	12.1	6.5	42.9
RR-12 in LPS (1:1)	59.1	26.9	0.3	13.7
RR-12 in LPS (1:2)	57.4	42.6	0.0	0.0
FL-13 in water	1.8	21.2	20.2	56.8
FL-13 in LPS (1:0.5)	62.8	11.3	13.6	12.3
FL-13 in LPS (1:1)	78.9	21.1	0.0	0.0

FL-13 in LPS (1:2)	77.6	22.4	0.0	0.0

Table E3. MD simulations of peptides (RR-12, FL-13) in the presence and absence of membrane mimics (micelle or bilayer). The initial structural model, simulation box size, composition, and sampling (a total of 15.2 μs) are given.

Sl. No	System	Replicas	Box Size (Å^3)	Number of molecules	Sampling (ns)
	Random coil peptide				
1	**Free RR-12**	3	70×70×70	Peptide: 1 Chloride: 5 Solvent: 11136	3000 (1000×3)
2	**Free FL-13**	3	70×70×70	Peptide: 1 Chloride: 6 Solvent: 11122	3000 (1000×3)
3	**RR-12: SDS**	3	100×100×140	Peptide: 1 SDS: 60 Sodium: 60 Chloride: 5 Solvent: 47400	600 (200×3)
4	**FL-13: SDS**	3	100×100×140	Peptide: 1 SDS: 60 Sodium: 60 Chloride: 6 Solvent: 47399	600 (200×3)
	Helical peptide				
5	**RR-12: SDS** Set-up A (0 mM NaCl) Set-up B (0 mM NaCl) Set-up C (150 mM NaCl)	 3 1 1	 100×100×100 110×110×110 100×100×100	Peptide: 1 SDS: 60 Sodium: 60/60/149 Chloride: 5/5/94 Solvent: 31712/44597/31534	1000 (200×5)
6	**FL-13: SDS** Set-up A (0 mM NaCl) Set-up B (0 mM NaCl) Set-up C (150 mM NaCl)	 3 1 1	 100×100×100 110×110×110 100×100×100	Peptide: 1 SDS: 60 Sodium: 60/60/149 Chloride: 6/6/95 Solvent: 31701/44577/31523	1000 (200×5)
7	**RR-12: Bilayer** (Outer Leaflet: 28 Lipid A of *P. aeruginosa*; Inner Leaflet: 60 PE, 16 PG and 4 CL)	3	67.5×67.5×110	Peptide: 1 Lipids: 108 Sodium: 80 Chloride: 5 Solvent: 11509	3000 (1000×3)

8	**FL-13: Bilayer** (Outer Leaflet: 28 Lipid A of *P. aeruginosa*; Inner Leaflet: 60 PE, 16 PG and 4 CL)	3	67.5×67.5×110	Peptide: 1 Lipids: 108 Sodium: 80 Chloride: 6 Solvent: 11609	3000 (1000×3)

Abbreviations

Naturally occurring amino acids with abbreviations and single letter codes

Amino acids	Abbreviations	One letter code
Alanine	Ala	A
Arginine	Arg	R
Asparagine	Asn	N
Aspartic acid	Asp	D
Cysteine	Cys	C
Glutamine	Gln	Q
Glutamic acid	Glu	E
Glycine	Gly	G
Histidine	His	H
Isoleucine	Ile	I
Leucine	Leu	L
Lysine	Lys	K
Methionine	Met	M
Phenylalanine	Phe	F
Proline	Pro	P
Serine	Ser	S
Threonine	Thr	T
Tryptophan	Trp	W
Tyrosine	Tyr	Y
Valine	Val	V

Unnatural amino acid

Amino acids	Abbreviations
α-Amino-3-guanidino-propionic acid	Agp
Diaminobutyric acid	Dab
Diaminopropanoic acid	Dap
Norleucine	Nle
Octahydroindolecarboxylic acid	Oic
Ornithine	Orn
Tetrahydroisoquinolinecarboxylic acid	Tic

ACN	Acetonitrile
ABSSSI	Acute bacterial skin and skin structure infections
AMBPs	Antimicrobial bridged bicyclic peptides
AMP	Antimicrobial peptide
AMR	Antimicrobial resistance
AO	Acridine orange
Boc	tert-Butyloxycarbonyl
CD	Circular dichroism
CFU	Colony-forming unit
CL	Cardiolipin
CMC	Critical micelle concentration
CMS	Colistin methanesulfonate
CRE	Carbapenem-resistant Enterobacterales
cSSSI	Complicated skin and skin structure infections
DCM	Dichloromethane
DIPEA	N,N-diisopropylethylamine
DiSC3(5)	3,3'-Dipropylthiadicarbocyanine iodide
DMF	N,N-Dimethylformamide
DNA	Deoxyribonucleic acid
DPC	Dodecylphosphorylcholine
D8PG	1,2-dioctanoyl-sn-glycero-3-phospho-(1'-rac-glycerol)
EDTA	Ethylenediaminetetraacetic acid
ESI-MS	Electrospray ionization mass spectrometry
FACS	Fluorescence-activated cell sorting
FDA	The Food and Drug Administration
FESEM	Field emission scanning electron microscope
FETEM	Field emission transmission electron microscope
FITC	Fluorescein isothiocyanate
Fmoc	9-Fluorenylmethyloxycarbonyl
GABA	Gamma-aminobutyric acid
HABP	Hospital-acquired and ventilator-associated bacterial pneumonia
HBTU	2-(1H-Benzotriazol-1-yl)-1,1,3,3-tetramethyluronium hexafluorophosphate
hBD	Human beta-defensins
HCCA	α-Cyano-4-hydroxycinnamic acid
HDF	Human dermal fibroblasts
HNP	Human neutrophil peptide
HOBt	1-hydroxybenzotriazole
HPLC	High-performance liquid chromatography
ITC	Isothermal titration calorimetry

LPS	Lipopolysaccharide
LTA	Lipoteichoic acid
MALDI	Matrix-assisted laser desorption/ionization
MD	Molecular dynamics
MDR-TB	Multidrug-resistant tuberculosis
MeOH	Methanol
MIC	Minimum inhibitory concentration
MMPBS	Molecular Mechanics Poisson-Boltzmann Surface Area
MRSA	Methicillin-resistant *Staphylococcus aureus*
MSSA	Methicillin- susceptible *Staphylococcus aureus*
MTT	3-(4,5-dimethylthiazol-2-yl)-2,5-diphenyltetrazolium bromide
NMR	Nuclear magnetic resonance
NPN	N-Phenyl-1-naphthylamine
OD	Optical density
PBS	Phosphate buffer saline
PC	Phosphatidylcholine
PE	Phosphatidylethanolamine
PG	Phosphatidylglycerol
PI	Phosphatidylinositol/ Propidium iodide
POPE	1-palmitoyl-2-oleoyl-phosphatidylethanolamine
POPG	1-Palmitoyl-2-oleoyl-sn-glycero-3-(phospho-rac-(1-glycerol))
PS	Phosphatidylserine
RBC	Red blood cell
RNA	Ribonucleic acid
RMSF	Root mean square fluctuation
RT	Room temperature
SASA	Solvent accessible surface area
SDS	Sodium dodecyl sulfate
SM	Sphingomyelin
Spp.	Species pluralis
TFA	Trifluoroacetic acid
TFE	2,2,2-Trifluoroethanol
TIS	Triisopropylsilane
VAP	Ventilator-associated pneumonia
VRE	Vancomycin-resistant Enterococci
UV	Ultraviolet

Microbes used in the study

Microbes	**Full names**
A. baumannii	*Acinetobacter baumannii*
E. coli	*Escherichia coli*
C. albicans	*Candida albicans*
K. pneumoniae	*Klebsiella pneumoniae*
P. aeruginosa	*Pseudomonas aeruginosa*
S. aureus	*Staphylococcus aureus*

List of publications

Part of the thesis

1. **Sarkar, T.**; Chetia, M.; Chatterjee, S. Antimicrobial Peptides and Proteins: From Nature's Reservoir to the Laboratory and Beyond. *Front. Chem*. **2021**, *9*, 691532. DOI: https://doi.org/10.3389/fchem.2021.691532

2. **Sarkar, T.**; Ghosh, S.; Sundaravadivelu, P.K.; Pandit, G.; Debnath, S.; Thummer, R.P.; Satpati, P.; Chatterjee, S. Mechanism of Protease Resistance of D-Amino Acid Residue Containing Cationic Antimicrobial Heptapeptides. *ACS Infect. Dis*. **2024**, *10* (2), 562-581. DOI: https://doi.org/10.1021/acsinfecdis.3c00491

3. **Sarkar, T.**; Vignesh, S.R.; Sehgal, T.; Ronima, K.R.; Thummer, R.P.; Satpati, P.; Chatterjee, S. Development of protease resistant and non-cytotoxic Jelleine analogs with enhanced broad spectrum antimicrobial efficacy. *Biochim. Biophys. Acta Biomembr*. **2024**, *1866* (6), 184336. DOI: https://doi.org/10.1016/j.bbamem.2024.184336

4. **Sarkar, T.**; Vignesh, S.R.; Sundaravadivelu, P.K.; Thummar, R.P.; Satpati, P.; Chatterjee, S. *De novo* Design of Tryptophan containing Broad-Spectrum Cationic Antimicrobial Octapeptides. *ChemMedChem* **2024**, *20* (2), e202400566. DOI: https://doi.org/10.1002/cmdc.202400566

5. Sarkar, T.; Rajalakshmi, V.S.; K R, R., Thummer, R.P., Chatterjee, S. Serum-Stable, Cationic, α-Helical AMPs to Combat Infections of ESKAPE Pathogens and *C. albicans*. *ACS Appl. Bio Mater*. **2025**, *8* (5), 3941-3957. DOI: https://doi.org/10.1021/acsabm.5c00126

6. Ghosh, S.; **Sarkar, T.**; Chatterjee, S.; Satpati, P. Alchemical Simulation Aided *De novo* Design of Membrane Active Antimicrobial Hepta-Peptides. (Revised)

Other than the thesis

7. Pandit, G.; **Sarkar, T.**; Vignesh, S.R.; Debnath, S.; Satpati, P.; Chatterjee, S. Delineating the Mechanism of Action of a Protease Resistant and Salt Tolerant Synthetic Antimicrobial Peptide against *Pseudomonas aeruginosa*. *ACS Omega* **2022**, *7* (18), 15951-15968. DOI: https://doi.org/10.1021/acsomega.2c01089

8. Ghosh, S.; **Sarkar, T.**; Chatterjee, S.; Satpati, P. Bridging Thermodynamics, Antimicrobial Activity, and pH Sensitivity of Cationic Membranolytic Heptapeptides-A Computational and Experimental Study. *J. Chem. Inf. Model*. **2023**, *63* (8), 2393-2408. DOI: https://doi.org/10.1021/acs.jcim.2c01419

9. Chetia, M.; **Sarkar, T.**; Yadav, M.; Dey, C.; Sundaravadivelu, P. K.; Thummer, R. P.; Chatterjee, S. Tuning of hydrophobic–hydrophilic balance for the development of a salt-tolerant and protease-resistant lipopeptide AMP. *New J. Chem.* **2024**, *48*, 2764-2777. DOI: https://doi.org/10.1039/D3NJ04815B